# OPTICAL AMPLIFIERS AND THEIR APPLICATIONS





*Cosponsored by*
IEEE/Lasers and Electro-Optics Society
Optical Society of America

**1991 TECHNICAL DIGEST SERIES VOLUME 13**

**JULY 24–26, 1991**
**SNOWMASS VILLAGE, COLORADO**

# REPORT DOCUMENTATION PAGE

Form Approved
OMB No. 0704-0188



| 1. AGENCY USE ONLY (Leave blank) | 2. REPORT DATE | 3. REPORT TYPE AND DATES COVERED |
|---|---|---|
| | May 22, 1992 | Final 1/1/91-12/31/91 |

**4. TITLE AND SUBTITLE**
Organization of the 1991 Optical Society of America Photonic Science Topical Meeting Series

**5. FUNDING NUMBERS**
G - AFOSR-91-0176

**6. AUTHOR(S)**
Jarus W. Quinn

**7. PERFORMING ORGANIZATION NAME(S) AND ADDRESS(ES)**
Optical Society of America
2010 Massachusetts Ave. NW
Washington, DC 20036

**8. PERFORMING ORGANIZATION REPORT NUMBER**
AFOSR-TR- 92 0521

**9. SPONSORING/MONITORING AGENCY NAME(S) AND ADDRESS(ES)**
US Air Force Office of Scientific Research
Department of the Air Force
Bolling Air Force Base
Washington, DC 20332-6448
NE
Scalossberg

**10. SPONSORING/MONITORING AGENCY REPORT NUMBER**
2305/A1

**11. SUPPLEMENTARY NOTES**

**12a. DISTRIBUTION/AVAILABILITY STATEMENT**
Approved for public release
Distribution unlimited

**12b. DISTRIBUTION CODE**

**13. ABSTRACT** (Maximum 200 words)

Attach list of reports supported by Optical Society of America
Photorefractive Materials, Effects, and Devices
Integrated Photonics Research
Nonlinear Guided Wave Phenomena
Optical Amplifiers and Their Applications
Optical computing
Picosecond Electronics and Optoelectronics
Quantum Optoelectronics
Photonic Switching
Microphysics of Surfaces: Beam Induced Processes
Soft X-ray Projection Lithography
Short Wavelength Coherent Radiation, Generation & Applications
Presistent Spectral Hole-Buring: Science & Applications

| 14. SUBJECT TERMS | 15. NUMBER OF PAGES |
|---|---|
| | 16. PRICE CODE |

| 17. SECURITY CLASSIFICATION OF REPORT | 18. SECURITY CLASSIFICATION OF THIS PAGE | 19. SECURITY CLASSIFICATION OF ABSTRACT | 20. LIMITATION OF ABSTRACT |
|---|---|---|---|
| [redacted] | [redacted] | [redacted] | [redacted] |

Summaries of papers presented at the
Optical Amplifiers and Their Applications Topical Meeting

# Optical Amplifiers and Their Applications

1991 Technical Digest Series
Volume 13

CONFERENCE EDITION
July 24–26, 1991 — Snowmass Village, Colorado



Cosponsored by
IEEE/Lasers and Electro-Optics Society
Optical Society of America

Optical Society of America
2010 Massachusetts Avenue, NW
Washington, DC 20036

Articles in this publication may be cited in other publications. In order to facilitate access to the original publication source, the following form for the citation is suggested:

> Name of Author(s), "Title of Paper," in Technical Digest on Optical Amplifiers and Their Applications, 1991 (Optical Society of America, Washington, D.C., 1991), Vol. 13, pp. xx-xx.

ISBN Number

| | |
|---|---|
| Conference Edition | 1-55752-198-0 (softcover) |
| Postconference Edition | 1-55752-199-9 (hardcover) |
| (Note: Postconference Edition includes postdeadline papers.) | |
| 1991 Technical Digest Series | 1-55752-192-1 (hardcover) |

Library of Congress Catalog Card Number

| | |
|---|---|
| Conference Edition | 90-64488 |
| Postconference Edition | 90-64487 |

# CONTENTS

## GENERAL COCHAIRS

**Kiyoshi Nakagawa**
NTT Transmission Systems Laboratories, Japan

**David Payne**
University of Southampton, United Kingdom

**N. Anders Olsson**
AT&T Bell Laboratories, USA

## TECHNICAL PROGRAM COMMITTEE

### PROGRAM COCHAIRS

**Mike O'Mahony**
British Telecom Research Laboratories, United Kingdom

**Richard E. Wagner**
Bellcore, USA

### FIBER AMPLIFIERS AND FIBER COMPONENTS

**R. I. Laming,** *Chair*
University of Southampton, United Kingdom

**W. L. Emkey**
AT&T Bell Laboratories, USA

**E. Desurvire**
AT&T Bell Laboratories, USA

**G. Grasso**
Societa Cavi Pirelli SpA, Italy

**D. W. Hall**
Corning, Inc., USA

**C. A. Millar**
British Telecom Research Laboratories, United Kingdom

**W. J. Miniscalco**
GTE Laboratories, USA

**M. Nakazawa**
NTT Transmission Systems Laboratories, Japan

**M. Ogai**
The Furukawa Electric Company Ltd., Japan

**S. Poole**
University of Sydney, Australia

**H. Tanaka**
Mitsubishi Cable Industries Ltd., Japan

### SEMICONDUCTOR AMPLIFIERS AND PUMP LASERS

**K. Kurumada,** *Chair*
NSC Electronics Laboratories, Japan

**M. J. Adams**
British Telecom Research Laboratories, United Kingdom

**D. P. Bour**
David Sarnoff Research Center, USA

**G. Eisenstein**
Technion-Israel Institute of Technology, Israel

**T. Kamijoh**
OKI Electric Industry Company Ltd., Japan

**T. Kamiya**
University of Tokyo, Japan

**I. Mito**
NEC Corporation, Japan

**K. E. Stubkjaer**
University of Denmark, Denmark

**M. Suyama**
Fujitsu Ltd., Japan

**C. E. Zah**
Bellcore, USA

### SYSTEMS APPLICATIONS AND INSTALLATIONS

**C. R. Giles,** *Chair*
AT&T Bell Laboratories, USA

**K. Aida**
NTT Transmission Systems Laboratories, Japan

**J. Auge**
CGE, Marcoussis, France

**T. Hadjifotiou**
STC Technology Ltd., United Kingdom

**E. Eichen**
GTE Laboratories, USA

**R. Heidemann**
SEL/Alcatel, Federal Republic of Germany

**C. Lin**
Bellcore, USA

**J. J. O'Reilly**
University of Wales, United Kingdom

**Y. K. Park**
AT&T Bell Laboratories, USA

**S. Yamamoto**
KDD Meguro R&D Laboratories, Japan

## TUESDAY, JULY 23, 1991

### CABARET LOBBY

**6:00 pm–9:00 pm REGISTRATION**

### ELDORADO ROOM

**7:00 pm–8:30 pm INFORMAL RECEPTION**

## WEDNESDAY, JULY 24, 1991

### CABARET LOBBY

**7:00 am–5:00 pm REGISTRATION/SPEAKER CHECK-IN**

### ANDERSON ROOM (Conference Center)

**7:00 am–8:00 am BREAKFAST**

### CABARET ROOM

**8:00 am**
**OPENING REMARKS**
David Payne, *University of Southampton, United Kingdom*

**8:15 am–8:45 am**
**WA, PLENARY SESSION**
David Payne, *University of Southampton, United Kingdom, Presider*

**8:15 am (Invited)**
**WA1 Toward network transparency with photonic amplifiers,** Peter Cochrane, Christopher J. Todd, *British Telecom Research Laboratories, U.K.* Optical amplifiers will revolutionize telecommunications and make possible new classes of virtually lossless network with a dual digital-analog capability and almost infinite split ratios. **(p. 2)**

**8:45 am–10:00 am**
**WB, DOPED FIBER AMPLIFIERS**
R. I. Laming, *University of Southampton, United Kingdom, Presider*

**8:45 am (Invited)**
**WB1 Progress in erbium doped fiber amplifiers,** J. R. Simpson, D. J. DiGiovanni, *AT&T Bell Laboratories.* The performance of erbium doped fiber amplifiers continues to be challenged by applications requiring output powers of tens of milliwatts, high gain-bandwidth products and quantum limited noise. Progress in realizing these goals will be discussed. **(p. 8)**

## WEDNESDAY, JULY 24, 1991—*Continued*

**9:15 am (Invited)**
**WB2 Prospects for fiber amplifiers at 1.3 $\mu$m,** Mike Brierley, *British Telecom Research Laboratories, U.K.* For fiber amplifiers at 1.3 $\mu$m two practical possibilities present themselves, neodymium doped ZBLAN and praseodymium-doped ZBLAN. Recent results show praseodymium to be the better prospect. **(p. 12)**

**9:45 am**
**WB3 $Nd^{3+}$ doped fluoride fiber amplifier module with 10-dB gain and high pump efficiency,** Yoshiaki Miyajima, Tomoki Sugawa, Tetsurou Komukai. *NTT Transmission Systems Laboratories, Japan.* A gain of 10 dB was obtained in a neodymium-doped fluoride fiber amplifier by using bidirectional 25-mW pumping and a 1.05-$\mu$m rejection filter. **(p. 16)**

### CABARET LOBBY

**10:00 am–10:30 am COFFEE BREAK/EXHIBITS**

### CABARET ROOM

**10:30 am–12:00 m**
**WC, LASER DIODE PUMP SOURCES**
K. Kurumada, *NSC Electronics Laboratories, Japan* and M. O'Mahony, *British Telecom Research Laboratories, United Kingdom, Presiders*

**10:30 am (Invited)**
**WC1 1.48 $\mu$m and 0.98 $\mu$m high-power laser diodes for erbium-doped fiber amplifiers,** Ikuo Mito, Kenji Endo, *NEC Corporation.* Reported here is recent progress in the development of 1.48 $\mu$m and 0.98 $\mu$m wavelength high-power laser diodes. Multi-quantum well or strained quantum well structures, employed as active layers, have facilitated both high power operations and reliable long-time aging tests under high output conditions of up to 100 mW. **(p. 22)**

**11:00 am**
**WC2 0.98-$\mu$m strained single quantum well lasers launching high optical power in a single-mode fiber,** Masato Wada, Kaoru Yoshino. *Tokai-mura, Japan;* Masanobu Okayasu, Jiro Temmyo, *NTT Opto-electronics Laboratories, Japan.* Optical power as high as 58 mW in a single-mode fiber is obtained using narrow-ridge waveguide 0.98-$\mu$m lasers on the basis of an investigation of epitaxial layer structures. **(p. 26)**

**11:15 am**
**WC3 High power operation of 1.48-$\mu$m GaInAsP/GaInAsP strained-layer multiple quantum well lasers,** H. Kamei, M. Yoshimura, H. Kobayashi, N. Tatoh, H. Hayashi, *Sumitomo Electric Industries, Ltd., Japan.* 1.48-$\mu$m GaInAsP/GaInAsP MQW lasers were fabricated by OMVPE. Maximum light output power of 236 mW was obtained for a 900-$\mu$m long laser with 1% compressive strain in quantum wells. **(p. 30)**

**11:30 am**
**WC4 Single-mode 980-nm pump lasers for fiber amplifiers,** F. D. Crawford, W. F. Sharfin, B. Elman, R. B. Lauer, P. Mabrahtu, E. Eichen, *GTE Laboratories, Inc.* Ridge waveguide 980-nm wavelength, InGaAs/GaAs lasers that lase as high as 170 mW have been fabricated to pump $Er^{3+}$ optical fiber amplifiers. **(p. 34)**

**11:45 am**
**WC5 High power 980-nm ridge waveguide laser in a single-mode fiber coupled package,** Richard F. Murison, Shuyen R. Lee, Nigel Holehouse, Alan H. Moore, Kenneth M. Dzurko, *EG&G Canada Ltd;* Aldo Righetti, Giorgio Grasso, Flavio Fontano, *Societa Cavi Pirelli spa, Italy;* Christian F. Schaus, Shangzhu Sun, *U. New Mexico;* Nancy A. Dinkel, John C. Connolly, *David Sarnoff Research Center.* A 980-nm strained layer ridge waveguide laser is described, exhibiting 54-mW coupled power into a single-mode fiber pigtail. Systems performance in an EDFA power amplifier is described. **(p. 38)**

**12:00 m–1:30 pm LUNCH (on your own)**

## CABARET LOBBY

**12:00 m–1:30 pm EXHIBITS**

## CABARET ROOM

**1:30 pm–3:00 pm**
**WD, MATERIAL EFFECTS IN FIBER AMPLIFIERS**
G. Grasso, *Societa Cavi Pirelli SpA, Italy, Presider*

**1:30 pm (Invited)**
**WD1 Materials for erbium-doped fiber amplifiers,** William J. Miniscalco, *GTE Laboratories, Inc.* The composition of the host glass significantly affects the characteristics of $Er^{3+}$ fiber amplifiers. For silica, codoping with $Al_2O_3$ has particularly important optical and material implications. **(p. 44)**

**2:00 pm**
**WD2 Nonlinear excited state absorption in $Er^{3+}$-doped fiber with high power 980-nm pumping,** M. G. Sceats, P. A. Krug, G. R. Atkins, S. C. Guy, S. B. Poole, *U. Sydney, Australia.* We report the measurement of nonlinear excited state absorption in $Er^{3+}$-doped fibers pumped at 980 nm. The implications for high power high-gain amplifiers are discussed. **(p. 48)**

**2:15 am**
**WD3 Amplification reduction in fiber amplifiers due to up-conversion at $Er^{3+}$ concentrations below 1000 ppm,** P. Blixt, J. Nilsson, B. Jaskorzynska, *Royal Institute of Technology, Sweden;* T. Carlnas, *Ericsson Cables AB, Sweden.* We show that up-conversion drastically reduces amplification for $Er^{3+}$-doping concentrations of 70–840 ppm by weight. Comparing experimental and simulated characteristics, we obtain an up-conversion coefficient of $10^{-22}$ $m^3/s$. **(p. 52)**

WEDNESDAY, JULY 24, 1991—*Continued*

**2:30 pm**
**WD4 Erbium-doped fiber amplifiers pumped in the 800-nm band,** B. Pedersen, *Technical U., Denmark;* S. Zemon, W. J. Miniscalco, M. P. Singh, *GTE Laboratories, Inc.* The performance of $Er^{3+}$-doped silica and fluorophosphate fiber amplifiers pumped at 800 nm has been analyzed using measured parameters, including excited state absorption cross sections. **(p. 56)**

**2:45 pm**
**WD5 Gain characteristics of a lanthanum co-doped erbium fiber amplifier,** Yasuo Kimura, Masataka Nakazawa, *NTT Transmission Systems Laboratories, Japan.* A lanthanum co-doped erbium fiber amplifier has a gain of 35–43 dB at 1.535 $\mu$m. A moderate gain flattening effect was observed at 1.552 $\mu$m. **(p. 60)**

## CABARET LOBBY

**3:00 pm–3:30 pm COFFEE BREAK/EXHIBITS**

## CABARET ROOM

**3:30 pm–4:30 pm**
**WE, SEMICONDUCTOR OPTICAL AMPLIFIERS**
J. J. O'Reilly, *University of Wales, United Kingdom*
and M. Suyama, *Fujitsu Ltd., Japan, Presiders*

**3:30 pm (Invited)**
**WE1 The future role of semiconductor optical amplifiers,** I. W. Marshall, *British Telecom.* Despite the development of $Er^{3+}$ doped fiber amplifiers, semiconductor amplifiers still have important applications at 1.3$\mu$m and as fast optical switches for routing, timing extraction and wavelength conversion.
**(p.66)**

**4:00 pm**
**WE2 Laser structure for polarization insensitive semiconductor amplifier with low current consumption,** P. Doussiere, B. Mersali, A. Accard, P. Garabedian, G. Gelly, J. L. Lafragette, F. Leblond, G. Michaud, M. Monnot, B. Fernier, *Alcatel Alsthom Recherche, France.* Using a high yield process polarization insensitive amplifiers are made with 18-dB fiber to fiber gain for low forward current and reflectivities below $10^{-4}$. **(p. 68)**

**4:15 pm**
**WE3 Strained layer quantum well semiconductor optical amplifiers: polarization insensitive amplification,** M. Joma, H. Horikawa, M. Nakajima, M. Kawahara, T. Kamijoh, *Oki Electric Industry Co., Japan.* Polarization insensitive optical amplification was demonstrated in newly developed semiconductor amplifiers that have strained GaInAsP quantum well structures as active layers. **(p. 72)**

**4:30 pm–5:50 pm**
**PP, PRODUCT PRESENTATIONS**
S. Poole, *University of Sydney, Australia, Presider*

**4:30 pm–4:50 pm**
**PP1 EDFA Consultants,** *Kingston, RI,* Dr. Harish R. D. Sunak, President, is author of "Bibliography on Erbium-doped fiber amplifiers 1987–1990" with 600 references and subject index and Fundamentals of EDFA's with learning software.

**4:50 pm–5:10 pm**
**PP2 Santec USA Corp.,** *Saddlebrook, NJ,* Roseanee DeBlack. The tunable semiconductor laser TSL-80 is available in 1.55 μm or 1.30 μm wavelength with tunability of more than 80 nm. Front keypad allows easy manual operation GP-1B provides external control of all keypad functions. Most suitable for applications such as devices as isolators, waveguides, switches, filters, couplers, amplifiers, fibers. Optical amplifier testing is made easy with the OAT-3000 from Santec. One engineer can operate the system and measure parameters for EDFA and SLA. Chips for SLA can also be characterized using a test fixture with a precise positioning stage. Accurate. Reliable. User-friendly.

**5:10 pm–5:30 pm**
**PP3 JDS Fitel, Inc.,** *Canada,* Joseph Straus. JDS Fitel will present several passive components for design and manufacturing of fiber amplifiers, including couplers/wdm's, blocking filters and polarization beamsplitters/combiners. Self-contained fiber amplifier modules will also be presented.

**5:30 pm–5:50 pm**
**PP4 Pirelli Cable Corp.,** *Lexington, SC,* Alan Guest. Pirelli Cable Corporation, world leader in designing and manufacturing Erbium Doped Fiber Amplifiers, presents Ampliphos; a self-contained EDFA designed for lab use with 15 dBm saturated output power and 30 dB gain.

**CABARET LOBBY**

**6:00 pm–7:00 pm EXHIBITS**

**ROOF GARDEN (Conference Center)**

**7:00 pm–8:30 pm RECEPTION**



**CABARET LOBBY**

**7:00 am–5:00 pm REGISTRATION/SPEAKER CHECK-IN**

**ANDERSON ROOM (Conference Center)**

**7:00 am–8:00 am BREAKFAST**

**CABARET ROOM**

**8:00 am–10:00 am**
**ThA, ULTRA-LONG DISTRANCE TRANSMISSION SYSTEMS**
C. R. Giles, *AT&T Bell Laboratories, USA, Presider*

**8:00 am (Invited)**
**ThA1 System limitations for fiber amplifier cascades,** Takeshi Ito, *NTT Transmission Systems Laboratories, Japan.* Fiber dispersion, amplifier performance, and noise accumulation limitations on amplifier cascade system performance as defined by (bit rate) × (distance) are evaluated from a system design viewpoint. **(p. 78)**

**8:30 am**
**ThA2 Erbium-doped fiber amplifier spectral behavior in transoceanic links,** J. P. Blondel, J. F. Marcerou, J. Auge, H. Fevrier, P. Bousselet, A. Dursin, *Alcatel Alsthom Recherche, France.* A model giving complete output spectra has been experimentally validated and simulations have been done for long haul links, in various configurations such as autofiltering. **(p. 82)**

**8:45 am**
**ThA3 Evaluation of theoretical limits of cascaded EDFA transmission systems,** O. Audouin, L. Prigent, J. P. Blondel, J. P. Hamaide, J. M. Gabriagues, *Alcatel Alsthom Recherche, France.* We have investigated some limits of multiamplifier transmission systems, by performing numerical simulations taking into account dispersion, Kerr effects, and amplified-spontaneous-emission. **(p. 86)**

**9:00 am**
**ThA4 Characteristics of single-carrier fiber-optic transmission systems using optical amplifiers,** S. Yamamoto, H. Taga, Y. Yoshida, H. Wakabayashi, *KDD R&D Laboratories, Japan.* The effect of variations around zero dispersion of a single-carrier optical fiber transmission system using optical amplifiers was characterized by numerical simulations and by a circulating loop. **(p. 90)**

**9:15 am**
**ThA5 Bit-error-rate measurements of a multithousant-kilometer fiber-amplifier transmission system using a circulating loop,** Neal S. Bergano, Jennifer Aspell, C. R. Davidson, P. R. Trischitta, B. M. Nyman, F. W. Kerfoot, *AT&T Bell Laboratories.* We expand on the method and results of a circulating loop experiment used to demonstrate the feasibility of ultralong distance transmission employing EDFA at high bit rates. **(p. 94)**

**9:30 am (Invited)**
**ThA6 Ultralong distance soliton transmission using erbium fiber amplifiers,** L. F. Mollenauer, *AT&T Bell Laboratories.* We report soliton transmission through a chain of dispersion shifted fiber segments and low gain erbium amplifiers, with measured bit error rate $\leq 10^{-10}$ over transoceanic paths at 2.5 Gbits/s. **(p. 98)**

## CABARET LOBBY

**10:00 am–10:30 am COFFEE BREAK/EXHIBITS**

## CABARET ROOM

**10:30 am–12:00 m**
**ThB, SPECTRAL CHARACTERISTICS OF FIBER AMPLIFIERS**
W. J. Miniscalco, *GTE Laboratories, USA, Presider*

**10:30 am (Invited)**
**ThB1 Spectral gain cross saturation and hole burning in wideband Er-doped fiber amplifier amplifers,** M. Tachibana, *Seiko Instruments, Inc., Japan;* R. I. Laming, P. R. Morkel, D. N. Payne, *Southampton U., U. K.* Cross saturation characteristics are investigated in broadband 1.48-$\mu$m pumped and 980-nm pumped gain-shaped EDFAs. Gain-shaping is shown to give a more uniform spectral gain compression on saturation. **(p. 104)**

**11:00 am**
**ThB2 Multichannel amplification characteristics of saturated erbium-doped fiber amplifiers,** Y. H. Cheng, N. Kagi, A. Oyobe, K. Nakamura, *Furukawa Electric Co., Ltd., Japan.* The amplification characteristics of a Ge/Er-doped and a Ge/Al/Er-doped silica fiber post amplifiers are compared experimentally in a multichannel system. **(p. 108)**

**11:15 am**
**ThB3 Diode-pumped, electrically tunable erbium-doped fiber ring laser with a fiber Fabry-Perot etalon,** J. L. Zyskind, J. W. Sulhoff, J. Stone, D. J. DiGiovanni, L. W. Stulz, H. M. Presby, A. Piccirilli, P. E. Pramayon, *AT&T Bell Laboratories.* A diode-pumped erbium-doped fiber laser tuned by a fiber Fabry-Perot etalon has low threshold (2.9 mW), high slope efficiency (0.15), and wide tuning range (60 nm). **(p. 112)**

**11:30 am**
**ThB4 Widely tunable actively mode-locked erbium fiber ring laser,** T. Pfeiffer, H. Schmuck, *SEL Alcatel Research Center, F.R.G.* A widely tunable actively mode-locked erbium-doped fiber ring laser pumped by a 980-nm laser diode is presented. It emits picosecond pulses in the range 1529–1562 nm at variable repetition rates up to 6 GHz. **(p. 116)**

THURSDAY, JULY 25, 1991—*Continued*

**11:45 am**
**ThB5 Femtosecond soliton collapse by frequency modulation instability in erbium-doped fiber amplifiers,** I. R. Gabitov, *L. D. Landau Institute for Theoretical Physics, U.S.S.R.;* M. Romagnoli, S. Wabnitz, *Fondazione Ugo Bordoni, Italy.* A frequency modulation instability leads to femtosecond soliton collapse in erbium fiber amplifiers, generating a train of pulses that collide under Raman self-scattering. **(p. 120)**

**12:00 m–1:30 pm LUNCH (on your own)**

## CABARET LOBBY

**12:00 m–1:30 pm EXHIBITS**

## CABARET ROOM

**1:30 pm–2:45 pm**
**ThC, CARRIER DYNAMICS AND NONLINEARITIES IN SEMICONDUCTOR AMPLIFIERS**
G. Eisenstein, *Technion-Israel Institute of Technology, Israel, Presider*

**1:30 pm (Invited)**
**ThC1 Nonlinear effects in semiconductor optical amplifiers,** Takaaki Mukai, Tadashi Saitoh, *NTT Basic Research Laboratories, Japan.* Nonlinear effects in semiconductor optical amplifiers, such as signal gain saturation and nearly degenerate four-wave mixing, are reviewed from the viewpoints of physical mechanism and use. **(p. 126)**

**2:00 pm**
**ThC2 Characterization of high speed phase modulators based on semiconductor optical amplifiers,** T. N. Nielsen, U. Gliese, B. Mikkelsen, K. E. Stubkjaer, *Technical U. Denmark;* B. Fernier, P. Doussiere, J. L. Lafragette, *Alcatel Alsthom Recherche, France.* Optical phase modulation with a semiconductor optical amplifier is investigated. By equalizing the phaseresponse, the 3-dB bandwidth is extended from 600 MHz to 2.5 GHz. **(p. 130)**

**2:15 pm**
**ThC3 Coupling between barrier and quantum well energy states in a multiple quantum well optical amplifier,** N. Tessler, R. Nagar, G. Eisenstein, *Technion-Israel Institute of Technology;* U. Koren, G. Raybon, *AT&T Bell Laboratories.* We report broadband static pump-probe measurements of interactions between carriers at energy levels in the barrier and quantum wells in 1.5 $\mu$m multiple quantum well amplifier. **(p. 134)**

**2:30 pm**
**ThC4 Phase modulation and optical switching by a semiconductor laser amplifier,** A. C. Labrujere, *PTT-Research Neher Laboratories, The Netherlands;* C. A. M. Steenbergen, C. J. van der Laan, *Delft U. Technology, The Netherlands.* Operation of a semiconductor laser amplifier simultaneously as phase modulator and optical switch is proposed. Theoretical and experimental results on performance in saturation are reported. **(138)**

**2:45 pm–3:45 pm**
**ThD COMPONENTS AND NOVEL AMPLIFIER CONFIGURATIONS**
M. Nakazawa. *NTT Transmission Systems Laboratories, Japan, Presider*

**2:45 pm**
**ThD1 Fiber Bragg filters for pump rejection and recycling in erbium doped fiber amplifiers,** M. C. Farries, C. M. Ragdale, D. C. J. Reid, *Plessey Research Caswell, Ltd., U.K.* Broadband chirped fiber Bragg filters centered at 980 nm with 99% reflectivity are reported. The filters are used to reject and recycle unabsorbed pump light from a fiber amplifier. **(p. 144)**

**3:00 pm**
**ThD2 Gain enhancement in reflected-pump erbium-doped fiber amplifiers,** C. R. Giles, J. Stone, L. W. Stulz, K. Walker, C. A. Burrus, *AT&T Bell Laboratories.* Improved performance of EDFAs is achieved using wavelength-selective reflective filters to double-pass the pump beam. In low-gain amplifiers these filters can increase the saturation output power by 2 dB or reduce the pump power requirements. **(p. 148)**

**3:15 pm**
**ThD3 Accurate modeling of distributed erbium-doped fiber amplifiers with bidirectional pumping,** E. Desurvire, D. Chen, *Columbia U.* An accurate model for low-gain erbium-doped fiber amplifiers with fiber background loss is presented. An exact analytical expression is derived for the gain as a function of input pump power in the cases of unidirectional or bidirectional pumping. **(p. 152)**

**3:30 pm**
**ThD4 73.6-km attenuation free concatenated fibers doped with distributed erbium,** D. Tanaka, A. Wada, T. Sakai, T. Nozawa, R. Yamauchi, *Fujikura, Ltd., Japan.* Based on a theoretical investigation of lengthwise erbium distribution, 73.6-km attenuation-free fiber doped with distributed erbium has been achieved by 66-mW × bidirectional pumping. **(p. 156)**

## CABARET LOBBY

**3:45 pm–4:15 pm COFFEE BREAK/EXHIBITS**

THURSDAY, JULY 25, 1991—*Continued*

## CABARET ROOM

**4:15 pm–5:15 pm**
**ThE, HIGH EFFICIENCY AND SATURATED AMPLIFIERS**
E. Desurvire, *AT&T Bell Laboratories, USA, Presider*

**4:15 pm**
**ThE1 Noise characteristics of the EDFA in gain saturation regimes,** J. F. Marcerou, H. Fevrier, J. Hervo, J. Auge, *Alcatel Alsthom Recherche, France.* Noise properties of EDFA are studied in various signal regimes. New experimental behaviors are theoretically confirmed for 1.48-$\mu$m pumped amplifiers. **(p. 162)**

**4:30 pm**
**ThE2 Characteristics of 1.48-$\mu$m pumped erbium-doped fiber amplifier with high efficiency,** Tomonori Kashiwada, Masayuki Shigematsu, Takashi Kougo, Hiroo Kanamori, Masayuki Nishimura, *Sumitomo Electric Industries, Ltd., Japan.* An erbium-doped fiber amplifier pumped at 1.48 $\mu$m with high efficiency has been developed. A slope efficiency of 86% and a gain coefficient of 6.3 dB/mW have been achieved. **(p. 166)**

**4:45 pm**
**ThE3 Conversion efficiency and noise in erbium-doped fiber power amplifiers,** B. Pedersen, *Technical U. Denmark;* M. L. Dakss, W. J. Miniscalco *GTE Laboratories, Inc.* A comprehensive analysis of $Er^{3+}$-doped fiber power amplifiers pumped at 980 nm and 1480 nm is presented. The effects of waveguide design and erbium confinement on conversion efficiency and noise figure are elucidated. **(p. 170)**

**5:00 pm**
**ThE4 Pump configuration and length optimization of an erbium-doped fiber amplifier for low-noise and high power operation,** M. Suyama, I. Yokota, S. Watanabe, H. Kuwahara, *Fujitsu Laboratories, Ltd., Japan.* We obtained an erbium-doped fiber amplifier (EDFA) with 15-dBm output power and 6-dB noise figure by a proper choice of pump configuration and length optimization of EDFA. **(p. 174)**

**5:15 pm–7:00 pm**
**PD, POSTDEADLINE PAPER SESSION**
R. E. Wagner, *Bellcore, USA, Presider*

## FRIDAY, JULY 26, 1991

### CABARET LOBBY

**7:00 am–5:00** REGISTRATION/SPEAKER CHECK-IN

### ANDERSON ROOM (Conference Center)

**7:00 am–8:00 am** BREAKFAST

### CABARET ROOM

**8:00 am–9:45 am**
**FA, SYSTEM PERFORMANCE CONSIDERATIONS**
Y. K. Park, *AT&T Bell Laboratories, USA, Presider*

**8:00 am (Invited)**
**FA1 The appropriateness of squeezed light for long-distance communication,** Bernard Yurke, *AT&T Bell Laboratories.* Squeezed light allows suitable optical systems to operate below the shot-noise limit. The usefulness of squeezed light for long-distance communication will be assessed. **(p. 180)**

**8:30 am**
**FA2 Preamplified direct detection versus heterodyne detection: can they be equivalent?** Ozan K. Tonguz, *SUNY-Buffalo;* Richard E. Wagner, *Bellcore.* The interrelationship of heterodyne receivers and preamplified direct-detection receivers is explained. We show that under certain conditions these two lightwave receiver types have equivalent performance. **(p. 183)**

**8:45 am**
**FA3 Comparison of direct and coherent detection systems with optical amplifiers,** S. W. Granlund, Y. K. Park, *AT&T Bell Laboratories.* We report on an experimental and theoretical comparison of direct and coherent 1.7-Gbit/s detection systems using practical system components including erbium-doped fiber amplifier modules. **(p. 187)**

**9:00 am**
**FA4 High receiver sensitivity at 2.5 Gbit/s obtained with a highly efficient low noise diode pumped erbium-doped fiber amplifier,** B. Mikkelsen, C. G. Joergensen, T. Durhuus, K. E. Stubkjaer, *Technical U. Denmark;* J. A. van den Berk, *Telecom Denmark;* C. F. Pedersen, *NKT Elektronik, Denmark;* C. C. Larsen, *Lycom, Denmark.* A preamplifier-receiver sensitivity of −43.0 dBm is obtained at 2.5 Gbit/s using an erbium-doped fiber amplifier pumped bidirectionally with laser diodes at 980 and 1480 nm. The total pump power is 14 mW and the noise figure 3.1 dB. **(p. 192)**

## FRIDAY, JULY 26, 1991—*Continued*

**9:15 am**
**FA5 Signal statistical effects from stimulated Brillouin scattering in a CPFSK repeaterless transmission system with optical booster amplifier,** Toshihiko Sugie, *NTT Transmission Systems Laboratories, Japan.* For a 2.5-Gbit/s CPFSK transmission system with an EDF-booster amplifier, the bit error rate and the penalty-improvement by signal randomization are clarified in the presence of stimulated Brillouin scattering along a 280-km dispersion shifted fiber. **(p. 196)**

**9:30 am**
**FA6 Combined effect of self-phase modulation and dispersion in SLA post-amplified transmission systems,** C. R. Medeiros, J. J. O'Reilly, *U. Wales-Bangor, U.K.* We consider the performance implications of using semiconductor laser amplifiers as post-transmitter power amplifiers in long-haul directly modulated optical systems operating in the 1.55-$\mu$m region. **(p. 200)**

### CABARET LOBBY

**9:45 am–10:15 am** COFFEE BREAK/EXHIBITS

### CABARET ROOM

**10:15 am–12:00 m**
**FB, BROADBAND OPTICAL NETWORK APPLICATIONS**
C. Lin, *Bellcore, USA, Presider*

**10:15 am (Invited)**
**FB1 Optical fiber amplifiers for multi-channel video transmission and distribution,** W. I. Way, *Bellcore.* This paper reviews the previous work on fiber amplifier applications to analog video transmission and distribution, and compares the different technology aspects of analog and direct-detection digital video systems. The paper also addresses potential evolutionary problems of using optical fiber amplifiers in a subscriber loop that may need upgrading when the distribution signals change from AM-VSB video to future digital video services. **(p. 206)**

**10:45 am**
**FB2 Simultaneous distribution of analog AM-TV and multi-gigabit HDTV with an optical amplifier,** R. Heidemann, B. Junginger, H. Krimmel, J. Otterbach, D. Schlump, B. Wedding, *SEL Alcatel Research Center, F.R.G.* We demonstrate the feasibility of flexible TV/HDTV distribution using simultaneous analog AM and digital PCM transmission over optical amplifiers without any mutual quality degradation. **(p. 210)**

**11:00 am**
**FB3 High power and low noise transmitter for AM-VSB transmission using an erbium-doped fiber post amplifier,** Masayuki Shigematsu, Masayuki Nishimura, Toshio Okita, Kazuo Iizuka, *Sumitomo Electric Industries, Ltd., Japan.* An AM-VSB transmitter with 14-dB loss budget for CNR of 51 dB was developed using a bidirectionally pumped erbium-doped fiber post amplifier with a long-wavelength-pass filter. **(p. 214)**

**11:15 am**
**FB4 Forty-channel AM-VSB distribution system with a 21-dB link budget,** G. R. Joyce, R. Olshansky, R. Childs, T. Wei, *GTE Laboratories, Inc.* An AM-VSB fiber video distribution system utilizes an erbium-doped fiber power amplifier and a low-noise receiver and attains a 21-dB link budget for forty channels. **(p. 218)**

**11:30 am**
**FB5 Noise performance of bus-configured optical networks with distributed fiber amplification,** Evan L. Goldstein, *Bellcore.* A simple closed-form analysis shows that bus-configured lightwave networks with distributed gain can support thousands of nodes, spanning thousands of km. However, in networks of this size the end-to-end gain and loss must be well matched. **(p. 222)**

**11:45 am**
**FB6 Optically preamplified 1-Gbit/s/channel multichannel grating demultiplexer receiver,** J. P. King, Y. Kanabar, J. Brannan, N. Baker, *STC Technology, Ltd, U.K.* Optical preamplification of an HDWDM multichannel receiver improved sensitivity beyond −33 dBm at 1 Gbit/s; IM crosstalk allows up to eight 1-gbit/s channels. **(p. 226)**

**12:00 m–1:00 pm LUNCH (on your own)**

## CABARET LOBBY

**12:00 m–1:00 pm EXHIBITS**

## CABARET ROOM

**1:00 pm–2:15 pm**
**FC, APPLICATIONS OF SEMICONDUCTOR OPTICAL AMPLIFIERS**
K. E. Stubkjaer, *Technical University of Denmark, Denmark, Presider*

**1:00 pm (Invited)**
**FC1 Optical amplifiers used as functional components,** Lars Thylen, Mats Gustavsson, *Ericsson Telecom, Sweden;* Lars Gillner, *Royal Institute of Technology, Sweden.* Semiconductor laser amplifiers can be used for detection, switching or gating as well as frequency translation, and broadband amplification. Device and applications aspects are reviewed. **(p. 232)**

**1:30 pm**
**FC2 GaAlAs/GaAs vertical cavity surface emitting active filter,** F. Koyama, S. Kubota, K. Iga, *Tokyo Institute of Technology, Japan.* An active filter/amplifier based on a vertical cavity surface emitting laser has been demonstrated, giving a filter bandwidth as narrow as 0.08 nm. **(p. 237)**

FRIDAY, JULY 26, 1991—*Continued*

**1:45 pm**
**FC3 Dynamics of DFB semiconductor laser amplifiers,** Z. Wang, T. Durhuus, B. Mikkelsen, K. E. Stubkjaer, *Technical U. Denmark.* A dynamic model for DFB amplifiers is established and used to assess amplification of short pulses. Both strong and weak input pulses are considered for different operating conditions. **(p. 241)**

**2:00 pm**
**FC4 Low-loss packaged, 2 × 2 semiconductor optical amplifier switch,** E. Eichen, R. Boudreau, R. Morrison, C. Frost, B. Foley, J. Schlafer, K. Vo, *GTE Laboratories, Inc.* A packaged 2 × 2 semiconductor optical amplifier switch that utilizes a novel imaging configuration for fiber coupling has been demonstrated: average insertion loss 4 dB, optical isolation >40 dB, rise/fall time 0.5 ns. **(p. 245)**

**2:15 pm–3:15 pm**
**FD, FIBER AMPLIFIER ENGINEERING**
W. L. Emkey, *AT&T Bell Laboratories, USA, Presider*

**2:15 pm**
**FD1 Amplified integrated star couplers with zero loss,** Herman M. Presby, C. Randy Giles, *AT&T Bell Laboratories.* We compensate the loss of a 19 × 19 integrated star coupler with erbium-doped fibers connected to the output channels and pumped with one source distributed through the star itself. **(p. 250)**

**2:30 pm**
**FD2 Compact size and high output power Er-doped fiber amplifier modules pumped with 1.48-μm MQW LDs,** H. Takenaka, H. Okuno, M. Fujita, Y. Odagiri, Y. Sunohara, I. Mito, *NEC Corp.* We have developed an Er-doped fiber booster amplifier module that can deliver signal output power as high as +22.3 dBm. **(p. 254)**

**2:45 pm**
**FD3 High efficiency erbium-doped fiber amplifiers using a mode field diameter adjusting technique,** A. Wada, T. Sakai, D. Tanaka, T. Nozawa, R. Yamauchi, *Fujikura, Ltd., Japan.* Nearly 100% performance has been achieved from the high-NA EDF using a mode field diameter adjustment technique at the spliced parts with external fibers. **(p. 258)**

**3:00 pm**
**FD4 Effect of pump-induced temperature variation on erbium-doped fiber amplifiers,** S. Nishi, H. Masuda, J. Nakajima, K. Aida, *NTT Transmission Systems Laboratories, Japan.* The temperature increase of an erbium-doped fiber by 1.48-μm pumping was measured. The mechanism of heat generation and its influence on amplification characteristics are discussed. **(p. 262)**

## CABARET LOBBY

**3:15 pm–3:30 pm COFFEE BREAK**

## CABARET ROOM

**3:30 pm–5:00 pm**
**FE, NOVEL SYSTEM TECHNIQUES AND APPLICATIONS**
E. Eichen, *GTE Laboratories, USA, Presider*

**3:30 pm**
**FE1 OTDR in optical amplifier transmission systems using EDFAs containing optical circulators,** Yoshiaki Sata, Shigendo Nishi, Koh-ichi Aoyama, *NTT Transmission Systems Laboratories, Japan.* OTDR fault location using a return transmission line is demonstrated in a 1.8-Gbit/s signal transmission system. The 280.9-km transmission line contains three Er-doped fiber amplifiers. **(p. 268)**

**3:45 pm**
**FE2 Measurement of polarization dispersion in the components of in-line erbium-doped fiber amplified links,** J. J. Bernard, F. Bruyere, J. Guillon, *Alcatel Alsthom Recherche, France.* An experiment investigation of polarization dispersion of an in-line erbium-doped fiber amplified link has been carried out. Results show a non-negligible contribution of the isolators. **(p. 272)**

**4:00 pm**
**FE3 Automatic gain control of an erbium-doped fiber amplifier by detecting spontaneous emission along the fiber,** Kazuo Aida, Hiroji Masuda, *NTT Transmission Systems Laboratories, Japan.* EDFA gain control is achieved by detecting the spontaneous emission radiated along the EDF and modulating the pump LDs with optoelectronic feedback. **(p. 276)**

**4:15 pm**
**FE4 Optimized nonregenerative repeater using cascaded erbium-doped and Raman fiber amplifier,** S. L. Zhang, J. J. O'Reilly, *U. Wales-Bangor, U.K.* A cascaded configuration for fiber amplifier nonregenerative repeater is proposed and optimized, providing better performance that can be achieved using either amplifier alone. **(p. 280)**

**4:30 pm**
**FE5 All-optical remote gain switching scheme for Er-doped fiber amplifiers,** M. Zirngibl, *AT&T Bell Laboratories.* We demonstrate all-optical feedback scheme that allows remote optical gain switching over the transmission fiber in Er-doped fiber amplifiers; gain bistability (on-off ratio) 26 dB at 1530 nm switching time 10-50 ms. **(p. 284)**

**4:45 pm**
**FE6 Optical amplifiers operating in a random access fiber loop optical memory,** G. Grosskopf, L. Kuller, R. Ludwig, W. Pieper, R. Schnabel, H. G. Weber, *Heinrich-Hertz-Institut fur Nachrichtentechnik Berlin GmbH, F.R.G.* In a fiber loop optical memory the use of semiconductor laser amplifiers as switching elements and of erbium-doped fiber amplifiers as gain controlling elements are investigated. **(p. 288)**

**5:00 pm–5:15 pm**
**CLOSING REMARKS**
Mike O'Mahony. *British Telecom Research Laboratories, United Kingdom*

# Plenary Session

**WA** 8:15am–8:45am
Cabaret Room

David Payne, *Presider*
*University of Southampton, United Kingdom*

# TOWARDS NETWORK TRANSPARENCY WITH PHOTONIC AMPLIFIERS

Peter Cochrane* and Christopher J Todd**

## PROLOGUE

Over the past 15 years optical fibre transmission systems have largely replaced their copper forebears on a point to point basis. The approach has been, quite simply, to overlay one-on-one the copper and radio systems by an optical fibre network with improved repeater spacing, smaller physical size, increased capacity and lower cost being the key benefits gained so far. With the advent of the optical amplifier and the possibility of access to the total fibre bandwidth, insensitivity to 'lossy' components and the eradication of much of the electronics necessary in transmission, there now exists an opportunity for radically new forms of network. The key feature that an optical amplifier has to offer is transparency. The ability to convey a number of wavelengths that can act as independently-modulated orthogonal carriers for a diverse mix of traffic in both digital and analogue forms offers a revolutionary step in the evolution of telecommunication networks.

Much of today's thinking with respect to photonic amplification is still concerned with the one-on-one replacement of opto-electronic 3R repeaters, coupled with the achievement of higher launch powers and pre-amplifiers for optical receivers. However, the optical amplifier in all its diverse forms offers a much greater opportunity when we consider equipment, system and network realisation more deeply. In this paper, we briefly comment on the state-of-the-art of today's optical amplifier technology and then go on to postulate future advances and applications for local, short, and long haul applications.

## PROGRESS TO DATE

Semiconductor and fibre based amplifiers are now commercially available covering a wide range of wavelengths spanning the entire 1.3 and 1.5 um windows. In the case of the semiconductor devices, it has now been established that the sensitivity to polarisation can largely be overcome by attention to device geometry, but the reduction in available gain due to coupling losses and their inherent ability to generate intermodulation products has led many people to discount them as a viable component. However, their small size makes them an ideal element in future integrated optic applications. Fibre to fibre gains up to 30dB and power levels up to +5dBm have been reported but 15dB and 0dBm are more typical and representative of available production devices [1].

In contrast, the development of fibre amplifiers to date has been dominated by Er doped devices that return a negligible sensitivity to polarisation and very low coupling losses. Their physical length can span between 1m and 100 km with gains up to 40dB, and launch powers in excess of +20dBm have been reported. More typically, production items are realising 15-25dB gain with output powers of <+5dBm. It is interesting to note that both the semiconductor and Er doped amplifiers require a similar pump power and with suitable dopants and geometries can achieve similar bandwidths. However, the Er devices appear to realise the highest linearity, the lowest level of noise and intermodulation accumulation and have their key characteristics defined by their atomic composition. More recently there has been a surge of activity with fluoride fibre hosts and fibre amplification centred on 1.3um has been reported [2].

The development of the Raman amplifier has also seen some remarkable results with gains up to 40dB and power outputs up to +25dBm reported. The pump power required is, however, far higher than that of the semiconductor and Er doped amplifier. In addition, the essential non-linear nature of this device also renders it prone to the generation of intermodulation products and higher noise levels.

---

* *British Telecom Laboratories, Martlesham Heath, Ipswich, Suffolk, IP5 7RE*
** *Department of Electronics & Electrical Engineering, University College London, WCE 7JE*

Experimental results with both linear (WDM) and non-linear (Soliton) propagation have shown that amplified systems are, in principle, capable of providing a global point to point capability The level of confidence may be gauged by the determined efforts of both European and North American companies who wish to span both the North Atlantic and Pacific oceans with amplified systems from about 1996 onwards. On the terrestrial scene, the prime interest has been expressed by the cable TV industry who see major benefits with optical amplifiers on their trunk distribution systems. There are, however, a growing number of demonstrations and papers being published on long and short haul network uses.

**NEW FORMS**

The fibre amplifier can be extended in space to become the entire transmission medium. With a bus network of weakly amplifying fibre, and using say D-fibre taps (Fig 1), the optical equivalent of the classic '50 Ohm tapped bus' has now been demonstrated (Fig 2). Although noise accumulation will eventually dominate, it is anticipated that such buses can be grown organically with need to >1000 taps. Put this together with the recent demonstrations of fibre power amplifiers to offset splitter losses in a PON or branching network to allow tens of thousand or even million fold fan outs (Fig 3), and a new field of Virtually LOssless Networks (VLONs) has been generated [3]. The implications of the VLON concept on the design of small or large network architectures has yet to be fully explored. Consider the possibilities of configurations of extended and lumped amplification, transparent in both the 1.3 and 1.5um windows, with a distance elasticity that bridges between cities and wavelength selective taps or fan out to reach all the local exchanges in a metropolis. Such configurations are multidimensional in that space, time and wavelength/frequency may be accessed and traded to extents depending on the availability/cost and relative functionality of the evolving portfolio of optical components. When the VLON concept is configured as a switching node the multidimensionality allows bandwidth to be traded for simplicity, as has recently been demonstrated in the powerful MONET switch/interconnect concept [4].

**POINT TO POINT TRANSMISSION**

There are a number of interesting break points in point to point transmission related to undersea and terrestrial networks. In the undersea case about 40% of all systems can be served with repeater spans <350 km. In the specific case of the UK, terrestrial spans seldom exceed 200 km between major conurbations. These distances are also pertinent to much of Continental Europe and parts of North America. Although such distances can in principle be bridged without repeaters at the lower bit rates, the demand for increased transmission rates (>600 Mbit/s)and provision of practical operating margins reduces the fundamental reach. In satisfying these demands, the undersea network will probably see the first extensive application of optical amplification. In this respect Raman amplification produced by pumping standard fibre from the ends of a link provides a simple means of increasing the capacity of installed repeaterless systems. In a recent demonstration of direct capacity increase a 20x rate upgrade has been demonstrated on a short (132 km) route from the UK to the Channel Islands, by the addition of doped amplifiers to the land terminals [5].

Plans are now building in a number of laboratories world wide to introduce cascaded fibre amplifiers in place of conventional repeaters on future trans-oceanic routes to coincide with capacity needs up to and beyond 2.5 Gbit/s. This has provoked the concern that for distances > 5000km non-linear effects cannot be neglected. Groups at BTRL and AT&T Bell Labs have predicted the essential non-linearity of amplifier systems in this distance x bit rate regime. The issue is whether such systems planned as conventional linear transmission lines will suffer catastrophic losses of data if small , but uncontrolled, non-linearities are created during propagation. Perhaps the safest approach is to launch solitons and thereby control the non-linearity by using it to advantage. Certainly practical soliton sources are now being demonstrated in the laboratory based on mode locked semiconductor and Er doped fibre lasers generating 3ps pulses [6]. There is however a significant additional cost for such a system as the distance between fibre amplifiers would probably have to be at least halved to maintain the power level for soliton propagation, thereby putting up both the cost and complexity of the undersea system.

## THE ULTIMATE BIT RATE

Today, we use <0.001% of the inherent transmission capacity of any optical fibre in service. It has been demonstrated that pulse transmission up to 30 Gbit/s is both feasible and possible whilst WDM up to 100 Gbit/s has also been demonstrated. So a ~0.2% capacity has been practically demonstrated whilst theoretical studies suggest a further order of magnitude to be feasible. If there is such a future capacity demand, it unlikely to be accessible without the use of doped fibre amplifiers.

## NEW NETWORKS AND APPLICATIONS

The use of amplifiers for CATV + telecommunications in the traditional sense is axiomatic. What is interesting is the prospects for removing the need for electronic multiplex and switching. It has been shown that a central office can be eradicated (theoretically) for ~200,000 lines, but then the need for switching systems in the traditional sense arises [7]. We might thus anticipate a future network with multi-layer ether operation and intermediate steering and switching between levels.

With a growing mobile periphery to all networks a new opportunity arises with the optical amplifier. It is now possible to transport sections/sectors of the radio spectrum from one physical location to another without the need for demodulation to baseband. So groups of common interest users could be conveniently linked across large distances in a more direct manner and the utility of the radio spectrum enhanced. A further possibility is that of "optical radio" with leaky feeder or fish eye radiators and distributed fibre amplification. A new, and similar, subset of applications is now also evident when we consider both terrestrial and satellite radio systems where the complex station equipment could be more centrally located and the Tx|Rx sites considerably simplified. The coupling of these various options into a universal ether with the ability to simultaneously support analogue and digital modulation will also assist the process of services and technology migration with PDH, SDH and WDH coexisting for a number of years. It will also be an important feature for future self-organising networks and perhaps the realisation of Neural Networks.

## FINAL COMMENTS

Overall, the optical amplifier is poised to contribute to a continuing trend of increased capacity, longer reach, less equipment, greater utility, lower cost and higher reliability that has been the story of transmission since it began in the late 19th century. As we move into the 21st century, we can expect to see optical amplification as the next facilitator of new opportunities in telecommunications. Optical amplifiers will release the network designers from the historic rigidity of the link power budget, and allow him to mix and match bus and fan out topography to suite his application. In time the extended fibre amplifier will help overcome node inertia, by removing throughput limits and allowing modular growth of switch blocks. The massive achievements in optical communications during the last decade are likely to be be eclipsed in the future by the opportunities that will flow from networking with optical amplifiers.

## REFERENCES

1] COCHRANE P & HEATLEY D J T: BT Engineering, Vol 1, Jan 1991, pp 268 - 280.

2] BRIERLEY M C: Invited paper at this conference.

3] HILL J R et al: IEE Electronics Letter, Vol 26, No22 , Oct 1990, pp 1882 - 1883.

4] HEALEY M C et al: SPIE Proc Optical Digital Computing, Vol. 2, Jan 1990, pp 191-197.

5] LEWIS R B et al: BTTJ, Vol 8, No 4 Oct 1990, pp 10 - 17.

6] SMITH K et al: IEE Electronics Letter - to be published.

7] BRAIN M C & COCHRANE P: IEEE ComSoc Mag, Vol 26, No 11, Nov 88, pp 45 - 60.

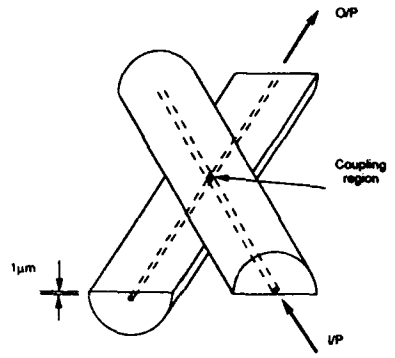


Fig 1. D fibre coupling

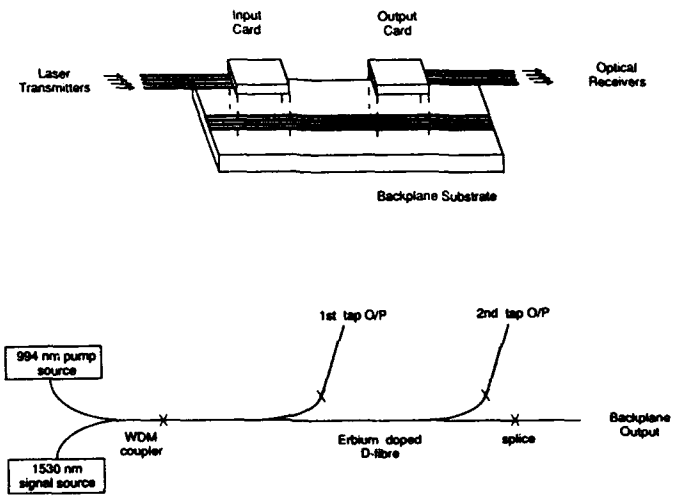


Fig 2. The D fibre back plane

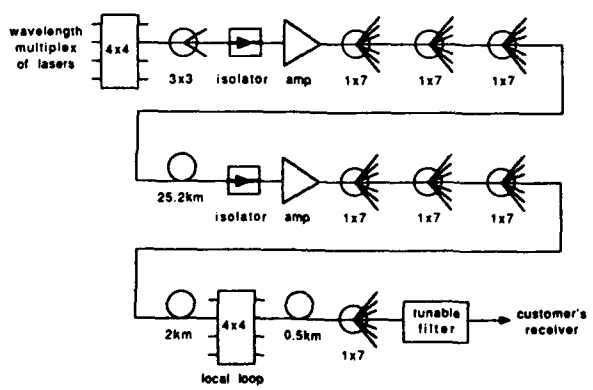


Fig 3. A 39 million split VLON

# Doped Fiber Amplifiers

**WB** 8:45am–10:00am
Cabaret Room

R. I. Laming, *Presider*
*University of Southampton, United Kingdom*

# Progress in Erbium Doped Fiber Amplifiers

J.R. Simpson and D.J. DiGiovanni
AT&T Bell Laboratories, Murray Hill, New Jersey, 07974

Erbium fiber amplifiers are entering a fourth year of development with six commercial offerings now available, the result of rapid improvements in pump lasers, wavelength division multplexers, isolators and doped fiber designs. A number of challenges remain however to improve the performance and ensure reliability in field applications.

Improvements in the rare earth doped fiber, itself, remain a challenge. Rare earth doped fiber fabrication has been dominated by variations on traditional low loss telecommunications fiber using $GeO_2$, $Al_2O_3$, and $P_2O_5$ co- dopants yielding fiber which is fusion splice compatible with telecommunications fiber [1]. It has long been realized that alternate host compositions may improve the efficiency and gain-bandwidth products at the expense of compatibility with telecommunications fiber. Host materials of compound glasses, phosphates, fluorophosphates and others have recently been reported [2,3,4,5]. The incorporation of Ca in a $GeO_2$-$Al_2O_3$-$SiO_2$ or $Al_2O_3$-$SiO_2$ host has, for example, also been shown to improve the efficiency of 813 nm pumping [3].

New fabrication methods have also been described which incorporate these alternate host dopants by such techniques as coating the inside of an MCVD tube with a polymer like sol-gel material or methods which deliver dopants for flame or MCVD reactions in the form of aerosols or vaporized chelates [6,7,8]. An older method of double crucible fiber drawing has also been revisited to explore the compound glass materials as hosts [2]. The use of fluoride host compositions also remaines especially promising as recently demonstrated by a 1.3μm amplifier using a ZBLAN fluoride host and Pr dopant [9]. Pump wavelengths other than those provided by the Er transitions may be made possible by co-doping with other rare earths. A Yb/Er phosphate fiber amplifier has recently demonstrated this with an 85% energy transfer using a 1064 nm YAG laser pump [4].

In addition to experimental means to understand the performance of these amplifiers there have also been a number of theoretical and modeling methods. One approach offers the ability to extend only a few amplifier measurements into many operating conditions of pump power, wavelength and signal power [10,11,12]. Some models have also been used to predict the performance of fiber designs and host glass compositions [13,14]

As fiber amplifiers approach commercial applications issues which address performance over a broad temperature range and reliability become more important. Temperature effects the gain and noise figure as a result of a change in the population inversion which is intern dependent on pump power, wavelength and host composition to name a few [15,16,17]. Typically the gain will change on the order of -0.1 dB per degree centigrade or less and the noise figure will change by -0.02 dB per degree centigrade [17]. The issue of fiber strength must be considered when packaging requires small coils of the doped fiber. One such reliable high gain

amplifier coil consisting of a 200 meter length of hermetic coated fiber wound to a dimension of 32 mm outside diameter by 20 mm high has been demonstrated [18].

Application of erbium fiber amplifiers have made use of both the ability of these devices to amplify many independent wavelength channels (up to 100 [19]) and the ability to amplify, with little distortion, short duration pulses (as short as 53 femtoseconds [20]). Schemes have been proposed to flatten the gain response with wavelength including a two stage amplifier where each stage has a different wavelength dependent gain function [21], insertion of a notch filter within the amplifier [22], using optical feedback [23], and choosing operating conditions to saturate the effect [24].

The amplification of short pulses tens of femtoseconds in duration begins to reach the near 30 nm bandwidth limits of these amplifiers [20]. Pulse trains of 350 Ghz have however been amplified with little distortion [25] indicating that, for the near future, the bandwidth required from modulation will not represent a limitation.

High bit rate long distance spans employing fiber amplifiers reach a limit from the fiber dispersion, a constraint which may be relaxed by the use of soliton pulse propagation. There is however an additional constraint then of the signal power excursion along the span and the separation of repeaters [26]. This constraint can be handled by the use of many low gain amplifiers closely spaced or by the use of a distributed amplifier. Progress in realizing a practical distributed amplifier, tens of kilometers in length has been reported with the required pump power for transparency now approaching 1 mW per kilometer for low signal levels [27,28]. Although this type of erbium amplifier is more difficult to fabricate it will likely provide the greatest opportunity for ultra high bit rate communications systems.

References


1. B.J. Ainslie "A Review of the Fabrication and Properties of Erbium-Doped Fibers for Optical Amplifiers," J. Lightwave Tech., Vol. 9, No. 2, pp. 220-227, (1991)
2. M. Yamada, M. Shimizu, M. Horiguchi, M. Okayasu and E. Sugita, "Gain Characteristics of an $Er^{3+}$-Doped Multicomponent Glass Single-Mode Optical Fiber," Photonics Tech. Lett., Vol. 2, No. 9, pp. 656-658, (1990)
3. M.A. Saifi, M.J. Andrejco, W.I. Way, A. Von Lehman, A.Y. Yan, Chinlon Lin, F. Bilodeau and K.O. Hill, "$Er^{3+}$- doped $GeO_2$-CaO-$Al_2O_3$ Silica Core Fiber Amplifier Pumped at 813 nm" Proceedings of OFC'91, paper FA6, (1991)
4. S.G. Grubb, R.S. Cannon, T.W. Windhorn, S.W. Vendetta, P. A. Leilabady, D.W. Anthon, K.L Sweeney, W.L. Barnes, E.R. Taylor, J.E. Townsend, "High Power Sensitized Erbium Optical Fiber Amplifier," Proceedings of OFC'91, paper PD7, (1991)
5. W.J. Miniscalco, "Erbium-Doped Glasses for Fiber Amplifiers at 1500 nm". J. Lightwave Tech., Vol. 9., No. 2, pp. 134-250, (1991)
6. D.J. DiGiovanni and J. B. MacChesney, " New Optical Fiber Fabrication Technique Using Sol-Gel Dipcoating," Proceedings of OFC '91, paper WA2, (1991)

7. T.F. Morse, A. Kilian, L. Reinhart, Wm. Risen, Jr., and J.W. Cipolla, Jr., "Aerosol Technique for Fiber Core Doping," Proceedings of OFC '91, ppaper WA3, (1991)
8. R.P. Tumminelli, B.C. McCollum and E. Snitzer, "Fabrication of High Concentration Rare Earth Doped Optical Fibers Using Chelates, J. Lightwave Tech., 8, No. 11, pp. 1680-1683, (1990)
9. Y. Ohishi, T. Kanamori, T. Kitagawa, S. Takahashi, E. Snitzer and G.H. Sigel, "$Pr^{3+}$ Doped Fluoride Fiber Amplifier Operating at 1.31μm," Proceedings of OFC '91, paper PD2, (1991)
10. A.A.M. Saleh, R.M. Jopson, J.D. Evankow and J. Aspell, "Modeling of Gain in Erbium-Doped Fiber Amplifiers," IEEE Photonics Tech. Lett., Vol. 2, No. 10, pp. 714-717, (1991)
11. C.R. Giles and E. Desurvire, "Modeling Erbium-Doped Fiber Amplifiers," J. Lightwave Tech. Vol. 9, No. 2, pp. 271-283, (1991)
12. B. Pedersen, K. Dybdal, C.D. Hansen, A Bjarklev, J.H. Povlsen, H.V. Pommer and C.C. Larsen, "Detailed Theoretical and Experimental Investigation of High-Gain Erbium-Doped Fiber Amplifier," IEEE Photonics Tech, Lett., Vol. 2, No. 12, (1990)
13. E. Desurvire, J.L Zyskind and C.R. Giles, "Design Optimization for Efficient Erbium-Doped Fiber Amplifiers," J. Lightwave Tech., Vol. 8, No. 11, pp. 1730-1741, (1990)
14. M. Ohashi and M. Tsubokawa, "Optimum Parameter Design of $Er^{3+}$-Doped Fiber for Optical Amplifiers," IEEE Photonics Tech. Lett., Vol. 3, No. 2, (1991)
15. C.A. Millar, T.J. Whitley, and S.C. Fleming, "Thermal Properties of an Erbium-Doped Fibre Amplifier," IEE Proceedings, Vol. 137, Pt. J, No. 3, pp. 155-162, (1990)
16. N. Kagi, A, Oyobe, K. Nakamura, "Temperature Dependence of the Gain in Erbium Doped Fibers," J. Lightwave Tech., Vol. 9, No. 2, pp. 251-265, (1991)
17. Y.H. Chen, N. Kagi, A. Oyobe, H. Hiramatsu and K. Nakamura, "Temperature Characteristics of Noise Figure of Erbium-Doped Fiber Amplifiers," Proceedings of OFC'91, paper ThM4, pg. 179, (1991)
18. A. Oyobe, K. Hirabayashi, N. Kagi and K. Nakamura, "Hermetic Erbium-Doped Fiber Coils for Compact Optical Amplifier Modules," Proceedings of OFC '91, paper WL8, (1991)
19. K. Inoue, H. Toba, S. Sekine, H. Sugiyama and K. Nosu, "100- Channel Common Amplification Using an $Er^{3+}$ Doped Fiber Amplifier,"in Technical Digest, Optical Amplifiers and Their Applications, Monterey, paper TuA3, (1990)
20. E.M. Dianov, A.B. Grudinin, I.Y. Khrushchev, D.V. Korobkin, Jr., A.Y. Makarenko, A.M. Prokhorov, "Nonlinear Dynamics of Femtosecond Soliton Amplification in Erbium Doped Fibers," Proceedings of CLEO '90, paper JTUA7, (1991)
21. C.R. Giles and D.J. DiGiovanni, "Dynamic Gain Equalization in Two-Stage Fiber Amplifiers," Proceedings of Optical Amplifiers and Their Applications," paper MD2, Monterey,CA, (1990)

22. G. Grasso, F. Fontana, A. Righetti, P. Scrivener, P. Turner, and P. Maton, "980-nm Diode-Pumped Er-Doped Fiber Optical Amplifiers with High Gain-Bandwidth Product," Proceedings of OFC '91, paper FA6, (1991)
23. M. Zirngibil, P.B. Hansen, G. Raybon, B. Glance and E. Desurvire, "Passive Gain Control by All-Optical Feedback Loop in Erbium- Doped Fiber Amplifiers," Proceedings of OFC'91, paper PD21, (1991)
24. R.I. Laming, J.E. Townsend, D.N. Payne, F. Meli, G. Grasso, and E.J. Tarbox, "High-Power Erbium-Doped-Fiber Amplifiers Operating in the Saturated Regime," IEEE Photonics Tech. Lett. Vol. 3, No. 3, pp. 253-255, (1991)
25. M.C. Wu, Y.K. Chen, J.R. Simpson, T.Tanbun-Ek, R.A. Logan, and M.A. Chin, "Fiber Transmission of 650-fs Pulses at 350 GHz. Generated by Monolithic Colliding-Pulse Mode-Locking Quantum-Well Lasers," Proceedings of CLEO '91, (1991)
26. L.F. Mollenauer, S.G. Evangelides and H. A. Haus, "Long-Distance Soliton Propagation Using Lumped Amplifiers and Dispersion Shifted Fiber," J. Lightwave Tech., Vol. 9, No. 2, pp. 194-197, (1991)
27. S.T. Davey, D.L. Williams and B.J. Ainslie, "Distributed Erbium- Doped Fiber for Lossless Link Applications," Proceedings of OFC'91, paper FA8, (1991)
28. J.R. Simpson, H.T. Shang, L.F. Mollenauer, N.A. Olsson, P.C. Becker, K.S. Kranz, P.J. Lemaire and M. J. Neubelt, "Performance of a Distributed Erbium-Doped Dispersion-Shifted Fiber Amplifier," J. Lightwave Tech., Vol. 9, No. 2, pp. 228-233, (1991)

# Prospects for Fiber Amplifiers at 1.3μm

Mike Brierley

Technology Research, MLB 1/29, BT Laboratories

Martlesham Heath, Ipswich, IP5 7RE

U.K.

## Summary

*Introduction*

The erbium doped silica fiber amplifier for the 1.55μm telecommunications has now become a well established research laboratory tool. It offers high gain, high efficiency, low noise, low cross-talk, and high saturation power. It has been used in both land and under-sea systems demonstrations, and is commercially available from a number of manufacturers. In distribution experiments splits of up to 39 million ways have been demonstrated for only two stages of amplification [1]. In short it has revolutionised thinking on future optical fibre networks. Unfortunately the vast majority of current operational systems are deployed in the 1.3μm window, and some fiber designs may prohibit upgrading to 1.55μm. A similar amplifier for 1.3μm has been much more elusive. Examination of the observed energy levels of the trivalent rare-earth ions reveals three principal candidates; neodymium with a known laser transition around 1.32μm, praseodymium with known laser transitions but not until very recently at 1.3μm, and promethium with known laser transitions at 0.933μm and 1.098μm, but not around 1.3μm. Promethium is radioactive and has not been studied in fibers, leaving two practical possibilities for fiber amplifiers for 1.3μm.

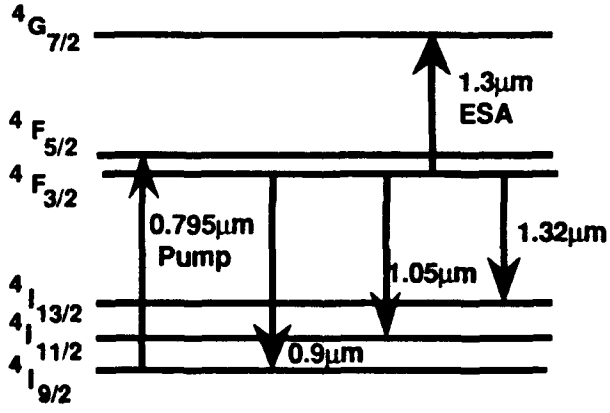


Figure 1: Energy level diagram for neodymium in glass showing only relevant levels and transitions.

*Neodymium amplifiers*

The most obvious candidate for amplification in a fiber for 1.3μm is the $^4F_{3/2} \rightarrow {}^4I_{13/2}$ transition (figure 1) in neodymium doped silica, with the fluorescence band centred around 1.32μm. However it is known that in glass hosts this transition suffers from excited state absorption (ESA) from $^4F_{3/2} \rightarrow {}^4G_{7/2}$ which occurs in the same wavelength range. Hak·ni et al [2] report that

even with the core glass of a silica fiber heavily doped with phosphorous, ESA dominates, limiting gain to beyond 1.36μm, which is out of the communications window. However in a ZBLAN fibre the wavelength of ESA is shifted to shorter wavelengths, and is reduced in strength, allowing gain from 1.32μm to 1.38μm [3-6] with the peak gain occurring near 1.345μm. The limiting factor then becomes competition from the $^4F_{3/2} \rightarrow {}^4I_{9/2}$ 0.9μm transition and the $^4F_{3/2} \rightarrow {}^4I_{11/2}$ 1.05μm transition. This limits gain to a maximum of about 7dB at 1.345μm in a single stage device, due mainly to the buildup of amplified spontaneous emission at 1.05μm causing population clamping in $^4F_{3/2}$. The noise figure of this device has only been measured in the low-gain case, but theoretical modelling suggests that the ESA will give a noise figure between 3dB and 6dB for high gain, dependent on wavelength. Sugawa et al [7] have reported that 10dB can be achieved by cascading amplifiers with 1.05μm filtering to bypass this problem. Recent mathematical modelling [8] suggests that significant increase in this performance may achieved by use of a single pump source and multiple ASE filters. However this amplifier is still sufficiently far from the desired systems wavelength to be of only limited use.

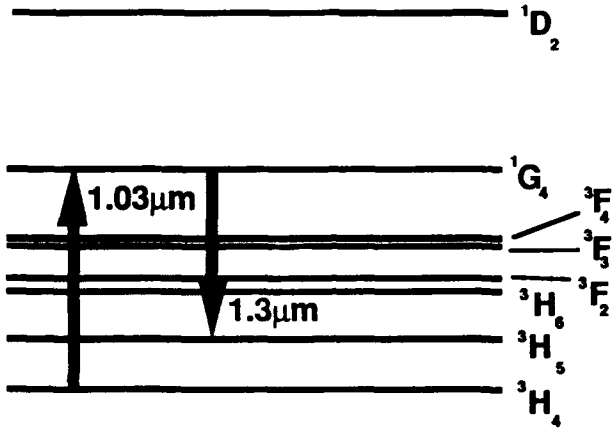


Figure 2. Partial energy level diagram for praseodymium in glass showing relevant transitions

*Praseodymium Amplifiers*

Examination of the energy level diagram for praseodymium reveals a 1.3μm transition $^1G_4 \rightarrow {}^3H_5$ which can be directly pumped around 1.03μm. However the energy gap $^1G_4 \rightarrow {}^3F_4$ is only about 2700cm$^{-1}$ ( 3.7μm) so in a silica fiber the multiphonon decay from $^1G_4$ will prohibit radiative emission, and in a ZBLAN fiber will severely limit the fluorescence lifetime of that level. Fluorescence measurements on bulk glass samples [9] indicate that there is sufficient 1.3μm emission in praseodymium doped ZBLAN to merit further investigation. We have constructed an amplifier using 17m of singlemode ZBLAN fibre doped with 560ppmw $Pr^{3+}$ [10]. The background loss of this fibre was approximately 2dB. Although the peak absorption is near 1.015μm, pumping at 1.007μm by a Ti:Sapphire laser yielded maximum gain, due mainly to the higher power available at that wavelength because of the reflectivity of beam steering mirrors. Figure 3 shows the net small signal gain spectrum of the amplifier, with 0.55W pump power, taking into account the background loss and the short wavelength edge of the ground state $^3H_4 \rightarrow {}^3F_4$ absorption, which accounts for the negative region beyond 1.34μm. It can be seen that the peak gain is around 10.5dB at 1.3μm, which corresponds to ~13dB internal gain.

The 3dB bandwidth is 35nm. Figure 4 shows the small signal gain evolution at 1.3μm with pump power. Again the background loss of the fibre accounts for the negative figures at low pump powers (<0.1W). Under these conditions the efficiency of the amplifier is 0.019dB/mW.

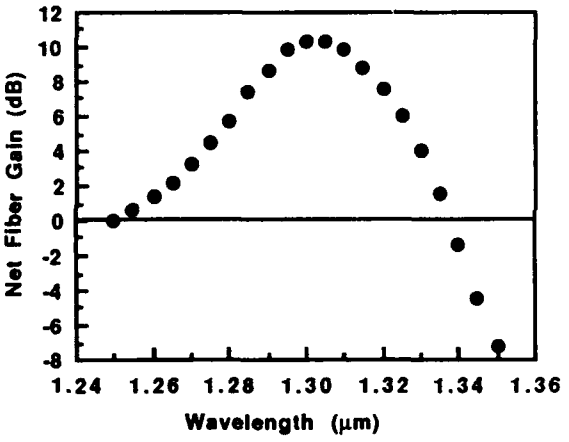


Figure 3. Net fiber gain spectrum with 0.55W pump power at 1.007μm

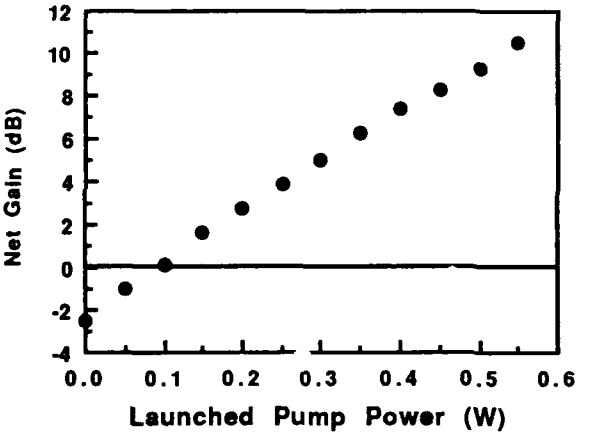


Figure 4. Gain evolution at 1.3μm pumped at 1.007μm.

The maximum gain achieved was 10.5dB with the available pump power, but figure 4 shows that there is no sign of small signal gain saturation even at these pump powers. Greater pump power would therefore result in greater gain. The efficiency of the amplifier is low due to the high non-radiative decay from $^1G_4 \rightarrow {}^3F_4$, but some improvement could be expected from reduction in the fibre loss and optimisation of fibre parameters. The system suffers some slight ESA as the orange glow of the fibre shows.

Other groups [11,12], also report recent work on this transition, with largely similar results. [12] reports higher efficiency due to pumping at the absorption peak, but limited pump power results in net gain of 5.2dB. [11] uses a Nd:YAG laser at 1.064μm and reports internal gain of up to 15dB.

*Conclusions:*

At present it is not possible to realise an amplifier based on silica fibres for 1.3μm. ZBLAN or similar heavy metal fluoride glass fibres offer a choice of transitions, due to shifted energy bands and much lower phonon energies. Neodymium has shown that amplifiers of at least 10dB are possible at 1.345μm, with prospects of 15dB for the future. Praseodymium is at a much earlier stage of development but has already demonstrated internal gains of 15dB, and net gains of >10dB at 1.3μm. Noise has not yet been measured in these devices, though as a 4-level system with small ESA it should be low. Although the efficiency is low at present, prospects are good that this will be improved to make diode pumping a practical proposition. (The development of high-power long-lived strained-layer MQW AlGaAs/InGaAs 980nm lasers as pump sources for erbium doped silica fibre amplifiers will be of direct benefit here since only a small change in process conditions will allow operation in the 1.015μm band.) Since no gain saturation has been observed, and there are no stronger competing transitions, significant improvement in gain should also be possible. For the immediate future then, praseodymium doped fluoride glasses offer the best prospect for fibre amplifiers at 1.3μm.

*Acknowledgements:*

The author would like to acknowledge the contributions made to this work by R Wyatt, S F Carter, D Szbesta, S T Davey, M H Hunt, J E Pedersen, and C A Millar. M Monerie is also thanked for providing a preprint of his group's work.

*References:*

[1] Hill A M, Wyatt R, Massicott J F, Blyth K J, Forrester D S, Lobbett R A, Smith P J, Payne D B, "39.5 Million Way WDM Broadcast Network Employing Two Stages of Erbium-Doped Fibre Amplifiers", Electronics Letters, vol 26, pp1182-1184 (1990).

[2] Hakimi F, Po H, Tumminelli R, McCollum B C, Zentino L, Cho N M, Snitzer E, "Glass fiber laser at 1.36μm from $SiO_2$:Nd", Optics Letters, vol 14, p 1060 (1989)

[3] Pedersen J E, Brierley M C, Carter S F, France P W, "Amplification in the 1300nm telecommunications window in a Nd-doped fluoride fibre", Electronics Letters, vol 26, pp 329-330 (1990)

[4] Pedersen J E, Brierley M C, "High saturation output power from a neodymium-doped fluoride fibre amplifier operating in the 1300nm telecommunications window", Electronics Letters, vol 26, pp 819-820 (1990)

[5] Miyajima Y, Sugawa T, Komukai T, "Efficient 1.3μm-band amplification in a $Nd^{3+}$-doped single-mode fluoride fibre", Electronics Letters, vol 26, pp 1397-1398 (1990)

[6] Brierley M C, Pedersen J E, Lobbett R A, France P W, "Amplification in the 1.3μm telecommunications window using a singlemode neodymium-doped fluorozirconate fibre", Digest of IEEE First International Workshop on Photonics Networks, Applications, and Components, Montebello, Quebec, Canada, October 1990.

[7] Sugawa T, Miyajima Y, Komukai T, "10dB gain and high saturation power in a $Nd^{3+}$-doped fluorozirconate fibre amplifier", Electronics Letters, vol 26 pp 2042-2044 (1990)

[8] Øbro M, Pedersen B, Bjarklev A, Povlsen J H, Pedersen J E,"Highly improved fibre amplifier for operation around 1300nm" Electronics Letters, vol 27, pp 470-472 (1991)

[9] Davey S T, France P W," Rare earth doped fluorozirconate glasses for fibre devices", British Telecom Technology Journal, 1989, no 7, pp 58-68.

[10] Carter S F, Szebesta D, Davey S T, Wyatt R, Brierley M C, France P W, " Amplification at 1.3μm in a $Pr^{3+}$doped single-mode fluorozirconate fibre", Electronics Letters, vol 27, no 8, 11 April 1991.

[11] Durteste Y, Monerie M, Allain J Y, Poignant H, "Amplification and lasing at 1.3μm in praseodymium-doped fluorozirconate fibres", Electronics Letters, vol 27, no 8, 11 April 1991.

[12] Ohishi Y, Kanamori T, Kitagawa T, Takahashi S, Snitzer E, Sigel G H, "$Pr^{3+}$-doped fluoride fiber amplifier operating at 1.31μm", Postdeadline paper at OFC '91, Feb 1991

# $Nd^{3+}$-doped Fluoride Fiber Amplifier Module With 10 dB Gain and High Pump Efficiency

Yoshiaki MIYAJIMA, Tomoki SUGAWA, and Tetsurou KOMUKAI
NTT Transmission Systems Laboratories
Tokai, Ibaraki-ken, 319-11, Japan

**Introduction:** Recently, $Nd^{3+}$-doped fluoride fiber has attracted much interest, because it has the potential for optical amplification around the 1.3 μm communication band[1]. In terms of the effect of ESA(excited state absorption) and the probability of radiative transition, fluoride fiber is preferable to silica fiber as a host glass[2]. However, some problems must be solved for the development of a practical amplifier. First, gain has not been sufficiently large for a practical pump power to be obtained from diode lasers. Second, gain has been obtained in wavelengths longer than 1.31 μm.

In this report, we focus on the first problem. This work reports that a gain of 10 dB was obtained by using bidirectional 25 mW pumpings and by applying a 1.05 μm rejection filter in doped fiber.

**Amplifier configuration:** The amplifier configuration is shown in Fig.1. The pump source was a commercially available AlGaAs diode laser operated at 0.82 μm. A maximum pump power of 50 mW was launched into the fiber simultaneously in both the forward and backward directions. Pump and signal light were coupled by a dichroic mirror.

A 4 m long $Nd^{3+}$-doped fluoride fiber with a concentration of 2000 ppm in the core were used. The fiber glass matrix was ZBLAN($ZrF_4$-$BaF_2$-$LaF_3$-$AlF_3$-NaF). Its core and outer diameters were 4 μm and 125 μm, respectively. The cut-off wavelength of the fiber was 1.22 μm. The transmission loss was 0.1 dB/m at 1.30 μm. Fiber ends were polished to make 8 degree endfaces to suppress the cavity effect.

To improve the pump saturation, the competitive transition of 1.05

μm (from $^4F_{3/2}$ to $^4I_{11/2}$ shown in Fig.2) should be suppressed. A dielectric multilayer coated filter is positioned in the middle of Nd-doped fiber. This filter has 98% reflectivity for 1.05 μm light and allows 1.3 μm and 0.8 μm light to pass through. Therefore, it can suppress the 1.05 μm transition activated by the increased ASE(amplified spontaneous emission). The signal coupling losses in the two dichroic mirror systems are 1.5 dB and 1.1 dB, and the fiber loss including filter insertion loss is 1.2 dB. Therefore, the total insertion loss in this amplifier module is 3.8 dB.

**Pump efficiency and gain limit:** To improve pump efficiency, fiber with a high NA and a small core was examined. The calculated pumping efficiency dependence on the core diameter of the doped fiber is shown in Fig.3 for several ESA ratios, $\varepsilon$, which is the ratio of the ESA transition to the 1.3 μm band transition. We assumed a transition cross-section of $0.8\times10^{-20}cm^2$, a metastable-state lifetime of 450 μs and a fiber cut-off wavelength of 1.30 μm. It is understood that the pumping efficiency for 6.5 μm core fiber is 0.16 dB/mW and that it increases for a small core fiber.

Two kinds of fiber were prepared. Fiber A has a core diameter of 6.5 μm and a relative refractive index difference of 0.5 % and a cut-off wavelength of 1.30 μm. Fiber B has a core diameter of 4.0 μm and a relative refractive index difference of 1.18 % and a cut-off wavelength of 1.22 μm. Measured gain vs. pump power without a 1.05 μm rejection filter are shown in Fig.4. Pump efficiencies of 0.13 and 0.28 dB/mW are obtained(plotted in Fig.3), respectively.

Gain saturation is observed at pumping powers of 40 and 20 mW, respectively. This saturation is caused by the activation of the 1.05 μm transition from $^4F_{3/2}$ to $^4I_{11/2}$. As the strong 1.05 μm emission will stimulate the further 1.05 μm emission from $^4F_{3/2}$, the 1.3 μm transition from the same upper level will not increase. Pump saturation may be improved by rejecting out the 1.05 μm fluorescence.

The amplifier module presented in this report has a 1.05 μm rejection filter in the middle of the doped fiber. This filter prevents the transmission of 1.05 μm fluorescence. Therefore two sections of fiber can operate without pump saturation. The results of gain measurement with different signal output levels are shown in Fig.5. The maximum gain of 10 dB is observed at a signal wavelength of 1.343 μm with forward and backward pump powers of 25 mw. Also, the saturation output signal power of 3 dB compression gain is estimated to be over +10 dBm. Pump efficiency is 0.20 dB/mW in this system.

This 10 dB gain in large signal region is almost twice the maximum gain in Fig.4. From this result, we can confirm the usefulness of the cascade structure amplifier with a 1.05 μm rejection filter. If we insert more filters in doped fiber, high gain over 20 dB is attainable for 100 mW pumping power.

**Conclusion:** A 10 dB gain has been achieved in a $Nd^{3+}$-doped fluoride fiber by using simultaneous forward and backward pumping with a 25 mW AlGaAs diode laser. In order to attain high gain, it is important not only to use small core fiber but also to apply a 1.05 μm rejection filter between the fibers.

**References:**

[1]Y.Miyajima, et al., Electron. Lett., vol.26, pp.1397-1398, (1990),

[2]W.J.Miniscalco, et al., Electron. Lett., vol.24, pp.28-29, (1988),

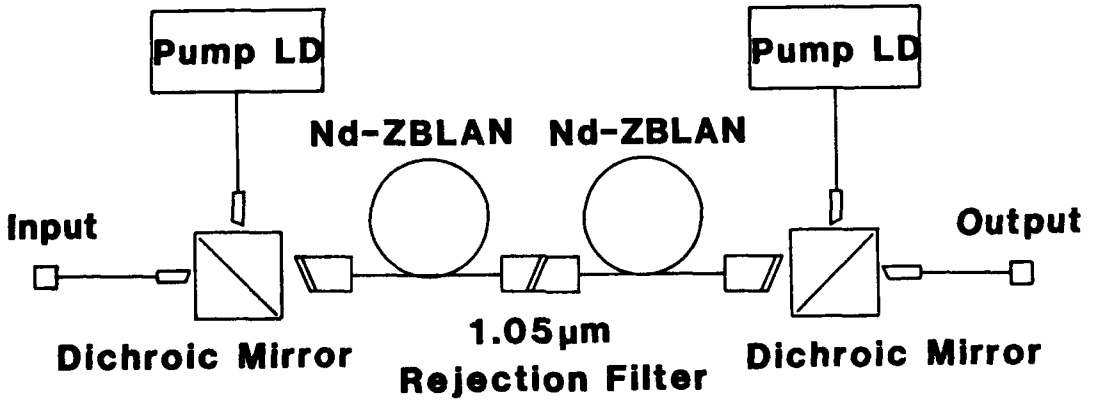


Fig.1 Amplifier configuration

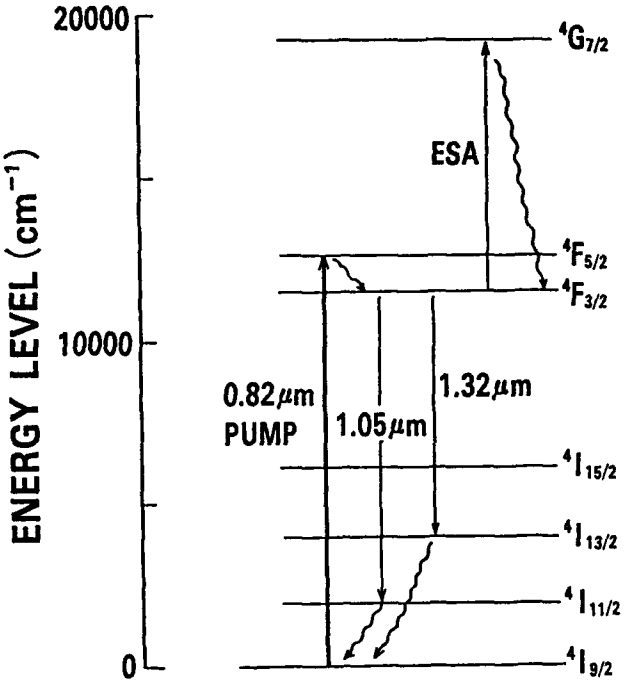


Fig.2 Energy diagram of $Nd^{3+}$

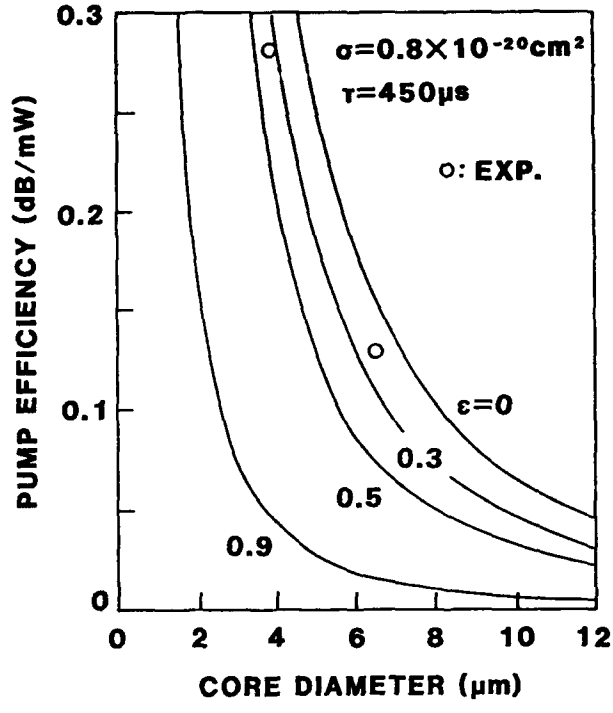


Fig.3 Pumping efficiency dependence on core diameter

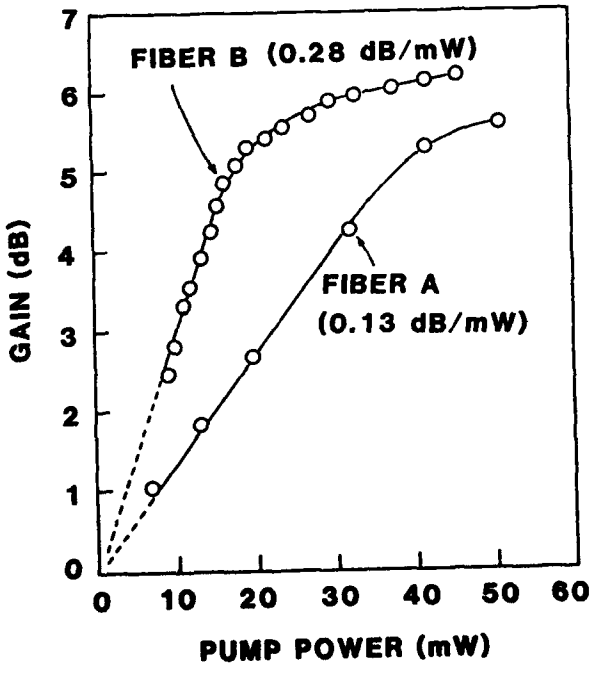


Fig.4 Gain vs.pump power

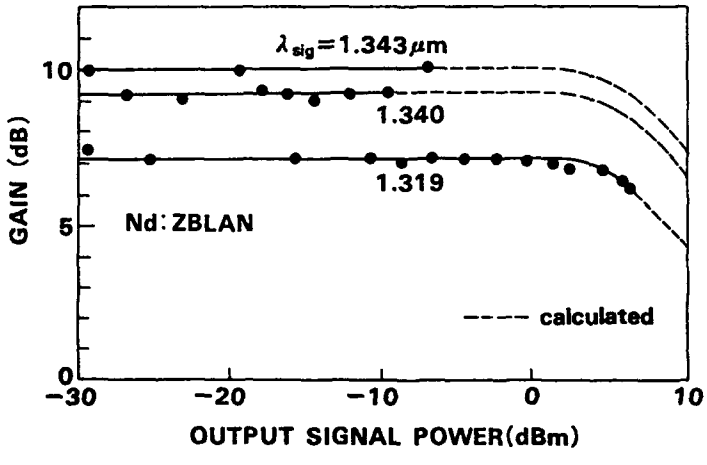


Fig.5 Output signal power vs. gain

# Laser Diode Pump Sources

**VC** 10:30am–12:00m
**abaret Room**

**.. Kurumada,** ***Presider***
***'SC Electronics Laboratories, Japan***

# 1.48μm and 0.98μm High-Power Laser Diodes for Erbium-Doped Fiber Amplifiers

Ikuo MITO and Kenji ENDO
Opto-electronics Research laboratories, NEC Corporation
4-1-1, Miyazaki, Miyamae-ku, Kawasaki-shi, 216 Japan

## 1.INTRODUCTION

The development of erbium-doped fiber amplifiers has recently progressed rapidly. Highly efficient power conversion for 1.48μm wavelength pumping enables a post-amplifier to achieve output power greater than 100mW[1]. When pumped in 0.98μm wavelength, the erbium-doped fiber amplifiers showed very low noise property[2], which permits high receiver sensitivity as a pre-amplifier.

High power laser diodes (LDs), operating at 1.48μm and 0.98μm wavelength, are essential as pumping light sources. Recently, multi-quantum well (MQW) structures have been employed as active layers for 1.48μm wavelength LDs[3]. We have obtained the highest cw output power reported so far, 250mW[4]. Lasing at 0.98μm wavelength was achieved with InGaAs strained quantum well structures grown on GaAs substrates[5]. Low internal absorption loss helped these devices to emit 240mW cw power[6].

This paper reports recent progress in the development of 1.48μm and 0.98μm wavelength high power LDs for erbium-doped fiber amplifiers.

## 2. 1.48um WAVELENGTH InGaAs MULTI-QUANTUM WELL LDs

The development on high power InGaAsP LDs has been conducted on an approach to lengthen the LD cavity from a view point of heat dissipation. 700-800μm long cavity devices was fabricated to be effective for maximum cw power improvement. 190mW cw power at 1.48μm wavelength was reported and constant power aging tests of 100mW at 25℃, 65mW at 50℃ were conducted[7]. We demonstrated a new approach to reduce the internal absorption loss of LD cavity by employing InGaAs MQW structure[3]. Less than 10cm$^{-1}$ internal absorption loss was achieved. Low threshold current and high quantum efficiency for about 1mm long MQW-LDs greatly enhanced high power cw operation.

A schematic device structure of 1.48μm wavelength InGaAs MQW DC-PBH LD is shown in Fig.1. 5 QW layers, stacked with InGaAsP barrier layers on an n-InP substrate, were grown by MO-VPE. DC-PBH LD structure was adopted for the purpose of both current confining and stabilizing the lateral mode. Front and rear facet reflectivities were controlled to 10% and 90% by dielectric film coating.

Device parameter optimization was carried out experimentally on the quantum well number. As shown in Fig.2, an optimal well number of 5 existed among 3-7 quantum well devices tested. The result was attributed to a trade-off relation between the internal absorption loss and the threshold current density.

Light output and injection current (L-I) curves for 800μm and 1800μm devices are depicted in Fig.3(a),(b). Due to the low internal absorption loss of 8cm$^{-1}$, both low threshold

current and high quantum efficiency were obtained for such a long cavity devices. 250mW maximum cw light output was obtained for very long 1800μm cavity device. More than 150mW cw light output was maintained up to 70°C.

The reliability has been under examination. Figure 4 shows the driving current traces for 100mW constant power aging tests at 20°C, 50°C, 70°C. All the devices aged were operated stably under such a high stress conditions. Drive current increasing rate of $2x10^{-6}$/hr was obtained for 20°C-100mW aging. This result indicates a possibility that these devices have a few 100 thousand hour median life-time to failure at 20°C.

## 3. 0.98μm WAVELENGTH InGaAs STRAINED QUANTUM WELL LDs

0.98μm wavelength pumping is important due to high absorption efficiency and low noise property of erbium doped fiber amplifier. Although 0.98μm wavelength is separate from the lasing wavelength regions of both AlGaAs/GaAs LDs and InGaAsP/InP LDs, InGaAs strained quantum well on GaAs substrate has been developed as an active layer covering 0.9-1.0μm wavelength region. 0.98μm lasing, aimed at pumping light sources, was achieved by Uehara et al. with ridge-waveguide structure[5]. They showed promising long term aging test at 50°C-10, 20, 30mW constant power conditions. Recently, preliminary life test of 100mW output power was presented by Welch[8].

We have developed 0.98μm wavelength LDs, characterized by both a strained double-quantum well (DQW) and a flat device surface. Figure 5 shows the schematic device structure. On an n-GaAs substrate, a separate-confinement heterostructure (SCH) including two InGaAs strained quantum wells was grown by MO-VPE. The cladding layers were n-, and p-$Al_{0.4}Ga_{0.6}As$. A flat wafer surface was achieved by embedding a mesa stripe with n-GaAs burying layers. Figure 6 is an L-I curve and its temperature dependence was shown in Fig.7. 140mW cw power was obtained. The DQW active structure resulted in large $T_0$ value of 145K. It was superior to 75-120K, typically reported for the LDs with an active layer of InGaAs strained single quantum well. A reliability test was conducted at 50°C-30mW constant power condition. After 8000hr aging, these devices operated stably. We have studied the reliability feature on InGaAs strained QW LDs. It was different from the conventional AlGaAs LDs. Sudden death was much reduced in InGaAs strained QW LDs and a very small growth velocity of dark-line defects was observed[9].

We demonstrated a low noise performance of erbium doped fiber amplifier pumped by a 0.98um InGaAs strained QW LD. An optical receiver was composed of an erbium doped fiber pre-amplifier and InGaAs pin-PD. Excellent receiver sensitivity of -37.2dBm at $10^{-9}$ bit error rate was observed for 10Gb/s direct detection as shown Fig.8. The receiver sensitivity was improved by 15dB from the detection without the pre-amplifier[10].

## 4.CONCLUSION

The development of pumping light sources for erbium doped fiber amplifiers has been focused on both 1.48μm wavelength MQW LDs and 0.98μm strained QW LDs. Their low internal absorption loss resulted in low threshold and high power cw operation.

REFERENCES

1)T.Sugie et al.: Technical Digest of Topical Meeting on Optical Amplifiers and Their Applications, Monterey, PDP2 (1990).
2)R.I.Laming and D.N.Payne: IEEE Photonics Technol. Lett., vol.2, pp.418 (1990)
3)I.Mito et al.:Technical Digest of IOOC'89, Kobe, PDP-B12 (1989).
4)H.Asano et al.: Technical Digest of OFC'91, San Diego, WG-1 (1991).
5)M.Okayasu et al.: IEEE Photonic Technol. Lett., vol.2, pp.689 (1990).
6)A.Larsson et al.,: Technical Digest of Topical Meeting on Optical Amplifiers and Their Applications, Monterey, WA-2 (1990).
7)K.Yamada et al.:Technical Digest of Topical meeting on Optical Amplifiers and Their Applications, Monterey, WA-3 (1990).
8)D.F.Welch et al.: Technical Digest of OFC'91, WB1.
9)K.Fukagai et al.: Jpn. J. Appl. Phys., vol.30, pp.L371 (1991).
10)T.Saito et al.: Technical Digest of OFC'91, San Diego, PDP-14 (1991).

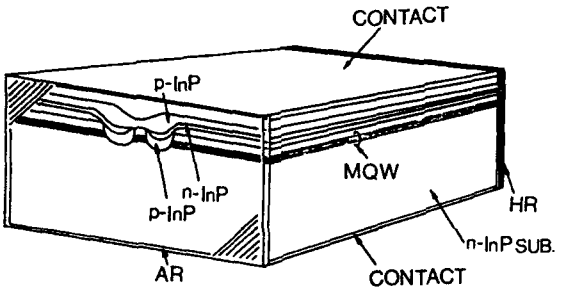


Fig.1 Schematic structure of 1.48μm InGaAs MQW DC-PBH LD.

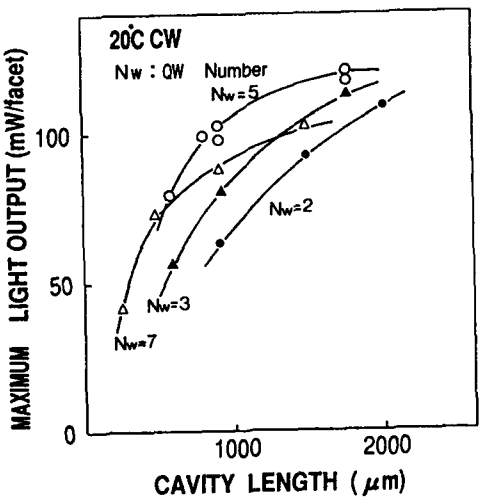


Fig.2 Maximum cw light output power per facet plotted as a function of cavity length for 1.48μm MQW DC-PBH LDs with both facets as-cleaved. Nw is quantum well number.

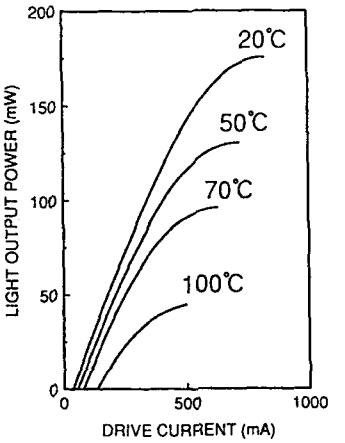


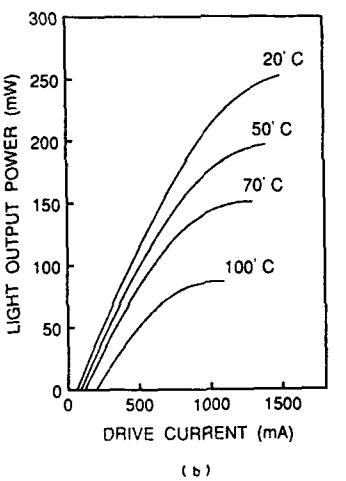


Fig.3 Light output power versus injection current for 1.48μm DC-PBH LDs. (a) 800μm long cavity device. (b) 1800μm long cavity device.

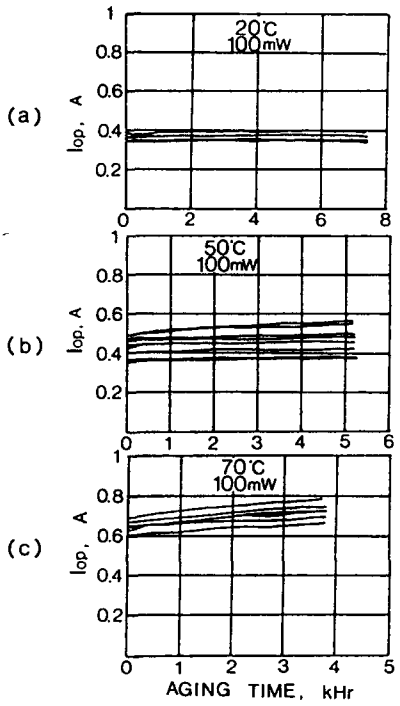


Fig.4 Driving current traces for 1.48μm MQW-DC-PBH LDs.
(a) 20℃-100mW: 800μm long cavity devices.
(b) 50℃-100mW: 800μm long cavity devices.
(c) 70℃-100mW: 1800μm long cavity devices.

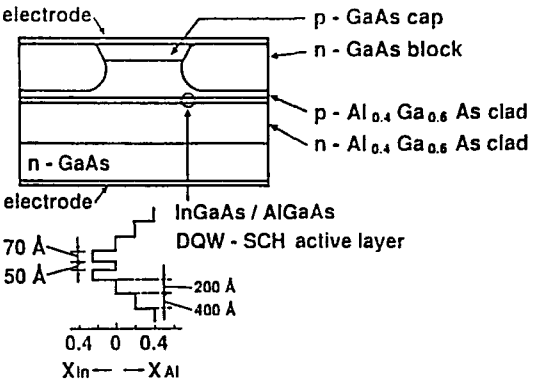


Fig.5 Schematic cross section of 0.98μm InGaAs strained double-quantum well LD.

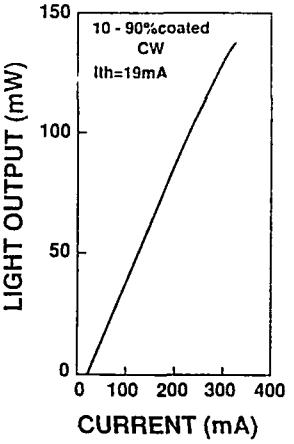


Fig.6 Light output power versus injection current for a 0.98μm InGaAs strained DQW LD.

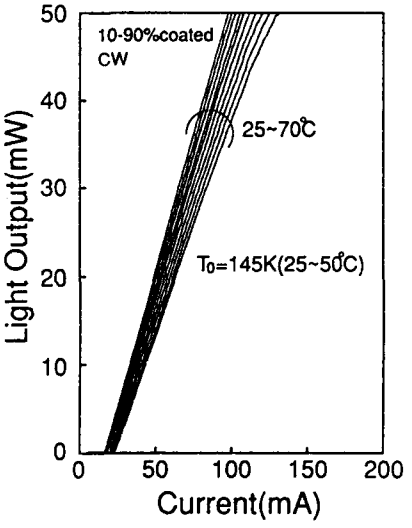


Fig.7 Temperature dependence of L-I curves for a 0.98μm InGaAs strained DQW LD. $T_0$ value between 25℃ and 50℃ is 145K.

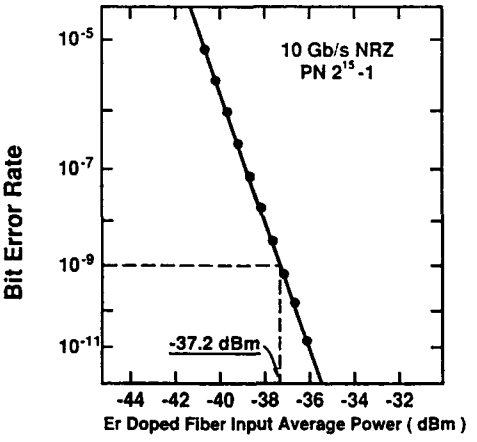


Fig.8 Bit error rate curve for an optical receiver composed of an pre-amplifier pumped 0.98μm InGaAs strained DQW-SCH LD and InGaAs pin-PD. Receiver sensitivity for 10Gb/s direct detection is -37.2dBm at $10^{-9}$ error rate.

# 0.98-μm Strained Single Quantum Well Lasers Launching High Optical Power in a Single-Mode Fiber

Masato Wada, Kaoru Yoshino*, Masanobu Okayasu and Jiro Temmyo

NTT Opto-electronics Laboratories
Morinosato Wakamiya, Atsugi-shi, Kanagawa 243-01 Japan
*Tokai-mura, Naka-gun, Ibaraki 319-11 Japan

## I. INTRODUCTION

Erbium-doped optical fiber amplifiers (EDFA) pumped by 0.98-μm laser diodes exhibit a small noise figure (1) and small temperature-induced variation in amplification compared with pumping by 1.47-μm laser diodes (2). Recently, considerable research interest has focused on 0.98-μm laser diodes (3)-(8).

For practical application of EDFAs, however, optical power coupled to a single-mode fiber (SMF) is the key issue, a subject that few studies have addressed. In order to obtain high optical power in a SMF, we have improved the mode field emitted from lasers. Employing narrow-ridge waveguide lasers, we have sought to realize transverse lateral mode stabilization. We have also investigated epitaxial layer structures to enlarge optical spots for stabilizing the mode field and also for decreasing the vertical beam divergence. Aging test results are also described.

## II. EXPERIMENT

Epitaxial layers were grown by low pressure metalorganic vapor phase epitaxy at 750°C on n-type GaAs substrates. We prepared four different epitaxial structures:

Table 1 Epitaxial layer structures (x: Al composition, t: layer thickness)

| | GRIN SCH I | | GRIN SCH II | | SCH | | guided SCH | |
|---|---|---|---|---|---|---|---|---|
| | x | t (μm) | x | t (μm) | x | t (μm) | x | t (μm) |
| p-$Al_xGa_{1-x}As$ | 0.5 | 1.0 | 0.4 | 1.0 | 0.4 | 1.0 | 0.4 | 1.0 |
| p-$Al_xGa_{1-x}As$ | | ------ | | ------ | | ------ | 0.3 | 0.3 |
| non-$Al_xGa_{1-x}As$ | 0.5-0 | 0.17 | 0.4-0 | 0.06 | | ------ | | ------ |
| non-GaAs | | ------ | | ------ | | 0.06 | | 0.06 |
| $In_{0.21}Ga_{0.79}As$ | | 0.011 | | 0.011 | | 0.011 | | 0.011 |
| non-GaAs | | ------ | | ------ | | 0.06 | | 0.06 |
| non-$Al_xGa_{1-x}As$ | 0-0.5 | 0.17 | 0-0.4 | 0.06 | | ------ | | ------ |
| n-$Al_xGa_{1-x}As$ | | ------ | | ------ | | ------ | 0.3 | 0.3 |
| n-$Al_xGa_{1-x}As$ | 0.5 | 1.0 | 0.4 | 1.0 | 0.4 | 1.0 | 0.4 | 1.0 |

[1] two different graded index separate confinement heterostructures (GRIN SCH-I and -II), [2] a separate confinement heterostructure (SCH), and [3] a separate confinement heterostructure with guide (guided SCH). Common epitaxial layers shared by these four structures are a $In_{0.21}Ga_{0.79}As$ strained active layer (11 nm) and a p-GaAs cap layer (0.3 μm). The details of the four structures are summarized in Table 1.

Ridge waveguide structures were formed using electron cyclotron resonance reactive ion etching. The stripe width was 2 μm and the cavity length was 600 μm. Suitable ridge depth (the thickness of the residual cladding and confining layer) was determined on the basis of the transverse-mode calculation. A low-reflection coating of $Al_2O_3$ (~3%) and a high-reflection coating of $Al_2O_3/TiO_2$ (~70%) was applied on front and rear facets of the lasers, respectively. For the metalization, Ti/Pt/Au was used for the p-contact and AuGeNi was used for the n-contact.

For coupling to a SMF ( $\lambda c$=0.85 μm, $\Delta$=0.3%), an aspheric glass lens for laser module (9) was used.

## III. RESULTS AND DISCUSSION

The epitaxial layer structures were designed to enlarge the vertical spreads of the optical field intensity; this is to decrease the optical density for lateral mode stabilization and also to decrease vertical beam divergence $\theta_\perp$. Calculated vertical optical field intensity spreads in the waveguide at the full width at half maximum (FWHM) are listed in Table 2 together with other experimental results. Both $\theta_{//}$ and $\theta_\perp$ are obtained from far field patterns. Coupling efficiency is calculated from the optical power of the laser itself and that in a SMF at an applied current of 150 mA. Maximum power in a SMF obtained near maximum applicable current for each laser is also listed. For the GRIN SCH-II, SCH, and guided SCH structures, smaller $\theta_\perp$ and larger coupling efficiency were obtained at the expense of threshold current, compared with the GRIN SCH-I case. Threshold currents for GRIN SCH-I, GRIN SCH-II, SCH, and the guided SCH were 8, 35, 30, 14 mA, respectively.

Table 2 Experimental results

| | | GRIN SCH-I | GRIN SCH-II | SCH | guided SCH |
|---|---|---|---|---|---|
| $\theta_{//}$ at FWHM | (deg) | 12 | 11 | 12 | 14 |
| $\theta_\perp$ at FWHM | (deg) | 54 | 42 | 47 | 49 |
| calculated spread at FWHM | (μm) | 0.24 | 0.40 | 0.28 | 0.31 |
| coupling efficiency at 150 mA | (%) | 22 | 37 | 36 | 36 |
| maximum power in SMF | (mW) | 29 | 43 | 45 | 52 |

Figure 1 shows the optical power in a SMF as functions of applied current under continuous-wave (CW) operation. Except for the GRIN SCH-I structure, the characteristics are smooth and their linearity up to about 25 mW is quite good, showing high stability of the beam emitted from the narrow-ridge lasers.

The GRIN SCH-I structure lasers yielded the smallest coupling efficiency of 22% at 150 mA, probably due to the relatively large $\theta_\perp$. In this case a gradual decrease in gradient is obvious and hence only relatively small power could be launched into a SMF even at high

applied current. This can probably be attributed to the instability of the transverse lateral mode, such as spatial hole-burning, that occurs at smaller applied current than the other three cases due to smaller spread of the optical field intensity. In case of the wider (3.6 μm) ridge laser with GRIN SCH-I structure, the coupling efficiency at 150 mA was even smaller at 19%. A narrow ridge structure is effective for reducing the astigmatism that must exist in the present cases; this may have also served to enhance the coupling efficiency.

Maximum power was obtained in the guided SCH structure, reaching 58 mW with less smoothness at high operating current.

Randomly selected lasers adopting the GRIN SCH-I structure have operated in an aging test at 70 mW in 50 °C ambient for more than 2500 hours. Activation energy calculated from a 3000-hour test at 10 mW in 30, 50 and 70 °C ambient is 0.3 eV. Lasers with larger optical field intensity spread such as shown in Table 2 are expected to perform even more reliably under aging tests.

## IV. CONCLUSION

We realized high optical power in a SMF launched by narrow-ridge waveguide structure lasers on the basis of an investigation of epitaxial layer structures. High optical power of well over 50 mW in a SMF was obtained for a 2-μm-width ridge waveguide laser with guided SCH epitaxial structure. Further investigation of epitaxial layer structures is needed to increase the vertical spreads of optical field at the expense of small increases in threshold currents to enhance coupling efficiency.

## ACKNOWLEDGEMENT

We would like to thank M. Fukuda, S. Uehara and M. Horiguchi for their invaluable discussion and K. Kurumada, M. Nakahara and T. Ikegami for continuous encouragement.

## References

(1) M. Shimizu et al., Erbium-doped fiber amplifiers with an extremely high gain coefficient of 11.0 dB/mW, Electron. Lett., 26, 1641(1990).
(2) M. Yamada et al., Temperature insensitive $Er^{3+}$-doped optical fibers, Electron. Lett., 26, 1649(1990).
(3) S. Uehara et al., 0.98-μm InGaAs strained quantum well lasers for erbium-doped fiber optical amplifiers, Proc. IOOC'89, 20PDB-11, 58(1989).
(4) P. K. York et al., InGaAs-GaAs strained-layer quantum well buried heterostructure lasers ($\lambda$>1μm) by metalorganic chemical vapor deposition, Appl.Phys.Lett., 54, 499(1989).
(5) A. Larsson et al., A 980nm Pseudomorphic Single Quantum Well Laser for Pumping Erbium-Doped Optical Fiber Amplifiers, Optical Amp. and Their Application, 210/WA(1990).
(6) D. P. Bour et al., 980 nm Diode Laser for Pumping $Er^{3+}$-Doped Fiber Amplifiers, IEEE Photonics Technol.Lett., 2, 153(1990).
(7) D. F. Welch et al., High-power, 980-nm, single-mode laser diodes, OFC'91, Technical Digest, 66 WB1(1991).
(8) T. Saito et al., High Receiver Sensitivity at 10 Gb/s using an Er-doped Fiber Preamplifier pumped with a 0.98 μm Laser-diode, OFC'91, PD14-1.
(9) K. Kato and I. Nishi, Low-Loss Laser Diode Module Using a Molded Aspheric Glass Lens, IEEE Photonics Technol. Lett., 2, 473(1990).

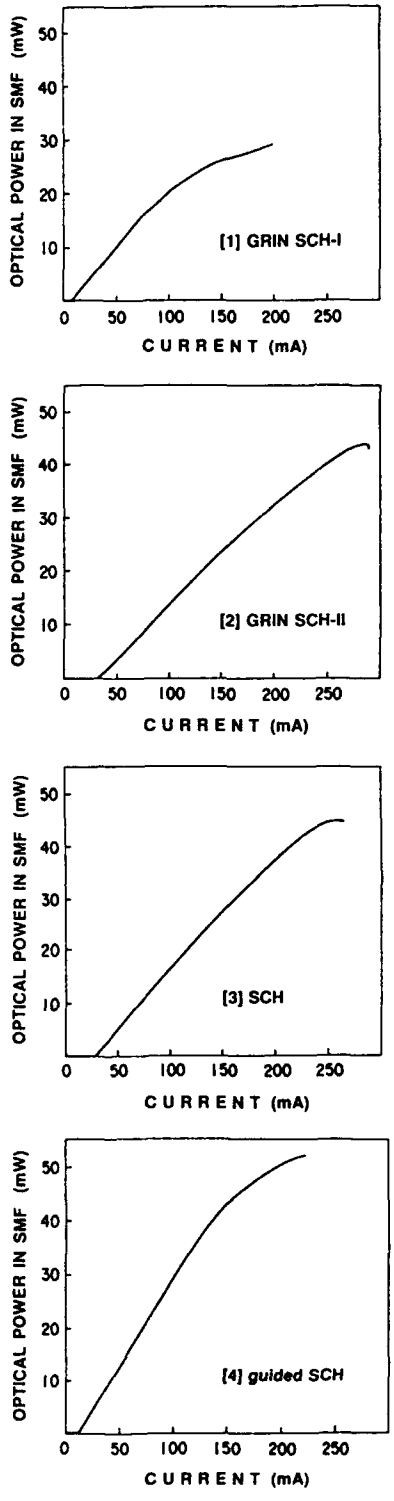


Fig. 1 Optical power launched in a SMF by [1] GRIN SCH-I, [2] GRIN SCH-II, [3] SCH, and [4] guided SCH structure 2-μm ridge waveguide lasers under CW operation.

# High-power Operation of 1.48 $\mu$m GaInAsP/GaInAsP Strained-layer Multiple Quantum Well Lasers

H.Kamei, M.Yoshimura*, H.Kobayashi, N.Tatoh, and H. Hayashi

Optoelectronics R&D Laboratories

*Information and Electronics R&D Laboratories

Sumitomo Electric Industries, Ltd.
1 Taya-cho, Sakae-ku, Yokohama 244, Japan

## Intoduction

High-power semiconductor lasers emitting at 1.48 $\mu$m wavelength have been increasingly important as pumping light sources for $Er^{3+}$-doped fiber amplifiers [1, 2]. In this paper we report high power operation of 1.48 $\mu$m GaInAsP/GaInAsP multiple quantum well (MQW) lasers which utilize strained-layer MQW structures as active layers.

## Laser structure

Three types of GaInAsP/GaInAsP SCH (separate confinement hetero-structure) MQW structures were formed by low pressure OMVPE (organometallic vapor phase epitaxy). The SCH-MQW structure is shown in Fig. 1. Well number is five. Quaternary well composition and well thickness for three types of MQW structures are summarized in Table 1. Amount of compressive strain are 0 % (unstrained), 0.5 %, and 1 %, respectively. Thickness of barrier and guide layers,whose bandgap wavelength are both 1.2$\mu$m, are 150Å and 500Å, respectively. PBH (planar buried heterostructure) lasers were fabricated for these three types of MQW structures as shown in Fig. 2. All the crystal growth including the burying growth were performed by OMVPE.

## Characteristics

Threshold currents are less than 10 mA for 300 $\mu$m-long lasers and about 13 mA even for 900 $\mu$m-long lasers. There is little difference of threshold current for three types of lasers. Inverse of external differential quantum efficiency as a function of cavity length for three types of lasers are shown in Fig. 3. Values of



internal loss and external differential quantum efficiency are shown in the table of Fig. 3. Internal loss is as low as around 8 $cm^{-1}$ due to the utilization of quantum well structures. External differential quantum efficiency of strained-layer MQW lasers is higher than that of unstrained-layer MQW lasers.

I-L (current-light output) curves for three types of 900 $\mu$m-long lasers with HR (highly reflective) and AR (anti-reflective) coatings are shown in Fig. 4. Maximum light output of unstrained-layer, 0.5 % strained-layer, and 1 % strained-layer lasers are 192 mW, 207 mW, and 236 mW, respectively. Higher light output power could be obtained by introducing compressive strains into MQWs. The value of 236 mW is the highest value for 1.48 $\mu$m lasers with cavity length of 900$\mu$m. Temperature dependence of I-L curves of a MQW laser with 1 % compressive strain is shown in Fig. 5. 100 mW of output power can be obtained with input current of 300 mA at 20°C, and even at 70°C output power of 100 mW can be obtained at fairly low input current of 480 mW. Parallel and perpendicular beam divergence, $\theta_{\parallel}$ and $\theta_{\perp}$, of these MQW lasers are 25° and 30°, respectively. The almost circular far field patterns promise high coupling coefficiency of lightwave into optical fibers.

## Summary

1.48$\mu$m GaInAsP/GaInAsP MQW lasers were fabricated by OMVPE growth technique. Maximum light output power of 236 mW was obtained for a 900 $\mu$m-long laser with 1 % compressive strain in quantum wells.

## References

[1] K. Yamada, S. Oshiba, T. Kunii, Y. Ogawa, T. Kamijoh, T. Nonaka and Y. Kawai, in : Proc. of 1990 Topical Meeting on Optical Amplifiers and Their Applications, WA3, 214-217 (1990).

[2] H. Asano, S. Takano, M. Kawaradani, M. Kitamura and I. Mito, in : Technical Digest of Optical Fiber Communication Conference 1991, WG1, 88 (1991).

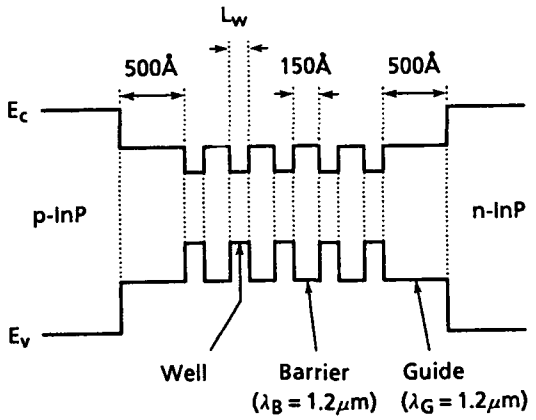


Fig. 1 GaInAsP/GaInAsP SCH-MQW structure

Table 1. Well composition and thickness of three types of strained-layer MQW structures

| Well composition | Compressive strain | Well thickness : $L_W$ |
|---|---|---|
| $Ga_{0.42}In_{0.58}As_{0.9}P_{0.1}$ ($\lambda$ = 1.55$\mu$m) | Unstrained | 68 Å |
| $Ga_{0.34}In_{0.66}As_{0.9}P_{0.1}$ | 0.5 % | 47 Å |
| $Ga_{0.27}In_{0.73}As_{0.9}P_{0.1}$ | 1 % | 36 Å |

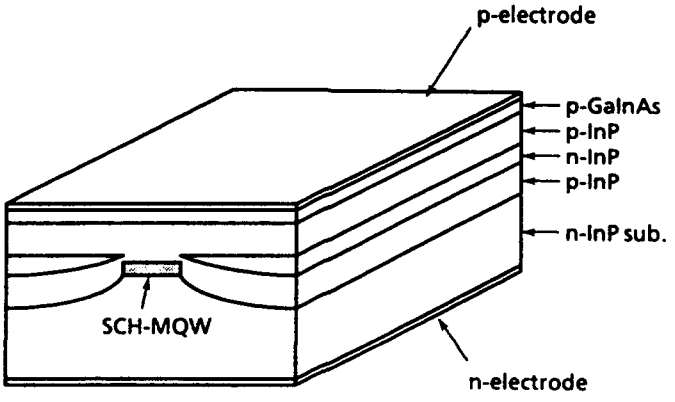


Fig. 2 Schematic cross-section of PBH strained-layer MQW laser

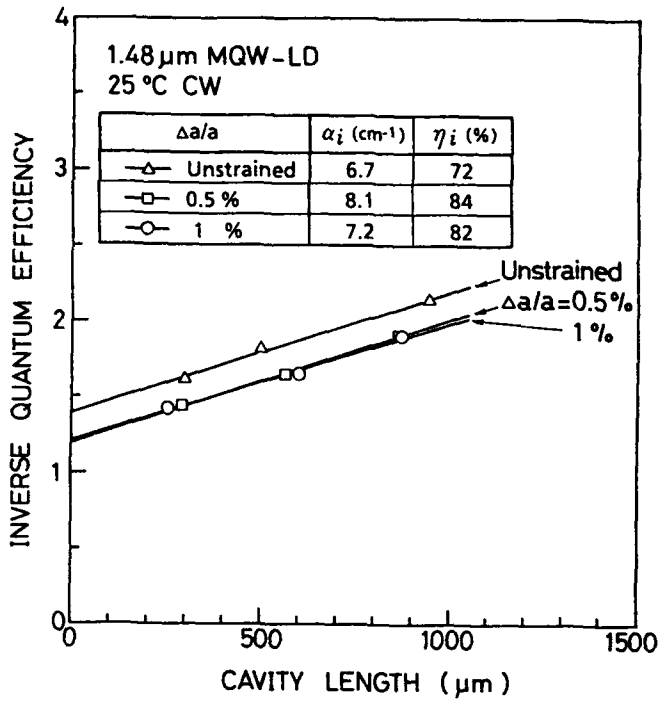


Fig. 3 Internal loss and external differential quantum efficiency of MQW lasers

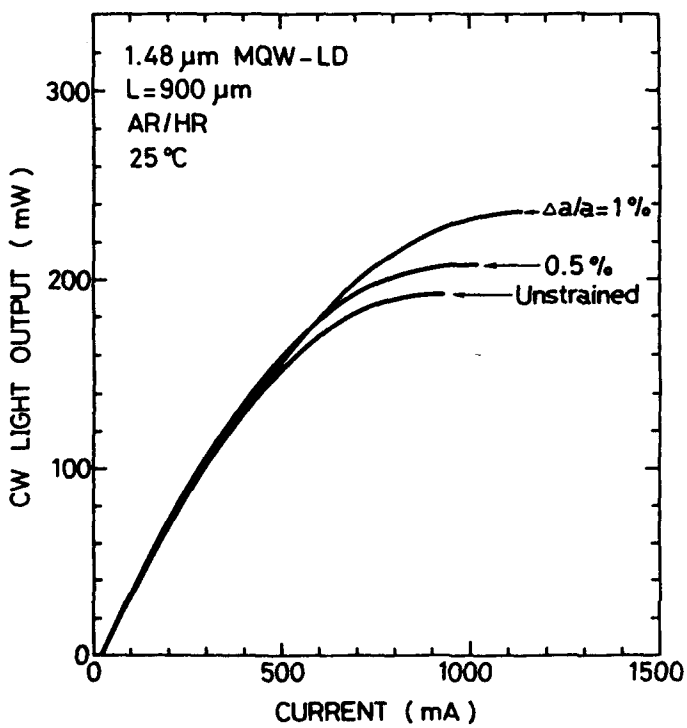


Fig. 4 I-L curves of three types of MQW lasers

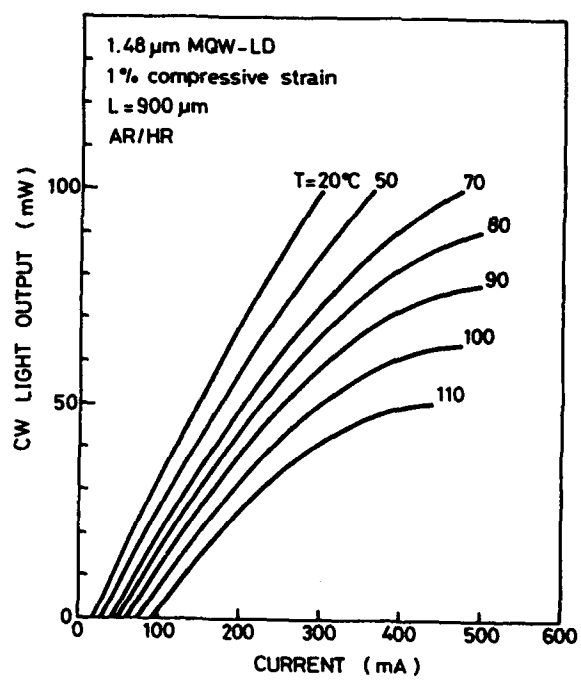


Fig. 5 Temperature dependence of I-L curves of a MQW laser with 1.0% compressive strain

# Single-Mode, 980 nm Pump Lasers for Fiber Amplifiers

*F. D. Crawford, W. F. Sharfin, B. Elman, R. B. Lauer, P. Mebrahtu, and E. Eichen*

GTE Laboratories Incorporated
40 Sylvan Road
Waltham, MA 02254
Telephone: (617) 466-2403
FAX: (617) 890-9320

Pump lasers for $Er^{3+}$-doped silica fiber optical amplifiers must demonstrate excellent spatial mode stability to high output power levels in order to achieve useful gain.[1,2] The pump band at 980 nm is the most efficient of the principle $Er^{3+}$ absorption bands in terms of gain per input optical power.[3] Pumping at 980 nm is also preferred in comparison to pumping at 1480 nm because it reduces the noise introduced into the amplified optical signal.[4]

In this paper we describe the design, fabrication, and characteristics of a high power, MBE-grown 980 nm laser with a simple, weakly-index-guided structure. The geometry of the laser's lateral waveguide is carefully controlled to ensure that all of the power is in the fundamental spatial mode. Far field patterns of these devices are single lobed and stable to the highest measured powers. These Fabry-Perot lasers exhibit single frequency operation to output powers as high as 170 mW, with linewidths as narrow as 5 MHz.

## *Design and Fabrication*

In order to ensure high output power, we chose a separate confinement heterostructure (SCH) design in which the waveguide region perpendicular to the p-n junction plane is relatively wide (410 nm). A single quantum well of InGaAs with a nominal thickness of 10 nm and a nominal InAs concentration of 20% was sandwiched between two 200 nm thick GaAs guide layers. This separate confinement and quantum well region was centered between n- and p-type layers of $Al_{0.22}Ga_{0.78}As$. A thin (~100 nm) Be-doped GaAs cap served as the p-contact layer. All layers were grown by MBE, with the InGaAs quantum well grown at a substrate temperature of 530°C, the GaAs layers grown at a substrate

temperature of 600°C, and the $Al_{0.22}Ga_{0.78}As$ layers grown at a substrate temperature of 650°C.

Accurate and reproducible definition of the lateral waveguide region is necessary to achieve a single lateral spatial mode to high output powers. For this purpose, we chose a ridge waveguide structure with a nominal 4 μm wide ridge. A SEM photograph of the ridge structure is shown in Figure 1; the facet has been etched to delineate the layers. The critical step in the fabrication of ridge waveguide lasers is control of the etch depth, which determines the lateral mode confinement. The preferred etch depth was empirically determined to be about150±50 nm above the active layer. A fast etch of $Na_4OH$: $H_2O_2$:$H_2O$ was followed by a slow $H_2SO_4$:$H_2O_2$:$H_2O$ etch to control the ridge height. If the ridge is not etched deeply enough, the laser is essentially gain-guided; in this case, excessively high threshold current densities (greater than 5 $kA/cm^2$) arise because of strong anti-guiding from the carrier-induced change in refractive index. On the other hand, if the ridge is etched too deeply, the waveguide will support numerous spatial modes.

The ridge was isolated from the rest of the chip by the use of sputtered $SiO_2$. n- and p-contacts were formed using alloyed AuSn and AuZn, respectively. The p-contact had a TiPtAu overlay.

***Characteristics***

A single-facet power-current curve is shown in Figure 2 for an uncoated 1000 μm long laser. The total output power is 170 mW at 200 mA. The laser operates in a single frequency for bias currents between 80 and 200 mA. The characteristic temperature $T_o$ ranged from 90 to 100 K. External efficiencies were 85 to 95%, due to extremely low cavity losses. The internal loss was estimated at 3 $cm^{-1}$ from the slope of a plot of the inverse of the external quantum efficiency versus cavity lengths from 400 to 1000 μm.

Figure 3 demonstrates that the far field pattern of a typical laser is single lobed and remains in a stable pattern up to high powers. While the far field pattern is a good indication of modal purity, a far more sensitive measure of mode quality can be obtained by monitoring the emission spectra of the laser. An emission spectrum is shown in Figure 4 for the laser of figure 2, biased at 200 mA. The lasers typically emitted in a single frequency and had side mode suppression ratios greater than 20 dB, with linewidths as low as 5 MHz.

**Summary:**

The design, fabrication, and lasing properties of high power, single mode, ridge waveguide lasers will be described in detail. The excellent modal purity of these devices is demonstrated by the stimulated emission spectrum, which shows single frequency operation with side mode suppression of more than 20 dB and linewidths as narrow as 5 MHz at powers of up to 170 mW. These lasers are ideally suited as optical pumps for $Er^{3+}$ doped fiber amplifiers.

**References:**

1. M. Okayasu, T. Takeshita , M. Yamada, O Kogure, M. Horiguchi, M. Fukuda, K. Oe, and S. Uehara, Electron. Lett. 25, 1564 (1989).
2. M. Okayasu, M. Fukuda, T. Takeshita, S. Uehara, Photon. Tech. Lett. 2, 689 (1990).
3. M. Shimizu, M. Yamada, M. Horiguchi, T. Takeshita, and M. Okayasu, Electron. Lett. 26, 1641, (1990).
4. M. Yamada, M. Shimizu, M. Okayasu, T. Takashita , M. Horiguchi, Y. Tachikawa, and E. Sugita, Photon. Tech. Lett. 2, 205 (1990).

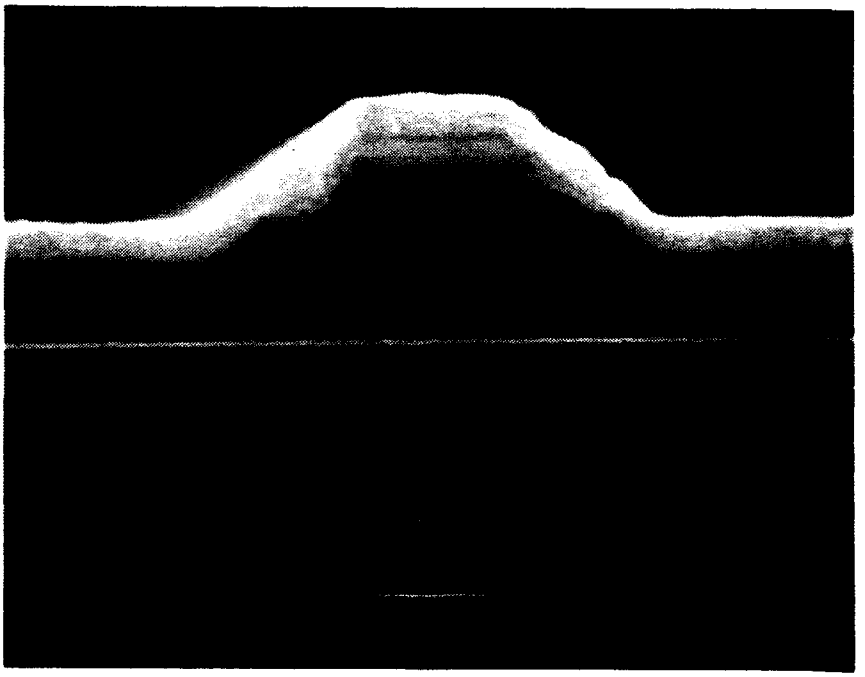

*Figure 1.* SEM photograph of the facet of a 980 nm ridge waveguide laser. The facet has been etched to delineate the layers.

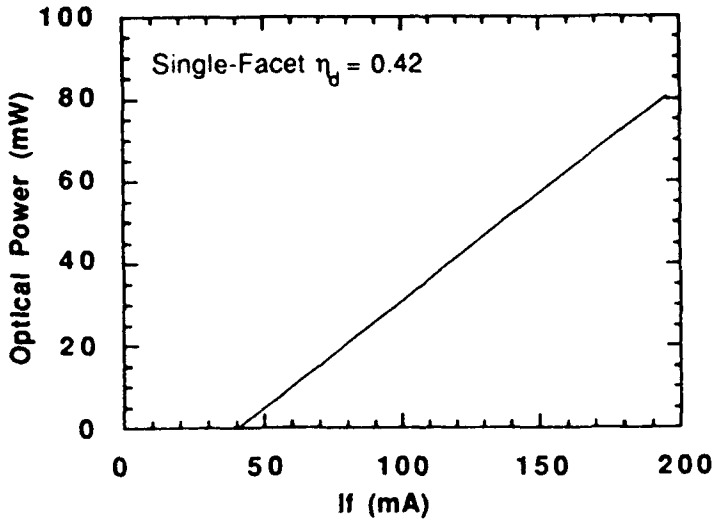


*Figure 2.* Single-facet power-current characteristic for an uncoated 980nm diode laser.

*Figure 3.*

Far field pattern for a typical 980 nm ridge waveguide laser. The output beam is single lobed and stable at high power.

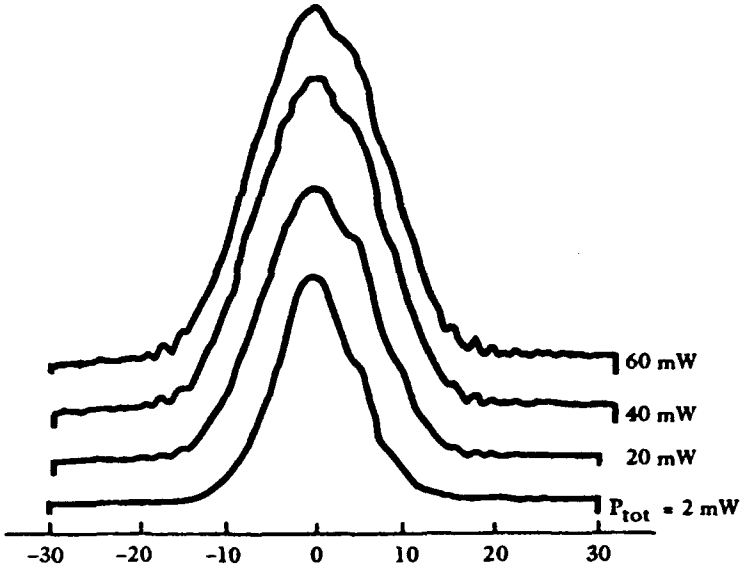


*Figure 4.*

The lasing spectrum shows single frequency operation.

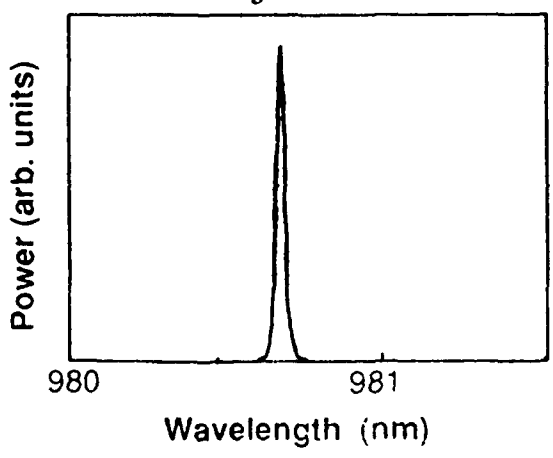

# High Power 980 nm Ridge Waveguide Laser in Single Mode Fiber Coupled Package

Richard F. Murison, Shuyen R. Lee, Nigel Holehouse,
Alan H. Moore, Kenneth M. Dzurko
EG&G Canada Ltd., Optoelectronics Division
Vaudreuil, Quebec, Canada

Aldo Righetti, Giorgio Grasso, Flavio Fontano
Societa Pirelli Cavi, Milano, Italy

Christian F. Schaus, Shangzhu Sun
University of New Mexico
Center for High Technology Materials
Albuquerque, NM

Nancy A. Dinkel, John C. Connolly
David Sarnoff Research Center
Princeton, NJ

Rapid progress in strained quantum well InGaAs/AlGaAs laser diodes has led to the wide acceptance of 980 nm diodes as potential pump sources for $Er^{3+}$-doped fiber amplifiers (EDFA). In particular, ridge waveguides have proven to be ideal structures for such devices[1,2], promising ease of manufacture, and potentially high reliability[3]. In this paper, we report high coupled power from ridge waveguide lasers into large NA single-mode fiber designed for use in EDFA systems, using an industry-standard 14-pin DIL package outline. We also report systems performance obtained using these lasers as the pump source in a broad-band EDFA power amplifier.

The epitaxial structure is a graded-index separate confinement heterostructure, grown in a low pressure MOCVD reactor. A single quantum well was employed, using a strained InGaAs layer whose composition and thickness were engineered to provide lasing at a wavelength of 980 nm. The threshold current density, measured on a 50 μm oxide stripe structure with 500 μm cavity length, was 272Acm$^{-2}$.

The ridge waveguide structure employed is illustrated in the SEM photomicrograph reproduced in Figure 1. The ridges were defined by wet chemical etching, resulting in a typical U-shaped channel profile, with a ridge width of 2.5 μm measured at the top of the ridge. Following etching, a thin film of Silicon Nitride, chosen for its excellent thermal properties, was deposited over the entire structure using PECVD. Contact stripes were photolithographically defined on the tops of the ridges, and opened by Plasma Etching. Contacts comprising a Ti:Pt:Au tri-metal were deposited conformally in an E-beam evaporator equipped with a planetary substrate motion. Finally, the wafer was mechanically thinned to 100 μm and a conventional AuGeNi alloyed contact applied to the n-surface.

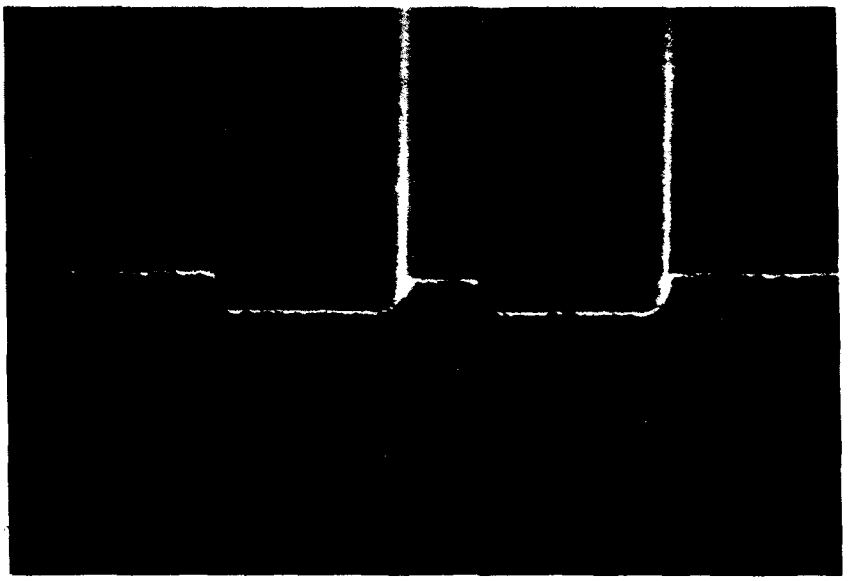

Figure 1

Individual devices were cleaved with a cavity length of 750 μm, and coatings applied to the front and rear facets to produce modal reflectivities of around 5% and 95% respectively. The dice are bonded p-side down onto Copper-Tungsten submounts using 60:40 Sn:Pb solder. The threshold current is typically 20 mA, although the lowest value measured to date is 9 mA. The output power slope efficiency is 0.87 mW/mA, measured from zero to 100 mW (the maximum value permitted by our calibrated power meter). Uncalibrated measurements of total output power at 200 mA indicate a value of 150 mW. The series resistance above threshold is 2Ω, and the measured total power conversion efficiency is typically 40% at operating power levels.

The packaging approach is illustrated in Figure 2. A 14-pin, dual-in-line flanged body is used, and both rear facet monitor and TE cooler are present. The optical fiber is soldered into a supporting tube which is clamped firmly in place against the laser submount. This arrangement has been engineered to permit sub-micron fiber alignment accuracy, while retaining a high degree of immunity from typical thermal and environmental hazards.

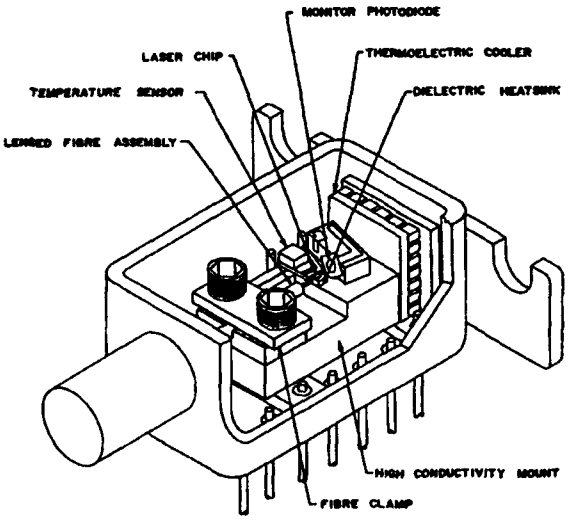


Figure 2

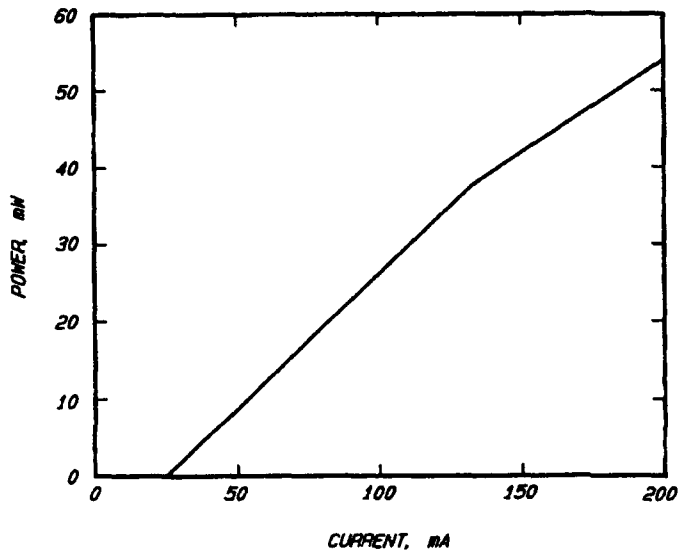


Figure 3

Figure 3 shows the light-current characteristic measured from the end of a single mode fiber having 0.22 nA, a cutoff wavelength of 920 nm, and mode field diameter of 3.8 μm. The power rises to 54 mW at 200 mA. There is a slope change at 38 mW in this device, caused by the onset of higher order transverse modes in the laser diode, but this has not resulted in a severe power drain from the fundamental mode. Devices of this type are rated for continuous operation at a drive current of 200 mA.

We calculate that a differential fiber coupling efficiency of 38% has been achieved below the slope change, reducing to 31% at higher power.

The laser illustrated in Figure 3 was evaluated as a pump source for an EDFA power amplifier optimized for flat spectral response[4]. The signal source comprised a high coherence tunable semiconductor laser whose output was preamplified to +3 dBm. The measured spectral gain characteristic shows a flat response, within 1.5 dB from 1530 nm to 1560 nm. The gain characteristic was measured at 1547 nm, and is shown in Figure 4.

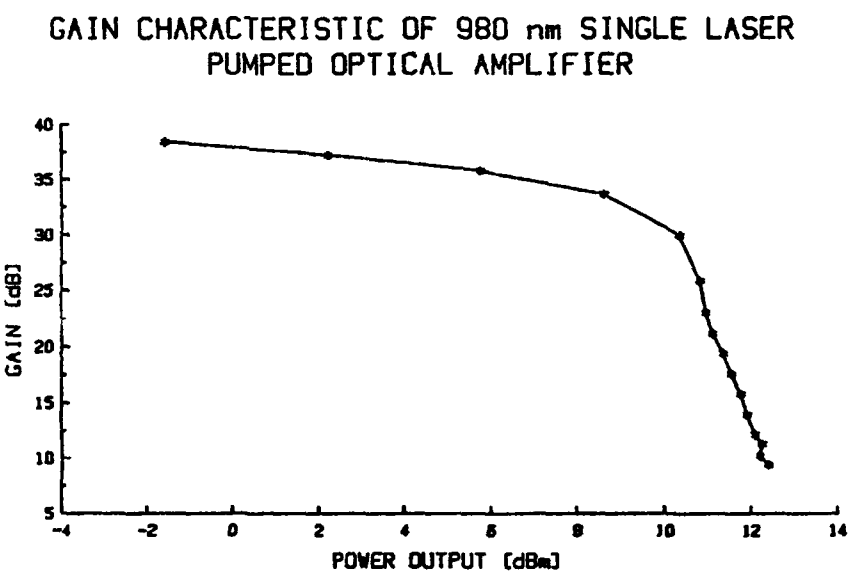


Figure 4

The saturation output power of + 12.8 dBm is the highest reported to date using a single 980 nm laser diode pump source. Direct measurement of amplifier noise shows that in saturation condition, the Noise Figure is lower than 3.5 dB. From these results we obtain a total power conversion efficiency of 48% (90% quantum efficiency), which is very close to that reported using an *"ideal"* Ti:Sapphire pump source[5].

The use of these high power 980 nm ridge waveguide lasers as pump sources for EDFA power amplifiers permits an ideal balance of low noise and high output power, leading to improved systems performance in both digital and analogue optical signal distribution.

**References**

[1] D. Bour, N. Dinkel, et al; *"980 nm diode laser for pumping Er-doped fiber amplifiers"*; IEEE Photon. Tech. Lett., Vol 2, p153, 1990.

[2] A. Larsson, S. Forouhar, J. Cody, R. Lang, P. Andrekson; *"A 980 nm Pseudomorphic Single Quantum Well laser for pumping Erbium-doped Optical Fiber Amplifiers"*; IEEE Photon. Tech. Lett., Vol 2, p540, 1990.

[3] M. Okayasu, M. Fukuda, T. Takeshita, S. Uehara; *"Stable Operation (over 5000h) of High-Power 0.98 μm InGaAs-GaAs Strained Quantum Well Ridge Waveguide lasers for pumping Er-doped Fiber Amplifiers"*; IEEE Photon. Tech. Lett., Vol 2, p689, 1990.

[4] G. Grasso, F. Fontana, A. Righetti, et al; *"980 nm diode-pumped Er-doped fiber optical amplifiers with high gain-bandwidth product"*; OFC '91, San Diego CA, February 1991, Paper FA-3.

[5] R. Laming, D. Payne, F. Meli, et al; *"Highly saturated Erbium doped fiber power amplifiers"*; Optical Amplifiers and their Applications, First Topical Meeting, Monterey CA, July 1990, Paper MB-4.

# Material Effects in Fiber Amplifiers

**WD** 1:30pm–3:00pm
Cabaret Room

G. Grasso, *Presider*
*Societa Cavi Pirelli SpA, Italy*

# Materials for Erbium-Doped Fiber Amplifiers

William J. Miniscalco
GTE Laboratories Incorporated
40 Sylvan Road, Waltham, MA 02254

## 1. Introduction

Fiber offers an extremely favorable geometry for optical devices, and fiber lasers [1] and amplifiers [2] were reported only shortly after the first bulk glass laser [3]. The choice of host composition has always been an important consideration. Silicates are the oldest and best understood glasses, and the first glass lasers used silicate compositions selected for high rare earth solubility and long lifetimes for the metastable state. The use of phosphate glass significantly improved the performance of early bulk $Er^{3+}$ lasers [4] and it has become the most common host for bulk glass lasers doped with $Er^{3+}$ and $Nd^{3+}$. Although outstanding performance has been achieved using single-mode silica fiber, silica is a poor host for most activator ions, particularly rare earths. The influence of glass composition on the properties of $Er^{3+}$ fiber amplifiers will be considered with particular emphasis placed upon silica; a more detailed discussion can be found in Ref. [5].

## 2. Radiative Efficiency

The relative strengths of the relaxation channels available to an excited ion have an important effect upon the characteristics of an optical amplifier. Nonradiative relaxation is the overriding consideration in determining which of the excited states can be used to provide gain. For rare earths nonradiative decay occurs through electronic relaxation to the next lower state accompanied by multiphonon emission to conserve energy. The smaller the energy gap and the larger the characteristic phonon frequency, the faster the rate. For most oxide glasses the phonon frequencies are large enough to quench all but the $^4I_{13/2}$ level responsible for 1540 nm emission of $Er^{3+}$. The lower phonon frequencies of fluoride glasses lead to additional metastable states and amplifiers have been demonstrated at 2700 nm [6] and 850 nm [7] using fluorozirconate fibers.

Another class of dissipative processes involves cooperative interactions or energy transfer between $Er^{3+}$ ions, phenomena which are sensitive to the distance between ions. This can lead to fast energy migration among the ions until the energy is lost at a trap such as an $OH^-$ complex [8]. Being the lowest excited level, the $^4I_{13/2}$ cannot relax to an intermediate state but can undergo cooperative upconversion, a process in which two excited ions combine their energy leaving one in the ground state and the other in an undesired highly excited state. Because cooperative upconversion requires two interacting ions in the excited state it only manifests itself at high pump powers where it appears as accelerated and nonexponential decay, the latter due to variations in coupling strength between excited ions. This behavior has been observed [9] and further evidence has been the detection of upconverted luminescence [9,10]. Moreover, the decay kinetics expected for a process involving two ions in the $^4I_{13/2}$ state were also seen [9]. The pump power dependence of the upconversion mechanism has important device consequences since the quenching process will be most deleterious at the high population inversions required for $Er^{3+}$ amplifiers to achieve high gain and good signal-to-noise ratio.

## 3. $Er^{3+}$ Solubility

If the rare earth dopant is uniformly dispersed, as is the case for multicomponent glasses, concentrations can greatly exceed $10^{19}$ $cm^{-3}$ (≈1000 ppm-wt) before cooperative processes become significant. Pure silica, however, can incorporate only very small amounts of rare earths before microscopic clustering appears. Rare earth ions require large coordination numbers, and Arai *et al.* have explained the solubility problem with a model in which the absence of a sufficient number of nonbridging oxygens to coordinate isolated rare earths in the rigid silica network causes them to cluster in order to share nonbridging oxygens [11]. Indeed, fiber amplifier experiments have revealed significant $Er^{3+}$–$Er^{3+}$ interactions at an average concentration of ≈$10^{18}$ $cm^{-3}$ in pure silica [12]. Four-coordinated Ge is not expected to alter the tetrahedral silica network sufficiently to alleviate the problem, and power amplifier [13,14] and small-signal amplifier [10] investigations have indicated that performance degrades at similar $Er^{3+}$ levels for Ge-doped silica.

The addition of $Al_2O_3$ to silica eliminates the clustering problem and provides solubilities similar to multicomponent silicate glasses [11]. This has been explained in terms of $Al_2O_3$ forming a solvation shell around the rare earth ion and the resultant complex being readily incorporated into the silica network [11]. Power amplifier studies found $Er^{3+}$ levels $\approx 10^{19}$ $cm^{-3}$ in Al-doped silica provided approximately the same efficiency as found for concentrations an order of magnitude lower in Ge silica [14]. By comparison, levels $<10^{19}$ $cm^{-3}$ in Ge silica reduced the efficiency by roughly an order of magnitude from the low concentration limit [13,14]. The correlation between the positions of the rare earth and Al ions implied by this model is consistent with the small Al-to-Er ratio (≈50) required to eliminate quenching effects in fiber amplifiers [13]. No comparable benefits are derived from P doping: for $P_2O_3$ levels up to 1 mol%, $Er^{3+}$ concentrations $<10^{18}$ $cm^{-3}$ are still required to prevent quenching [13].

4. Operation at 1540 nm

The electronic structure of rare earth ions is dictated by electron-electron interactions, with the host principally affecting the splitting of the Stark levels of the J multiplets. Odd-symmetry terms in the host ligand field potential at the ion site introduce an electric-dipole component to the radiative transition strength between the multiplets. For most transitions this dominates the oscillator strength although the important $^4I_{15/2} \leftrightarrow {}^4I_{13/2}$ transitions of $Er^{3+}$ have a significant magnetic dipole component. The strength of the $^4I_{15/2} \rightarrow {}^4I_{13/2}$ absorption varies by only a factor of two among glass compositions [5,15], while oscillator strengths for $Nd^{3+}$ can vary by as much as a factor of four [16]. The smaller range for $Er^{3+}$ is due in part to the relatively host-independent magnetic dipole contribution. For rare earth ions it is common practice to connect the oscillator strength in absorption, $f_{12}$, and emission, $f_{21}$, employing the Einstein relations generalized to account for the finite linewidth (also referred to as the Landenburg-Fuchtbauer relationship). However, experimental evidence indicates that this approach leads to significant error for the 1540 nm transitions [17] because the assumptions needed to generalize the Einstein relations are not satisfied. Recently a less restrictive analysis procedure has been presented [18]. Table 1 compares measured absorption and emission oscillator strengths as well as peak cross sections, $\sigma$, for several glasses. Although the Einstein relations predict that oscillator strengths and cross sections should be larger in emission than absorption, the opposite is generally true.

Cross section spectra are important in determining amplifier characteristics, particularly efficiency and gain bandwidth. Figure 1 illustrates the extreme diversity that can be found in the shape of the $Er^{3+}$ emission spectrum. These variations are not due to inhomogeneous broadening but rather to differences in the distribution of transition strength among the 56 Stark transitions that comprise the emission band. Sharper spectra result in higher peak cross sections and gain efficiencies (dB/mW), while broader spectra yield wider gain bandwidths under conditions of high inversion. Table 2 lists full-widths at half-maximum (FWHM) for representative glass compositions; pure silica and fluoride glasses lie at the opposite extremes of the observed values. Also indicated is the 3-dB gain bandwidth for a fully inverted amplifier with a peak gain of 30 dB. This serves as the lower bound on what is expected in actual operation since high gain amplifiers are usually incompletely inverted. Note that the emission spectrum of Al/P silica in Figure 1 is anomalous for a silicate glass, being more characteristic of a fluorozirconate or high-fluorine-content fluorophosphate. This is reflected in the wide gain bandwidth for this composition seen in Table 2.

5. Pump Bands

The performance of a fiber amplifier is extremely sensitive to the characteristics of the pump band used, properties that are also dependent on host. Exciting at 980 nm has produced the best results for 1540 nm amplifiers. This is a consequence of the relatively large ground state absorption (GSA) cross section and the complete absence at this wavelength of excited state absorption (ESA) for the $^4I_{13/2}$ metastable state. For this pump band most glass compositions have peak cross sections ranging from 2.0 to 2.5 x $10^{-21}$ $cm^2$ and FWHMs of 15–20 nm. Excellent results have also been obtained directly exciting the $^4I_{13/2}$ by pumping at ≈1480 nm. The absorption cross section is comparable to that at 980 nm, but the finite value of the stimulated emission cross section at the pump wavelength prevents complete inversion. This manifests itself as reduced gain efficiency and a noise figure penalty that has a minimum value of 1–2 dB. The magnitude of the penalty appears to be relatively independent of glass composition [5].

$Er^{3+}$ also has an absorption band at 800 nm which suggests the possibility of pumping with high-power AlGaAs diode lasers, but relatively poor performance has been achieved at this band because of the low strength of the GSA transition ($0.6–1 \times 10^{-21}$ $cm^2$) and an intense, overlapping ESA transition. High gains have been achieved with silica fibers by pumping the long-wavelength wing of the GSA band at ≈820 nm [19], thereby avoiding the ESA at shorter wavelengths. Alternatively, one can utilize glasses with a more advantageous ratio between the cross sections, $\sigma_{ESA}$ and $\sigma_{GSA}$ [20]. ESA measurements have been used to identify compositions more favorable than silica [21,22]. Using the data of Zemon *et al.* [22], Figure 2 compares the spectral dependence of the ratio of $\sigma_{ESA}$ to $\sigma_{GSA}$ for Al/P silica and a fluorophosphate glass. Not only is the fluorophosphate better at all wavelengths, but $\sigma_{GSA}$ exceeds $\sigma_{ESA}$ even at the peak of the pump band. Model calculations indicate this translates into an improvement in gain and efficiency in small-signal amplifiers, and an even more significant increase in conversion efficiency for power amplifiers [23].

6. Operation at Other Wavelengths

Another important transition of $Er^{3+}$ is the $^4I_{11/2} \rightarrow {}^4I_{13/2}$ at 2700 nm which requires a nonoxide glass for the fiber to be transparent and the $^4I_{11/2}$ to be metastable. The long lifetime of the upper level lends itself to small-signal amplification and a gain of 18 dB has been reported for a fluorozirconate fiber amplifier [6]. Because the terminal level is also metastable, a technique for emptying it is essential to good performance. An effective approach, first demonstrated by Brierley *et al.*, is to pump at a wavelength with appreciable ESA [24]. Carrying this process still further, Whitley *et al.* have used upconversion pumping at 800 nm to achieve 23 dB gain on the $^4S_{3/2} \rightarrow {}^4I_{13/2}$ transition at 850 nm in a fluorozirconate fiber [7]. Rather than being deleterious, here the 800 nm ESA enables a single excitation wavelength to perform multiple functions: populate the upper level and deplete all other metastable states, including the terminal level.

I wish to acknowledge experimental assistance by B. Thompson, data provided by R. Quimby, S. Zemon, M.P. Singh, and B. Pedersen, and stimulating discussions with L. Andrews, M. Dakss, R. Folweiler, T. Wei, and R. Klein.

1. E. Snitzer, Proc. 3rd Intl. Conf. Quant. Elect., Paris, 1963, p. 999.
2. C.J. Koester and E. Snitzer, Appl. Opt. **3**, 1182 (1964).
3. E. Snitzer, Phys. Rev. Lett. **7**, 444 (1961).
4. E. Snitzer *et al.*, IEEE J. Quant. Electron. **QE–4**, 360 (1968).
5. W.J. Miniscalco, J. Lightwave Technol. **9**, 234 (1991).
6. D. Roarc'h *et al.*, Electron. Lett. **26**, 903 (1990).
7. T.J. Whitley *et al.*, Electron. Lett. **27**, 184 (1991).
8. V.P. Gapontsev *et al.*, Optics and Laser Tech. **14**, 189 (1982).
9. R. Wyatt, Proc. SPIE **1171**, 54 (1990); B.J. Ainslie *et al.*, IEE Proceed. **137**, Pt. J, 205 (1990).
10. N. Kagi *et al.*, IEEE Photon. Technol. Lett. **2**, 559 (1990).
11. K. Arai *et al.*, J. Appl. Phys. **59**, 3430 (1986).
12. M. Shimizu *et al.*, IEEE Photon. Techn. Lett. **2**, 43 (1990).
13. S.P. Craig-Ryan *et al.*, ECOC'90, Proc. Vol. **1**, 571 (1990); J.F. Massicott *et al.*, Proc. SPIE **1373**, 93 (1991).
14. R.I. Laming *et al.*, OSA 1990 Tech. Digest Series Vol. **13**, p. 16; R.I. Laming *et al.*, IEEE Photon. Technol. Lett., in press.
15. J.N. Sandoe *et al.*, J. Phys. D **5**, 1788 (1972).
16. S.E. Stokowski *et al.*, Lawrence Livermore National Laboratory Report M-095, Rev. 2, Nov. 1981.
17. K. Dybdal *et al.*, Proc. SPIE **1171**, 209 (1990); P.R. Morkel and R.I. Laming, Optics Lett. **14**, 1062 (1989); W.L. Barnes *et al.*, OSA 1990 Tech. Digest Series, Vol. **7**, 50 (1990).
18. W.J. Miniscalco and R.S. Quimby, Optics Lett. **16**, 258 (1991).
19. K. Suzuki *et al.*, Electron. Lett. **26**, 948 (1990); Y. Kimura *et al.*, ECOC'90, Proc. Vol. **1**, 103 (1990).
20. L.J. Andrews *et al.*, in *Proc. of the First Intl. School on Excited States of Transition Elements*, (World Scientific, Singapore, 1989) p. 9.
21. S. Zemon *et al.*, Mat. Res. Soc. Proc. Vol. **172**, 335 (1990).
22. S. Zemon *et al.*, Proc. SPIE **1373**, 21 (1991).
23. B. Pedersen, private communication.
24. M.C. Brierley and P.W. France, Electron. Lett. **24**, 935 (1988).

**Table 1**
**1540 nm TRANSITION STRENGTHS**

| Glass | Emission | | Absorption | |
|---|---|---|---|---|
| | $f_{21}$ ($10^{-6}$) | Peak σ ($10^{-21}$ $cm^2$) | $f_{12}$ ($10^{-6}$) | Peak σ ($10^{-21}$ $cm^2$) |
| Al/P silica | 1.07 | 5.12 | 1.17 | 5.28 |
| Silicate L22 | 0.821 | 7.27 | 0.737 | 5.80 |
| Fluoro-phosphate (low fluorine) | 1.38 | 7.16 | 1.53 | 6.99 |
| Fluoro-phosphate (high fluorine) | 1.33 | 5.79 | 1.48 | 5.76 |
| Fluoro-zirconate | 1.26 | 4.95 | 1.29 | 4.98 |

Sources: Lifetimes for Al/P silica this work, all other lifetimes R.S. Quimby, private communication; absorption for Al/P silica M.P. Singh, private communication.

**Table 2**
**1540 nm BANDWIDTHS**

| Glass | BANDWIDTHS (nm) | |
|---|---|---|
| | FWHM | 30 dB Gain |
| Pure silica | 7.94 | 2.2 |
| Ge silica | 24.9 | 4.2 |
| Al/P silica | 43.3 | 6.4 |
| Silicate ED2 | 20.4 | 3.3 |
| Phosphate L27 | 27.1 | 3.6 |
| Fluorophosphate (low fluorine) | 32.0 | 3.7 |
| Fluorophosphate (high fluorine) | 43.3 | 5.8 |
| Fluorozirconate | 63.3 | 11.7 |
| Ba-Zn-Lu-Th fluoride | 59.2 | 10.1 |
| Borate L87 | 41.2 | 5.6 |

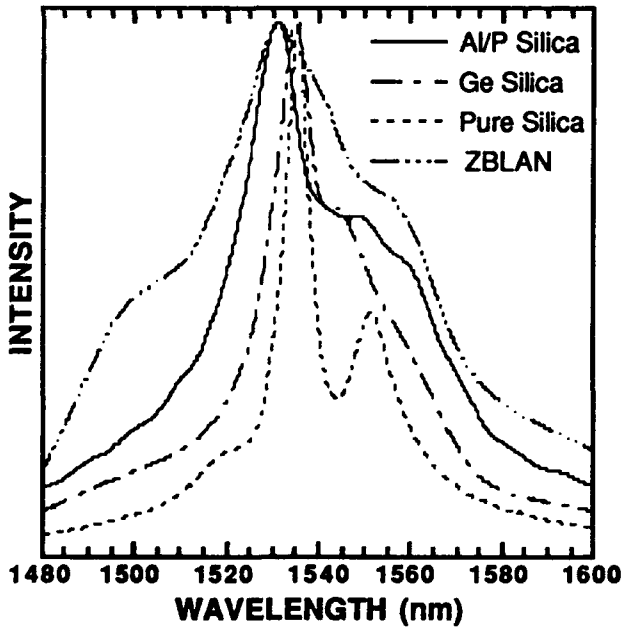


**Figure 1:** $Er^{3+}$ emission band for ZBLAN fluorozirconate and doped and undoped silica. Spectra were scaled to same peak value to facilitate comparison.

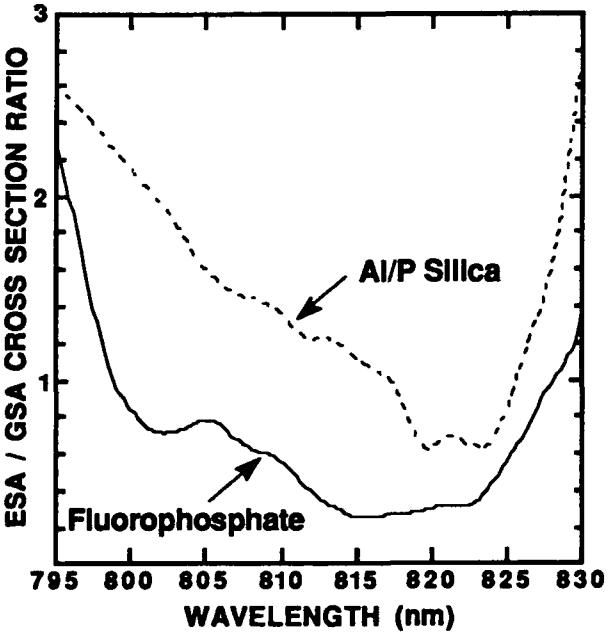


**Figure 2:** Ratio of the ESA to the GSA cross section over the range of the 800 nm pump band; based on data of Zemon *et al.* [22]. Comparison is for Al/P silica and low-fluorine fluorophosphate.

# Non-linear excited state absorption in $Er^{3+}$-doped fibre with high-power 980nm pumping

M.G.Sceats*, P.A.Krug, G.R.Atkins*, S.C.Guy** and S.B.Poole

Optical Fibre Technology Centre
University of Sydney, NSW 2006
Australia

## ABSTRACT

We report the measurement of non-linear excited state absorption (ESA) in $Er^{3+}$-doped fibres pumped at 980nm. The implications for high-power high-gain amplifiers are discussed.

## INTRODUCTION

The performance of erbium doped optical fibre amplifiers[1,2] can be significantly degraded by excited state absorption (ESA) of the pump light from the metastable $^4I_{13/2}$ state. Laming *et al*[2] showed that ESA was negligible for pumping into the 980nm and 530nm absorption bands, whilst Snitzer *et al*[3] showed that pumping directly into the $^4I_{13/2}$ band was also possible. These deductions were based on linear ESA experiments in which the small signal absorption spectrum was measured in a regime in which the population was fully inverted.

Recently, high-power, high-gain amplifiers have been reported[5,6] with 50% slope efficiency, corresponding to a quantum efficiency of 80%, and with linear characteristics up to injected pump powers of 1.1W at 980nm. In this paper, we show that there is a non-linear ESA from the 980nm pump, and suggest that it arises from the short-lived $^4I_{11/2}$ state which is pumped directly by 980nm light. It is of interest to determine whether the non-linear ESA has a detrimental effect on amplifier performance at high power.

## EXPERIMENT

The experimental configuration consisted of a Ti:sapphire laser, giving up to 1W at 980nm in the TEM-00 mode, injected into Erbium doped germanosilicate fibre with an $LP_{11}$ cut-off of 850nm, a NA of 0.22 and a doping level of ca 50ppm. The maximum power injected into the fibre was 340mW. At these powers, the fibre glowed with the green fluorescence characteristic of emission from the $^4S_{3/2}$ and $^2H_{11/2}$ states. Fig 1 shows the fluorescence spectra from these states.

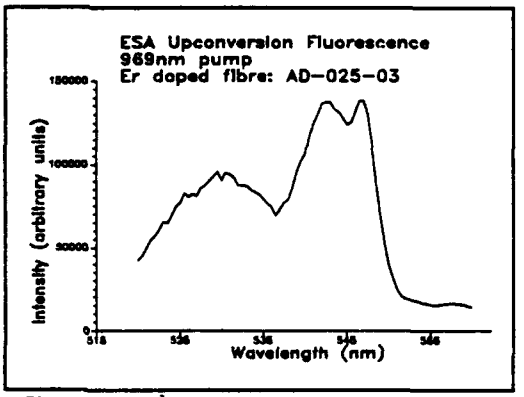


Figure 1 $Er^{3+}$ fluorescence around 540nm.

* School of Chemistry, University of Sydney
** School of Electrical Engineering, University of Sydney

Providing reabsorption can be neglected, the fluorescence intensity is a measure of the ESA. This was confirmed by comparing the side-scattered and transmitted fluorescence intensities at 546 nm as a function of pump power for a 20m length of fibre in which the fluorescence was uniform along the fibre length. In the log-log plot of Figure 2, the power law which characterises this ESA is shown to be 1.4. The same law applied to both results. The fibre, when pumped with 340mW, exhibited significant ASE generation, but was not lasing. The fluorescence power was measured to be 20nW from one end of the fibre of length 20m.

The small signal gain properties were measured in a 100m length of fibre up to 60mW of pump. The results are shown in Figure 3.

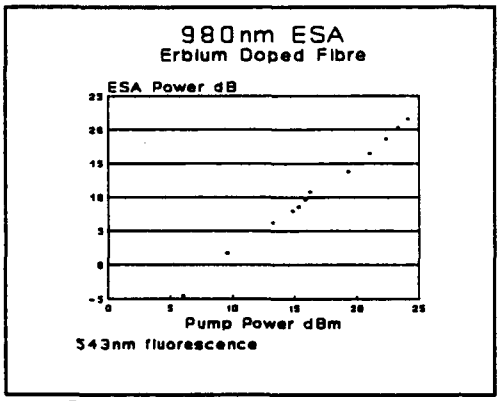


Figure 2 Log:Log plot of 540nm fluorescence against pump power.

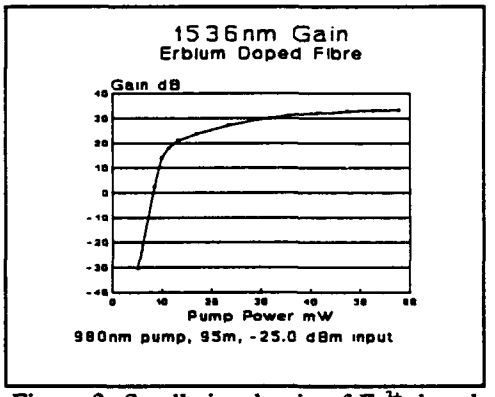


Figure 3 Small signal gain of $Er^{3+}$-doped amplifier

The onset of the normal saturation behaviour is shown by the knee at 10mW. It is noted that there is an onset of a second saturation process observed by the flattening of the gain at about 40mW of injected power. It is noted that this change of slope occurs at pump powers which roughly mark the "onset" of both the non-linear ESA reported above in Figures 2 and the observation of significant Amplified Spontaneous Emission (ASE).

The lifetimes of emission from both the $^4S_{3/2}$ state at 546nm and the $^2H_{11/2}$ states were measured using gated photon counting techniques to be 980ns. These states are, as expected, in quasi-thermal equilibrium. Assuming that the radiative lifetime is similar to that in crystals, namely 0.7ms[7], the quantum yield is $\sim 1.4 \times 10^{-3}$.

## DISCUSSION

The issues raised by the results obtained in this paper primarily relate to the performance of 980nm light as a pump source for erbium doped fibres as power amplifiers. Generally, ESA will degrade amplifier performance.

Firstly, we consider the mechanism of the observed ESA. From the energy level diagram in Figure 4, the observed emission from the $^4S_{3/2}$ and $^2H_{11/2}$ states ***cannot*** arise from single photon absorption from the metastable $^4I_{13/2}$ state because of the energy mismatch. It is noted that all previous reports of ESA can be attributed to single photon absorption from the metastable state. We therefore attribute the origin of the non-linear ESA observed in the experiments to absorption from the short lived $^4I_{11/2}$ state which is the state directly pumped by 980nm from the ground state. The ESA is assigned to the $^4I_{11/2}$ to $^4F_{7/2}$ transition. The $^4F_{7/2}$ state rapidly relaxes to the $^4S_{3/2}$ and $^2H_{11/2}$ states from which emission is observed.

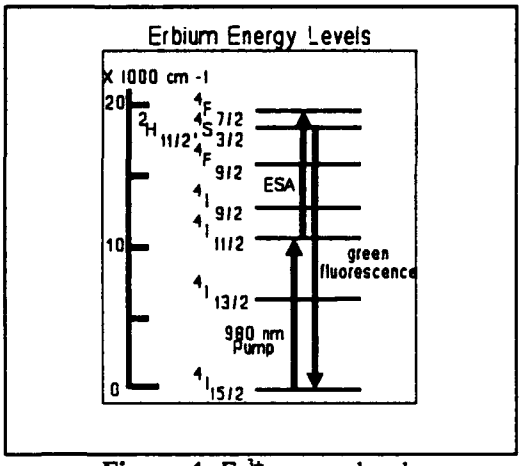


**Figure 4** $Er^{3+}$ energy levels

Consider next the observed pump power-law dependence of 1.4. We will show that a detailed model of ESA from short lived states gives the following pump power dependencies:-

*Low Power:* A quadratic dependence on pump power is expected at low power for a sequential two-photon absorption process from the undepleted ground state.

*Intermediate Power:* At these powers, above about 10mW, population inversion depletes the ground state. The ground state is replenished by spontaneous radiative decay. The pump power dependence falls to linear in this saturation regime.

*High Power:* Above about 40mW pump power, significant build up of Amplified Spontaneous Emission (ASE) is observed in the fibre. This leads to a more rapid population cycling, and hence an increase of the steady-state ground state population with pump power. A simple model of ASE build up shows that the power law for the ESA approaches 1.5. This is in accord with the 1.4 power dependence observed at powers above the saturation power.

For the pump powers used to obtain the power law results of Figure 2, the system is in the high power regime. The observed power law of 1.4 is in good accord with the expected 1.5 law in this regime. More details of the model will be presented at the conference.

A significant issue is the efficiency of the ESA process, as it determine whether the effect is deleterious in high power amplifiers. 20nW emission is observed at the end of the fibre with 340nW of pump. With a collection efficiency of $3.6 \times 10^{-3}$, the total

radiated power is 6μW and, for the quantum yield of $1.4x10^{-3}$, this corresponds to 4mW of dissipated power. For an amplifier with no signal input, this is not a significant loss.

However, it is noted that the ESA from short-lived intermediate states depends on the steady-state ground state population, and a high power amplifier operating in the heavily saturated regime has a population inversion in the presence of the signal which is clamped in the same manner as a laser oscillator. If so, any ESA loss will be linear in pump power, and will be manifest by a reduction of slope efficiency. It is possible that the observed quantum extraction efficiency of 80% for 980nm pumping can be attributed to ESA from short-lived intermediate states.

## CONCLUSIONS

We report for the first time evidence of non-linear ESA in erbium-doped fibres. The process is attributed to absorption from short-lived intermediate states. Further experiments are required to determine whether the mechanism plays a role in limiting the efficiency of high power erbium doped amplifiers.

## ACKNOWLEDGMENTS

GRA acknowledges the award of an APRA Scholarship, SCG acknowledges the award of an APRA Scholarship and Telecom Australia Postgraduate Fellowship. Part of this work was supported by OTC Limited, who are also acknowledged as Sponsor of the OFTC.

## REFERENCES

[1] R.J.Mears, L.Reekie, I.M.Jauncey and D.N.Payne, *Low noise erbium-doped fibre amplifier operating at 1.54μm*, Electron. Lett., **23**, 1027 (1987)

[2] E.Desurvire, J.R.Simpson and P.C.Becker, *High gain erbium-doped travelling-wave fiber amplifier*, Opt.Lett., **12**, 888 (1987)

[3] R.I.Laming, S.B.Poole and E.J.Tarbox, "*Pump excited state absorption in erbium doped fibres*, Opt. Lett., **13**, 1084-6 (1988)

[4] E.Snitzer, H.Po, F.Hakimi, R.Tuminelli and B.C.MacCollum, *Erbium fiber laser amplifiers at 1.55μm with pump at 1.49μm and Yb sensitized Er Oscillator*, Proc OFC'88, paper PD2

[5] E.G. Bryant, S.F. Carter, A.D. Ellis, W.A. Stallard, J.V. Wright and R. Wyatt, *Unrepeatered 2.4 Gbit/s transmission experiment over 250km of step-index fibre using erbium power amplifier*, Electron. Lett., **26**, 528-30 (1990)

[6] J.F. Massicott, R. Wyatt, B.J.Ainslie and S.P. Craig-Ryan, *Efficient, high power, high gain $Er^{3+}$ doped silica fibre amplifier*, Electron. Lett.,**26**, 1038-9 (1990)

[7] R.Reisfeld and C.K.Jorgensen, *Lasers and Excited States of Rare-Earths*, Springer Verlag, New York (1977)

# Amplification Reduction in Fiber Amplifiers Due to Up-Conversion at $Er^{3+}$-Concentrations Below 1000 ppm.

*P. Blixt[a], J. Nilsson[a], T. Carlnäs[b], and B. Jaskorzynska[a]*

## Introduction

One of the key parameters for optimizing erbium-doped fiber amplifiers (EDFAs) is the $Er^{3+}$-concentration profile. Below the concentration for onset of component clustering, up-conversion may play a significant role [1]. Recent experiments have shown that up-conversion is a considerable deteriorating mechanism even below an erbium concentration of 1000 ppm by weight [2,3].

In this paper, we have made an extensive study of eight different fibers in order to examine the up-conversion as a function of erbium concentration below 1000 ppm by weight. From these experiments and a computer model of up-conversion, we have been able to estimate the up-conversion coefficient used in our rate-equation model. These results are necessary for accurately modelling EDFAs with erbium concentrations down to approximately 100 ppm by weight and for erbium profile optimizations.

## Up-conversion model

Up-conversion of $Er^{3+}$-has previously been studied in bulk-crystal materials [4]. In a recent paper [5], the up-conversion coefficient for $Er^{3+}$ in YAG has been estimated to be $1.5-4\times10^{-23}$ m$^3$/s and shown to be independent on erbium concentration.

The energy diagram for two atoms is shown schematically in Fig. 1. The sequence of up-conversion in our model is the following: 1) two neighbouring atoms are excited to the $^4I_{13/2}$-level by two photons with a wavelength of 1.48 μm. 2) energy is transferred non-radiatively from one of the atoms (donor) to the other atom (acceptor). The energy-transfer results in a de-excited donor atom and an acceptor atom in the $^4I_{9/2}$-state. 3) the acceptor atom relaxes to the $^4I_{11/2}$-state within a few nanoseconds. At this level there is a non-negligible splitting ratio which we estimate to be of the order of 1:10000 from our computer model. The most probable decay is to the upper lasing level (4a). Roughly, one out of ten thousand atoms relaxes down to the ground state under emission of a photon at a wavelength of 980 nm (4b).

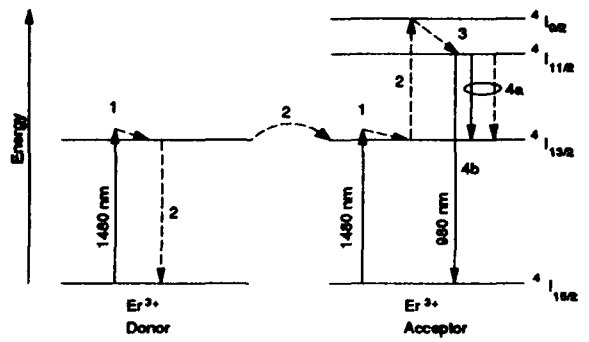


**Fig. 1** *Up-conversion in erbium-doped fibers. 1) two neighbouring atoms are excited. 2) energy is transferred from the donor atom to the acceptor atom via phonons. 3) the acceptor atom immediately relaxes to a lower lever and either 4a) relaxes down to the upper lasing level or 4b) relaxes down to the ground level under emission of a photon.*

In Fig.1, all dashed arrows represent non-radiative transitions while solid arrows represent radiative transitions. Due to up-conversion one or both ions involved in the process return to the ground level. The closer the atoms are, the easier energy is transferred. Thus up-conversion is concentration dependent. The process can be modelled by incorporating a quadratic term ($-2C\cdot n_1^2$)

a Institute of Optical Research and Department of Physics II, Royal Institute of Technology, S-100 44, Stockholm, Sweden

b Ericsson Cables AB, S-172 87 Sundbyberg, Sweden

in the rate-equation for the upper lasing level and the term $C \cdot n_1^2$, in the rate-equation for both the ground level and the $^4I_{9/2}$-level [5]. $n_1$ is the concentration of atoms in the upper lasing level and $C$ is a material constant. Here, we will restrict the investigation to obtain an order of magnitude estimation of $C$ in erbium-doped fibers.

**Characterization of fibers at 1.5 μm**

The fibers were made by Ericsson Cables AB using the solution doping technique. Care was taken to keep all parameters constant except the erbium-concentration. Fibers with two different co-dopants were made, namely $GeO_2$ and $GeO_2$-$Al_2O_3$-$P_2O_5$. The $e^{-1}$ mean mode-field radius was 4.9 μm and the mean core diameter was 8.8 μm with standard deviations of 0.3 μm and 0.7 μm, respectively. The $^4I_{13/2}$ level fluorescence lifetime at $e^{-1}$ was measured for low pump-powers to be 10-11 ms for the Ge-core fibers and 7-8 ms for the Ge-Al-P-core fibers. The flourescence lifetime was independent of $Er^{3+}$-concentration, showing absence of concentration quenching [1]. Only the host material affected the lifetime. The maximum amplification was measured for the optimum length at a pump power of 25-26 mW at 1.48 μm. The set-up used for amplification characterization consisted of one laser diode for pumping and a tunable signal laser diode. The signal was always kept at the wavelength for maximum amplification, i.e. around 1.535 μm. Both the signal laser and the pump laser had optical isolators to prevent feedback. The pump and the signal was launched into the erbium-doped fiber via a wavelength division multiplexer (WDM). At the end of the erbium-doped fiber, an additional optical isolator was used to prevent feedback from the end facet. Input and output signals were measured with an optical spectrum analyzer and the amplification within the fibers were calculated taking into account input and output coupling losses for each fiber. The input signal power was in the range -40 to -35 dBm to avoid amplification saturation.

**Characterization of fibers at 980 nm**

We measured the 980 nm luminescence due to up-conversion in the backward direction at the 1.5 μm input/output port of the WDM. In the forward direction stray light from the pump at 1.48 μm severely reduced the sensitivity in our set-up so that the signal at 980 nm was flooded by the pump. The fiber lengths were several absorption lengths at 980 nm to ensure that maximum luminescence power was detected. Unfortunately, the WDM attenuated the 980 nm luminescence by approximately 10 dB. The resolution of the optical spectrum analyzer was set to 5 nm during all measurements of the luminescence at 980 nm. The full-width at half-maximum spectral width at 980 nm was approximately 30 nm, thus roughly 1/6 of the total power at 980 nm was measured. When pumping at 807 nm, there have been luminescence at 800 nm due to up-conversion [1]. However, in our case, there was no detectable luminescence at 800 nm. Furthermore, we were not able to detect higher order up-conversion luminescence at 670 nm. By plotting the maximum amplification for 25-26 mW pump at 1.48 μm as a function of detected up-conversion luminescence at 980 nm, we see a strong correlation between the parasitic effect of up-conversion and amplification. See Fig. 2.

Up-conversion depends on the $Er^{3+}$-concentration. However, the exact dependence has never been investigated in silica fibers. The $Er^{3+}$-concentration profile was measured on the preforms using electron probe microanalysis in a scanning electron microscope at SGU, Uppsala, Sweden. The spatial resolution was $6 \times 6$ μm$^2$ at an energy of 20 keV. The accuracy was ± 10 % at these levels. The erbium profile is assumed to be the same in the fiber as in the preform because out-diffusion of $Er^{3+}$ is negligible during pulling of the fiber [6]. As in Ref. 6, the erbium concentration followed the Ge-concentration and a dip in the middle of the core was clearly seen for both germanium and erbium. Contrary to Ref. 6, there was a similar dip in the Ge-Al-P-core fibers. Then a mean erbium concentration was calculated by averaging the erbium concentration profile within the full-width at half-maximum of the scan. Moreover, a standard deviation was calculated for the same region. This standard deviation should not be confused with the accuracy of profile measurements, it is only a measure of the profile variation. The mean erbium concentration with its standard deviation was then plotted versus the 980 nm luminescence. See Fig. 3. It is the same values of the power at 980 nm as in Fig. 2, but they are given in pW instead of dBm in Fig. 3.

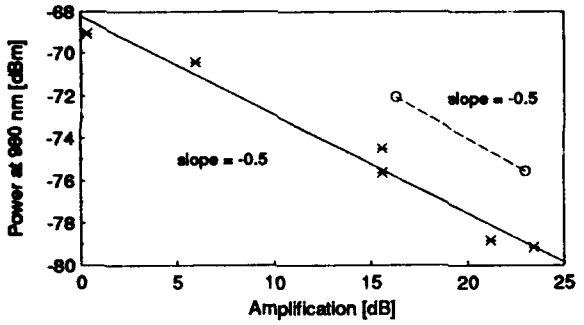


**Fig. 2.** *Up-conversion at 980 nm as a function of maximum amplification with 25-26 mW pump power at 1480 nm. The solid line represents fibers with Ge-core and the dashed line represents fibers with Ge-Al-P-core.*

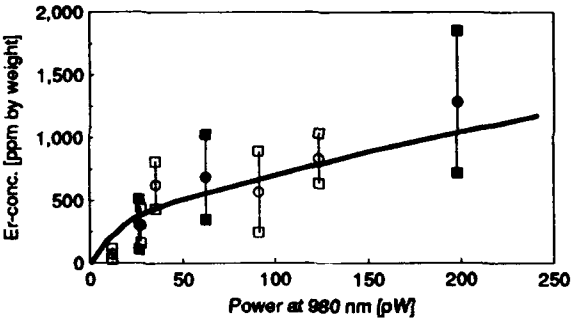


**Fig. 3.** *The up-conversion luminescence at 980 nm as a function of erbium concentration. The mean $Er^{3+}$-concentration with its standard deviation is plotted for Ge-core fibers (open symbols) and for Ge-Al-P-core fibers (filled symbols). A guide-line for the eye is drawn to show the tendency.*

We also measured the lifetime of the 980 nm luminescence, which was less than 0.15 ms. (The temporal resolution was limited by our mechanical chopper.) This rougly agrees with Ref. 5, where the lifetime of the 980 nm luminescence in $Er^{3+}$-doped YAG has been measured to be approximately 100 μs.

**Determination of the up-conversion coefficient**

The effect of up-conversion was included in our numerical model by adding a loss term $(-2C \cdot n_1^2)$ in the rate-equation for the upper lasing level and the term $C \cdot n_1^2$, in the rate-equation for both the ground level and the $^4I_{9/2}$-level [5]. We were primarily interested in obtaining a value for the up-conversion constant $C$. In order to achieve this, we correlated simulations with measurements of the 980 nm luminescence transverse to approximately 6 mm of fiber. The measurements were performed with a sensitive silicon detector with negligible responsitivity of the signal at 1.5 μm. We measured the 980 nm luminescence as a function of pump power at 1.48 μm. In this case, we used a short fiber (<1 m). Hence, amplified spontaneous emission was negligible. However, there is a non-negligible emission cross-section at 1.48 μm, which was included in the simulations. Using measured values for mode-field radius, core diameter, pump-power threshold and erbium-doping profile, we were able to preliminary determine the up-conversion coefficient to be around $10^{-22}$ $m^3/s$. This order of magnitude of the up-conversion coefficient reduces the maximum amplification in a similar way as in Fig. 2 according to our preliminary simulations. Additionally, we obtained an order of magnitude estimate of the splitting ratio (1:10000) between radiative transitions to the ground level and transitions to the upper lasing level at the $^4I_{11/2}$-level by fitting both amplitude and curvature of the pump *vs.* 980 luminescence dependence. We used literature values for the ratio of the emission and absorption cross-sections. We are now working on an improved model incorporating measured cross-sections for the specific fibers. The simulated and measured up-conversion luminescence at 980 nm is shown in Fig. 4.

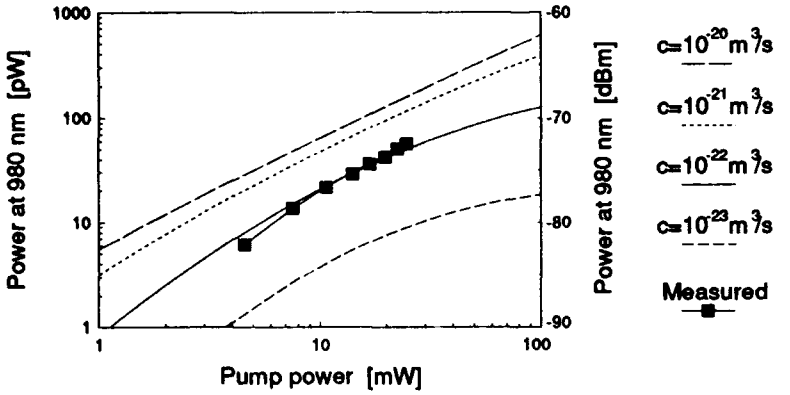


**Fig. 4.** *Simulated (lines) and measured (squares) emission at 980 nm transverse to the fiber. The best fit was for an up-conversion coefficient of $10^{-22}$ $m^3/s$ and a splitting ratio of 1:10000.*

## Conclusions

We have found strong correlation between amplification and deteriorating up-conversion in fibers with both Ge- and Ge-Al-P-cores when the erbium-doping concentration is in the range 70 to 840 ppm by weight. When plotting the 980 luminescence *vs.* maximum amplification in a logarithmic scale, the slope was ~ -0.5 irrespective of the host material. Furthermore, we have investigated the up-conversion efficiency as a function of erbium concentration as well as measured an upper limit of the 980 nm luminescence lifetime (< 150 μs). By computer simulations, we have been able to establish a value of the up-conversion coefficient around $10^{-22}$ $m^3/s$ as well as a splitting ratio at the $^4I_{11/2}$-level of roughly 1:10000 between radiative transitions to the ground level and transitions to the upper lasing level. These results should be helpful for optimizing the erbium doping profile and for modelling of the amplification.

## Acknowledgments

We wish to thank Ericsson Cables AB for the erbium-doped fibers and characterization of "passive" parameters. Also Ericsson Telecom AB is acknowledged for supplying pump and signal lasers. Financial support is gratefully acknowledged from the Swedish Board for Technical Development (STU), Ericsson Telecom AB and the Swedish Telecom. We would also like to thank Anne Lidgard for helpful discussions.

## References

1. B.J. Ainslie, S.P. Craig-Ryan, S.T. Davey, J.R. Armitage, C.G. Atkins, and R. Wyatt, "Optical analysis of $Er^{3+}$ doped fibres for efficient lasers and amplifiers," in *Proc. 7th Integrated Optics and Optical Commun. Conf. (IOOC)* (Kobe, Japan), 1989, paper 20A3-2
2. M. Shimizu, M. Yamada, M. Horiguchi, and E. Sugita, "Concentration effect on optical amplification characteristics of Er-doped silica single-mode fibers," IEEE Photon. Technol. Lett., **2**, 43 (1990).
3. N. Kagi, A. Oyobe, and K. Nakamura, "Efficient optical amplifier using a low-concentration erbium-doped fiber," IEEE Photon. Technol. Lett., **2**, 559 (1990).
4. L.F. Johnson, H.J. Guggenheim, T.C. Rich, and F.W. Ostermayer, "Infrared-to-visible conversion by rare-earth ions in crystals," J. Appl. Phys., **43**, 1125 (1972).
5. W.Q. Shi, M. Bass, and M. Birnbaum, "Effects of energy transfer among $Er^{3+}$ ions on the fluorescence decay and lasing properties of heavily doped Er:$Y_3Al_5O_{12}$," J. Opt. Soc. Am. B, **7**, 1456 (1990).
6. B.J. Ainslie, J.R. Armitage, S.P. Craig, and B. Wakefield, "Fabrication and optimisation of the erbium distribution in silica based doped fibres," in *Proc. 14th European Conf. Optical Commun. (ECOC)*, pp.62-65, 1988.

# Erbium-Doped Fiber Amplifiers Pumped in the 800-nm Band

B. Pedersen*, S. Zemon, W. J. Miniscalco and M. P. Singh
GTE Laboratories Incorporated, 40 Sylvan Road, Waltham, MA 02254, USA

*Permanent address: Technical University of Denmark, Electromagnetics Institute, Dk-2800 Lyngby, Denmark

The performance of fiber amplifiers is extremely sensitive to the material-dependent properties of the pump band. High-power, reliable, low-cost diode lasers are currently only available at 800 nm, a poor pump band for $Er^{3+}$ due to the low strength of the ground state absorption (GSA) transition and an intense, overlapping excited state absorption (ESA) band. High gains have been achieved with silica fibers by pumping the long-wavelength wing of the GSA band at ≈820 nm [1,2], thereby avoiding the ESA at shorter wavelengths but introducing another problem by reducing the already low GSA cross section at the pump wavelength. Alternatively, the use of other glass host compositions with reduced ESA has been proposed [3]. We have examined both approaches using experimentally determined parameters in a highly quantitative numerical model to compare the performance of Al/P-silica, Ge/P-silica, and fluorophosphate fiber amplifiers. The analysis was performed for co- and bi-directional pumping and included treatments of waveguide design, $Er^{3+}$ confinement, pump-wavelength dependence of gain and noise figure, and quantum conversion efficiency for power amplifiers.

**Experimental:** The Al/P-silica and Ge/P-silica fibers were drawn from solution-doped MCVD preforms. The previously described procedure for determining the GSA cross sections from cut-back measurements and the $Er^{3+}$ doping profile [4] was augmented by neutron activation analysis to provide a more accurate value of the $Er^{3+}$ concentration. Because measurement difficulties prevented a determination of the absolute values of the cross sections for Ge/P silica, the absorption spectra were converted to cross section by setting their oscillator strengths equal to the mean of published values for three silica preforms [5] and the Al/P silica. Cross sections for the fluorophosphate were determined using the absorption spectra of bulk samples with known concentrations. Stimulated emission cross sections were determined from emission spectra and excited-state lifetimes using established techniques [6]. The ESA cross sections, $\sigma_{24}$, were measured for single-mode silica fibers and multimode fluorophosphate fibers using procedures discussed in Ref. 7. Fig. 1 illustrates $\sigma_{24}$ and the GSA cross sections, $\sigma_{13}$, for the three glasses; the 800-nm pump band is always dominated by a strong ESA band centered at 790 nm. For the silicas, the extended long-wavelength tails of the GSA bands lead to a region ≈820 nm where $\sigma_{13} \approx \sigma_{24}$. In contrast, beyond ≈800 nm $\sigma_{13} > \sigma_{24}$ for the fluorophosphate even at the peak of the pump band.

**Theory:** The analysis was performed using a full-scale, large-signal, numerical model [8] that has been shown to accurately reproduce experimental results [9]. Actual LP modes calculated from the fiber index profiles were used for the pump and signal. The values for all other inputs to the calculation were experimentally determined. Pump ESA was included and the full spectrum of the forward and backward amplified spontaneous emission (ASE) was treated.

**Gain Coefficient:** The signal wavelengths was chosen to lie at the peak of the emission for each composition. The emission and absorption cross sections used were, respectively, 5.5 and 5.2 x $10^{-25}m^2$ at 1532 nm for the Al/P silica, 8.6 and 8.9 x $10^{-25}m^2$ at 1536 nm for the Ge/P silica, and 7.5 and 6.8 x $10^{-25}m^2$ at 1533 nm for fluorophosphate. The corresponding radiative lifetimes were measured to be 10.8, 11.0, and 8.25 ms, respectively. For a given waveguide geometry and pumping scheme, the gain coefficient is defined as the maximum of the ratio between the small signal gain in dB and the total pump power launched in the fundamental mode in mW. It was found by iteratively changing the pump power, finding the fiber length that gives the maximum small-signal gain, and plotting the gain to pump power ratio until the maximum ratio was reached. In Fig. 2 the gain coefficient is shown as a function of cutoff wavelength for a (a) Al/P-silica fiber pumped at 815 nm, (b) Ge/P-silica fiber pumped at 810 nm, and (c)

fluorophosphate fiber pumped at 805 nm. Results are displayed for co-directional (dashed curves) and bi-directional (solid curves) pumping. Similar gain-coefficient curves were calculated for a series of pump wavelengths at intervals throughout the 800-nm band, and those depicted in Fig. 2 are for the pump wavelengths yielding the highest value for each host. As seen from the figure, the fluorophosphate fiber is predicted to give the highest gain coefficient, 3.5 dB/mW. This is not surprising, since both $\sigma_{13}$ and $\sigma_{13}/\sigma_{24}$ are higher for this composition. However, the Ge/P-silica fiber has a gain coefficient that is only slightly lower. This is because the emission cross section at the signal wavelength is higher for Ge/P silica and the excited state lifetime is 25% longer, resulting in a smaller threshold pump power needed to obtain population inversion. In the presence of ESA the gain coefficient can be improved up to 50% by applying the bi-directional pumping scheme. When the pump power is high enough to reach inversion, a significant fraction of any additional pump power will be attenuated by ESA and will be of no use further on in the fiber. Therefore, splitting the power by pumping from both fiber ends causes the amplifier to become more efficient. Additional analysis of the bi-directional pumping scheme shows that, of all the possible options for dividing a given total pump power, the highest gain is achieved when the pump power is divided equally.

**Gain and Noise:** The small-signal gain is presented in Fig. 3 as a function of pump wavelength for the three compositions. The profile is step-index with an NA of 0.3. The cutoff is chosen to be 800 nm, the optimum value from Fig. 2. Results are shown for total launched pump powers of 10, 25, 50, and 100 mW for both co-directional (dashed curves) and bi-directional (solid curves) pumping. As seen from the figure, the small-signal gain for the bi-directional case can exceed that for the co-directional case by as much as 10 dB. For the silica fibers in particular, the gain difference is most pronounced at shorter pump wavelengths where the ESA is more significant. With a pump power of 100 mW the maximum gain for the fluorophosphate fiber is predicted to be 2 dB higher than that for the Ge/P-silica fiber, and 6-8 dB higher than that for the Al/P-silica fiber. The noise figures, corresponding to the small-signal-gain values in Fig. 3, were observed to increase with increasing pump wavelength, i.e., for 50-mW, co-directional pumping the noise figure for the Al/P-silica fiber increases from 3.3 dB, when pumping at 800 nm, to 5.8 dB, when pumping at 825 nm. For the Ge/P-silica fiber it increases from 3.3 to 7.2 dB and for the fluorophospate fiber from 3.5 to 6.8 dB. The increasing noise figures are due to the decrease in $\sigma_{13}$. However, the noise figure for the fluorophosphate exceeds those for the silicas at shorter wavelengths, even though the former composition has higher $\sigma_{13}$ values. This is because the excited state lifetime for the fluorophosphate is 25% shorter.

**Erbium Confinement:** For step index fibers with an NA of 0.3, Fig. 4 plots the gain coefficient as a function of the confinement factor, which is defined as the ratio of the radius of the erbium concentration profile to that of the refractive index profile.The pump wavelengths are chosen as in Fig. 2. As seen from Fig. 4, the gain coefficient is improved by more than 50% when the confinement factor is decreased from 1.0 to 0.1, and it reaches values close to the maxima found for step index fibers with an NA of 0.4 and a confinement factor of 1.0 (shown in Fig. 2). For practical applications this means that the gain coefficient can be improved without affecting the splice loss between the amplifier fiber and a standard telecommunications fiber. The primary impact of a change in the gain coefficient is on the launched pump power and not on the gain. Thus, decreasing the confinement factor will reduce the pump power required for a given net gain in inverse proportion to the increasing gain coefficient. In contrast, when improving the gain coefficient by increasing the NA, the improvement in the ratio of the net gain to launched pump power will be countered by the increasing splice losses. It should be noted that when the confinement factor is decreased from 1.0 to 0.1, the optimum cutoff wavelength was observed to increase from 800 nm to 920 nm for bi-directional pumping and from 830 nm to 950 nm for co-directional pumping.

**Power Amplifiers:** A power amplifier is best characterized by the quantum conversion efficiency (QCE) which is defined as the the number of photons added to the signal divided by the total number of launched pump photons. The QCE is plotted in Fig. 5 as a function of the pump wavelength for bi-directional pumping with total launched powers of 25 and 100 mW for the pump and 1 mW for the signal. The fluorophosphate fiber is predicted to have a QCE that is 50% higher than that of the two other types of fibers. This is because the major loss mechanism is ESA when the amplifier is highly saturated by the signal. Since the effects of ESA are

reduced at longer wavelengths, especially for the fluorophosphate, the QCE approaches the theoretical limit of 1. This also explains why the optimum pump wavelength is longer in comparison to that for the small-signal regime, where the efficiency is limited not only by ESA but also by ASE, spontaneous emission and residual pump power.

**Conclusion:** A full-scale numerical model was used to analysize 800 nm pumping of $Er^{3+}$-doped fibers. Three glass host compositions, Al/P silica, Ge/P silica and fluorophosphate, were compared and all model input parameters, including the excited-state-absorption cross sections, were experimentally determined. The highest gain coefficient, 3.5 dB/mW, was found for a fluorophosphate fiber with an NA of 0.4. The bi-directional pumping scheme was determined to be the most efficient, with a gain coefficient of up to 50% higher than that for co-directional pumping. The small-signal gain can be as much as 10 dB higher for the bi-directional pumping scheme. The noise figure was observed to increase by up to 3.5 dB with increasing pump wavelength. The noise figure for bi-directional pumping is predicted to be 2 dB higher than that for co-directional pumping. The use of a confined erbium doping yielded improvements in the gain coefficient of more than 50%. When used as a power amplifier, the fluorophosphate fiber was predicted to have a 50% higher quantum conversion efficiency than those of the two silica fibers.

We thank L. J. Andrews and T. Wei for helpful contibutions, and G. Lambert, B. Thompson, B. Hall, and R. Hammond for technical assistance.

## References

[1] K. Suzuki et al, Electron. Lett.,vol. 26 (1990), no. 13, pp. 948-949.
[2] Y. Kimura et al, Proc. Eur. Conf. Optical Commun. (1990), pp.103-106.
[3] L. J. Andrews et al, Proc. First Intl. School on Excited States of Transition Elements (World Scientific, Singapore, 1989), pp. 9-30.
[4] M. P. Singh et al, Symp. on Opt. Fiber Meas., NIST Sp. Publ. 792 (1990), pp. 93-96.
[5] K. Dybdal et al, Proc. SPIE Symp. on Fiber Laser Sources and Ampl., vol. 1171 (1990), pp. 209-218.
[6] W. J. Miniscalco and R. S. Quimby, Optics Lett., vol. 16 (1991), pp. 258-260.
[7] S. Zemon et al, Proc. SPIE Symp. on Fiber Laser Sources and Ampl. II , vol. 1373 (1991), pp. 21-32.
[8] B. Pedersen et al, Opt. Commun., vol. 81 (1991), no. 1, pp. 23-26.
[9] B. Pedersen et al., Techn. Dig. Opt. Amp. and Their Appli. (1990), vol. 13, pp. 653-655.

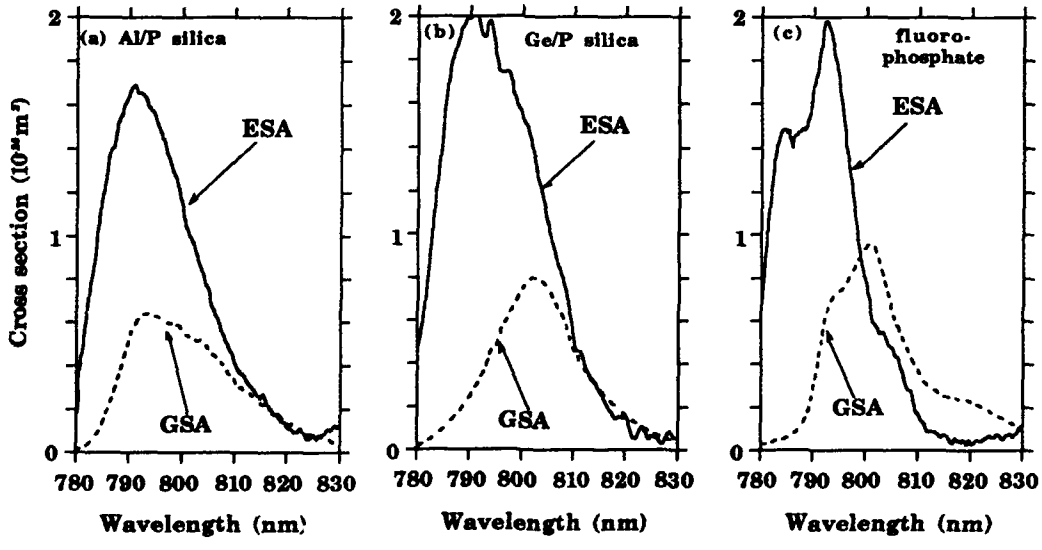


Fig. 1 Experimentally determined ESA and GSA cross sections for erbium-doped (a) Al/P silica, (b) Ge/P silica, and (c) fluorophospate.

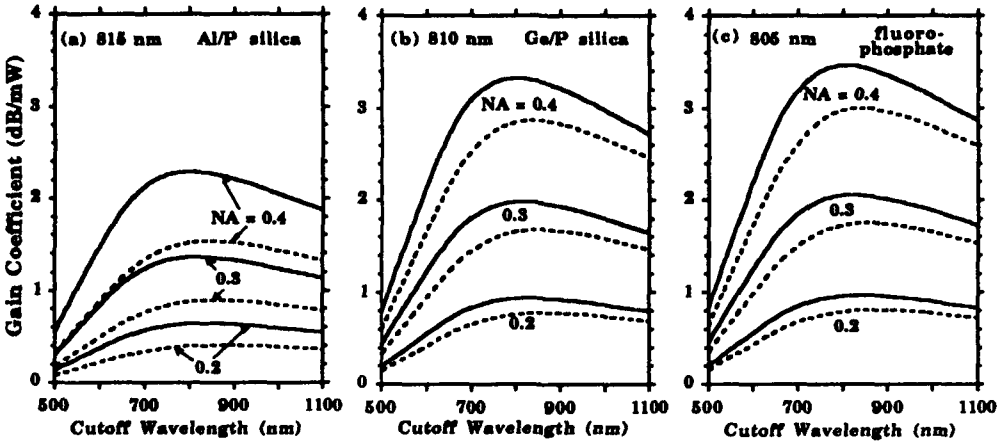


Fig. 2 Gain coefficient vs cutoff wavelength in step-index, erbium-doped (a) Al/P-silica fiber, (b) Ge/P-silica fiber, and (c) fluorophosphate fiber. Results are shown for co-directional (dashed curves) and bi-directional (solid curves) pumping, and for NA's of 0.4, 0.3 and 0.2.

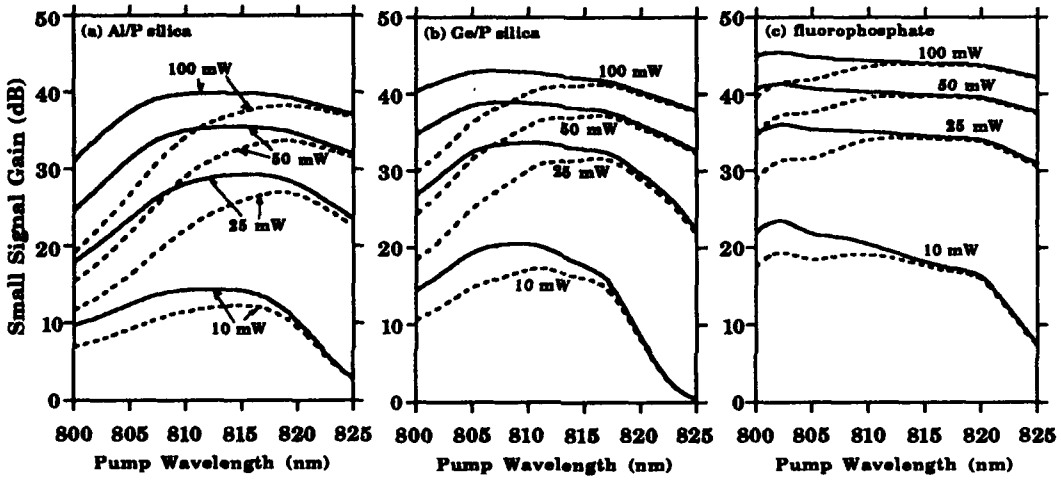


Fig. 3 Small-signal gain vs pump wavelength for erbium-doped (a) Al/P-silica fiber, (b) Ge/P-silica fiber and (c) fluorophosphate fiber. Results are shown for co-directional (dashed curves) and bi-directional (solid curves) pumping with total launched powers of 10 mW, 25 mW, 50 mW and 100 mW.

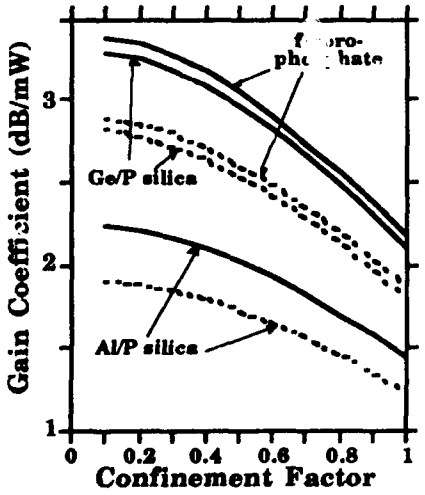


Fig. 4 Gain coefficient vs confinement factor in step-index fibers with an NA of 0.3. Results are presented for bi-directional (solid curves) and co-directional (dashed curves) pumping.

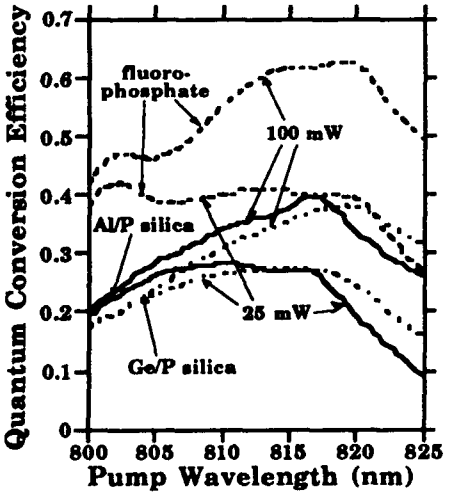


Fig. 5 Quantum conversion efficiency vs pump wavelength for 1-mW signal input power and launched pump powers of 25 mW and 100 mW in a bi-directional pumping scheme.

# Gain Characteristics of Lanthanum Co-Doped Erbium Fiber Amplifier

Yasuo Kimura and Masataka Nakazawa

NTT Transmission Systems Laboratories
Lightwave Communication Laboratory
Tokai, Ibaraki-Ken 319-11, Japan
Tel. +81-292-87-7317 Fax. +81-292-87-7874

Recent progress on erbium-doped fiber amplifiers (EDFAs) and their application to optical communications has been very rapid since the EDFA has many advantages such as polarisation-insensitive high gain, a low noise-figure, and low insertion loss.[1] It is well known that in order to obtain a broader and relatively flatter gain profile, Aluminum ($Al_2O_3$) is co-doped into the core of the fibers.[2,3] To make a wavelength independent flat gain profile is very important from the viewpoint of ultrashort pulse amplification and wavelength division multiplexing technique. Payne and Laming investigated a Borolanthanate co-doped EDFA.[4] Although $LaF_3$ or $La_2O_3$ were used as hosts for Nd ions[5~7], detailed gain characteristics of a Lanthanum co-doped $Er/SiO_2$ fiber amplifier have not yet been clarified.

In this paper, we describe for the first time the detailed gain characteristics of a Lanthanum (La) co-doped EDFA and compare then with those of Al co-doped and non co-doped EDFAs.

La co-doped silica-based erbium fibers were made by the VAD method and the solution doping technique, where the refractive-index difference between the core and the cladding was made by doping $GeO_2$. Figure 1 shows gain as a function of launched pump power at 1.48 μm. Fiber A is a La co-doped EDFA. The doping concentrations of erbium and lanthanum ions are 420 ppm and 4000 ppm, respectively. The relative refractive index difference, the cut-off wavelength and the modefield diameter are 1.11 %, 1.27 μm, and 5.6 μm, respectively. The fiber length is 20 m, so that the product of the fiber length and the Er concentration is 8400 mppm. Fiber B is an Al-$Er/SiO_2$ fiber, in which the doping concentrations of the erbium and aluminum ions are 220

ppm and 2000 ppm, respectively. The relative refractive-index difference, the cut-off wavelength, and the modefield diameter are 1.02 %, 1.18 μm, and 5.8 μm, respectively. Fiber C is an $Er/SiO_2$ fiber which has no codopant. The erbium concentration for Fiber C is 450 ppm. The relative refractive-index difference, the cut-off wavelength, and the core diameter are 1.06 %, 1.17 μm, and 5.8 μm, respectively.

A 38 m-long fiber is chosen so that the product of the fiber length and the Er concentration is the same as that of Fiber A. Fibres B and C are measured for comparison with $La\text{-}Er/SiO_2$ fiber. The signal input level for the gain measurement is - 40 dBm. It is found from Fig. 1 that the gain at 1.535 μm for Fiber A is the highest among them and the gain at 1.552 μm for Fiber A is between those of Fibres B and C. These results indicate that La is promising as a co-dopant for erbium fibers.

Figure 2 shows gain vs. amplified output power for a 1.48 μm pump power of 50 mW. - 3 dB saturation powers at 1.535 μm for Fibres A, B, and C are + 1.2 dBm, + 2.0 dBm, and + 0.4 dBm respectively. Those at 1.552 μm are + 4.6 dBm, + 5.4 dBm, and + 4.4 dBm, respectively. Although the gain saturation is slightly bigger in Fiber A, a high power La co-doped EDFA at 1.55 μm is possible since the amplified output power easily reached around + 5 dBm.

Important roles of the Al co-doping are to remove the concentration quenching ( cooperative up-conversion) and to flatten the gain profile. We have investigated how La ions flattened the EDFA gain profile as compared with $Al\text{-}Er/SiO_2$ or $Er/SiO_2$ fibers. The results are shown in Fig. 3. The pump power and the signal power for the gain profile measurement are 50 mW and - 40 dBm, respectively.

As can be seen, a gain flattening effect exists in Fiber A in comparison with non co-doped Fiber C. That is, the gain flattening effect is improved by co-doping La ions. The biggest gain flattening effect was obtained in Fiber B ($Al_2O_3$ co-doping). The gain peak at 1.535 μm is shifted to 1.531 μm and that at 1.552 μm is considerably flattened in comparison to Fiber C( No co-doping). - 3 dB gain bandwidths for Fibres A, B, and C at around 1.535 μm are 3.3, 5.6, and 2.9 nm, respectively, and those at around 1.552 μm are 8.8, 23.5, and 5.1

nm, respectively. The gain peak shift at 1.552 μm for Fiber A is 0.5~1 nm compared with the gain peak for Fiber C. To evaluate the effectiveness of the gain flattening in the 1.552 μm band, the gain difference between 1.542 μm (gain bottom) and 1.552 μm (gain peak) in each fiber was compared. The gain differences for Fibres A, B, and C are 8.5, 3.5, and 14.7 dB, respectively. Furthermore, the gain at 1.541 μm (gain bottom) for Fiber A is clearly higher than that for Fiber C, which means that a moderate gain flatness effect exists due to the co-doping of La ions.

Fluorescence curves for Fibres A, B, and C are also measured to make sure the above-mentioned results. As seen in Fig. 4, the wavelength dependence of the gain characteristics completely reflects these fluorescence profiles.

We have also investigated gain characteristics for a La co-doped EDFA with a La concentration of 2000 ppm, in which a gain as high as 43 dB was obtained at 1.535 μm for a pump power of 92 mW. The relative refractive-index difference, the cut-off wavelength, and the modefield diameter are 1.02 %, 1.33 μm, and 5.8 μm, respectively. The erbium concentration and the fiber length are 100 ppm and 100 m, respectively. For a signal wavelength of 1.552 μm, the output power exceeds + 10 mW.

These results indicate that co-doping of La ions into erbium fibers is one of the alternative approaches for improving the EDFA gain characteristics The authors would like to express their thanks to Drs. S. Shimada and H. Ishio for their encouragement.

**References**

[1] Topical meeting on "*Optical amplifiers and their applications*" Proceedings, (Optical Society of America), Monterey, California 1980.

[2] S. B. Poole, ECOC'88, 1988, pp. 433-436.

[3] B. J. Ainslie, J. R. Armitage, J. P. Craig, and B. Wakefield, ECOC'88, 1988, pp. 62-65.

[4] D. N. Payne and R. I. Laming, Tutorial Talk, OFC'90, (OSA/IEEE) San Francisco, 1990, pp. 331-353.

[5] M. J. Weber, *Handbook of Laser Science and Technology,* vol. **1**, *Lasers and Masers,* (CRC Press, 1982) Section 2.

[6] P. B. Mauer, Appl. Opt., 1964, **3**, p. 153.

[7] R. H. Hoskins and B. H. Soffer, J. Appl. Phys., 1965, **36**, pp. 323-324.

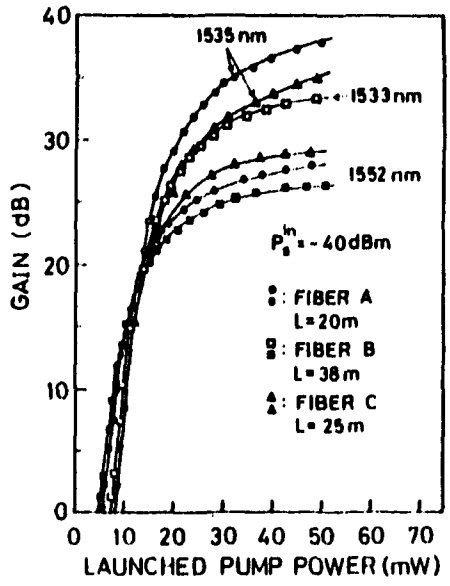


Figure 1 Gain vs. launched pump power for La co-doped EDFA. Fiber A: Er=420 ppm and La=4000 ppm, Fiber B: Er=220 ppm, Al=2000 ppm. Fiber C: Er=450 ppm. The pump wavelength is 1.48 μm.

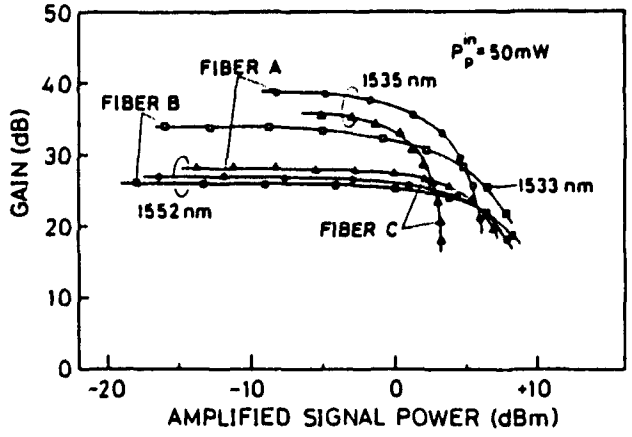


Figure 2 Gain vs. amplified output power for La co-doped EDFA. Fiber A: Er=420 ppm and La=4000 ppm, Fiber B: Er=220 ppm, Al=2000 ppm. Fiber C: Er=450 ppm. The pump wavelength is 1.48 μm.

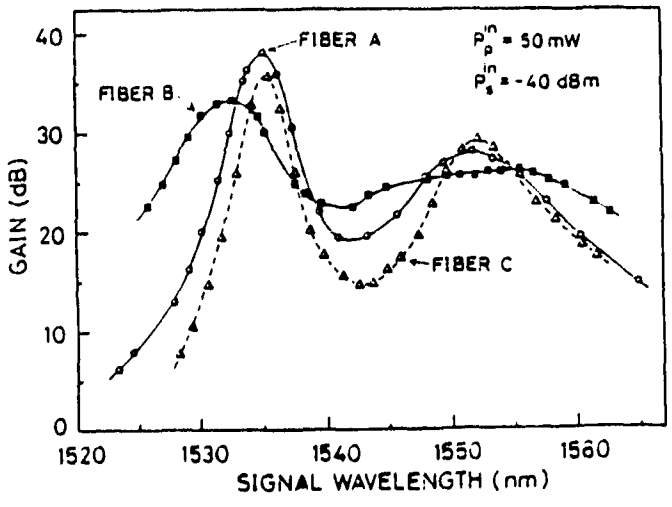


Figure 3 Changes in gain profile due to co-doping. Fiber A: Er=420 ppm and La=4000 ppm, Fiber B: Er=220 ppm, Al=2000 ppm. Fiber C: Er=450 ppm. The pump wavelength is 1.48 μm.

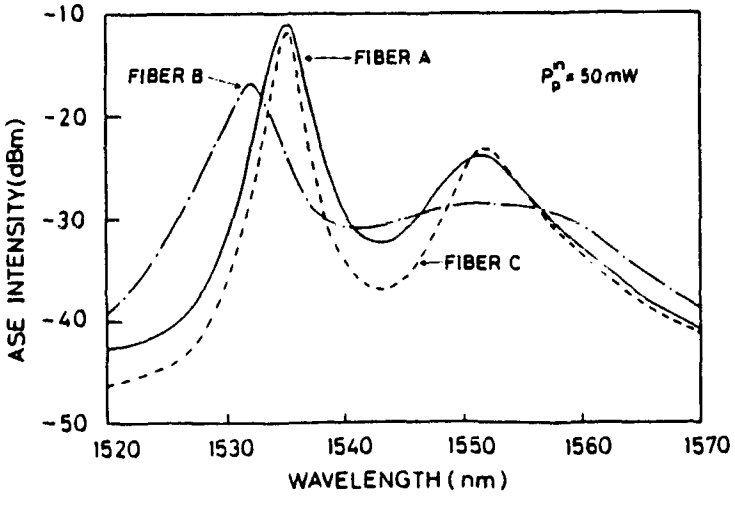


Figure 4 Fluorescence characteristics for Fibres A, B, and C.

# Semiconductor Optical Amplifiers

**WE** 3:30pm–4:30pm
Cabaret Room

J. J. O'Reilly, *Presider*
*University of Wales, United Kingdom*
M. Suyama, *Presider*
*Fujitsu Ltd., Japan*

# The future role of semiconductor optical amplifiers

by

I.W.Marshall

British Telecom, 11-13 Holborn Viaduct, London EC1A 2AT, U.K.
Tel. +44 71 356 9226, Fax +44 71 248 1635

## Summary

The recent rapid development of Erbium doped fibre amplifiers with high gains, high saturation powers and low noise figures [1,2] has deflected the attention of system engineers from the older semiconductor technology [3] and it is thus now hard to find new published papers which use semiconductor amplifiers in a system context. Device development has not ceased however [4] and the performance of semiconductor amplifiers has improved considerably. In addition there are important applications for which doped fibre amplifiers are not suitable at present e.g. at 1.3 μm, and others for which they will never be suitable, e.g. as fast optical switches. This presentation attempts to review these possibilities for future practical application of semiconductor optical amplifiers in the light of the recent developments of the technology.

The most obvious immediate application for optical amplifiers is as linear gain blocks in optical telecommunications systems. Amplifiers are already competitive with conventional regenerators on cost and are even more competitive when deployment of WDM is considered. If the system operates at 1.53-6μm the characteristics of Erbium doped fibre amplifiers are superior to those of semiconductor amplifiers in many respects and are likely to remain so, thus it is not likely that semiconductor amplifiers will be used as linear gain blocks in the 1.5μm window. At present, however most telecom systems operate at 1.3μm, and for a variety of reasons (fibre/connector transparency, dispersion etc.) this situation is likely to continue for at least the next ten years (till existing fibre plant is replaced). The immediate requirement is thus for optical amplifiers operating at 1.3μm. Whilst it is true that recent developments using Praesodymium doped Flouride fibre [5] are very promising for this application, the technology is extremely immature and it is not clear whether similar technical advantages to those of Erbium doped silica will be realised, or whether the amplifiers will prove to be limited by issues such as splice loss and fibre fragility. Either way it will take another 5 years or so to find out. We are thus left with the semiconductor amplifier as the only alternative in the short term and possibly still the best alternative in the long term. I will describe how a practical amplifier can be made for immediate application using high saturation power MQW amplifiers. This device, which is based on previous work [6], has a gain of > 30 dB, a polarisation sensitivity of ~1 dB and a saturated output power of 10-100 mW. The projected cost is less than £10k and the predicted reliability is >50000 hours.

Perhaps a more promising future role for semiconductor optical amplifiers is as fast optical switches. There is a potential requirement for broadband circuit switches in future telecommunications networks. Such a switch could be used for call set-up or route protection and a switching time of ~μs would be required. It may prove most effective to meet this requirement using an optical switch. Optical amplifiers would be ideal since only a single element is required to provide switching without introducing losses. However, since the recombination time of doped fibre amplifiers is ~ms they are too slow to meet the performance specifications for a broadband circuit switch in a telecommunications network (~10 μs). Semiconductor optical amplifiers, on the other hand are easily fast enough (switching time ~ns [7]) to meet even an enourmously improved

performance specification. In addition they are integrable into large arrays. An example is the 16 x 16 switch recently developed by Ericsson [8]. Assuming it is possible to develop larger arrays (at least 64 x64) and these prove cheaper than combining Erbium doped fibre amplifiers with liquid crystal arrays, semiconductor optical amplifiers could be used for this type of application within 10 years.

The most exciting future role for semiconductor amplifiers is in applications requiring all optical processing, e.g. delay free routing, timing extraction from broadband signals and wavelength conversion. There have recently been a number of publications describing the use of optical amplifiers (in particular a derivative with two electrical contacts rather than the usual one) for this type of application [9-12] and the work seems extremely promising. Recent results will be presented and discussed in detail.

To conclude; Although Erbium doped fibre amplifiers are superior in many respects to semiconductor optical amplifiers there remains a great deal of scope for future application of the semiconductor technology, particularly in non-linear optical devices.

**References**

1 E Desurvire et al "Recent advances in Erbium doped fibre amplifiers at 1.5 μm", Digest OFC '90 paper FA1

2 M Yamada et al, "Noise characteristics of $Er^{3+}$ doped fibre amplifiers", IEEE Photon Tech Lett, 2 page 205 (1990)

3 M J O'Mahony "Semiconductor optical amplifiers for use in future fibre systems" J Lightwave Tech 6, pp531-44, 1988

4 M Bagley et al "MQW amplifier with 115 mW output power" Electron Lett, 26, p512 (1990)

5 Y Ohishi et al "$Pr^{3+}$ doped flouride fibre amp @ 1.31 μm", Digest OFC '91, PD2

6 I W Marshall and P D Constantine, "High gain semiconductor laser amplifier package", Proc ECOC 1989 page 54

7 B P Cavanagh et al, "Comparison of laser amplifier switches" Electron Lett, 27, p263 (1991)

8 L Thylen "Devices for photonic switching", Proc. ECOC '89 (Gothenburg)

9 M Kuznetsov "High speed frequency modulation of two segment DFBs", Digest CLEO '90, paper ThA3

10 P E Barnsley and P J Fiddyment "Wavelength conversion from 1.3 μm to 1.5 μm using split contact optical amplifiers", IEEE Photon Tech Lett, 3, March 1991

11 R M Fortenberry et al, "Photonic fast packet switch with gain" Digest Photonic Switching topical meeting, March 1991, paper ThA2-1

12 P E Barnsley et al, "Clock extraction using an optical non-linearity", Digest CLEO '91 paper CTuT4

# NEW LASER STRUCTURE FOR POLARIZATION INSENSITIVE SEMICONDUCTOR AMPLIFIER WITH LOW CURRENT CONSUMPTION

P. DOUSSIERE, B. MERSALI, A. ACCARD, P. GARABEDIAN, G. GELLY, J.L. LAFRAGETTE, F. LEBLOND, G. MICHAUD, M. MONNOT, B. FERNIER

ALCATEL ALSTHOM RECHERCHE - Route de Nozay - 91460 MARCOUSSIS (France)

**INTRODUCTION :** Due to their low current consumption and their intrinsic simplicity polarization insensitive semiconductor travelling wave amplifiers (TWAs) are very attractive components for long haul non regenerated fiber transmissions systems. It appears up to now that only buried stripe with width less than one micron has enabled to obtain high gain and polarization insensitivity for low bias current [1 - 4]. However realization of such narrow stripe leads to poor reproducibility in case of conventional laser structure. We have investigated a new structure, called modified double channel planar buried heterostructure (MDCPBH), which allows to process very narrow stripe with much better reproducibility than previously obtained.
Recently high fiber to fiber gain and low polarization sensitivity have been published [4] using buried window structure but for current higher than 150 mA and it was necessary to use bulk optics for packaging. MDCPBH structure with small area square active stripe section and $TiO_2/SiO_2$ two layers coating has enabled to achieve simultaneously for TE and TM modes reflectivities as low as $10^{-4}$ and reproducible fiber to fiber gains higher than 14 dB using lensed fiber for bias current lower than 100 mA.

**DEVICE STRUCTURE :** The structure is similar to those of double channel buried heterostructure (DCPBH) but doesn't include any blocking layer in order to diminish the number of critical steps in the process. Two additive lateral channel are used for leakage current reduction. Since it is based on poor selectivity between mesa and lateral channels, LPE regrowth of blocking layers is extremely critical in case of stripe narrower than one micron width and leads to poor reproducibility. So unselective regrowth of p doped InP makes the process much more easier and thus more suited to amplifier realization than conventional DCPBH or BH process are. In addition angled buried window [3] can be easily realized with MDCPBH structure. Basic heterostructures are grown by gas source molecular beam epitaxy (GSMBE) which allows very good control of InGaAsP active layer thickness. Lasers with nearly square active layer section as shown on figure 1 have been processed on several wafers.
$TiO_2/SiO_2$ two layers coatings are used for facet coating with step by step in-situ monitoring[5]

**RESULTS AND DISCUSSION :** Nearly square active stripe sections with 0.45 and 0.3 micron active layer thickness basic heterostructure have been processed and characterized before and after antireflection coatings. Laser characteristics obtained for the smaller active stripe section size (0.3 µm) are surprisingly good and remarkably homogeneous. Figure 2 shows continuous threshold current as low as 15 mA and power more than 15 mW for 400 µm length. Owing to the simplified regrowth process 56 percent of the cleaved lasers have pulsed threshold current below 40 mA. Average pulsed threshold current of 23 mA with only 2 mA standard deviation measured over 120 lasers 600 µm length clearly shows the high level of homogeneity that MDCPBH structure can provide (figure 3). As expected from nearly square active sections, circular far field patterns (figure 4) are observed and clearly show the influence of active section size over the beam output divergence value: 0.45 µm square section exhibits half maximum divergence more than 60 degrees leading to poor fiber coupling efficiency (9±1 dB / facet) whereas 0.3 µm square section exhibits values about 35 degrees leading to better fiber coupling efficiency (5.3±0.5 dB / facet). This last value corresponds to common values for laser with standard active layer thickness.

Gain and reflectivity are measured after coating using injection technique and tunable source already described in ref [6]. Reflectivity as low as $10^{-4}$ for both TE and TM polarizations have been obtained with $TiO_2/SiO_2$ coating on square active stripe laser for both 0.45 µm (figure 5) and 0.3 µm (figure 6) square size. Reflectivities below $10^{-4}$ are obtained on both TE and TM modes over a 30 nm spectral range for 0.3 µm structure and correspond to system requirements. Average internal gains up to 25 dB with 1 dB polarization sensitivity have been measured at 1.55 µm on amplifier with 0.3 µm square section for bias current in the range of 63/80 mA whereas gains between 25 and 30 dB with 1 dB polarization sensitivity are obtained with 0.45 µm square section for bias current up to 120 mA. This gain difference can be attributed to the significantly smaller modal confinement factor ($\Gamma \simeq$ 0.2) for 0.3 square section compared to those of 0.45 µm square section ($\Gamma \simeq 0.5$). Notice that TM gain is slightly higher than TE gain for each structure. This behaviour has been observed for each component tested and cannot be attributed to active layer structure because it is found independent of bias current. This is probably due to residual stress induced by combination of dielectric film and two additive lateral channels used for current confinement. This effect is expected to be reduced in the future.

Fiber to fiber gain up to 18.5 dB has been measured using bulk optic at only 100 mA bias current which is two times lower than previously published [4]. Average coupling efficiency of 5.3 ± 0.5 dB with minimum value up to 4 dB has been measured over 20 amplifiers using bulk optics. Several packaged modules have been realized using lensed fiber. Typical characteristics are 14 dB fiber to fiber gain with 2 dB gain ripple and 2 dB polarization sensitivities for less than 100 mA bias current. Three of them have been successfully inserted with no penality in 2.3 Gbit optical link with 10 dB minimum practical gain and no polarisation controller [7].

**CONCLUSION :** A new MDCPBH structure has been investigated and has enabled us to realize a large number of TWAs with very narrow stripe (< 0.5 µm). Using $TiO_2/SiO_2$ antireflection coating the reflectivity is below< $10^{-4}$ leading to low polarization sensitivity (< 1 dB) and a high gain (> 25 dB) for low current consumption (< 100 mA).

**ACKNOWLEDGMENTS** : We wish to thank O.BRISSON, D.DUFRESNE,V. COLSON, J. MAGNABAL, M. MATABON and A.PERALES for laser technology and characterization. Parts of this work were supported by FRANCE TELECOM and RACE 1027 CEC contracts.

## REFERENCES

[1] B. MERSALI *et al* "1.55 µm high gain polarisation insensitive semiconductor travelling wave amplifier with low driving current", Electron. Lett. 26, pp. 124-125 (1990)

[2] T. TSUJI *et al* "High gain polarization independent semiconductor optical amplifier with a large optical cavity and angled buried facets", Technical digest, Optical Amplifiers and their applications, Monterey (1990)

[3] T. TOYONAKA *et al* "Polarization independent semiconductor optical amplifier module using twin graded-index rod lenses", Technical digest, OFC (1991)

[4] I. CHA *et al* "1.5 µm band travelling-wave semiconductor optical amplifiers with window facet structure" Electron. Lett. 25, pp. 1241-1249 (1991)

[5] A. BODERE *et al* "Ion assisted deposition of optical coatings for III-V devices". Le vide, les couches minces, Supplèment au n° 246, Mars-Avril 1989, pp. 139-141

[6] J-C. SIMON *et al* "Gain polarisation sensitivity and saturation power of 1.5 µm near travelling wave semiconductor amplifier", Electron. Lett. 23, pp. 332-334 (1987)

[7] P.GABLA Internal report

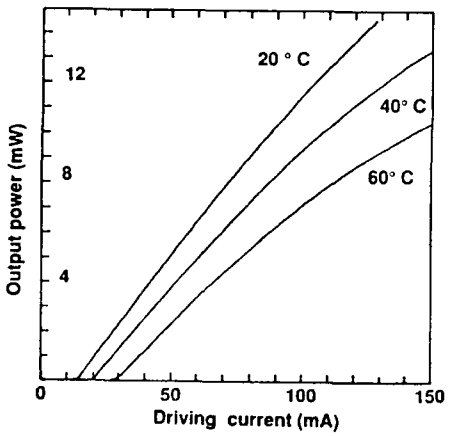


**Figure 2 :** Ligth / current characteristic of 400 µm length MDCPBH square active stripe laser

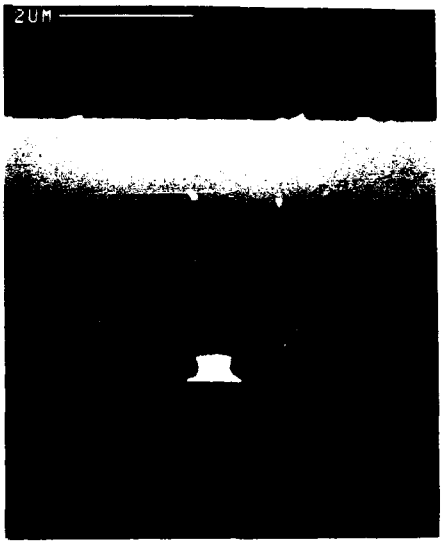


**Figure 1 :** Cross section view of MDCPBH square active stripe laser

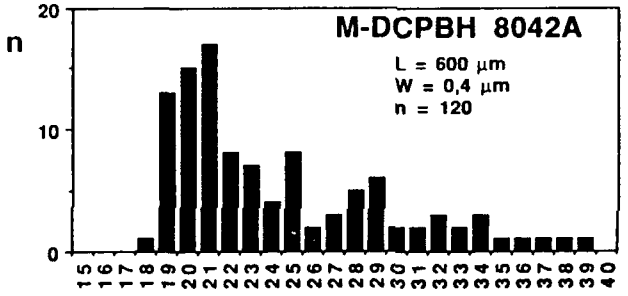


**Figure 3 :** Pulsed threshold of 120 unselected MDCPBH square active stripe lasers

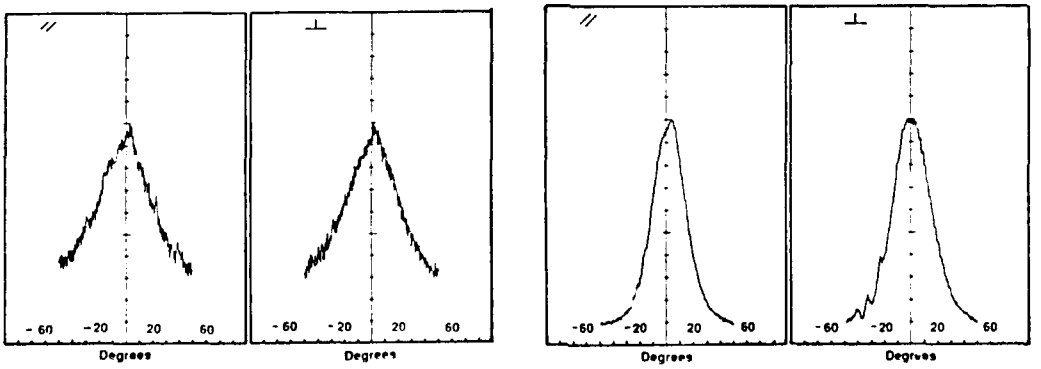


**Figure 4 :** Far field patterns of 0.45 µm (left) and 0.3 µm (rigth) size square active stripe MDCPBH lasers

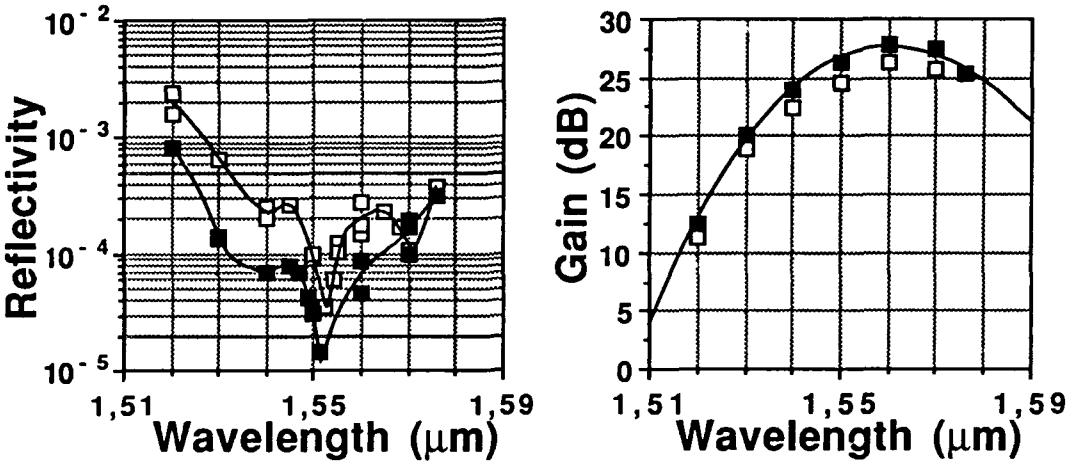


**Figure 5 :** Gain and reflectivity of 0.45 μm square amplifier for 120 mA bias current

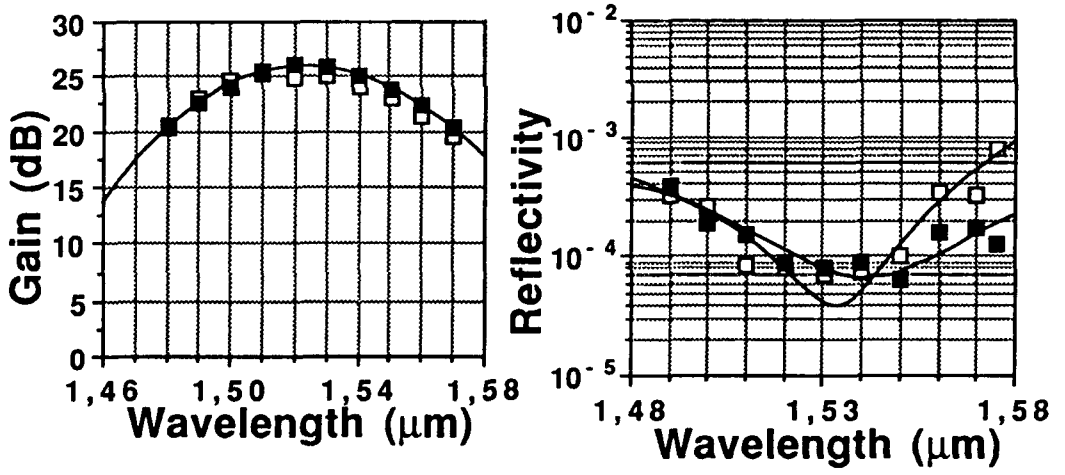


**Figure 6 :** Gain and reflectivity of 0.3 μm square amplifier for 65 mA bias current

# STRAINED LAYER QUANTUM WELL SEMICONDUCTOR OPTICAL AMPLIFIERS: POLARIZATION INSENSITIVE AMPLIFICATION

M. JOMA, H. HORIKAWA, M.NAKAJIMA, M.KAWAHARA AND T.KAMIJOH

R&D Group, Oki Electric Industry Co., Ltd., Higashiasakawa, Hachioji Tokyo 193, Japan

***Polarization insensitive optical amplification was demonstrated in newly developed semiconductor optical amplifiers which have strained GaInAsP quantum well structures. We tailored the active region of the quaternary strained layer quantum well structure with small biaxially tensile strain of 0.2% in the well layers for polarization insensitive operation.***

## 1. Introduction

Optical amplifiers are important devices for future optical fiber transmission and other photonic technologies. Semiconductor laser amplifiers are attractive candidates for these applications because of theirs high gain, compactness, possibility of integration with light source and so on. In comparison with fiber amplifiers such as $Er^{+}$-doped fibers, the semiconductor laser amplifiers have a disadvantage which is large difference between TE and TM gain. Therefore, to control the TE/TM mode gain is a key item in the development of semiconductor amplifiers. For polarization insensitive amplification in the semiconductor laser amplifier, several approaches have been proposed by geometric designing of active layers. [1-3] In this paper, we describe an approach to the polarization insensitive optical amplifier in which active layer consisted of GaInAsP multiple quantum well structures with biaxially tensile strains within well layers. A group has reported a strained layer quantum well amplifier with tensed barriers. [4] In this work, we investigated the effects of biaxially tensile strain on amplification in the quaternary strained quantum well amplifiers. The polarization insensitive amplification was successfully demonstrated.

## 2.Device Structure and Fabrication

In the view points of material design, TE and TM modes can be controlled by modulating the valence band structures, because the optical transition processes related to the TE and the TM mode are governed heavy and light hole bands in III-V materials, respectively. The TE and the TM gain are based on the transition probability of electron -to-heavy hole and electron-to-light hole. In unstrained quantum well structure, the

heavy hole mass and the undegenerated band structure cause the TE mode dominant amplification. When the biaxially tensile strain is applying on the well layer, the light hole band lifts up in the potential and then the TM gain is enhanced

A device structure is shown in Figure 1. Buried heterostructures were grown on (001)-oriented InP substrates by 3-step MOVPE growth. The active layers were made of strained quantum well structures in which five InGaAsP (0.95 eV) wells and six InGaAsP (0.77 eV) barriers, which were sandwiched by InGaAsP (1.1 eV) confinement layers. [5] Throughout this work, band gap energies of InGaAsP of the well, barrier, and confinement layers were kept at constant. The tensile strain in the well layers was varied by only changing the composition of InGaAsP. The quaternary materials would be suitable and attractive for the flexible design in the materials. The device length and cavity width were 350 and 1.5 μm, respectively. The cleaved facets were coated with anti-reflection films of SiOx.

3. Characteristics

Amplified spontaneous emission (ASE) spectra were measured with the amplifiers by varying tensile strain up to 0.4 % The ASE spectra of TE and TM mode at a biaxially tensile strain of 0.2 % for a driving current of 100 mA are shown in Fig. 2. Full widths of half maximum (FWHMs) of ASE spectra are about 80nm for TE and 60nm for TM modes. The emission intensities of TE and TM modes are much the same around 1.45μm. From this result, it is expected to be the polarization insensitive operation. At a biaxially tensile strain of 0.4 %, we observed an enhancement of the TM mode, while the TE mode emission was dominate in the conventional (no strain) quantum well amplifier. The enhancement of the TM mode can be explained by valence band modulation around the zone center (**k**=0) by the tensile strain.

The signal gains of TE and TM modes were measured as a function of driving current. The signal light at a wavelength of 1.4573μm and 1.4562μm was coupled into the amplifiers using fiber optics. Both a λ/2 plate and a polarizer were used to adjust the TE and the TM modes. The measured signal gain characteristics of the amplifiers are shown in Fig. 3. The TM mode gain increased with increase of the tensile strain. The polarizaion insensitive operation was successfully obtained at the strain of 0.2 % until the driving current of 90 mA. The TE mode gain saturated above 90 mA, whereas the TE mode increased. More gains under polarization insensitive condition will be expected by optimizing the device parameters such as ultra-low anti-reflection coatings, longer cavity lengths, and efficient current confinement within the the active layers.

4. Conclusion

Polarization insensitive optical amplification was successfully demonstrated on the semiconductor amplifiers with the active region of tailored strained layer quantum well structure. Gains of TM mode were enhanced with increase in biaxially tensile strain within well layer. When the strain was 0.2 %, the gain of the TM mode was completely same as that of the TE modes. We would like to pronounce that the quaternary InGaAsP strained layer quantum well structures with the biaxially tensile strain within well layer will be attractive for the polarization insensitive optical amplification, although details in amplification should be studied.

References

1 I. Cha et al., "1.5μm Band Traveling-Wave Semiconductor Optical Amplifier with Window Facet Structure", Electron. Lett. **25**, 1241 (1990).

2 S. Cole et al., Polarization-Insentive Near-Traveling-Wave Semiconductor Laser Amplifier", Electron. Lett. 25, 314 (1989).

3 W. J. Devlin et al., "Polarization-Insentive, High Output Power 1.3μm and 1.5μm Optical Amplifier Made by MOVPE.", Tech. Digest, IOOC '89, p.148, Kobe Japan, (1989).

4 K. Magari et al., "Polarization Insensitive Traveling Wave Type Amplifier with Strained MQW Structure.", Tech. Digest on Optical Amplifiers and Their Applications, **13**, 30 (1990).

5 M. Joma et al., "High-power Laser Diodes at 1.48μm with Strained Quaternary Quantum Well Structures.", CLEO '91, Baltimore, CWF14 (1991).

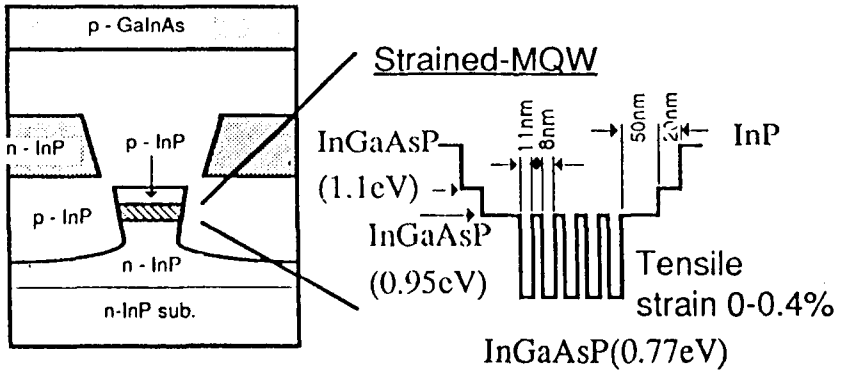


Fig.1 Schematic diagram of strained MQW Laser amplifier

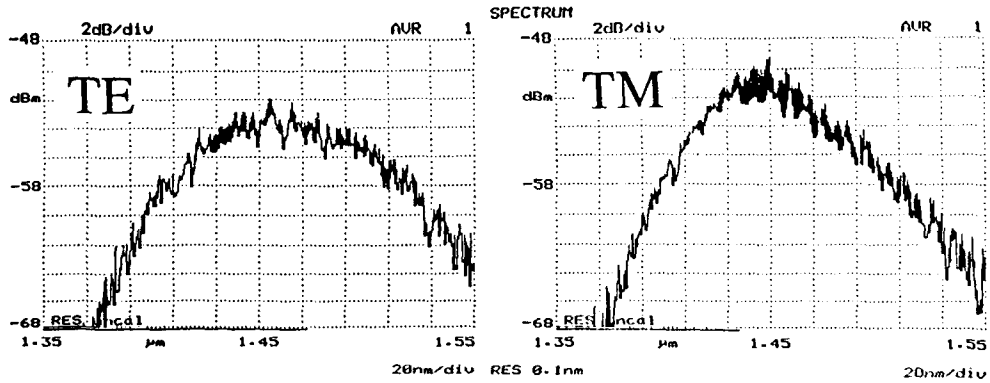


Fig. 2 Amplified spontaneous emission spectra.

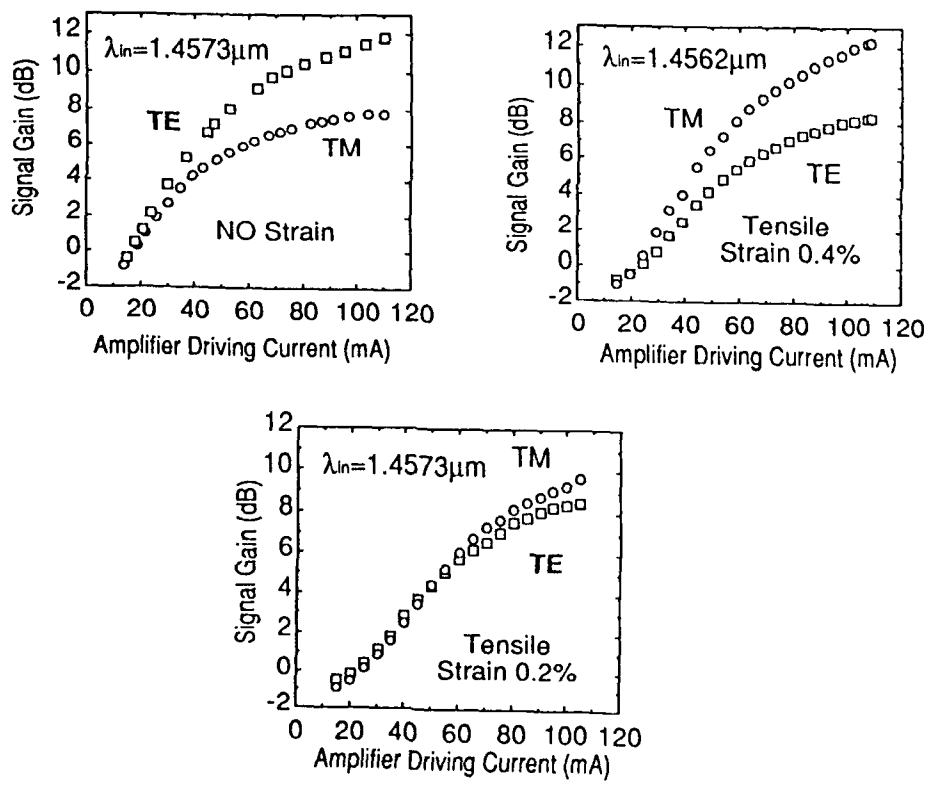


Fig. 3 Signal gain characterristics

# Ultra-Long Distance Transmission Systems

**ThA** 8:00am–10:00am
Cabaret Room

C. R. Giles, *Presider*
*AT&T Bell Laboratories, USA*

# System Limitations for Fiber Amplifier Cascades

Takeshi Ito

NTT Transmission Systems Laboratories
1-2356 Take, Yokosuka-shi, Kanagawa-ken. 238 Japan

## 1. System Performance and Amplifier Performance

The performance of an amplifier cascade system is taken to be the product of transmission bit rate, B, and transmission distance, L. In amplifier cascade systems using the IM/DD scheme, signal spontaneous beat noise, spontaneous-spontaneous beat noise and shot noise are present in addition to receiver thermal noise, while local oscillator shot noise and local oscillator-spontaneous beat noise are additional factors in coherent systems. Signal-spontaneous and spontaneous-spontaneous beat noises generally predominate in IM/DD systems if many cascaded amplifiers are used. Conversely, in coherent systems, local oscillator-spontaneous beat noise predominates. In such cases, system performance is approximated by

$$B \times L = f_{mod}(SNR, l) \times (P_s/NF), \quad (1)$$

where $f_{mod}(SNR, l)$ is a function of required SNR and amplifier spacing, $l$, depending on the mod/demod scheme, $P_s$ is the amplifier output power, and NF is the amplifier noise figure. Therefore, the system performance depends on amplifier spacing and amplifier performance given as $P_s$/NF. As the spacing decreases and/or amplifier performance increases, system performance increases. However, it is limited by four conditions: (i) Fiber dispersion, (ii) Amplifier performance, (iii) Noise accumulation, and (iv) No cascaded amplifier. These limits are plotted in Fig.1.

In order to achieve required system performance within the allowable region, the relationship between repeater spacing and amplifier performance should be optimized from a system cost viewpoint.

## 2. Fiber Dispersion Limit

Waveform distortion due to fiber dispersion is a serious problem in a cascaded amplifier system because the optical signal is transmitted without regeneration over a long distance. The limit of B×L depends on the mod/demod scheme, and the maximum B×L is achieved by IM/DD. The limit could be greater increased by using delay equalization in an IF band with heterodyne detection as shown in Fig.2. An FSK modulation/heterodyne detection system with IF delay equalization would be superior

below ~10 Gbit/s to optical soliton transmission. Experimental data are also shown in the figure. Recirculating transmission experiments [1],[2] for an IM/DD system and soliton transmission experiments [3] closely approached very near to the respective limits. On the other hand, ample margins remained in long span transmission experiments at 1.2 [4], 2.5 [5] and 10 Gbit/s [6].

An example of observed fiber dispersion is shown in Fig.3. Fibers used in a 2200 km transmission experiment [5] was specified by the zero-dispersion wavelength within $1.55 \pm 0.01\ \mu$m. Submarine cables with six cores of ~250 km long divided into three sections, which was recently installed for FS-1.8G submarine repeatered system connecting between Fukuoka and Hamada, was specified by dispersion coefficients within $\pm 2.5$ ps/nm/km from 1.54 to 1.56 $\mu$m wavelength. Wavelength dependency of dispersion coefficients ranged from 0.055 to 0.08 ps/nm/km/nm. A number of fibers with dispersion coefficients within $\pm 0.5$ ps/nm/km around 1.552 $\mu$m were obtained.

*3. Amplifier Performance Limit*

Available amplifier output power is limited by the maximum allowable fiber input power, which depends on modulation scheme and speed. For example, it is 20 dBm for CPFSK, and 13 dBm for IM at 2.5 Gbit/s. The limit of net $P_S$/NF is 17 dBm, and 10 dBm, respectively [7]. The performance measured in a 2200 km transmission experiment is shown as an example in Fig.4. In the high $P_S$ region, NF was degraded. The maximum net $P_S$/NF was 0 dBm.

Optical amplifiers are constructed with optical components such as couplers, isolators, filters, and so on. In addition, optical components for a supervisory and an APC circuit are needed to realize a practical system. Insertion loss of these components degrades the net $P_S$/NF mentioned above. Amplifier performance should be evaluated by the overall $P_S$/NF.

*4. Noise Accumulation Limit*

As amplifier spacing decreases, accumulated noise decreases and more amplifiers can be cascaded. When the spacing is 0 km, although it is not realistic, the maximum B×L is achieved as shown in Fig.5. The wide width, $B_{opt}$, of the ASE noise rejection filter lowers B×L in an IM/DD system, while the broad spectrum, $\Delta\nu$, of the signal and local lasers does the same in a CPFSK/heterodyne system. B×L with $B_{opt}/B = 100$ is about 50 % of B×L with $B_{opt}/B = 1$, and B×L with $\Delta\nu/B = 10^{-3}$ is about 70 % of B×L with $\Delta\nu/B = 0$. However, the noise accumulation limit exceeds the typical system performance of $B \times L = 10^5$, which means a 10 Gbit/s transoceanic transmission system. In addition, these limits far exceed the fiber dispersion limits.

*5. Amplifier Spacing*

Assuming $B_{opt}/B = 100$ or $\Delta\nu/B = 10^{-3}$, attainable B×L can be calculated as shown in Fig.6. The achieved bit error rate at the receiver is $10^{-11}$ with a 6 dB margin. Limiting conditions are as follows: ① Fiber dispersion limit is given at 5 Gbit/s for an IM/DD system, and at 10 Gbit/s for a CPFSK/heterodyne system. Those bit rates correspond to the maximum available speed for a transoceanic transmission system, respectively. ② Amplifier performance limit is $P_S/NF$ = 5 dBm and is an optimistic estimation. ③ Amplifier spacing should be longer than ~ 40 km from a system cost reduction viewpoint. This spacing corresponds to the repeater spacing of 1.3 $\mu$m wavelength transoceanic transmission systems now in commercial use.

A CPFSK/heterodyne system can achieve the required B×L at an amplifier spacing which is longer by about 20 km than an IM/DD system. This value is due to the fact that CPFSK/heterodyne receiver sensitivity is intrinsically higher by about 3 dB than IM/DD receiver sensitivity. The difference of 20 km may be important from a system cost reduction viewpoint.

The relationship between B×L and $P_S/NF$ was experimentally obtained as shown in Fig.7. The experimental system was a 2.5 Gbit/s CPFSK/heterodyne system with an amplifier spacing of 80 km. The two estimated points around $P_S/NF$ = -8 dBm were determined by allowing for the measured SNR and a bit error rate of at least $10^{-11}$ assured after 2200 km transmission. The observed performance agrees quite well with the calculated performance, although some unidentified degradation is noticed.

Multi-gigabit/s transoceanic transmission systems can be realized by cascading amplifiers of $P_S/NF$ = 0 dBm with ~ 80 km spacing and possibly by applying CPFSK/heterodyne technology.

*References*

[1] N.S.Bergano et al, OFC'91, PDP13 (1991)
[2] D.J.Malyon et al, Electronics Letters, 27, 2, pp.120-121 (1991)
[3] L.F.Mollenauer et al, Optics Letters, 15, 21, pp.1203-1205 (1990)
[4] N.Edagawa et al, Electronics Letters, 26, 1, pp.66-67 (1990)
[5] S.Saito et al, OFC'90, PDP2 (1990)
[6] K.Hagimoto et al, IEEE/OSA JLT, 8, 9, pp.1387-1395 (1990)
[7] T.Sugie, ibid., (to be published)

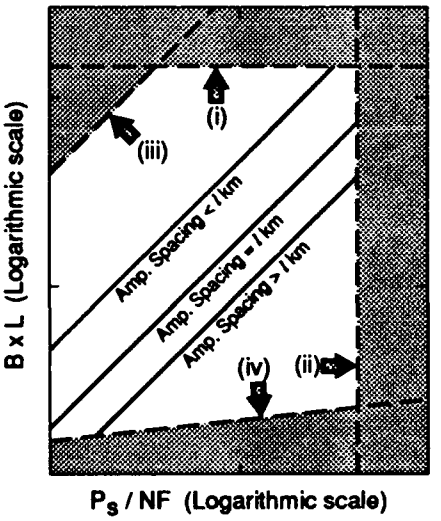


Fig.1 Limitation Factors

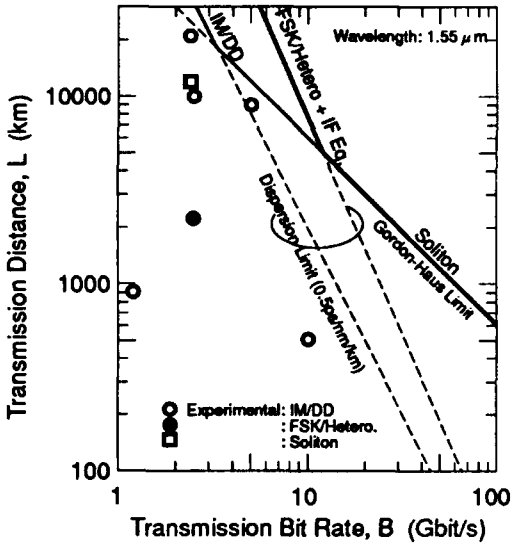


Fig.2 Fiber Dispersion Limit

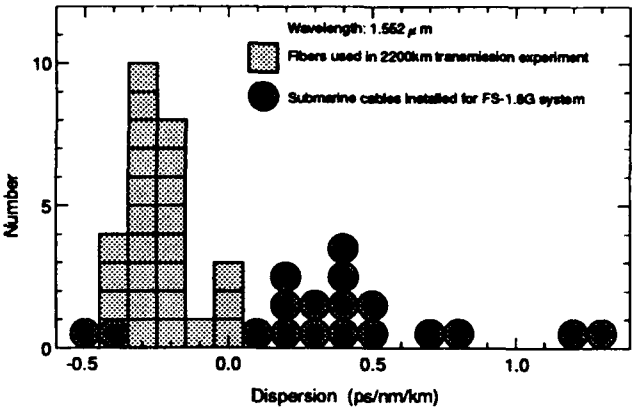


Fig.3 Observed Fiber Dispersion

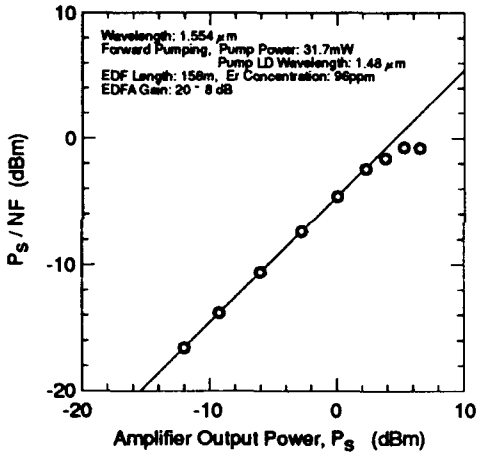


Fig.4 Observed Amplifier Performance

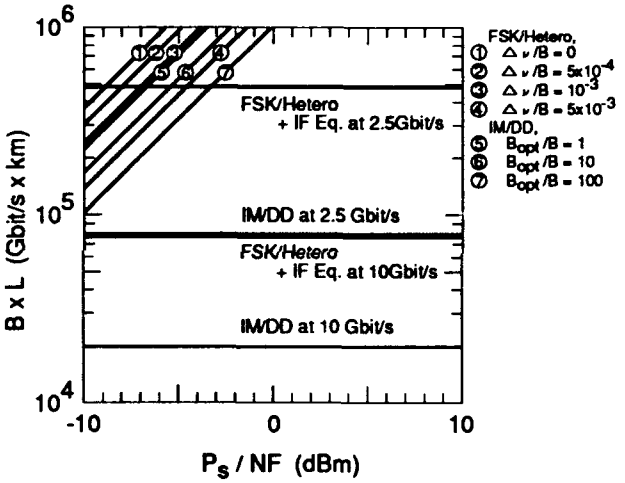


Fig.5 Noise Accumulation Limit

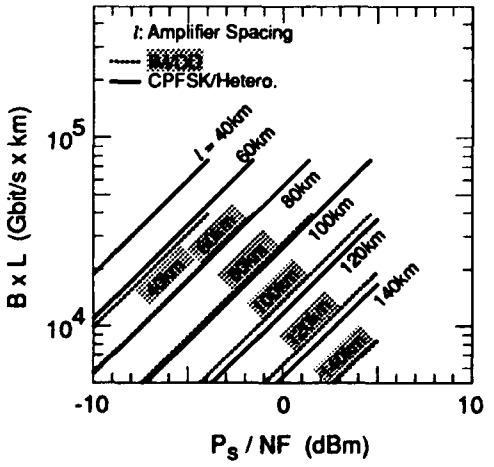


Fig.6 System Performance

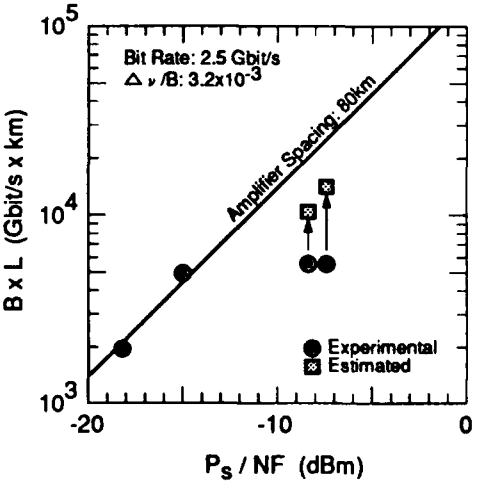


Fig.7 Observed System Performance

# Erbium-Doped Fiber Amplifier Spectral Behavior In Transoceanic Links

J-P. BLONDEL, J-F. MARCEROU, J. AUGE, H. FEVRIER, P. BOUSSELET, A. DURSIN

*ALCATEL ALSTHOM RECHERCHE, Route de Nozay, 91460 Marcoussis, France*

## 1. INTRODUCTION

Some experiments have already been presented for long haul transmission using in-line Erbium-Doped Fiber Amplifiers (EDFA) [1,2]. However, the question is to determine the actual system limitations for transoceanic links (up to 10,000 km), such as EDFA maximum output power, amplifier spacing, optical filter design. Some theoretical [3] and experimental [4] works have been published mainly with a recirculating loop.

A specific problem is to predict the evolution of signal and Amplified Spontaneous Emission (ASE) powers along the link. To our knowledge, the calculations published so far have assumed that an optical filter was set after each amplifier. In this case, the cascaded EDFA behavior can be described by scalar values without spectral dependence, and an analytical calculation is possible.

In order to predict the cascaded EDFA behavior in a more general case, spectral characteristics have to be considered, especially if there is no optical filter after each amplifier. The subject of this paper is to examine these specific aspects without taking into account the dispersive and non linear effects. Calculations for very long links are presented along with an experimental validation of the modeling.

## 2. MODELING VALIDATION AND AUTO-FILTERING DEMONSTRATION

By using an efficient theoretical modeling of the complete EDFA behavior [5], the output spectrum is obtained as a function of the input spectrum, including ASE and signal powers outcoming from the previous amplifiers. For our purpose, an active fiber with a $SiO_2/Al_2O_3/GeO_2$ matrix was used both for calculations and experiments. The other parameters are a 2.6 µm core diameter, a 2 % relative index difference and a 3 dB/m absorption peak value.

Some general evolutions of ASE and signal power have been observed with the modeling. Then, in order to validate these results, an experimental set-up has been especially designed.

Fig. 1 presents the experiment with ten amplifiers. For each EDFA, the erbium-doped fiber length is 25 m and the pump wavelength is close to 1475 nm. An optical isolator is inserted at each output end to suppress the counterpropagating ASE from the following EDFA. The variable attenuator takes the place of the link fiber with a loss A. The tunable source is modulated at 20 kHz and allows to choose the signal wavelength. Just after a 1 nm bandwidth filter, the receiver includes a lock-in amplifier to discriminate the signal from the ASE noise. The optical spectra are recorded by an optical spectrum analyzer placed before the optical filter.

The main observed spectral phenomenon is auto-filtering occuring at various wavelengths related to the EDFA configuration. Fig. 2 illustrates the output spectrum obtained with a signal wavelength at 1533 nm. The launched pump power Pp is high relatively to the erbium-doped fiber length so that the signal wavelength is in a spectral domain where the EDFA power grows up naturally. Then the ASE peak increases at this wavelength without strongly reducing the signal which nearly benefits from the same gain. Because of the saturated amplifiers auto-regulation, the total output power converges to an equilibrium value. After this stabilization, there is no more energy spectral fluctuations,which demonstrates auto-filtering effects.

As shown in Fig. 3, the same auto-filtering phenomenon can be obtained around 1558 nm if the pump power is relatively low. The EDFA configuration allows to avoid the 1533 nm peak appearance by favouring the 1558 nm peak.

If the signal is placed around 1550 nm, the auto-filtering does not profit to signal. One of the peak at 1533 or 1558 nm increases as shown in Fig. 4 and our simulations show that after a large number of amplifiers, the signal power will quickly decay contrary to the previous cases.

Agreement between theory and experiment is quite good. For example, Fig. 5 gives the simulated output spectrum after ten amplifiers in the case of auto-filtering at 1533 nm. Fig. 6 shows the evolution of output signal power (Ps) and ASE power per nm below the signal (NASE) in the case of auto-filtering at 1558 nm. The difference between the total power after the filter, and the signal power detected by the lock-in amplifier was below the measurement accuracy, confirming that NASE was far below Ps.

## 3. APPLICATION TO LONG HAUL LINKS

Confident of this modeling, calculations were made for very long haul transmissions with identical co-pumped EDFA. The criterion used to assess the signal to noise ratio quality of the link was the ratio ß between the signal power and the ASE power through an optical filter in reception. When the beat noises are dominant, the BER can be directly related to this ratio ß. For example, at a 2.5 Gb/s data rate, with an infinite extinction ratio, a 1 nm filter bandwidth in reception and a BER floor equal to $10^{-13}$, the ß value is 1.28 [3].

Fig. 7 and 8 demonstrate respectively the auto-filtering at 1533 and 1558 nm. Fig. 9 describes the evolution of Ps, Nase, and of the total output power Pt in the case of auto-filtering at 1533 nm. The signal power decreases slightly after each amplifier due to the ASE addition, the total output power remaining constant. Fig. 10 represents a different configuration with the signal at 1550 nm and a quasi-rectangular filter of 5.5 nm width at the output end of each EDFA. The power evolution is the same in both cases of auto-filtering or optical filtering. In all these cases, the ß obtained values lead to very low BER floor. Moreover, the equilibrium output powers are realistic from the point of view of dispersive and non linear effect limitations and the required launched pump powers are below 12 mW.

## 4. CONCLUSION

This work shows that a spectral treatment of the EDFA behavior is necessary to predict the evolution of signal and ASE powers in all possible cases. This evolution strongly depends on the relation between the EDFA configuration and the signal wavelength. For a $SiO_2/Al_2O_3/GeO_2$ matrix, a demonstration of realistic transoceanic links using auto-filtering has been made at 1533 nm and 1558 nm. For the same matrix, no realistic configuration could be found with a signal wavelength at 1550 nm without adding optical filters. The solution choice will be conducted by system requirements, such as link fiber design, supervision facilities and multiplexing possibility. Calculations are in progress to study more cases such as contra-pumped or non-identical amplifiers, insertion of an optical filter after every n EDFA, use of other erbium-doped fiber matrices.

## ACKNOWLEDGEMENTS

This work was supported by France Telecom.

## REFERENCES

[1] S. SAITO, T. IMAI, T. SUGIE, N. OHKAWA, Y. ICHIHASHI and T. ITO, paper PD2, OFC'90, San Francisco (1990).

[2] N. EDAGAWA, Y. YOSHIDA, H. TAGA, S. YAMAMOTO, K. MOCHIZUKI and H. WAKABAYASHI, paper PDA-8, postdeadline ECOC 89, Gothenburg (1989).

[3] C. R. GILES, E. DESURVIRE, J. Lightwave Technology, Vol. 9, No. 2, Feb. 91.

[4] D. J. MALYON, T. WIDDOWSON, E. G. BRYANT, S. F. CARTER, J. V. WRIGHT and W. A. STALLARD, Electron. Lett., Vol 27, No. 2, Jan. 91.

[5] L. F. MOLLENAUER, B. M. NYMAN, M. J. NEUBELT, G. RAYBON and S. G. EVANGELIDES, Electron. Lett., Vol. 27, No. 2, Jan. 91.

[6] J. F. MARCEROU, H. FEVRIER, J. AUGE, C. CLERGEAUD, S. LANDAIS, A. M. BRIANCON and B. JACQUIER, Topical Meeting on Optical Amplifiers and Their Applications, Monterey, CA, Aug. 90

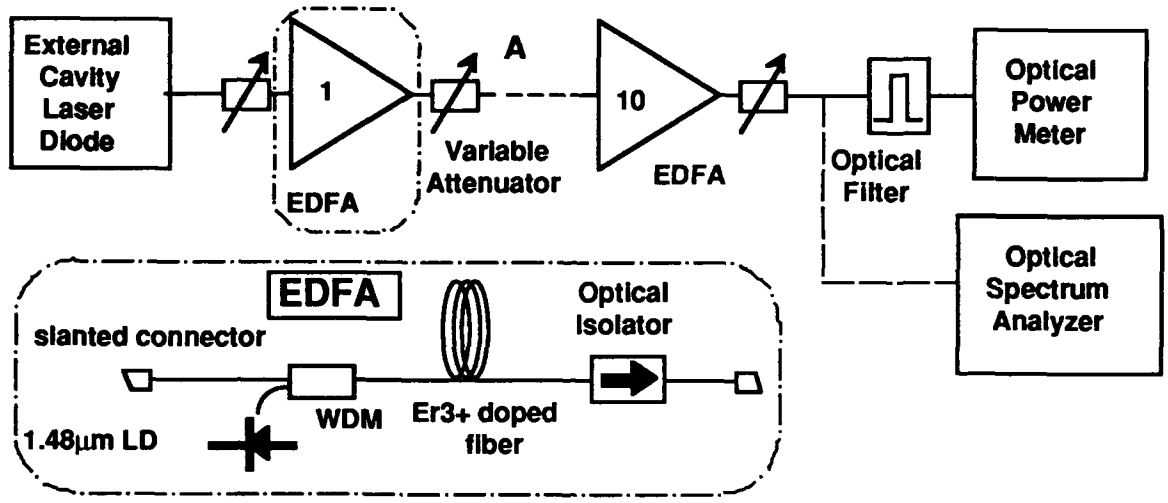


**Figure 1 :** Experimental set-up

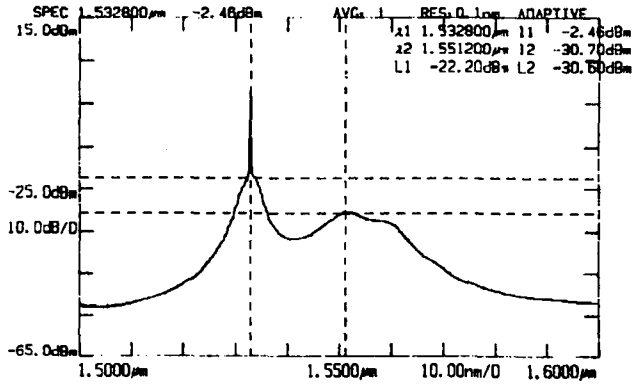


**Figure 2 :** Experimental output spectrum
$\lambda_s$ = 1532.8nm - A = 20.5dB - $P_p$ = 15mW
(after 10 EDFA)

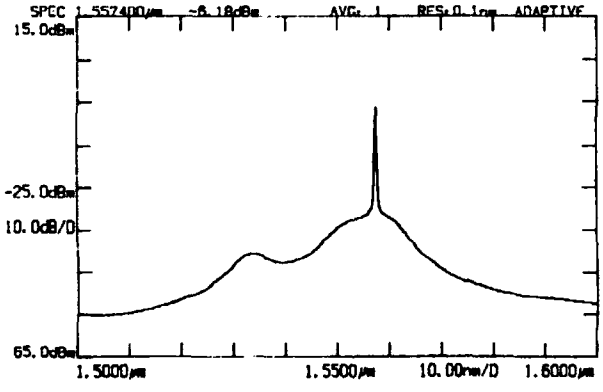


**Figure 3 :** Experimental output spectrum
$\lambda_s$ = 1557.4nm - A = 13dB - $P_p$ = 7mW
(after 10 EDFA)

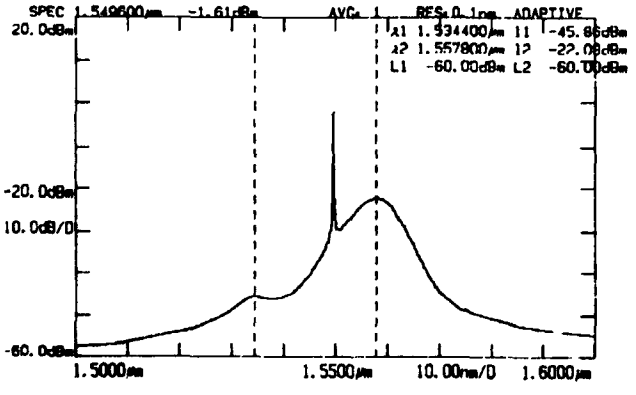


**Figure 4:** Experimental output spectrum
$\lambda_s$ = 1549.6nm - A = 13dB - $P_p$ = 10mW
(after 10 EDFA)

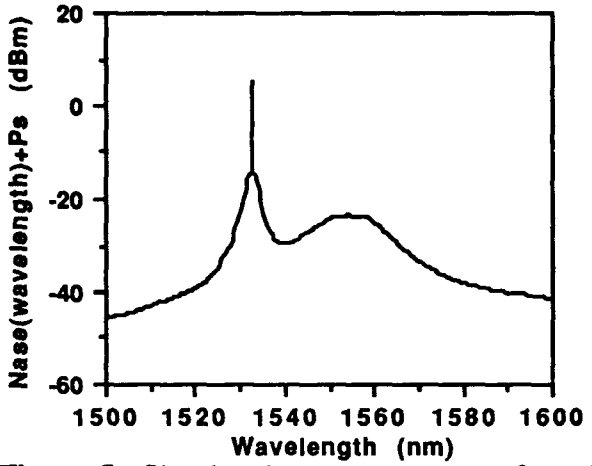


Figure 5 : Simulated output spectrum after 10 amplifiers (same conditions as in Fig. 2)

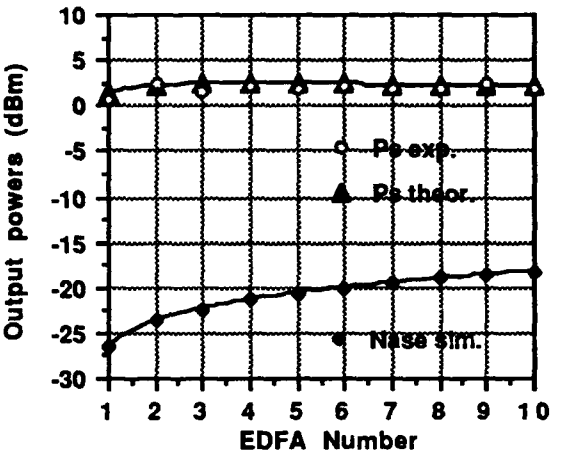


Figure 6 : Output powers evolution (same conditions as in Fig. 3)

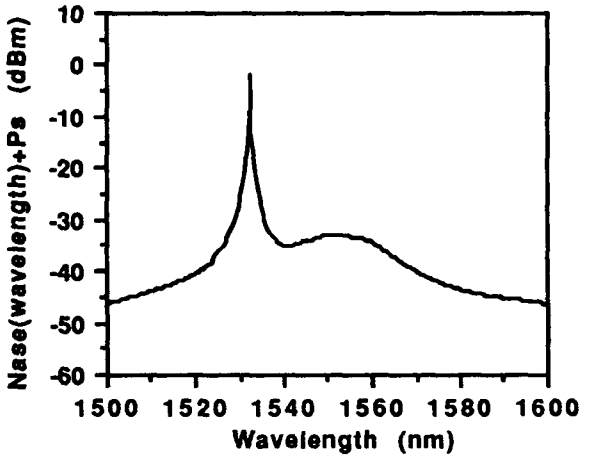


Figure 7 : Simulated output spectrum after 10000 km (Amplifier spacing : 40 km)

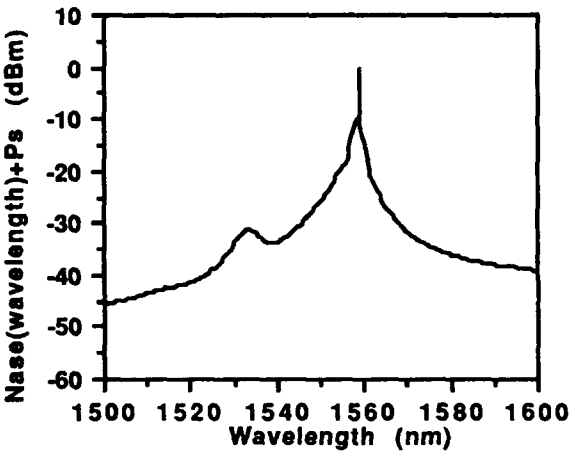


Figure 8 : Simulated output spectrum after 10000 km (Amplifier spacing : 40 km)

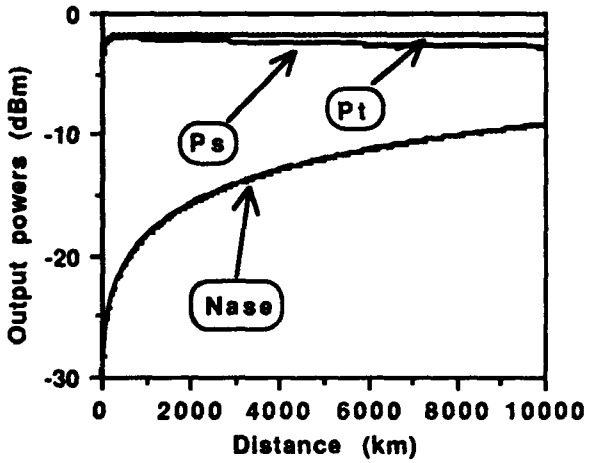


Figure 9 : Output powers evolution (same conditions as in Fig. 7)

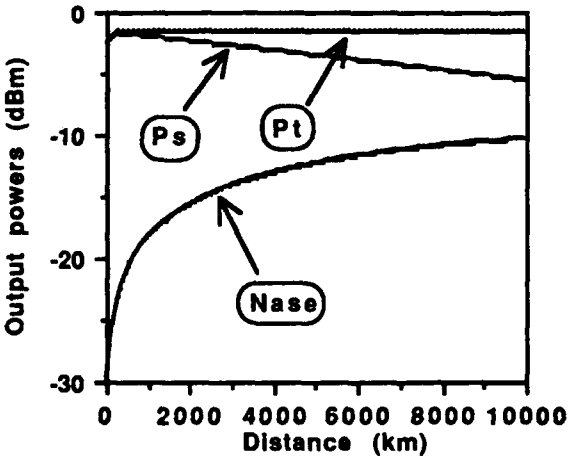


Figure 10 : Output powers evolution (Amp. spacing : 60 km, with optical filter, signal wavelength : 1550nm)

# EVALUATION OF THEORETICAL LIMITS OF CASCADED EDFA TRANSMISSION SYSTEMS

O. AUDOUIN, L. PRIGENT, J.P BLONDEL, J.P HAMAIDE, J.M GABRIAGUES
Alcatel Alsthom Recherche, Route de Nozay, F-91460 MARCOUSSIS (FRANCE)

## SUMMARY

### Introduction

In the future optical transmission systems, it is likely that Erbium doped fiber optical amplifiers will replace present electrical regenerators. Both experimental studies (1, 2) and computer simulations (3-5) have investigated the feasability of non-regenerated optical long haul systems. A considerable number of parameters are determining the overall performances of the transmission link. In this paper, we report on theoritical studies carried out using numerical simulations in order to investigate the limits of such systems. We have considered both cases of 5 Gbit/s and 10 Gbit/s transmission. The theoretical limit value of the amplifier spacing, as imposed by group velocity dispersion (GVD), self phase modulation (SPM) and accumulated amplified spontaneous emission (ASE) has been evaluated.

### System parameters

We consider here the case of an optical link, based on intensity modulation and direct detection over 9000 km using dispersion shifted fiber with periodical optical amplification.The wavelength of the transmitter is choosen so as to be in the normal dispersion domain (negative dispersion). The simulations of the propagation in the fiber link are taking into account attenuation (0,2 dB / km), dispersion and Kerr nonlinearity (4) and is based on the resolution of the nonlinear Schrödinger equation.The Kerr constant is 2,67 $10^{-20}$ $m^2/W$ and the fiber mode field radius is 4µm.

The total output power of each amplifier is kept at a constant level by using an automatic gain control loop (7). ASE is added to the amplified signal at each amplifier. The spontaneous emission noise factor ($n_{sp}$) is taken as $n_{sp}$=1.5. An in-line filter is used at the output of the amplifiers in order to reject most of the ASE noise.

At the transmitter, a repetitive pattern of 16 bits (0011100110101010) is launched at the input of the fiber (4) . The receiver is composed of a narrow-band optical filter, a quadratic detection (modeling an ideal photodiode) and an electrical low-pass second order Butterworth filter (bandwidth: 0,65 * Bit rate).

### Limits on the bit rate due to dispersion

In a first step, we only took into account the limitations imposed by linear dispersion (d). Figure 1 shows the eye opening penalty at the receiver as a function of dispersion for two values of the bit rate BR (10 Gb/s and 5 Gb/s). These results have been found in complete agreement with those of ref. (3), which allowed us to check the validity of our model and the choice of the bit pattern sequence. For BR = 10 Gb/s, an important increase of the penalty appears when d > 0,15 ps/nm.km. Considering that the actual fluctuations of the dispersion of real fiber sections are in the range of 1 ps/nm.km (9), we deliberately exclude the single channel transmission at 10 Gb/s. Thus we have evaluated limits due to GVD, SPM and ASE for a bit rate of 5Gbit/s only.

### Limits on power due to nonlinear effect

In a second step, we have introduced the contribution of the Kerr nonlinearity.

It is well known that the nonlinear phase-shift $\Phi_{NL}$ due to SPM is proportional to the integrated optical power along the fiber

$$\phi_{NL} = \gamma . P_o . (1 - \exp(-\alpha z)) / \alpha$$

where $\gamma$ contains the nonlinear Kerr index, $P_O$ is the initial power, $\alpha$ the linear loss and z the distance along the fiber (6). We now define the average power along a section separating two amplifiers as:

$$<P> = P_{out}(1 - \exp(-\alpha z_a)) / \alpha z_a$$

where Pout is the output power of the amplifiers and $z_a$ the amplifier spacing.

The combined effect of dispersion and Kerr nonlinearity on the performances of the transmission link is represented in figure 2. The upper curve shows the calculated eye opening penalty as a function of the amplifier spacing, ie $z_a$, when the output power of the (noiseless) amplifiers $P_{out}$ is kept constant. When the amplifier spacing $z_a$ increases, <P> decreases and the nonlinear effect becomes less intense. The lower curve has been drawn the same way, except that the integrated signal power along a section <P> has been kept constant : it comes out that the nonlinear penalty now remains almost constant. We thus conclude that, with a good approximation, the influence of $z_a$ and $P_{out}$ can be represented by the single parameter <P>, just as in the case of soliton propagation.

We have then calculated the eye penalty versus <P> for different values of the dispersion (fig 3). This set of curves can be used to determine, at a given value of the fiber dispersion, the maximum allowable average power along a section $<P_{max}>$ as imposed by the Kerr non-linearity. For instance, a maximum allowable penalty of 4 dB corresponds to a maximum average power $<P_{max}>$=-8 dBm. Also, for a given value of the amplifier spacing, the corresponding maximum output power at each amplifier $P_{max}$ can be derived easily.

## Limits on amplifier spacing due to amplified stimulated emission

In the third step, we have taken into account the amplifier noise (ASE) as well.

We have considered the case where all amplifiers were operated at constant total output power; as a consequence, the signal power will decrease along the link at the expense of an increase of ASE (7). Assuming that the system must operate at a nominal value of the bit error rate (BER), say $BER=10^{-13}$, there is a minimum limit value of the ratio between the signal power at the receiver and the cumulated ASE noise power, and thus, a minimum allowable value of the total output power at each amplifier Pmin: this value has been calculated, at given values of the in-line filter bandwidth B, as described in ref (7). The results are shown in figure 4, where $P_{min}$ has been calculated for B=2 nm and B=5 nm.

The maximum limit power $P_{max}$, as defined in §IV, has been superimposed on the same figure: It corresponds to an average power $<P_{max}>$ = -8 dBm.

These two sets of curves ($P_{min}(B)$,$P_{max}$) are delimiting the range of values of the amplifier spacing satisfying both ASE- and SPM-induced constraints: their intersection gives the absolute maximum limit $Z_{max}$ of amplifiers spacing .

## Overall limits of a 9000-km 5 Gbit/s non-regenerated transmission system

The last step consists in performing numerical simulations of the transmission over the fiber link, taking into account GVD, SPM and ASE. The total output power at each amplifier, $P_{out}$, has been taken equal to $P_{min}(z_a)$, as defined in §V, when $z_a$ (amplifier spacing) is smaller than $Z_{max}$. Considering the random nature of the noise, we have performed a number of simulations of the propagation with ASE in order to obtain statistical results : the average behaviour has been summarised in figure 5.

The upper curve shows the average eye opening penalty as a function of the amplifier spacing, for a 2 nm filter bandwidth B (corresponding to Z max=70 km). In comparison, the lower curve shows the penalty resulting only from the ASE contribution.

The quasi constant penalty (about 2,5 dB) when only ASE is taken into account can be associated to a value of the bit error rate equal to $10^{-13}$. We can thus evaluate the

supplementary penalty introduced by all other effects during the propagation : from 2,5 dB for $z_a$ = 30 km to 3,5 dB for $z_a$ = 70 km.

## Conclusion

Using a step-by-step approach, we have investigated the limitations imposed by normal dispersion, Kerr Nonlinearity and amplifier noise in a 9000-km non-regenerated transmission system. Our results suggest that :

- 10 Gbit/s single channel does not seem to be feasible,
- 5 Gbit/s transmission can be theoretically envisaged with amplifier spacings smaller than 70 km, at the expense of significant eye opening penalties.

We have shown that the average power over a section separating amplifiers was the most useful parameter for the evaluation of the impact of fiber nonlinearities on transmission performances.

## References

(1) S. SAITO et al., Technical Digest OFC '90, post-deadline paper PD2, 1990.
(2) D.J. MAYLON et al., Electron. Lett., vol. 27, 1990, p 120
(3) A.F. ELREFAIE et al., IEEE J. Lightwave Tecchnol., vol. 6, 1988, p 704
(4) J.P. HAMAIDE et al., Electron. Lett., vol. 26, 1990, p 1451
(5) D. MARCUSE et al., IEEE J. Lightwave Technol., vol 9, 1991, p 121
(6) G.P. AGRAWAL, Non Linear Fiber Optics, Academic Press, 1989, p 75
(7) C.R. GILES et al., IEEE J. Lightwave Technol., vol. 9, 1991, p 147
(8) N.A. OLSSON, IEEE J. Lightwave Technol., vol. 7, 1989, p 1071
(9) D. MARCUSE, IEEE J. Lightwave Technol., vol. 9, 1991, p 356

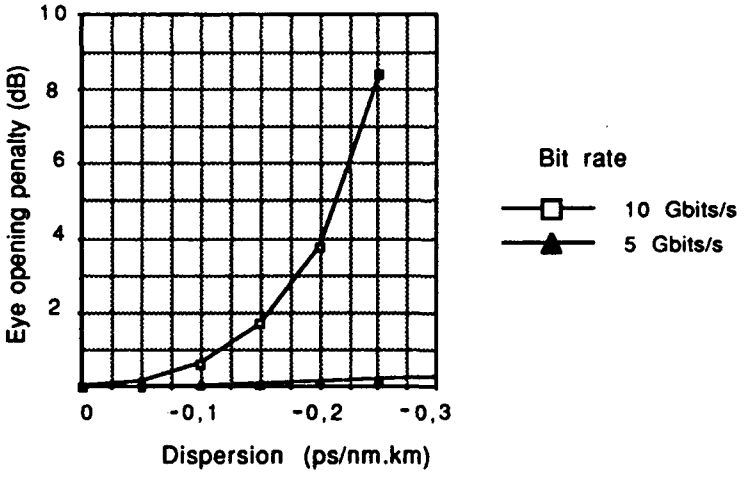


Fig.1 : Eye opening penalty due to dispersion (only) after propagation along a 9000-km dispersion-shifted-fibre transmission link

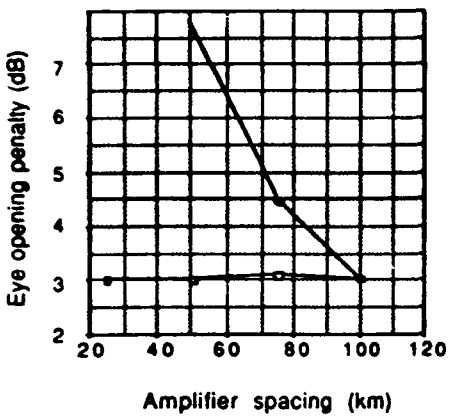


Fig. 2 : Eye opening penalty vs amplifier spacing :
full circles : at fixed Pout
open squares : at fixed <P>

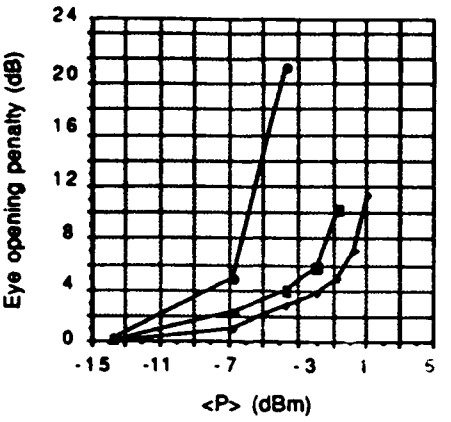


Fig. 3 : Eye opening penalty vs average power <P> :
open circles : d=-0.2 ps/nm.km
full squares : d=-0.1 ps/nm.km
crosses : d=-0.05 ps/nm. km

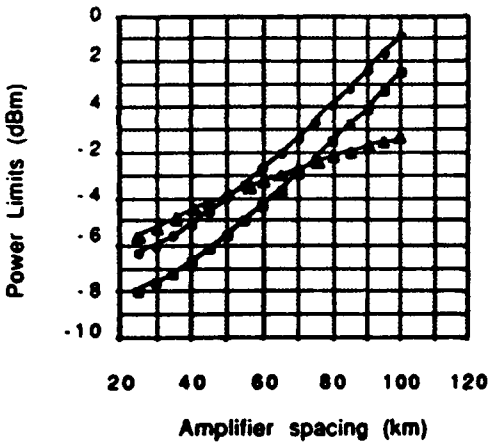


Fig 4 : Power limits versus amplifier spacing:
open squares : Minimum output power of amplifier, with 2 nm filter, required to ensure $10^{-13}$ BER in linear case
full circles : Minimum output power of amplifier, with 5 nm filter, required to ensure $10^{-13}$ BER in linear case
triangles : Maximum output power required to ensure less than 4 dB penalty due to GVD and Kerr nonlinearity.

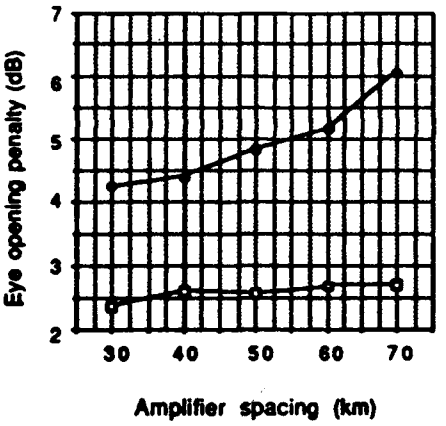


Fig 5 : Eye opening penalty due to combined GVD, SPM and ASE (upper curve) or ASE only (lower curve), vs amplifier spacing. Filter bandwidth : B=2 nm.

# Characteristics of Single-Carrier Fiber-Optic Transmission Systems using Optical Amplifiers

*S.Yamamoto, H.Taga, Y.Yoshida and H.Wakabayashi*
KDD R&D Laboratories

2-1-15 Ohara Kamifukuoka-shi, Saitama 356, Japan

## Introduction

The capability of a very long-distance transmission using erbium-doped fiber amplifiers (EDFAs) has been demonstrated by using a circulating loop.[1],[2] In a single-carrier long-distance fiber transmission system, the signal wavelength will usually be tuned to the zero dispersion wavelength of the fiber to avoid the pulse waveform distortion due to chromatic dispersion. It has also been reported that when the signal wavelength is located exactly at the zero dispersion wavelength, the mixing of the signal with the spontaneous emission from the optical amplifiers will produce four-wave mixing sidebands.[3] However, in the practical systems, the fiber chromatic dispersion varies along the long transmission path and may alleviate the effect of the four-wave mixing.[3]

We have investigated the effect of the dispersion variations on long-distance optical amplifiers transmission by numerical simulations. The results show that variation of the fiber dispersion well maintain the signal quality. In addition, this consequence was confirmed by a circulating loop experiment including the fibers with +/- 1ps/km/nm dispersion.

## Numerical Simulations

The characteristics of optical pulse propagation through optical fiber with lumped amplifiers was numerically simulated by using the nonlinear Schrodinger equation.[4] In the simulation, a 16bits NRZ pulse sequence with a bit rate of 2.5Gbit/s was assumed. The carrier wavelength and the average power at fiber input power were assumed to be 1.55μm and -3dBm, respectively.

The amplifier spacing was here assumed to be 30km to be consisted with the experiments. The first order chromatic dispersion of a 30km length fiber was chosen from Gaussian distribution with zero mean and the second order chromatic dispersion was fixed to be 0.08ps/km/nm$^2$. The Kerr coefficient and the effective area were assumed to be $3.2\times10^{-20}$m$^2$/W and 50μm$^2$, respectively.

The optical amplifier was assumed to compensate the fiber span loss having a loss of 0.23dB/km. The amplifier population inversion factor $n_{sp}$ and noise bandwidth were assumed to be 2.3 and 640GHz, respectively. To avoid the accumulation of amplifier

spontaneous emission, an optical filter with a bandwidth of 500GHz was inserted after each amplifier.

Fig.1 shows the simulated eye diagrams after 9000km transmission for the standard deviations of dispersion of 0, 0.5 and 1ps/km/nm. Fig.2 shows the optical power spectrum for each corresponding eye. The results show that when the deviation is zero, the signal energy is broadened by the four wave mixing generated between the signal and the amplifier spontaneous emission. On the other hand, it is suggested that the variation of fiber dispersion suppress the spectrum broadening. In addition, although the large deviation of fiber dispersion is expected to distort the pulse waveform together with fiber nonlinearity, it is found that the eye diagram is still open.

## EXPERIMENT

To confirm the feasibility of long-distance transmission with large deviation of fiber dispersion, a circulating loop experiment was carried out. The loop consisted of four EDFAs and three 30km fiber spans as shown in Fig.3. The chromatic dispersions of each fiber span were chosen to be +1ps/km/nm, 0ps/km/nm and -1 ps/km/nm, respectively. The DFB laser was tuned to the average zero dispersion wavelength of 1.550μm and intensity modulated with 2.5Gbit/s $2^{11}$-1 NRZ signal by a $LiNbO_3$ Mach-Zehender modulator. The signal was recirculated in the fiber loop. Fig.4 shows the bit error rate versus the propagation distance. The bit error rate of less than $10^{-9}$ was successfully obtained at 9000km.

## CONCLUSION

We have shown that the variation of fiber dispersion is effective to avoid the effect of the four-wave mixing in the long-distance transmission around zero dispersion. Next the possibility of long-distance transmission over fibers with large deviation of dispersion was presented by the circulating loop.

However, we could not demonstrate the experimental confirmation of the phase matched four-wave mixing. Therefore the further investigation of the characteristics of the transmission around zero dispersion will be remained as the future works.

## ACKNOWLEDGEMENTS

We wish to thank Dr.K.Ono, Dr.T.Yamamoto and Dr.T.Kushiro of KDD R&D Laboratories for their encouragements.

**REFERENCES**

[1] N.S.Bergano, J.Aspell, C.R.Davidson, P.R.Trischitta, B.M.Nyman and F.W.Kerfoot, Paper PD13-1, OFC'91, San Diego(1991)

[2] N.A.Olsson, P.A.Anderkson, J.R.Simpson, T.Tanbun-Ek, R.A.Logan and K.W.Wecht, Paper PD1-1, OFC'91, San Diego(1991)

[3] D.Marcuse, J. of Lightwave Technol., LT-9, No.3, (1991)

[4] G.P.Agrawal, *Nonlinear Fiber Optics*, Academic, 1989

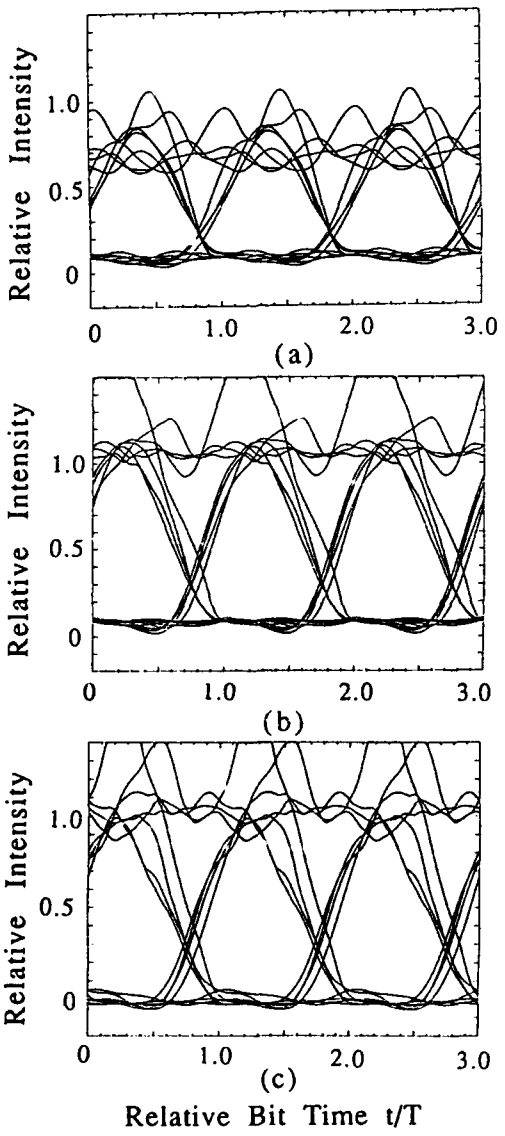


Fig.1 Simulated Eye Diagrams after 9000km Transmission (T=400ps)
(a) Standard Deviation of D, $\sigma_D$=0
(b)$\sigma_D$=0.5 (c)$\sigma_D$=1.0 ps/km/nm

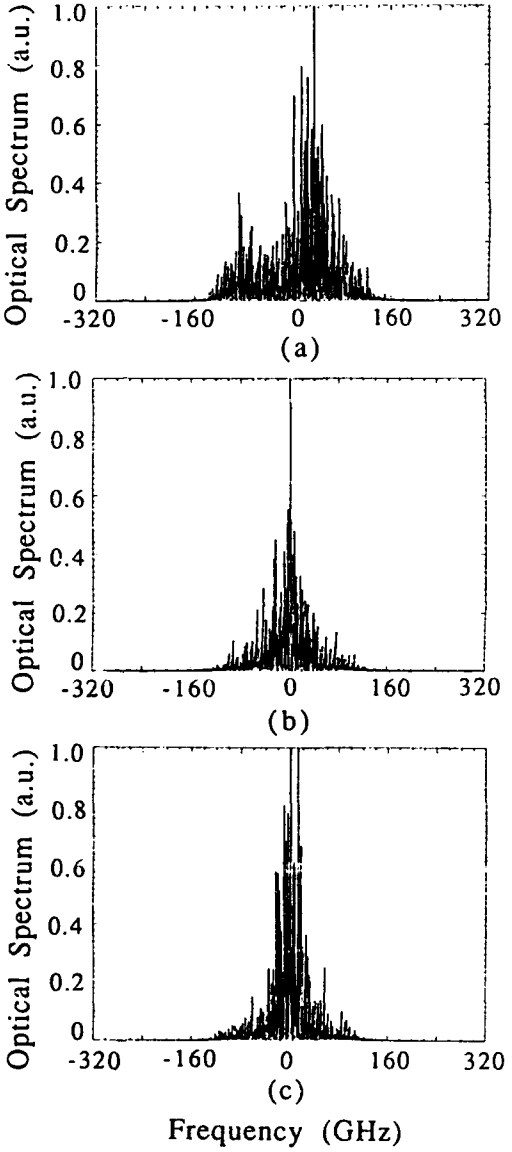


Fig.2 Optical Spectrum corresponding to the Eye Diagrams in (a), (b) and (c).

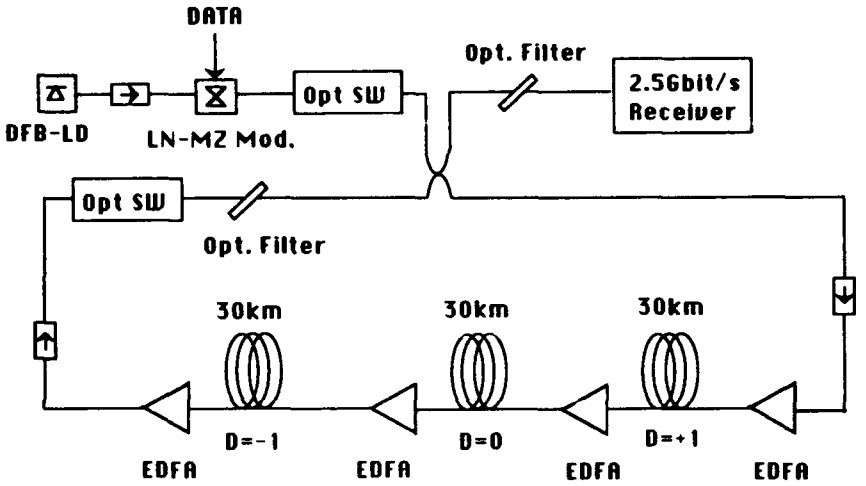


Fig.3 Schematic Diagram of Circulating Loop Experiment

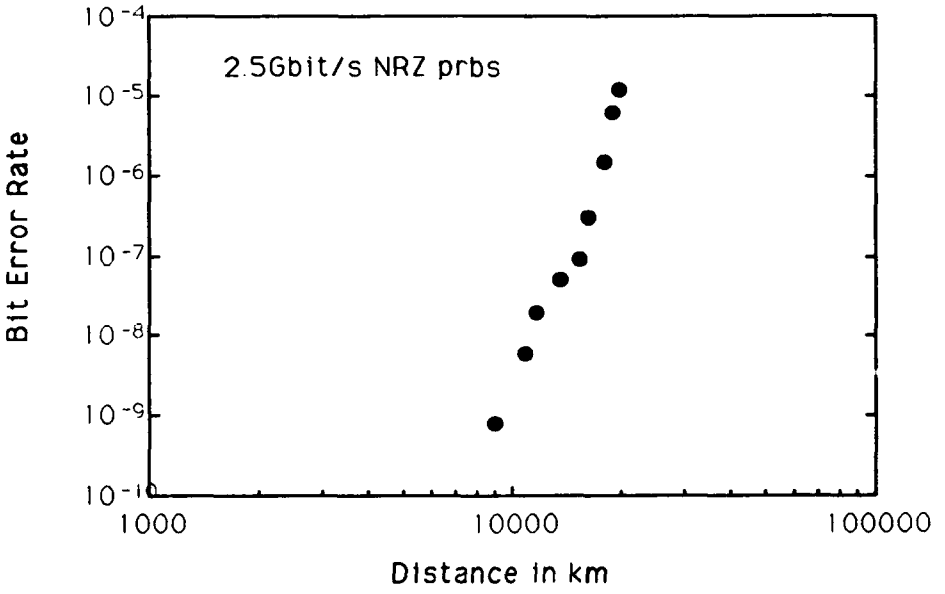


Fig.4 Bit-Error Rate as a function of Transmission Distance

# Bit-Error-Rate Measurements of a Multi-Thousand-Kilometer Fiber-Amplifier Transmission System Using a Circulating Loop.

Neal S. Bergano, Jennifer Aspell, C. R. Davidson,
P. R. Trischitta, B. M. Nyman and F. W. Kerfoot

AT&T Bell Laboratories
Crawfords Corner Road
Holmdel, New Jersey 07733

**INTRODUCTION** - Recently, we reported the results of a 2.4 Gb/s and 5 Gb/s feasibility demonstration of long distance erbium-doped fiber amplifier (EDFA) transmission systems using a circulating loop.[1] The significance of this experiment was threefold. First, it demonstrated that high bit rate all-optical EDFA transmission systems are capable of achieving transoceanic distances. Second, it demonstrated a new measurement technique in which bit-error-rate (BER) is measured in a circulating loop. And, third, it achieved a new record in bit rate distance products.

In this paper, we expand on the previously reported results by giving details of the experiment along with new transmission results. At 2.4 Gb/s and 9000 km, we have found that the transmitter's wavelength could be tuned over a 2 nm region while maintaining low BER. In addition, at 2.4 Gb/s we have measured a BER of $10^{-9}$ at 16,000 km, using a transmitter with direct laser modulation.

**EXPERIMENT** - A block diagram of the experiment and a timing diagram are shown in Figure 1. (For a more detailed description of the optics in the loop, see reference 1.) The basic principles of the circulating loop experiment are as follows. With the transmitter switch closed and the loop switch opened ("load state"), an integer number of data words is launched into the loop, then both switches toggle ("loop state"), thereby allowing the data to circulate. The data circulates for a specified time, after which the state of the switches changes again and the experiment repeats. By counting bit errors made on the $N^{th}$ pass of data around the loop, BER as a function of received optical power and transmission length is measured.

Synchronization of the two optical switches and the bit error counter is the key to performing successful bit error rate measurements. In the experiment, synchronization is achieved by counting the number of data words transmitted from the bit error rate test set. The input to the synchronization circuit (the word frame signal) is counted down by the number of words needed to fill the loop with data (44 for the 2.4 Gb/s experiment), and the number of revolutions needed in the experiment (74 for 9000 km). The basic unit of time in the experiment is the round trip-time for the loop, or $\tau$ = 590 μs. As indicated in the timing diagram in Figure 1, the optical switches are held in the "load" state for $2\tau$ and in the "loop" state for $74\tau$ for the 9000 km experiment. The synchronization circuit also provides an "error gate" signal as a time aperture to count bit errors that occur only in the final revolution of the experiment.

At any given time, there is an integer number of words in the loop. The relationship among the clock frequency (f), the loop delay time ($\tau$), and the number of words in the loop (N) is given by:

$$f = \frac{N\,M}{\tau} \qquad (1)$$

where M is the number of bits per word. When the loop was constructed, a coarse adjustment were made by cutting the fiber to have the appropriate delay time. Then a fine adjustment is made by changing the clock frequency to meet the condition of Equation 1.

The BER for long distance transmission is calculated as the number of errors detected in the error gate period, divided by the total number of bits transmitted during the observation. The effective duty cycle for the error rate measurement is the ratio of the error gate duration to the switch cycle time. For the 9000 km experiment, the duty cycle is 0.9%; therefore, on average, an experiment with a BER of $10^{-10}$ counts one error every 7.5 minutes.

**MEASUREMENTS AND RESULTS -** We have measured BER vs. transmission distance at a fixed wavelength ($\lambda_{sig}=\lambda_0$), the wavelength dependence on BER at a fixed distance (9000 km), and, finally, the transmission performance using a directly modulated DFB laser. For operation at $\lambda_0$, we have obtained a bit error rate of $10^{-9}$ at 9000 km for 5 Gb/s and 21,000 km at 2.4 Gb/s (Figure 2).

Figure 3 shows BER vs. wavelength for 2.4 Gb/s transmission at 9000 km. The circles indicate a measured point, and the arrows indicate an error rate less than $10^{-10}$. The x-axis is the wavelength offset from the zero dispersion wavelength of the fiber. The data shows a working window of low error rate of about 2 nm, roughly centered around the fiber's zero dispersion wavelength. The apparent offset of the low error rate region of 0.5 nm to the long wavelength side of $\lambda_0$ is not significant because of the uncertainty of the fiber's average dispersion. The low error rate window, expressed in fiber dispersion units, extends over a range of ±500 ps/nm.

The 2.4 Gb/s experiment has been repeated using a directly modulated laser transmitter. An AT&T CMBH DFB laser[2] is directly modulated in a 50Ω strip-line package, using a modulation current of 10 mA, and a zero state current at the laser's threshold. All other parameters of the experiment are similar to those listed in reference 1. The BER vs. distance (Figure 2) for direct modulation intersects the $10^{-9}$ point at 16,000 km, and has a slope similar to the external modulated source. The low error rate operation at long distances is probably due to the low fiber dispersion over the spectral width of the chirped laser.

**CONCLUSIONS -** The circulating loop experiment has proven its usefulness in the development of long distance optical amplifier transmission systems. We have demonstrated the importance of operating close to the dispersion minimum of the transmission fiber. In addition, we have demonstrated low error rate over long distances using a directly modulated laser transmitter.

**ACKNOWLEDGEMENTS -** We thank P. K. Runge for his enthusiastic support. We also thank D. Marcuse, R. Kimball, and S. Evangelides for enlightening discussions of optical propagation modeling.

*REFERENCES*

1. Neal S. Bergano et al., "A 9000 km 5 Gb/s and 21,000 km 2.4 Gb/s Feasibility Demonstration of Transoceanic EDFA Systems Using a Circulating Loop," Post-deadline paper PD13, OFC'91.

2. J. L. Zilko et al., "Growth and Characterization of High-Yield Reliable High-Power High-Speed InP/InGaAsP Capped Mesa Buried Heterostructure Distributed Feedback (CMBH-DFB) Lasers," JQE, Vol. 25, No. 10, p. 2091, Oct. 1989.

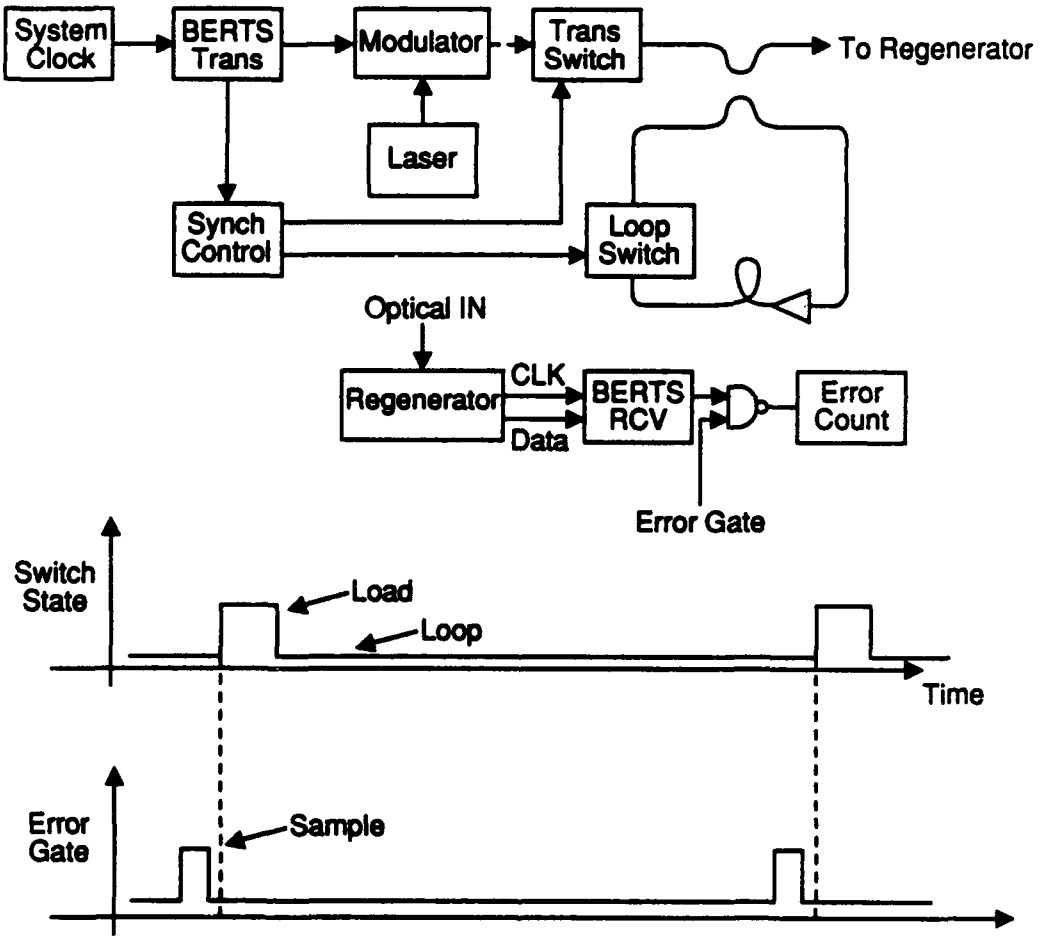


FIGURE 1 - BLOCK DIAGRAM.

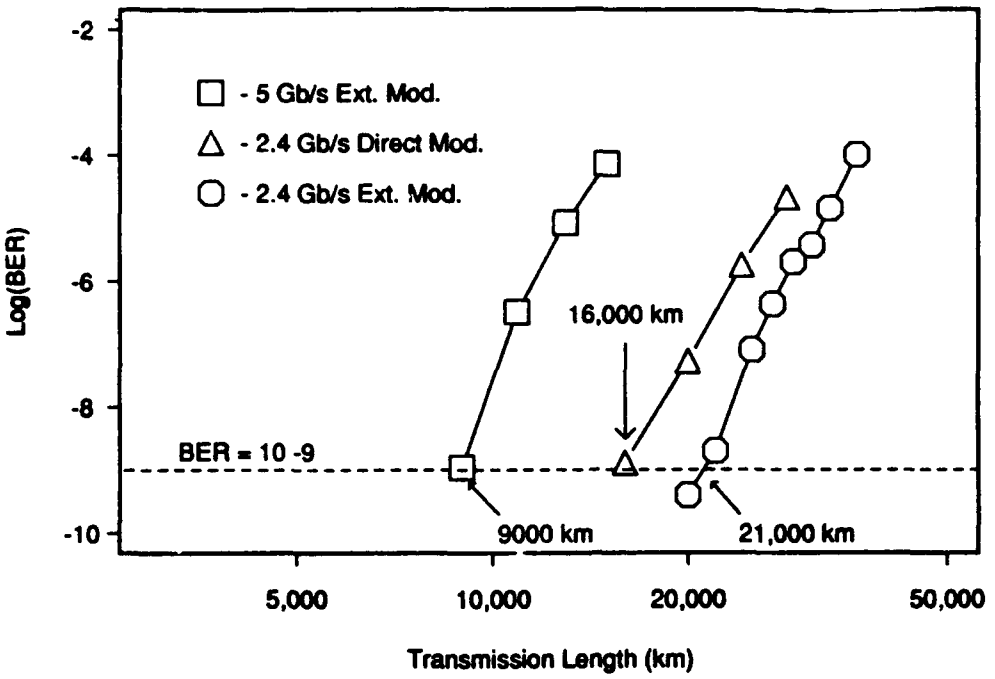


FIGURE 2 - BIT ERROR RATE VS. DISTANCE

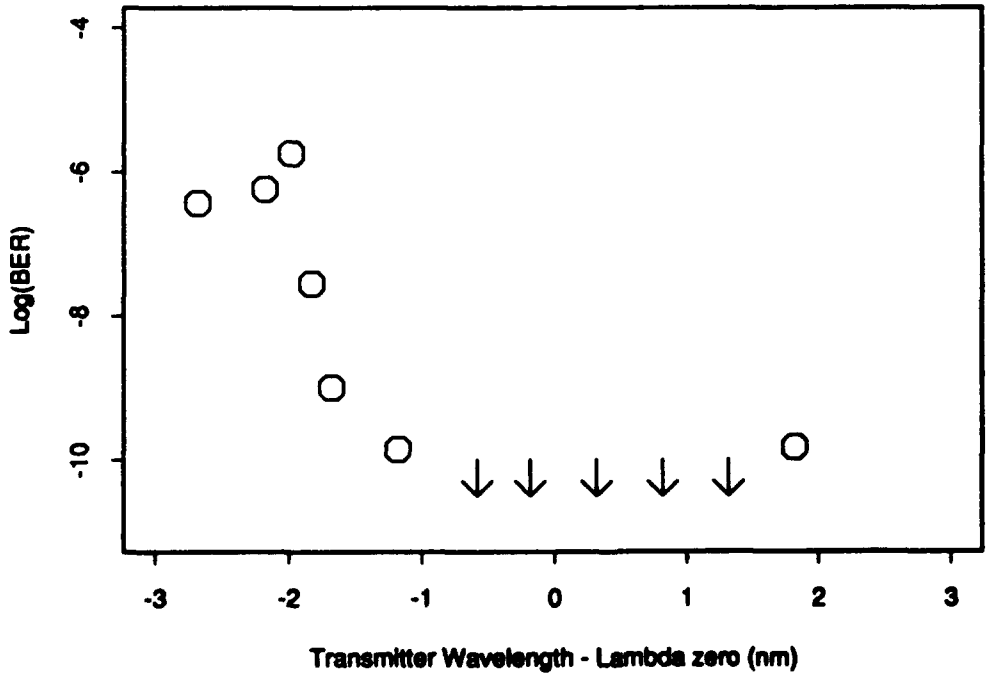


FIGURE 3 - BIT ERROR RATE VS. WAVELENGTH

# ULTRALONG DISTANCE SOLITON TRANSMISSION USING ERBIUM FIBER AMPLIFIERS

L. F. Mollenauer
Rm 4C-306
AT&T Bell Laboratories
Holmdel, NJ 07733

*Summary*

Long distance transmission using a chain of optical amplifiers is potentially much cheaper and faster than with conventional electronic regenerators. Erbium doped fiber amplifiers, with their low pump-power requirements, lack of pulse chirping, independence of gain on polarization, built in automatic gain control, and perfect compatibility with transmission fibers, have done much to make this "all-optical" approach truly practical. It can be shown, however, that the full capacity of such a system can be realized only by using solitons.

Solitons can be transmitted perfectly well through a chain of low gain amplifiers and dispersion shifted fiber segments, as long as the characteristic dispersion distance, $(2/\pi)z_0$, is great enough with respect to the amplifier spacing [1]. For such transmission, it is necessary only to make the path-average power over each amplification period equal to the usual soliton power in lossless fiber. We have verified this point experimentally [2,3] over paths as great as 12,000 km and at pulse rates to 2.5 Gbits/s by using the recirculating loop shown in Fig. 1. In all cases, broadening of the ~50 ps pulse train can be explained almost entirely by a modest jitter in pulse arrival times from the Gordon-Haus effect [4]; furthermore, at about 5000 or 6000 km, the pulse shapes look more nearly text book perfect than they do at the beginning. Thus there is no significant broadening or other distortion of the individual pulses. Our experiments [2] have also shown no significant interaction between soliton pairs spaced 5 or more pulse widths apart, and a complete absence of the long distance interaction discovered earlier in experiments using high dispersion fiber [5].

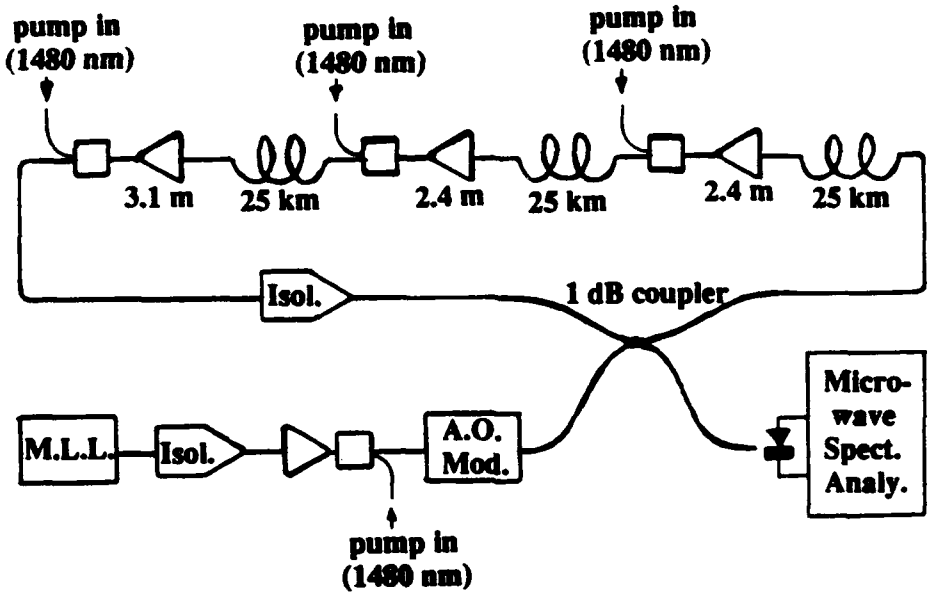


Fig. 1: Schematic of the recirculating loop. The 25 km lengths of AT&T dispersion shifted fiber had $\bar{D}$ = 1.38 ps/nm/km, $A_{eff}$ = 35 $\mu m^2$, 0.25 dB/km loss at $\lambda_{sig.}$ = 1532 nm, and a polarization dispersion parameter less than 0.2 ps/km$^{1/2}$. The acousto-optic modulator is used for its ability to reject the signal pulse stream >80 dB once the loop has been filled.

The ultimate test, however, lies in direct bit error rate measurements. Recently, we have devised a novel technique to facilitate such measurements in a recirculating loop. First, with an electro-optic modulator, we impose a $2^{12}$ bit pseudo random word, followed by its logical complement, onto the stream of pulses emerging from a mode-locked external cavity diode laser, and fill the loop with that repeated pattern. We then split the loop output into two parts, delay one part by exactly one word length, and then detect and regenerate each part. The two sets of complementary, regenerated data are then compared in an ultrafast *exclusive nor* gate, whose output goes high only when an error is present. Finally, those errors corresponding to the final round trip are gated out with an *and* gate and sent to a counter. Figure 2 shows the best results we have obtained to date at 2.5 Gbits/s. Note that we have achieved essentially "error-free" transmission (error rate $\leq 10^{-10}$) over 7500 km, the undersea distance between New Jersey and England.

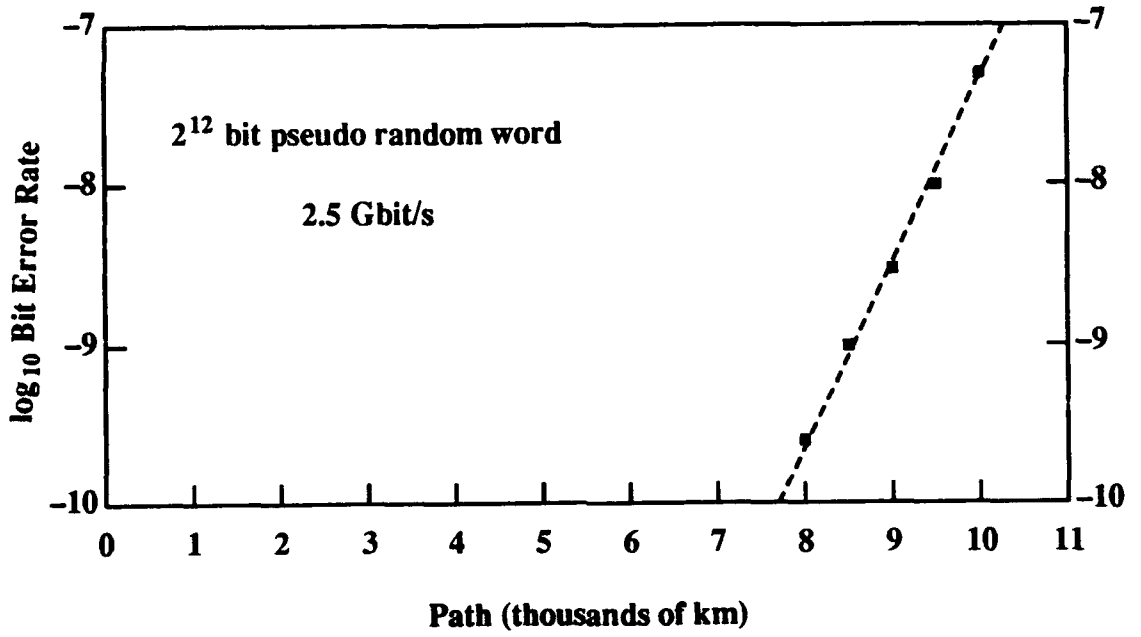


Fig. 2: Measured bit error rate for soliton transmission at 2.5 Gbits/s as a function of the total path traversed.

While that error free distance is a good beginning, it is considerably less than predicted by the simplest theory [6]. We speculate that the difference can be explained in terms of a less than 100% amplitude margin of the regenerators, and in terms of excess noise at the signal frequency created by dispersive wave radiation shed by the initially imperfect pulses fed into the transmission line. Nevertheless, with improved fiber ($A_{eff}$ = 50$\mu$m$^2$, loss rate 0.21 dB/km, as opposed to the parameters cited above in the caption to Fig. 1), and with the lower $n_{sp}$ possible with operation at 1550 nm rather than at 1532 nm, we expect soon to be able to extend error free transmission to well beyond the trans-Pacific undersea distance of 9000-10000 km.

Finally, we believe that the 2.5 Gbit/s rate can be at least doubled through a novel technique [7] involving combined polarization and time division multiplexing, as we have shown, both theoretically and experimentally, that solitons maintain a nearly complete degree of polarization over trans- oceanic distances. Furthermore, the interaction between adjacent, orthogonally polarized pulses is greatly reduced. That single channel rate can then be further multiplied by wavelength division multiplexing. That is, we have shown [8] that the well-known transparency of solitons to each other in collisions can be maintained, as long as the collision length (the distance solitons of different channels must travel down the fiber in order to pass through each other) is greater than two or more times the amplifier spacing.

## REFERENCES

[1] L. F. Mollenauer, S. G. Evangelides, and H. A. Haus, "Long distance soliton propagation using lumped amplifiers and dispersion shifted fiber," *J. Lightwave Technol.* **9**, pp. 194-197 (Feb. 1991).

[2] L. F. Mollenauer, M. J. Neubelt, S. G. Evangelides, J. P. Gordon, J. R. Simpson, and L. G. Cohen, "Experimental study of soliton transmission over more than 10,000 km in dispersion-shifted fiber," *Opt. Lett.* **15**, pp. 1203-1205 (1990).

[3] L. F. Mollenauer, B. M. Nyman, M. J. Neubelt, G. Raybon, and S. G. Evangelides, "Demonstration of soliton transmission at 2.4 Gbits/s over 12,000 km," *Electron. Lett.* **27**, pp. 178-179 (Jan. 1991).

[4] J. P. Gordon and H. A. Haus, "Random walk of coherently amplified solitons in optical fiber transmission," *Opt. Lett.* **11**, pp. 665-667 (1986).

[5] K. Smith and L. F. Mollenauer, "Experimental observation of soliton interaction over long fiber paths: discovery of a long-range interaction," *Opt. Lett.* **14**, pp. 1284-1286 (1989).

[6] J. P. Gordon and L. F. Mollenauer, "Effects of fiber nonlinearities and amplifier spacing on ultra long distance transmission," to be pub. in the *J. Lightwave Technol.* **9**, pp. 170-173 (Feb. 1991).

[7] S. G. Evangelides, L. F. Mollenauer, J. P. Gordon, and N. S. Bergano, "Polarization division multiplexing with solitons," submitted to *J. Lightwave Technol.*.

[8] L. F. Mollenauer, S. G. Evangelides, and J. P. Gordon, "Wavelength Division Multiplexing with Solitons in Ultra Long Distance Transmission Using Lumped Amplifiers," *J. Lightwave Technol.* **9**, pp. 362-367 (March 1991).

# Spectral Characteristics of Fiber Amplifiers

**ThB** 10:30am–12:00m
Cabaret Room

W. J. Miniscalco, *Presider*
*GTE Laboratories, USA*

# SPECTRAL GAIN CROSS SATURATION AND HOLE-BURNING IN WIDEBAND ERBIUM-DOPED FIBRE AMPLIFIERS

M.Tachibana*, R.I.Laming, P.R. Morkel and D.N. Payne
Optoelectronics Research Centre, The University, Southampton, UK.
Tel: (+703) 593583 Fax: (+703) 593142

*Now at Seiko Instruments Inc., 563 Takatsuka-Shinden, Matsudo, Chiba 271, Japan,
Tel: (+473) 91 3126, Fax: (+473) 92 2026

**ABSTRACT** Cross saturation characteristics are investigated in broadband 1.48$\mu$m pumped and 980nm pumped, gain-shaped" EDFAs. "Gain-shaping" is shown to give a more uniform spectral gain compression on saturation. In addition room temperature spectral gain hole-burning is observed for the first time.

**INTRODUCTION** One of the major applications of erbium-doped fibre ampliifers (EDFA) is likely to be in WDM systems[1]. In this case it is desirable to flatten and maximise the gain bandwidth of the EDFA. To date two techniques have been employed, either by the use of a pump wavength of ~1.48$\mu$m combined with careful choice of pump power and fibre length[2] or by "gain-shaping", incorporating an optical filter in the middle of the amplifier[3]. Applied to either alumino-silicate, germano-alumino-silicate or ZBLAN[4] EDFAs results in 3dB gain bandwidths of ~35nm. In addition it is important to understand and optimise the cross saturation characteristics of the EDFA. Thus the number of WDM channels can be maximised whilst the gain penalty for each channel and interchannel crosstalk effects are minimised.[5,6].

In this paper, we report an efficient, 1.48$\mu$m diode pumped fibre amplifier. The use of a germano-alumino-silicate erbium-doped fibre aswell as careful choice of pump power, pump wavelength and fibre length creates an amplifier characterised by a 25dB gain and 35nm 3dB bandwidth for only 15mW of pump power. Cross saturation characteristics are investigated for saturating signals at various wavelengths across the gain band and different pump powers. In general the gain spectrum decreases non-uniformly, with shorter wavelengths suffering the largest penalty. In addition saturation characteristics show little dependence on the saturating wavelength, only small spectral gain hole-burning is observed confirming the near homogeneous nature of the erbium transition in germano-alumino-silicate glass. Comparison with similar results for a "gain-shaped", 980nm pumped EDFA shows this to be a preferable technique yielding a more uniform decrease in gain spectrum.

**EXPERIMENTAL** The amplifier consisted of 35m of germano-alumino-silicate erbium-doped fibre which was characterised by an $Er^{3+}$-doping level of ~160ppm, a NA of 0.2 and $\lambda_{cutoff}$ at 930nm. The signal source was an ELED which allowed measurement of gain spectra between 1.52$\mu$m and 1.57$\mu$m. Its power was maintained to be less than 200nW within the gain band of $Er^{3+}$, thus ensuring small-signal operation. A further signal from either a DFB-LD or a tunable external cavity LD was mixed with the probe signal through a 3dB fibre coupler. This large signal was sufficient to saturate the amplifier and permitted the measurement of spectral gain under saturated conditions[3]. Pump light at ~1.485$\mu$m was obtained from 2 diode lasers. This was combined with the two signals via a dichroic fibre coupler and injected into the amplifier fibre. All free fibre ends were angle-polished to suppress optical feedback.

The amplifier output was coupled to a monochromator and detected with lock-in techniques to allow discrimination of the broad-band (ELED), saturating signals (DFB or tunable laser) and ASE by virtue of their different modulation frequencies. Output spectra were obtained for various pump powers, under both small-signal and saturated operation and for several wavelengths of saturating signal. At the end of experiments, the fibre was cut back and spectrum of the broad-band (ELED) signal measured such that the gain spectrum could be obtained.

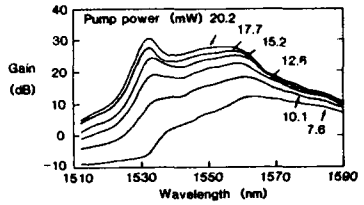


**Figure 1 Gain spectra of EDFA in small signal operation for different pump powers at 1485nm.**

**RESULTS** Figure 1 shows small-signal gain spectra obtained for various pump powers. It can be seen that a pump power between 15.2 to 17.7mW gives the broadest gain. In the case of a pump power of 15.2mW a peak gain of 25dB and 3dB bandwidth of 35nm are obtained. This corresponds to a gain efficiency of ~1.6dB/mW.

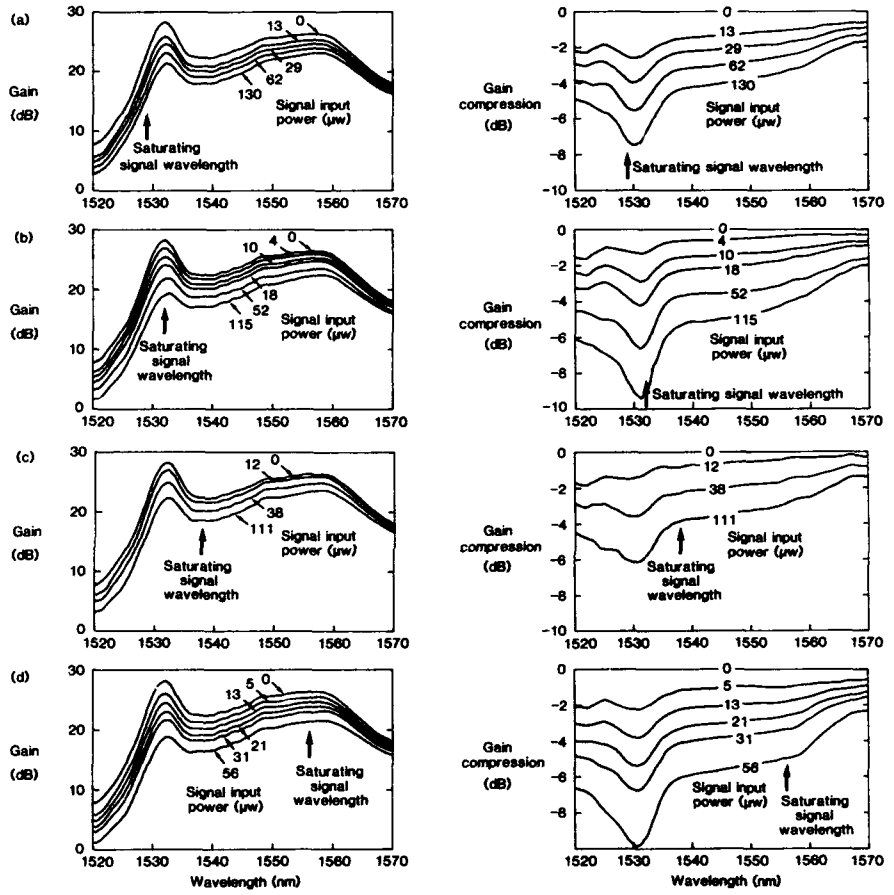


**Fig. 2 Gain spectra and corresponding gain compression obtained with a pump power of 17.7mW and increasing saturating signal power at the wavelengths (a) 1529nm, (b) 1432nm, (c) 1538nm and (d) 1556nm.**

Figure 2 shows gain spectra and corresponding gain compression obtained with a pump power of 17.7mW and increasing signal input power at the wavelengths (a) 1529nm, (b) 1532nm, (c) 1538nm and (d) 1556nm. These were selected to correspond to either a peak or dip in the homogeneous emission profile[7] and thus maximise any inhomogeneous effects observed. From the figure it is clear that for all signal wavelengths the gain spectrum distorts on saturation, with the shorter signal wavelengths around 1.532$\mu$m incurring the largest gain compression. This is undesirable for WDM systems. Also from the figure it can be seen that the gain compression

curves for different signal wavelengths are similar, thus confirming the homogeneous character of erbium in germano-alumino-silicate glass.

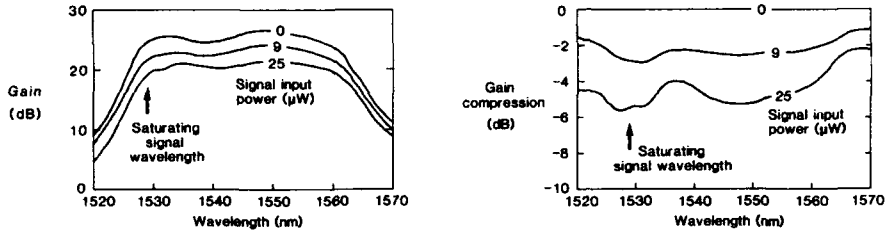


**Fig.3 Gain spectra and corresponding gain compression for a "gain-shaped" amplifier[3] and with saturating signal at the wavelength of 1529nm.**

Figure 3 plots similar data for a "gain-shaped", 980nm pumped amplifier[3]. In this case the gain spectrum decreases more uniformly making it a preferable technique. In addition it may be possible to further optimise the performance by exact location of the "gain-shaping" filter.

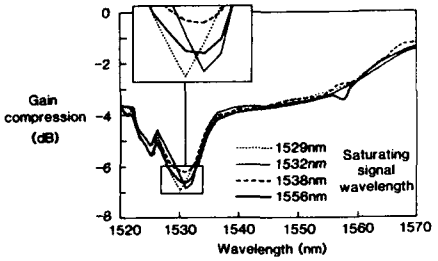


**Fig. 4 Gain compression for different wavelengths of saturating signal but with the same degree of saturation. Small spectral hole burning can be observed.**

Figure 4 compares in more detail gain compression data of figure 2. Data is selected for the four saturating wavelengths and at the same degree of saturation. The differences are subtle with the saturating signals at 1529, 1532 and 1556nm creating a spectral hole at each of their respective wavelengths, whilst the signal at 1538nm results in a reduced gain compression at 1532nm. This is the first observation of room temperature spectral hole-burning in alumina co-doped EDFAs. However the effect is small, resulting in a less than 1dB change in gain compression across the gain band and will thus be of little consequence in future WDM systems.

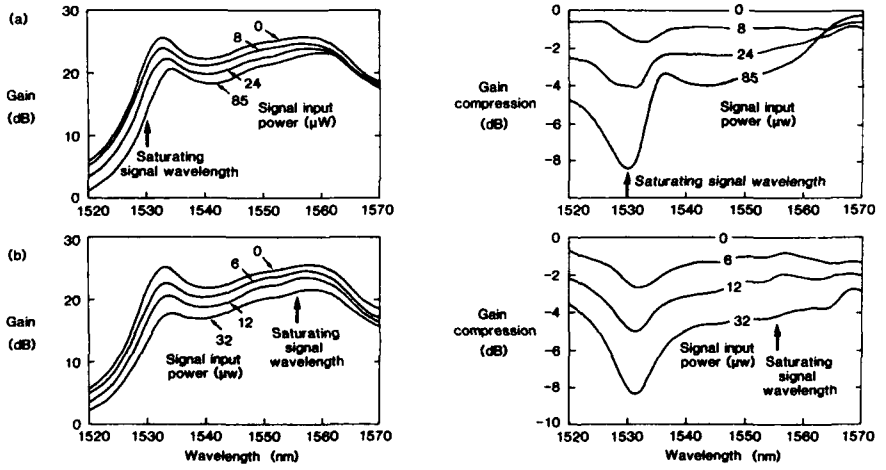


**Fig.5 Gain spectra and corresponding gain compression obtained with a pump power of 15.2mW and increasing saturating signal power at the wavelengths (a) 1530nm and (b) 1555nm. A shift in the wavelength of maximum gain compression is observed in curve (a) due to spectral hole burning.**

Figure 5 shows additional data obtained for a reduced pump power of 15.2mW. In this case the saturating signal wavelength was (a)1530nm and (b) 1556nm. For the saturating signal at 1556nm we note that the compession data is similar to that presented previously in figure 2(d). The wavelength of maximum gain compression, 1532nm, is seen to correspond to both the peak emission and absorption wavelength. However for the saturating signal at 1530nm we note that for small gain compression the peak compression occurs at 1532nm, whilst at deeper compression a spectral hole occurs and the peak gain compression occurs at the signal wavelength. In addition gain compression is relieved around 1538nm, a wavelength corresponding to a midpoint between Stark components[7].

**CONCLUSION** Either "gain-shaping" and 980nm pumping or 1.48$\mu$m pumping can be used to give a broad spectral gain. Both types of EDFA exhibit gain spectra which change when saturated. However, a 980nm "gain-shaped" amplifier exhibits a lower cross-saturation effect than a 1.48$\mu$m pumped amplifier. For example, for 1.48$\mu$m pumping a large signal at 1556nm sufficient to cause 5dB of gain compression at that wavelength, causes 10dB of gain compression at 1530nm. On the other hand for a "gain-shaped", 980nm pumped amplifier a 5dB compression at 1556nm gives only a 5.5dB compression at 1530nm.

In addition, we have made the the first observations of room temperature spectral gain hole-burning in EDFAs pumped by broad linewidth ($\sim$10nm) pump sources. The effect is small and gives rise to a less than 1dB change in gain compression across the gain band and confirms the near homogeneous nature of the erbium transition in germano-alumino-silicate glass. This effect will be of little consquence to future WDM systems.

**ACKNOWLEDGEMENTS** This work was supported by Societa Cavi Pirelli. M. Tachibana acknowledges Seiko Instruments Inc. for financial support and R.I. Laming acknowledges The Royal Society for provision of a Research Fellowship. The authors would like to thank J.E.Townsend for fabricating the fibre and J.D.Minelly for supplying the fibre couplers.

**REFERENCES**

1. R.Welter, R.I.Laming, R.S.Vodhanel, W.B.Sessa, M.W.Maeda and R.E.Wagner: Proc. CLEO '89, Paper PD22, Baltimore, 1989
2. J.R. Armitage: IEEE J. Quuantum Electronics, Vol. 26, pp. 423, 1990.
3. M.Tachibana, R.I.Laming, P.R.Morkel and D.N.Payne: Proc. Topical Mtg on Optical Amplifiers and their Applications, Paper MD1, Monterey, 1990
4. Y. Miyajima, T. Sugava, T. Komukai: Electronics Letters, Vol. 26, pp. 1527, 1990.
5. R.I.Laming, L.Reekie, P.R.Morkel and D.N.Payne: Electronics Letters, vol.25, no.7, p.455, 1989
6. K.Inoue, H.Toba, N.Shibata, K.Iwatsuki and A.Tahada: Electronics Letters, vol.25, no.9, p.594, 1989
7. E.Desurvire, J.W.Sulhoff, J.L.Zyskind and J.R.Simpson: IEEE Photonics Technology Letters, vol.2, no.9, p.653, 1990

# Multichannel amplification characteristics of saturated erbium-doped fiber amplifiers

Y.H.Cheng, N.Kagi, A.Oyobe and K.Nakamura

Opto-technology Laboratory, Furukawa Electric Co., Ltd.
6, Yawata-kaigandori, Ichihara, Chiba 290, Japan

## INTRODUCTION

Erbium-doped fiber amplifiers (EDFAs) are attractive for various optical fiber transmission systems and networks owing to their several advantages such as high gain and low noise. A EDFA with its high output saturation power and wide gain profile is specially suitable for wavelength-division multiplexing (WDM) applications such as multichannel CATV distribution systems [1]. In these applications, the EDFA is normally used as a post (or a booster) amplifier and operates at a saturated region. Although it has been demonstrated that the EDFA is immune to patterning effects and interchannel interference, and has low gain saturation induced crosstalk [2], [3], there is little information about effects of wavelength spacing and fiber length in a saturated EDFA for multichannel applications. In this paper, we report the experimental results on wavelength and fiber length dependence of gain for saturated EDFAs in a two-channel amplification system. The experimental results show that when an EDFA operates at the saturated region in a multichannel system, a shorter fiber length than that in single-channel should be selected to get a flat gain profile, and that the Ge/Al/Er-doped silica fiber is desirable for multichannel amplification use since a gain hole-burning is observed for the Ge/Er-doped silica fiber.

## EXPERIMENTAL SETUP

Figure 1 shows the experimental setup used for the two channel CW signal amplification. A single-mode tunable external cavity laser (ECL) (Channel 1) and a DFB laser (Channel 2) were used. In the measurements, the wavelength, $\lambda_1$, of the ECL was changed from 1530nm to 1560nm, and that of the DFB laser, $\lambda_2$, was fixed at 1552nm. Outputs of the two lasers were combined through a fiber coupler, and coupled into the EDFA by a filter type WDM coupler having flat loss characteristics in the concerned wavelength regions. The signal input power to the EDFA was -4.5dBm for both channels. A 1480nm laser was used as a pump source, and a pump power of 22.6mW was launched into the EDFA. Two polarization insensitive isolators were used to avoid the laser oscillation. The gain characteristics were measured using an optical spectrum analyzer.

A Ge/Er-doped and a Ge/Al/Er-doped silica fibers were tested in the experiment. The former (hereafter Fiber 1) had an $Er^{3+}$ core concentration of 77ppm by weight, a cutoff wavelength of 1.19μm, and an MFD of 5.9μm. The latter (hereafter Fiber 2) had an $Er^{3+}$ core concentration of 260ppm by weight, an $Al^{3+}$ concentration of 5000ppm, a cutoff wavelength of 0.96μm, and an MFD of 6.1μm. The peak absorption coefficients are 0.7dB/m and 2.5dB/m for Fibers 1 and 2, respectively. In the experiment, the gains for both channels were measured changing the fiber length and the wavelength of the ECL.

## RESULTS AND DISCUSSION

First, the gain characteristics of Fibers 1 and 2 operated at the saturated region were measured in a single channel system. The measured results are shown in Fig.2 for different fiber lengths. As shown in Fig.2(a), the gain of Fiber 1 was dependent on the signal wavelength and fiber length even operated at the saturated region, whereas in Fiber 2, a quite flat gain profile was obtained over a wavelength range of 30nm (from 1530nm to 1560nm) for a wide range of fiber length (Fig.2(b)).

The measured gain characteristics of Fibers 1 and 2 in the case of a two channel amplification are shown in Figs.3 and 4. Figures 3(a) and 4(a) show the gains for Channel 1 as a function of $\lambda_1$, and Figs.3(b) and 4(b) are those for Channel 2 as a function of the relative wavelength $\lambda_1$-$\lambda_2$.

It can be seen that in both fibers when the fiber length is long and $\lambda_1$ is located at the 1530nm region, no gain can be obtained in Channel 1 (Figs.3(a) and 4(a)), and the gain of Channel 2 is independent of the presence of Channel 1 (Figs.3(b) and 4(b)). When $\lambda_1$ is located at the 1550nm region and close to $\lambda_2$, a gain hole-burning effect [4] appeared in Fiber 1 due to gain competition (Fig.3(b)), and the hole shifted toward the shorter wavelength for shorter fiber length.

On the other hand, in the case of Fiber 2, no gain hole-burning appeared even $\lambda_1$ and $\lambda_2$ were located very closely (Fig.4(b)) [5], and the channel located at the longer wavelength has always larger gain. It can also be seen from Figs.4(a) and 4(b) that although the gains for both channels are smaller than that for single channel, a flat gain profile can be obtained in the 1550nm region, suggesting that the use of the Ge/Al/Er-doped silica fiber is desirable in a multichannel use.

## CONCLUSIONS

The multichannel amplification characteristics of saturated EDFAs are investigated for the Ge/Er-doped and Ge/Al/Er-doped silica fibers. A gain hole-

burning was observed in the Ge/Er-doped silica fiber, whereas a flat gain profile was obtained in the Ge/Al/Er-doped silica fiber. The experimental results suggest the uses of a shorter length Ge/Al/Er-doped silica fiber and 1550nm wavelength region for multichannel amplifications with a saturated EDFA.

REFERENCES

[1] K.Nakagawa, S,Nishi, K.Aida, and E.Yoneda, J. Lightwave Technol., vol.9, no.2, pp.198-208, 1991.

[2] R.I.Laming, L.Reekie, P.R.Morkel, and D.N.Payne, Electron. Lett., vol.25, no.7, pp.455-456, 1989.

[3] E.Desurvire, C.R.Giles, and J.R.Simpson, J. Lightwave technol., vol.7, no.12, pp.2095-2104, 1989.

[4] J.L.Zyskind, E.Desurvire, J.W.Sulhoff, and D.J.DiGiovanni, IEEE Photon. Technol. Lett., vol.2, no.12, pp.869-871, 1990.

[5] E.Desurvire, J.L.Zyskind, and J.R.Simpson, IEEE Photon. Technol. Lett., vol.2, p.246, 1990.

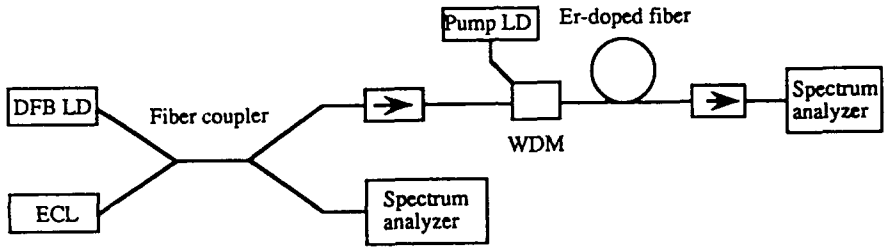


Fig.1 Experimental setup.

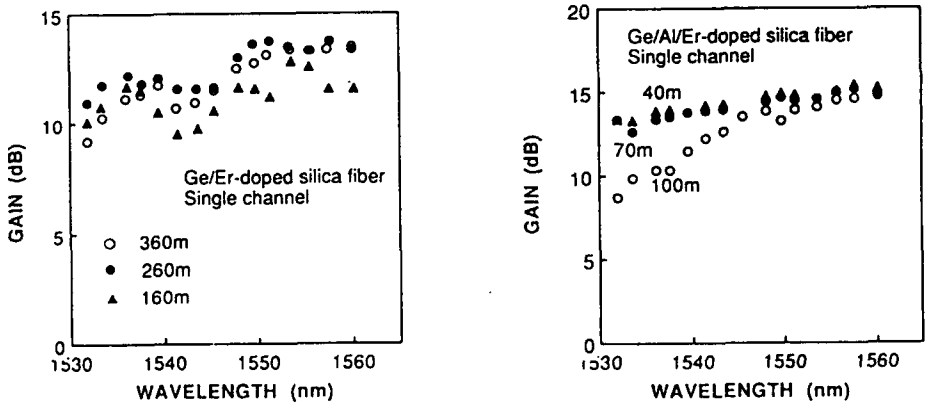


(a) (b)

Fig.2 Gain characteristics of Fibers 1 and 2 as a function of signal wavelength in the single channel amplification experiment.

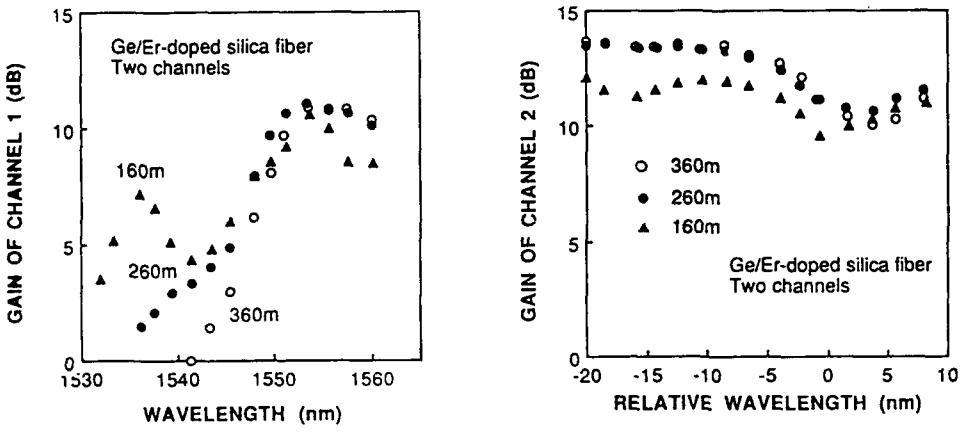


(a) (b)

Fig.3 Gain characteristics of Fiber 1 in the two-channel amplification experiment, (a) gain for Channel 1 as a function of the wavelength of Channel 1, (b) gain for Channel 2 as a function of the relative wavelength between Channels 1 and 2.

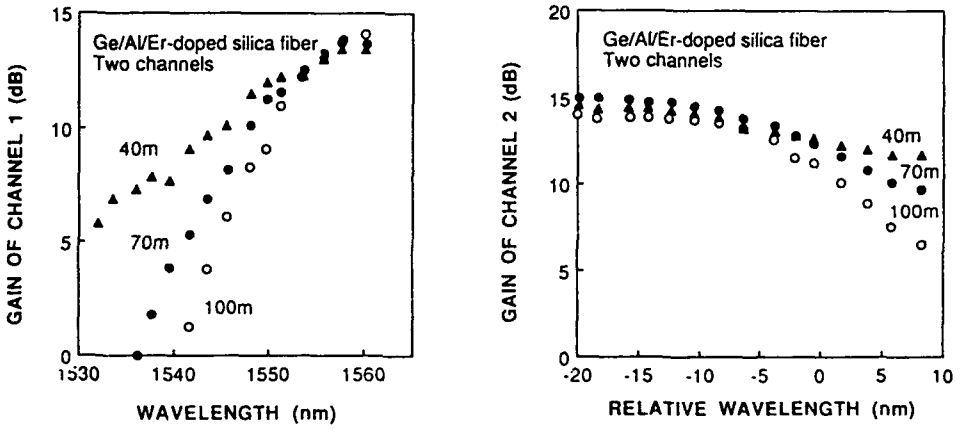


(a) (b)

Fig.4 Gain charecteristics of Fiber 2 in the two-channel amplification experiment, (a) gain for Channel 1 as a function of the wavelength of Channel 1, (b) gain for Channel 2 as a function of the relative wavelength between Channels 1 and 2.

# Diode-Pumped, Electrically Tunable Erbium-Doped Fiber Ring Laser with Fiber Fabry-Perot Etalon

J. L. Zyskind*, J. W. Sulhoff*, J. Stone*, D. J. DiGiovanni+, L. W. Stulz*, H. M. Presby*, A. Piccirilli+ and P. E. Pramayon*

*AT&T Bell Laboratories
Crawford Hill Laboratory
Holmdel, NJ 07733, USA
Phone: (908) 888-7238

+AT&T Bell Laboratories
Murray Hill, NJ 07974, USA

*Abstract*

An all fiber, diode-pumped, electrically tunable ring laser is reported. Gain is provided by an erbium-doped fiber and tuning by a Fiber Fabry-Perot etalon. The threshold at 1.566 $\mu$m is 2.9 mW, the slope efficiency is 0.15 and the output power is 4.2 mW with 32 mW of pump power. The output wavelength can be tuned from 1.525 to 1.586 $\mu$m with a variation in power of less than 3.5 dB.

*Introduction*

Tunable lasers have applications in a wide variety of fields, including optical communications, optical fiber sensors, and spectroscopy. The high performance of erbium-doped fiber (EDF) amplifiers and lasers pumped with modest powers[1,2,3] offers the possibility, with a suitable tuning element, of compact, diode-laser pumped tunable fiber lasers for the wavelengths near 1.5 $\mu$m of interest for optical fiber communications.

The Fiber-Fabry Perot (FFP) etalon[4] is a compact all-fiber, electrically tunable, polarization independent filter. It cannot be used in a standing wave resonator because the FFP will reflect wavelengths outside the pass band, and act as a resonator end-mirror for these wavelengths. However, in a ring cavity an optical isolator will prevent the formation of a resonator for wavelengths outside the FFP pass band and lasing should occur only within the FFP pass band. We report here a low threshold ($I_{th} < 3$ mW), electronically tunable, all fiber, diode pumped ring laser using this scheme. A tunable laser utilizing a similar approach with a liquid-crystal etalon filter has recently been reported.[5]

*Experiment*

The tunable fiber laser is shown in Figure 1. The laser cavity is a fiber ring including an erbium-doped fiber and a wavelength multiplexer to combine the pump and the circulating laser light. The pump light is provided by a 1.48 $\mu$m laser diode, the emission of which is coupled into a laser-machined fiber micro-lens.[6] A 99:1 fused

fiber coupler is included to permit monitoring of the coupled pump power. The EDF had a length of 30m, a cut-off wavelength of 1.0 $\mu$m, a core diameter of 2 $\mu$m and an index difference $\Delta n = 0.045$. The core had an Er concentration of 100 ppm and was co-doped with Ge and Al. The EDF was followed by a 50:50 fused fiber coupler acting as an output coupler.

The ring is completed with the FFP tuning element and a polarization independent pig-tailed optical isolator, both of which are necessary to assure wavelength selectivity of the ring cavity. The FFP interferometer[4] has a free spectral range of 66 nm, a finesse of 55 and an insertion loss of 0.7 dB on resonance. A single polarization controller is included in the loop, and is adjusted to maximize output power.

*Results*

With injection currents up to 300 mA, as much as 32 mW of pump power was launched into the ring laser. The light-light curve measured for a wavelength of 1.566 $\mu$m is shown in Figure 2. The threshold is 2.9 mW. The slope efficiency is 0.15, with an output power of 4.2 mW for 32 mW of pump power.

The tuning characteristics of the laser are shown in Figure 3. The spectral power density of the laser line exceeds that at other wavelengths in the erbium gain spectrum by more than 50 dB over most of the tuning range (correcting for the 0.5 nm measurement resolution and laser line width $< 0.1$ nm). The tuning range exceeds 60 nm, from 1.525 $\mu$m to 1.586 $\mu$m (Figure 4). Over this range the power of the laser line varies by less than 3.5 dB.

The laser wavelength can be tuned continuously over the 60 nm tuning range by adjusting only the bias of the FFP (Figure 5), without the need to adjust the polarization. The continuous tuning is demonstrated over a portion of the gain spectrum in the inset to Figure 5. The change in FFP bias necessary to tune over the full 60 nm range in the second order is about 10 V. In the first order the laser wavelength initially changes slowly with bias but beyond the starting bias of about 50V, the dependence of wavelength on bias is similar. The departures of the tuning curve from linearity arise from effects of FFP loading friction and the shape of the FFP piezoelectric translator hysteresis curve at low bias ($V_{FFP} < 50$ V), and from gain pulling near the limits of the tuning range.

As a result of the low loss of the FFP etalon and the low threshold of the EDF, the FFP EDF ring laser reported here has substantially improved threshold power, slope efficiency, output power and tuning range compared to other reported designs for tunable, erbium-doped fiber ring lasers.[5,7,8] The FFP EDF ring laser is thus especially well suited for pumping by semiconductor diode lasers. The polarization independence of the FFP permits simpler operation with continuous tuning over 60 nm by adjusting only the FFP bias. As an all fiber, polarization independent diode pumped device, the FFP EDF is inherently simpler and more compact.

*Conclusions*

We have presented an all fiber 1.5 $\mu$m laser which is electrically tunable. An erbium-doped fiber pumped by a 1.48 $\mu$m laser diode provides the gain and the tuning

element is a Fiber-Fabry Perot etalon. The laser has a low threshold of 2.9 mW and a slope efficiency of 15%. The tuning range is 60 nm, over which the laser output power varies by less than 3.5 dB.

*References*


[1] W. L. Barnes, P. R. Morkel, L. Reekie and D. N. Payne, "High-Quantum-Efficiency $Er^{3+}$ Fiber Lasers Pumped at 980 nm", Opt. Lett., *Vol. 14,* p. 1002 (1989).

[2] E. Desurvire, C. R. Giles, J. R. Simpson and J. L. Zyskind, "Efficient Erbium-Doped Fiber Amplifier at a 1.53-$\mu$m Wavelength with a High Output Saturation Power", Opt. Lett., *Vol. 14,* p. 1266 (1989).

[3] J. L. Zyskind, D. J. DiGiovanni, J. W. Sulhoff, P. C. Becker and C. H. Brito Cruz, "High Performance Erbium-Doped Fiber Amplifier Pumped at 1.48 $\mu$m and 0.97 $\mu$m", in *Technical Digest on Optical Amplifiers and Their Applications, 1990* (Optical Society of America, Washington, D. C., 1990), *Vol. 13,* p. PdP6-1.

[4] J. Stone and L. W. Stulz, "Pigtailed High-Finesse Tunable Fibre Fabry-Perot Interferometers with Large, Medium and Small Free Spectral Ranges", Electronics Letters, *Vol. 23,* p. 781 (1987).

[5] M. W. Maeda, J. S. Patel, D. A. Smith, C. Lin, M. A. Saifi and A. Von Lehman, "An Electronically Tunable Fiber Laser with a Liquid-Crystal Etalon Filter as the Wavelength-Tuning Element", IEEE Photonics Technology Letters, *Vol. 2,* p. 787 (1990).

[6] H. M. Presby, A. F. Benner and C. A. Edwards, "Laser Micromachining of Efficient Fiber Microlenses", Applied Optics, *Vol. 29,* p. 2692 (1990).

[7] D. A. Smith, M. W. Maeda, J. J. Johnson, J. S. Patel, M. A. Saifi and A. Von Lehman, "Acoustically Tuned Erbium-Doped Fiber Ring Laser", Optics Letters, *Vol. 16,* p. 387 (1991).

[8] K. Iwatsuki, H. Okamura and M. Saruwatari, "Wavelength-Tunable Single Frequency and Single-Polarization Er-Doped Fibre Ring-Laser with 1.4 kHz Linewidth", Electron. Lett., *Vol. 26,* p. 2033 (1990).

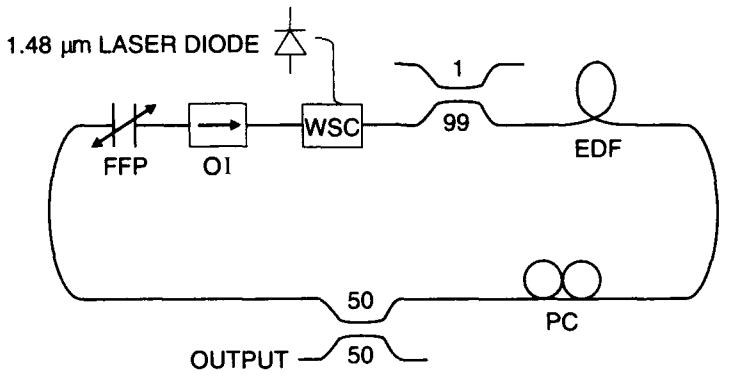


FIGURE 1 Tunable, diode pumped fiber laser. FFP: fiber Fabry-Perot etalon. OI: optical isolator. WSC: wavelength selective coupler. EDF: erbium-doped fiber. PC: polarization controller.

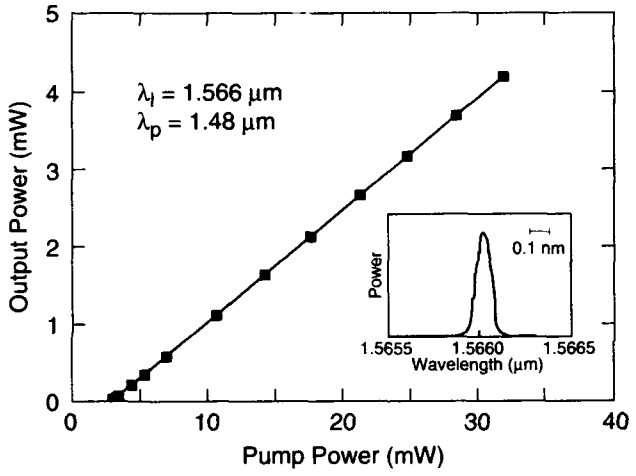


FIGURE 2 Pump power versus laser output power. Inset shows laser line measured with 0.1 nm resolution.

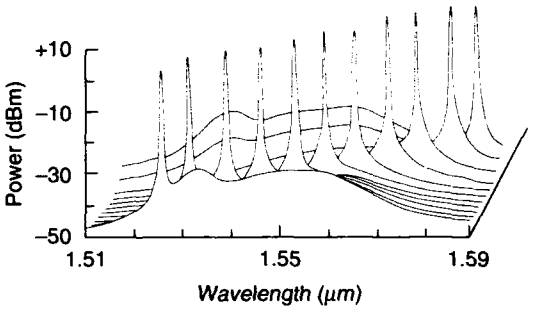


FIGURE 3 Output spectra for laser wavelengths between 1.526μm and 1.584 μm. Measurement resolution is 0.5 nm.

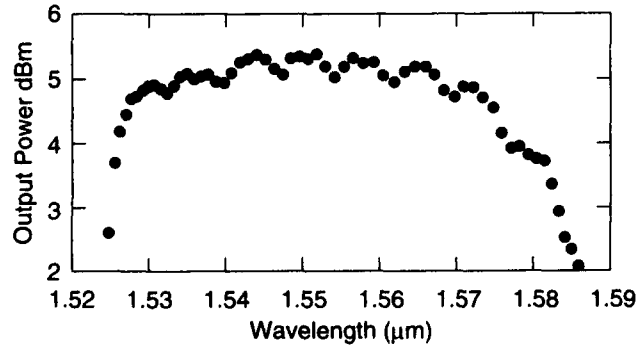


FIGURE 4 Laser output power versus wavelength.

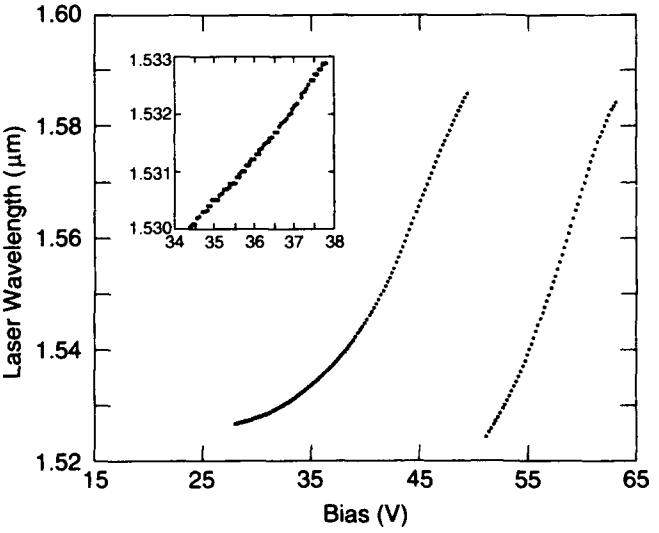


FIGURE 5 Laser wavelength versus FFP bias. Inset shows detail of first order tuning near 1.531 μm.

# Widely Tunable Actively Modelocked Erbium Fibre Ring Laser



by

Th. Pfeiffer, H. Schmuck
SEL Alcatel Research Centre
Lorenzstrasse 10
D-7000 Stuttgart 40, FRG

## INTRODUCTION

Erbium fibre lasers offer a large variety of features such as large tuning range /1/, high output power /1/, modelocking at repetition rates beyond 10 GHz /2/, Q-switching /3/ and single longitudinal mode operation /4/. In this paper we present a 980 nm laser diode pumped erbium-doped fibre ring laser that combines a large tuning range of 33 nm with picosecond pulse generation by active modelocking at repetition rates up to 6 GHz.

## EXPERIMENTAL

The active element in the ring cavity (fig. 1) was an $Al^{3+}$-codoped $Er^{3+}$-doped silica fibre with $\Delta n = 30 \cdot 10^{-3}$, core diameter of 2.3 µm and length of 30 m. It was pumped by 10 mW optical power at 980 nm provided by a semiconductor laser diode. Travelling wave operation of the ring laser was accomplished by the introduction of a polarization insensitive optical isolator with an isolation of better than -60 dB. Part of the optical power (22 %) in the ring was coupled out via an asymmetric fused fibre coupler. The tuning element was a fibre-pigtailed GRIN lens Fabry-Perot filter /5/. The lens facets were coated by a high reflection coating with R = 95.6 % around 1.55 µm. The free spectral range was adjusted to be FSR = 75 nm, the filter finesse was F = 62. The total insertion loss of the filter was less than -3 dB. Active modelocking in the ring laser cavity has been performed by periodical loss modulation using

a $LiNbO_3$ electro-optic amplitude modulator. It was driven by an electrical bipolar square wave signal with 16 V peak-to-peak voltage. This resulted in a repetition rate of the optical pulses of twice the electrical driving frequency. Limited by the bandwidth of the electro-optic modulator (3 GHz) the repetition rate could be varied up to 6 GHz. Both before the optical isolator and before the electro-optic modulator manual polarization controllers were introduced in order to adjust the state of polarization for good modelocking and continous wavelength tuning /6/. The free spectral range of the ring cavity was 4.7 MHz, corresponding to a round trip time of 213 ns. The total loss including all optical elements, splices and output coupling was estimated to be -15.9 dB. The output signals were analyzed by means of a 10 GHz PIN diode/20 GHz sampling oscilloscope/electrical spectrum analyzer system and by an optical spectrum analyzer, respectively.

## RESULTS

When the ring laser is operated continuous wave the output power varies between -12.8 dBm and -9.8 dBm in the wavelength range 1529.7-1563.2 nm (fig. 2). The power minima fall into a small window between 1539-1545 nm and are due to non-optimized gain saturation in this wavelength range. When the electro-optic amplitude modulator is switched on, pulsed operation is achieved (at 2.2 GHz in fig. 2) within 1529.0-1562.1 nm with less than 6 dB variation of average output power. The determination of the pulsewidth was limited by the bandwidth of the PIN diode (10 GHz) sampling oscilloscope (20 GHz) detection system. The detected pulsewidth was always less than 60 ps (fig. 3a). Spectral measurements using a grating monochromator (resolution 0.1 nm) showed a 3 dB-bandwidth of 0.13-0.14 nm (fig. 3b). Scanning Fabry-Perot measurements revealed a line spectrum with 2.2 GHz spacing and an envelope of 14.3 GHz width. Assuming a time bandwidth product of 0.315 for $sech^2$-shaped pulses this corresponds to an optical pulse width of $\geq$ 22 ps. While tuning the emission wavelength of the laser from 1529 nm to 1562 nm, the modulation frequency of the amplitude modulator had to be increased by 261 kHz (fig. 4) to achieve good modelocking. With this fine frequency tuning the pulses became more stable, the amplitude was increased and the optical spectrum was broadened to 0.13-0.14 nm. The relative frequency

tuning rate was $7.1 \cdot 10^{-6}$/nm. The same relative tuning rate ($7.2 \cdot 10^{-6}$/nm) was measured with a shorter $Er^{3+}$ doped fibre (22.5 m) at a modulation frequency of 231.1 MHz. It is assumed that this effect is due to the combined dispersion properties of the different elements in the ring cavity, such as filter, modulator and amplifier fibre. This will be investigated in more detail in the next future. It was possible to increase the modelocking rate of the optical pulses up to 6 GHz. This was the upper limit set by the modulator, but it has already been shown at a fixed wavelength that modulation rates up to 30 GHz are possible /2/.

We would like to thank R. Rossberg for preparing low-loss fibre splices.

REFERENCES

/1/ K. Smith et al.: Electr. Lett. 26, 1149-151 (1990)

/2/ A. Takada et al.: Electr. Lett. 26, 216-217 (1990)

/3/ R. J. Mears et al.: Electr. Lett. 22, 159-160 (1986)

/4/ K. Iwatsuki et al.: Electr. Lett. 26, 2033-2035 (1990)

/5/ H. Schmuck, G. Veith: Proc. 16th ECOC, Amsterdam 1990, Vol. 1, 585-588

/6/ M.W. Maeda et al.: Phot. Techn. Lett. 2, 787-789 (1990)

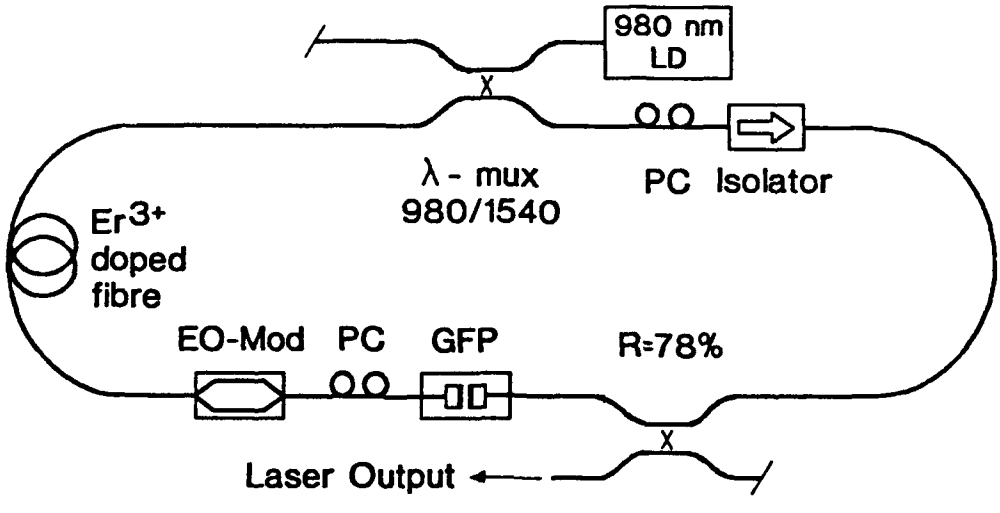


Fig. 1 Set-up of erbium doped fibre ring laser
(PC: manual polarization controller, GFP: GRIN lens Fabry-Perot filter)

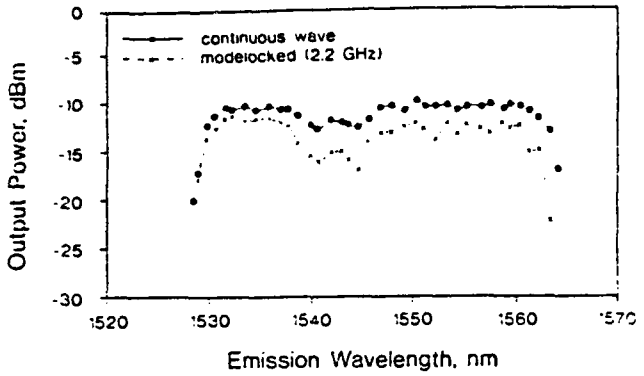


Fig. 2 Tuning curve of erbium ring laser.

(dots) continous wave,
(crosses) modelocked (2.2 GHz)

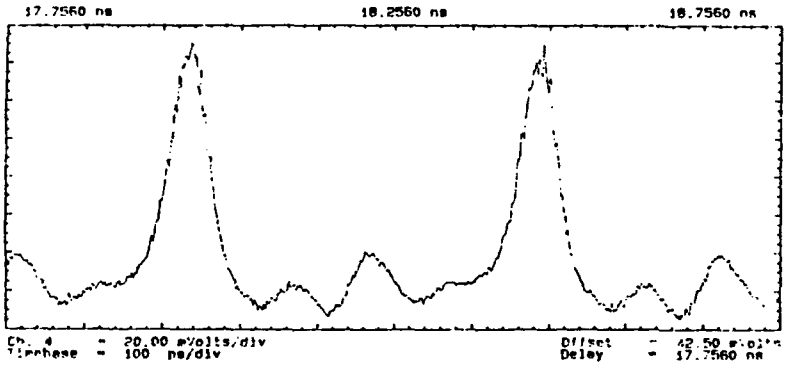


a)

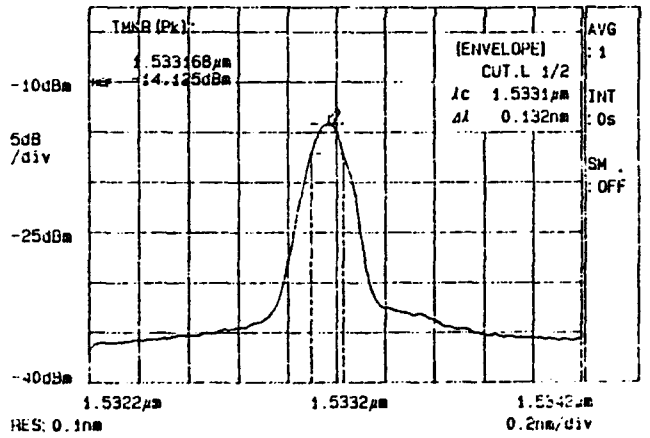


b)

Fig. 3 Output pulses at 1533 nm (a) and spectrum (b). Repetitionrate 2.2 GHz.

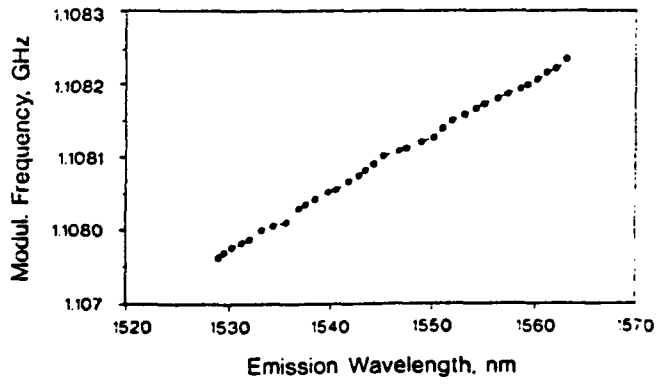


Fig. 4 Variation of modulation frequency with emission wavelength.

# Femtosecond Soliton Collapse by Frequency Modulation Instability in Erbium-Doped Fiber Amplifiers

**I.R. Gabitov**

*L.D. Landau Institute for Theoretical Physics, Kosygina 2, 117334 Moscow, USSR*

**M. Romagnoli, and S. Wabnitz**

*Fondazione Ugo Bordoni, Via B. Castiglione 59, 00142 Rome, Italy*

## 1. INTRODUCTION

Recent experiments [1-3] have reported the amplification of femtosecond solitons in erbium doped optical fibers. Whenever the spectral width of the soliton is as wide as the linewidth of the amplifier, the gain that is seen by the pulse is reduced with respect to that of a weak continuous wave signal. However, it has been observed that the pulse width remains virtually unchanged, at least over some initial stage of the amplification process. Physically, this is due to the fact that the pulse shape is determined by two competing effects. From one side, the amplified pulse tends to remain a soliton and therefore to compress its time width. On the other hand, the finite spectral width of the gain leads to preferential amplification of the central part of the pulse spectrum and this would lead to pulse broadening. If these two effects balance each other, the output pulse width may remain almost undistorted. This compensation is however an unstable phenomenon.

In fact, in ref.[3] it was observed that an initial stage of undistorted soliton pulse amplification may be followed by a relatively sudden temporal compression, that is accompanied by substantial spectral reshaping. We will show here that this pulse collapse phenomenon is activated by a frequency modulation instability. In fact, the finite phase memory of the amplifier introduces a temporal asymmetry, where the leading edge of the pulse is sharper than its tail. This in turn leads, through self-phase modulation, to a frequency modulation along the pulse profile that breaks the uniformity of the soliton phase. As we shall see, the consequence of this instability is the generation of a train of ultrashort pulses of different amplitudes. In the presence of Raman self-scattering [6-7], the leading pulse of the train is subject to the largest self-frequency shift. After multiple collisions, a single compressed and amplified soliton may emerge from the fiber.

## 2. THEORY

Soliton propagation in the presence of finite bandwidth gain may be studied by introducing linear gain and gain dispersion in the nonlinear Schrödinger (NLS) equation [3-4]. This description is only valid in the case where the spectral width of the pulse is much narrower than the amplifier bandwidth [5]. This condition is clearly not satisfied for pulsewidths of 200 fs or shorter [1-3]. Moreover, the observed soliton instability leads to compression of the soliton down to 50 fs. Therefore the coherent interaction between field and atoms must be taken into account, as well as the presence of self-stimulated Raman scattering in the fiber [6-7].

The coupled equations for the single mode electric field $E$ in the fiber and the polarization $P$ and population inversion $W$ of the homogeneously broadened system of two-level atoms in the active fiber read, in dimensionless units,

$$\begin{aligned}\frac{\partial E}{\partial z}+\frac{i\beta''}{2}\frac{\partial^2 E}{\partial t^2} &= iR\left(\rho|E|^2+(1-\rho)\int_{-\infty}^{t}|E(\tau)|^2 f(t-\tau)d\tau\right)E+P \\ \frac{\partial P}{\partial t} &= \frac{P}{T_2}+EW \\ \frac{\partial W}{\partial t} &= -\frac{1}{2}(PE^*+EP^*)\,.\end{aligned} \tag{1}$$

where $1-\rho \simeq 0.2$ is the fractional Raman contribution to the nonlinear index [6-7], $R$ is the self-phase modulation (SPM) coefficient, and $\beta''$ is the group velocity dispersion (GVD). Furthermore, $f(t)$ is the Raman response function of silica [6-7], and $T_2$ is the dephasing time of the atomic polarization.

## 3. RESULTS

In the numerical simulations, we chose the following input boundary conditions

$$\begin{aligned}&E(z=0,x,t)=A_0\sqrt{\beta/R}sech(t)\\ &P(z,t=-T)=0, W(z,t=-T)=1,\end{aligned} \tag{2}$$

where $T$ is half of the computational temporal window. Note that for $A_0=1$ one has at the input a $N=1$ soliton of the NLS equation. Figures (1-2) show the calculated pulses and spectra whenever the experimental values of ref.[3] are considered. The fiber dispersion was set equal to $D=-5ps/nm\cdot km$, and the input pulse width at half maximum was $\tau_0=250fs$. We considered a spectral width of the amplified spontaneous emission line of erbium at $\lambda=1.55\mu m$ of $10nm$, which leads, in real units, to $T_2\simeq 250fs$. The doping concentration was $N=5\times 10^{18}cm^{-3}$, whereas the erbium dipole moment is $\wp=2.5\times 10^{-20}esu$.

Figure (1) shows the output pulse profile after 1.5 and 3 m of erbium doped amplifier, for a linear gain of 4.2 dB/m and with $A_0=1.4$. As can be seen, in the frequency domain the signature of soliton collapse is the appearence of three spectral peaks. The central frequency peak is associated with the long tail of the pulse and increases when $T_2$ grows larger, whereas the two sidebands originate from the frequency modulated narrow pulse.

Figure (2) shows the effects of Raman self-scattering: here the fiber length is 6m and the gain is 7 dB/m. The top figure has been calculated without the Raman term in eqs.(1), whereas in the lower figure the Raman effect is included. In the absence of the Raman effect, a train of pulses is generated. These are not independent solitons: rather, the train may be thought as a chain of infinitely many coupled solitons, in analogy with the self-similar pulse trains that are generated by a two-level amplifier in the absence of GVD and SPM. As can be seen, owing to the Raman effect the leading pulse of the train has gained energy from the multiple collisions with the other pulses and eventually it separates from the broken-up background because of the slowing down due to soliton self-frequency shift.

## 4. CONCLUSIONS

We have shown that the recently observed femtosecond soliton compression and soliton train generation phenomena in erbium doped fiber amplifiers result from the interplay between nonlinearity and dispersion of the composite glass/two-level system medium.

This work was carried out in the framework of the agreement between Fondazione Ugo Bordoni and the Istituto Superiore Poste e Telecomunicazioni.

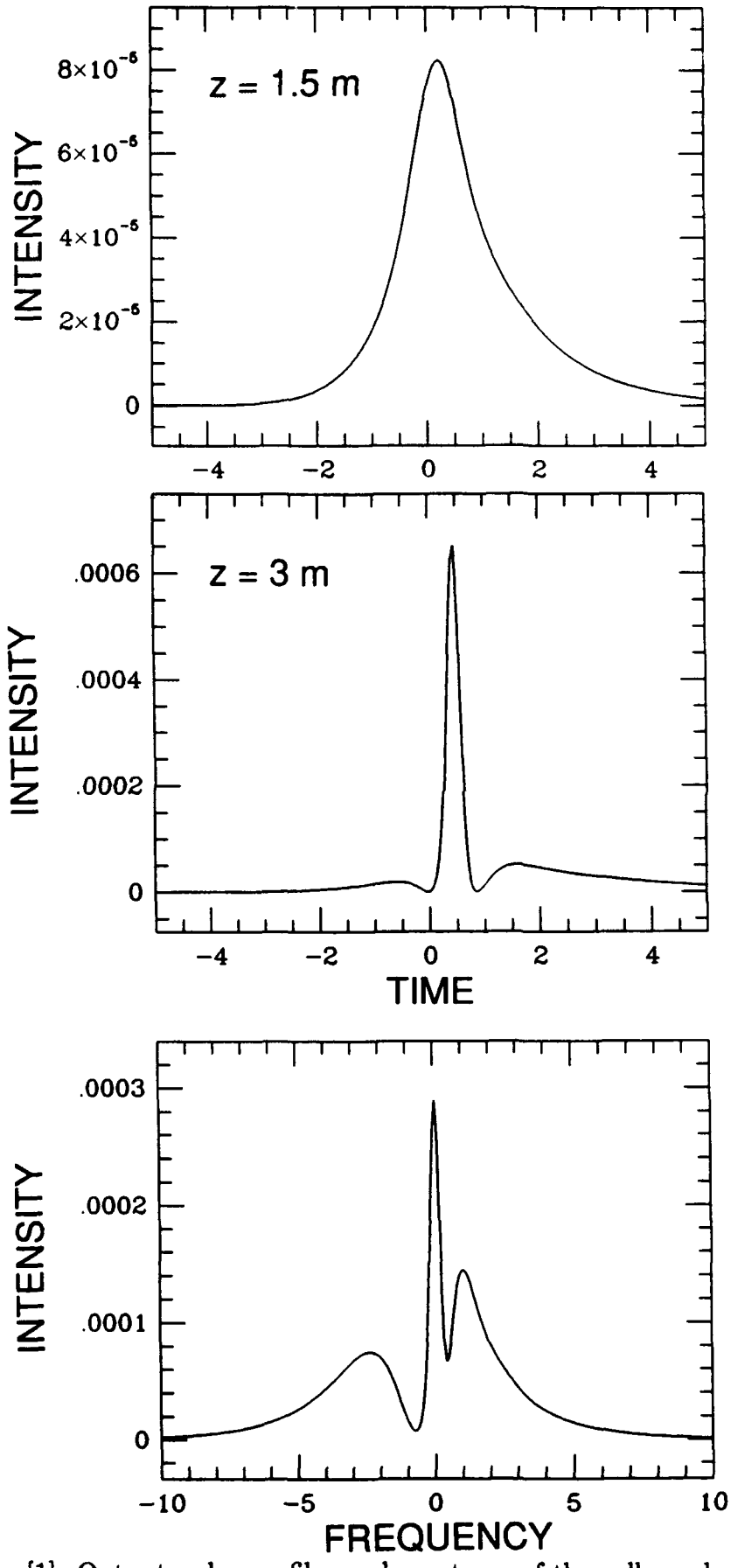


Figure [1]: Output pulse profiles and spectrum of the collapsed pulse.

**REFERENCES**
[1] B.J. Ainslie, K.J. Blow, A.S. Gouveia-Neto, P.G.J. Wigley, A.S.B. Sombra, and J.R. Taylor, Electron. Lett. **26**, 186 (1990).
[2] I.Yu. Khrushchev, A.B. Grudinin, E.M. Dianov, D.V. Korobkin, V.A. Semenov, and A.M. Prokhorov, Electron. Lett. **26**, 456 (1990); A.B. Grudinin, E.M. Dianov, D.V. Korobkin, A.Yu. Makarenko, A.M. Prokhorov, and I.Yu. Khrushchev, JETP Lett. **51**, 135 (1990).
[3] M. Nakazawa, K. Kurokawa, H. Kubota, K. Suzuki, and Y. Kimura, Appl. Phys. Lett. **57**, 653 (1990); M. Nakazawa, K. Kurokawa, H. Kubota, and E. Yamada, Phys. Rev. Lett. **65**, 1881 (1990).
[4] G.P. Agrawal, Opt. Lett. **16**, 226 (1991).
[5] I.V. Mel'nikov, R.F. Nabiev, and A.V. Nazarkin, Opt. Lett. **15**, 1348 (1990).
[6] E.M. Dianov, A.Ya. Karasik, P.B. Mamyshev, A.M. Prokhorov, V.N. Serkin, M.F. Stelmakh, and A.A. Fomichev, JETP Lett **41**, 294 (1985).
[7] F.M. Mitschke, and L.F. Mollenauer, Opt. Lett. **11**, 659 (1986).

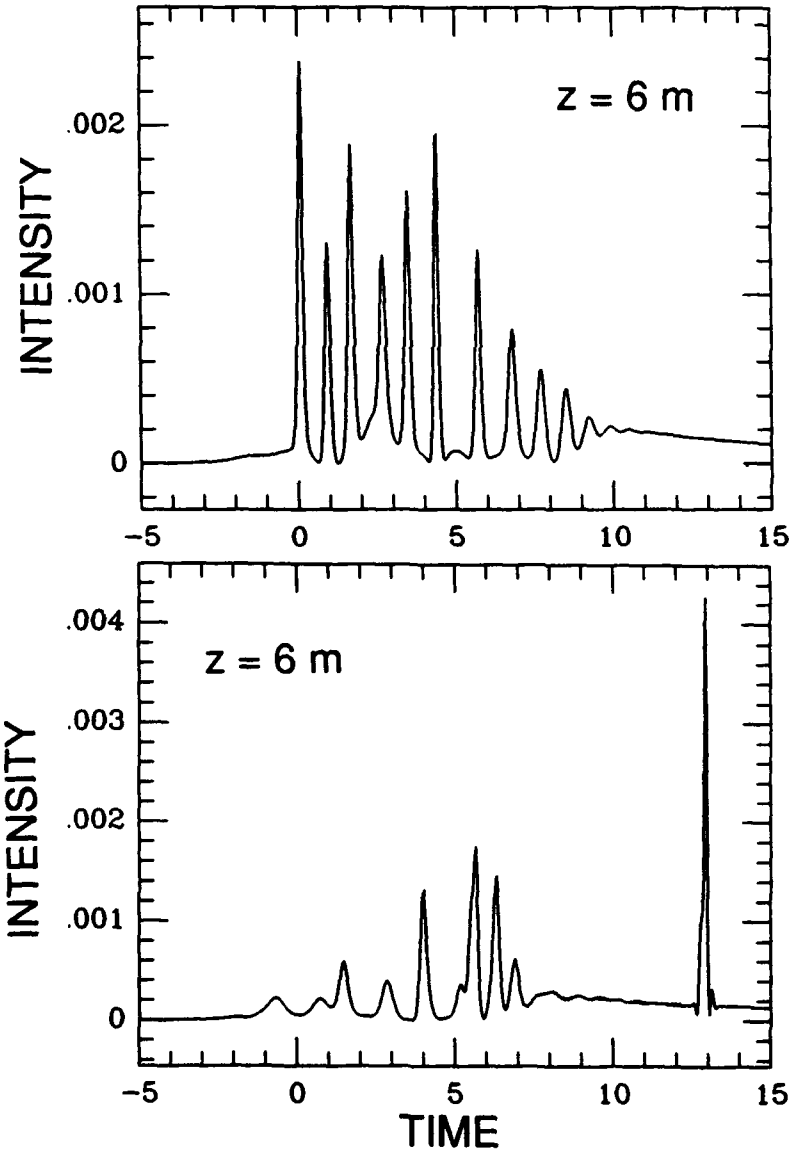


Figure [2]: Output pulses without (top) and with (bottom) Raman effect.

# Carrier Dynamics and Nonlinearities in Semiconductor Amplifiers

**ThC** 1:30pm–2:45pm
Cabaret Room

G. Eisenstein, *Presider*
*Technion–Israel Institute of Technology, Israel*

# Nonlinear Effects in Semiconductor Optical Amplifiers

**Takaaki Mukai and Tadashi Saitoh**

NTT Basic Research Laboratories
Nippon Telegraph and Telephone Corporation
Midori-cho 3-9-11, Musashino-shi, Tokyo 180, Japan

A traveling-wave semiconductor laser amplifier (TWA) [1]-[4] can greatly simplify optical repeaters used in wavelength-division-multiplexed (WDM) systems, since its wide gain bandwidth allows a single TWA to simultaneously amplify signals of different wavelengths. Even though such system performance in the linear gain regime is determined only by amplifier noise properties [5],[6], the onset of nonlinear effects in optical amplifiers result in crosstalk [7].

Nonlinear effects in optical amplifiers have opposite aspects; (1) unfavorable for linear amplification where any nonlinearity impairs the performance and should be avoided, but (2) favorable for highly efficient nonlinear operation [8],[9] due to a large optical gain compared with passive/absorptive nonlinear materials. Two significant nonlinear effects are signal gain saturation [10] occurring for a large input signal and nearly degenerate four-wave mixing (NDFWM) [11],[12] occurring for multifrequency input signals, as summarized in Fig. 1 [13]. The dominant nonlinearity in the semiconductor laser amplifiers (SLAs) results from changes in the injected-carrier density as a result of signal amplification. Signal gain saturation arises from the reduction in DC carrier component $\Delta n_{dc}$, while the NDFWM is attributed to the generation of a carrier beat component $\Delta n_{\Omega}$ at the beat frequency $\Omega$.

Signal gain decreases with an increase in amplified signal output due to the reduction of injected carrier density from the unsaturated gain level through stimulated emission. Signal gain is suppressed by 4.34 dB from the unsaturated value when the output signal power $P_{out}$ is equal to the saturation power $P_{sat}$ [4]. Changes in the carrier density not only change the gain of an amplifier but also change the amplifier refractive index due to the $\alpha$-parameter, resulting in shifts in the phase of the Fabry-Perot (FP) ripple in the amplifier gain spectrum. The effect of FP resonance peak shift becomes significant in uncoated FP amplifiers, which can be utilized for bistable optical gates [14]-[16].

Since the amplifier gain is homogeneously broadened [17], in multichannel amplification systems the saturation of the amplifier gain by any one channel reduces the gain for all channels. In amplitude-modulated WDM systems, this saturation causes crosstalk between channels regardless of the amount of channel separation [18]-[20]. This saturation-induced (SI) crosstalk can be partially reduced by using an electronic feedforward linearization method which maintains a constant carrier density [21].

In the case of high-energy pulse amplification, signal gain saturation also causes pulse waveform distortion simply because the leading pulse edge saturates the amplifier and reduces the gain available for the trailing edge. The pulse duration variation depends on the input pulse shape, *i.e.*, a Gaussian pulse is broadened by amplification, while a rectangular pulse is compressed [22]-[24]. The pulse waveform distortion is accompanied by the self phase modulation occurring as a result of the SI refractive index change. The instantaneous

frequency of the amplified pulse is down-shifted. The chirped pulse can be compressed by a factor of $\sim 2$ if it is passed through a dispersive delay line (*e.g.* fiber) having anomalous dispersion [25].

Nearly degenerate four-wave mixing (NDFWM) [9],[26]-[30] is a different kind of nonlinear effect occurring for multifrequency CW input signals when the frequency separation between two signal channels is reduced to the reciprocal of the carrier lifetime ($\sim$ GHz). The physical mechanism behind NDFWM is carrier density modulation $\Delta n_\Omega$ induced at the beat frequency between two incident light waves. This carrier density modulation generates two new light waves, which are frequency shifted from the two input waves by the beat frequency. The NDFWM also causes intermodulation distortion (IMD) in closely spaced FDM systems [11],[12],[31]-[36]. Operation of a TWA well below $P_{sat}$ as well as enough channel-spacing more than a few GHz is required to prevent signal degradation from the IMD [33].

In contrast to the crosstalk point of view, this new frequency generation due to efficient NDFWM interaction [9] is attractive for other applications. Optical frequency exchange between two frequency channels [37], and wideband optical frequency conversion with a 1.5 THz conversion range by introducing a second pump wave at a desired frequency within the amplifier bandwidth [38],[39], have been demonstrated.

Since saturation recovery time of Er-doped fiber amplifiers (EDFAs) is extremely slow ($\sim$ 10 milliseconds) compared with that of SLAs, any kind of nonlinearity in EDFAs ceases to be a problem for high speed signals. However, SLAs still have an important role to play as they possess new functions based on the efficient nonlinear effects and can be integrated to form functional components.

## References


[1] T. Saitoh and T. Mukai, "1.5 $\mu$m GaInAsP traveling-wave semiconductor laser amplifier," IEEE J. Quantum Electron., **QE-23**, 6, 1010-1020 (1987).

[2] J. C. Simon "GaInAsP semiconductor laser amplifiers for single-mode fiber communications," IEEE J. Lightwave Technol., **LT-5**, 9, 1286-1295 (1987).

[3] M. J. O'Mahony, "Semiconductor laser optical amplifiers for use in future fiber systems," IEEE J. Lightwave Technol., **6**, 4, 531-544 (1988).

[4] T. Saitoh and T. Mukai, "Traveling-Wave Semiconductor Laser Amplifiers," in *"Coherence, Amplification, and Quantum Effects in Semiconductor Lasers,"* (Y. Yamamoto, ed.), John Wiley & Sons, New York, pp. 257-322 (1991).

[5] T. Mukai, Y. Yamamoto and T. Kimura, "S/N and error rate performance in AlGaAs semiconductor laser preamplifier and linear repeater systems," IEEE J. Quantum Electron., **QE-18**, 10, 1560-1568 (1982).

[6] N. A. Olsson, "Lightwave system with optical amplifiers," IEEE J. Lightwave Technol., **7**, 7, 1071-1082 (1989).

[7] R. M. Jopson and T. E. Darcie, "Semiconductor Laser Amplifiers in High-Bit-Rate and Wavelength-Division-Multiplexed Optical Communication Systems," in *"Coherence, Amplification, and Quantum Effects in Semiconductor Lasers,"* (Y. Yamamoto, ed.), John Wiley & Sons, New York, pp. 323-366 (1991).

[8] M. J. Adams, H. J. Westlake, M. J. O'Mahony, and I. D. Henning,"A comparison of active and passive optical bistability in semiconductors", IEEE J. Quantum Electron., **QE-21**, 9, 1498-1504 (1985).

[9] T. Mukai and T. Saitoh, "Detuning characteristics and conversion efficiency of nearly degenerate four-wave mixing in a 1.5 $\mu$m traveling-wave semiconductor laser amplifier," IEEE J. Quantum Electron., **QE-26**, 5, 865-875 (1990).

[10] T. Mukai, Y. Yamamoto and T. Kimura, "Optical Amplification by Semiconductor Lasers," in *"Semiconductors and Semimetals,"* (R. K. Willardson and A. C. Beer, eds.), Academic Press, New York, vol. 22-E, pp. 265-319 (1985).

[11] G. P. Agrawal, "Amplifier-induced crosstalk in multi-channel coherent lightwave systems", Electron. Lett., **23**, 22, 1175-1177 (1987).

[12] K. Inoue, "Observation of crosstalk due to four-wave mixing in a laser amplifier for FDM transmission," Electron. Lett., **23**, 24, 1293-1295 (1987).

[13] T. Mukai and T. Saitoh,"Nonlinear phenomena in traveling-wave semiconductor laser amplifiers," Trans. IEICE, **E73**, 1, 46-52 (1990).

[14] K. Otsuka and S. Kobayashi, "Optical bistability and nonlinear resonance in a resonant-type semiconductor laser amplifier", Electron. Lett., **19**, 7, 262-263 (1983).

[15] W. F. Sharfin and M. Dagenais, "Femtojoule optical switching in nonlinear semiconductor laser amplifiers", Appl. Phys. Lett., **48**, 5, 321-322 (1986).

[16] K. Inoue, "High-speed all-optical gate switching experiment in a Fabry-Perot semiconductor laser amplifier," Electron. Lett., **23**, 18, 921-922 (1987).

[17] T. Mukai, K. Inoue and T. Saitoh, "Homogeneous gain saturation in 1.5$\mu$m InGaAsP traveling-wave semiconductor laser amplifiers," Appl. Phys. Lett., **51**, 6, 381-383 (1987).

[18] G. Großkopf, R. Ludwig and H. G. Weber, "Crosstalk in optical amplifiers for two-channel transmission," Electron. Lett., **22**, 17, 900-902 (1986).

[19] T. Mukai, K. Inoue and T. Saitoh, "Signal gain saturation in two-channel common amplification using a 1.5 $\mu$m InGaAsP travelling-wave laser amplifier," Electron. Lett., **23**, 8, 396-397 (1987).

[20] M. G. Öberg and N. A. Olsson, "Crosstalk between intensity-modulated wavelength-division multiplexed signals in a semiconductor laser amplifier," IEEE J. Quantum Electron., **QE-24**, 1, 52-59 (1988).

[21] T. E. Darcie, R. M. Jopson and A. A. M. Saleh, "Electronic compensation of saturation-induced cross-talk in optical amplifiers," Electron. Lett. **24**, 18, 1154-1156 (1988).

[22] I. W. Marshall and D. M. Spirit, "Observation of large pulse compression by a saturated travelling wave semiconductor laser amplifier," in Tech. Digest CLEO'88, Anaheim, CA, April 1988, paper: TuM64.

[23] A. J. Lowery, "Pulse compression mechanisms in semiconductor laser amplifiers," IEE Proc., **136-J**, 3, 141-146 (1989).

[24] T. Saitoh and T. Mukai, "Gain saturation characteristics of traveling-wave semiconductor laser amplifiers in short optical pulse amplification," IEEE J. Quantum Electron., **26**, 12, 2086-2094 (1990).

[25] G. P. Agrawal and N. A. Olsson, "Self-phase modulation and spectral broadening of optical pulses in semiconductor laser amplifiers," IEEE J. Quantum Electron., **25**, 11, 2297-2306 (1989).

[26] H. Nakajima and R. Frey, "Collinear nearly degenerate four-wave mixing in intracavity amplifying media", IEEE J. Quantum Electron., **QE-22**, 8, 1349-1354, (1986).

[27] K. Inoue, T. Mukai and T. Saitoh, "Nearly degenerate four-wave mixing in a traveling-wave semiconductor laser amplifier," Appl. Phys. Lett., **51**, 14, 1051-1053 (1987).

[28] G. Großkopf, R. Ludwig, R. G. Waarts and H. G. Weber, "Four-wave mixing in a semiconductor laser amplifier," Electron. Lett., **24**, 1, 31-32 (1988).

[29] G. P. Agrawal,"Population pulsations and nondegenerate four-wave mixing in semiconductor lasers and amplifiers," J. Opt. Soc. Amer. B, **5**, 1, 147-159 (1988).

[30] F. Favre, D. Le Guen, J. C. Simon, and P. Doussiere, "Four-wave mixing in traveling-wave semiconductor laser amplifier", Electron. Lett., **25**, 4, 272-273 (1989).

[31] T. E. Darcie, R. M. Jopson and R. W. Tkach, "Intermodulation distortion in optical amplifiers from carrier-density modulation," Electron. Lett., **23**, 25, 1392-1394 (1987).

[32] R. M. Jopson, T. E. Darcie, K. T. Gayliard, R. T. Ku, R. E. Tench, T. C. Rice and N. A. Olsson, "Measurement of carrier-density mediated intermodulation distortion in an optical amplifier," Electron. Lett., **23**, 25, 1394-1395 (1987).

[33] T. E. Darcie and R. M. Jopson, "Nonlinear interactions in optical amplifiers for multifrequency lightwave systems," Electron. Lett., **24**, 10, 638-640 (1988).

[34] R. M. Jopson and T. E. Darcie, "Calculation of multicarrier intermodulation distortion in semiconductor optical amplifiers," Electron. Lett., **24**, 22, 1372-1374 (1988).

[35] T. G. Hodgkinson and R. P. Webb, "Application of communication theory to analyze carrier density modulation effects in traveling-wave semiconductor laser amplifiers," Electron. Lett., **24**, 25, 1550-1552 (1988).

[36] R. P. Webb and T. G. Hodgkinson, "Experimental confirmation of laser amplifier intermodulation model", Electron. Lett., **25**, 8, 491-493 (1989).

[37] K. Inoue, "Optical frequency exchange utilizing LD amplifiers and Mach-Zehnder filters," Electron. Lett., **25**, 10, 630-632 (1989).

[38] G. Großkopf, R. Ludwig and H. G. Weber, "140 Mbit/s DPSK transmission using an all-optical frequency converter with a 4000 GHz conversion range," Electron. Lett., **24**, 17, 1106-1107 (1988).

[39] G. Großkopf, L. Küller, R. Ludwig, R. Schnabel and H. G. Weber, "Semiconductor laser optical amplifiers in switching and distribution networks," Opt. Quantum Electron., **21**, S59-S74 (1989).

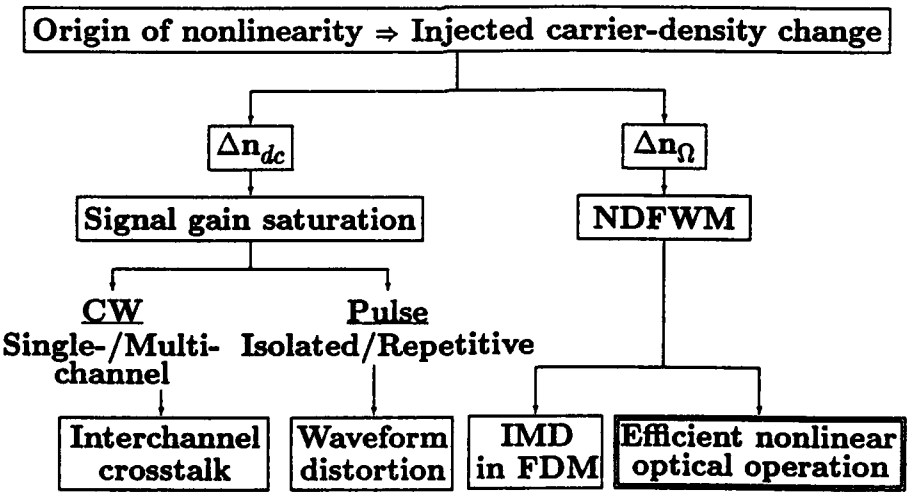


Fig. 1 Nonlinear effects in semiconductor optical amplifiers.

# Characterization of high bit rate phase modulators based on semiconductor optical amplifiers

T.N. Nielsen, U. Gliese, B. Mikkelsen and K.E. Stubkjaer
Center for Broadband Telecommunications, Electromagnetics Institute
Technical University of Denmark, Building 348, DK-2800 Lyngby, Denmark

B. Fernier, P. Doussiere and J-L. Lafragette
Alcatel Alsthom Recherche, F-91460 Marcoussis, France

**Abstract**

Optical phase modulation with a semiconductor optical amplifier is investigated. By equalizing the phase response, the 3 dB bandwidth is extended from 600 MHz to 2.5 GHz.

## Introduction

Various experiments have demonstrated the feasibility of using semiconductor optical amplifiers (SOA's) as optical phase modulators in coherent optical communication systems [1]-[4]. Compared to traditional phase modulators (e.g. $LiNbO_3$ phase modulators) the SOA provides the advantages of gain and fairly low modulation power requirements.

For performance optimization it is important to know how the different parameters of the SOA influence the phase modulation properties. Therefore, a numerical model of the SOA is developed to calculate both amplitude and bandwidth of the phase and amplitude responses under various driving conditions. To establish the accuracy of the model, the phase and amplitude responses are measured. The major drawback of using SOAs as optical phase modulators is the limited modulation bandwidth. It is determined by the carrier lifetime and is normally less than 600 MHz [1]-[4]. Here it is, however, demonstrated that the SOA can be used as phase modulator at up to 2.5 Gbit/s by equalizing the phase response.

## Numerical amplifier model

The model used for the calculations is based on a transmission line description of the SOA [6]. For precise modelling of the longitudinal electron distribution the SOA is divided into sections. The phase and amplitude modulation is then calculated from the phase and amplitude difference between the optical input and output electrical fields of the SOA, where the electrical field at the output facet is calculated from a recursive expression given by:

$$A(t) = \sqrt{G_{\Delta L}} \cdot e^{-j\phi} \cdot \left[1 + 2j\Gamma A_\omega \cdot (\omega - \omega_p(N))\,\Delta L \frac{\partial}{\partial t}\right] \cdot A^0(t-\tau) \quad (1)$$

$$\phi = \frac{\Delta L}{c} \cdot \left[\omega_r n_r + n_g \cdot (\omega - \omega_r) + \omega_r \Gamma \cdot (N - N_r)\frac{\partial n}{\partial N}\right] \quad (2)$$

$G_{\Delta L}$ is the single pass gain in one section, $\phi$ the phase of the field, $\Gamma$ the confinement factor, $A_\omega$ a gain constant and $\omega$ is the angular frequency of the light, while $\omega_p$ is the angular frequency corresponding to the gain peak wavelength. $N$ is the carrier concentration, $\Delta L$ the length of one section and $\tau$ is the corresponding transit time. $c$ is the light velocity in vacuum, $n_g$ the group index and $n$ the refractive index. The indices $r$ designates reference values of the variables. Furthermore,

$A^0$ is the electric field at the beginning of each section and is calculated using (1) and (2) on the preceding section. Finally, $N$ is calculated using the rate equations with a detailed model of the recombination rate [7].

## Phase and amplitude response

To estimate the performance of the phase modulator, the numerical model is used to calculate the phase and amplitude responses of the SOA. Subsequently, measurements using both a Fabry-Perot and a self heterodyne measurement setup [8] is performed to verify the validity of the calculations.

The SOA investigated here is a 400 $\mu$m long BH-type amplifier with an active layer thickness of 0.4 $\mu$m and a width less than 1 $\mu$m [5]. For reference the gain peak is at 1532 nm for a bias current of 85 mA and the lasing threshold after AR-coating is 110 mA.

When using the SOA as external modulator there is a trade off between amplitude and bandwidth of the phase response. This is seen from Fig. 1 where the calculated and measured phase response is shown for three different values of output power level at 1530 nm wavelength. In trace A and B the SOA is biased at 70 and 85 mA, respectively, while the input power level (in the fibre) is -15 dBm. In trace C the SOA is biased at 85 mA and the input power level is -7 dBm. The modulation bandwidth of the SOA is determined by the effective carrier lifetime and can, as calculations and measurements show (c.f. Fig. 1 and 2), be increased by using higher bias current or by saturating the SOA. As the SOA is driven into saturation the number of stimulated recombinations is increasing and hence the effective carrier lifetime is decreasing with the result of a higher modulation bandwidth. As seen, the highest bandwidth (600 MHz) is achieved when the SOA is saturated and also provides the highest output power level (3 dBm). Since the SOA will be placed directly after a laser in a real system, high input power levels are easily obtained.

The measured and calculated amplitude responses corresponding to trace A and B of the phase response are depicted in Fig. 2. The bandwidth of the amplitude response is seen to be equal to the bandwidth obtained for the phase response. This indicates that the linewidth enhancement factor $\alpha$, giving the ratio between the phase and amplitude modulation [8], is independent of the modulation frequency. The ratio between the measured phase and amplitude response indicates an $\alpha$ of approximately 6. Furthermore, $\alpha$ is found to increase with increasing wavelength.

From Fig. 1 and 2 it is seen that there is good agreement between the calculated and measured phase and amplitude responses. This has great importance since the model then can be used to

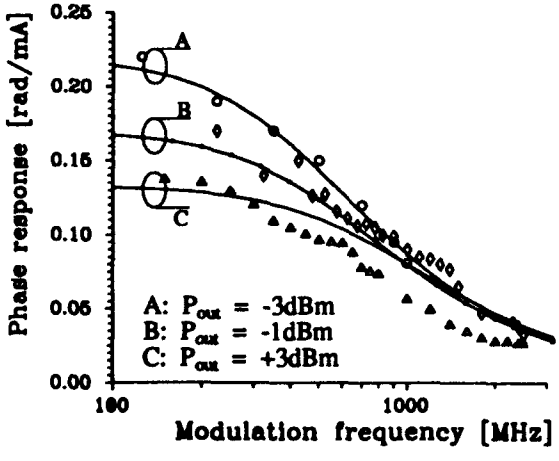


Figure 1: Phase response.

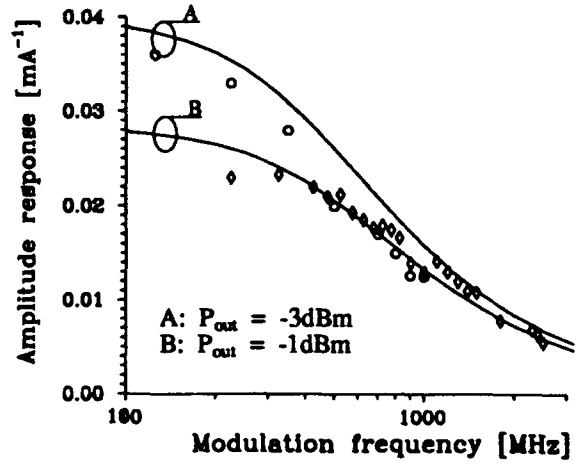


Figure 2: Amplitude response.

investigate how the different SOA parameters influence the performance of the phase modulator.

Finally, it should be noted that the amplitude response is measured using the self heterodyne measurement setup only. This is due to the fact that the phase and amplitude modulation are found to be in quadrature, which means that the amplitude modulation can not be estimated from the spectrum recorded by the Fabry-Perot interferometer even though the amplitude modulation is quite large. This is seen from Fig. 3 where the power spectra obtained at a modulation frequency of 400 MHz is shown. If the phase and amplitude modulation were not in quadrature, the symmetrical spectrum would indicate a very low amount of amplitude modulation and thereby a linewidth enhancement factor $\alpha$ greater than 40, which is not a realistic value for ordinary SOA structures.

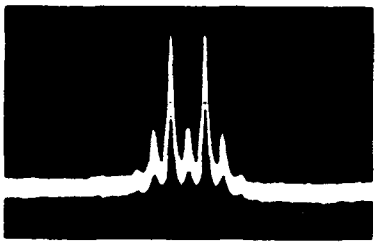

Figure 3: Power spectrum.

## High bit rate performance

In order to improve the modulation bandwidth and thus making PSK modulation above 900 Mbit/s possible, a passive equalizer has been designed and implemented (c.f. Fig. 4). In Fig. 5 the measured values of the modulation power required to obtain the PSK phase shift of $\pi$ radians are depicted for a wavelength of 1552 nm. This high wavelength was chosen to obtain a higher value of $\alpha$ (approximately 10). The non-equalized phase response (dotted line) corresponds to trace C in Fig. 1. The equalized phase response (solid line) exhibits a ripple less than 3 dB up to more than 2.5 GHz, and the modulation power requirements indicates a $V_\pi$ of 7 V, which is comparable to reported values for wideband $LiNbO_3$ modulators.

The modulation bandwidth of 2.5 GHz indicates modulation capabilities of up to 3.8 Gbit/s. It is however, only possible to obtain PSK modulation speeds slightly above 2 Gbit/s since the measured time delay variation between the electrical and optical phase modulation is around 300 ps. This is demonstrated in a 2.5 Gbit/s DPSK semi-coherent system experiment where the demodulation is achieved with an optical delay line demodulator [9] and subsequent detection with a direct detection system. The demodulated bit pattern and corresponding 'eye' diagram are shown in Fig. 6 and Fig. 7, respectively.

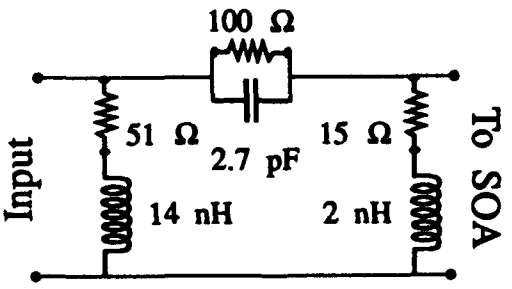


Figure 4: Circuit diagram of the equalizer.

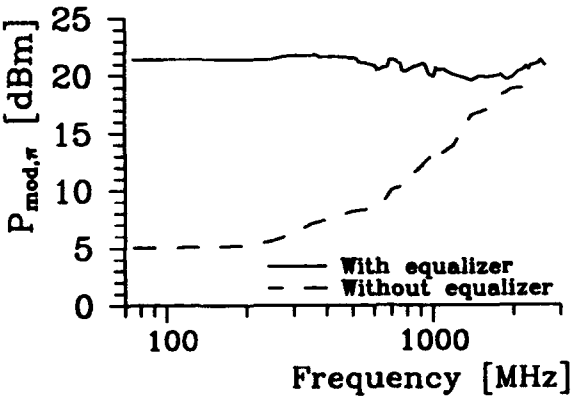


Figure 5: Required modulation power to obtain the PSK phase shift of $\pi$ radians.

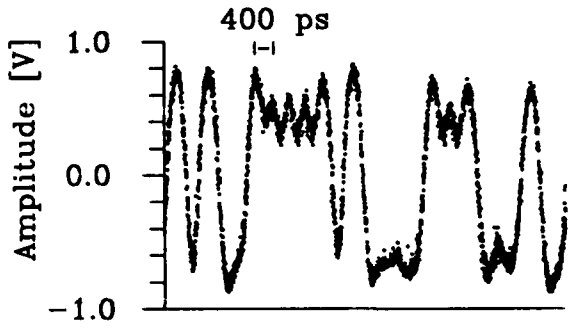


Figure 6: Demodulated bit pattern.

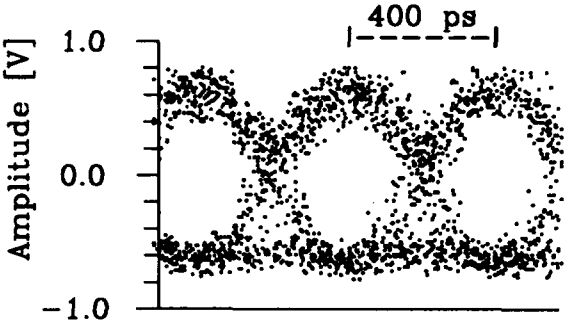


Figure 7: Eye diagram.

The observed ripple between succeeding 'ones' in the demodulated bit pattern is not necessary due to bandwidth limitations in the equalizer/SOA since a DPSK 'one' represents a real phase shift between two succeeding bits. A BER of $10^{-9}$ at a sensitivity of -23.5 dBm is obtained, with the sensitivity being limited by the frontend. The optical output power of the SOA was 3 dBm and the fibre-to-fibre gain 10 dB. To the best of our knowledge, it is the first time that phase modulation at 2.5 Gbit/s has been demonstrated using a SOA as phase modulator. Penalties induced by the inherent amplitude modulation can be substantially reduced using special techniques and is therefore not expected to be a major problem.

## Conclusion

Optical phase modulation using a semiconductor optical amplifier has been investigated theoretically and experimentally. Good agreement has been obtained between calculated and measured results. The phase and amplitude modulation has been observed to have equal shape and to be in quadrature. Furthermore, it has been shown that output power levels of up to 3 dBm is obtainable with a fibre-to-fibre gain of 10 dB. This makes phase modulation by optical amplifiers promising since high output power and gain is not available from traditional $LiNbO_3$ phase modulators. Finally, it has been demonstrated that the SOA can be used as phase modulator at very high bit rates (2.5 Gbit/s) by equalizing the phase response. Since the SOA in addition provides the potential of future optoelectronic integration, it is very promising for use as phase modulator in coherent optical communications systems.

**Acknowledgement:** Part of this work was supported by RACE project 1027.

## References

[1] J. Mellis et al.: Electronics Letters, vol. 25, no. 10, pp. 679-682, 1989.
[2] G. Großkopf et al.: Electronics Letters, vol. 25, no. 17, pp. 1188-1189, 1989.
[3] G. Großkopf et al.: In Proceedings of IOOC, 1989, paper 21B4-2.
[4] D. Hui Bon Hoa et al.: Journal of Ligthwave Technology, vol. 9, no. 2, pp. 266-270, 1991.
[5] B. Mersali et al.: Electronics Letters, vol. 26, no. 2, pp. 124-125, 1990
[6] T. Durhuus et al.: Electronics Letters, vol. 27, no. 4, pp. 310-312, 1991
[7] J. Wang et al.: Journal of Lightwave Technology, vol. LT-5, no. 1, pp.184-189, 1987
[8] N. Storkfelt et al.: Submitted for publication in Photonics Technology Letters, 1991.
[9] R.J.S. Pedersen et al.: Electronics Letters, vol. 25, no. 17, pp. 1108-1109, 1989

# COUPLING BETWEEN BARRIER AND QUANTUM WELL ENERGY STATES IN A MULTIPLE QUANTUM WELL OPTICAL AMPLIFIER

N. Tessler, R. Nagar and G. Eisenstein

Department of Electrical Engineering
Technion — Israel Institute of Technology
Technion City, Haifa 32000, Israel
Tel: +972 -4-294694 Fax: +972 -4-323041

U. Koren and G. Raybon
AT&T Bell Labs.
Holmdel, NJ 07733 U.S.A.

## I. Introduction

Multiple quantum well (MQW) optical amplifiers have recently been demonstrated. It has been shown that these MQW amplifiers have excellent characteristics such as high gain, large saturation power and low noise [1—3]. In addition to being excellent devices, they can serve as convenient tools to study the gain dynamics in an inverted MQW media.

The energy band diagram of a typical 1.5 μm InGaAs/InGaAsP MQW optical amplifier is shown in Fig. 1. When an electrical pump (DC current) is applied to the device, the allowed states of the structure fill up as the quasi Fermi level rises. Since the amplifier never reaches lasing threshold, there is no pinning of the Fermi level which may rise to a level far in the barrier. In that case, the barrier serves as a carrier reservoir [4]. When a strong optical pump is injected at an energy level inside the QW, carriers from higher energies relax to the newly generated empty states. Replenishing of the removed carriers comes first from higher energy levels which are inside the QW (this process has a sub-ps time constant). Then the carriers in the barriers diffuse towards the QW and are captured with a mean time of several ps [4],[5]. And finally, conventional recombination dominated by Auger processes, with time constants of ~250 ps take place in the barrier region [4].

Many dynamical gain processes in an inverted MQW media depend upon the interaction between the carriers in the three dimensional barrier region and the two dimensional QW. Several studies of these processes which use short pulse luminescence and single wavelength pump — probe gain evaluation have been reported [4—6].

Here we report, for the first time, on the use of a broad band static pump-probe technique to study the coupling of barriers and QW states in an InGaAs/InGaAsP MQW amplifier. We study the effect of a pump signal at an energy near the QW gain peak (1.51 μm) on the device gain by probing at various energies and by measuring its broad band amplified spontaneous emission spectrum. The measurements map out the energy (wavelength) dependence of

the interaction between carriers in the barrier and the quantum well and thus yield details of the density of states function in the vicinity of the QW top. As will be shown, the great difference between the relaxation time inside the QW and the barrier to QW capture time, creates a dip in the carrier distribution near the top of the QW.

## II. Experimental Set Up

The experimental schematic is shown in Fig. 2. For the pump probe measurements we use two lasers. The pump is a high power 1.51 μm DBR laser and the probe is an extended cavity laser. Each laser output can be chopped and its polarization controlled. The two lasers are combined in a fiber directional coupler and injected through a microlens to the amplifier under test. The output of the amplifier was filtered by a spectrometer, tuned to the probe wavelength, and measured by an optical spectrum analyzer or by a lock in amplifier. In the pump probe measurements, we used as the probe source two different lasers to cover the ranges 1.32 — 1.37 μm (in the barrier) and 1.45 — 1.5 μm (in the QW). For the measurements of the reduction in the amplified spontaneous emission (ASE) power, only the pump laser was used. The pump power was chosen to cause a 2 dB saturation of the amplifier gain.

The interaction between the regions of interest was characterized by measuring the cross talk between the pump signal at 1.51 μm and the higher energy levels near the top of the QW or in the barrier. First we used, a chopped probe signal whose gain is measured with and without a cw pump. The chopped probe wavelength was tuned over the above mentioned ranges and the reduction of the gain (due to the pump) was recorded as a function of probe wavelength. Next we use a chopped pump signal with no probe and measured the effect of the pump on the ASE power over the spectral range of 1.32 — 1.5 μm, namely, from high in the barrier to well inside the QW.

## III. Results

In Fig. 3 the ASE of the amplifier at a drive current of 140 mA is shown. It can be seen that the ASE extends to wavelengths as short as 1.25 μm. This implies that most of the quantum well states are filled and also many in the barrier. In Fig. 4 we present the effect of the pump (at 1.515 μm) on the ASE spectrum. The data in Fig. 4 represents the difference between the ASE spectra with and without the pump. In the region near the top of the QW the density of state functions of the barrier and QW regions merge. Since the two functions extend into one another, the transition regions take a complicated form. The addition of a strong pump signal creates a dip near the top of the QW. This dip starts at a wavelength of 1.365 μm and is mapped out in Fig. 4. Since the capture time of carriers in the barrier is acting as a bottle neck for the

relaxation process, this dip is maximized below the barrier energy at 1.43 μm. At wavelength longer than 1.43 μm (which is well inside the QW), the cross talk signal decreases. This is due to the fact that the saturation energy increases as the wavelength of interest approaches the gain peak at 1.51 μm from the short wavelength side [7].

Cross talk measurements similar to the ones described in Fig. 4 were performed at several drive currents. The general shape of the cross talk spectrum repeated itself but the fine features and the wavelength of maximum cross talk were bias dependent. The only feature which is bias independent is the first edge on the short wavelength side of the dip. That portion of the measured dip is shown in detail in Fig. 5. The dip edge at the short wavelengths (1.36$\mu m$—1.37$\mu m$) is marked by an arrow found to be bias independent and is therefore identified as the energy at which the QW and the barrier's states meet.

We also performed static pump-probe measurements at the wavelength ranges 1.32—1.37 and 1.45—1.5. The reduction of the gain in the presence of the pump resembles the reduction of the ASE spectrum (Fig. 4). Next we measured the cross talk dependence on the drive current. In Fig. 6 we see that up to a 140 mA drive, the cross talk increases with the current and at higher currents it decreases. This effect is, probably, the result of two mechanisms that oppose each other. First, as the current is increased there are more carriers in the reservoir and hence the effect is stronger. However, at high currents the QW are filled more so that less carriers are needed from the reservoir and the effect decreases.

**IV.References**

[1] G. Eisenstein, U. Koren, G. Raybon, T.L. Koch, J. M. Wiesenfeld, M. Wegener, R.S. Tucker, B.I. Miller, Appl. Phys. Lett., 56, 1201, (1990)

[2] M. Bagley, G. Sherlock, D.M. Cooper, L.D. Westbrook, D.J. Elton, H.J. Wickes, P.C. Spurdens, W.J. Devlin, Electron. Lett., 26, 512, (1990)

[3] T. Saitoh, Y. Suzuki, H. Tanaka, Photonic Technol. Lett., 2, 794, (1991)

[4] G. Eisenstein, J.M. Wiesenfeld, M. Wagener, G. Sucha, D.S. Chemla, S. Weiss, G. Raybon, U. Koren, Appl. Phys. Lett., 58, 158, (1991)

[5] P.W.M. Blom, R.F. Mols, J.E.M. Haverkort, M.R. Leys, J.H. Wolter, 16th European Conference On Optical Communication, Amsterdam 1990.

[6] B. Deveaud, F. Clerot, A. Regreny, K. Fujiwara, K. Mitsunaga, J. Ohta, Appl. Phys. Lett., 55, 2646, (1989)

[7] G. Eisenstein, U. Koren, G. Raybon, J. M. Wiesenfeld, M. Wegener, Appl. Phys. Lett., 57, 333, (1990)

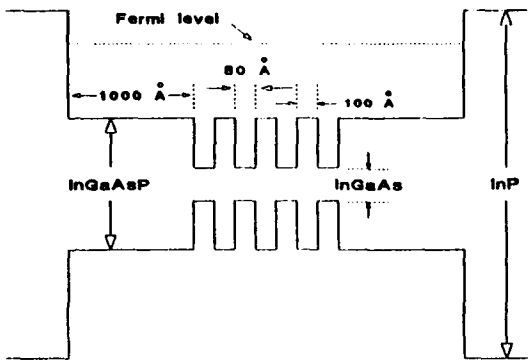


Fig.1 - Energy band diagram of the MQW amplifier.

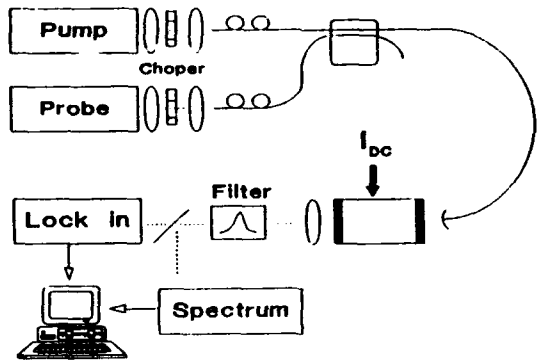


Fig.2 - Experimental setup.

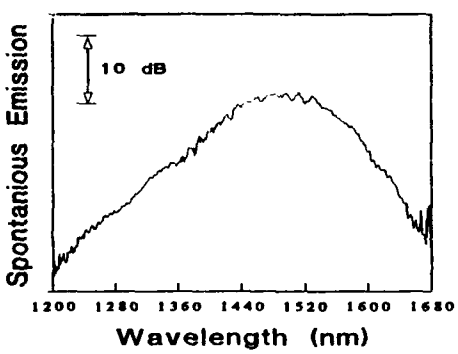


Fig.3 - Measured amplified spontanious emission of the MQW amplifier. At 140 mA.

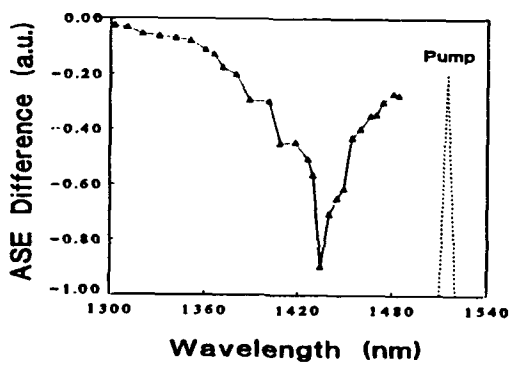


Fig.4 - The ASE cross talk spectrum measured as the ASE spectrum with pump minus the spectrum without it.

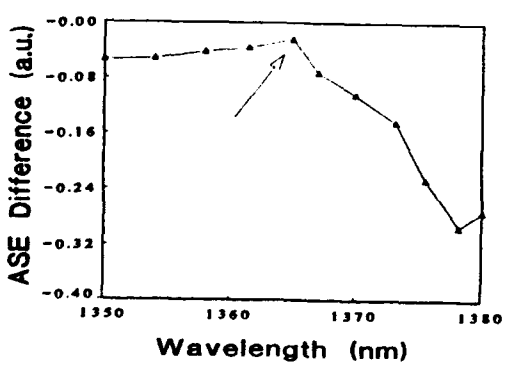


Fig.5 - The ASE cross talk near the QW top. The "dip" edge (marked by arrow) is clearly seen at 1365 nm.

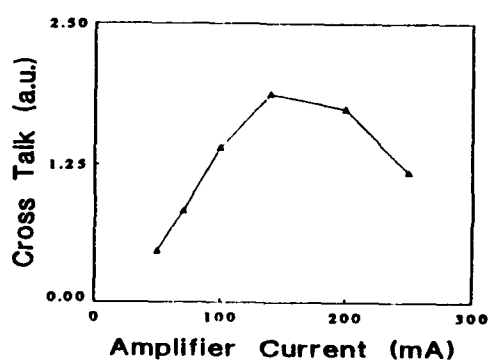


Fig.6 - ASE cross dependence on drive current.

# Phase Modulation and Optical Switching by Semiconductor Laser Amplifier

A.C. Labrujere[1], C.A.M. Steenbergen[2], and C.J. van der Laan[2]

[1] PTT-Research Neher Laboratories, P.O. Box 421, 2260 AK Leidschendam, The Netherlands
[2] Delft University of Technology, Dept. of Applied Physics, P.O. Box 5046, 2600 GA Delft, The Netherlands

**Abstract**

Operation of a semiconductor laser amplifier simultaneously as phase modulator and optical switch is proposed. Theoretical and experimental results on performance in saturation are reported.

## Introduction

Phase modulation by semiconductor laser amplifiers is a promising technique, as has been demonstrated in coherent transmission links [1,2]. A semiconductor laser amplifier can also be applied as fast optical on/off switch. This can be realized by turning off the bias current, so making the amplifier to become highly absorbant for signal radiation. The combination of both functions can be applied in a coherent multi-channel system, in which (D)PSK modulation format is used, and a fast optical switch is required to accomplish TDMA on each channel. Such an application at the transmitter of a coherent system provides a very flexible approach, as being demonstrated in the ESPRIT 2054:UCOL project [3].

The main advantage of this approach is the signal gain of the amplifier/switch, in contrast to e.g. $LiNbO_3$ devices that introduce signal attenuation. This feature enables a significant increase of the coherent system capacity, even when amplifier saturation, and receiver sensitivity degradations due to intensity modulation and amplified spontaneous emission noise are taken into account [4].

In this paper the switching and phase modulation performance of a semiconductor laser amplifier is described theoretically. Experimental results are given as well to validate the modeling work. Special attention is given to operation in saturation.

## Amplification and Switching

A semiconductor laser amplifier basically is a laser diode (AR coated) operating just below threshold. Light injected into the amplifier experiences gain if a population inversion of carriers is created. The intrinsic amplifier gain is in approximation given by [5]:

$$G = \exp\left[\left(\frac{\Gamma g_m}{1+S} - \alpha\right) L\right], \tag{1}$$

in which $\Gamma$ is the optical confinement factor, $L$ is the length of the amplifier, $S$ is the saturation parameter that depends on the light intensity in the amplifier and the saturation intensity. $\alpha$ is the internal loss coefficient and is responsible for all internal loss processes apart from band gap absorption [6].
The material gain coefficient depends on the carrier density and is given by [5]:

$$g_m = a(n_e - n_0) - a_2(\lambda - \lambda_p)^2, \tag{2}$$

with $n_e$ the carrier density, and $n_0$ the transparency density. $a$ and $a_2$ are empirical constants. $\lambda$ is the wavelength of the injected light, and $\lambda_p$ is the peak gain wavelength of the amplifier (dependent on the carrier density). In this approximation, the gain profile is assumed to be parabolic and the center shifts linearly with carrier density. All parameter values used in the model, are listed in Table 1.

The carrier density is related to the bias current $I_b$ by the rate equation:

$$\frac{dn_e}{dt} = \frac{\gamma I_b}{eV} - (A_{nr} n_e + B n_e^2 + C n_e^3) - \frac{\Gamma g_m P}{Ewd} \tag{3}$$

with $\gamma < 1$ the factor for the leakage current in the amplifier, $e$ the electronic charge, $V$ the volume of the active region. The second term on the right is the carrier recombination rate, which is dominated by Auger recombination for large carrier density. The empirical constants $A_{nr}$, $B$, and $C$ to describe the

relaxation processes are also given in Table 1. The third term describes the optical amplification of light with optical power $P$. $E$ is the photon energy, and $w$ and $d$ are the width and the thickness of the active region, respectively.

From the stationary situation, one may derive the relation between the bias current and carrier density. In combination with equations (1) and (2) one can derive the bias current dependency of the amplifier gain. Theoretically an attenuation of about 80 dB at zero bias current compared to a gain of 20 dB at 60 mA bias current is possible. This ideal 100 dB isolation can however not be obtained for a saturated amplifier, as gain and absorption saturation cause a significant decrease of isolation.

We have experimentally determined the switching operation of a heavily saturated amplifier. A DBR laser operating at 1522 nm with 3 dBm optical power in fiber was used as signal source. The optical amplifier gain maximum was around 1500 nm at 60 mA bias current (3 dB ripple point). The unsaturated fiber to fiber gain at this particular wavelength was about 6 dB. In Fig. 1a the isolation degree of the amplifier (relative to the power level at 60 mA bias current), is plotted versus the bias current. One can see that an isolation degree of more than 60 dB can be achieved by switching the bias current between 60 mA and 0 mA. The solid line in the figure represents the theoretical curve and is in good agreement with the measurements.

The time response as derived from the rate equation (3) is simulated and plotted in Fig. 1b. One can see that the decay is not exponential resulting from the higher order carrier density terms in the recombination rate. For the situation of Fig 1a the time to establish an isolation degree of 50 dB is about 10 nanoseconds.

## Phase modulation

Phase modulation by a semiconductor amplifier arises from the carrier density dependence of the index of refraction in the active region. Modulation of the bias current results hence in modulation of the optical path of the amplifier and thus in phase modulation. Besides the phase of the signal, also the gain is modulated. The expression for the E-field after amplification $E_m$ is given by [2]:

$$E_m = E_0\sqrt{G}\exp\left(\frac{\Delta g L}{2}(1-i\beta)\right). \tag{4}$$

$E_0$ is the E-field of the unmodulated signal, and $\Delta g$ is the gain modulation and $\beta$ is the linewidth enhancement factor. One can see that the phase modulation index is larger than the amplitude modulation index by a factor $\beta$.

Sinusoidal phase modulation of a laser results in sidebands of the spectrum, and can be analyzed by a Fabry-Perot interferometer. In Fig. 2 the intensity of the central line and the first two sidebands are plotted versus the modulation index. One can see that up to a modulation index of 2, the relative intensities are in good agreement with the theoretical Bessel intensities (solid lines). At higher modulation index, the non-linear relation between amplifier gain and bias current dominates, resulting in a distortion of the ideal performance. However in a realistic system, digital phase modulation makes use of phase shifts equal to $-\pi/2$ and $\pi/2$ for which good performance is expected.

We have determined the linewidth enhancement factor $\beta$ by measuring both the amplitude and phase modulation response of the amplifier. It turns out that $\beta$ shows a rippled pattern with period equal to the FSR of the amplifier diode (see Fig. 3). For the amplifier based at 50 mA (at which the gain ripple was 2.5 dB), $\beta$ varies between 3.4 and 7.6. The average value of $\beta$ is 5.3.

An expression for the phase modulation response $d\phi/dI_b$ can be derived to be:

$$\frac{d\phi}{dI_b} = -\frac{a^*\gamma\Gamma\beta L\tau_n}{2eV}\frac{1}{\sqrt{(1+S)^2+\omega_m^2\tau_n^2}}. \tag{5}$$

$\omega_m$ is the modulation frequency, and $\tau_n = \partial\tau/\partial n_e = A_{nr} + 2Bn_e + 3Cn_e^2$ is the differential carrier lifetime of the amplifier. $a^* = \partial g/\partial n_e$ is equal to $a$ at $\lambda = \lambda_p$.

In Fig. 4 the (unsaturated) modulation response of the semiconductor laser amplifier is shown. The modulation response is about 0.08 rad/mA for 60 mA bias current, and increases with decreasing bias current. This effect is caused by the carrier dependency of the differential recombination time. If we insert the values of Table 1 and assume $\beta = 5.3$ the differential carrier lifetime is calculated to 0.3 nsec.

| | | | | | |
|---|---|---|---|---|---|
| $n_0$ | $1.1 \times 10^{18}$ cm$^{-3}$ | $\lambda_0$ | 1580 nm | $\alpha$ | 50 cm$^{-1}$ |
| $L$ | 500 $\mu$m | $w$ | 1.5 $\mu$m | $d$ | 0.14 $\mu$m |
| $\Gamma$ | 0.3 | $a$ | $2.7 \times 10^{-16}$ cm$^2$ | $a_2$ | 0.15 cm$^{-1} \times$ nm$^{-2}$ |
| $a_3$ | $2.7 \times 10^{-17}$ nm $\times$ cm$^{-3}$ | $A_{nr}$ | $10^8$ s$^{-1}$ | $B$ | $10^{-10}$ cm$^3$/s |
| $C$ | $3 \times 10^{-29}$ cm$^6$/s | $\gamma$ | 0.6 | | |

Table 1: Parameters used to model a DCPBH semiconductor laser amplifier.

The 3 dB bandwidth of the amplifier is determined by the differential lifetime. For 60 mA bias current ($\tau_n$ = 0.3 nsec) the calculated bandwidth is about 900 MHz. From Fig. 4 the bandwidth for phase modulation by the amplifier is deduced as about 700 MHz. The difference may be ascribed to the frequency response of the electrical connections, which were optimised for 300 Mbit/s DPSK transmission.

From Equation (5) it appears that the phase modulation response decreases with increasing saturation parameter. In Fig. 5a experimental results on saturation effects on phase modulation are plotted. The response of the 50 mA biased amplifier starts to decay at about -8 dBm input power (in fiber). This input power corresponds to -3 dBm output power in fiber (see Fig 5b on gain saturation).

In Fig. 5a the theoretical response of Equation (5) is plotted. One can see that the experimental results differ from the theoretical model. This is due to residual facet reflections, causing a ripple on the phase modulation response [4]. As the gain ripple shifts with saturation parameter, deviations from the expected response appear. At an input power of -9 dBm and 0 dBm the wavelength of the signal laser coincides with the optimal wavelength for phase modulation.

## Conclusions

In this paper it is proposed to deploy semiconductor laser amplifiers in coherent multi-channel systems to combine phase modulation and optical switching for DPSK-modulation and TDMA at the transmitters. We have set up a model to describe the switching and phase modulation performance of the amplifier. Experimentally an isolation degree of 60 dB is observed, and theoretically a switching time of 10 nsec is derived for an amplifier operating in saturation.

We have shown the feasibility of phase modulation for a modulation index up to about 2, and in a bandwidth up to 700 MHz. The phase modulation response decreases when operating in saturation. The response depends on the gain ripple.

## References

[1] J. Mellis, and M.J. Creaner, *Coherent Detection of 565 Mbit/s DPSK Data, using Semiconductor Laser Amplifier as Phase Modulator, Electron. Lett. 25, (1989), 680*

[2] G. Grosskopf, R. Ludwig, R. Schnabel, and H.G. Weber, *Characteristics of Semiconductor Laser Optical Amplifier as Phase Modulator, Electron. Lett. 24, (1988), 551*

[3] A. Fioretti, E. Neri, O.J. Koning, A.C. Labrujere, J.P. Bekooij, B. Hillerich, E. Weidel, and G. Veith, *An Evolutionary Configuration for an Optical Coherent Multichannel Network, GLOBECOM'90, San Diego, (1990)*

[4] A.C. Labrujere, J.P. Bekooij, C.A.M. Steenbergen, and C.J. van der Laan, *System Aspects of Phase Modulation and Optical Switching by Semiconductor Laser Amplifier, submitted to ECOC'91*

[5] M.J. O'Mahony, I.W. Marshall, and H.J. Westlake, *Semiconductor Laser Amplifiers for Optical Communication Systems, Brit. Telecom. Technol. J. 5, (1987), 9*

[6] G.P. Agrawal, and N.K. Dutta, *Long Wavelength Semiconductor Lasers, Van Nostrand Reinhold Company, (1986)*

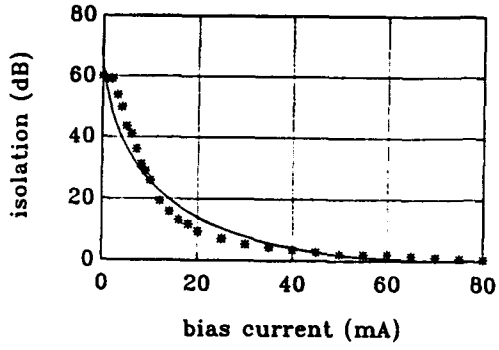


Fig. 1a: Measured and theoretical isolation semiconductor laser amplifier.

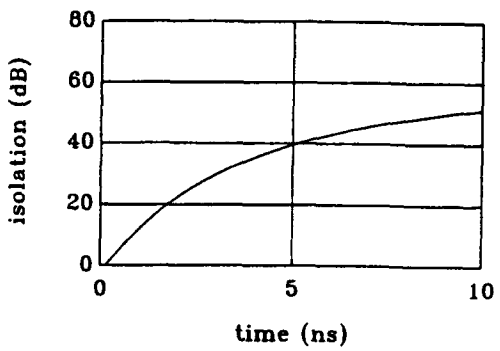


Fig. 1b: Simulated switching time.

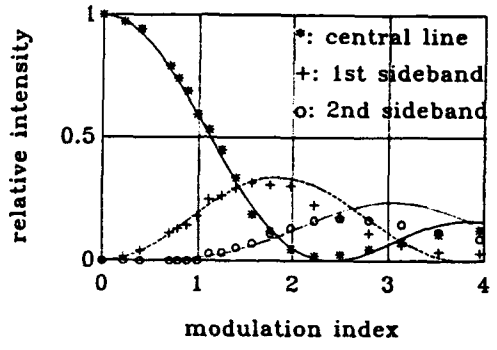


Fig. 2: Relative intensity of central line and sidebands for sinusoidal phase modulation.

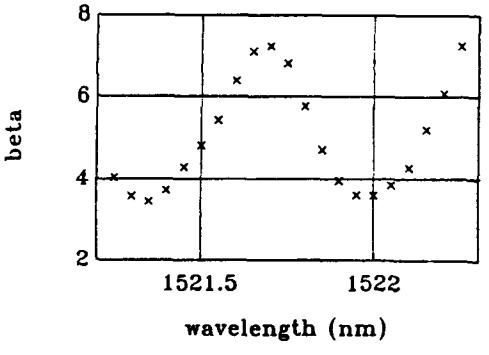


Fig. 3: Effective linewidth enhancement factor $\beta$.

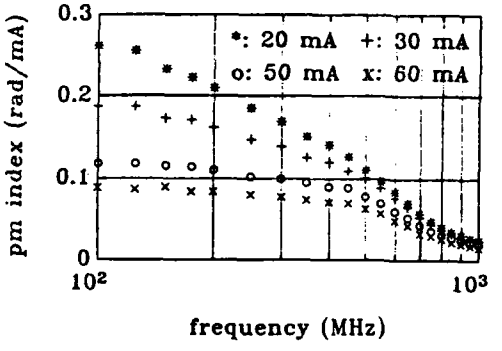


Fig. 4: Phase modulation index versus frequency.

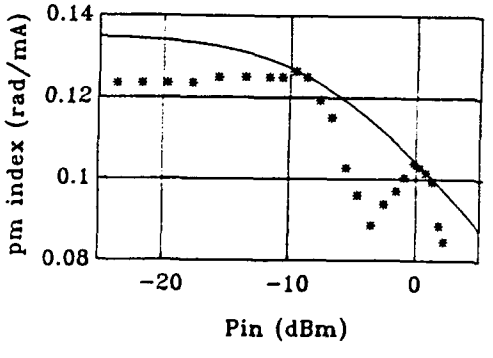


Fig. 5a: Saturation of phase modulation index.

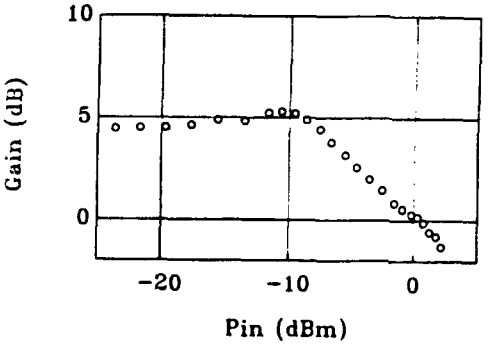


Fig. 5b: Gain saturation.

# Components and Novel Amplifier Configurations

**ThD** 2:45pm–3:45pm
Cabaret Room

M. Nakazawa, *Presider*
*NTT Transmission Systems Laboratories, Japan*

# Fibre Bragg filters for pump rejection and recycling in erbium doped fibre amplifiers.

by M.C. Farries, C.M. Ragdale, D.C. J. Reid.

Plessey Research Caswell Ltd,
Caswell, Towcester, Northants, NN12 8EQ.

## Summary

Residual pump light emitted from an optical fibre amplifier can be a problem in a telecommunication system. The performance of a receiver can be adversely affected by the residual pump power emitted from a pre-amplifier, which is usually larger than the signal power, because it can cause excess noise and receiver saturation. A pre-amplifier which is designed for optimum gain and minimum noise figure will therefore have a large emission of unabsorbed pump light. If the unabsorbed pump light can be reflected back into the amplifier then the amplifier performance will be increased and the receiver will be free from pump light. We show for the first time how this can be achieved with an efficient wavelength dependent fibre reflection filter.

Efficient fibre based filters have been made by fabricating a Bragg grating on a polished fibre by two beam interference and then etching the grating into the fibre [1]. The reflection bandwidth of these filters can be determined by the chirp of the grating to be from 0.3 nm to 22 nm [2]. A high efficiency of 95% of the grating is maintained by increasing the interaction length of the grating as the chirp is increased. The gratings described here have an interaction length of 10 mm but narrow band gratings have interaction lengths of 3 mm. The efficiency of the filter is maintained by increasing the interaction length of the Bragg grating from 3 mm to 10 mm. The filters are fabricated by creating a grating in photoresist on a polished half coupler by 2 beam interference [1]. The grating is then etched into the fibre by ion beam milling and then coated with a layer of high index material in order to pull the fibre field to the grating. We have previously reported [2] a filter optimised for the 1480 nm pump band of a fibre amplifier and now we show that filters with similar performance, but optimised for 980 nm can be fabricated.

The performance of the 980 nm fibre grating was measured in both reflection and transmission is shown in figures 1 and 2. The filter is characterised by a peak reflectivity of 99% back into the input fibre and a reflection bandwidth of 12 nm. There is a ripple on the reflection spectrum but the reflectivity is greater than 75% over a bandwidth of 10 nm. These filters are particularly advantageous due to their coverage of the 980 nm pump band of an erbium amplifier. The filter has a low insertion loss of less than 0.5 dB at all wavelengths between 1.1 μm and 1.6 μm. This is particularly advantageous for telecommunication applications such as pump rejection after weak signal pre-amplification. The filter has a loss of 8 dB at wavelengths shorter than reflection band due to out-coupling by the Bragg grating, but this will not affect most applications. An important feature of the fibre filter for optical amplifier applications is its low reflectivity at the signal wavelength.

The 980 nm filter was tested in an experimental fibre amplifier as shown in figure 3. The amplifier is pumped with a 980 nm diode laser fabricated in house. The signal and pump are multiplexed with a fibre coupler which was spliced to erbium doped fibre supplied by Southampton University. The filter was spliced to the end of the doped fibre and the output was monitored on a spectrum analyser. Figure 4 shows the output spectrum of the emission form the amplifier including the pump, signal and amplified spontaneous emission with and without the fibre filter attached to the doped fibre. Without the fibre filter an unabsorbed pump power of 1 mW was measured and this is seen to be larger than the signal output power of 0.25 mW . While this residual pump power is small compared with the input pump power it is wasted and will cause degradation of the sensitivity of the receiver. With the filter spliced to the output the residual pump power is reduced by 30 dB to 1 μW and there is a small increase in the signal power. The broad bandwidth of the filter is sufficient to cover the 5 nm spread of the multimode pump laser and most of the pumps spontaneous emission as well.

Fibre Bragg filters have been shown to be very efficient in the rejection of residual pump power from fibre amplifiers. They have the added advantage that there is no insertion loss penalty at the signal wavelength and if there is significant unabsorbed pump power then an improvement in amplifier gain from 20 dB to 30 dB may be achieved.

## Acknowledgements.

This work was supported by GEC-Plessey Telecommunications Ltd Erbium doped optical fibre was supplied by Southampton University.

## References

1. I. Bennion, D.C.J. Reid C.J. Rowe, W.J. Stewart 'High-reflectivity monomode-fibre grating filters', Electron. Lett 22, p341,1986.

2. M.C. Farries, C.M. Ragdale, D.C. J. Reid. 'Chirped Bragg optical fibre filter with 22 nm bandwidth.' Paper MC 2 Workshop on active and passive fibre components, Monterey 1991.

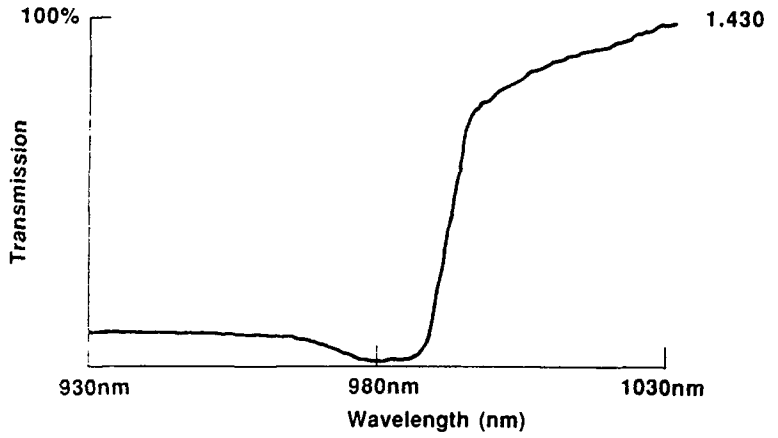


Figure 1 TRANSMISSION SPECTRUM OF BRAGG FIBRE FILTER

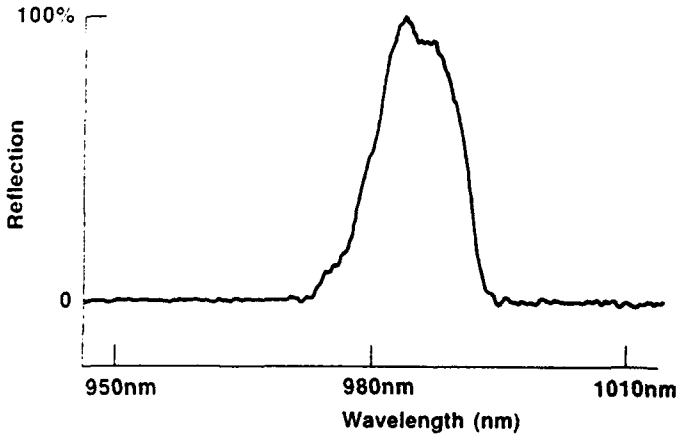


Figure 2 REFLECTION SPECTRUM OF BRAGG FIBRE FILTER

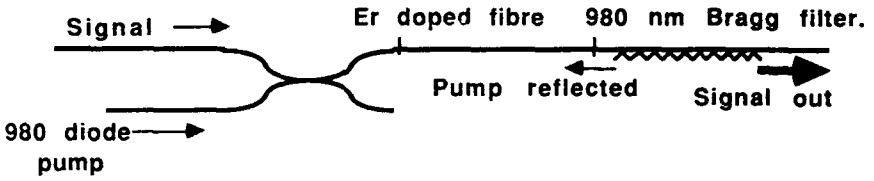


FIGURE 3. ASSESSMENT OF BRAGG FIBRE FILTER FOR PUMP REJECTION.

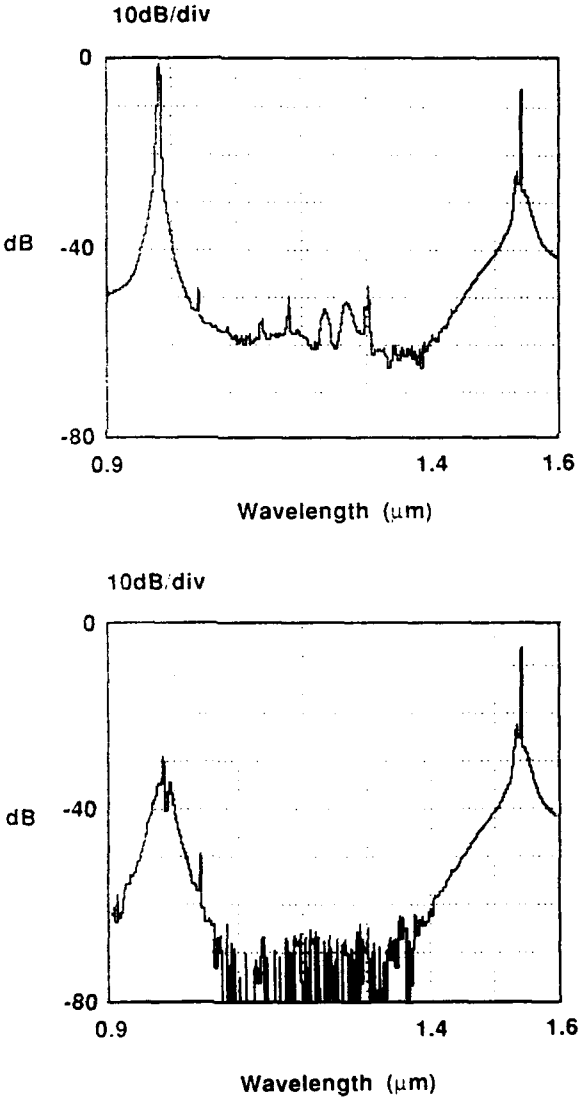


Figure 4 EMISSION SPECTRUM OF FIBRE AMPLIFIER WITHOUT (UPPER) AND WITH (LOWER) A BRAGG FIBRE FILTER

# Gain Enhancement in Reflected-Pump Erbium-Doped Fiber Amplifiers

C. R. Giles, J. Stone, L. W. Stulz, K. Walker*, C. A. Burrus

AT&T Bell Laboratories
Crawford Hill Laboratory
Holmdel, NJ 07733

* AT&T Bell Laboratories
Murray Hill Laboratory
Murray Hill, NJ 07974

Abstract

Improved performance of EDFAs is achieved using wavelength-selective reflective filters to double-pass the pump beam. In low-gain amplifiers these filters can increase the saturation output power by 2 dB or reduce the pump power requirements.

*Summary*

The performance of erbium-doped fiber amplifiers can be enhanced using reflectors and optical circulators to double-pass the pump and signal beams through the erbium-doped fiber [1,2]. However, reflecting only the pump light is simpler to implement and increases the amplifier gain and saturated output power and lowers the amplifier noise. These reflected-pump amplifiers (RPA) are well-suited as low-gain (10-15 dB) amplifiers for ultra-long distance systems where the amplifiers are closely spaced to limit impairments caused by fiber nonlinearities and amplified spontaneous emission [3,4].

Three reflector-type amplifiers were compared to the conventional EDFA using a model of amplifier gain based on the Er-doped fiber absorption coefficient, $\alpha(\lambda)$, gain coefficient, $g^*(\lambda)$ and saturation parameters, $\zeta$ [5,6]. In this analytical model reflecting the pump or signal has the same effect on gain as doubling $\alpha(\lambda)$ and $g^*(\lambda)$ at the reflected wavelength in a single-pass amplifier (this is not the same as doubling the amplifier length). Figure 1(a) is the calculated small-signal gain for a 14 m length of our high efficiency Er-doped fiber pumped at wavelength $\lambda_p$ = 1475 nm and amplifying a signal $\lambda_s$ = 1549 nm. Use of a signal reflector doubles the small-signal gain while a pump reflector lowers the threshold pump power. The pump reflector also increases the saturated output signal power, as shown in Figure 1(b) for 7.5 mW pump power. The output power at 3-dB gain compression, $P_{3dB}$, ranged from -1.6 dBm with the signal reflector to +3.2 dBm with the pump reflector. Double-passing the signal is less helpful in highly-saturated amplifiers, especially because of the need for an optical circulator to isolate the input and output ports.

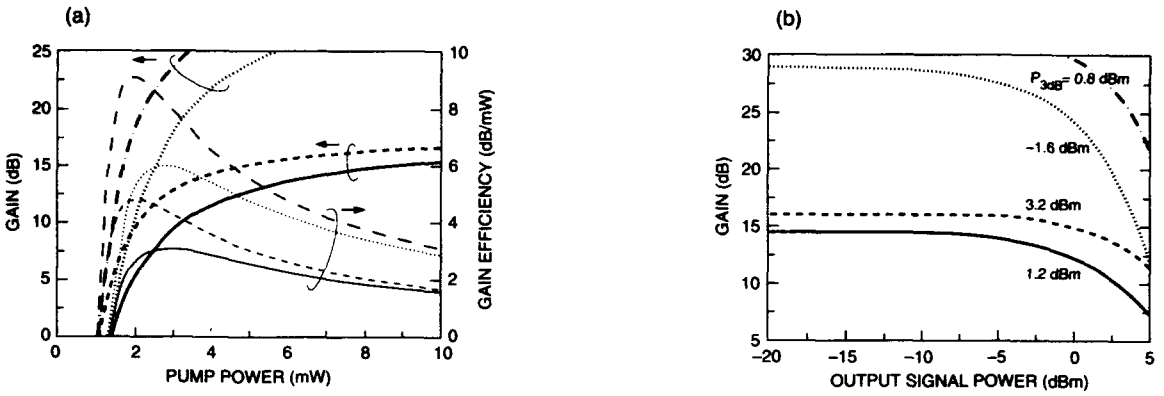


**1. Calculated gain characteristics of conventional EDFA (——), EDFA with signal reflector (....), EDFA with pump reflector (- - -) and EDFA with pump and signal reflector (-·-·-). (a) Gain and gain efficiency vs pump power for $P_s = 1\ \mu W$ and (b) gain vs signal output power for $P_p = 7.5$ mW. Amplifier parameters are $L = 14$ m, $\lambda_p = 1475$ nm, $\lambda_s = 1549$ nm, $\alpha_p = 0.86$ dB/m, $g_p^* = 0.264$ dB/m, $\alpha_s = 1.52$ dB/m, $g_s^* = 2.14$ dB/m and $\zeta = 1.21\times10^{15}\text{m}^{-1}\text{s}^{-1}$.**

The experimental amplifier consisted of a 14 m length of Er-doped fiber which was pumped with 7.5 mW from a 1475 nm semiconductor laser by means of a 1480 nm/1550 nm WDM coupler. Two types of pump reflector as shown in Figure 2 were tested; a wavelength multiplexer-coupler with a reflector on the pump port, and a multilayer silica/silicon fiber-end edge filter [7]. A disadvantage of this particular fiber-end reflector was the filter reflectance $R_s = 0.29$ at the signal wavelength $\lambda_s = 1549$ nm, causing a 1.5 dB reduction in the net amplifier gain.

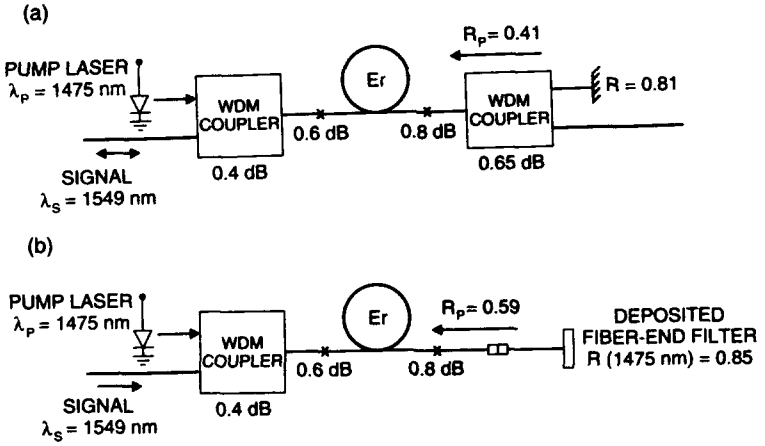


**2. Erbium-doped fiber amplifiers with pump reflectors consisting of (a) multiplexer-coupler with reflective pump port and (b) fiber-end reflective filter. The pump reflectance, $R_p$, is the net reflectance including component and splice losses.**

Figure 3 compares the measured gain and noise factors of conventional amplifiers to RPAs using multiplexer-reflectors for both co-directional and counter-directional pumping. In the co-directionally pumped amplifiers the small-signal internal gain at 1549 nm increased from 12.6 dB to 13.4 dB once the multiplexer reflector was in place. At $G = 9.5$ dB, the 3-dB saturated gain of the conventional amplifier, the output signal power increased from -0.5 dBm to 0.9 dBm upon adding the reflector. The amplifier noise factor also improved. Similar gain saturation was

achieved using counter-directional pumping but the noise improvement for the RPA was more noticeable; $n_{sp}$ = 1.9 at small signal in the conventional amplifier was lowered to 1.75 in the RPA.

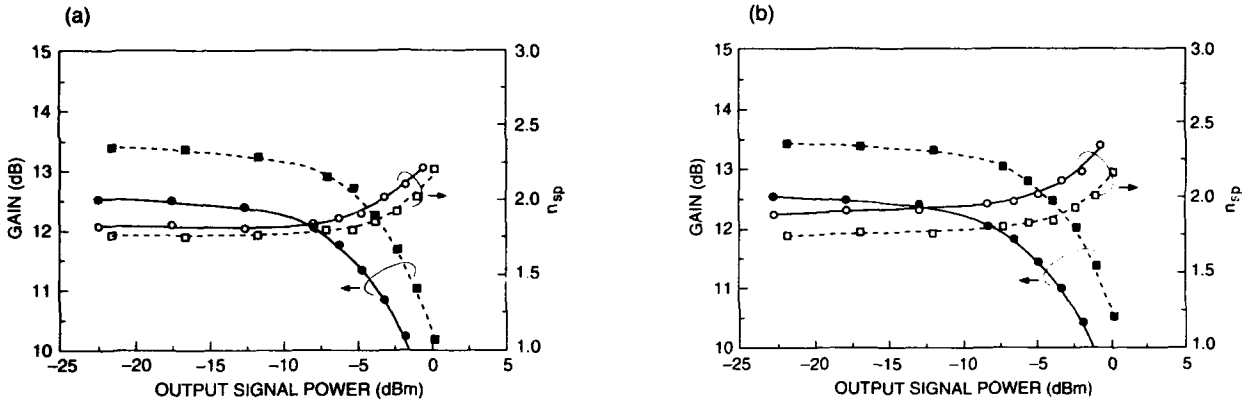


**3. Gain and noise factors of EDFA (——) and RPA (- - -) for (a) co-directionally pumped amplifiers and (b) counter-directionally pumped amplifiers.**

Improvements in amplifier performance were also achieved using the fiber-end filter in a co-directionally pumped RPA. Figure 4 shows the increase in the amplified signal at 1549 nm and the modification of the ASE spectrum. The observed increase in signal gain, 0.9 dB, might improve to 2.4 dB using filters having high-transmission at the signal wavelength. A 2.4 dB increase in gain is close to the limit calculated for this particular amplifier using a large-signal spectrally-resolved amplifier model [6]. We also calculated that if $R_p$ = 1, this RPA with $P_p$ = 4.8 mW would have the same small-signal gain as the conventional amplifier with $P_p$ = 7.5 mW. This reduction in required pump power could significantly improve the reliability of a pump laser.

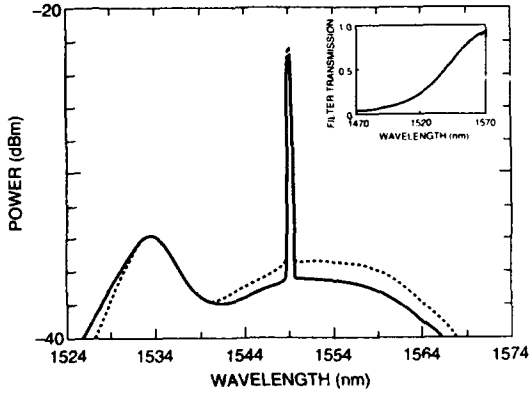


**4. Amplified signal and ASE for EDFA (——) and RPA (- - -). The RPA has a fiber-end reflective filter with $R_p$ = 0.59. Inset is transmission spectrum of the reflective filter.**

*Conclusions*

Pump reflectors having 40-60% reflectance were used with 12-13 dB gain amplifiers to increase the gain by 0.9 dB and reduce the noise factor by 0.4 dB. Better reflectors would increase the gain and saturated output power by 2 dB. Pump reflectors might be very low cost items and could be incorporated into other amplifier components such as optical isolators or ASE filters.

*References*

1. S. Nishi, K. Aida and K. Nakagawa, "Highly efficient configuration of erbium-doped fiber amplifier", ECOC '90, Amsterdam, Proc. Vol. I, pp. 99-102 (1990).

2. V. Lauridsen, R. Tadayoni, A. Bjarklev, J. H. Povlsen and B. Pedersen, "Gain and noise performance of fibre amplifiers operating in new pump configurations", Electron. Lett., Vol. 27, No. 4, pp. 327-329 (1991).

3. J. P. Gordon and L. F. Mollenauer, "Effects of fiber nonlinearities and amplifier spacing on ultra-long distance transmission", J. Lightwave Tech., Vol. 9, No. 2, pp. 170-173 (1991).

4. C. R. Giles and E. Desurvire, "Propagation of signal and noise in concatenated erbium-doped fiber optical amplifiers", J. Lightwave Tech., Vol. 9, No. 2, pp. 147-154 (1991).

5. A. A. M. Saleh, R. M. Jopson, J. D. Evankow and J. Aspell, "Modeling of gain in erbium-doped fiber amplifiers", Photonics Tech. Lett., Vol. 2, No. 10, pp. 714-717 (1990).

6. C. R. Giles and E. Desurvire, "Modeling erbium-doped fiber amplifiers", J. Lightwave Tech., Vol. 9, No. 2, pp. 271-283 (1991).

7. J. Stone and L. W. Stulz, "FiEnd filters: Passive multilayer thin-film optical filters deposited on fibre ends", Electron. Lett., Vol. 26, pp. 1290-1291 (1990).

# Accurate modeling of distributed Erbium-doped Fiber Amplifiers with bidirectional pump

by E. Desurvire and D. Chen,
Department of Electrical Engineering, Columbia University
500 W. 120th Street, New York, NY 10027, USA

In this paper, we present an analysis of unsaturated erbium-doped fiber amplifiers (EDFA) with fiber back-ground loss and bidirectional pumping. This analysis provides an *exact* closed-form expression for the amplifier gain as a function of input pump power. This model is useful to study distributed EDFA's [1,2] and to determine the optimal $Er^{3+}$ concentration and pumping configuration that minimizes the required pump power, as shown in this paper. In the case of forward pumping, it is also shown that a simple relation exists between the input pump power required for EDFA transparency and pump threshold, which can be usefully applied to EDFA characterization.

## Theory

Let $q^{\pm}(z) = P^{\pm}(z)/P_p^{th}$ be the relative forward (+) and backward (-) pump powers, where $P_p^{th}$ is the pump threshold. In the unsaturated gain regime, and assuming confined $Er^{3+}$ doping, the pump equations are [3]:

$$\frac{dq^{\pm}}{dz} = \mp a_p q^{\pm}\left(\frac{1}{1+q^{+}+q^{-}} + \varepsilon_p\right) \qquad (1)$$

where $a_p$ is the pump $E_r^{3+}$ absorption coefficient, $\varepsilon_p = a'_p/a_p$, and $a'_p$ is the fiber background loss coefficient at the pump wavelength $\lambda_p$. One derives from eq.(1) the relation $d(q^+q^-)/dz = 0$ which yields $q_o^+ q_o^- = q_L^+ q_L^- = q^+(z)q^-(z)$, where $q_o^{\pm} = q^{\pm}(z = 0)$ and $q_L^{\pm} = q^{\pm}(z=L)$ and L is the fiber length. This relation enables decoupling between $q^+$ and $q^-$ in eq.(1), which can be integrated, taking the forward pump $q^+$ as example, into the following expression:

$$Ln\frac{q_L^+}{q_o^+} - \frac{1}{\varepsilon_p}\int_{q_o^+}^{q_L^+}\frac{dx}{x^2+bx+a} + a'_p L = 0 \qquad (2)$$

with $a = q_L^+ q_L^-$ and $b = (1+\varepsilon_p)/\varepsilon_p$. Solution (2) can be fully expressed in terms of elementary functions, depending on the sign of $\Delta = 4a - b^2$ [4].

Let $P^{\pm}(z)$ be the forward or backward signal powers (amplified signal + ASE). The rate equations for $P^{\pm}$ are [3]:

$$\frac{dP^{\pm}}{dz} = \pm\frac{a_s}{1+Q}\left\{\frac{\eta_s}{1+\eta_p}Q(P^{\pm}+P_o) - \left|1+\frac{\eta_p}{1+\eta_p}Q+\varepsilon_s(1+Q)\right|P^{\pm}\right\} \qquad (3)$$

where $Q = q^+ + q^- = q^+ + a/q^+$ is the total input pump power, $\eta_{s,p} = \sigma^e_{s,p}/\sigma^a_{s,p}$ are the ratios of emission to absorption cross-sections at $\lambda_{s,p}$, $\varepsilon_s = a'_s/a_s$, $a_s$ and $a'_s$ being the $Er^{3+}$ absorption and fiber background loss coefficients at $\lambda_s$, and $P_o = 2h\nu\delta\nu$. Substitution of the relation $(1+Q)^{-1} = -(dq^+/dz)/a_p q^+(1+\varepsilon_p+\varepsilon_p Q)$ obtained from eq.(1) into eq.(3) yields a z-independent equation:

$$\frac{dP^{\pm}}{dq^+} = \pm\frac{a_s}{a_p}\frac{1}{q^+(1+\varepsilon_p+\varepsilon_p Q)}\left\{\left(\frac{\eta_p-\eta_s}{1+\eta_p}Q+1+\varepsilon_s+\varepsilon_s Q\right)P^{\pm} - \frac{\eta_s}{1+\eta_p}QP_o\right\} \qquad (4)$$

Equation (4) is linear in $P^{\pm}$ and integratable, as shown in [3]. The quality relevant to study is the EDFA gain $G_t(q)$, which, from eq.(4), takes the form:

$$G_{\pm}(q) = exp\left\{ \pm \frac{a_s}{a_p} \frac{1+\varepsilon_s}{\varepsilon_p} \int_{q_{o,L}^{\pm}}^{q} \frac{x+C(a+x^2)}{x(a+bx+x^2)}\, dx \right\} \qquad (5)$$

with $C = [\varepsilon_s + (\eta_p - \eta_s)/(1+\eta_p)]/(1+\varepsilon_s)$. We focus now on the simpler unidirectional pump case (i.e. $q_L^- \sim a = 0$, $\Delta < 0$). After integration in eq.(5), the EDFA gain at z = L takes the explicit form:

$$G = G_+(q_L^+) = exp\left\{ \frac{a_s}{a_p} \frac{1+\varepsilon_s}{\varepsilon_p} \left| C\,Ln\left( \frac{1+\varepsilon'_p q_L^+}{1+\varepsilon'_p q_o^+} \right) + 2\varepsilon'_p\, Arth\left( \frac{q_L^+ - q_o^+}{q_L^+ + q_o^+ + 2\varepsilon'_p q_L^+ q_o^+} \right) \right| \right\} \qquad (6)$$

This result combined with pump solution (2) yields, after integration, a relation between the output and input pump powers:

$$1 + \varepsilon'_p q_L^+ = (1 + \varepsilon'_p q_o^+) e^{-AL} \quad with \quad A = \varepsilon_p (1+\varepsilon_s) \frac{1+\eta_p}{1+\eta_s} \left( 1 + \frac{Ln\, G}{(a_s + a'_s)L} \right) a_p \qquad (7)$$

Using then relation (7) to eliminate $q_L^+$ in eq.(6) yields a second-degree equation in $q_o^+$, whose solution is:

$$\boxed{q_0^+ = \frac{1+\varepsilon_p}{\varepsilon_p} e^{BL} \frac{e^{AL} - 1}{e^{BL} - 1}} \qquad (8)$$

$$with \quad B = (1+\varepsilon_p) \left| \left( \frac{\eta_s - \eta_p}{1+\eta_p} - \varepsilon_s \right) \frac{1+\eta_p}{1+\eta_s} - \frac{Ln\, G}{(a_s + a'_s)L} \right| a_p \qquad (9)$$

The output pump power $q_L^+$ is found from eqs. (7),(8):

$$q_L^+ = e^{-(A+B)L} q_o^+ \qquad (10)$$

The EDFA gain, input and output pump powers are thus related by the simple closed-form expressions (8),(10). Similar expressions can be obtained in the more general bidirectional pumping case, by using the same method.

Application

The gain G can be studied as a function of input pump power $q^+_o$ using eq.(8), plotted as $q^+_o = f(G)$. Figure 1 shows such plots in the case of $\lambda_p$ = 1.48 μm-pumped distributed EDFA with lengths L = 5 to 20 km, for the unidirectional and bidirectional pump case. The fiber background loss coefficient is $a'_s$ = 0.5 dB/km, and the $Er^{3+}$ absorption coefficients $a_s$(1.53 μm) = 4 dB/km and $a_p$(1.48 μm) = 1.6 dB/km. The Er-doped fiber is assumed to be of the aluminosilicate type with parameters $\eta_p$(1.48 μm) = 0.37, $\eta_s$(1.531 μm) ≈ 1.0 [5]. Figure 1 shows that as expected, for increasing EDFA lengths the total input pump power required to achieve transparency (G=1) is increasing, the value being always lower in the case of bidirectional pumping. The difference in power requirement between unidirectional and bidirectional pumping for transparency is further illustrated in fig. 2, which shows plots of the total input pump for transparency as a function of the ratio $r = q^-_L/q^+_0$ (r = 0 corresponds to unidirectional pumping, while r = 1 corresponds to bidirectional pumping with equal inputs). As the figure shows, this ratio is not critical for the shorter lengths (L=5-15 km). For the longer lengths, however, changing from unidirectional pumping to bidirectional, symmetric pumping reduces the total input pump power from $q^+_o$ = 35 to $q^+_o + q^-_L$ = 20, which represents a 43% reduction in required power. Obviously,

bidirectional pumping with $q^-_L > 0.5\ q^+_0$ is advantageous for long EDFA's ($L \geq 20$ km), as the effect of fiber background loss becomes significant.

Another important issue is the optimization of $Er^{3+}$ absorption coefficient for a given distributed EDFA length, fiber background loss, glass host, pump and signal wavelengths and pumping scheme. The $Er^{3+}$ absorption coefficient is related to the concentration $\rho_o$ through $a_s \approx \rho_o \Gamma_s \sigma_s^a$ where $\Gamma_s$ is a filling factor [6]. Thus, any $Er^{3+}$ absorption coefficient $a_s$ corresponds to different possibilities for $\rho_o$ and $\Gamma_s$. Figure 3 shows plots of $q^+_0 + q^-_L = f(a_s)$ for different EDFA lengths L = 10 to 25 km, with same other parameters as previously, and $a_p \sim 0.40\ a_s$ [5]. The figure shows that there exists a minimum value $a^*_s$ below or at which EDFA transparency *cannot* be achieved. Such critical value is given by B = 0 in eq.(8), i.e., $a^*_s = a'_s(1 + \eta_p)/(\eta_s - \eta_p) \approx 1.09$ dB/km. Below this value, the $Er^{3+}$ ions cannot generate enough gain to compensate for the signal background loss, independently of pump power. For $Er^{3+}$ absorption just above the critical value $a^*_s$, the pump power has to be set to a high level in order to obtain total loss compensation, as there is an unsufficient number of $Er^{3+}$ ions to provide gain. On the other hand, if the $Er^{3+}$ absorption is too large, the pump power required to bleach it has to be high as well. Thus, there exists an optimum value for the $Er^{3+}$ absorption coefficient $a_s^{opt}$ which minimizes the required pump power, as shown by the plots in Figure 3.

Using the condition G=1, eq.(8) yields directly the input pump power $q_o^+$ required for achieving transparency. In the particular case where the fiber background loss is negligible in comparison to the $Er^{3+}$ absorption, i.e., $\varepsilon_{p,s} \sim 0$ (as it is actually the case in most EDFA applications) the input pump power in eq.(8) is simply:

$$P_p^{in}(trans.) = \gamma a_p L \frac{T}{T-1} P_p^{th} \qquad (10)$$

and for the output pump: $P_p^{out}(trans.) = P_p^{in}(trans.)/T$, where $T = \exp[(1-\gamma)a_p L]$, and $\gamma = (1+\eta_p)/(1+\eta_s)$. These expressions establish the relation between pump threshold $P_p^{th}$ and the input and output pump powers for transparency, which is useful to characterize EDFA's, as these can be experimentally measured.

In conlusion, the analytical expressions for the input/output pump powers and EDFA gain derived in this study provide a very practical tool to design and optimize fiber systems using chains of distributed EDFAs with unidirectional or bidirectional pumping.

*This work was supported by the Center for Telecommunications Research, Columbia University, Department of Electrical Engineering, 500 W. 120th Street, New York, NY 10027, and IBM T.J. Watson Research Center, P.O. Box 704, Yorktown Heights, NY 10598.*

References

[1] J.R. Simpson et al., Proc. OFC '90, paper PD19.
[2] M. Nakazawa et al., Optics Lett., vol. 15, no. 21, 1200 (1990).
[3] E. Desurvire et al., IEEE Photonics Technology Lett., vol. 3, no. 2, 127 (1991).
[4] I.S. Gradshteyn et al., "Table of integrals, series and products, Academic Press, New York 1980.
[5] C.R. Giles et al., Photonics Technology Lett., vol. 2, no. 11, 797 (1990).
[6] E. Desurvire et al., J. Lightwave Technology, vol. 7, no. 12, 2095 (1989).

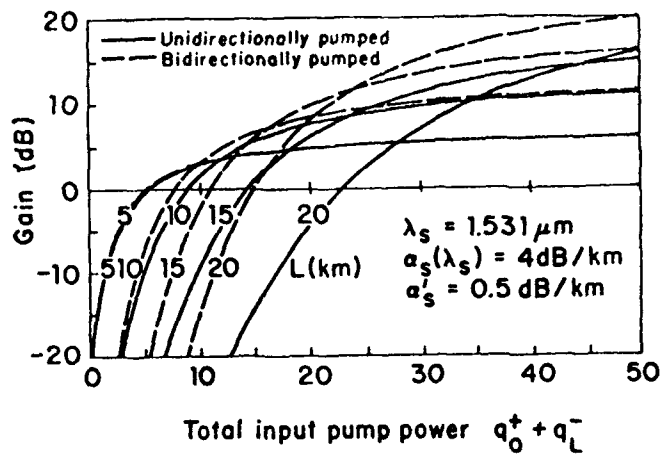


**Figure 1.**
Gain G as a function of total input pump power $q^+_0+q^-_L$ (normalized to pump threshold) at $\lambda_p$=1.48 μm for different EDFA lengths, as plotted directly from analytical solution (8), for unidirectional ($q^-_L$=0) or bi-directional ($q^-_L=q^+_0$) pumping.

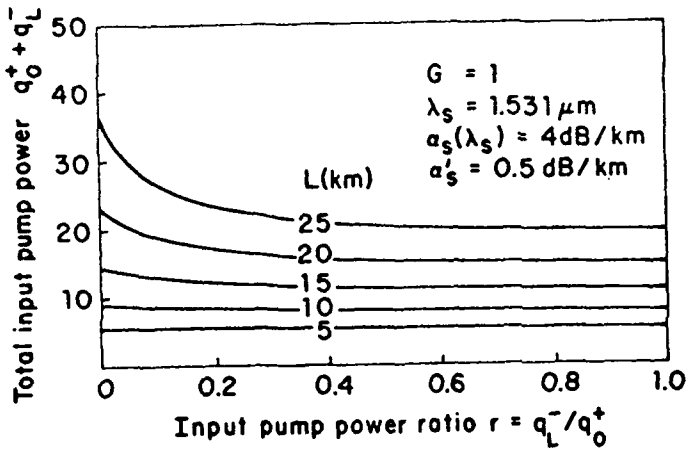


**Figure 2.**
Total input pump power $q^+_0+q^-_L$ required for EDFA transparency as a function of the backward to forward input pump power ratio r, for different fiber lengths. The cases r=0 corresponds to forward pumping and r=1 to symmetrical bidirectional pumping.

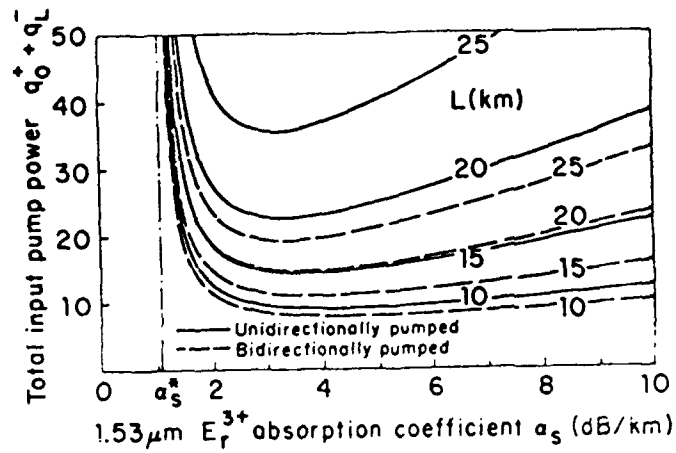


**Figure 3.**
Total input pump power $q^+_0+q^-_L$ required for EDFA transparency (G=1) at $\lambda_s$=1.531 μm, as a function of $Er^{3+}$ absorption coefficient $\alpha_s$ for different fiber lengths, with uni-directional ($q^-_L$=0) or bi-directional ($q^-_L=q^+_0$) pumping.

# 73.6km ATTENUATION FREE CONCATENATED FIBERS DOPED WITH DISTRIBUTED ERBIUM

D. Tanaka, A. Wada, T. Sakai, T. Nozawa and R. Yamauchi
FUJIKURA Ltd.
1440 Mutsuzaki, Sakura-shi, Chiba 285, Japan

## 1.Introduction

Recently, distributed Er-doped fiber amplifiers have become of great interest.[1)-5)] Intrinsic fiber loss can be compensated by the distributed gain. As a result, a fiber which is free from the attenuation can be realized.[2)] Due to its small gain, the distributed EDFA also has the advantage of low amplified spontaneous emission(ASE). Moreover, no isolator to prevent lasing is necessary, so bi-directional transmission is possible. This kind of fiber is also applicable to soliton transmission.[5)]

In this paper, we describe a design of lengthwise-distribution of Er-concentration for long length attenuation-free fibers. An attenuation-free length of 73.6km has been realized at the signal level of -10dBm.

## 2.Lengthwise-distribution of Er-concentration for attenuation-free fiber

In the case of a long length, distributed EDFA, the intrinsic fiber attenuation of pump wavelength cannot be ignored. 1.48μm pumping is preferable because its intrinsic fiber loss is the lowest among the possible pump wavelengths. Modifying the equations in Ref.(6), we solved the rate equations of a two-level laser model of 1.48μm pumping. They are described as follows;

$$\frac{dQ_p(z)}{dz} = -\left(\frac{1}{1+\varepsilon Q_p(z)}\alpha_{pEr}+\alpha_{pi}\right)Q_p(z) \quad (1a) \qquad \frac{dQ_s(z)}{dz} = \left(\frac{Q_p(z)-1}{1+\varepsilon Q_p(z)}\alpha_{sEr}+\alpha_{si}\right)Q_s(z) \quad (1b)$$

where $Q_s(z)=P_p(z)/P_{th}$, $Q_s(z)=(\sigma_{sa}\nu_p)/(\sigma_{pa}\nu_s)P_s(z)/P_{th}$, $\varepsilon=(1+\mu_p)/(\mu_s-\mu_p)$

$\mu_p$, $\mu_s$ ; ratios of emission cross section to absorption cross section
$P_p(z)$, $P_s(z)$ ; the pump power and the signal intensity at fiber length z
$P_{th}$ ; threshold pump power
$\sigma_{ps}$, $\sigma_{ss}$ ; absorption cross sections
$\alpha_{pi}$, $\alpha_{si}$ ; intrinsic fiber losses
$\alpha_{pEr}$, $\alpha_{sEr}$ ; erbium absorption losses

Suffix p and s denote pump and signal wavelengths, respectively. $dQ_s(z)/dz=0$ gives the optimum condition for attenuation-free line as follows,

$$(Q_p(z)-1) / (1+\varepsilon Q_p(z))\,\alpha_{sEr}(\rho) - \alpha_{si} = 0 \qquad (2)$$

Here, $Q_p(z)$ is determined by eq.(1a). If the emission and absorption cross sections and the intrinsic fiber loss are known, the Er concentration along the attenuation free fiber can be calculated. In order to estimate Er concentration of the attenuation free fiber, we evaluated the absorption cross section, the emission cross section and the intrinsic fiber loss, measuring 10.4km attenuation free fiber of Ref.2). Fig.1 shows the total loss, background loss and Er absorption loss around the wavelength of 1.55μm. Here, the background loss and the Er absorption loss were decomposed of the total fiber loss. The absorption cross sections are $0.96\times10^{-21}cm^2$ and $2.72\times10^{-21}cm^2$ while emission cross sections are $0.39\times10^{-21}cm^2$ and $4.14\times10^{-21}cm^2$ at the pumping and signal wavelengths, respectively. By substituting these values into eq.(2), lengthwise-distribution of Er-concentration, which gives an attenuation free fiber is deduced. Fig.2 shows a result. In this figure, Er concentration is represented by Er absorption loss at the wavelength of

1.55μm. In the region where the pumping power is strong, Er-concentration is lengthwise increased very slowly(nearly constant). On the contrary, as the signal approaches the output end, Er-concentration should be increased rapidly, because the pumping power become small toward the output end. For example, If available pumping power is 100mW, the maximum length of attenuation free fiber is estimated to be 39km.

### 3.Experimental set-up

As mentioned above, it is required for an attenuation free fiber to increase Er-concentration along the fiber length, however, it is not easy to control such a lengthwise Er distribution. Then we approximated it by concatenating two distributed EDFAs of different Er-concentration. In this case, the signal intensity change is not equal to zero throughout the fiber, however, it is not significantly large. In an attenuation-free fiber, spontaneous emission is hardly amplified due to the small gain. Therefore, signal to noise ratio is kept large even if backward pumping is employed. If we splice two sets of concatenated attenuation-free fibers as shown in Fig.3, the total attenuation-free length can be doubled by bi-directional pumping, without serious degradation of signal to noise ratio. Table 1 shows the constituent fibers of experimental set-up. Er concentration of fibers #1 and #4 is 0.7wt ppm, and #2, #3, 1.8 wt ppm.

### 4.Gain characteristics

The gain characteristics of the fibers were investigated by pumping at 1.48μm with laser diodes. Fig.4 and 5 show results of OTDR measurement for each set with 70mW, forward pumping. A signal wavelength of OTDR is not agreed with the optimal wavelength of the EDFA. Therefore observed gain is a little bit lower than that at wavelength of 1.535μm. This gain decrease causes signal intensity drop near the far end. However, attenuation free length of each set exceeds 30km within 1dB ~ 1.2dB of signal intensity deviation. From the OTDR measurement, if bi-directional pumping is employed, more than 60km of attenuation free fiber is expected within 1.2dB of signal intensity deviation throughout the fiber.

We also investigated the gain characteristics of long series of concatenated fibers at the optimal wavelength for EDFA, i.e., 1.536μm. Fig.5 shows output spectra after 36.8km transmission (set #1), and 73.6km (a series of set #1 and #2) with 1×66 mW and 2×66mW(bi-directional) pumping, respectively. Input signal intensity was -10dBm. Though pumping power was smaller than that in OTDR measurement, the signal intensity was maintained to the fiber end. The amplified spontaneous emission was fairly low even after 73.6km transmission, and a large S/N ratio has been achieved. Noise suppression at shorter wavelength is also observed in the output spectrum of 73.6km transmission. This decrease, however, is caused by wavelength characteristics of a dichroic mirror at the end of set #2, not by amplifier characteristics.

### 5.Conclusion

The optimal lengthwise Er distribution for the attenuation free fiber has been theoretically investigated. Based on this calculation, 73.6km attenuation-free fiber is realized.

**Reference**
1)J.R.Simpson, L.F.Mollenauer, K.S.Kranz, P.J.Lemaire, N.A.Olsson, H.T.Shang, P.C.Becker, OFC'90, PD19, (1990)
2)D.Tanaka, A.Wada, T.Sakai, R.Yamauchi, Topical Meeting on Optical Amplifiers and Their Applications, TuB4, (1990)
3)S.T.Davey, D.L.Williams, B.J.Ainslie, OFC'91, FA8, (1991)
4)J.R.Simpson, H.T.Shang, P.C.Becker, L.F.Mollenauer, N.A.Olsson, M.J.Neubelt, K.S.Kranz, P.J.Lemaire, OFC'91, FA7, (1991)
5)M.Nakazawa, Y.Kimura, K.Suzuki, Topical Meeting on Optical Amplifiers and Their Applications, TuA7, (1990)
6)E.Desurevire, Photo. Tech. Lett., vol.1, No.10, p.293, (1989)

Table 1 Fiber parameters of the distributed EDFAs

| fiber | length (km) | erbium concentration (wt ppm) | cutoff wavelength (μm) | MFD (μm) |
|---|---|---|---|---|
| #1 | 16.5 | 0.7 | 1.24 | 7.4 |
| #2 | 20.3 | 1.8 | 1.38 | 7.5 |
| #3 | 19.7 | 1.8 | 1.24 | 7.5 |
| #4 | 17.1 | 0.7 | 1.19 | 7.4 |

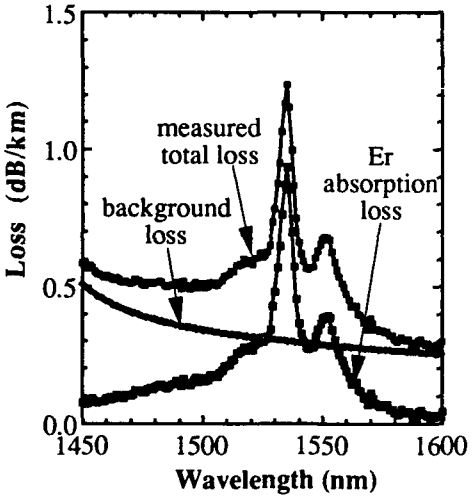


Fig.1 Spectral losses of loss components in an erbium doped fiber.

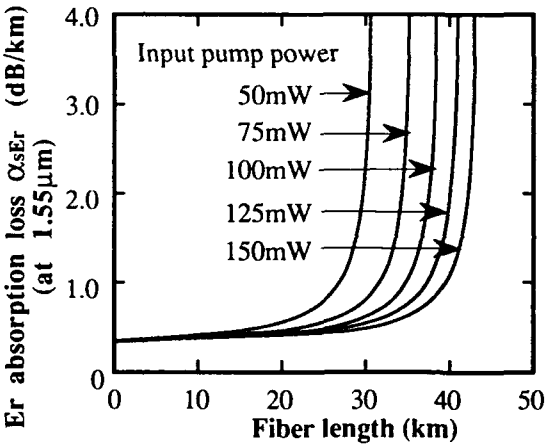


Fig.2 Lengthwise-distribution of Er-concentration for the attenuation-free fiber.

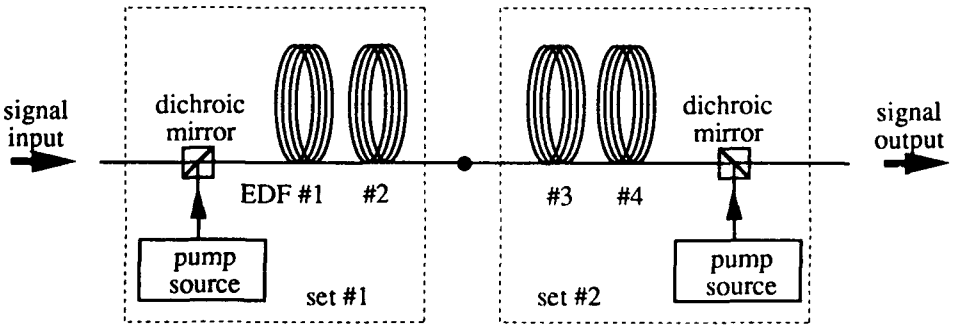


Fig.3 Experimental set-up.

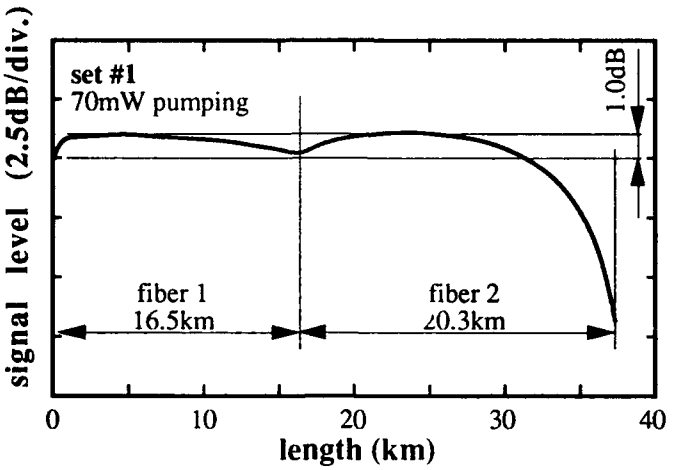


Fig.4 Result of the OTDR measurement (set #1).

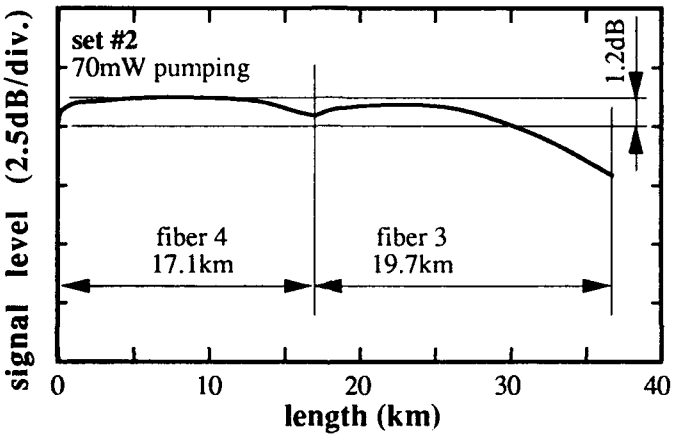


Fig.5 Result of the OTDR measurement (set #2).

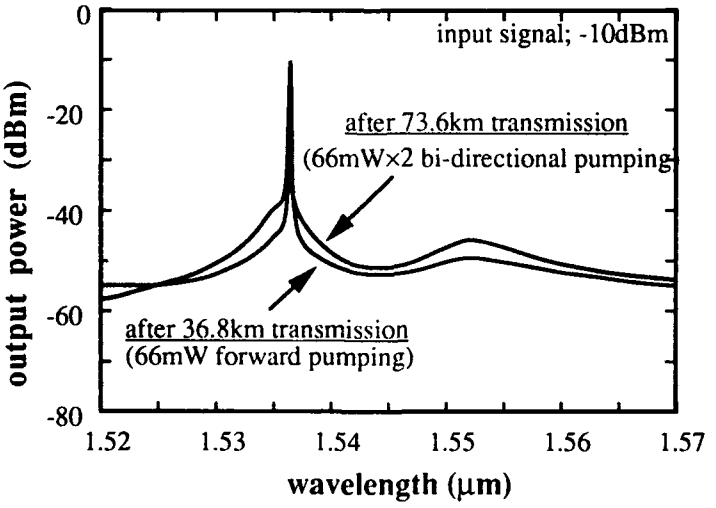


Fig.6 Output spectra after 36.8km (set #1)
and 76.8km (set #1 and #2) signal transmission.

# High Efficiency and Saturated Amplifiers

**ThE** 4:15pm–5:15pm
Cabaret Room

E. Desurvire, *Presider*
*AT&T Bell Laboratories, USA*



# Noise Characteristics of the EDFA in Gain Saturation Regimes

J.F. MARCEROU, H. FEVRIER, J. HERVO and J. AUGE

ALCATEL ALSTHOM RECHERCHE, Route de Nozay, 91460 Marcoussis, France.

Though erbium-doped fiber amplifiers (EDFA) are very attractive candidates for optical transmissions, one of their important characteristics is the noise properties. These amplifiers generate low noise levels and corresponding noise figures are close to the quantum limit[1,2]. However, a number of applications, such as CATV and transoceanic links, will be highly sensitive to excess noise above this limit. Up to now, noise figures have been experimentally [1,3,4] and theoretically studied in several conditions, such as small-signal or highly-pumped amplifiers[2,5]. But when looking at the behavior of the noise figure in various signal regimes as a function of the amplifier working point, important variations appear [6]. This indicates a highly complex reciprocal influence of the different propagating beams through the amplifying medium. In this paper, we study the noise propertics of the EDFA, especially in the transition from small-signal regimes to saturated gain ones. Theoretical results are shown to explain experimental observations.

Previously published papers have pointed out theoretically that noise figure should exhibit complex form when the EDFA is based on highly performing doped fibers[7,8]. We have experimentally observed such an unusual behavior of the noise figure in several modules based on optimized fibers. For example, we report in Fig.1 the noise figure of a both-end 1.48μm-pumped amplifier. In both cases, small-signal fiber net gain were between 38 and 39dB. The fiber is an alumino-germano-silicate one[9] and the signal wavelength is 1.550μm. We may see that the noise figure exhibits a significant minimum located near a -10dBm input signal level. This was attributed to the influence of noise saturation of the medium.

Due to the great number of parameters governing the amplification processes, we use a complete modeling of the EDFA to carefully analyze these effects. This theoretical tool agrees with any experimental result with an accuracy better than 1dB both in terms of gain and noise[7]. However, any other comprehensive approach of the EDFA taking into account the complete ASE treatment will give the same behavior[5,8].

To have a comprehensive view of the noise behavior in various signal regimes, we report on fig.2 to fig.4 some typical theoretical noise figures versus the fiber length and the input signal level. These three figures refer to the same fiber as for fig.1, the amplifier configuration being a copropagative one and the pump wavelength set at 1.48μm. For Pp=10mW and λs=1.550μm (fig.2), we observe for long fiber lengths a slight minimum near -17dBm, while the small-signal gain is actually 28.2dB at 40m. When increasing pump power up to 50mW (fig.3), we see for long lengths (G=35.9dB at 50m) a significant degradation of the noise figure in small-signal regimes. However, an improvement of the noise figure appears for input signals above -15dBm and become more significant at 0dBm. This is due to the increase of pump power leading to a higher inversion factor at high signal levels. Furthermore, the minimum of the noise figure is shifted to -8dBm. This behavior is characteristic of a saturation of the amplifying medium by the ASE beams, essentially the counter-propagating one. This occurs when the launched signal is sufficiently high to break down the equilibrium established by the pump and ASE beams. By changing the signal wavelength to 1.533μm where the gain per unit length is higher, we must see the same kind of noise saturation quenching occuring for lower input levels. Actually, on fig.4, corresponding to λs=1.533μm and Pp=50mW, this quenching appears above-35dBm of input signal. Furthermore, it must be pointed out that, as it is the case for highly-pumped amplifiers in small-signal regime[5], the noise figure is always slightly worse at 1.533μm than at 1.550μm.

Another important point is the noise figure sensitivity to the pump wavelength. In small-signal regimes[5], the noise is reduced by lowering the pump wavelength down to 1.46μm, even if the efficiency is lowered. But for strong input signals, we see on fig.5 that the optimum is shifted due to absorption cross-section values becoming too small below 1.47μm.

Other specific observations related to different amplifier configurations, such as the strong signal counter-propagative configuration, will be discussed.

We analyze the noise of the EDFA in various signal regimes. Experimental observations of unusual noise figure behaviors near the gain saturation regime are explained by the effects of the counterpropagating ASE beam. This effect being relatively important in high gain fibers, it appears that fiber length must be carefully chosen to avoid an increase of the noise figure without any significant gain benefit. However, the use of an in-line filter in the middle of the erbium-doped fiber [10,11] will avoid noise penalties as well as the use of an in-line isolator.

This work was supported by France-Telecom and Alcatel.

**References :**

[1] R.I. LAMING, W.L. BARNES, L. REEKIE, P.R. MORKEL and D.N. PAYNE, in Proc. SPIE 1171, 82-92 (1990).
[2] E. DESURVIRE, IEEE Photon. Technol. Lett., 2, 208-210 (1990).
[3] W.I. WAY, A.C. VON LEHMAN, M.J. ANDREJCO, M.A. SAIFI and C. LIN, in Technical Digest on Optical Amplifiers, (OSA), Vol.13, 134-137 (1990).
[4] E. DESURVIRE, M. ZIRNGIBL, H.M. PRESBY and D. DI GIOVANI, in Proc. OFC'91, 176 (1990).
[5] C.R. GILES and E. DESURVIRE, J. Lightwave Technol., 9, 271-283 (1991).
[6] J.F. MARCEROU, H. FEVRIER, J. AUGE, C. CLERGEAUD, S. LANDAIS, A.M. BRIANCON and B. JACQUIER, in Technical Digest on Optical Amplifiers, (OSA), Vol.13, 68-71 (1990).
[7] J.F. MARCEROU, H. FEVRIER, J. RAMOS, J. AUGE and P. BOUSSELET, in Proc. SPIE 1373, 168-186 (1990).
[8] H. VENDELTORP,-POMMER, B. PEDERSEN, A. BJARKLEV and J.H. POVLSEN, in Proc. SPIE 1373, 254-265 (1990).
[9] J.F. MARCEROU, H. FEVRIER, J. AUGE, J.RAMOS and A. DURSIN, Electron. Lett., 26, 1102-1104 (1990)
[10] M. TACHIBANA, R.I. LAMING, P.R. MORKEL and D.N. PAYNE, in Technical Digest on Optical Amplifiers, (OSA), Vol.13, 44-47 (1990).
[11] G. GRASSO, F. FONTANA, A. RIGHETTI, P. SCRIVENER, P. TURNER and P. MATON, in Proc. OFC'91, 195 (1990).

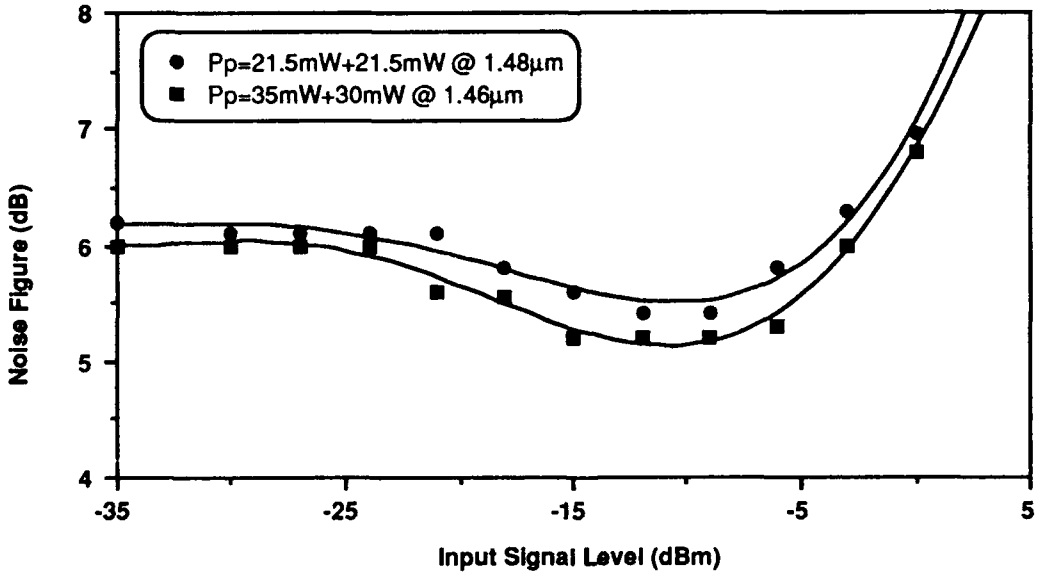


**Figure1 :** Example of noise figure behavior in a both-end 1.48µm-pumped amplifier. The signal is @ 1.550µm.

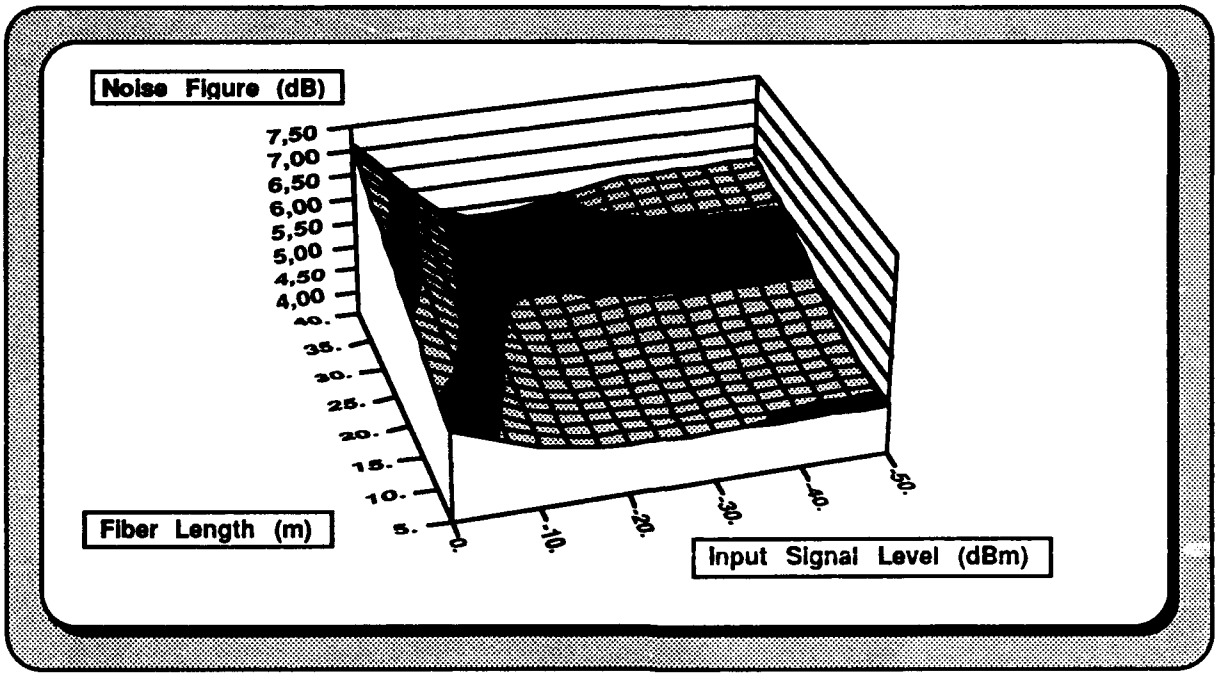


**Figure 2 :** Noise figure versus the input signal regime and the fiber length.
Signal @ 1.550µm, $P_p$=10mW @ 1.48µm

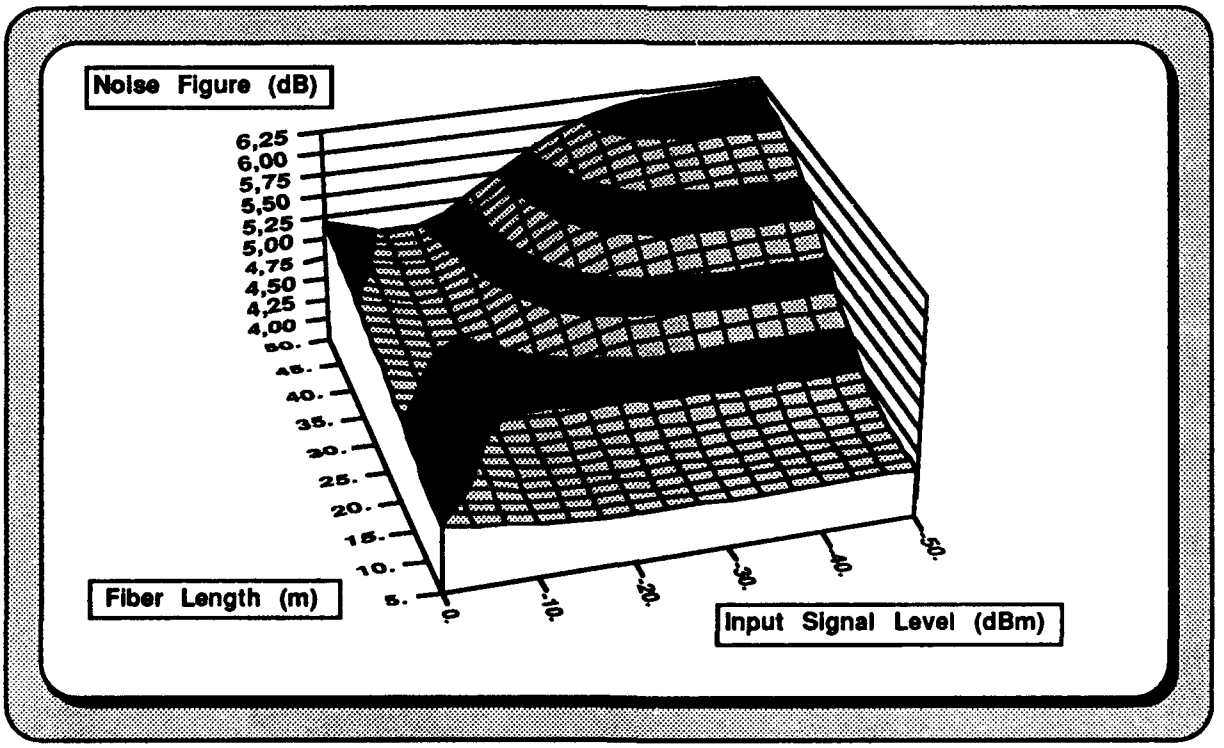


**Figure 3 :** Noise figure versus the input signal regime and the fiber length.
Signal @ 1.550µm, $P_p$=50mW @ 1.48µm

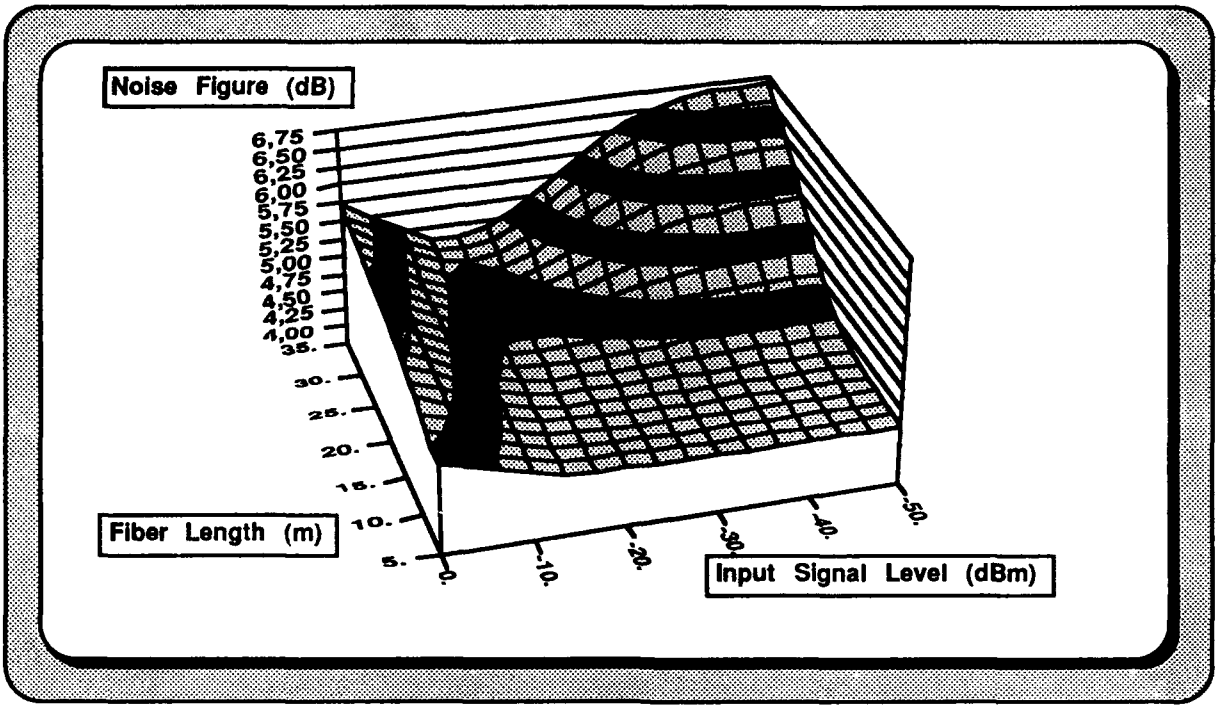


**Figure 4 :** Noise figure versus the input signal regime and the fiber length.
Signal @ 1.533μm, $P_p$=50mW @ 1.48μm

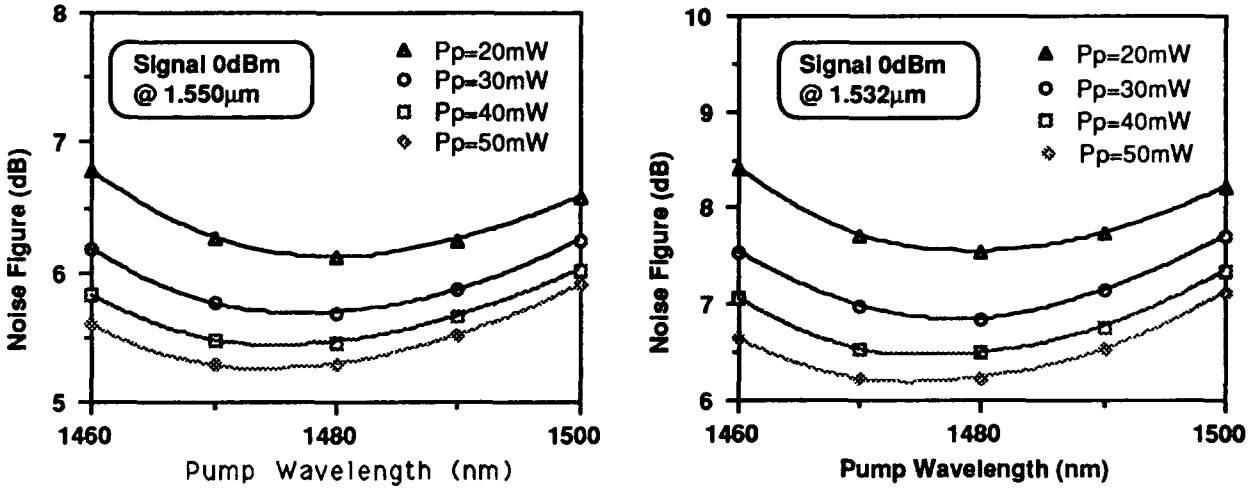


**Figure 5 :** Noise figure sensitivity of the pump wavelength for highly saturated amplifiers.
The optimum fiber length is taken for each pump power and wavelength.

# Characteristics of 1.48 μm pumped erbium-doped fiber amplifier with high efficiency

Sumitomo Electric Industries, LTD
1, Taya-cho, Sakae-ku, Yokohama, 244, Japan

## 1.INTRODUCTION

Erbium-doped fiber amplifiers(EDFAs) are very attractive devices for single-mode fiber communication systems operating in the 1.55 μm wavelength band. [1] The main advantages of EDFAs are polarization-insensitive high gain, high amplification efficiency, low insertion loss, low noise and wide bandwidth. [2] There are two important parameters to evaluate EDFA's performance; an energy conversion efficiency and a gain coefficient.

In this paper, we report an extremely high efficiency EDFA with a slope efficiency of 86% and a gain coefficient of 6.3dB/mW at 1.48 μm by increasing the numerical aperture(NA) of the erbium-doped fiber and concentrating the doped $Er^{3+}$ ions near the center of the core. [3] [4] Both are the highest values reported to date for EDFAs pumped at 1.48 μm. [5] [6]

## 2.FABRICATED FIBERS

The glass composition of the core is Er:$GeO_2$-$SiO_2$-$Al_2O_3$. The concentrations of $Er^{3+}$ ions and aluminium are approximately 300ppm and 0.3wt%, respectively. Both $Er^{3+}$ ions and alumina are doped only in the central area with the radius less than one half of the core radius. Relative refractive index difference of 2.0% has been achieved by doping Ge in the core and adding F in the cladding. The core diameter, the cutoff wavelength, and the mode field diameter at 1.55 μm are 2.9 μm, 1.17 μm, and 3.7 μm, respectively.

## 3.RESULT AND DISCUSSION

Fig.1 shows amplified signal output as a function of launched pump power in the forward and backward pumping configurations when input signal power was relatively high. The input signal power was 1mW in the forward pumping and 0.1mW in the backward pumping. The signal wavelength was 1.554 μm. It was found that the output signal power increased linearly as the launched pump power increased in both cases. The slope efficiency was 80% in the forward pumping configuration and 86% in the backward pumping configuration. The latter value is very close to the quantum-limited efficiency of 95% for the pump wavelength of 1.48 μm and the signal wavelength of 1.554 μm, and it is the highest slope efficiency ever reported for EDFAs, to our best knowledge.

Spectral signal output at 18mW forward pump power is indicated by open circles in Fig.2. Input signal power was -3dBm. In order to examine effects of alumina doped in the core, [7] another $Er^{3+}$-doped fiber having a similar structure but with no alumina doped was tested for comparison. Results obtained at 28mW pump power are plotted in the same figure by solid squares. The input signal power was -5dBm. It was found that wavelength-independent high signal output was obtained from the alumina-codoped fiber in a broad wavelength

range(1.53 μm to 1.57 μm), while two peaks existed in the output signal spectrum of the alumina-nondoped fiber.

Fig.3 shows the signal gain observed at 1.554 μm as a function of the launched pump power in the small input signal regime and in the forward pumping configuration. The input signal power was -39dBm. The gain exceeded 30dB when the pump power was above 5mW. The pump threshold was as small as 2.5mW. The gain coefficient was calculated to be 6.3dB/mW and this is also the highest value reported so far for EDFAs pumped at 1.48 μm.

The amplifier noise figure was also measured through an amplified spontaneous emission(ASE) power measurement. The noise figure(NF) is given by the following equation, when the signal-spontaneous beat noise is dominant, [8]

$$NF = P_{ASE} / h \nu_S \Delta \nu G, \quad (1)$$

where $P_{ASE}$ is the power of the ASE through an optical filter with a bandwidth of $\Delta \nu$, $\nu_S$ is the signal frequency and G is the gain of the EDFAs. Fig.4 shows the noise figure measured as a function of the signal wavelength in the forward pumping scheme. The input signal power and the pump power were -35dBm and 17mW, respectively. The noise figure was found to be around 5dB and almost independent of the signal wavelength in a wavelength range of 1.525 μm to 1.57 μm, in spite of the wavelength dependence of the gain.

The developed erbium-doped fiber has an extremely small mode field diameter(MFD). Therefore, splice loss could become unacceptably large when spliced with standard fibers. Fig.5 shows measured splice loss as a function of the discharge duration in fusion-splicing of the erbium-doped fiber and a standard dispersion-shifted fiber. MFD of the dispersion-shifted fiber used in the experiment was 8.0 μm at 1.55 μm. It was found that the splice loss decreased as the discharge duration increased and that the splice loss could be reduced to 0.5dB by simply adjusting the discharge conditions, although the splice loss predicted theoretically from the MFD mismatch was as high as 2.4dB. This is possibly because fluorine doped in the cladding of the erbium-doped fiber is diffused fairly quickly by heat and the MFD expands locally at the fiber end. [9]

## 4.CONCLUSION

An erbium-doped fiber amplifier pumped at 1.48 μm with extremely high efficiency has been developed. The slope efficiency is as high as 86% at a signal wavelength of 1.554 μm. The gain coefficient reaches 6.3dB/mW at the same signal wavelength in the small signal input regime. In the large signal regime, signal output is almost constant in a broad wavelength range of 1.53 μm to 1.57 μm. The noise figure is also nearly constant in the same wavelength range. It has also been found that, in spite of its small MFD, the erbium-doped fiber can be fusion-spliced to standard dispersion-shifted fibers with low loss possibly because of quick diffusion of fluorine doped in the cladding.

## REFERENCES

(1) M.Shigematsu, et al. :Technical Digest on Optical Amplifiers and Their

Applications, paper WB3, pp240-243(1990)
(2) E.Desurvire, et al. :Journal of Lightwave Technol., Vol.7, pp2095-2104 (1989)
(3) M.Shimizu, et al. :Technical Digest on Optical Amplifiers and Their Applications, paper MB2, pp12-13(1990)
(4) E.Desurvire, et al. :Journal of Lightwave Technol., Vol.8, pp1730-1741 (1990)
(5) S.P.Craig-Ryan, et al. :16th ECOC, pp571-574(1990)
(6) J.L.Zyskind, et al. :Technical Digest on Optical Amplifiers and Their Applications, paper PDP6(1990)
(7) C.G.Atkins, et al. :Electron. Lett., Vol.25, pp910-911(1989)
(8) P.R.Morkel, et al. :Opt. Lett., Vol.14, pp1062-1064(1989)
(9) J.T.Krause, et al. :11th ECOC, pp629-632(1985)

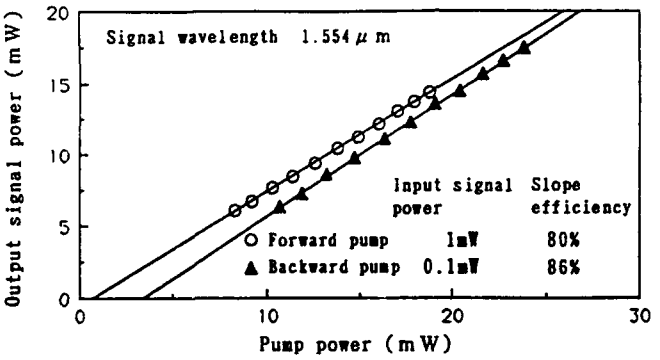


Fig.1. Amplified signal output as a function of launched pump power

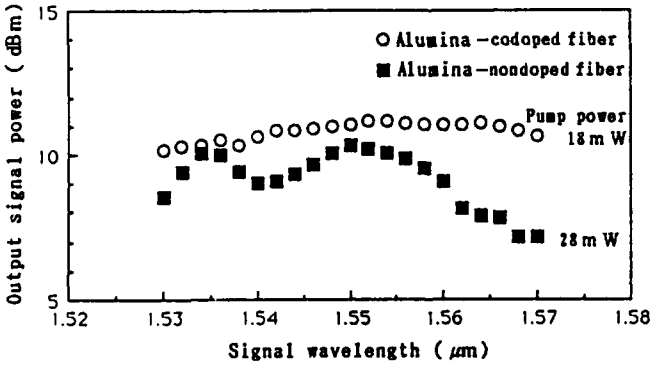


Fig.2. Spectral signal output in the large input signal regime

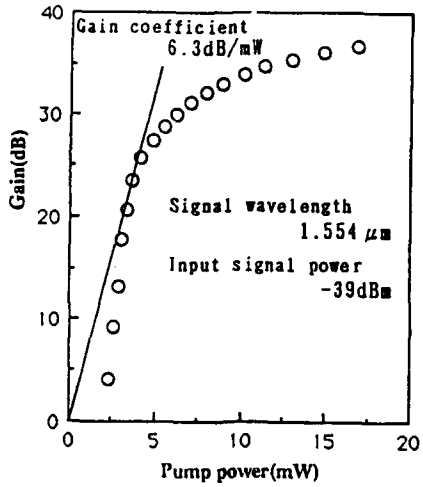


Fig.3. The gain as a function of launched pump power

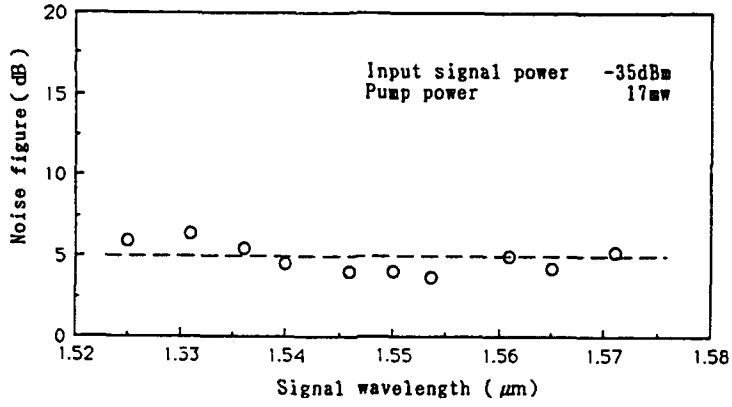


Fig.4. Noise figure vs signal wavelength

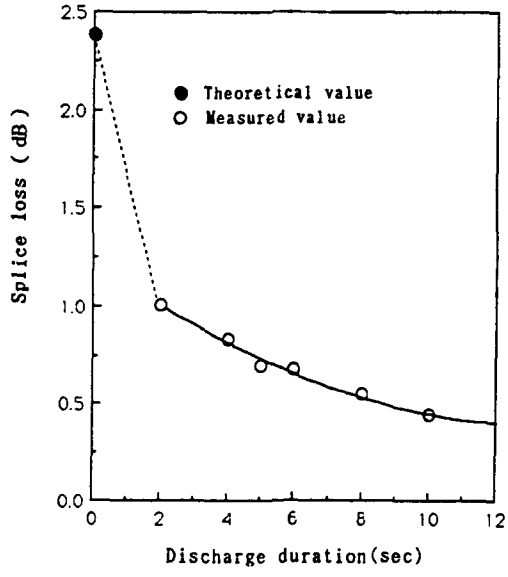


Fig.5. Splice loss as a function of the discharge duration in fusion-splicing of the erbium-doped fiber and a standard dispersion-shifted fiber

# Conversion Efficiency and Noise in Erbium-Doped Fiber Power Amplifiers



**B. Pedersen*, M.L. Dakss and W.J. Miniscalco**

GTE Laboratories Incorporated
40 Sylvan Road
Waltham, MA 02254

*Permanent address:
Technical University of Denmark
Electromagnetics Institute
ter for Broadband Telecommunications
DK-2800 Lyngby, Denmark

There has been a growing awareness of the importance of $Er^{3+}$-doped fibers as power amplifiers in many applications including wavelength- and frequency-multiplexed systems as well as distribution systems with large fanouts [1]. This is a consequence of their excellent behavior under highly saturated conditions: immunity to crosstalk and high signal output powers. The characteristics of fiber power amplifiers, however, have not been extensively investigated. Relevant parameters include the operational configuration (forward, backward or bidirectional pumping), the signal and pump wavelength, fiber composition, fiber index and $Er^{3+}$-doping profile. Due to the high cost of pump lasers and their limited power, the paramount consideration for a power amplifier is efficiency. The signal-to-noise ratio is also of importance, particularly in analog applications such as the AM-VSB systems now favored for video distribution [2]. We have investigated both these properties using an accurate numerical model and measured input parameters. The optimum waveguides have been determined for both 980 nm and 1480 nm pumping, and the effects of confined $Er^{3+}$-doping have also been elucidated.

## Theory

The analysis is based on a full scale numerical model that has been shown to predict the properties of the $Er^{3+}$-doped fiber with high accuracy [3]. To treat 1480 nm pumping the model was extended to include resonant pumping of the emitting $^4I_{13/2}$ level. The model uses the actual LP-modal distributions of the signal and pump modes that are calculated from the fiber index profiles. The complete spectrum of the forward and backward amplified spontaneous emission (ASE) is retained throughout the calculation. The analysis uses the excited state lifetime and emission and absorption cross section spectra that were experimentally determined for an Er/Al/P-doped silica fiber. The most important values are as follows: $\tau$ = 10.8 ms, $\sigma_a$(980 nm) = 2.1 x $10^{-25}$ $m^2$, $\sigma_a$(1480 nm) = 2.0 x $10^{-25}$ $m^2$, $\sigma_a$(1532 nm) = 5.2 x $10^{-25}$ $m^2$, $\sigma_a$(1555 nm) = 1.9 x $10^{-25}$ $m^2$, $\sigma_e$(1480 nm) = 0.73 x $10^{-25}$ $m^2$, $\sigma_e$(1532 nm) = 5.5 x $10^{-25}$ $m^2$, $\sigma_e$(1555 nm) = 3.3 x $10^{-25}$ $m^2$. Absorption and emission cross sections are indicated by $\sigma_a$ and $\sigma_e$, respectively.

We consider the quantum conversion efficiency (QCE) as the most important figure of merit for a power amplifier and define it as the average number of photons added to the signal divided by the number of launched pump photons. The QCE was chosen because, being independent of wavelength, it is a more fundamental measure than the more practical power conversion efficiency. The latter is obtained by multiplying the QCE by the ratio of the pump wavelength to the signal wavelength. The second figure of merit considered is the amplifier noise figure, F, defined as

$$F = (S^{+}_{ASE}(\nu_s,L) + 1)/G \qquad (1)$$

where $S^{+}_{ASE}(\nu_s,L)$ is the power spectral density of the ASE co-propagating with the signal, evaluated at the signal frequency, $\nu_s$, at the output of the fiber of length L. G is the gain.

**Waveguide Optimization**

Waveguide design plays an important role in the QCE of a power amplifier just as it does in the gain efficiency of a small-signal amplifier. Pump photons not converted to signal photons are lost as spontaneous emission photons, ASE photons, and residual pump photons exiting the fiber. If the amplifier is highly signal-saturated, the number of photons lost to ASE is negligible compared to the total number of photons lost to residual pump and spontaneous emission. The loss to residual pump photons can be reduced by minimizing the threshold pump power, defined as the pump power needed to obtain 0 dB of gain in a fiber of infinitesimal length [4]. For a given pump wavelength, this is accomplished by increasing the overlap between the pump mode and the $Er^{3+}$ doping profile. The number of photons lost to spontaneous emission is related to the overlap between the signal mode and the profile of excited $Er^{3+}$ ions. Decreasing this overlap decreases the amount of local stimulated emission for a particular amount of spontaneous emission. This increases the overall spontaneous emission for a particular signal output power and leads to a less efficient amplifier.

Fig. 1 shows the QCE versus the cutoff wavelength of the $LP_{11}$ mode for signal wavelengths, $\lambda_s$, of 1532 nm (emission peak) and 1555 nm. Step-index fibers with NAs of 0.15, 0.25 and 0.35 were used with $Er^{3+}$ doped uniformly throughout the core. The pump and signal were launched from the same fiber end with powers of 50 mW and 1 mW, respectively, and for each point on the curves the fiber length was optimized to give maximum QCE. Figs. 1a and 1b are for pump wavelengths, $\lambda_p$, of 980 nm and 1480 nm, respectively, and it is seen that pump wavelength makes a difference of less than 150 nm in optimum cutoff wavelength. This indicates that the overlap between the signal and the $Er^{3+}$ profile is more important than the overlap between the pump mode and the $Er^{3+}$ profile. Moreover, QCE is not very sensitive to the cutoff wavelength over the range from 700 nm to 900 nm for the 980 nm pumping case, and over the range from 800 nm to 1000 nm for the 1480 nm pumping case. It is also observed that the QCE for the signal wavelength of 1555 nm is higher than that for the signal wavelength of 1532 nm when pumping at 1480 nm, while the opposite is true when pumping at 980 nm. This can be explained by the difference in population inversions developed. Since 980 nm pumping produces a relatively high inversion, the effects of reabsorption are small and the highest QCE is expected near the peak of the stimulated emission cross section. In contrast, the lower inversion achieved by 1480 nm pumping increases the significance of reabsorption and the best efficiencies are expected at longer wavelengths where the ratio of the absorption to the stimulated emission cross section is lower.

**Conversion Efficiency and Noise Figure**

Fig. 2 plots the QCE and the noise figure, F, versus the launched pump power for an input signal power of 1 mW. For the 980 nm pumping case (Fig. 2a), the cutoff wavelength is fixed at 750 nm when the signal wavelength is 1532 nm and at 800 nm when the signal wavelength is 1555 nm. For the 1480 nm pumping case (Fig. 2b), the cutoff wavelength is fixed at 900 nm . All other conditions are the same as in Fig. 1, including fiber lengths that have been optimized with respect to QCE. As seen from the figures, QCE and F improve with increasing pump power. It is also observed that the F is up to 3 dB higher for the signal wavelength of 1532 nm than for 1555 nm. This follows from the incomplete inversion due to saturation combined with the higher absorption to emission cross section ratio at 1532 nm. Moreover, as 1480 nm pumping leads to a lower inversion than 980 nm pumping, noise figures are up to 3 dB higher when 1480 nm is used.

Although increasing the NA is observed to increase the QCE, the NA does not affect the F significantly

for the cases treated in Fig. 2. At first glance this appears surprising since a higher NA improves the overlap between the pump mode and the $Er^{3+}$ doping profile and is expected to increase the inversion. However, it also improves the overlap between the signal mode and the excited $Er^{3+}$ profile, thereby increasing the stimulated emission rate which acts to reduce the inversion. It appears that for fibers with lengths and cutoff wavelengths that have been optimized for QCE, these two effects largely cancel each other.

### $Er^{3+}$ Confinement

In actual operation the $Er^{3+}$-doped fiber must be fusion spliced to a standard telecommunications fiber, and the improvement in QCE from using a higher NA is countered by increasing splice losses. For a fixed NA, however, QCE can be improved without affecting splice loss by constraining the $Er^{3+}$ doping profile to lie within the core. Fig. 3 plots QCE and F versus the launched pump power for a series of confinement factors ranging from 0.2 to 1.0. The confinement factor is defined as the ratio of the radius of the $Er^{3+}$ step doping profile to that of the refractive index step profile. In the figure, which treats the case of an NA of 0.15, the solid and dashed curves are for pump wavelengths of 980 nm and 1480 nm, respectively. Results for signal wavelengths of 1532 nm (Fig. 3a) and 1555 nm (Fig. 3b) are illustrated. For each point on the curves, both the fiber length and the cutoff wavelength have been optimized. As expected, decreasing the confinement factor results in a higher QCE with the greatest improvement realized at low pump powers. It is also observed that the F is not significantly affected by the confinement.

### Summary and Conclusions

A comprehensive analysis of the quantum conversion efficiency and noise figure of $Er^{3+}$-doped fiber power amplifiers has been performed. All input parameters used in this analysis were experimentally determined. The investigation included the effects of waveguide design, signal wavelength, pump wavelength, pump power, and $Er^{3+}$ confinement. The analysis indicates that pump wavelength has only a minor effect upon the cutoff wavelength for maximum QCE, and that for a given pump wavelength QCE is relatively insensitive to cutoff wavelength. Efficiency can be greatly improved by increasing the fiber NA, with the largest enhancements at lower pump power levels where QCE can be more than doubled by increasing the NA from 0.15 to 0.25. Noise figure, however, is not significantly affected by changes in NA for fibers with lengths and cutoff wavelengths that have been optimized with respect to QCE. The use of confined $Er^{3+}$ doping has little effect on F but can improve QCE by as much as 60% in cases where inversion is critical, e.g. low pump powers, 1480 nm pumping, and 1532 nm signal. Because of signal saturation, complete inversion is not achieved even at very high pump powers. This manifests itself as noise figures exceeding 3 dB and through higher values at 1532 nm than at 1555 nm due to the difference in relative sizes of the absorption and emission cross sections. A further penalty in F of up to 3 dB is realized when pumping at 1480 nm as compared to 980 nm.

We wish to thank M.P. Singh for providing his absorption cross sections prior to publication, and acknowledge L.J. Andrews for encouragement and helpful discussions.

### References

1. J. F. Massicott et. al., Proc. SPIE Vol. 1373 Fiber Laser Sources and Amplifiers II (1990), M. Digonnet, ed., pp. 93-102.
2. P. M. Gabla et. al., IEEE Phot. Technol. Lett. (1991), vol. 3, pp. 56-58.
3. B. Pedersen et. al., OSA/Techn. Dig. Optical Amplifiers and Their Applications (1990), vol.13, pp. 653-655.
4. J.Hedegaard Povlsen et. al., Electronics. Letters. (1990), vol. 26, pp. 1419-1420.

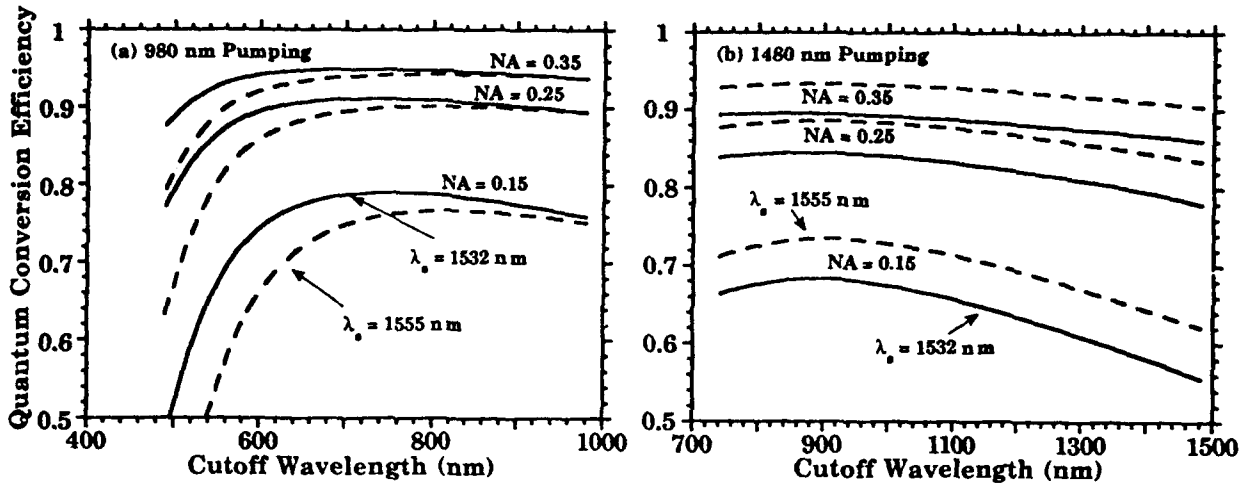


Fig. 1. Conversion efficiency versus cutoff wavelength for a step-index fiber with uniform $Er^{3+}$ doping over the core. NAs of 0.15, 0.25 and 0.35 and signal wavelengths of 1555 nm (dashed) and 1532 nm (solid) are shown. Pumping is at (a) 980 nm and (b) 1480 nm.

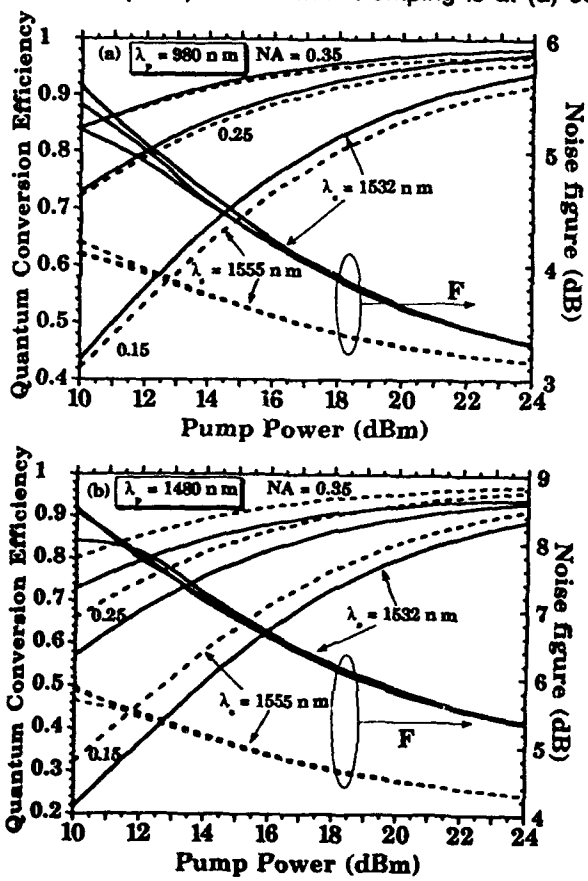


Fig. 2 Conversion efficiency and noise figure versus launched pump power for pump wavelengths, $\lambda_p$, of (a) 980 nm and (b)1480 nm. Fiber has step-index profiles with NAs of 0.15, 0.25 and 0.35; the $Er^{3+}$ is doped uniformly over the core.

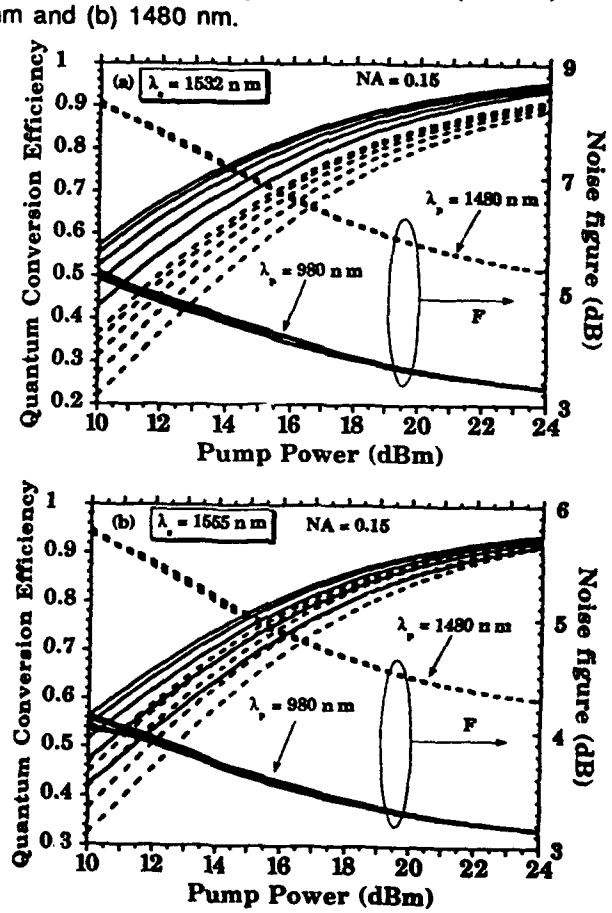


Fig. 3 Conversion efficiency and noise figure versus launched pump power for signal wavelengths, $\lambda_s$, of (a)1532 nm and (b)1555 nm. Confinement factors of 1.0, 0.8, 0.6, 0.4 and 0.2 (increasing QCE with decreasing confinement factor).

# Pump Configuration and Length Optimization of Erbium-doped Fiber Amplifier for Low Noise and High Power Operation

M.Suyama, I.Yokota, S.Watanabe and H.Kuwahara
Fujitsu Laboratories Ltd.
1015, Kamikodanaka, Nakahara, Kawasaki, 211, Japan

## Introduction

In a ultra-long system with cascaded erbium-doped fiber amplifiers[1] (EDFAs), in order to keep a signal-to-noise ratio (SNR) as high as possible, EDFA[2] having high output power and low noise is highly required as a post-amplifier or as an in-line-amplifier. Such an EDFA is also important for optical pre-amplifiers with large dynamic ranges. Although Way et al. reported a low noise figure (NF) in a saturation region under the condition of sufficiently high pump power[3], the relationship between lowering the NF and optimizing the gain of EDFA was not clear. In this paper, we report that an EDFA having both a high output power (+15dBm) and a low NF (6dB) can actually be realized using 1.48μm pump LDs when the EDFA length is optimized to give a maximum gain for large signal power. In addition, we also show that there is a remarkable difference between forward and backward pump in terms of NF characteristics of EDFA in a deep saturation.

## Experiment

The erbium-doped fibers (EDFs) used in the experiment were germano-silicate fibers with a mode-field diameter of 7μm and a cutoff wavelength of 1.1μm. 500ppm erbium was doped in the central region of the core with Al. The EDFs were pumped by 1.48μm LDs which launched 60mW pump power into it. Having a very high power-conversion efficiency, our EDFA[4] gives a signal output power of +16dBm (40mW) with only 60mW backward pump. We measured a gain and an NF characteristics at saturation for backward and forward pump using two fibers of different lengths. One fiber length was 72m, which was optimized for a small-signal gain of -30dBm input, while the other was 49m, optimized for a large input signal of 0dBm. In the NF measurement, we employed a heterodyne technique[5] with a balanced optical receiver used to make the local-spontaneous beat noise more dominant. The signal was from a three-electrode DFB-LD[6] with an emission wavelength of 1552nm and a relative intensity noise (RIN) of -155dB/Hz. Uncerntainty in the NF measurement is estimated to be around ±0.5dB.

## Gain saturation characteristics

A striking difference between the forward and backward pump is that while almost the same output power is obtained from both long

and short fibers using the backward pump (Fig.1), the short fiber delivers a higher output power than the long one using the forward pump (Fig.2). The latter characteristics can be easily understood when one notes that depleting the population inversion, a strong signal produces a lossy region. Therefore, a short fiber is suitable for high output power operation at the expense of reduced small-signal gain. This description was confirmed by a simple two-level model of the EDFA[7]. The calculated characteristics (inset of Fig.2) using experimentally determined parameters qualitatively agrees with the data. On the other hand, the characteristics of backward pump is not understood yet, because the simple two-level model predicts the same characteristics as the forward pump. The mechanisms which should be included in the simple model to explain this difference would be those mentioned in ref.8 such as signal excited absorption or fiber loss.

**Noise figure (NF) in saturation region**

The difference of NF characteristics between backward (Fig.3) and forward (Fig.4) pump is found in the modest output power region (i.e. less than +10dBm) and the high output power or saturation region (i.e. more than +10dBm).

In the modest output power region, the NF of the backward pump is 5-6dB depending on the fiber length, while that of the forward pump is 4-5dB almost independent of length. This behaviour is consistent with previous analyses[9,10].

Noise figure degradation in the saturation region is caused by the depleted inversion due to a strong signal[11]. In the backward pump, 1dB NF degradation point is +15dBm for both fibers. It is noteworthy that even with backward pump, an NF of 6dB with an output power of +15dBm was obtained using a short EDF. In the forward pump, 1dB NF degradation point of the short fiber is +13.5dBm, 2.5dB higher than the longer one, a result which can be explained qualitatively by the two-level model (inset of Fig.4). A higher output power could be achieved without degrading the NF by increasing the pump power in both pump configurations. Interestingly, the differences being the reflection of gain saturation, a close correlation between the NF degradation and gain saturation in each pump configuration is observed.

The above results highlight the importance of the proper choice of pump configuration and the length optimization of the EDFA in system applications. If a large small-signal gain, low noise EDFA, a frequent requirement for optical pre-amplifier, is required, a long EDFA with a forward pump would be a good choice. On the other hand, if a high output power, low noise EDFA with limited available pump power, a frequent requirement for in-line-amplifier, is required, a backward pump with a short EDFA can be one solution.

## Conclusion

We described that length optimization plays an important role in the gain and NF characteristics of an EDFA. In particular, we have found that NF degradation characteristics in saturation region is dependent not only on the pump configuration but also on the EDFA length. Based on these investigations, we have realized an EDFA with a high output power of +15dBm and low NF of 6dB using a backward pump by 60mW power from 1.48μm LDs. These results are quite important in designing EDFAs suitable for various requirements of optical transmission systems with EDFAs.

## Acknowledgements

We thank S.Inagaki for fabricating a highly efficient erbium-doped fiber and S.Kinoshita for measuring RIN of three-electrode DFB-LD. Also one of the authors (M.S.) is grateful to Dr.Laming of the University of Southampton for fruitful discussions while he stayed at the University.

## References

(1) S.Saito et al., OFC'90, PD2
(2) R.J.Mears et al., Electron. Lett., **23**, 1026, 1987
(3) W.I.Way et al., Optical Amp. and Their Applications, TuB3, 1990
(4) S. Inagaki et al., submitted to this conference
(5) R.S.Vodhanel et al., OFC'90, WL4
(6) H.Onaka et al., OFC'90, FD4
(7) M.Suyama et al., Electron. Lett., **26**, 1756, 1990
(8) R.I.Laming et al., Optical Amp. and Their Applications, MB3, 1990
(9) R.Olshansky, Electron. Lett., **24**, 1363, 1988
(10) P.R.Morkel et al., Opt. Lett., **14**, 1062, 1989
(11) R.I.Laming et al., Photon. Technol. Lett., **2**, 418, 1990

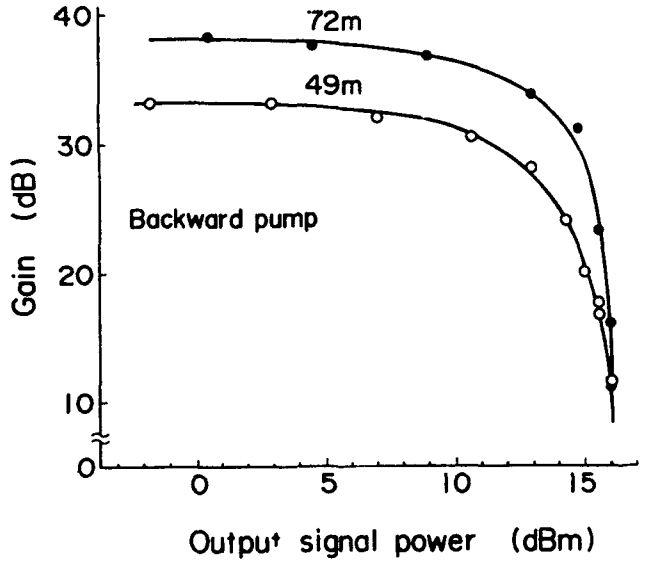


Fig.1. Gain saturaion characteristics with backward pump. Pump input power is 60mW.

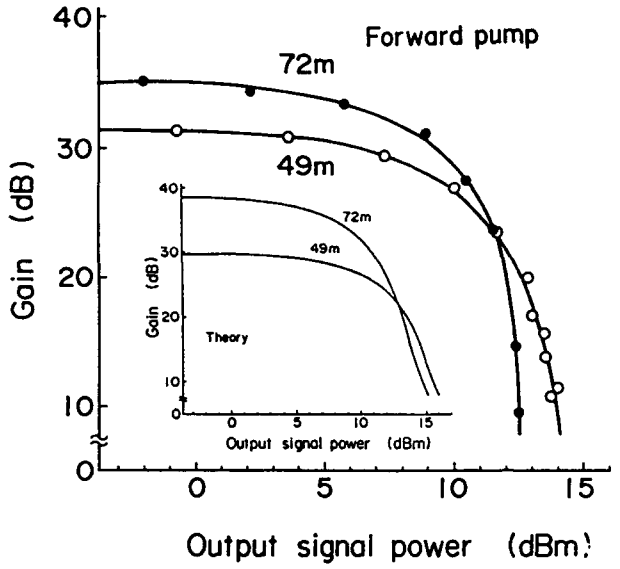


Fig.2. Gain saturaion characteristics with forward pump. Pump input power is 60mW. Inset is the calculation based on two-level model.

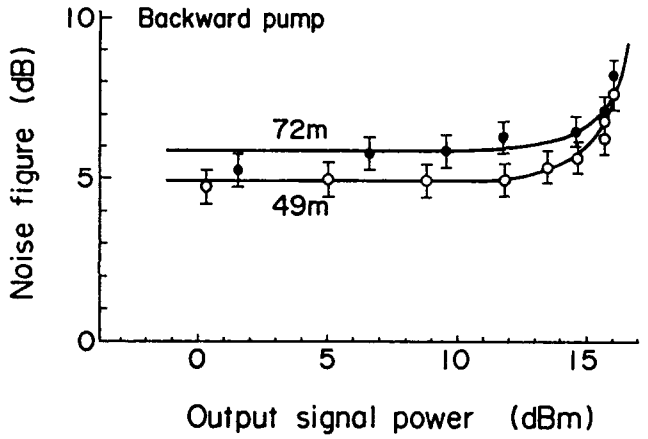


Fig.3. NF characteristics with backward pump. Pump input power is 60mW.

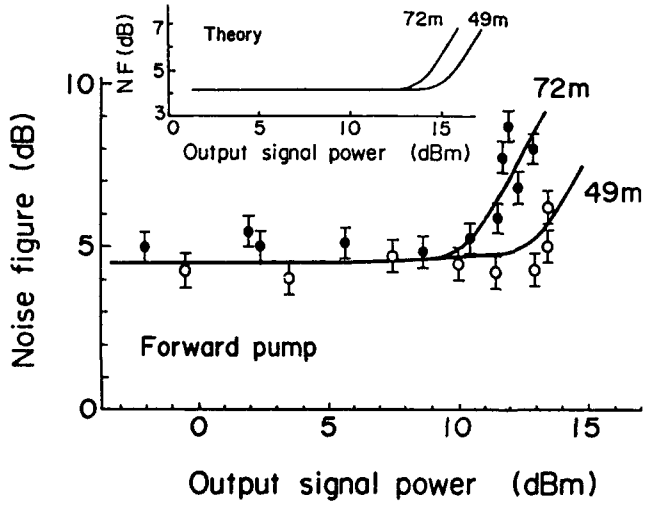


Fig.4. NF characteristics with forward pump. Pump input power is 60mW. Inset is the calculation based on two-level model.

Friday, July 26, 1991

# System Performance Considerations

**FA** 8:00am–9:45am
Cabaret Room

Y. K. Park, *Presider*
*AT&T Bell Laboratories, USA*

# The Appropriateness of Squeezed Light for Long-Distance Communication

BERNARD YURKE

AT&T Bell Laboratories, Murray Hill, NJ 07974

Squeezed light allows suitable optical systems to perform at below the standard shot-noise level. Below shot-noise performance of optical interferometers employing squeezed light has been demonstrated in the laboratory [1,2] and it is clear that squeezed state enhanced microscopes and spectrometers could be constructed. There is also considerable interest in the issue of whether optical communications systems could benefit from the use of squeezed light. In fact, much of the early work on squeezed light [3-5] was motivated by quantum communications issues, particularly those involving coherent communication.

Two parameters of considerable use in characterizing the performance of a communications system are channel capacity and bit error rate. The optimal channel capacity of a lossless optical communications channel, given a mean power constraint, is achieved when photon number operator eigenstates are transmitted and the photons are counted at the receiver. In practice, coherent states are generally transmitted and photon counting or coherent detection such as homodyne or heterodyne detection is employed at the receiver. The channel capacity of such a system comes within a factor of two of the optimal channel capacity. If amplitude and phase modulation are simultaneously employed, the channel capacity closely approaches the ideal channel capacity. Hence, conventional detection techniques can in principle come close to achieving the ideal channel capacity. Employing squeezed state transmitters will thus not dramatically increase the channel capacity of an optical communication system [6]. The expense of the extra hardware involved in making a squeezed state transmitter is thus likely to make squeezed state enhanced communication uneconomical if channel capacity were the only relevant figure of merit.

Squeezed light can reduce homodyne detection noise to below the shot-noise level. Squeezed light can thus, at least in principle, dramatically reduce the bit error rate of a coherent communication system. It should be kept in mind, however, that one can, in principle, make the bit error rate as small as desired and still transmit at the rate set by the channel capacity by using error corrective coding. Whether one uses squeezed light or the more conventional technique of error corrective coding will boil down to the issue of which technology is more economical to implement.

In the discussion so far it has been assumed that the communications channel is lossless and that the only noise present in the communication channel is that due to the quantum statistics of light. For long-distance communication one expects the transmitted light to be heavily attenuated by the time it arrives at the receiver.

Squeezed states consist of carefully engineered superpositions of photon number operator eigenstates. The superposition is delicate and is easily destroyed by the losses as they randomly remove photons from the light beam. Thus, in contrast to coherent states which can be arbitrarily attenuated and still remain coherent states, squeezed light that has suffered $3dB$ loss can exhibit no more than 50% squeezing below the shot noise level. In fact, letting $\eta$ denote the quantum efficiency of a communications system, i.e., $\eta$ equals the number of photons transmitted divided by the number of photons "seen" by the receiver, the noise floor measured in shot noise units is no lower than $1-\eta$ at the receiver [7]. So, when the quantum efficiency goes to zero, the noise floor approaches the shot noise floor and no benefit is realized in using squeezed light. The penalty exacted by losses on squeezed light can be made graphic by considering current generation squeezed state experiments. The chief losses one has to consider in these experiments are: the reflection losses from the optics $\eta_T$, the mode-matching efficiency $\eta_M$, and the detector efficiency $\eta_D$. Each of these efficiencies individually can be fairly good. Typically $\eta_T = 0.9$, $\eta_M = 0.8$, and $\eta_D = 0.9$. The overall efficiency of such a system is obtained by multiplying these efficiencies together, $\eta = \eta_T\eta_M\eta_D \approx 0.6$, so that even if one had an ideal squeezer the useful noise reduction would be no more than $4dB$. A typical squeezed state system is hardly a communications system, however. In a communications system there are likely to be many more components through which the squeezed light must pass (modulators, switches, multiplexers, etc.), each of which will have losses of its own. Hence, to take advantage of the bit error rate reduction that is made possible by using squeezed light, one will have to do one's optics very very well and insure that nearly every photon transmitted arrives at the receiver. Clearly, in a long-distance communication system where the light suffers many $dB$ of loss before reaching the receiver, there will be little benefit from using squeezed light. Using phase insensitive repeater amplifiers along the length of the fiber to reamplify the light only makes the performance of a squeezed light communication system worse. The spontaneous emission noise associated with reamplifying the light is every bit as bad as the random deletion noise associated with the loss.

To summarize, a lossless communication channel employing coherent detection could benefit from squeezed light in that the bit error rate could be reduced. However, losses severely limit the degree of noise reduction that can be realized using squeezed light. Squeezed light is thus likely to find very limited use in communications systems, particularly long-distance communication. For short-distance communication a poor signal-to-noise ratio or bit error rate is generally not a problem, making the use of squeezed light unnecessary. However, it is possible to imagine circumstances where squeezed light would be useful for short-distance communication. For example, consider optical communication between chips in a computer. One can imagine that for such a system power consumption might be a major concern so that one would want to communicate with as few photons as possible. For such a system, size is also generally a concern so one may not want to give up the chip real estate necessary to implement error corrective coding in hardware. In addition, speed is generally a chief concern so one may not want to slow the

computer down by implementing error corrective coding in software. In this circumstance, squeezed state communication may become economical. One generally finds this same pattern when considering the viability of any proposed application for squeezed light. There is nearly always a conventional means of accomplishing the same thing. Hence, one must have additional restrictions such as bandwidth and power constraints that prevent the more conventional approach from being as cost effective as the squeezed light approach.

1 Min Xiao, Ling-An Au, and H. J. Kimble, "Precision measurement beyond the shot-noise limit," *Phys. Rev. Lett.*, vol. 59, pp. 278-281, 1987.

2 P. Grangier, R. E. Slusher, B. Yurke, and A. La Porta, "Squeezed-light - enhanced polarization interferometer," *Phys. Rev. Lett.*, vol. 59, pp. 2153-2156, 1987.

3 H. Takahashi, "Information theory of quantum-mechanical channels," in *Advances in Communication Systems*, A. V. Balakrishnan, Ed., Academic, 1965, p. 227.

4 H. P. Yuen and J. H. Shapiro, "Optical communication with two-photon coherent states - Part I: Quantum-state propagation and quantum-noise reduction," *IEEE Trans. Inform. Theory*, vol. IT-24, p. 657, 1978; also vol. IT-26, p. 78, 1980.

5 J. H. Shapiro, H. P. Yuen, and J. Machado Mata, "Optical communication with two-photon coherent states - Part II: Photoemissive detection and structured receiver performance," *IEEE Trans. Inform. Theory*, vol. IT-25, p. 179, 1979.

6 Y. Yamamoto and H. A. Haus, "Preparation, measurement, and information capacity of optical quantum states," *Rev. Mod. Phys.*, vol. 58, pp. 1001-1020, 1986.

7 R. E. Slusher and B. Yurke, "Squeezed Light for Coherent Communications," *J. Lightwave Technol.*, vol. 8, pp. 466-477, 1990.

# PREAMPLIFIED DIRECT DETECTION VERSUS HETERODYNE DETECTION: CAN THEY BE EQUIVALENT?

**Ozan K. Tonguz**
**State University of New York at Buffalo, Amherst, NY, USA**

**Richard E. Wagner**
**Bellcore, Red Bank, NJ, USA**

**Abstract**

In this paper the interrelationship of heterodyne receivers and preamplified direct-detection receivers is explained. We show that under certain conditions these two lightwave receiver types have equivalent performance. Furthermore, it is shown that this is a general result which is independent of the modulation format used.

**Introduction:** There is a growing debate in the lightwave research community concerning whether direct-detection lightwave systems using optical preamplifiers can be a substitute for heterodyne lightwave systems [1], [2]. This paper contributes to this debate by establishing a fundamental equivalence between these two receiver schemes. The established mathematical equivalence uses a comparison made by Oliver [3] between the SNR of the optical field at the output of an ideal optical amplifier and the output current of a balanced photomixer. Oliver's analysis, however, did not include laser phase noise or demodulation effects, and did not make an attempt to compare heterodyne receivers with direct-detection receivers. More recent work by Olsson [4] compares the performance degradations caused by in-line optical amplifiers on ASK heterodyne and direct detection receivers, but does not establish a general equivalence between the two receiver schemes.

The contribution of this paper is in comparing the performance of the two lightwave receiver schemes such that:

- the realistic case of laser phase noise is included in the formulation of the problem;
- the non-linear demodulation effects are included in the analysis of both receivers;
- the specific conditions of the mathematical equivalence between the two are identified;
- the established equivalence is generalized for all modulation formats including ASK, FSK, and PSK.

Even with these realistic effects included in the analysis, the two receivers have mathematically equivalent performance. This equivalence suggests that both analytical and practical design criteria already established for one scheme can be applied directly to the other scheme. For instance, both schemes have the same sensitivity, require the same linewidth and frequency control, and suffer the same degradations from bandwidth limitations, chromatic dispersion, and modulation imperfections. In particular, an ideal preamplified direct-detection receiver has a sensitivity of 20 photons/bit for DPSK modulation, the same as a heterodyne DPSK receiver [5].

**Receiver Description:** Figure 1 shows a heterodyne lightwave receiver with a delay-and-multiply demodulator. The received signal at the input of the IF filter can be represented as

$$e_h(t) = A_h(t)cos[\omega_{IF}t + \psi_h(t) + \phi_{nh}(t)] + n_h(t) \qquad (1)$$

where the subscript $h$ refers to the heterodyne receiver; $A_h(t) = 2R\sqrt{P_S(t)P_{LO}}$ is the signal amplitude, $\mathcal{R}=\eta e/h\nu$ is the detector's responsivity, $\eta$ is the quantum efficiency, $e$ is the electron charge, $h\nu$ is the photon energy, $P_S(t)$ and $P_{LO}$ are the powers of the optical signal and of the local oscillator (LO), respectively, measured at the input of the 3-dB coupler; $\omega_{IF}$ is the intermediate frequency; $\psi_h(t)$ is the angle modulation; $\phi_{nh}(t)$ is the combined phase noise of the transmitter and LO; and $n_h(t)$, which has a single-sided power spectral density of $\eta_h = 2eRP_{LO}$, is the additive noise due to LO shot noise. The LO is assumed to have a power level $P_{LO}$ sufficiently high that thermal noise is

negligible compared to shot noise, and a polarization state that matches the signal polarization.

Figure 2 shows a direct-detection lightwave receiver with an optical preamplifier, assumed to be either a semiconductor or a fiber-based traveling wave amplifier, which is followed by a polarizer that matches the signal polarization and eliminates the orthogonal polarization of the amplified spontaneous emission (ASE) noise. The optical signal is demodulated with a Mach-Zehnder interferometer, as has been used recently to demodulate CPFSK signals with $\tau < T$ [6] and DPSK signals when $\tau = T$ [7], where T is the bit period. The same arrangement also demodulates ASK signals when $\tau = 0$, but in a practical ASK receiver the interferometer and one photodiode can be eliminated without changing the performance.

The signal at the input of the optical bandpass filter can be represented as

$$e_d(t) = A_d(t)cos[\omega_d t + \psi_d(t) + \phi_{nd}(t)] + n_d(t) \tag{2}$$

where the subscript $d$ refers to the preamplified direct-detection receiver, $A_d(t) = \sqrt{2GP_S(t)}$ is the signal amplitude; G is the gain of the optical amplifier; $P_S(t)$ is the optical signal power; $\omega_d = 2\pi\nu$ is the carrier frequency, $\nu$ is the optical frequency; $\psi_d(t)$ is the angle modulation; $\phi_{nd}(t)$ is the laser phase noise of the transmitter laser; and $n_d(t)$, which has a single-sided PSD of $\eta_d = h\nu n_{sp}(G-1)$, is the ASE noise of the optical amplifier, where $n_{sp}$ is the spontaneous emission parameter.

The two noise processes, the shot noise $n_h(t)$ and ASE noise $n_d(t)$, are both Poisson processes. Each is assumed to have white power spectral density within the filter bandwidth. The laser phase noise processes, $\phi_{nh}(t)$ and $\phi_{nd}(t)$, are identical Wiener processes.

**Analysis:** The signals $e_h(t)$ and $e_d(t)$ differ by a proportionality constant and by their carrier frequencies $\omega_{IF}$ and $\omega_d$, respectively, but they have the same mathematical signal form and noise statistics. The demodulation processes produce baseband signals that differ only by a proportionality constant that is immaterial for receiver performance. This result depends on the assumption that the non-linear elements in the demodulation processes (i.e. the electrical mixer and the photodiodes following the interferometer) do not add significant noise.

In a heterodyne receiver, the output of the IF filter is $f_h(t)$, which is a filtered version of the heterodyne signal $e_h(t)$. After delay demodulation, the output $g_h(t)$ is

$$g_h(t) = f_h(t)f_h(t-\tau_h) \tag{3}$$

This product term contains the sum and difference frequencies of the IF frequency $\omega_{IF}$. The sum frequency components are filtered out by the low pass filter following the demodulator, leaving the baseband term $s_h(t)$. The baseband term contains the demodulated signal and noise originating from $n_h(t)$ and $\phi_{nh}(t)$ as processed through the IF filter, and low pass filter.

In a similar way, the signal for the preamplified direct-detection receiver $e_d(t)$ is filtered by the optical bandpass filter $H(\omega - \omega_d)$, which is assumed to have the same spectral shape and noise bandwidth, $BW_{IF}$, as the IF filter $H(\omega - \omega_{IF})$ of the heterodyne receiver but centered at a different carrier frequency. The resulting signal $f_d(t)$ is the same as $f_h(t)$, but differs by a proportionality constant and by the carrier frequency. In this case, the demodulation is performed on the optical signal using the Mach-Zehnder interferometer. Assuming that the interferometer beam splitters are ideal, the optical field in each arm of the interferometer is $f_d(t)/\sqrt{2}$. The interferometer produces the sum and difference terms of the fields $f_d(t)$ and $f_d(t-\tau_d)$ at its two outputs. The signal $g_d(t)$, which is the difference of the outputs of the two photodetectors, is

$$\begin{aligned} g_d(t) &= R\left|\frac{1}{\sqrt{2}}\{\frac{1}{\sqrt{2}}f_d(t) + \frac{1}{\sqrt{2}}f_d(t-\tau_d)\}\right|^2 - R\left|\frac{1}{\sqrt{2}}\{\frac{1}{\sqrt{2}}f_d(t) - \frac{1}{\sqrt{2}}f_d(t-\tau_d)\}\right|^2 \\ &= Rf_d(t)f_d(t-\tau_d) \end{aligned} \tag{4}$$

assuming that the shot and thermal noises created by the two photodetectors are negligible compared to the ASE noise contained in the signal $f_d(t)$. The baseband term after the lowpass filter is $s_d(t)$. The two baseband signals, $s_h(t)$ and $s_d(t)$, differ only by a proportionality constant that depends on $P_{LO}$ and $G$, but are otherwise identical mathematically in their signal form and noise statistics. Both $s_h(t)$ and $s_d(t)$ have the same SNR, i.e.

$$(SNR)_h = (SNR)_d \tag{5}$$

We emphasize that the SNR relationship given in Eq.(5) is independent of $\tau$. Since the sampler and the decision device used is the same for both schemes, the receiver performance is identical in the two cases regardless of the modulation.

The conditions for obtaining equivalent performance for the two schemes are summarized in Table 1. More study is needed, however, to establish whether or not additional restrictions are required to obtain equivalent performance in multichannel systems.

**Conclusion:** It has been shown that the performance of heterodyne receivers and preamplified direct-detection receivers are identical, provided that the conditions listed in Table 1 are satisfied. This result is independent of the modulation format used.

## References


[1] R. E. Wagner and R. A. Linke, "Heterodyne Lightwave Systems: Moving Towards Commercial Use", IEEE Mag. of Lightwave Comm. Syst., Vol. 1, No. 4, pp. 28-35, Dec. 1990.

[2] P. E. Green and R. Ramaswami, "Direct Detection Lightwave Systems: Why Pay More?", IEEE Mag. of Lightwave Comm. Syst., Vol. 1, No. 4, pp. 36-49, Dec. 1990.

[3] B. M. Oliver, "Signal-to-Noise Ratios in Photoelectric Mixing", Proceedings of IRE, Vol. 49, pp. 1960-1961, December 1961.

[4] N. A. Olsson, "Lightwave Systems with Optical Amplifiers", IEEE/OSA Journal of Lightwave Technology, **LT-7**, No. 7, pp. 1071-1082, July 1989.

[5] R. A. Linke and A. H. Gnauck, "High-Capacity Coherent Lightwave Systems", IEEE/OSA Journal of Lightwave Technology, **LT-6**, pp. 1750-1769, Nov. 1988.

[6] H. Toba, et al., "A 100-Channel Optical FDM Transmission/Distribution at 622 Mb/s Over 50 km", IEEE/OSA Journal of Lightwave Technology, **LT-8**, p. 1396, Sept. 1990.

[7] R. S. Vodhanel, "5 Gb/s Direct Optical DPSK Modulation of a 1530-nm DFB Laser", IEEE Photonics Technol. Lett., 1, pp. 218-220 , August 1989.


**Table 1: Requirements for Equivalent Performance**

| Condition | Heterodyne | | Preamplified DD |
|---|---|---|---|
| Amplitude Modulation | $A_h(t)$ | = | $A_d(t)$ |
| Angle Modulation | $\psi_h(t)$ | = | $\psi_d(t)$ |
| Linewidth | $\Delta\nu_S + \Delta\nu_{LO}$ | = | $\Delta\nu_T$ |
| Dominant Noise | Shot noise | | ASE noise |
| Sensitivity Degradation | $\eta$ | = | $1/n_{sp}$ |
| Polarization | $P_{LO}$ matches $P_S(t)$ | | Single polarization mode |
| Optical Detectors | Dual balanced | | Dual balanced |
| Filters | $H(\omega - \omega_{IF})$ | = | $H(\omega - \omega_d)$ |
| Intermediate Frequency | $\frac{\omega_{IF}}{2\pi} \gg BW_{IF}$ | | Not applicable |
| Demodulation | $\tau_h$ | = | $\tau_d$ |

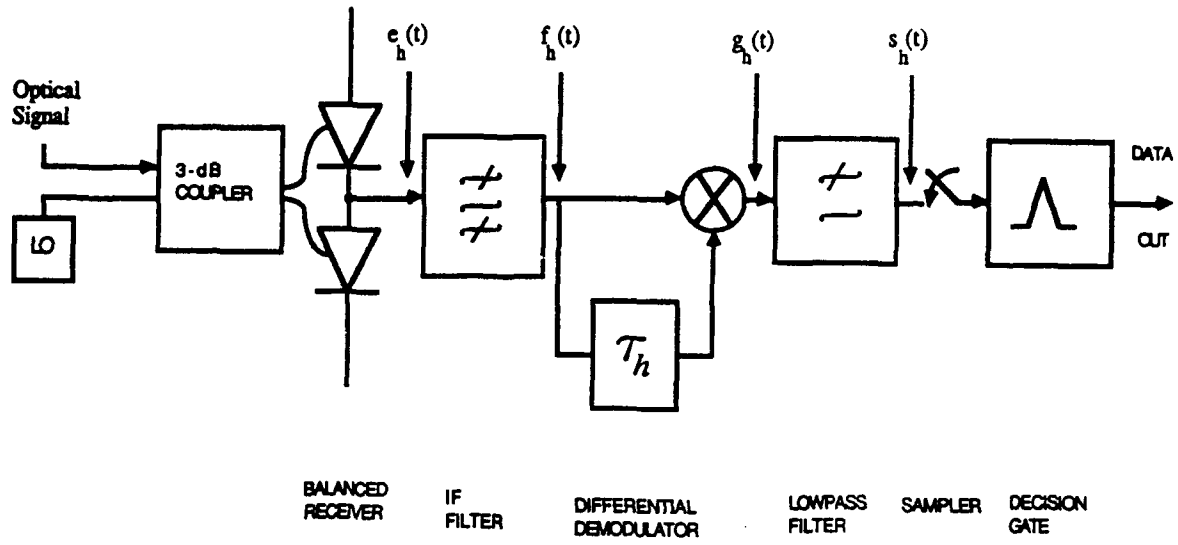


Fig. 1 Block diagram of a heterodyne lightwave receiver. When $\tau = 0$, this receiver structure corresponds to a heterodyne ASK receiver; when $\tau = T$, it corresponds to a DPSK receiver; and when $\tau$ is a fraction of T, it corresponds to a CPFSK receiver.

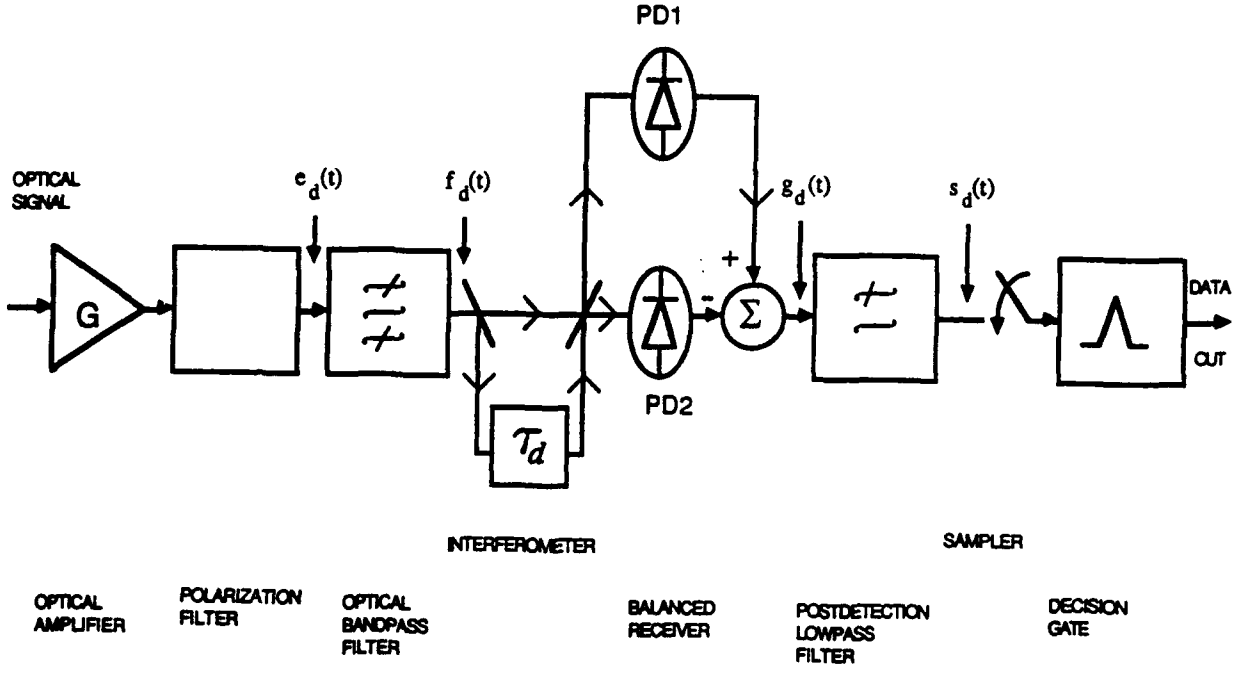


Fig. 2 Block diagram of a direct detection lightwave receiver using an optical preamplifier. Again the delay $\tau$ of the interferometer can be adjusted for the specific modulation format of interest.

# A Comparison of Direct and Coherent Detection Systems with Optical Amplifiers



S. W. Granlund and Y. K. Park

AT&T Bell Laboratories
Solid State Technology Center
9999 Hamilton Boulevard
Breiningsville, PA 18031

**1. Introduction:** The use of fiber amplifiers in future lightwave systems now appears certain. Many experiments have been published demonstrating both the long-distance and multi-channel capability of fiber amplifier-based systems. Most experiments have used conventional direct detection systems [1,2]; but some experiments, including a record transmission distance experiment, have used coherent detection systems [3,4]; and models of both systems have been developed. This paper will compare the two systems under the same conditions using both experiments and models. We will emphasize a practical comparison by using a direct detection regenerator from AT&T's commercial, 1.7 Gb/s system and a shelf-mounted, coherent detection regenerator from a recent AT&T field trial [5]. We will also emphasize a direct comparison by using transmitters of the same wavelength and identical optical paths including erbium-doped fiber amplifiers.

**2. Optical Subsystems:** The main direct detection subsystems are a 1.535 μm DFB laser transmitter and an APD receiver. Typical parameters which we will use in our model are a 13 dB extinction ratio (R) for the transmitter and an 8 $pA/\sqrt{Hz}$ noise spectral density ($I_c$), a gain (M) of 12, an excess noise factor (F) of 5, and a 0.6 dB coupling loss ($\eta$) for the receiver. Measurements of the receiver indicated the equivalent receiver bandwidth ($B_e$) was 1.2 GHz. A 1 nm optical bandpass filter ($B_{opt}$) in front of the receiver reduced the amount of detected amplified spontaneous emission from the optical amplifiers.

The main coherent detection subsystems are an FSK transmitter and a single-filter, polarization-diversity, heterodyne receiver. The transmitter consists of a two-electrode, 1.535 μm DFB laser, a driver from a conventional 1.7 Gb/s transmitter, and an equalizer. The receiver consists of polarization splitters and combiners, a local oscillator with automatic locking and tracking circuits, and a polarization-diversity receiver. The local oscillator power ($P_{lo}$=+3.0 dBm), receiver noise spectral density ($I_c$=15 $pA/\sqrt{Hz}$) and receiver coupling loss ($\eta$=1.0 dB) were measured. Values for the equivalent receiver bandwidth ($B_e$=1.2 GHz) and inter-symbol interference (ISI=2.5 dB) arising from imperfect filtering and polarization diversity detection were inferred.

The input coupling losses ($\eta_{in}$=2.3 dB) and internal noise figures (NF1=6.5 dB, NF2=7.5 dB) of the two erbium-doped fiber amplifiers used in this experiment were measured. These amplifiers were built with long erbium-doped fiber lengths and more counter than co-propogating pump power. We attribute these factors and the non-optimal signal wavelength to the relatively high noise figure measurements.

**3. Experimental Results:** The experimental setup for the direct detection system is shown in Fig. 1(a). Calibrated attenuators (ATT #1,2,3) were placed before the receiver and amplifiers. The first attenuator was calibrated using an optical power meter, the second and third were calibrated with an optical spectrum analyzer. During measurements of a single, in-line

amplifier, the other amplifier and attenuator were removed. Bit-error-rate (BER) curves were generated at step decreases in amplifier input optical power until error rates below $10^{-9}$ were unattainable. The receiver sensitivity ($\bar{P}$) at $10^{-9}$ BER versus amplifier input power ($\bar{P}_{in}$) for one amplifier (EDFA#1), the second amplifier (EDFA#2) and both amplifiers in series is plotted in Fig. 2. In the direct detection system, the minimum amplifier input power for a BER better than $1\times10^{-9}$ was -37.5 dBm.

Identical measurements using the coherent regenerator (requiring no optical filter) were made using the setup shown in Fig. 1(b). The results are plotted in Fig. 3. In the coherent detection system, the minimum amplifier input power was -32.5 dBm.

**4. Modeling Results:** The experimental results were analyzed with an optical amplifier model developed by N. A. Olsson [6]. Some modifications were required to accurately model our experiments.

In the direct detection system, we modeled the APD (vs. PIN) receiver by multiplying the expressions for signal power, signal-spontaneous noise power, and spontaneous-spontaneous noise power by $M^2$ and the shot noise power by $F\cdot M^2$. In both the coherent and direct detection models, we doubled the amplified spontaneous emission power to account for the two polarization modes of the fiber amplifier and added terms to account for receiver coupling loss.

In the FSK (vs. ASK) coherent system, we used a general expression for the coherent signal term ($S_{coh}$) without amplifiers:

$$S_{coh} = 144/N_p \cdot I_s I_{lo}$$

where $N_p$ is the average number of photons per pulse for a particular detection scheme [7], and $I_s$ and $I_{lo}$ are the photo-current equivalents of the optical signal and local oscillator powers. Note that for a given average optical signal power, the FSK photo-current equivalents are half the ASK equivalents. In single-filter, asynchronous, heterodyne FSK detection, $N_p$=80. Multiplication by the ISI penalty and inclusion of the amplifier terms completes our expression for the FSK signal power.

The model results for our direct and coherent detection systems with a single, in-line amplifier (EDFA#1) are shown by the solid lines in Figs. 2 and 3. A breakdown of the penalties leading to the minimum amplifier input powers and receiver sensitivities for our experiments is given in Tables I and II.

**5. Summary:** In comparing the results listed in Table I, we will focus on the regenerator contributions to the noise penalty and not on the common amplifier contributions.

The largest contribution to the direct detection noise penalty came from the optical bandpass filter (4 dB). However, none of the direct detection penalties is easily reduced. Our model indicates that a 0.2 nm filter is required to decrease the filter penalty by 2 dB, implying a tunable, possibly active, filter; signal degradation may result from attempts to reduce the equivalent receiver bandwidth penalty (1.0 dB); and an external modulator is required for substantial reduction of the extinction ratio penalty (0.7 dB).

The coherent system suffers from ISI (2.5 dB), receiver bandwidth (1.5 dB), and local oscillator power (1.1 dB) penalties. Again, these parameters are already close to current practical limits. The most straightforward improvement would be a change in modulation format. CPFSK or DPSK modulation would improve the theoretical limit by 6 dB.

We also modeled our direct detection system with a PIN receiver (M=F=1) and found no significant advantage over the APD receiver. In fact, APD receivers may be better for practical considerations since they require less optical gain, relaxing pump power and optical isolation requirements.

In summary, we found a 4 dB theoretical, and 5 dB experimental, advantage of our direct detection system over our single-filter, FSK coherent system. In the coherent system, CPFSK or DPSK detection would improve the minimum fiber input power limit by 6 dB, and more improvements would have to come from ISI penalty reductions. In the direct detection system, our model found no significant improvements of PIN over APD receivers. Narrow, tunable filters and external modulators will be needed to improve this limit. Finally, given the aforementioned improvements, we see no major advantage of either system and selection of one might be based needs like wavelength-division multiplexing and electronic dispersion equalization or on practical considerations like cost and manufacturability.

**6. Acknowledgements:** The authors would like to thank W. A. Asous and J. S. French for the direct detection transmitter and receiver, R. E. Tench and T. W. Cline for the optical amplifiers, and J.-M. P. Delavaux for the coherent regenerator. Discussions with J. S. French on receiver noise and C. R. Giles on the source of our high amplifier noise figures are greatly appreciated.

## REFERENCES

[1] H. Toba, K Nakanishi, N. Shibata, K. Nosu, N. Takato, M. Fukuda, "100-channel optical FDM transmission/distribution at 622 Mb/s over 50 km," PD1, Optical Fiber Communication Conference, San Francisco, CA, 22-26 January 1990.

[2] N. S. Bergano, J. Aspell, C. R. Davidson, P. R. Trischitta, B. M. Nyman, F. W. Kerfoot, "A 9000 km 5 Gb/s and 21,000 km 2.5 Gb/s feasibility demonstration of transoceanic EDFA systems using a circulating loop," PD13, Optical Fiber Communication Conference, San Diego, CA, 18-22 February 1991.

[3] S. Yamazaki, T. Ono, H. Shimizu, M. Kitamura, K. Emura, "2.5 Gb/s CPFSK coherent multichannel transmission experiment toward over 100 Gb/s communication system," PD12, Optical Fiber Communication Conference, San Francisco, CA, 22-26 January 1990.

[4] S. Saito, T. Imai, T. Sugie, N. Ohkawa, Y. Ichihashi and T. Ito, "Coherent transmission experiment over 7 223 km at 2.6 Gbit/s using erbium-doped fibre amplifiers," Electron. Lett., vol. 26, pp. 669-671, 1990.

[5] T. W. Cline, J.-M. P. Delavaux, N. K. Dutta, P. V. Eijk, C. Y. Kuo, B. Owen, Y. K. Park, T. C. Pleiss, R. S. Riggs, R. E. Tench, Y. Twu, L. D. Tzeng and E. J. Wagner,"A field demonstration of 1.7 Gb/s coherent lightwave regenerators," IEEE Photon. Technol. Lett., vol. 2, no. 6, pp. 425-427, 1990.

[6] N. A. Olsson, "Lightwave systems with optical amplifiers," IEEE J. Lightwave Technol., vol. LT-7, pp. 1071-1082, 1989.

[7] P. S. Henry, R. A. Linke, A. H. Gnauck, "Introduction to lightwave systems," in Optical Fiber Telecommunications II, San Diego: Academic Press, 1988.

| | Direct Detection | | Coherent Detection | |
|---|---|---|---|---|
| Source | Penalty (dB) | $\bar{P}_{in}$ (dBm) | Penalty (dB) | $\bar{P}_{in}$ (dBm) |
| Theo. Limit | | -50.3 | | -44.6 |
| NF1 | 3.5 | -46.8 | 3.5 | -41.1 |
| $N_{in}$ | 2.3 | -44.5 | 2.3 | -38.8 |
| $B_{opt}$ | 4.0 | -40.5 | | |
| $B_e$ | 1.0 | -39.5 | 1.5 | -37.3 |
| R | 0.7 | -38.8 | | |
| $P_{lo}$ | | | 1.1 | -37.2 |
| ISI | | | 2.5 | -34.7 |
| Exp. Result | | -37.5 | | -32.5 |

Table I - Amplifier Input Power Penalties

| | Direct Detection | | Coherent Detection | |
|---|---|---|---|---|
| Source | Penalty (dB) | $\bar{P}$ (dBm) | Penalty (dB) | $\bar{P}$ (dBm) |
| Theo. Limit | | -56.6 | | -47.6 |
| $I_c$, M, F | 17.2 | -39.5 | | |
| $B_e$ | 0.9 | -38.6 | 1.5 | -46.1 |
| R | 0.6 | -38.0 | | |
| $P_{lo}$, $I_c$ | | | 1.1 | -45.0 |
| ISI | | | 2.5 | -42.5 |
| $\eta$ | 0.6 | -37.4 | 1.0 | -41.5 |
| Exp. Result | | -37.4 | | -41.5 |

Table II - Receiver Sensitivity Penalties

## TABLES I AND II - SYSTEM NOISE PENALTIES

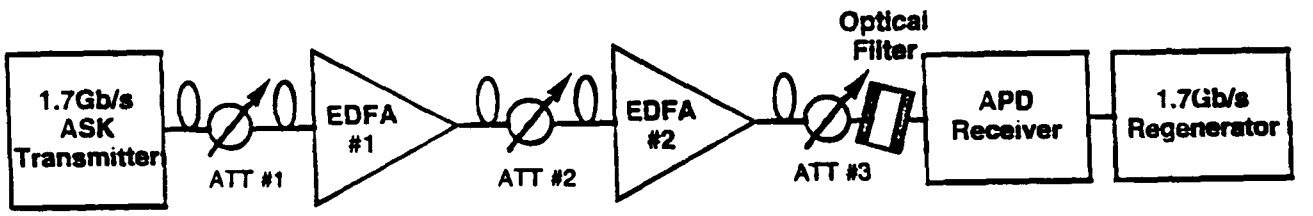


**Figure 1(a) – Direct Detection**

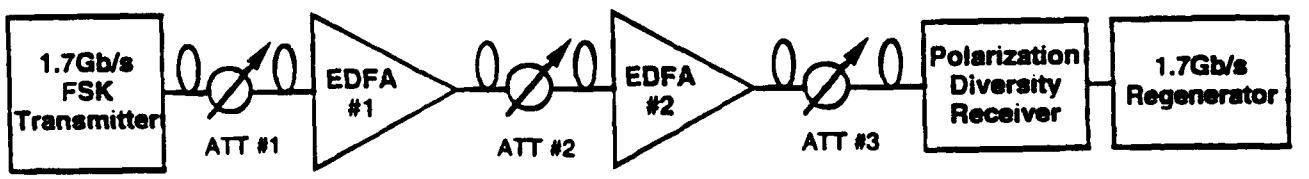


**Figure 1(b) – FSK Coherent Detection**

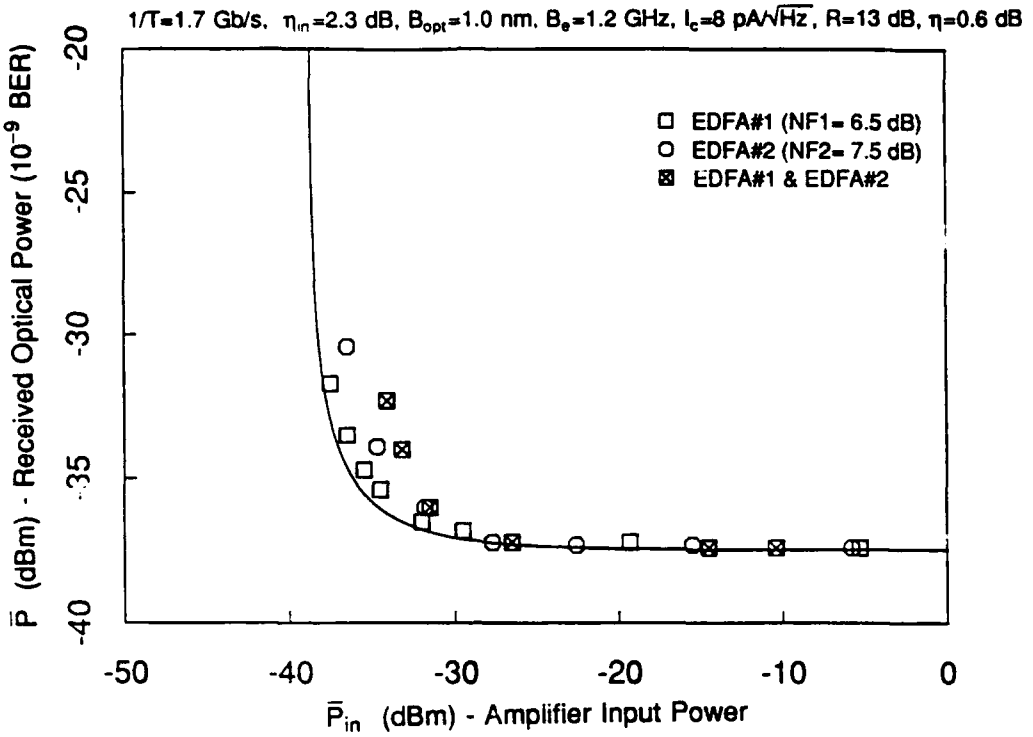


Figure 2. Direct Detection Receiver Sensitivity vs. Amplifier Input Power

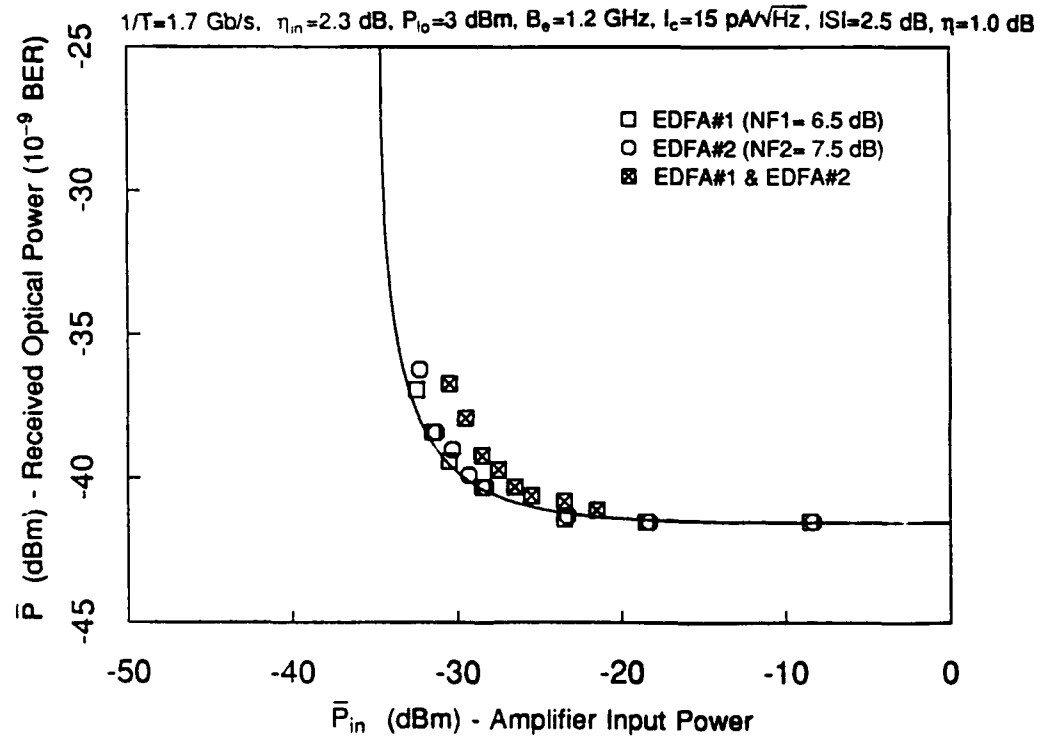


Figure 3. FSK Coherent Detection Receiver Sensitivity vs. Amplifier Input Power

# High Receiver Sensitivity at 2.5 Gb/s obtained with a Highly Efficient Low Noise Diode Pumped Erbium Doped Fiber Amplifier

B. Mikkelsen, C.G. Joergensen, J.A. van den Berk*, C.F. Pedersen**, C.C. Larsen***, T. Durhuus, and K.E. Stubkjaer

Center for Broadband Telecommunications, Electromagnetics Institute
Technical University of Denmark, DK-2800 Lyngby, Denmark
Phone no.: +45 42 88 14 44, Fax no.: +45 45 93 16 34
* Telecom Denmark, DK-2630 Taastrup, Denmark
** NKT Elektronik, DK-2605 Broendby, Denmark
*** Lycom, DK-2605 Broendby, Denmark

## Introduction

Laser diode pumped Erbium doped fiber amplifiers (EDFA) with low noise figures and high saturation powers are attractive because the ratio between the saturation power and the noise figure can be considered as a figure of merit for several applications [1]. These include multichannel receivers where high sensitivity and high saturation power increases the number of channels to be received and in-line applications where the dynamic range is proportional to the above mentioned figure of merit.

For 980 nm pumping the noise figure can reach the quantum limit of 3 dB [2], whereas the minimum noise figure obtainable with 1480 nm pumping is approximately 5 dB [3]. However, pumping at 1480 nm has the advantage of a better pump-to-signal conversion efficiency at high signal power levels leading to a higher saturation power compared to that achieved with 980 nm pumping [4]. Here we demonstrate that the advantages of the two pump wavelengths can be combined by pumping co-directionally at 980 nm and counter-directionally at 1480 nm. With this configuration the input end of the EDFA can be considered as a low noise preamplifier which determines the overall noise figure while the rear end serves as an efficient power amplifier.

Using this EDFA as a preamplifier in a 2.5 Gb/s direct detection system experiment a sensitivity of -43.0 dBm for a total coupled pump power of only 14 mW is achieved. This sensitivity is comparable to the best previously reported [2], but is achieved with a lower pump power. Also, it should be noticed, that the result presented here is obtained with system oriented components such as semiconductor pump sources and a polarization insensitive electrically tuneable filter.

## Active fiber and pump configuration

The Erbium doped fiber amplifier under consideration consists of 15 m of Er/Al/Ge doped fiber with an Er-doping concentration of $5.8 \cdot 10^{18}$ $cm^{-3}$, a core diameter of 3.7 μm and a refractive index step of 0.021. Co- and counter-directional pumping of the active fiber is provided by 980 and 1480 nm wavelength semiconductor lasers, respectively, as shown in Fig. 1. The EDFA is characterized at 1552 nm signal wavelength where the EDFA-bandwidth is largest. Also, this is in the low loss wavelength region, that is attractive for long haul links.

The gain and the noise figure of the EDFA are influenced by the total coupled pump power as well as the ratio of 980 nm to 1480 nm pump powers. The gain dependence on 980 nm pump power is shown in fig. 2 with the 1480 nm pump power as a parameter. The pump efficiencies for pumping separately by 1480 nm and 980 nm at optimized fiber lengths are 2.6 dB/mW and 2.7 dB/mW, respectively. Similarly, the noise figure dependence is shown in fig. 3. The noise figure is found by measuring the amplified spontaneous emission power in an optical bandwidth of 1 nm. A minimum noise figure of 3.1 dB is achieved at a gain of 29.5 dB for pump powers of 9 and 5 mW at 980 and 1480 nm pump wavelengths, respectively. This indicates, that no noise degradation is caused by 1480 nm counter-directional pumping. As expected, the noise figure increases to approximately 5 dB as the 1480 nm pump power is increased or the 980 nm pump is decreased.

Figure 4 gives the gain as a function of signal output power for various pump powers. It is seen that the saturation output power is increased with the 1480 nm pump power, so obviously, there is a trade-off between saturation output power and noise figure. Since a low noise figure is essential for a single channel preamplifier receiver the co- and counter-directional pump powers of 9 and 5 mW (i.e. a total pump power of 14 mW) are chosen in the system experiment described in the next section. The resulting gain, noise figure and saturation output power are 29.5 dB, 3.1 dB, and +2 dBm, respectively.

## System experiment

The EDFA with the proposed pump configuration is tested as a preamplifier in a 2.5 Gb/s system experiment as shown in fig. 1. Between the EDFA and the receiver, an electrically tuneable optical Fabry-Perot filter [5] with a 20 GHz FWHM bandwidth and a free spectral range of 18 nm is inserted. Maximum transmission is achieved by automatic control of the filter using the front-end photocurrent for feedback. The transmitter consists of a DFB-laserdiode at 1551.7 nm and an external modulator giving an extinction ratio better than 15 dB. The external modulator is used because the chirp associated with high extinction ratio direct modulation of the DFB-LD results in a spectral width larger than the filter bandwidth. The front-end has a bandwidth of 1.7 GHz, and a sensitivity of -27.5 dBm (BER equal to $10^{-9}$) at 2.5 Gb/s, using a directly modulated DFB-LD. With the external modulator the sensitivity is -26.2 dBm (see fig. 5), corresponding to a penalty of 1.3 dB relative to direct modulation.

The measured receiver sensitivity using the EDFA is also shown in fig. 5 and a sensitivity, $\eta P_{rec}$, of -43.0 dBm at a BER of $10^{-9}$ is achieved corresponding to an improvement of 16.8 dB. The input coupling efficiency, $\eta$, to the active fiber (wavelength multiplexer and splicing loss) is -1.5 dB and the output coupling efficiency from Er-fiber to receiver input (including isolator and filter insertion loss) is -4.5 dB. The 1.3 dB penalty for using the external modulator (relative to direct modulation) is attributed to insufficient electrical bandwidth (3 dB bandwidth of 1 GHz) which causes intersymbol interference (ISI). Since the main noise source of an EDFA-preamplifier receiver applying a narrowband optical filter is the signal-spontaneous beat noise, the ISI results in an extra penalty due to the ISI induced signal level in the neighbouring timeslots. It is therefore expected that the ISI penalty of 1.3 dB without an EDFA preamplifier will cause a penalty of 2-3 dB in this configuration. Using a better transmitter a sensitivity of about -45 dBm is expected.

## Conclusion

A diode pumped EDFA with a noise figure of 3.1 dB, a gain of 29.5 dB and a saturation output power of 2 dBm has been realized at a signal wavelength of 1552 nm by pumping co-directionally at 980 nm and counter-directionally at 1480 nm wavelength, with a total coupled pump power of only 14 mW. The proposed amplifier configuration with a low noise preamplifier section and an efficient power section is considered very attractive for practical applications. Finally, a receiver sensitivity, $\eta P_{rec}$, of -43.0 dBm is achieved at 2.5 Gb/s by using the EDFA as a preamplifier, showing that very high sensitivities can be realized in direct detection systems, using fiber preamplifiers implemented with low pump powers and systemoriented components.

## Acknowledgement

We would like to thank Mitsubishi Electric Corp., Itami, Japan, for kindly providing the 1480 nm pump source and the DFB-laser.

## References

[1] N.A. Olsson, Jour. Lightwave Technol., vol. 7, p. 1071, 1989.

[2] P.P. Smyth et al., in Proc. of ECOC '90, p. 91, Amsterdam, Sept. 1990.

[3] C. R. Giles et al., in Techn. Dig. of IOOC '89, paper 20 PDA-5, Kobe, July, 1989.

[4] E. Desurvire, Tutorial Session of OFC '91, San Diego, Feb. 1991.

[5] C. M. Miller, in Proc. of ECOC '90, p. 605, Amsterdam, Sept. 1990.

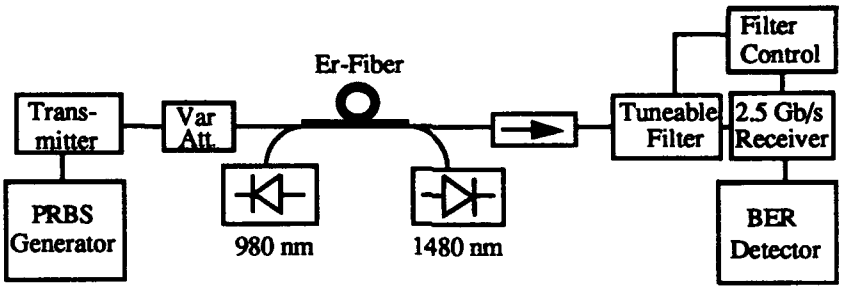


Fig. 1. Experimental set-up.

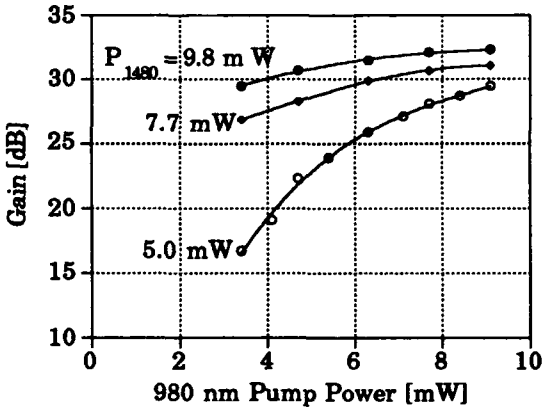


Fig. 2. Gain vs. 980 nm pump power with 1480 nm pump power as parameter.

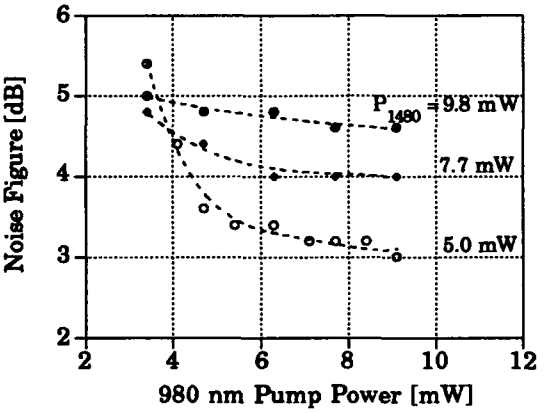


Fig. 3. Noise figure vs. 980 nm pump power with 1480 nm pump power as parameter.

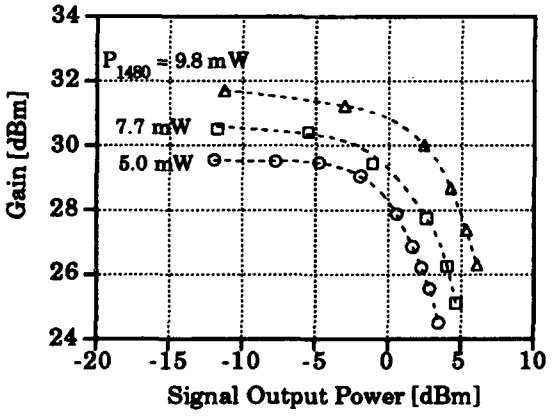


Fig. 4. Gain vs. signal output power for 9 mW pump power at 980 nm and with 1480 nm as a parameter.

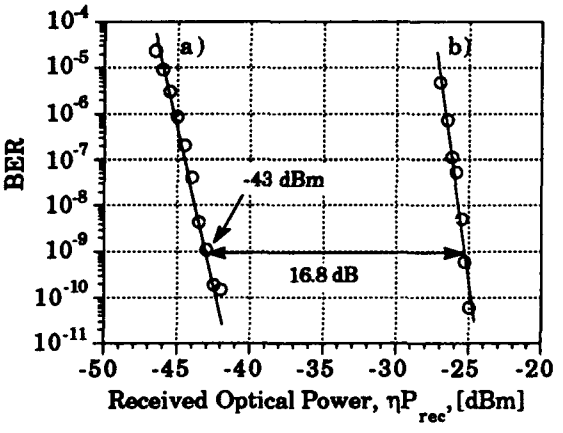


Fig. 5. BER (PRBS $2^7$-1) for a) fiber preamplifier receiver using 980 nm pump and 1480 nm pump, b) external modulation without fiber preamplifier.

# SIGNAL STATISTICAL EFFECTS FROM STIMULATED BRILLOUIN SCATTERING IN CPFSK REPEATERLESS TRANSMISSION SYSTEM WITH OPTICAL BOOSTER AMPLIFIER

Toshihiko SUGIE

NTT Transmission Systems Laboratories
1-2356, Take, Yokosuka-shi, Kanagawa, 238, JAPAN

ABSTRACT

For a 2.5 Gb/s CPFSK repeaterless transmission system with EDF-booster amplifier, the bit error rate performance and the penalty improvement by signal randomization are clarified in the presence of stimulated Brillouin scattering along a 280-km dispersion shifted fiber.

## 1. INTRODUCTION

Laser diode pumped erbium-doped fiber amplifiers (EDFAs) have recently demonstrated their potential for very long-haul transmission and distribution networks. Coherent transmission systems can enhance their overall link budget by using EDFAs[1-4]. However, at high EDF-booster amplifier output levels, stimulated Brillouin scattering(SBS) occurs and this restricts fiber launch power.

The impact of SBS on transmission characteristics has been investigated from the viewpoint of modulation format[5,6] and fiber parameters[7]. SBS suppression techniques for coherent systems using EDFAs were also proposed recently. They included a spread spectrum method[8] and the concatenation of fibers with different Brillouin shifts[3]. However, these techniques mainly focus on the fiber launch power and do not fully clarify the penalty degradation. The bit error rate performance of random signals affected by SBS must be further investigated before systems with EDF-booster amplifiers can be realized.

In this paper, we describe the bit error rate performance, in terms of signal randomness, of a 2.5 Gb/s CPFSK repeaterless transmission system using an EDF-booster amplifier and dispersion shifted fibers(DSFs) in the presence of SBS. A penalty improvement can be clarified by increasing signal randomness. A 2.5 Gb/s repeaterless transmission over 280-km dispersion shifted fiber is also confirmed by $2^7$-1 pseudorandom signal format.

## 2. EXPERIMENTAL CONFIGURATION

Figure 1 shows the experimental configuration. A 2.488 Gb/s CPFSK polarization diversity regenerator with a linewidth of 1 MHz at 1.545 μm[9] was used. The signal was amplified by an EDF-booster amplifier and transmitted over a 100-km or 280-km dispersion shifted fiber that had a loss of 0.2 dB/km and a dispersion of -0.45 ps/km/nm at 1:545 μm. The mode field diameter was 7.8 μm. The Brillouin threshold for cw light at 1.545 μm were found to be +5dBm for both fibers. The main Stokes with a Brillouin shift of 10.6 GHz and a linewidth of 28.9 MHz occurred at 0 dBm launch power, which was followed by three additional Stokes. Various random signals were generated at 2.488 Gb/s by a pulse pattern generator with pseudorandom format: $2^N$-1, where N=1- 23.

The EDF-booster amplifier consisted of two stages: a backward and a bidirectional pumping section as shown in Fig. 1 (b). A 49-m Al/EDF with high refractive index (1.4%, 300ppm-Er) was used in the first stage, which was backward

pumped by LDs with 82.8 mW at 1.46-1.49μm, to obtain high gain. In the 2nd stage, bidirectional pumping of a 17-m Al/EDF with relative refractive index of 0.35% achieved high saturated output power. Forward and backward pumping powers were 63.7 and 82.6 mW at 1.48μm, respectively.

## 3. RESULT AND DISCUSSION

(3-1) EDF-BOOSTER AMPLIFIER: The saturated output power of +19.6 dBm (EDF-out) with 12.2 dB gain was obtained at 1.545 μm. The maximum amplified spontaneous emission(ASE) occurred at 1.56 μm with a 28 dB ASE suppression ratio, i.e.,signal to maximum ASE ratio. This suggests that the penalty of the EDF-booster amplifier is less than 0.2 dB without any optical filter. The repeater gain of the system was 60 dB at $10^{-9}$, including the EDF-booster amplifier.

(3-2) TRANSMISSION EXPERIMENT: The optical link shown in Fig. 1 (a) was used. The 2.488Gb/s signal with +17.5 dBm optical power and modulation index of 0.8 was launched into the 100km dispersion shifted fiber. To ensure precise measurement, only the S-polarization branch of the received signal were maximized; the corresponding receiver sensitivity was -42.5 dBm at $10^{-9}$ for N=7. Fig. 2 shows the received optical power increase from the back-to-back performance with no EDF-booster amplifier and no fiber at a sensitivity of $10^{-9}$. The format of N=1 corresponds to the [1,0] fixed pattern. The received optical power at $10^{-9}$ apparently increases when N approaches 1, although it almost duplicates the received power under the 0-km transmission configuration when N >7. An obvious bit error rate floor was observed at N<5, and the penalty of less than $1 \times 10^{-4}$ was not achieved at the received power of -36 dBm for N=1. The optical power transmitted along the 100-km fiber is also shown in Fig.2. This is normalized by the cw output, which was restricted by SBS in the fiber. Transmitted signal output at N>9, increased by 7.8 dB from unmodulated signal(cw), was affected only by the fiber loss. The increase in the fiber output clearly depends on the penalty degradation. It is confirmed that the penalty degradation due to SBS is reduced by an increase in signal randomness, and is suppressed to less than 0.2 dB for N=7 even if optical signal at +17.5 dBm was launched into the fiber.

Fig. 3 shows the bit error rate at the received power of -43 dBm as a function of fiber launch power. The bit error rate degrades as the launch power increases. This is particularly evident at powers over +10 dBm for N=1, although bit error rate degrades from $2.5 \times 10^{-9}$ to only $4.4 \times 10^{-9}$ for N=7. The difference in bit error rate at the launch power of 0 dBm is caused by the regenerator performance with no EDF-booster amplifier and no fiber. To clarify the degradation due to SBS, the intermediate frequency(IF) spectrum and waveform after demodulation are shown in Fig.4. These correspond to (a) and (b) in Fig.3. It is observed that power spectrum components exceeding the SBS threshold were eliminated and the IF deviates from its initial value when the fiber launch power is +17.5 dBm. Observed waveform corresponds to the power spectrum obtained. These phenomena became less evident when N increases or launch power decreases. The penalty degradations shown in Fig. 2 and 3 are caused by SBS modifying the power spectrum.

To confirm these characteristics over long transmission spans, a 280-km long dispersion shifted fiber were tested. A signal with +17.5 dBm optical power modulated by N=7 and 3 pseudorandom pattern formats were used as shown in Fig.5. The bit error rate performance for the 100-km dispersion shifted fiber is also shown for comparison. No evident bit error rate floor was observed for the 280-km

transmission at N=7 except for penalty increase of about 0.2 dB. On the other hand, the degradation became significant at error rates less than $10^{-8}$ in the case of N=3. These characteristics duplicate those for the 100-km transmissions. This implies that there is no additional penalty for 280-km transmission except for SBS, and that it is important to use random signals that correspond to the formats where N>7 for repeaterless transmission employing optical booster amplifiers.

## 4. CONCLUSION

The bit error rate performance of a 2.5 Gb/s CPFSK repeaterless transmission system equipped with an EDF-booster amplifier was clarified from the viewpoint of signal randomness. It was confirmed that the random signal suppresses the penalty caused by SBS in long dispersion shifted fibers. For example, the signal randomness of N >7 must be applied to keep the penalty increase to less than 0.2 dB. We also confirmed that the degradation over 100 and 280-km dispersion shifted fibers is mainly caused by SBS when N≤7.

## ACKNOWLEDGEMENT

The author would like to thank Dr. Sadakuni Shimada and Dr. Hidehi Ishio for their encouragement. He also gratefully thanks Dr.Takeshi Ito for his support and suggestions, and Mr. Yoshihiro Hayashi and Mr. Norio Ohkawa for valuable discussions.

## REFERENCE

(1) M.J.Creaner,et.al.,Electron .Lett.,vol.26,no.7,pp.442-444,1990.
(2)Y.K.Park,et.al.,Topical Meeting on Optical Amplifiers and their Applications, 160-163/TuC4, Aug.6-8,1990.
(3)T.Sugie,et.al.,Topical Meeting on Optical Amplifiers and their Applications, pdp2,Aug.6-8,1990.
(4) B.Clesca, et.al.,Electron.Lett.,vol.26,no.18,pp.1426-1428,1990.
(5) Y.Aoki,et.al.,IEEE J.Lightwave Technol.,vol.6,pp.710-719,1988.
(6) E.Lichtman,et.al.,IEEE J.Lightwave Technol.,vol.7,pp.171-174,1989.
(7) N.Shibata,et.al.,Opt.Lett.,vol.13,pp.595-597,1988.
(8) A.Hirose,et.al.,ECOE'90,MoF3.6,pp.85-88,1990.
(9) T.Imai,et.al.,Electron.Lett.,vol.26,no.17,pp.1407-1408,1990.

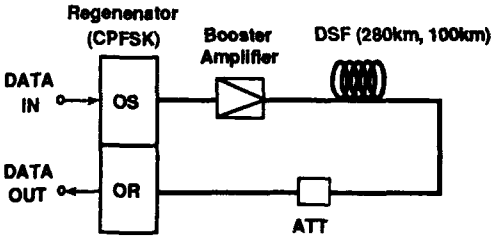


(a) 2.5 Gb/s CPFSK Transmission Experiment

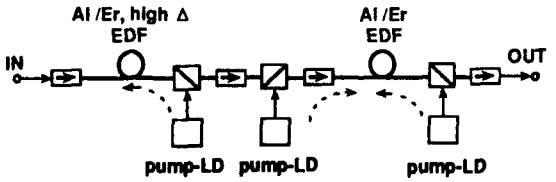


(b) EDF-Booster Amplifier

Fig. 1 Experimental Configuration

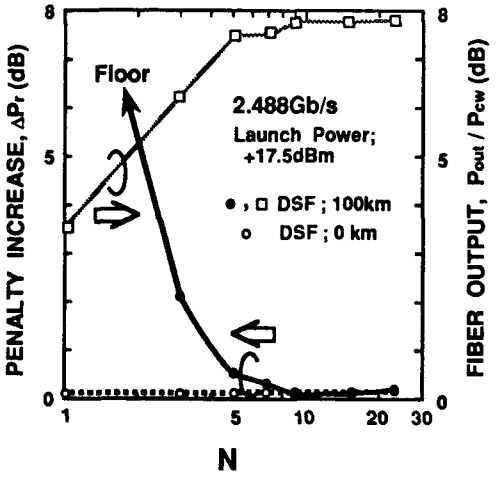


Fig. 2 Penalty Increase as a Function of Signal Randomness: $2^N-1$

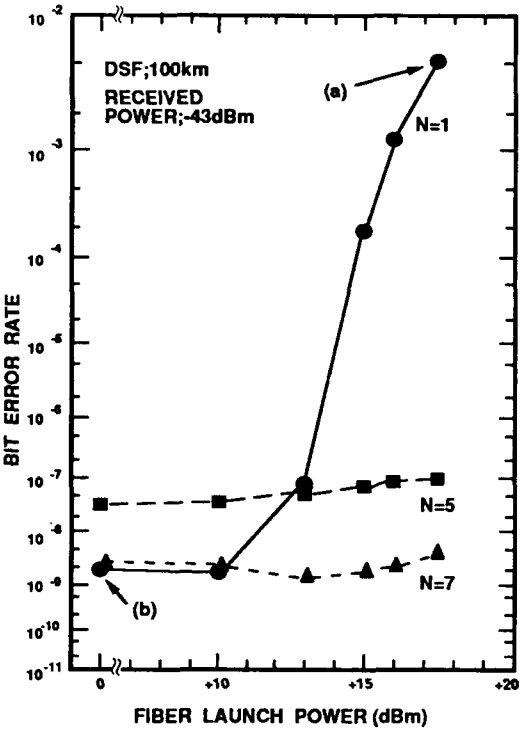


Fig. 3 Bit Error Rate as a Function of Fiber Launch Power

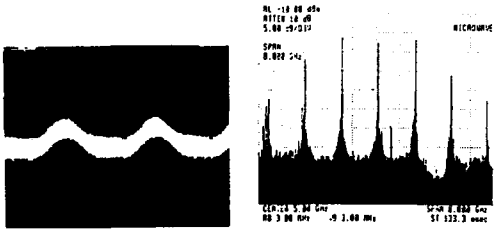

(1) Waveform (2) IF Spectrum

(a) Launch Power = 17.5 dBm

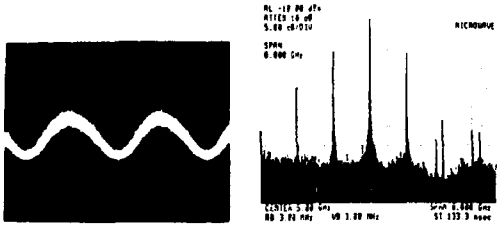

(1) Waveform (2) IF Spectrum

(b) Launch Power = 0 dBm

Fig. 4 IF Spectrum and Waveform

(1) Horizontal; 200ps/div, Vertical; arb. unit.
(2) Horizontal; center freq.=5 GHz, span=8 GHz
Vertical; 5 dB/div

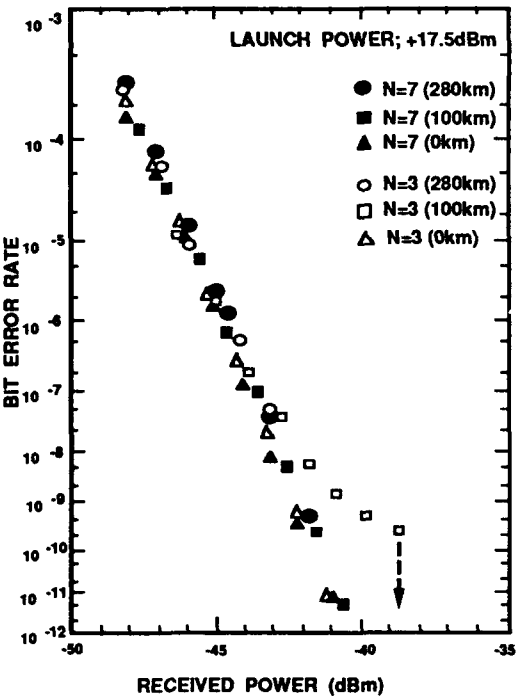


Fig. 5 Bit Error Rate as a Function of Received Power

# Combined Effect of Self-Phase Modulation and Dispersion in SLA Post-Amplified Transmission Systems

C. R. Medeiros and J. J. O'Reilly

## Abstract

In this paper we consider the performance implications of using semiconductor laser amplifiers (SLAs) as post-transmitter power amplifiers in long-haul directly modulated optical systems operating in the $1.55\mu m$ region. The combined effect of the dispersion, nonlinear self phase modulation, attenuation and the inherent SLA nonlinearity is numerically investigated.

## 1 Introduction

Semiconductor laser amplifiers are emerging as potentially useful components to be used in future optical communication systems [1], they are considered particularly attractive owing to their potential for integration.

Recently experimental work has successfully demonstrated the feasibility of post amplification by a semiconductor laser amplifier in directly modulated optical transmitters [2,3]. In these experiments a major concern has been the pattern effects due to gain saturation; here we will focus on the implications of such high power transmitters in long haul systems. Since the optical power at the output of such a transmitter is relatively high it must be determined whether the unavoidable nonlinear effects in the fibre play an important role and may modify the performance of the system.

Here using numerical simulation techniques we analyse and quantify the performance implications resulting from the combined effect of group velocity dispersion (GVD), nonlinear self phase modulation (SPM), attenuation and the inherent nonlinearity of the semiconductor laser amplifier. Specifically we show that the power launched into the fibre can be optimised taking into account the characteristics of the input signal.



## 2 System Model and Analysis

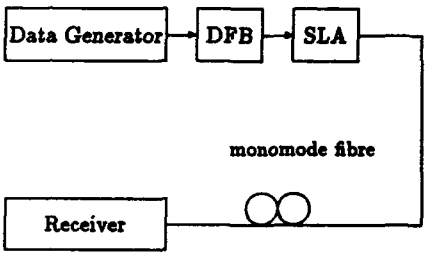


Figure 1: Block diagram of a direct detection optical communication system incorporating a SLA as post-transmitter-amplifier.

The block diagram of Fig. 1 shows the functional elements of the fibre system considered in this study. A 4.8 Gbit/s system transmitting NRZ data is considered. The optical source is considered to be a DFB laser which is directly modulated. The data patterns used are pseudorandom sequences of length $2^5 - 1$, relatively short sequences being selected to avoid unduly time consuming calculations. The dynamic response of the semiconductor laser in terms of optical power P(t), and phase $\phi(t)$, is determined by solving the large-signal rate equations and using the parameters of a typical DFB laser [4]. The complex envelope of the electromagnetic field of the laser output can be represented by, $E(t) = \sqrt{P(t)}\exp(j\phi(t))$. The behaviour of the SLA can be described by a pair of coupled equations [5], which relate the input and output fields, $E_{in}(t)$ and $E_{out}(t)$ respectively, to the physical parameters of the optical amplifier taking into account the effect of facet reflectivities and gain saturation.

$$E_{out}(t) = t_2 t_1 E_{in}(t-\tau)\exp A(t) + \\ + r_1 r_2 E_{out}(t-2\tau)\exp\left(A(t) + A(t-\tau)\right) \quad (1)$$

$$\frac{dG(t)}{dt} = \frac{G_0 - G(t)}{\tau_c} - \frac{t_2^{-2}|E_{out}(t)|^2}{E_{sat}}\left(1 - h(t)^{-1}\right) - \frac{r_2^2 t_2^{-2}|E_{out}(t-\tau)|^2}{E_{sat}}(h(t)-1) \quad (2)$$

where $A(t) = \left(\frac{1}{2}G(t) - i\left(\frac{\alpha}{2}G(t) + kL\right)\right)$ and $h(t) = \exp(G(t))$, $\tau$ is the single pass transit time, L (500 $\mu m$) is the amplifier length, $k$ the propagation constant, G(t) represents the response of the medium and is a measure of the total space integrated gain at each point of the pulse profile, $G_0$ is the unsaturated gain of the amplifier, $\alpha$ (5) is the linewidth enhancement factor, $\tau_c$ (100 ps) is the carrier lifetime, $E_{sat}$ (5 pJ) the saturation energy and $r_i$ and $t_i$ are the amplitude reflection and transmission coefficients of the laser amplifier facets ($r_i^2 = 10^{-4}$).

The propagation through the fibre is described by the nonlinear dispersive equation [6]:

$$i\frac{\partial E}{\partial z} + i\gamma E + \frac{1}{2}\beta_2\frac{\partial^2 E}{\partial t^2} + \frac{1}{2}\frac{n_2\omega_o}{cA_{eff}}|E|^2 E = 0 \quad (3)$$

where $z$ is the longitudinal coordinate of the fibre, $t$ represents time, $E$ is the slowly time varying amplitude of the electromagnetic field with $|E|^2$ the instantaneous power, $\gamma$ the fibre attenuation, $\beta_2$ the group velocity dispersion, $n_2$ the nonlinear index of refraction, $\omega$ the optical angular frequency, $A_{eff}$ the effective area and c the velocity of light. The numerical calculations were performed using the split-step Fourrier method whereby the fibre is divided into a number of segments. Within each segment the dispersive and nonlinear effects are assumed to act independently. More specifically, the optical field is first propagated for half of the segment with dispersion only, using the frequency domain. At the middle of the segment the field is multiplied by a nonlinear term which represents the effect of the nonlinearity over the whole segment, and finally the field is propagated the remaining distance with dispersion only. Variations in the fibre core size and polarisation dispersion were neglected as was spontaneous noise. The numerical values of the fibre parameter for pure silica core at the wavelength of 1.55$\mu m$ were considered as follows: $\gamma = 0.2\ dB/Km$, $|\beta_2| = 20 \times 10^{-27}\ s^2 m^{-1}$, $n_2 = 3.2 \times 10^{-20}\ m^2 W^{-1}$ and $A_{eff} = 50\ \mu m$.

In the receiver the complex envelope of the electromagnetic field at the fibre output is squared in magnitude by the action of a PIN photodetector and passed through a baseband receiving filter. Here the filter is assumed to provide 100 % *zero-forcing raised* cosine equalisation for rectangular input pulses with duration T, where T is the bit period. To assess the performance of the system, power penalties are estimated from the simulated eye diagram as $10\log(a)$, where $a$ is the eye opening relative to a distortion-free system.

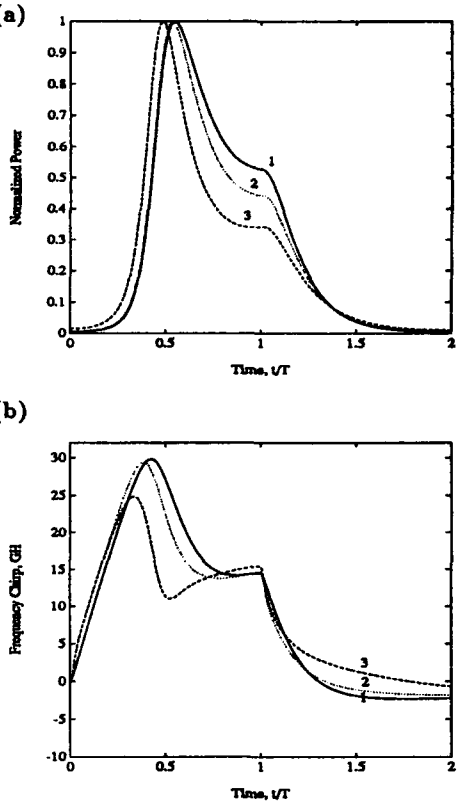


*Figure 2: SLA response to a laser pulse.* **(a)** Pulse shape. **(b)** Frequency chirp associated with the signal. 1 laser response 2 and 3 SLA response with 15 dB and 25 dB gain respectively.

## 3 Results

We consider two different situations. **(A)** where the laser is considered to operate with an unsaturated gain of 25 dB. In the other situation **(B)** the SLA is assumed operating with an unsaturated gain of 15 dB. In the latter case although the signal at the SLA input is relatively high the saturation effects are not very significant because the unsaturated gain is small and consequently the amplified signal is almost an amplified replica of the input signal. These considerations are illustrated in Fig. 2, which represents the amplification of an isolated 'one' and the frequency chirp associated with it. We note

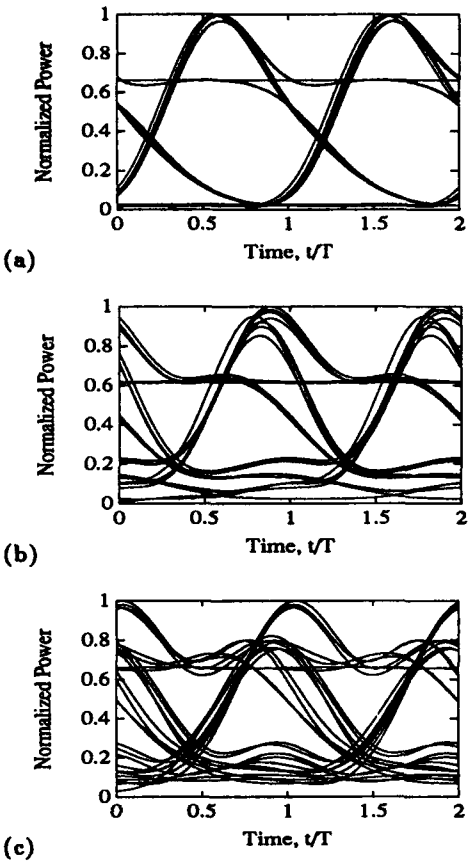


Figure 3: Received eye diagrams for different fibre lengths, SLA gain of 25 dB and coupling losses 5 dB. (a) Fibre length 0 Km. (b) Fibre length 100 Km. (c) Fibre length 200 Km.

that the effects of the SLA being operated under saturation are twofold, the amplified pulse becomes distorted and the frequency chirp associated with the signal is reduced.

The interaction between the optical signal and the fibre is accurately obtained by solving eqn. (3), but useful insight can be gained by understanding the effects of the various physical phenomena. In broad terms, the dispersion induces pulse broadening because different frequency components of the pulse travel at slightly different speeds. In the 1.55 $\mu m$ region ($\beta_2 < 0$) the short wavelength components travel faster than longer wavelengths, therefore the chirp associated with a directly modulated semiconductor laser enhances the effect of dispersion. Additionally, the nonlinear SPM process generates new frequency components as the pulse travels in the fibre, these components develop a frequency chirp which is proportional to the derivative of the signal pulse, and therefore counteract the initial chirp of a signal from a directly modulated laser. Therefore when the SLA is used as a post-amplifier in a directly modulated transmitter it reduces the effect of the fibre dispersion in two ways: by reducing the frequency chirp of the signal, and by increasing the power of the signal enabling the SPM process to be significant and counteract the dispersion.

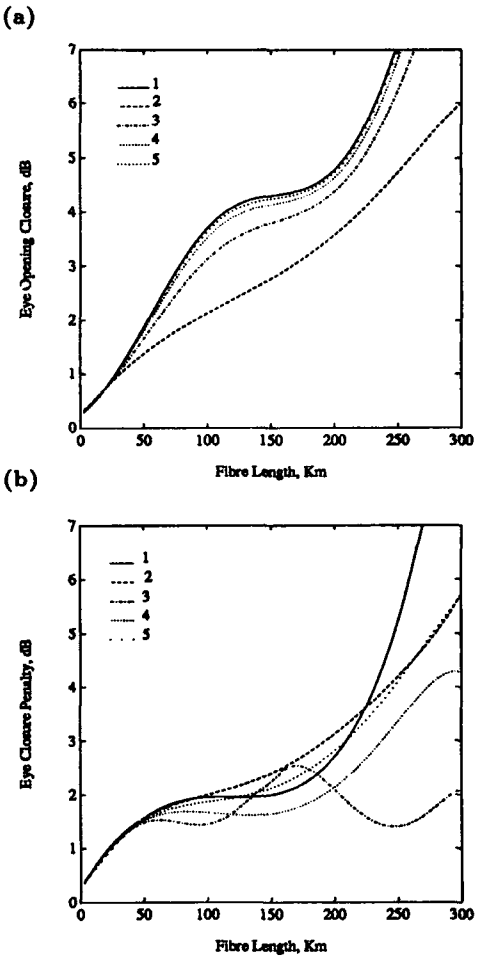


Figure 4: Eye closure penalty vs. the transmission distance. (a) SLA gain 15 of dB. (b) SLA gain of 25 dB. 1 only dispersion, 2 , 3, 4, 5, coupling losses , 0 dB, 5 dB, 10 dB, and 15 dB repectively.

Fig. 3 illustrates received eye diagrams for different fibre lengths, considering an SLA with 25 dB gain and coupling losses of 5 dB. Per-

formance results expressed as optical power penalty versus transmission distance are shown in Fig. 4 for cases (A) and (B). We consider various values for the coupling losses between the transmitter and the fibre thereby allowing for different signal powers at the fibre input. The solid line corresponds to a case where only the dispersion effects are considered, it shows the capability of the SLA to alleviate the fibre dispersion, which results from the reduction of the frequency chirp of the signal by the SLA and therefore depends on its degree of saturation. We note that this chirp compensation process is more effective for long distances since for small distances the system performance is dominated by the unavoidable pattern effects of the SLA when highly saturated. The broken lines corresponding to the coupling losses of 0dB, 5dB , 10dB and 15dB illustrate the interplay between signal frequency chirp, dispersion and self phase modulation. For the situation (A) the signal at the fibre input is more severely chirped and of lower power than in situation (B). The result is that in order to make the SPM process to counteract and compensate for the dispersion and signal chirp we need to minimise the coupling losses between the transmitter and the fibre. In contrast, in situation (B) minimal coupling losses do not yield best performance. Under these circumstances the self phase modulation process dominates inducing a frequency chirp of opposite sign and greater than the initial frequency chirp. Best performance can then only be achieved by an interplay between the launched power, fibre dispersion and signal frequency chirp.

## 4 Concluding Remarks

We have presented an analysis which quantifies the performance effects of using a semiconductor laser amplifier as a post-amplifier in long-haul systems operating in the 1.55 $\mu m$ region. Our results show that nonlinear fibre effects must be considered in the system design. In particular the power launched into the fibre must be optimised depending on the characteristics of the input signal.

## 5 Acknowledgments

This work has been supported by the UK Science and Engineering Research Council and by British Telecom.

## References

[1] M.J. O'Mahony. Semiconductor laser optical amplifiers for use in future fiber systems. *J. Lightwave Technol.*, Vol.LT-6:pp.531-544,1988.

[2] N.A. Olsson, T. Cella, L.O. Tseng and R.E. Tench. 1.3 $\mu$m semiconductor laser power amplifier. *IEEE Photon. Technol. Lett.*, Vol.1:pp.2-3, 1989.

[3] M. Le Ligne, Y. Sorel and J.F. Kerdiles. Theoretical and experimental study of a saturated near travelling wave amplifier working at 1 Gbit/s and 4.8 Gbit/s. *J. Opt. Comun.*, Vol.11:pp.104-106, 1990.

[4] T.L. Koch et al, 1.55 $\mu$m InGaAsP distributed feedback vapor phase transported buried heterostructure lasers. *Appl. Phys. Lett.*, Vol.47:pp.12-14, 1985.

[5] C.M. Medeiros, R.S. Fyath and J.J. O'Reilly. Nonlinear optical pulse propagation in semiconductor laser amplifiers. *IEE Colloquium on Non-Linear Effects in Fibre Communications*, November 1990.

[6] A. Hasegawa and F. Tappert. Transmission of stationary nonlinear pulses in dispersive dielectric fibres. I. Anomalous dispersion. *Appl. Phys. Lett.*, Vol.23:pp.142-144, 1973.

Friday, July 26, 1991

# Broadband Optical Network Applications

**FB** 10:15am–12:00m
Cabaret Room

C. Lin, *Presider*
*Bellcore, USA*

# Optical Fiber Amplifiers For Multichannel Video Transmission and Distribution

Winston I. Way
Bellcore, 331 Newman Springs Road, Red Bank, NJ 07701

**1. INTRODUCTION:** In the last three years, optical amplifiers have been successfully used in numerous analog fiber optic systems to transmit and distribute multiple AM-VSB or FM video channels. [1-14] Most technology issues regarding the usage of semiconductor optical amplifiers and erbium-doped fiber amplifiers (EDFAs) in those systems have been studied extensively.[8,15] Therefore, the main purpose of this paper is not only to review the previous work, but also to compare the different technology aspects of analog and direct-detection digital video broadcast systems. This paper also addresses the potential evolutionary problems of using optical amplifiers in a subscriber loop that may need upgrading when distribution signals change from AM-VSB video to future digital video services.

**2. GENERAL FORMULA FOR ANALOG/DIGITAL SYSTEMS USING LUMPED OPTICAL AMPLIFIERS:** A generalized formula for the carrier-to-noise-ratio (CNR) in analog systems and the signal-to-noise-ratio (SNR) in direct-detection digital systems with optical amplifiers is given below:

$$SNR\ (\ or\ CNR\ ) = \frac{i_s^2}{(i^2_{RIN} + i^2_{s-sp} + i^2_{sp-sp} + i^2_{shot} + i^2_{th})\cdot B_e} \tag{1}$$

where

$$i^2_{RIN} = RIN\cdot I_s^2, \qquad i^2_{shot} = 2eI_s, \qquad i^2_{sp-sp} = I^2_{ase}/B_o$$

$$Analog:\ i^2_{s-sp} = 2I_s I_{ase}/B_o, \qquad Digital:\ i^2_{s-sp} = 2I_1 I_{ase}/B_o \tag{2}$$

and $i_s^2$ is the mean-square signal photo-current, $i^2_{RIN}$, $i^2_{s-sp}$, $i^2_{sp-sp}$, $i^2_{shot}$, and $i^2_{th}$ are the equivalent current densities for relative-intensity-noise (RIN), signal-spontaneous beat noise, spontaneous-spontaneous beat noise, shot noise, and receiver thermal noise, respectively. In (1) and (2), $B_e$ and $B_o$ are the electrical and optical noise bandwidths, respectively; the photocurrents of the amplified spontaneous emission (ASE) noise, the analog signal, and the baseband digital signal are expressed as

$$I_{ase} = e\eta P_{ase} L/h\nu \tag{3}$$

$$Analog:\ I_s = e\eta P_s L/h\nu \qquad Digital:\ I_1 = 2e\eta P_s L/h\nu \tag{4}$$

$$i_s^2 = \frac{1}{2}m^2 I_s^2 \qquad i_s^2 = I_1^2$$

where e is the electron charge, $h\nu$ is the photon energy, m is the optical modulation index per channel (OMI/ch), $\eta$ is the photodetector quantum efficiency, and L is the loss between the amplifier and the photodetector. The average signal power $P_s$ and ASE power $P_{ase}$ ($\approx 2n_{sp}h\nu(G-1)B_o$) are measured at the amplifier output, as shown in Fig.1 (a). In the case of n-concatenated amplifiers, $P_s$ and $P_{ase}$ should be replaced by the signal and ASE power of the last stage amplifier, $P_{s,n}$ and $P_{ase,n}$, as shown in Fig.1 (b). Also, L should be replaced by $L_n$. The two key parameters $P_{s,n}$ and $P_{ase,n}$ can be obtained by iterative calculations given below[16]:

$$P_{s,n} = P_{s,n-1}\cdot L_{n-1}\cdot G_n \tag{5}$$

$$P_{ase,n} = P_{ase,n-1}\cdot L_{n-1}\cdot G_n + 2n_{sp}h\nu(G-1)B_o \tag{6}$$

## 3. SYSTEM DESIGN CONSIDERATIONS

**3.1 Different Input Power Requirements on Analog & Digital Systems:** For a single in-line amplifier and a preset CNR (analog systems) or bit-error-ratio (digital systems), the minimum required amplifier input signal power ($P_{in,min}$) can be estimated from the $P_{in}$ that causes 1 dB power penalty in the receiver sensitivity, as compared to the case when no amplifiers are used. If $P_o$ is the receiver sensitivity without an amplifier, $P_{in,min}$ is obtained from $10\cdot log\ (\ (P_{in,min}G + P_{ase})L\ /\ P_o\ ) = 1\ dB$. The calculated results are shown in Fig.2 for analog systems ( CNR=45 dB for AM, CNR=17 dB for FM), and in Fig.3 for digital systems (SNR= 16 dB). We notice that: (1) for a typical

OMI/channel in an AM system, the result is essentially the same with or without an optical filter; (2) the minimum required input power to the amplifier is about -10 dBm for an AM system with an OMI/ch = 5%; (3) an optical filter can significantly reduce $P_{in,min}$ for FM systems; (4) for the same filter bandwidth, $P_{in,min}$ for an FM system can be made comparable to that of a digital system by adjusting the OMI/ch[5]; and (5) the $P_{in,min}$ of an AM system is incompatible with that of a digital system -- a digital signal that traverses the same optical amplifier system as a multichannel AM-VSB signal will have to lose 20 to 35 dB power, depending on the bit-rate and optical filter bandwidth.

For systems with concatenated amplifiers, if we assume that each amplifier gain is adjusted to compensate for the optical loss before it (i.e., $G_n^{-1} = L_{n-1}$ ), the required $P_{in,min}$ (same for all amplifiers) is increased because of the increase in signal-spontaneous and spontaneous-spontaneous beat noise. For example, if we let $n_{sp,1} = n_{sp,2} = \cdots = n_{sp,n}$ for all stages, then from eq.(6), the total ASE power $P_{ase,n} = n \cdot P_{ase,1}$. Therefore, we can see from eqs.(2)-(3) that the signal-spontaneous beat noise will be increased by a factor of n, and the spontaneous-spontaneous beat noise will be increased by a factor of $n^2$. The calculated results (filter bandwidth = 0.1 nm) for the $P_{in,min}$ of n-cascaded amplifiers are shown in Fig.4. We see that due to the signal-spontaneous beat noise, $P_{in,min}$ increases linearly with the number of amplifiers for all modulation formats. It is also clear that multichannel FM video signals can be made compatible with the digital signals in terms of amplifier input power, while AM systems have the tightest power budget among all systems. Note that if any amplifier in the concatenation has its noise figure increased due to deep gain-saturation, $P_{in,min}$ will be further increased.

The required amplifier input power also depends on the signal wavelength when the pump power is not sufficiently strong.[17] This is true for both analog and digital systems. A higher noise figure near the high ground-state absorption region, i.e., 1531 nm for $Er^{3+}$–$Al$-codoped fiber, may necessitate higher input power to achieve the same SNR or BER performance. Hence, near 1555 nm is a better choice for a single laser system to operate.

3.2 **The 1.3/1.55 $\mu m$ WDM Subscriber Loop System:** Low-density WDM systems (1.3/1.55 $\mu m$ ) are described in Bellcore's fiber-in-the-loop (FITL) special report,[18] in which integrated digital signaling (up to 622 Mb/s) is proposed to be transported in the 1.3 $\mu m$ region, and multichannel AM-VSB video services are to be provided in the 1.55 $\mu m$ region. If EDFAs are used in such a system, several design aspects must be considered: first, the EDFAs for multichannel AM-VSB video transmission must have built-in optical isolators to prevent multiple optical reflections[19] and backward ASE noise from degrading the video signal quality. Therefore, to preserve bi-directional transmission which is necessary for interactive data/voice services, the 1.3 $\mu m$ digital signals will have to completely bypass all in-line EDFAs that are installed for AM-VSB signals. This in turn makes the cost of installing all the amplifiers not well-justified. The second consideration in the 1.3/1.55 $\mu m$ system concerns the introduction of the WDM mux/demux pair into the system. The optical reflectivities of these devices may cause severe degradations of the AM-VSB signal if the reflectivities are much higher than -40 dB.[19] In addition, we notice that the required received optical power for multichannel AM-VSB signals is typically between -5 dBm and 0 dBm, while it is less than -40 dBm for digital line-rates below 155 Mb/s; therefore, the typical -40 dB demux crosstalk from 1.55 $\mu m$ into 1.3 $\mu m$ may cause power penalties to line-rates lower than 155 Mb/s. The third consideration is the dispersion-induced second-order nonlinear distortions in an AM system that limit the distribution distance to less than 4 km of conventional single-mode fiber.[20,21] To overcome this problem, more studies are needed to determine if dispersion-shifted fiber should be installed in the subscriber loop, or if we can resort to alternative methods such as distortion-compensation techniques.

3.3 **High-Density WDM (HD-WDM) Systems:** Several HD-WDM systems using EDFAs to distribute a large number of digital and/or analog signals in the 1.53-1.56 $\mu m$ region have been reported.[4,5, 22-24] As in the case of 1.3/1.55 $\mu m$ system, because the amplifier input power is incompatible between digital and AM-VSB signals, and because the amplifiers are working uni-directionally, digital signals may not need the amplifiers which are installed for AM-VSB signals. As an example, Fig.5 shows the total number of optical amplifiers used in a subscriber loop versus the total optical branching number. The number of amplifiers used in a subscriber loop for distributing multichannel AM-VSB signals can be four orders of magnitude higher than that for distributing 155 Mb/s digital signals (e.g., 50 compressed NTSC digital videos with 2 Mb/s each), or over two orders of magnitudes higher than that for distributing 2.5 Gb/s signals (e.g., multiple compressed high-definition videos at 155 Mb/s, NTSC videos at 2 Mb/s, and other data services). This has important implications in the FITL evolutionary strategies, because almost all the optical amplifiers installed for AM video services may not be needed for future digital services. In addition to the amplifier input power compatibility and spectral dependent-noise figure issues (see Sec.3.1), the main

system concern is how to avoid gain spectrum unbalance due to gain saturation effects. This is especially critical for WDM channels spread over 30 nm. Amplifier gain saturation can be minimized by keeping the total power of the WDM channels before an amplifier low (e.g., less than -10 dBm[5,22,23] ) and/or by using very high pump power to increase the saturation power level.[22]

**4. CONCLUSIONS:** Based on typical erbium-doped fiber amplifier's characteristics and noise analysis, we have summarized several design considerations in low- and high-density WDM systems when EDFAs are used for the subscriber loop applications. The most critical system aspect we have emphasized is the power budget incompatibility between analog and direct-detection digital systems using EDFAs, and the uni-directional usage of EDFAs for multichannel AM-VSB video transmission which forbid future interactive digital services. This has important implications concerning evolutionary network planning strategies because broadcast analog AM-video is just a first-stage broadband service that will eventually have to be upgraded to all digital services. Therefore, even though EDFAs can transport multichannel AM video signals with satisfactory quality, their wide deployment may need careful network planning.

**5. ACKNOWLEDGMENT:** The author would like to thank C. Lin, M. Saifi, A. Yi-Yan, A. C. Von Lehmann, and M. Andrejco for their technical contributions in all the cited Bellcore EDFA experiments.

**REFERENCES:**

[1] W. I. Way, et al., Post-deadline Tech. Digest, p.37, ECOC'89.
[2] G. R. Joyce, V. Lanzisera, and R. Olshansky, Electron. Lett., p.499, 1989.
[3] W. I. Way, M. M. Choy, M. Andrejco, M. Saifi, and C. Lin, Photon. Tech. Lett., p.343, 1989.
[4] W. I. Way, M. W. Maeda, A. Yi-Yan, M. J. Andrejco, M. M. Choy, and C. Lin, Electron. Lett., pp.139, 1990.
[5] W. I. Way, S. S. Wagner, M. M. Choy, C. Lin, R. Menendez, H. Tohme, A. Von Lehman, A. Yi-Yan, M. Andrejco, M. Saifi, and H. Lemberg, PD21, OFC'90.
[6] K. Kikushima, E. Yoneda, and K. Aoyama, PD22, OFC'90.
[7] E. Eichen, J. McCabe, W. J. Miniscalso, R. Olshansky, and T. Wei, Photon. Technol. Lett., p.220, 1990.
[8] W. I. Way, C. E. Zah, and T. P. Lee, IEEE Trans. Microwave Theory and Tech., p.534, 1990.
[9] S. Y. Huang, T. W. Cline, L. C. Upadhyayula, R. E. Tench, and J. Lipson, paper BAM7, Summer Topical Meetings on Broadband Analog Optoelectronics, 1990.
[10] H. E. Tohme, C. N. Lo, and M. A. Saifi, paper WB4, Topical Meeting on Optical Amplifiers and Their Applications, 1990.
[11] M. Shigematsu, K. Nakazato, T. Okita, Y. Tagami, K. Nawata, paper WB3, Topical Meeting on Optical Amplifiers and Their Applications, 1990.
[12] K. Kikushima, E. Yoneda, K. Suto, and H. Yoshinaga, paper WB1, Topical Meeting on Optical Amplifiers and Their Applications, 1990.
[13] P. M. Gabla, V. Lemaire, H. Krimmel, J. Otterbach, J. Auge, and A. Dursin, IEEE Photon. Technol. Lett., p.56, 1991.
[14] D. R. Huber and Y. S. Trisno, PD16, OFC'91.
[15] W. I. Way and C. Lin, LEOS Summer Topical on Broadband Analog Optoelectronics, paper BAT4, 1990.
[16] C. R. Giles and E. Desurvire, J. Lightwave Technol., p.147, 1991.
[17] E. Desurvire, Photon. Technol. Lett., p.208, 1990.
[18] Bellcore Fiber In The Loop (FITL) Architecture Summary Report, SR-TSY-001681, Issue 1, June 1990.
[19] W. I. Way, C. Lin, C. E. Zah, R. Spicer, L. Curtis, and W. C. Young, Photon. Tech. Lett., p.360, 1990.
[20] M. R. Phillips, T. E. Darcie, D. Marcuse, G. E. Bodeep, and N. J. Frigo, paper TuC4, OFC'91.
[21] E. E. Bergmann, C. Y. Kuo, and S. Y. Huang, IEEE Photon. Technol. Lett., p.59, 1991.
[22] A. Hill, et al., Electron. Lett., p.1882, 1990.
[23] H. Toba, K. Inoue, K. Oda, and K. Nosu, paper ThC3, OFC'91.
[24] K. Inoue, H. Toba, and K. Nosu, J. Lightwave Technol., p.368, 1991.
[25] N. Henmi, S. Fujita, M. Yamaguchi, M. Shikada, and I. Mito, J. Lightwave Technol., p.936, 1990.

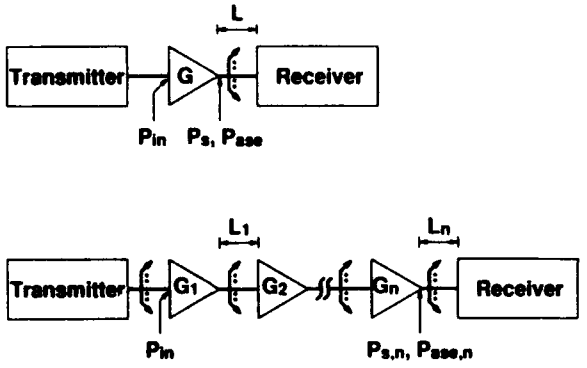


Fig.1. (a) Single and (b) cascaded optical amplifiers. An optical filter is integrated in each amplifier.

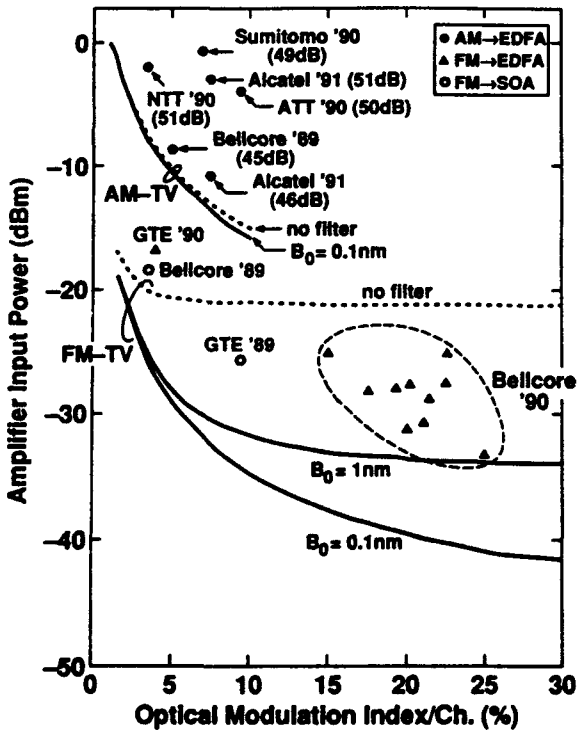


Fig.2. Minimum required amplifier input power versus OMI/ch for AM-VSB and FM video signals. The Minimum amplifier input power causes 1 dB power penalty to the receiver sensitivity. Solid and dashed lines are calculated results.

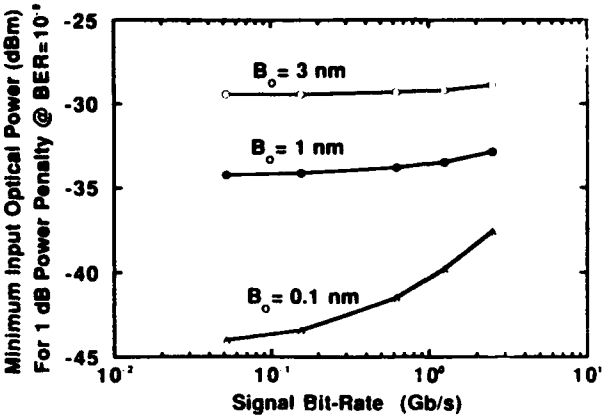


Fig.3. Minimum required amplifier input power versus digital bit-rates for three different optical filter bandwidths ( $B_o$ ).

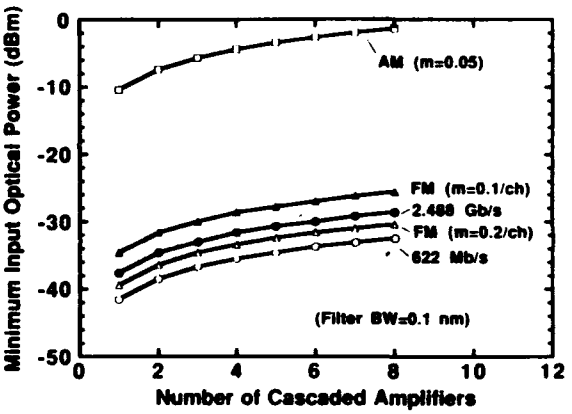


Fig.4. Minimum required input optical power versus the number of cascaded amplifiers for AM-TV, FM-TV, 622 Mb/s, and 2.488 Gb/s signals.

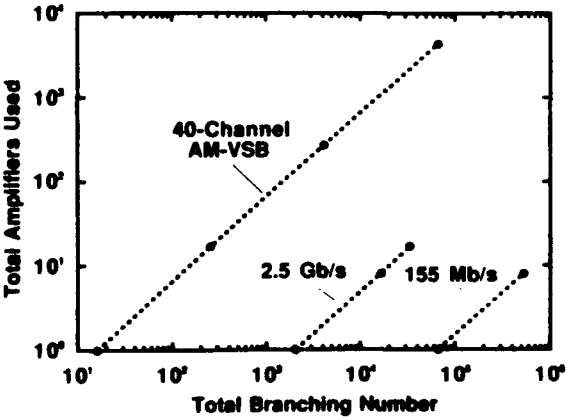


Fig.5. Total erbium-doped fiber amplifiers needed in a subscriber loop vs. total branching number (with 10 dB power margin). The 40-ch AM system data is from ref.[12].

# Simultaneous Distribution of Analogue AM-TV and Multigigabit HDTV with Optical Amplifier

R. Heidemann, B. Junginger, H. Krimmel, J. Otterbach,
D. Schlump, B. Wedding

SEL Alcatel Research Centre
Lorenzstrasse 10
D-7000 Stuttgart 40, FRG

## INTRODUCTION

Analogue FDM transmission of AM-VSB TV-channels over optical fibres is used today to upgrade existing copper-based CATV networks. With the aid of optical amplifiers (EDFA) cost competitive FTTC systems will be realized /1,2/. The strategy for the distribution of HDTV-channels is not so clear today, but in any case, digital transmission will yield the highest quality /3/. In this paper we demonstrate the feasibility of flexible TV/HDTV-distribution using simultaneous analogue AM and digital PCM transmission over optical amplifiers without any mutual quality degradation.

## SYSTEM APPLICATIONS

For high quality digital HDTV distribution the copper bottleneck in current FTTC system has to be avoided and the large-bandwidth fibre-pipe has to be layed to the home (FTTH) or even to the terminal ($FT^3$). Many experiments show that with purely digital transmission and extensive use of optical amplification extremely large transmitter sharing factors can be reached /4/.

On the way towards this ultimate target analogue AM-TV has to be provided to the customer in parallel. Furthermore not all customers in a neighbourhood will be fibred at the same time. Fig. 1 shows the block diagram of a tree-and-branch type distribution system enabling the evolution from analogue FTTC, via analogue and digital FTTH towards digital $FT^3$ without changing the access network or its key components, namely the optical amplifiers and power splitters.

In the CATV headend a conventional analogue FDM-signal (35xTV PAL-B/G, 30 x FM stereo-broadcast, 16 x Digital stereo-broadcast) is transmitted at 1550 nm wavelength. The digital HDTV-channels are time-division multiplexed (e.g. 64 x 140 Mbit/s → 10 Gbit/s), transmitted at 1536 nm and combined in a WDM coupler. This WDM/FDM/TDM signal is distributed in the network by successive optical amplification and optical splitting.

In the remote terminal at the curbe the TV/HDTV channels are routed via a WDM device, an analogue optical receiver and coaxial cable to the home (AM-TV only, FTTC), or via fibre to the home and to the coaxial in-house cabeling (FTTH), or via an extra optical amplifier and the fibre-based in-house cabling directly to the terminal ($FT^3$).

## FEASIBILITY EXPERIMENT AND RESULTS

The following key questions must be answered: Under which circumstances can FDM AM-VSB-signals and digital TDM PCM-signals be transmitted over a network containing Erbium-doped fibre-optic amplifiers as active, and possibly non-linear, components? Do the low frequency spectral components (starting at about 300 Hz at 2.488 Gbit/s $2^{23}$-1 PRBS) of the base-band PCM signal interfere, e.g. by gain modulation, with the sensitive analogue AM-TV

signal? Does the high power optical analogue signal degrade the bit-error rate of the PCM signal?

To answer these questions a system experiment depicted in fig. 2 has been carried out. The analogue optical transmitter uses a 1549 nm DFB-laser module with integrated optical isolator. This laser is modulated with the standard German BK 450 FDM-signal in the frequency band 47-450 MHz (35 x TV PAL B/G; 12 x FM stereo broadcast). At an optical output power of 0 dBm and a modulation index of 5.2 % a SNR of 55.6dB and a CSO and CTB less than -65 dBc are measured. The digital path comprises of a DFB laser transmitter at 1536 nm (P = -3.6 dBm), without optical isolator, driven by an Anritsu 10 Gbit/s pattern generator at the STM-16 bitrate of 2.488 Gbit/s with different PRBS ($2^7$-1,$2^{23}$-1) of different spectral content. Both signals are combined in a fused-fibre power combiner. To prevent CSO degradation by FM-AM conversion at optical fibre resonators in the system /5/ ultra low reflectivity fused-fibre WDM components are used in the whole system. The spectrum of the input signal to the Erbium-Doped-Fibre-Amplifier ($\lambda_{pump}$ = 1480 nm, $P_{pump}$ = +13.4 dBm, fused-fibre pump coupler, 50 m EDF, fluorescence spectrum see fig. 3) is shown in fig. 4a.

The output signal with a maximum level of +7.5 dBm is separated after 20 km of dispersion shifted fiber by a wavelength division demultiplexer consisting of cascaded fused-fibre wavelength selective couplers, (attenuation/crosstalk values, 1548 nm: E-A1 3 dB, E-A2 33 dB, 1536 nm: E-A2 5.5 dB, E-A1 24 dB). The crosstalk value of 24 dB from the digital to the analogue path is needed to separate any interference originating in the analogue optical receiver from such originating in the EDFA, whereas for the decoupling of the analogue CATV to the digital PCM signal 33 dB is sufficient for a BER $\leq 10^{-9}$. Details on requirements for the crosstalk in the wavelength demultiplexer will be reported elsewhere.

In fig. 4b and c the spectra of the optical input signals to the analogue and the digital receiver respectively are shown. The analogue CATV channels are not affected by the digital channel, neither is the SNR degraded beyond 47.6 dB, the value also measured with the modulation of the 1536 nm laser switched off, nor any interference occurs, even in the case of a $2^7$-1 PRBS where a data spectral line coincides with the channel S20 at 294.25 MHz.

On the other hand the bit-error rate curve (fig. 5) does not show any indication of degradation or error rate floor with the modulation of the analogue transmitter switched on.

**CONCLUSION**

We have demonstrated the feasibility of simultaneous transmission of standard CATV AM-VSB signals and digital multigigabit/s PCM signals in the same optical window, over a network containing Erbium-Doped-Fibre-Amplifiers as active elements. No mutual degradation neither of SNR, CSO and CTB nor of the bit-error rate could be measured. This is due to the fact that in the case of long PRBS the low frequency spectral density is very low and in the case of short PRBS the lowest frequency spectral line is above 100 kHz /6/.

## REFERENCES


/1/ M. Shigematsu, et al.: OFC 90, PD 22, WB3
/2/ K. Kikushima, et al: Optical Amplifiers and Their Applications Monterey 1990, WB1
/3/ R 1051: Multigigabit Transmission in the IBCN Subscriber Loop, RACE 90, Brussels
/4/ A. M. Hill, et al: OFC 91, ThD3
/5/ A. Lidgard, et al: IEEE Photonics, Technol. Lett. 2, 519, (1990)
/6/ R. I. Laming, et al: Electron. Lett. 25, (1989)


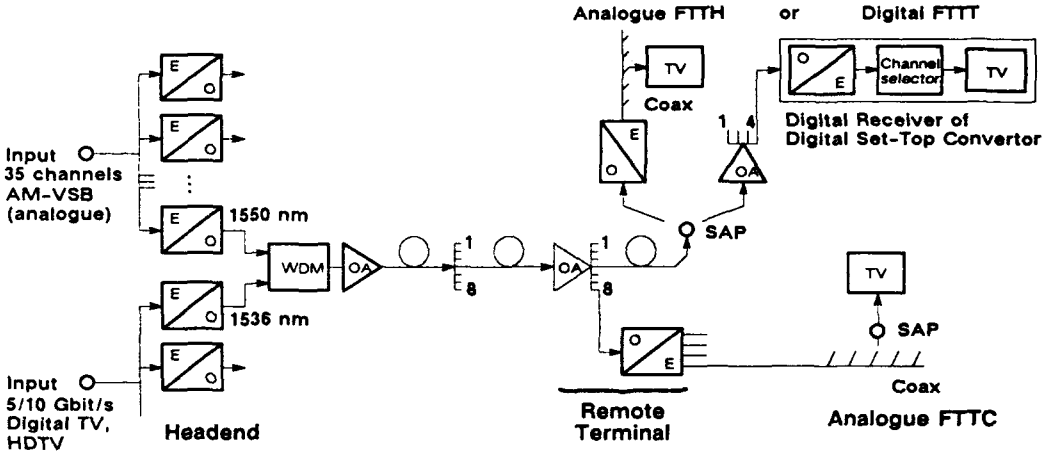


Fig. 1 Block diagram of TV/HDTV distribution network with simultaneous analog and digital transmission. Optical amplification allows implementation as FTTC, FTTH or even FT³ system.

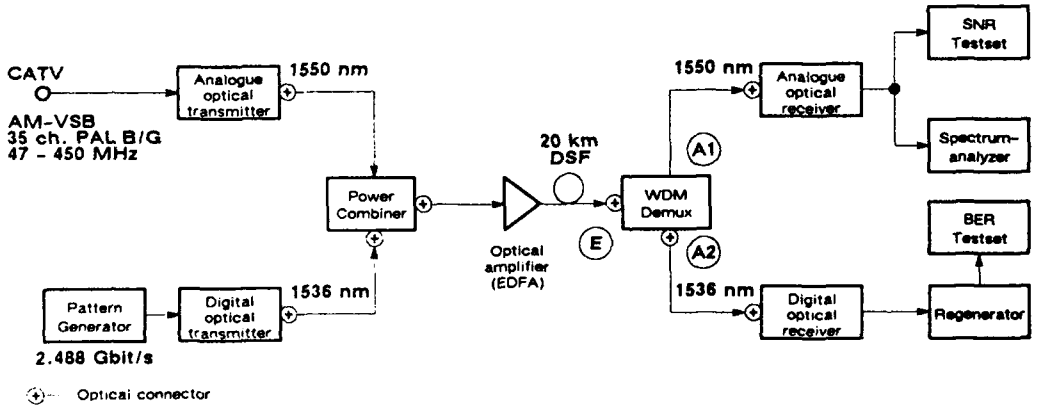


Fig. 2 Experimental set-up to demonstrate analog CATV and digital HDTV transmission using WDM and optical amplification.

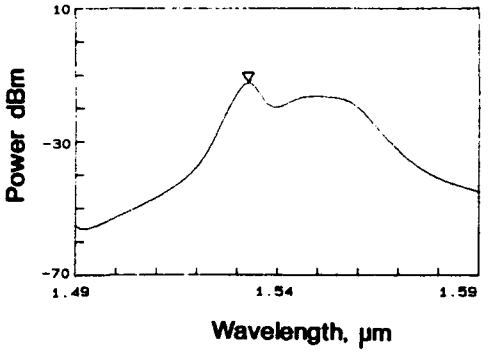


Fig. 3
Fluorescence spectrum of Erbium-doped-Fibre-Optic-Amplifier, 1480 nm pump wavelength.

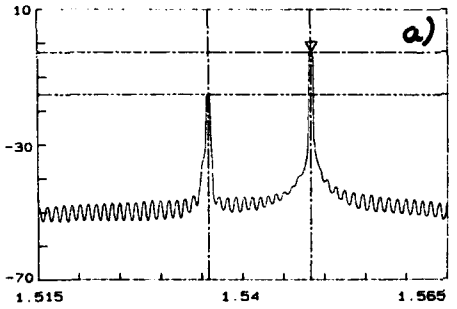


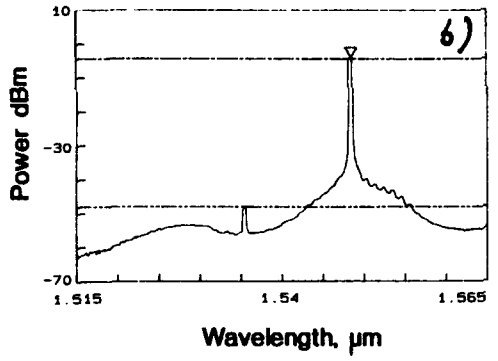


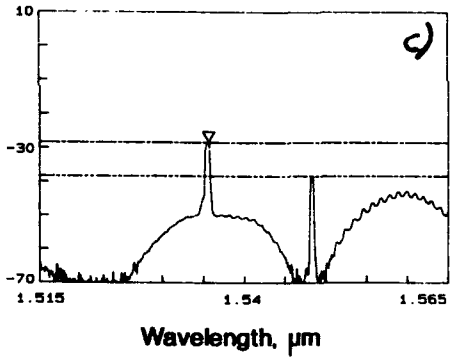


Fig. 4
Optical spectra of analogue (1549 nm) and digital (1536 nm) signal. a) input of optical amplifier, b) input of analogue optical receiver, c) input of digital optical receiver.

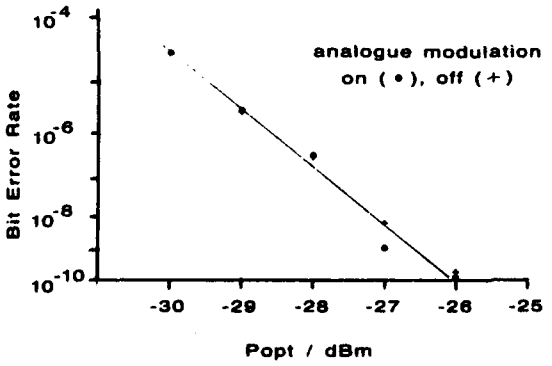


Fig. 5
Bit-error rate characteristic of digital 2.488 Gbit/s link with superimposed analogue CATV signal.

# A High Power and Low Noise Transmitter for AM-VSB Transmission Using Erbium-doped Fiber Post Amplifier

Masayuki Shigematsu, Masayuki Nishimura, Toshio Okita, Kazuo Iizuka

Sumitomo Electric Industries, Ltd.

1, Taya-cho, Sakae-ku, Yokohama, 244, JAPAN

## 1. Introduction

Erbium doped fiber amplifiers(EDFAs) with high output power and no distortion degradation are very useful for the amplitude-modulated vestigial-sideband(AM-VSB) transmission systems which require a relatively high received power for a preferred carrier to noise ratio(CNR) and a low distortion[1][2]. A field trial was conducted and feasibility of multi-distribution for trunk lines was confirmed[3].

We have developed an erbium doped fiber with a high conversion effeciency of 86 % and a small wavelength dependence. In this paper, by using this fiber as a post amplifier,we present a high power and low noise transmitter with monitoring functions for practical use. We also show the effectiveness of long-wavelength-pass filters which have a low insertion loss and no need for wavelength tuning unlike band-pass filters.

## 2. Theoretical Estimation

The CNR can be calculated as

$$CNR^{-1} = \left( \frac{2 \cdot RIN}{m^2} + \frac{4 \cdot e(Ro \cdot Pd + Id)}{(m \cdot Ro \cdot Pd)^2} + \frac{8 \cdot k \cdot T \cdot Fr}{Rl\,(m \cdot Ro \cdot Pd)^2} + \frac{4 \cdot E \cdot Fa}{m^2 \cdot Pin} \right) \cdot B$$

where RIN; relative intensity noise of transmitter, m; modulation index,
Id; dark current, Ro; sensitivity of receiver, Pd; received power, Rl; load resistance,
Fr; noise figure of receiver, E; photon energy of signal, Fa; noise figure of amplifier,
Pin; input signal power of amplifier, B; noise bandwidth of video channel

Fig.1 shows amplifier input signal power(Pin) dependence of the received power penalty for CNR of 51dB(preferred value for trunk lines), where RIN, m and Fa are -155 dB/Hz, 5 % and 7 dB respectively. The loss budget is also plotted when it is assumed that the output power of the transmitter and EDFA are +6 dBm(4 mW) and +13 dBm(20 mW). It is noted that the lower Pin increases the power penalty and when Pin is less than -2dBm, the preferred CNR cannot be satisfied. However, up to 20 dB loss budget is achievable when Pin is limited to -1 dBm or above. Although the total loss budget is slightly smaller than the possible maximum, it is one of the most practical configurations to use an EDFA as a post amplifier at the head end.

## 3. Characteristics of Erbium-doped Fiber

The developed erbium-doped fiber had a NA of 0.29 with germanium doped core and

fluorine added cladding. Erbium ions whose concentration was approximately 300 wt. ppm were doped with alumina in the central area of the core. The core diameter and the cut-off wavelength were 2.9 μm and 1.17 μm.

When 1.48 μm laser diodes(LDs) were used as a pump source, the slope efficiency was 80 % and 86% for forward and backward pumping configurations respectively at the signal wavelength of 1.554 μm. The gain coefficient of 6.3 dB/mW was also obtained at the same signal wavelength. The variation of output signal power in a range from 1.53 μm to 1.57 μm for foward pumping was 10.6 dBm +- 0.5 dB, when the input signal power and pump power were -3 dBm and 18 mW respectively.

## 4. Configuration of Fiber Amplifier

Fig.2 shows the optical block diagram of the developed EDFA. A 150 m erbium-doped fiber which was coiled into 65 mmϕ x 17 mmt was pumped bidirectionally by using two commercially available 1.48 μm pumping LDs and fiber couplers. The coupled pumping power levels were approximately 25 mW and 20 mW for copropagating and counterpropagating directions with respect to the signal.

A long-wavelength-pass filter(LWPF) whose insertion loss were 0.5 dB at 1.55 μm and more than 20 dB at 1.48 μm was used after the output optical isolator with no polarization dependence. The LWPF was fabricated by inserting a thin dielectric multi-layer filter into a 30 μm wide slit formed in optical fiber itself attached to a V-groove on Si substrate with an 8 degree tilt. The return loss and polarization dependence were less than -50 dB and 2 %.
In Fig.3, the input signal power dependence of noise figure(NF) when using the LWPF is shown. The signal wavelength was 1.556 μm. The NF was calculated from measurements of the RF electrical noise[4]. At the input signal power level more than -10 dBm, the NF was as low as 5 dB, which showed a close agreement with the value of 4.9 dB evaluated from ASE optical power measurements[4]. Considering that the ordinary received signal power is minus few dBm for AM-VSB transmission system, LWPFs with low insertion loss at signal wavelengths are sufficient and eliminate the necessity of wavelength tuning with the use of band-pass filters.

The output signal power level can be monitored by using a 2 % tapping coupler. The pump power and laser internal temperature can also be monitored by a photo-detector and a thermistor included in the pump LD modules.

## 5. Characteristics of 40 channel AM-VSB Transmission

A DFB LD(the output power of 4 mW) oscillating at 1.543 μm followed by the EDFA(rack mount type:see the photograph) was used as a transmitter. The output power of 16 mW(+12 dBm) was achieved. Fig.4 shows the relationship between transmission loss and CNR with and without the EDFA in the 40 channel (from 91.25 MHz to 337.25 MHz) transmission. The modulation index m was about 5 %. The carrier frequency used in the measurement was 97.25 MHz. For CNR of 51 dB, the loss budget of 14 dB was obtained with the post EDFA. The experimental data well coincided with theoretical values(solid lines) calculated from measured parameters (relative intensity noise of DFB LD : -155 dB/Hz, NF of EDFA : 7 dB [including the insertion losses of optical components on the input side])

## 6. Conclusions

A high output power and low noise transmitter for AM-VSB transmission was developed by using erbium-doped fiber post amplifier. The output power of 16 mW and 14 dB loss budget for CNR of 51 dB was achieved at 40 channel transmission. Effectiveness of the long-wavelength-pass filter was confirmed. This filter is very useful because of its low insertion loss and no need for wavelength tuning. The reliability test will be conducted for practical use.

## 7. References

[1] W. I. Way et al., IEEE Photonics Technol. Lett., Vol. 1, No. 10, pp343-345 (1989)

[2] K. Kikushima, E. Yoneda et al., OFC'90, PD22

[3] M. Shigematsu et al., Technical Digest on Optical Amplifiers and Their Applications, WB3 (1990)

[4] C. R. Giles et al., IEEE Photonics Technol. Lett., Vol. 1, No. 11, pp367-369 (1989)

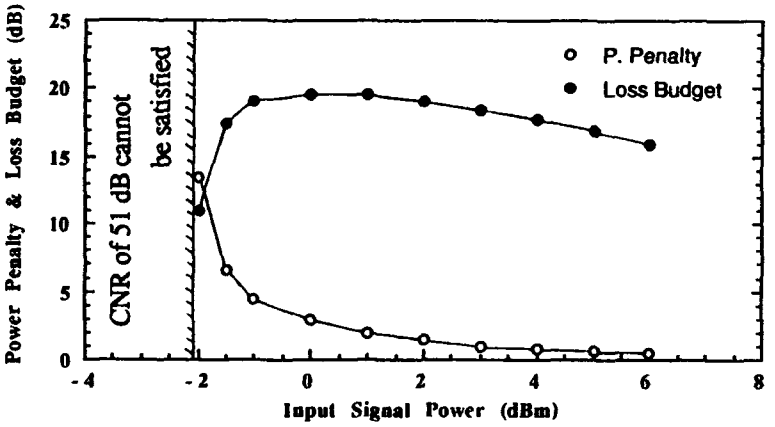


Fig.1 Input Signal Power of Amplifier vs. Received Power Penalty & Loss Budget

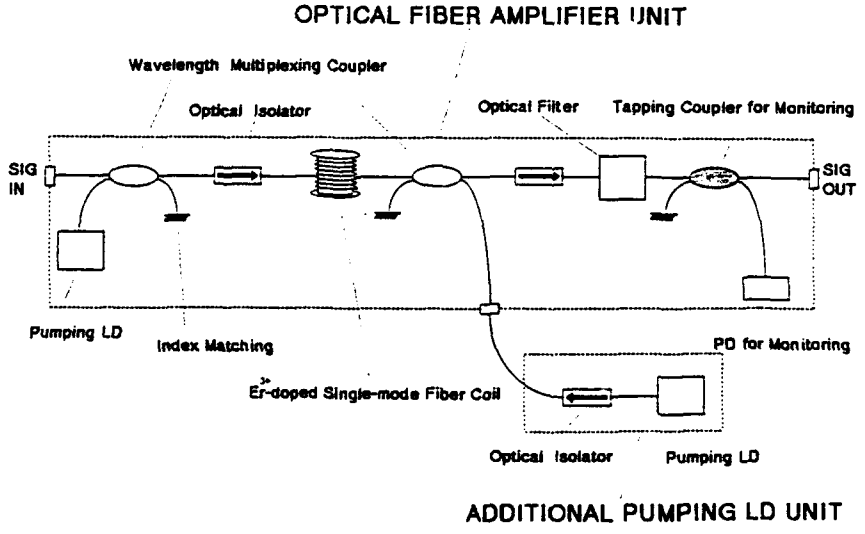


Fig.2 Optical Block Diagram of Developed EDFA

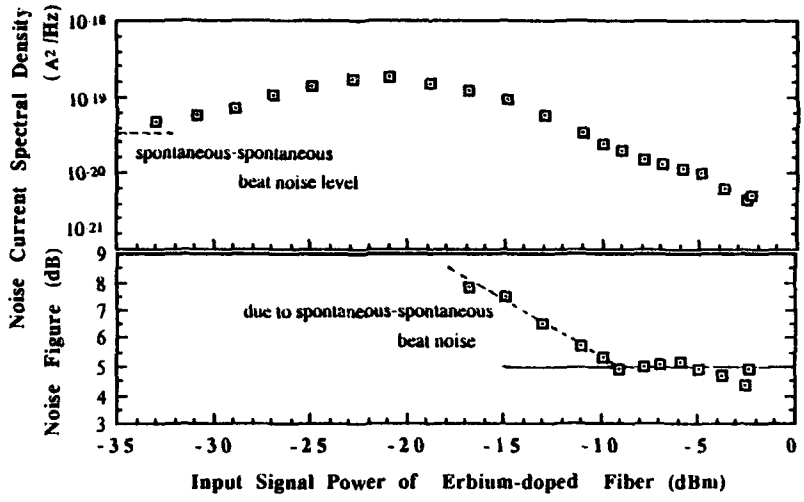


Fig.3 Input Signal Power Dependence of Noise Figure

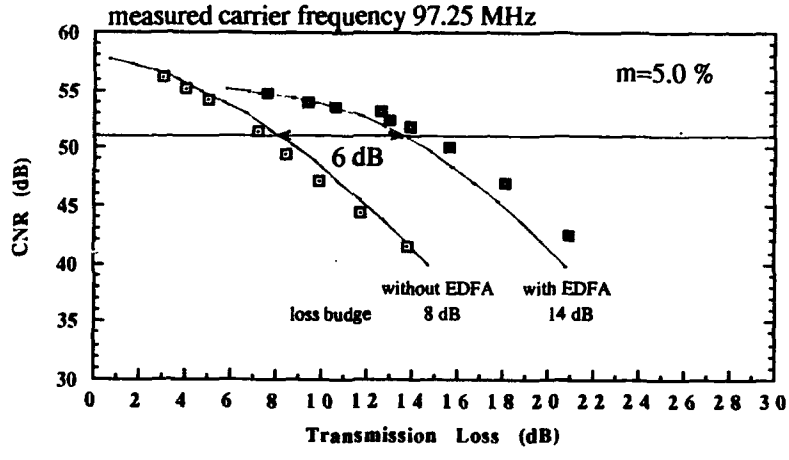


Fig.4 Transmission Loss vs. CNR

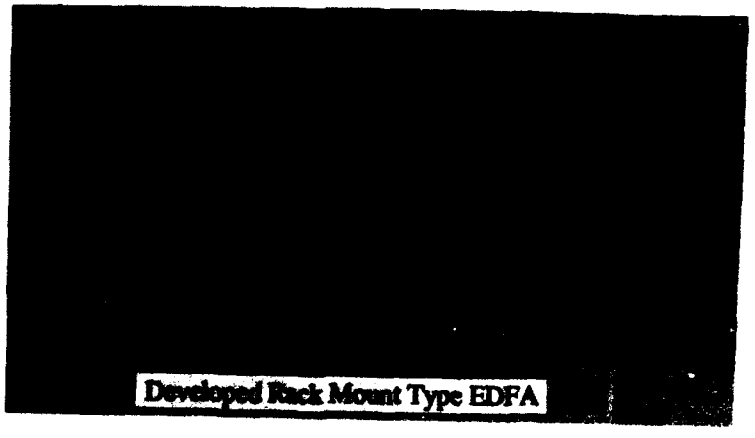

# A 40 Channel AM-VSB Distribution System with a 21 dB Link Budget

**G. R. Joyce, R. Olshansky, R. Childs and T. Wei**
GTE Laboratories Inc
40 Sylvan Road
Waltham, MA 02254
617-466-2346

**ABSTRACT** An AM-VSB fiber video distribution system combines an erbium-doped fiber power amplifier with a low-noise receiver to attain a 21 dB link budget for 40 channels.

**Introduction:** The combination of amplitude-modulated vestigial-sideband (AM-VSB) transmission with erbium doped fiber power amplifiers has proven useful for carrying video signals over fiber systems.[1,2,3,4,5] Highly linear, directly modulated lasers provide the high necessary carrier to noise ratio (CNR) at the CATV frequency range, and the fiber amplifiers provide the power necessary for a useful link budget despite the low modulation depth of the laser. By using optical splitting and shared optical receivers, the expense of the transmitter and amplifier pump lasers may be shared by many subscribers of an AM-VSB fiber video distribution system. By using a fiber booster amplifier and low noise hybrid receiver, we have acheived a 21 dB link budget for 40 channels with a 48 dB CNR.

**Experimental Setup:** Figure 1 shows the experimental setup. A "MATRIX generator" supplied high fidelity, unmodulated signals to directly modulate a highly linear DFB laser, simulating video sources at 6 MHz intervals, from 169.25 MHz to 283.25 MHz for 20 channels, and 139.25 MHz to 373.25 MHz for 40 channels. The laser (1561 nm) was biased at 43 mA (2.4 x threshold) so as to minimize laser nonlinearities, and had a measured relative intensity noise (RIN) coefficient of -153 dB/Hz. The modulation depth was limited to m = 7.75 % (20 channels) and m = 5.9% (40 channels) to avoid distortions due to clipping[6]. A 1.1 dBm signal was input to an erbium-doped fiber amplifier[7] which was pumped in the forward direction by 58 mW of 1480 nm light from two semiconductor lasers and was bracketed by pigtailed isolators. The fiber amplifier output was 13.6 dBm (10 dB into saturation), with a measured noise figure of approximately 5 dB[8], and a pump to signal power conversion efficiency of 39%. The output signal was passed through an optical bandpass filter (to remove residual pump light) and a variable

attenuator. A low-noise CATV hybrid receiver[9] featured a pigtailed detector (0.71 quantum efficiency) impedance matched to a highly linear amplifier and acheived a thermal noise of less than 6 pA/Hz$^{1/2}$ in this frequency range. Angled-facet connectors were used at all points in the system to minimize reflections. The composite second-order and composite triple-beat distortion were less than -60 dBc through the entire system.[10]

**Results:** Figure 2 shows the measured carrier to noise ratio for 20 channels operating at m=7.75%, for a 4 MHz bandwidth[10] versus received signal power, as well as the expected CNR due to RIN, signal spontaneous beat noise, shot noise, receiver thermal noise, and the combination of these. For a -3 dBm signal power the CNR was very high, 55 dB, and only fell to 48 dB for a signal power of less than -12 dBm. Figure 3 shows similar data for a 40 channel system operated at m=5.9%. Here the CNR was 53 dB for a -3 dBm signal and fell to 48 dB at -8.6 dBm, for a total system loss of 22 dB. In both cases the data fit the model very well. At the lower power levels, the dominant noise source is the receiver thermal noise, and the CNR performance in this range would have been impossible without the low noise receiver.

**Discussion:** By utilizing a fiber power amplifier and a low-noise receiver, a system budget of at least 21 dB was attained for a 40 video channel AM-VSB fiber distribution system, while delivering a 48 dB CNR. A 48 dB CNR is equivalent to very high quality video signal, similar to a laser disk player. This high system budget is important for the economies of scale for fiber based video distribution. Figure 4 shows an AM-VSB distribution network as a retrofit where the fiber, coax, pedestal and powering are already installed for narrowband services. The fiber booster amplifier and receiver have, as demonstrated, a +13 dBm output power and -8 dBm sensitivity (40 channels), for a 21dB system budget. A 1x16 splitter is assumed to have a 14 dB loss, and fiber, connector loss and margin account for the remaining 7 dB. If 8 homes are passed per optical receiver, the system serves 128 homes. If it is assumed that the outside plant for a fiber-to-the-curb narrowband network has already been installed (including pedestal, powering and coax drop), then one can estimate the incremental cost for adding a 40-channel AM broadcast capability. If the price of the opto-electronic components (DFB laser, fiber amplifier, isolators, optical receiver) is taken as a factor of two below today's low volume pricing and an additional 50% is budgeted for installation, then the incremental cost per home passed is about $250. Even lower costs could be realized as component prices decline further.

In conclusion, a 40-channel AM-VSB system has been demonstrated with a 21 dB link budget and 48 dB CNR. By allowing the use of a 1x16 optical splitter in a fiber-to-the-curb architecture, the system can distribute AM signals at an incremental cost per home which can be highly competitive with conventional coaxial systems.

[1] W. I. Way, M. M. Choy, A. Yi-Yan, M. Andrejco, M. Saifi and C. Lin, "Multichannel AM-VSB television signal transmission using an erbium doped optical fiber power amplifier," *IEEE Photonics Technology Lett.*, vol. 1, pp 343-345, 1989

[2] D. R. Huber, "40 Channel VSB-AM CATV link utilizing a high-power erbium amplifier," Optical Fiber Communication Conference 1991, San Diego, CA., paper TuC3

[3] P. M. Gabla, V. Lemaire, H. Krimmel, J. Ottrbach, J. Auge', and A. Dursin," 35 AM-VSB TV channels distribution with high signal postamplifier," *IEEE Photonics Technology Lett.*, vol. 3, pp 56-58, 1991

[4] M. Shigematsu, K. Nakazato, T. Okita, Y. Tagami and K. Nawata, "Field test of multichannal AM-VSB transmission using an erbium doped optical fiber amplifier at 1.55 μm wavelength range in the CATV network," Optical Amplifiers and Applications, Monterey, CA., 1990, paper WB3

[5] K. Kikushima, E. Yoneda, K. Suto, and H. Yoshinaga, "Simultaneous distribution of AM/FM FDM TV signals to 65,536 Subscribers using 4 stage cascade EDFA's," Optical Amplifiers and Applications, Monterey, CA., 1990, paper WB1

[6] A. A. M. Saleh, "Fundamental limit on number of channels in subcarrier multiplexed lightwave CATV systems," *Electron. Lett.*, vol. 25, pp 776-777, 1989

[7] W. J. Miniscalco, B. A. Thompson, E. Eichen, T. Wei, "Very high gain $Er^{3+}$ fiber amplifier pumped at 980 nm," Optical Fiber Communication Conference 1990, San Francisco, CA., paper FA2.

[8] W. I. Way, A. C. Von Lehman, M. J. Andrejco, M. A. Saifi and C. Lin, "Noise figure of a gain saturated erbium-doped fiber amplifier pumped at 980 nm," Optical Amplifiers and Applications, Monterey, CA., 1990, paper TuB3

[9] R. B. Childs, to be submitted

[10] T. E. Darcie and G. Bodeep, "Lightwave Subcarrier CATV Transmission Systems," *IEEE Trans. on Microwave Theory and Techniques*, vol. 38, pp 524-533, 1990.

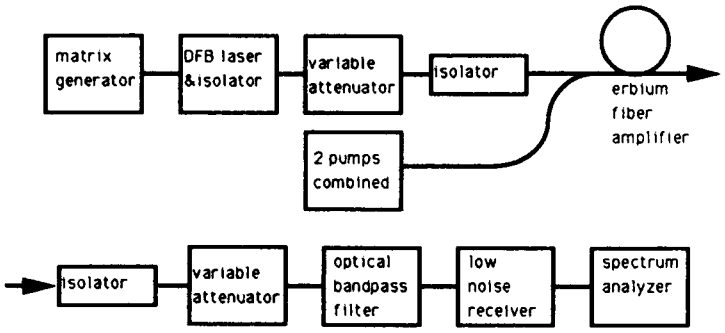


**Figure 1. Experimental setup**

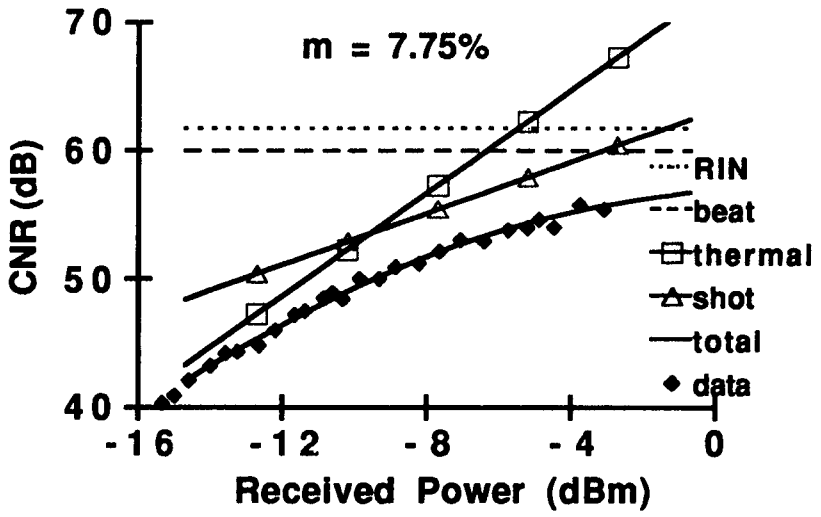


**Figure 2. System performance for 20 channels**

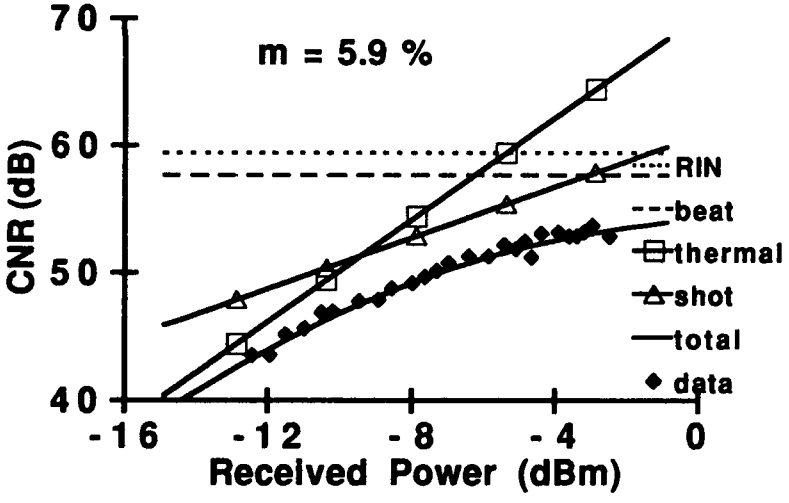


**Figure 3. System performance for 40 channels**

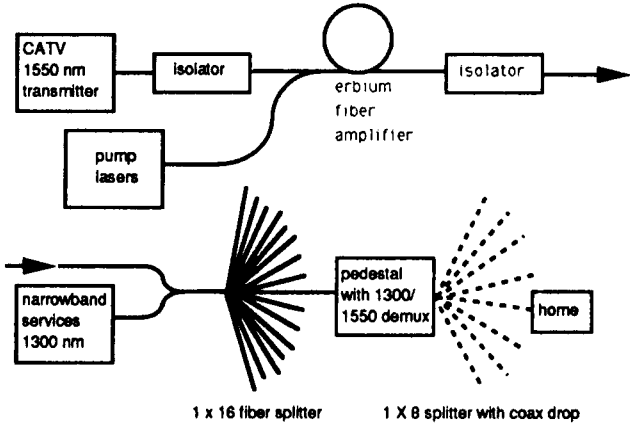


**Figure 4. Distribution system**

# NOISE PERFORMANCE OF BUS-CONFIGURED OPTICAL NETWORKS WITH DISTRIBUTED FIBER AMPLIFICATION

**Evan L. Goldstein**
*Bellcore, Red Bank, NJ 07701-7040*

**Introduction.** Optical bus networks with passive taps have attracted little attention because optical-power limits severely constrain their size. It has recently been realized, however, that such constraints may be overcome using $Er^{3+}$-doped fiber amplifiers. A numerical analysis [1],[2] has shown that buses with periodic amplification should be capable of supporting large numbers of nodes, even in the presence of saturating signals. Moreover, there is experimental evidence [3] that bus networks with uniformly distributed amplification generate low levels of amplified spontaneous emission (ASE). We here present a simple analysis yielding closed-form expressions showing that the amplified bus can indeed support thousands of nodes, that it can span thousands of kilometers (fiber dispersion and nonlinearity permitting), and that this excellent noise performance results from the slow growth of ASE in low-gain amplifying structures. To support large numbers of nodes, however, the bus's gain must be well matched to its loss.

**Spontaneous Emission in the Amplified Bus.** We consider networks of the sort depicted in Fig. 1, where a set of transceiving nodes is connected, via directional coupler, to a bus incorporating $Er^{3+}$-doped-fiber amplification. Practical implementations may use dichroic couplers and additional pump lasers. The network's amplifying elements are required to provide just enough gain to approximately overcome coupling and propagation losses. We focus on the evolution of ASE power along the bus, which in turn determines the network's crucial noise properties.

In practice, such buses are likely to contain lumped losses, at the couplers, spatially separated from lumped gain elements. Thus the local power gain per unit length $g(z)$, and the power loss per unit length $\alpha(z)$, will vary with distance $z$ from the input end of the bus. For computational purposes, we temporarily imagine a network whose local dopant concentration is precisely adjusted so that $g(z)$ and $\alpha(z)$ vary spatially while staying in fixed ratio $g/\alpha$; thus, local splitting losses, at couplers, are compensated by locally increased gain. The evolution of ASE in such a bus is easily calculated.

A traveling-wave optical amplifier of gain $G$ and optical bandwidth $B_0$, operating in a single transverse mode, is commonly assumed to generate ASE power $P_{sp} = n_{sp}h\nu(G-1)B_0$, where $n_{sp}$ is the population-inversion parameter and $h\nu$ is the photon energy. However, this expression plainly cannot apply to amplifiers with gain $G \leq 1$; it is in fact an approximation that fails when the waveguide's loss per unit length is comparable to its gain. Taking such loss into account yields a more accurate expression [4], which is easily generalized to the present case, where $g(z)$ and $\alpha(z)$ vary while preserving their ratio. The ASE power then evolves as

$$P_{sp}(z) = \frac{n_{sp}h\nu B_0}{1-(\alpha/g)}\left\{\exp\left[\int_0^z [g(\xi)-\alpha(\xi)]\,d\xi\right]-1\right\}, \tag{1}$$

valid for $g/\alpha \neq 1$. In the limit of negligible waveguide loss ($\alpha(z) \to 0$), (1) reduces, as it should, to the usual $P_{sp}$ expression mentioned above. On the other hand, at transparency, where $g(z)$ precisely equals $\alpha(z)$, the spontaneous power grows as

$$P_{sp}(z) = n_{sp}h\nu B_0 \int_0^z \alpha(\xi)d\xi, \tag{2}$$

obtained from (1) by taking the limit as $g$ approaches $\alpha$.

The evolution of bus ASE is shown graphically in Fig. 2, where $P_{sp}(z)$, given by (1) and (2), is plotted for distributed amplifying buses with $n_{sp} = 1$, $\lambda = 1.53$ $\mu$m, and $B_0 = 2.5$ THz, corresponding to the alumino-silicate $Er^{3+}$-fiber amplifier's noise-equivalent bandwidth of about 20 nm. The abscissa, scaled in dB, represents the total power loss $\mathcal{L} = 10\log_{10}\left[\exp\left(\int_0^z \alpha(\xi)d\xi\right)\right]$, from 0 to $z$, that would result from dissipation and tapping if the bus provided no compensating gain.

It is evident from Fig. 2 that the ASE power propagating along the bus increases only linearly with $\mathcal{L}$. More importantly, it rises quite slowly. A large bus with end-to-end loss $\mathcal{L}$ =1000 dB, for example, generates only about 80 $\mu$W of ASE over the full gain bandwidth. Consequently, the current-noise power generated in the network's receivers remains small, as shown below.

**Photocurrent Signal–to–noise Ratio of the Amplified Bus Network.** We calculate the bus's worst–case noise performance by supposing that the left–most node in Fig. 1 couples $P_{in}$ Watts of light onto the bus; we then compute the photocurrent signal–to–noise ratio that will result in the sender's own receiver. The mean signal photocurrent, given a mark, is $\langle i_s(t)\rangle = \frac{e\eta_d\kappa}{h\nu}P_{in}\exp\left[\int_0^L [g(\xi)-\alpha(\xi)]\,d\xi\right]$, where $L$ is the bus length, $e$ is the electronic charge, $\kappa$ is the directional coupler's power–coupling coefficient, and $\eta_d$ is the detector quantum efficiency. This signal is corrupted by photocurrent fluctuations due to beat noise, shot noise, and receiver–circuit noise. We write the signal field, at $z = L$, as $E_s(t) = \sqrt{2P_{in}}\exp\left[\frac{1}{2}\int_0^L [g(\xi)-\alpha(\xi)]d\xi\right]\cdot \cos(\omega_0 t)$, where $\omega_0$ is the optical angular frequency. Using (1), we write the spontaneous–emission field [5],[6] as $E_{sp}(t) = \left\{\frac{2n_{sp}h\nu}{1-(\alpha/g)}\left[\exp\left(\int_0^L [g(\xi)-\alpha(\xi)]\,d\xi\right)-1\right]\right\}^{1/2}\int_{-B_0/2}^{B_0/2}\cos\left[(\omega_0+2\pi\nu)t+\phi(\nu)\right]d\nu$, where $\{\phi(\nu)\}$ is a set of independent random variables, all uniformly distributed on $[0,2\pi]$, representing the optical phases associated with the spectral components of the spontaneous emission. By adding $E_s$ to $E_{sp}$, squaring, and taking second moments, it is straightforward to show that the received photocurrent variance due to beating of signal and spontaneous fields is

$$\mathrm{var}(i_{s-sp}(t)) = \frac{4n_{sp}e^2\eta_d^2\kappa^2\,P_{in}}{[1-(\alpha/g)]\,h\nu}\exp\left(\int_0^L [g(\xi)-\alpha(\xi)]d\xi\right)\left[\exp\left(\int_0^L [g(\xi)-\alpha(\xi)]d\xi\right)-1\right]B_e, \quad (3)$$

and that the variance due to spontaneous–spontaneous beating is

$$\mathrm{var}(i_{sp-sp}(t)) = \left\{\frac{\sqrt{2}e\eta_d\kappa n_{sp}}{1-(\alpha/g)}\left[\exp\left(\int_0^L [g(\xi)-\alpha(\xi)]d\xi\right)-1\right]\right\}^2 B_eB_0\left(1-\frac{B_e}{2B_0}\right), \quad (4)$$

where $B_e$ is the receiver's radio–frequency bandwidth. As an accuracy check, note that under the transformations $\alpha \to 0$ and $\int_0^L g(\xi)d\xi \to G$, our problem reduces to that of the ordinary lightwave amplifier with negligible waveguide loss; under these substitutions, (3) and (4) reduce to the well–known expressions for amplifier beat noise [5]–[8].

Beat noise generally dominates throughout the amplified bus, since the signal power remains high. However, the beat noise is accompanied by additional current fluctuations due to ASE shot noise, which generates photocurrent variance

$$\mathrm{var}(i_{sp-shot}(t)) = \frac{2e^2\eta_d\kappa n_{sp}}{1-(\alpha/g)}\left[\exp\left[\int_0^L [g(\xi)-\alpha(\xi)]d\xi\right]-1\right]B_0B_e, \quad (5)$$

and signal shot noise, which generates

$$\mathrm{var}(i_{s-shot}(t)) = \frac{2e^2\eta_d\kappa}{h\nu}P_{in}\exp\left[\int_0^L [g(\xi)-\alpha(\xi)]d\xi\right]B_e. \quad (6)$$

Finally, the receiver circuit generates a thermal-noise current with variance

$$\mathrm{var}(i_{th}(t)) = 4kT_eB_e/R, \quad (7)$$

where $k$ is Boltzmann's constant, $R$ is the detector–output impedance, and $T_e$ is the receiver's effective noise temperature, which is related to its noise figure $F$ by $T_e = 290(F-1)$.

This noise–component enumeration allows one to determine the network's worst–case photocurrent power signal–to–noise ratio, SNR. Since the five variance contributions may be viewed as arising from independent random processes, their sum is the total current variance, so that SNR is obtained by substituting (3)–(7) into $\mathrm{SNR} = \langle i_s(t)\rangle^2/[\mathrm{var}(i_{s-sp}(t)) + \mathrm{var}(i_{sp-sp}(t)) + \mathrm{var}(i_{s-shot}(t)) + \mathrm{var}(i_{sp-shot}(t)) + \mathrm{var}(i_{th}(t))]$.

Using this expression, one can plot SNR as a function of the total splitting and propagation loss $\mathcal{L}$. Figure 3 contains such plots for several values of $g/\alpha$, where we have taken $B_e = 1.5\,\mathrm{GHz}$ (sufficient for a 2.5 Gb/s receiver), $B_0 = 2.5\,\mathrm{THz}$ (representing alumino–silicate $Er^{3+}$ fiber), $T_e = 725$ K (corresponding to $F = 3.5$), $\lambda = 1.53\,\mu\mathrm{m}$, $R = 1000\,\Omega$, $P_{in} = 0.2$ mW, $\eta_d = n_{sp} = 1$, and $\kappa = 0.1$. For each value of

$g/\alpha$, the dashed curve represents the SNR of an amplifier–noise–limited system that is free of thermal noise ($T_e = 0$ K); the solid curve includes both amplifier and receiver noise. Also shown is the performance of the conventional, unamplified bus, obtained by setting $g(z) = 0$. Each curve decays with propagation distance $z$, or accumulated loss $\mathcal{L}$, because of the ASE build–up and, in buses with $g/\alpha < 1$, because of signal loss. In the unity–gain bus ($g/\alpha = 1$), SNR evolves solely under the influence of the ASE build–up and thus decays quite slowly. In the sub–unity–gain buses of Fig. 3, the SNR deterioration is dominated by loss of signal power.

Using Fig. 3, one can estimate the size limitations that ASE noise imposes on the amplified optical bus. Keeping the digital receiver's error rate $< 10^{-9}$ requires SNR $\geq$ 21.6 dB, since all photocurrent contributions from (3)-(7) result from narrowband–filtered random processes, so that the resulting photocurrent statistics are approximately Gaussian. For example, if $g/\alpha = 0.98$, then, from Fig. 3, the bus can tolerate $\mathcal{L} = 410$ dB of loss. This number represents the total propagation and splitting loss, absent amplification, that $P_{in}$ would undergo in traversing the entire bus. With power–coupling coefficients $\kappa$ optimized for the bus gain, this permits large networks. However, rather than optimizing, we instead set $\kappa = 0.1$ (-10 dB), which is near–optimal for the unamplified bus. Coupling losses then total $(2N-2)\cdot 10\log_{10}[(1-\kappa)\kappa_{ex}]$ dB, where $N$ is the number of nodes and $\kappa_{ex}$ is the coupler's excess loss. We assume fiber loss of 0.2 dB/km, and coupler excess loss of $10\log_{10}\kappa_{ex} = 0.05$ dB (high–quality fused–tapered couplers). An additional power margin of 6 dB is included. Using these assumptions, together with critical loss values read from Fig. 3, one can calculate size limits for the amplified bus.

The results are shown in Fig. 4, which plots the maximum bus length $L$ versus the network node count $N$, for various $g/\alpha$, including the special case $g/\alpha = 0$, representing the unamplified bus. Again, dashed curves include only beat– and shot–noise contributions; solid curves include receiver noise as well. For the unamplified bus, the dashed curve represents size constraints imposed by the standard quantum limit, with degradations due solely to signal shot noise.

Three features are clear from Fig. 4. First, the benefits of amplification are substantial: for $g/\alpha = 0.99$, about 800 nodes can be supported, spanning about 800 km. Second, size limits rise dramatically as the bus approaches transparency: a unity–gain bus can support over 4,000 nodes. Third, stating this dramatic improvement otherwise: the network's gain must nearly match its loss if the bus is to support upwards of 100 nodes. Large networks will thus require some form of gain control, which will perhaps be best implemented by exploiting saturation effects in the amplifiers. Finally, it should be mentioned that while the range of bus lengths plotted in Fig. 4 is feasible at 2.5 Gb/s using directly modulated DFB lasers, fiber dispersion on the order of 0.1 ps/nm km or less would be needed. Nonlinearities in such long fiber spans may of course impose additional limitations not addressed here.

**Conclusion.** A simple, closed–form analysis shows that the amplified, passive–access optical bus with near–unity gain has excellent noise properties, owing to the low ASE levels generated along its length. Consequently, networks supporting thousands of nodes spanning thousands of kilometers are feasible, so long as the bus's gain is well–matched to its loss.


[1] K. Liu and R. Ramaswami, *IEEE Summer Topical Meeting on Optical Multi–access Networks*, Monterey, 1990, paper OMTh12.

[2] R. Ramaswami and K. Liu, *Optical Fiber Communication Conference*, San Diego, 1991, paper FE5.

[3] T. J. Whitley, C. A. Millar, S. P. Craig–Ryan, and Paul Urquhart, *IEEE Summer Topical Meeting on Optical Amplifiers and their Applications*, Monterey, 1990, paper WB2.

[4] C. H. Henry, *IEEE J. Lightwave Technol.*, vol. LT-4, pp. 288–297, 1986.

[5] N. A. Olsson, *IEEE J. Lightwave Technol.*, vol. LT-7, pp. 1071–1082, 1989.

[6] P. S. Henry, *Optical Fiber Communication Conference*, Houston, 1989, paper THK3.

[7] A. Yariv, *Optics Lett.*, vol. 15, pp. 1064–1066, 1990.

[8] Y. Yamamoto, *IEEE J. Quantum Electron.*, vol. QE-16, pp. 1073–1081, 1980.

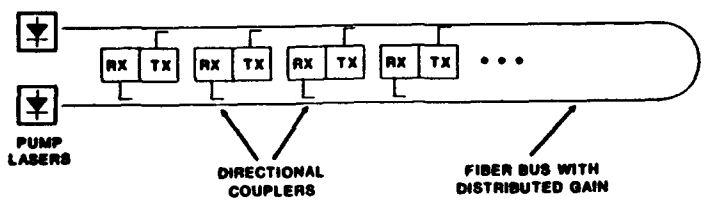


Fig. 1. Bus-configured optical network with distributed amplification.

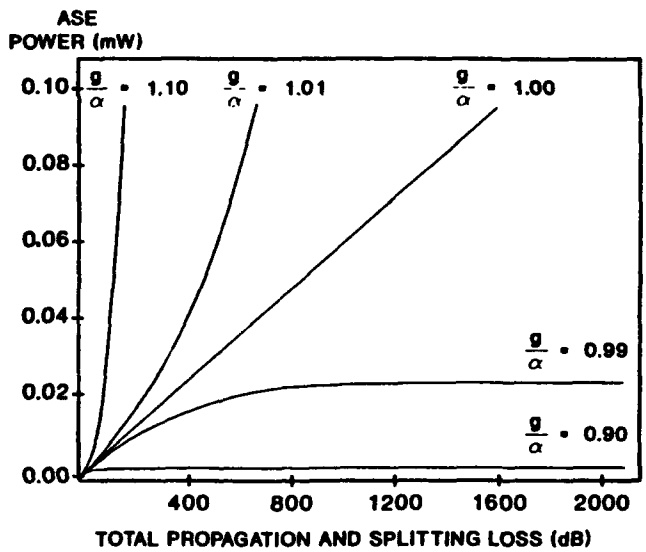


Fig. 2. Accumulated ASE power (in mW) as a function of $\mathcal{L} = 10\log_{10}\{\exp(\int_0^z \alpha(\xi)d\xi)\}$, representing (in dB) the total propagation and splitting loss, from 0 to $z$, that would occur if the network provided no compensating gain.

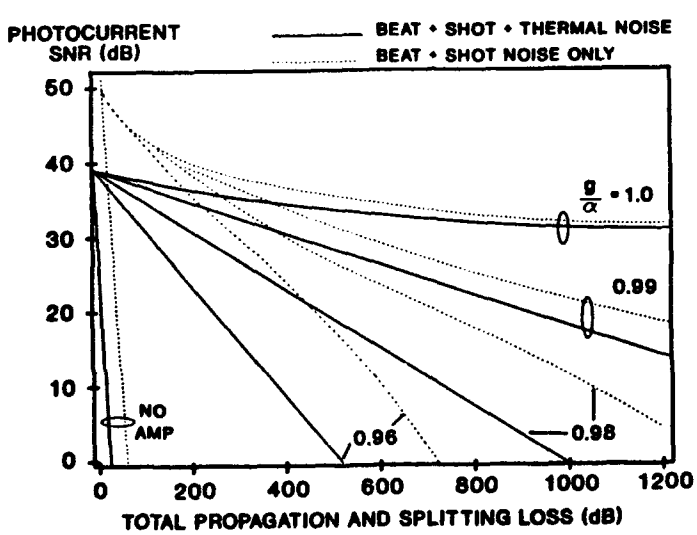


Fig. 3. Photocurrent signal-to-noise ratio as a function of total propagation and splitting loss $\mathcal{L}$ for various amplified-bus networks, and for the conventional, unamplified optical bus. Solid curves include all noise components; dashed curves exclude receiver noise, and thus represent limitations imposed solely by beat and shot noise (for the amplified bus), and by signal shot noise alone (for the unamplified bus).

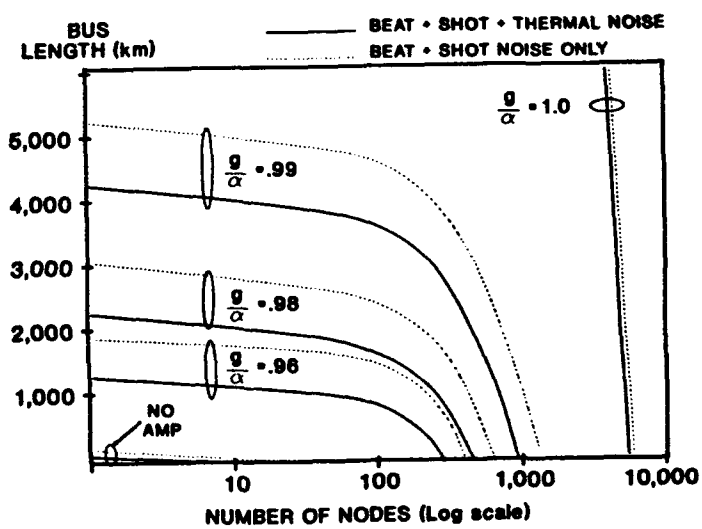


Fig. 4. Maximum bus length $L$ versus number of supported nodes $N$ for networks with SNR= 21.6 dB, sufficient for error rates $< 10^{-9}$. Noise limitations imposed by Eqs. (3)–(7) are depicted. Dashed curves include only beat-noise and shot-noise; solid curves also include thermal noise. The conventional, unamplified bus is represented by curves in the lower left corner.

# An Optically Preamplified 1 Gbit/s/channel Multichannel Grating Demultiplexer Receiver

by

J.P. KING, Y. KANABAR, N. BAKER, J. BRANNAN
STC Technology Ltd, London Road, Harlow, Essex, U.K. CM17 9NA
Telephone: 0279 429531 Telex: 81151 STL HW G Fax: 0279 441551

The Multichannel Grating Demultiplexer (MGD)[1] receiver is an attractive component for High Density Wavelength Division Multiplexing (HDWDM) systems. It combines a diffraction grating with an array receiver to provide multiple channel access. However, demultiplexer losses and the need for array operation may lead to insufficient receiver sensitivity for some applications. To improve sensitivity a semiconductor laser amplifier (SCLA) has been included before the MGD. The wide gain spectrum allows a single SCLA to preamplify many parallel HDWDM channels[2], while peak optical input, and consequently intensity modulation (IM) crosstalk, is minimised[3]. The MGD also provides a ~2.6 nm optical filter for the spontaneous emission, reducing its noise contribution at the receiver.

Fig. 1 shows the preamplified MGD arrangement. The MGD uses an InGaAs/InP 16-channel detector array (fabricated by the OEIC group at STL) and commercial GaAs receiver ICs[1]. A lens collimates light from the input fibre, and a diffraction grating separates the HDWDM channels, which the same lens refocusses onto the detector array.

The photodetectors are 107 μm x 40 μm in size, spaced at 167 μm. This gives 4 nm channel spacing with low optical crosstalk and >60% channel-width to spacing ratio. The optical preamplifier is a ridge waveguide structure with anti-reflection coated, angled facets to suppress

gain ripple[4]. For 150 mA bias the TE chip gain (at 1.55 μm signal wavelength) was 23 dB, with <1 dB ripple. Estimated coupling losses to and from the SCLA were -5 dB and -6 dB respectively. Preamplifier input signals were TE aligned.

For a single signal channel, sensitivity (measured at the preamplifier input fibre) was improved by over 8 dB to -35.7 dBm at 600 Mb/s and -33.5 dBm at 1 Gb/s (Fig. 2).

A second "crosstalk" channel at 500 Mb/s was added to simulate multiple channels with correlated data - a worst case condition. Signal channel BER was maintained at $10^{-9}$. Observed system penalties for various crosstalk channel powers and a simple model of IM crosstalk penalty are shown in figure 3. Electrical and optical crosstalk within the demultiplexer contributed <0.4 dB penalty at crosstalk/signal channel power ratios as high as +16.3 dB at 1 Gbit/s. The preamplifier IM crosstalk model assumes weak gain saturation: using an analytical expression for the gain saturation characteristic[5], the expected system penalty, $K_{Xt}$ , can be approximated to:

$$K_{Xt}\,[\mathrm{dB}] \quad \sim \quad 10.\mathrm{Log}_{10} \quad (\exp(G_0 \,.\, P_{in} \,.\, \ln 2/P_{sat}))$$

where $G_0 = 200$ is the unsaturated gain, $P_{sat} = 6.3$ mW is the 3 dB gain saturation output power, and $P_{in}$ is the peak crosstalk channel power coupled into the amplifier.

Measured penalties varied between upper and lower bounds because residual reflections (~0.02%) from the fibre lenses led to dynamic variation in the relative gains for the signal and crosstalk channels. Crosstalk channel powers in the preamplifier input fibre up to -16 dBm produced penalties 2 dB or less. Assuming 6 dB system margin and equal channel powers, this is equivalent to twelve 600 Mbit/s or eight 1 Gbit/s

HDWDM channels, with 6 dB nett sensitivity improvement over the unamplified MGD.

In conclusion: we have demonstrated that, even for moderate bit rate HDWDM systems, semiconductor optical preamplifiers can significantly improve multichannel receiver performance. IM crosstalk in the preamplifier limits the number of channels allowed.

REFERENCES

1. Kanabar, Y., Baker, N., "Demonstration of novel optical multichannel grating demultiplexer (MGD) receiver for HDWDM systems", Electron. Lett., 1989, Vol. 25, N°13, pp.817-818.
2. O'Mahoney, M.J., "Semiconductor laser optical amplifiers for use in future fiber systems", J. Lightwave Technology, Vol. 6, N°4, pp.531-544, April 1988.
3. Ogberg, M.G., and Olsson, N., "Crosstalk between intensity modulated wavelength division multiplexed signals in a semiconductor laser amplifier", J. Quantum Electronics, QE-24, 1, Jan 1988.
4. Collar, A.J., et al, "Fabrication and performance of 1.5 μm angled facet laser amplifiers", Proc. 11th IEE International Semiconductor Laser Conference, Boston, USA, 29 Aug - 1 Sept 1988.
5. Simon, J.C., "Semiconductor laser amplifiers for single mode fiber communications", J. Opt. Commun., 1983, 4, pp.51-62.

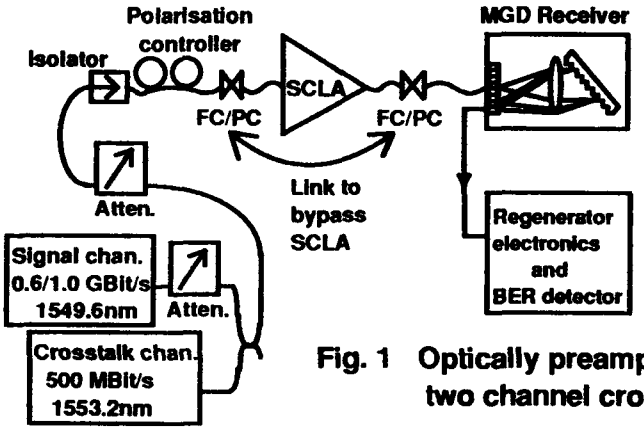


Fig. 1 Optically preamplified MGD: two channel crosstalk experiment

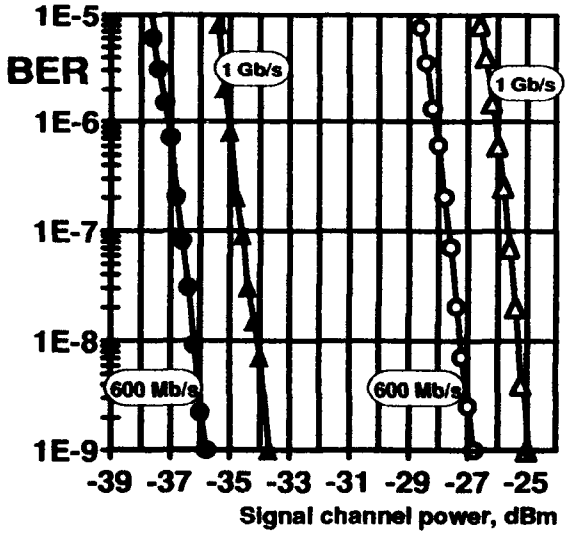


Fig. 2 MGD single channel sensitivity with (LHS) and without (RHS) optical preamplifier

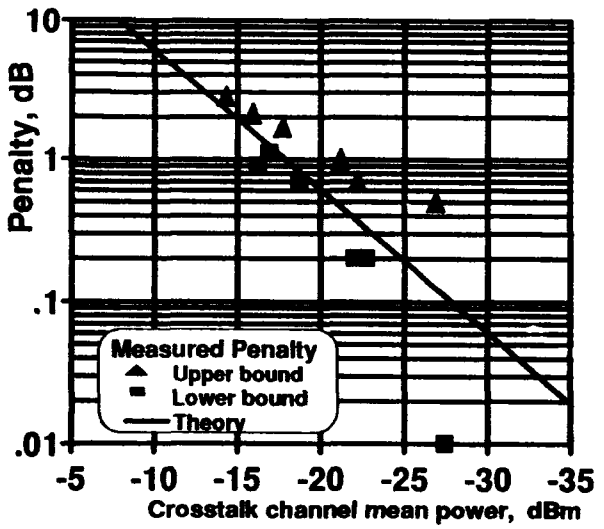


Fig. 3 Two channel crosstalk experiment: system penalty against crosstalk channel power at MGD input fibre

Fig. 4 Received eye diagram at 600Mb/s, crosstalk/signal channel ratio +16.3 dB

# Applications of Semiconductor Optical Amplifiers

**FC** 1:00pm–2:15pm
Cabaret Room

K. E. Stubkjaer, *Presider*
*Technical University of Denmark, Denmark*

# Optical Amplifiers Used as Functional Components

Lars Thylén and Mats Gustavsson
Ericsson Telecom
S-126 25 Stockholm
Sweden

Lars Gillner
Department of Microwave Engineering and Fiber Optics
Royal Institute of Technology
S-100 44 Stockholm
Sweden

## 1. INTRODUCTION

The optical amplifier is having a large impact on current research on optical networks, where the Er doped fiber amplifier (EDF) is the prime candidate for creating a transparent optical, analog network. The EDF will most likely be used for preamplification, power boosting, linear repeating because of its advantages of polarization insensitivity, extremely low "facet" reflectivity, good noise and saturation output power properties. However, the EDF amplifier is limited in versatility: In the semiconductor laser amplifier (SCLA), light amplification is effected by the coupling between the photon field and inverted electron population system, implying that the quasifermi level separation provides an electronic means of monitoring the optical field. Further, since the spontaneous recombination time is of the order of ns, the optical field can be **detected** (simultaneously with amplification), **frequency converted** and **gated** up to bandwidths of $\approx 1GHz$. In the EDF, there is no analog to the electrooptic interface (although the monitoring might be possible to perform optically) and the spontaneous recombination time is on the order of ms. Hence, the SCLA offer unique possibilities, and all of the above functions can be implemented by one single generic structure which is integrable, in contrast to the EDF. But it should also be noted that the ns time scale introduces severe crosstalk problems in multichannel systems.

## 2. SEMICONDUCTOR LASER AMPLIFIER AS DETECTOR

The operation of the SCLA in the forward biased detector mode of operation has been treated in a number of publications[1,2,3,4]. Recently, a quantum optics treatment was given[5]. From energy balance considerations, variations in the input power must be reflected in the quasifermi level separation (when the load resistance parallel to the junction$R_L \to \infty$) or in the injection current ($R_L \to 0$). In the latter case, for a travelling wave amplifier:

$$i_{junction} = (G-1) \cdot p_{in} \frac{e}{\hbar\omega} \frac{\Gamma g_m}{g} \tag{1}$$

$g_m$ is material gain coefficient, $g = \Gamma g_m - \alpha$ net gain coefficient, $\Gamma$ the confinement factor, $p_{in}$ is an input power change and $G$ the amplification factor. Fig 1 depicts calculated and measured responsivity and gain vs injection current[2], showing good agreement and the low current transition from reverse biased to forward biased detector operation. Fig 2 gives the quantum optics theoretical predictions[5] and measurements of BER, showing reasonable agreement. The detection bandwidth $B$ = 380 MHz, corresponding to a data rate in excess of 500 Mb/s. The theoretical sensitivity is roughly comparable to an ordinary PIN FET receiver at these data rates. Systems experiments have been carried out up to 900 Mb/s[3], in general, increasing the bias leads to shorter carrier lifetimes and larger bandwidths[2,3].

## 3. SEMICONDUCTOR LASER AMPLIFIER GATES AND SWITCH ELEMENTS

Gating of an optical signal by an SCLA is treated theoretically and experimentally in a number of papers[6,7,8,9]. When used as an integrated "external" modulator[7], the speed is, however, limited[9]. Fig 3a shows simulated bit patterns at 250 Mb/s for various input power levels. Higher input powers give higher modulation speed, but also mean less amplification, thus there is a trade off between amplification and speed. A few Gb/s can be attained with MQW SCLAs. SCLA modulators are far from ideal concerning chirp[9], fig 3b. But the chirp can instead be employed to realize a phase modulator[10]. Switches based on SCLAs are reported in different versions: Theoretically[11], and experimentally[12] as directional couplers, experimentally as gate switches[13]. Use of an SCLA based directional coupler as a wavelength filter has been suggested[14]

## 4. SEMICONDUCTOR LASER AMPLIFIER WAVELENGTH SHIFTER

The same mechanism that causes detrimental crosstalk in WDM systems can be employed for wide range frequency conversion[15,16]. This nonlinear FWM is based on beating between a signal ($P_s$) and a pump

($P_{p1}$), separated by less than 1 GHz; this beating creates a corresponding fluctuation in the carrier sea. A second pump ($P_{p2}$, where $\omega_{p2} - \omega_{p1} \gg 1GHz$) can then copy $P_s$ to a signal $P_{s1}$ at the new frequency: $\mid \omega_{s1} - \omega_{p2} \mid = \mid \omega_s - \omega_{p1} \mid$. Such a wavelength converter which retains all modulation formats is highly desirable in multiwavelength photonic switching networks, however, in order to remove $P_{p2}$, filters with very steep frequency response are required.

## 5. APPLICATIONS

SCLAs can be used to create switch arrays as in the suggested integrated photonic circuit of fig 4[17], where it performs routing and amplification and can be used to monitor the status of the switching fabric. Such a switch array could in principle be made quite large ($> 32 \times 32$ as an order of magnitude); the size will be limited by signal degradation as well as saturation effects due to accumulation of amplified spontaneous emission and further by technological constraints. A further advantage is the comparative insensitivity to waveguide losses, given the 3 dB losses at each Y-junction. However, from a noise point of view, it is more advantageous to use low loss passive switches and booster amplifiers. It is obvious that this type of switches has a potential to be superior to $LiNbO_3$ switches, and would be extremely useful in the photonicc transport network, however, like for $LiNbO_3$ devices, polarization independence is highly desirable. Fig 5 shows the measured amplification fiber-fiber in one of our integrated SCLAs, featuring passive-amplifying-passive sections, grown by MOCVD and with semi-insulating regrowth. Reasonable polarization independence is shown. Total fiber coupling losses $\approx$ 12 dB. Fig 6 shows another application of integrated SCLAs: Three interconnected SCLAs perform all the functions required in a bus node: Detection/amplification and transmission. A hybrid systems experiment with such configuration has been performed[18]. In an integrated version, detailed simulations show that transmit speeds of several Gb/s can be attained. It should be noted that the structure of fig 6 could be used in a variety of ways: By reverse biasing one of the SCLAs, we get a high frequency PIN detector; by introducing Bragg gratings frequency selective feed back, etc.

## 6. SUMMARY

The features which differentiate the SCLA from the EDF were identified; these features permit the use of the SCLA as a multifunctional device (as detector, gate, wavelength shifter). This versatility as well as the possibility for integration make the SCLA an important building block in lightwave transmission and switching systems.

## REFERENCES

1. A Alping, B Bentland, S T Eng: "100 Mb/s laser diode terminal with optical gain for fiber-optic local area networks", Electron. Lett., vol 20, (1984), p 794

2. M Gustavsson, A Karlsson, L Thylén, "Travelling wave semiconductor laser amplifier detectors", IEEE J Lightwave Techn, vol 8, (1990), p 610

3. M Gustavsson, L Thylén, A Djupsjöbacka, "System performance of semiconductor laser amplifier detectors", Electron. Lett., vol 25, (1989), p 1375

4. K T Koai, R Olshansky, P M Hill, "Dual-function semiconductor laser amplifier in a broad-band subcarrier multiplexed system", Phot. Techn. Lett., vol 2, (1990), p 926

5. Lars Thylén, Mats Gustavsson, T K Gustafson, Inho Kim and Anders Karlsson: "Calculation of photon and current fluctuations in travelling wave semiconductor laser amplifiers", to be published in J Quantum Electron.

6. R Rörgren, P A Andrekson, K Bertilsson, S T Eng: "Gain switching modulation of a semiconductor laser optical amplifier", Proc IEEE/LEOS Topical Meet on new semiconductor laser devices and applications, Monterey, USA, (1990), paper SCF3

7. G Eisenstein, U Koren, T L Koch, G Raybon, R S Tucker, B I Miller: "A multiple quantum well optical amplifier/modulator integrated with a tunable DBR laser", Proc IOOC '89, Kobe, Japan, (1989), paper 19C2

8. A F Elrefaie, H Izadpanah, A Alhamdan: "8 Gb/s current modulation of semiconductor optical amplifiers", Proc. ECOC '90, Amsterdam, Netherlands, (1990), p 625

9. Lars Gillner: "Modulation properties of a near travelling-wave semiconductor laser amplifier", submitted for publication

10. G Grosskopf, R Ludwig, R Schnabel, H G Weber: "Characteristics of semiconductor laser optical amplifier as phase modulator", Electron. Lett., vol 25, (1989), p 1188

11. C. J. Setterlind, Lars Thylén, "Directional Couplers with Optical gain" IEEE J. Quantum Electron., Vol. QE-22, (1986), pp 595

12. D Mace, M Adams, J Singh, M Fisher, I Henning, W Duncan, "Twin-ridge laser amplifier crosspoint switch", Electron. Lett., vol 25, (1989), p 987

13. S Oku, K Yoshino, M Ikeda, M Okamoto, T Kawakami, "Design and performance of monolithic LD optical matrix switches", Proc 1990 Int Top Meet on Photonic Switching, Kobe, (1990), paper 13C-17

14. Lars Thylén, "Wavelength and noise filtering characteristics of coupled and passive waveguides" IEEE J. Quantum Electron., Vol. QE-23, (1987), pp 1956

15. K Inoue, T Mukai, T Saitoh, "Nearly degenerate four-wave mixing in a travelling-wave semiconductor laser amplifier", Appl. Phys. Lett., vol 51, (1987), p 1051

16. G Grosskopf, R Ludwig, H G Weber, "140 Mbit/s DPSK transmission using an all-optical frequency converter with a 4000 GHz conversion range", Electron Lett, vol 24, (1988), p 1106

17. M Gustavsson, L Thylén, "Switch matrix with semiconductor laser amplifier gate switches: A performance analysis", Proc. OSA Top Meet Photonic Switching, (1989), paper FE5

18. M Gustavsson, L Thylén, "Multifunctional semiconductor laser amplifiers: Optical amplifier, detector, gate switch and transmitter", Proc OSA Top Meet Integrated Photonics Research, (1990), paper WI2

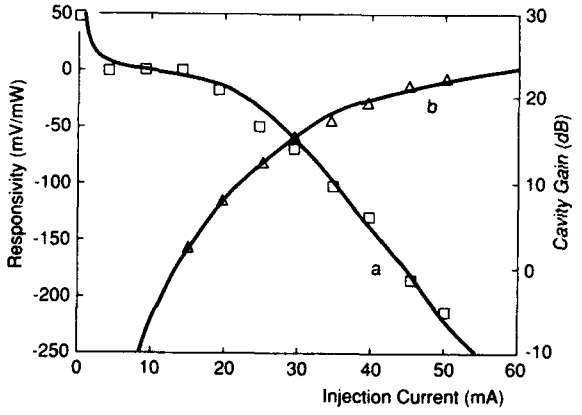


Fig 1: Calculated and measured responsivity and gain vs injection current[2] for an $1.3\mu m$ SCLA operating simultaneously as amplifier and detector. The responsivity increases with the gain (eq (1)).

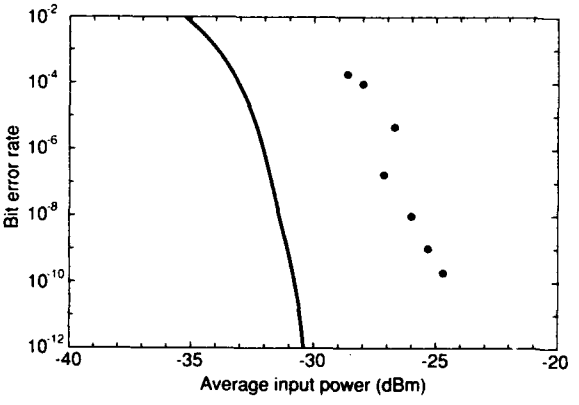


Fig 2 Quantum optics theory predictions[5] as well as measurements of BER for a $1.3\mu m$ discrete SCLA, showing reasonable agreement. The detection bandwidth $B$ = 380 MHz, corresponding to a data rate in excess of 500 Mb/s. Notice sensitivity in relation to a PIN-FET receiver.

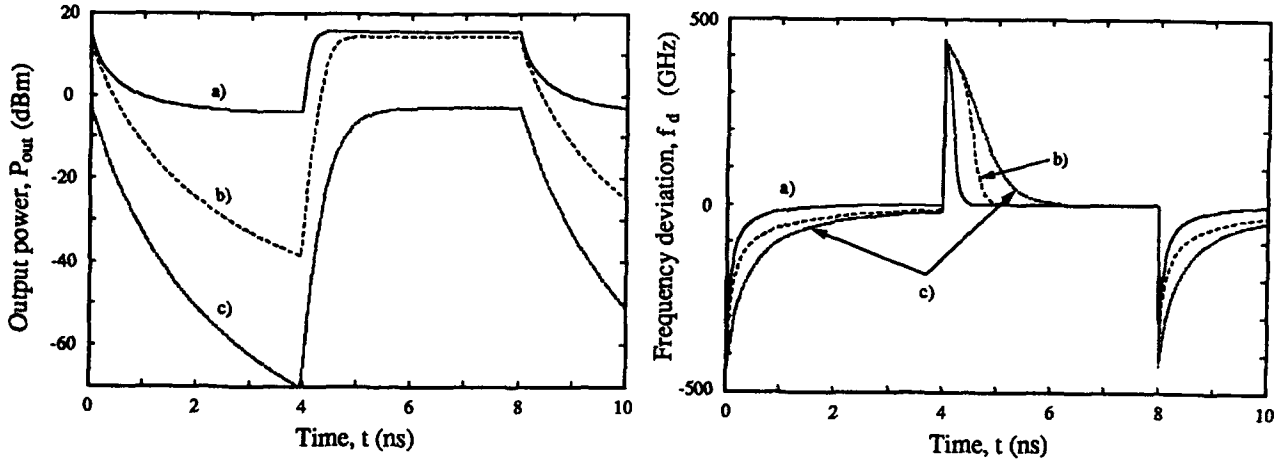


Fig 3: A: Output power of an SCLA for on-off modulation of the pump current at 250 Mb/s. $I_{off} = 0$ mA, $I_{on} = 60$ mA. $P_{in} = 10$ dBm (a), 0 dBm (b) and -30 dBm (c). B: Instantaneous frequency during the same conditions as in fig 3 A.

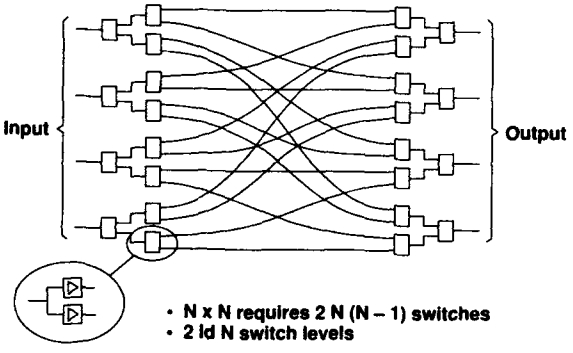


Fig 4: SCLA space switch architecture, with passive splitters, combiners and SCLA gates. The structure is strictly nonblocking and permits broad- and narrowcasting. The same architecture has been used for $LiNbO_3$ switch arrays.

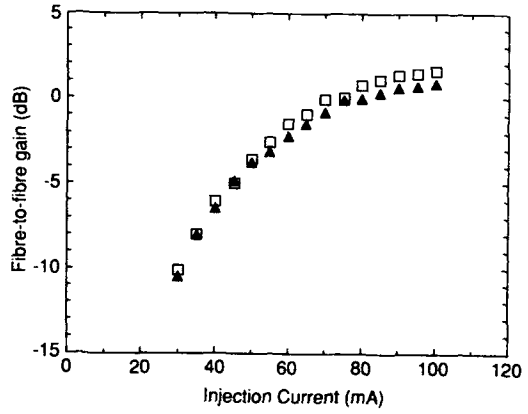


Fig 5: Fiber to fiber amplification in a 3-section integrated SCLA with passive amplifying passive sections; total coupling losses are roughly 12 dB. This is the basic building block for the switch array in fig 4.

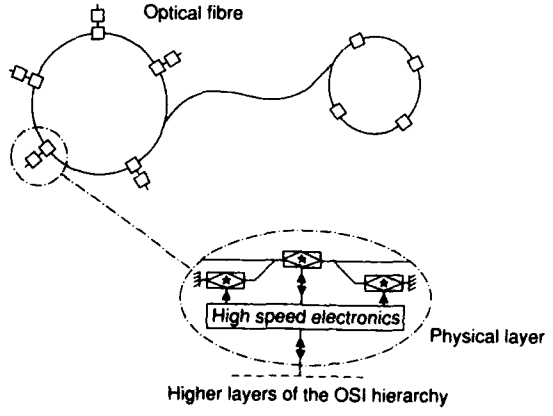


Fig 6: Three multifunctional semiconductor laser amplifiers connected as a node in a bus network. With only the center SCLA turned on, the node works in the amplifying and detection mode; with all amplifiers turned on in the transmission mode. In the latter case, the SCLAs with feedback operate as a laser.

# GaAlAs/GaAs Vertical Cavity Surface Emitting Active Filter

F. Koyama, S. Kubota and K. Iga

Tokyo Institute of Technology, Precision & Intelligence Lab.
Nagatsuta 4259, Midori-ku, Yokohama 227, Japan
Phone 81-45-922-1111 x2068, Fax 81-45-921-0898

## 1. Introduction

Semiconductor laser amplifiers are of interest for direct light amplification as well as functional operation such as wavelength filtering and so on. An optical filter with narrow bandwidth and wavelength tuning is one of key devices for dense wavelength division multiplexing (WDM) trunk lines and networks. So far, laser diode active filters using Fabry-Perot cavity or DFB/DBR laser structures have been studied [1]-[4]. There are remaining problems in these devices, such as large polarization sensitivity due to those rectangular waveguide structure and difficult coupling to optical fibers.

On the other hand, micro-cavity surface emitting (SE) lasers are now attracting much interest because of its ultra-low threshold and freedom in two-dimensional array [5]. In this laser structure, a circular cavity is used, resulting in low polarization selectivity [6]. If we use an SE laser structure for a resonance-type active filter/amplifier, we expect the following advantages; 1) low polarization sensitivity, 2) easy coupling to single mode fibers, 3) very low power consumption originated from ultra-low threshold, 4) large free spectral range due to ultra-short cavity structure, and so on.

In this paper, we propose a novel active filter/amplifier based on the SE laser structure. A GaAlAs/GaAs SE active filter has been realized and a preliminary result on wavelength filtering will be presented.

## 2. Device Structure

A proposed GaAlAs/GaAs active filter using a surface emitting laser structure is shown in Fig. 1. The device was fabricated by a two step MOCVD growth and processed by a fully

monolithic technology. The structure is similar to the SE laser device reported previously [7]. The circular mesa of 7 $\mu$ m in diameter was buried in the current blocking layers to confine injected current. In this device structure, the active region was not truncated and thus the injected current spreads in the active layer. The effective active region diameter was then extended to around 10$\mu$ m. A short cavity length of 5.5$\mu$ m was formed by chemically removing the GaAs substrate. A circular Au film/$SiO_2$/$TiO_2$/$SiO_2$ mirror and 7 pair $SiO_2$/$TiO_2$ dielectric multilayer reflector were used for p-side and n-side mirrors, respectively.

Figure 2 shows a current/light output characteristic and lasing spectrum as the filter was operated above the threshold. The threshold current was 63mA under pulsed condition. The differential quantum efficiency was $\sim$ 1%, which is much lower than the previous SE laser device [7]. This is due to the poor reflectivity of the p-side mirror, since a thin Au film ($\sim$ 20nm) is used for p-side mirror to reduce the transmission loss in the filter. Single mode operation with the lasing wavelength of 0.8855$\mu$ m was obtained. The longitudinal mode spacing was 16nm, which is 50 times larger than that of conventional horizontal cavity stripe lasers. We can expect a large free spectral range of the filter.

**3. Filter Characteristics**

The filtering characteristic of the fabricated device was measured, where the SE laser with the lasing wavelength of 0.8843 $\mu$ m was used as a light source. Both the filter and the SE laser were driven by synchronized pulsed currents (repetition rate:10kHz, pulse width:100nsec). The lasing wavelength of the light source was electrically tuned by applying small DC current, resulting in temperature change of the light source. The filter was biased at slightly below the threshold. The input light was coupled into the filter through a single mode fiber. The filter output through a single mode fiber was detected by an optical powermeter. The coupling loss between the filter and the fiber for the each side of the filter was estimated to be around 7dB.

Figure 3 show the filter transmission spectra. The 3dB filter bandwidth of 0.1nm was obtained with the bias current of

0.95 times the threshold. Figure 4 shows the 3dB bandwidth as a function of the filter bias current. The insertion loss of the filter including the coupling loss with the fibers was 10dB. Therefore, the internal gain of 4dB was estimated. We may improve the gain amplitude by introducing a loss-less reflector for the p-side and by reducing the coupling loss with single mode fibers. The detailed polarization dependence of the active filter is now under investigation.

## 4. Conclusion

We have demonstrated a GaAlAs/GaAs active filter based on a surface emitting laser structure for the first time. A bandwidth as narrow as 0.08nm was demonstrated. By introducing a micro vertical cavity structure, we can expect polarization insensitive and ultra-low power consumption device. We believe that this kind of device is promising for parallel wavelength multiplexing sub-systems for the future lightwave communications and optical interconnections.

## Acknowledgments

We would like to acknowledge Prof. Y. Suematsu, President of Tokyo Institute of Technology for his continuous encouragement.

## References

[1] H. Kawaguchi, K. Magari, K. Oe, Y. Noguchi and M. Fukuda, Appl. Phys. Lett., vol.50, pp.66-67, 1987.

[2] K. Kikushima, K. Sano and H. Nagai, IEEE J. Quantum Electron., vol.QE-23, p.1861-1867, 1987.

[3] T. Numai, M. Fujiwara, M. Shimosaka, K. Kaede, M. Nishio, S. Suzuki and I. Mito, vol.24, pp.236-237, 1988.

[4] T.L. Koch, F.S. Chao, F. Heismann and U. Koren, Electron. Lett., vol.25, pp.890-892, 1989.

[5] K. Iga, F. Koyama and S. Kinoshita, IEEE J. Quantum Electron., vol.24, pp.1845-1853, 1988.

[6] M. Shimizu, F. Koyama and K. Iga, Jpn. J. Appl. Phys., vol.27, pp.1774-1775, 1988.

[7] F. Koyama, S. Kinoshita and K. Iga, Appl. Phys. Lett., vol.55, pp.221-222, 1989.

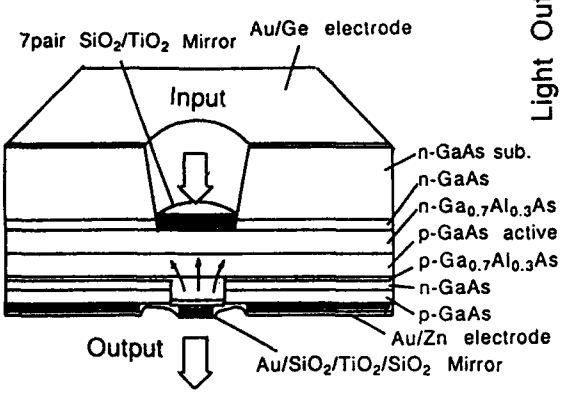


Fig.1 GaAlAs/GaAs surface emitting active filter

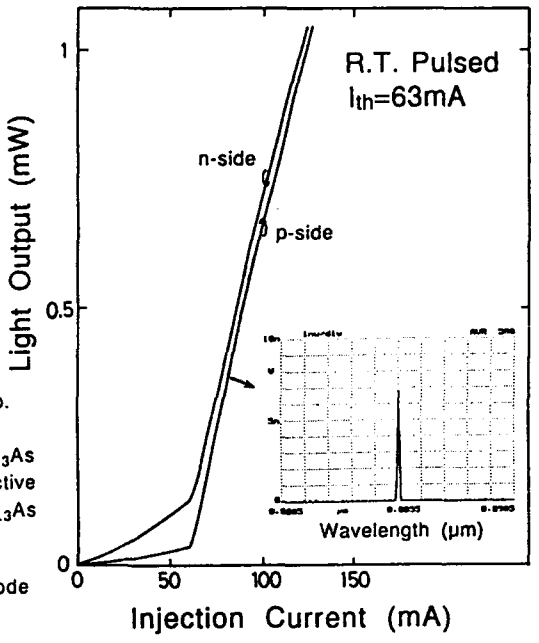


Fig.2 L/I characteristic and lasing spectrum

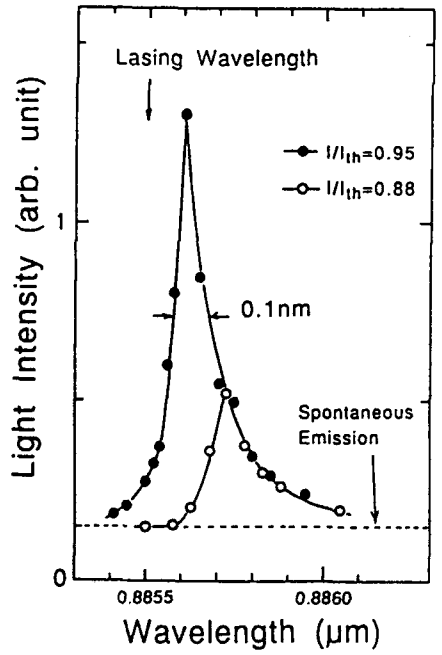


Fig.3 Filter profiles for different biases.

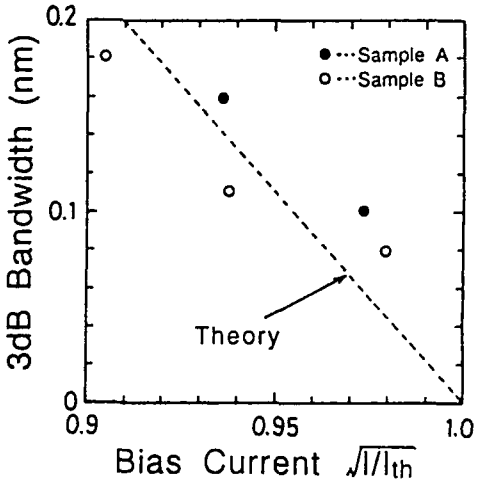


Fig.4 3-dB bandwidth against bias level. Dashed line shows theory with gain coeffcinet of $3.5\times 10^{-16}cm^{-2}$

# DYNAMICS OF DFB SEMICONDUCTOR LASER AMPLIFIERS

Z. Wang, T. Durhuus, B. Mikkelsen, and K. E. Stubkjaer

Center for Broadband Telecommunications, Electromagnetics Institute

Technical University of Denmark, DK-2800 Lyngby, Denmark

## INTRODUCTION

DFB laser amplifiers are very attractive for optical filtering because they can serve both as channel and noise filters and at the same time provide amplification. They may be used as filters in switching network or as receiver preamplifiers in multichannel direct detection systems [1]. Amplifiers incorporating DFB structures have also been suggested for wavelength converters [2]. For such applications it is important to understand the dynamic behaviour of DFB amplifiers when they are used in high speed systems. Especially, it is interesting to know the influence of the very narrow gain spectrum on short optical pulses.

Here we present a dynamic model for DFB amplifiers which takes both the time and longitudinal variations of the electric field distribution as well as the carrier distribution into account. Using this model the amplification of narrow optical pulses has been studied for both low and high pulse energies corresponding to pre- and booster-amplifier applications, respectively. Previously fast pulse amplification in travelling wave amplifiers has been reported in the literature [3], [4].

## THEORY

If ultra-fast phenomena, including amplification of very short optical pulses or fast optical switching, are considered then the terms which account for the variation of the electric fields with time have to be included in the coupled mode equations which are normally derived for DFB structures [5], [6]. Starting from Maxwell's equations and following the same procedure as in [5], the dynamic coupled mode equations are:

$$\frac{\partial A}{\partial z}+\frac{1}{v_g}\frac{\partial A}{\partial t}-\frac{1}{2}(1-j\alpha)(\Gamma g-\alpha_i)A = \kappa\exp(2j\delta z)(B+\frac{j}{\pi v}\frac{\partial B}{\partial t}) \quad (1)$$

$$-\frac{\partial B}{\partial z}+\frac{1}{v_g}\frac{\partial B}{\partial t}-\frac{1}{2}(1-j\alpha)(\Gamma g-\alpha_i)B = \kappa\exp(-2j\delta z)(A+\frac{j}{\pi v}\frac{\partial A}{\partial t}) \quad (2)$$

where $A(z,t)$ and $B(z,t)$ are the electric field distributions along the cavity for the waves propagating in the positive and negative z directions, respectively. $\delta$ is the detuning of the propagation constant from the Bragg condition, and $v_g$ is the group velocity of light inside the cavity. $\kappa$ is the mode coupling coefficient, $\alpha$ the linewidth enhancement factor, $\alpha_i$ the internal loss and $v$ the optical

frequency. $g$ is the material gain per unit length and it varies linearly with the carrier density, $N$, which is governed by [3]:

$$\frac{\partial N(z,t)}{\partial t} = \frac{I}{qV} - \frac{N(z,t)}{\tau_c} - \frac{a(N(z,t)-N_0)}{h\nu}(|A(z,t)|^2 + |B(z,t)|^2) \quad (3)$$

Where $I$ is the bias current, $q$ the electron charge and $V$ the volume of the active region. The carrier lifetime is denoted by $\tau_c$ and $a$ is the differential gain. $h$ is Plank's constant, and $N_0$ is the carrier density at transparency.

Equations 1 - 3 constitute the theoretical framework for the description of the dynamics of DFB laser amplifiers. In the following the facets are assumed to have zero reflectivity and the influence of spontaneous emission is ignored since it is not important for studies of fast phenomena [4]. The numerical simulations have been performed by adopting the method of characteristics [7]. In the calculations we have used wavelength: 1.55 μm, group index: 3.5, carrier lifetime: 2 ns, differential gain: $2.7 \cdot 10^{-20}$ $m^2$, confinement factor: 0.3, thickness of the active layer: 0.15 μm, width of the active layer: 3.0 μm, and cavity length: 500 μm.

## RESULTS

The steady state gain characteristics of DFB laser amplifiers can be investigated by using (1) and (2) with $\partial/\partial t = 0$. An example of a static gain spectrum for a DFB amplifier with $\kappa L = 3.0$ is seen in Fig.1 for a bias of 99% of the threshold. Since we consider an ordinary DFB structure without a $\lambda/4$ shift, the maximum gain of 36 dB is found for a detuning of -121 GHz from the Bragg frequency (only half of the spectrum is shown here). The high bias level results in a very sharp gain spectrum with a 3-dB bandwidth lower than 1 GHz.

The model accounts for both time and longitudinal variations of the field and carrier distribution. Fig. 2 gives the signal intensity and carrier density along the cavity 400 ps after the start of a -30dBm step input signal. Spatial hole burning is observed around the centre of the cavity, however, the depth is only around 0.5 %, and will not disturb the gain evolution significantly.

As examples, Fig. 3 and 4 show the transmitted and reflected pulses from the amplifier when weak and strong pulses, respectively, are injected. The input pulses are Gaussian-shaped with a width of 100 ps (full width half maximum) and the bias current is 99 % of threshold. For the weak input pulse, which has a peak power of 1 μW (energy 0.15 fJ), the output pulses are broadened to 235 ps due to the filtering characteristics of the amplifier. As seen from Fig. 4, this severe filtering is not observed when a strong input pulse with a peak power of 5 mW (energy 0.75 pJ) is injected because the gain is varied due to depletion of carriers by the front part of the pulse. In this case the width of the reflected pulse is reduced to 70 ps while the transmitted pulse is 85 ps wide. The lower gain in this case is also a result of carrier depletion.

In the case of a weak input the pulse broadening is very dependent on the bias current as seen from Fig. 5, where $\kappa L = 0.5$ and 3.0 are considered. Similar to Fig. 3, the input pulse is 100 ps wide with a peak power of 1 μW. For $I/I_{th} \leq 0.9$ the pulse broadening is insignificant in accordance with static gain spectra with 3-dB bandwidths of 19 and 6 GHz for $\kappa L = 0.5$ and 3.0, respectively. As $I/I_{th}$ increases from 0.90 to 0.99, the pulse width is broadened considerably, in agreement with a decrease in the filter bandwidth. The simulated results indicate that the DFB amplifier can be used as a combined filter and preamplifier even at high bitrates if the bias is not too close to threshold.

The pulse compression and the gain for the case of strong input is investigated in Fig. 6 as a function of the width of the input pulse. The input pulses have a constant pulse energy of 0.75 pJ and the results show that both the transmitted and the reflected pulses can be compressed provided that the input pulse width is larger than 40 ps. The wide input pulses are resonating more inside the cavity compared to the short pulses and are consequently undergoing a larger amplification.

## CONCLUSION

A dynamic model for DFB amplifiers has been established. The model accounts for the time and position dependence of both the electric fields and carrier density in the amplifier cavity. Simulations have shown that input pulses may be amplified and compressed for high signal levels due to saturation effects. For low input power it is possible to attain amplification without pulse broadening if the bias is not too close to threshold. We anticipate that DFB amplifiers can be used as combined preamplifiers and filters in high bit rate transmission systems.

## REFERENCE

[1] E. L. Goldstein et al., Proc. 11th IEEE Int. Semiconductor Laser Conf., p. 14, Boston, Aug. 1988.

[2] K.Kondo, et al., Tech. Dig. Photonic Switching, p. 199, Kobe, April 1990.

[3] G. P. Agrawal and N. A. Olsson, IEEE J. Quantum Electron., vol. QE-25, p. 2297, 1989.

[4] P. B. Hansen et al., IEEE J. Quantum Electron., vol. QE-25, p. 2611, 1990.

[5] A. Yariv: "Quantum Electronics", John Wiley & Sons, New York, 1987.

[6 W. Streifer et al., IEEE J. Quantum Electron., vol. QE-13, p.134, 1977.

[7] R. S. Bensen: "The thermodynamics and dynamics of internal combustion engines", Plenum, New York, 1982.

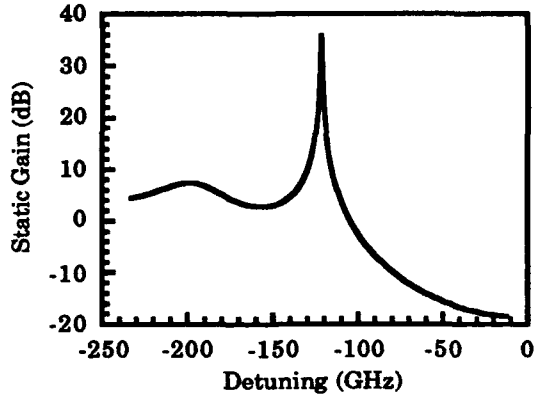


Fig. 1. Steady state gain spectrum of a DFB amplifier with $\kappa L = 3.0$ and $I/I_{th} = 99\%$.

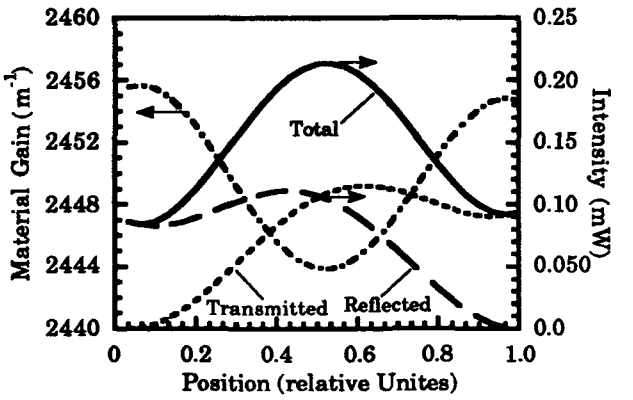


Fig. 2. Distributions of intensity and material gain 400 ps after the start of a -30 dBm step signal. $\kappa L = 3.0$, $I/I_{th} = 99\%$.

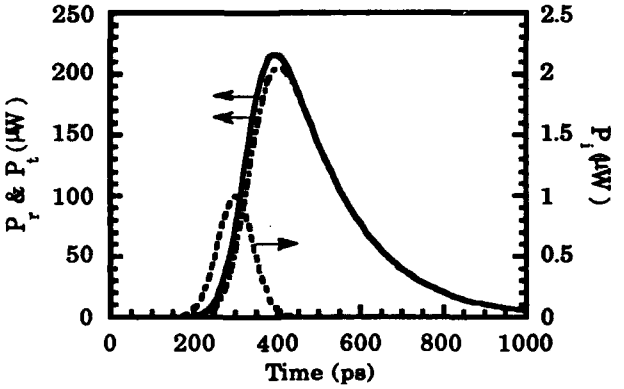


Fig. 3. Power of reflected (–·–·), transmitted (—) and input (---) pulses. The input pulse has a FWHM of 100-ps and a peak power of 1 μW. $\kappa L = 3.0$, $I/I_{th} = 99\%$.

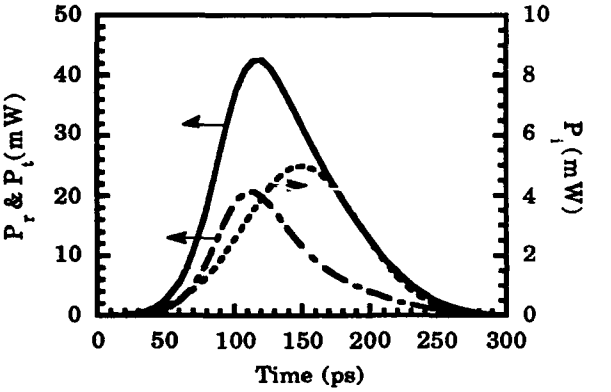


Fig. 4. Power of reflected (–·–·), transmitted (—) and input (---) pulses. The input pulse has a FWHM of 100-ps and a peak power of 5 mW. $\kappa L = 3.0$, $I/I_{th} = 99\%$.

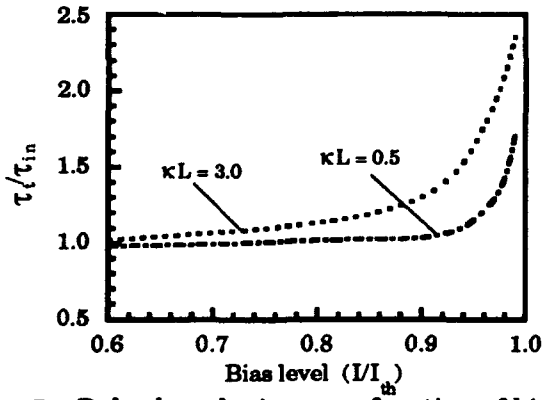


Fig. 5 Pulse broadening as a function of bias level for a 100-ps input pulse.

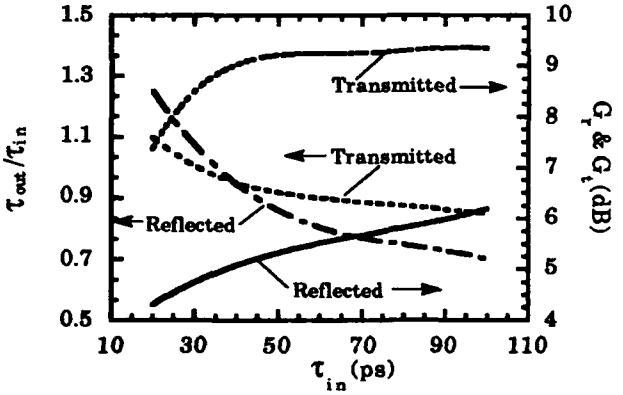


Fig. 6. Pulse compression and gain for transmitted and reflected pulses as a function of pulse width. The pulse energy is 0.75 pJ.

# Low-Loss, Packaged, 2 x 2 Semiconductor Optical Amplifier Switch

E. Eichen, R. Boudreau, R. Morrison, C. Frost,
B. Foley, J. Schlafer, and K. Vo
GTE Laboratories Incorporated, 40 Sylvan Road, Waltham MA 02254, USA
617-466-2301 / 617-890-9320 (facsimile)

## *Introduction*

Optical switching components based on semiconductor optical amplifiers have been investigated by a number of authors [1-3]. The combination of gain when the amplifier is pumped, and absorption when the amplifier is unpumped, provides the potential for low or zero insertion loss switches with large contrast ratios. In addition, simple switches based on traveling wave optical amplifiers are strictly nonblocking, have wide (~25-50 nm) optical bandwidths, and can be polarization insensitive. In this paper we discuss the performance and novel packaging of a 2x2 semiconductor optical amplifier switch which utilizes an imaging approach for fiber coupling. This switch had an average insertion loss of 4 dB, an optical isolation greater than 40 dB, and a 10-90% rise/fall time of approximately 0.5 ns. Moreover, the use of an imaging approach to fiber attachment may provide a solution for packaging other integrated photonic structures and switching components with multiple input/output waveguides that are too closely spaced to permit direct fiber pigtailing.

## *Packaging*

The experimental configuration (Figure 1) employed a single GRIN lens on either side of an array of 4 semiconductor optical amplifiers to image each element of the array onto separate cleaved single-mode fibers. The fibers were aligned to maximize coupling to the amplified spontaneous emission (ASE), and then epoxied in place. The use of a lens to provide magnification aids in matching the small amplifier near field with the larger mode size of the fiber, and also increases the fiber-to-fiber spacing in the image plane so that each fiber can be individually aligned. Using a lens or lens system also provides a region where a single bulk optical element, such as a bandpass optical filter or an optical isolator, can be placed and can function for all amplifier channels.

The magnification for the package shown in Figure 2 was approximately 3, and the single transverse mode, ridge waveguide amplifiers were spaced on 350 μm centers. Tilting the waveguide at 7° to the facet normal to reduce facet reflectivity results in light entering/exiting the amplifier at 23°, and this results in a variation in magnification across the image plane. Current to each amplifier is delivered through microstrip line, thus insuring that the response of the switch is limited by the carrier lifetime of the optical amplifiers, and minimizing electrical crosstalk caused by radiation.

*Performance*

The fiber-to-fiber gain of the packaged array varied between +8 dB for the best channel, and -5 dB for the worst channel (Figure 2). This results in an average insertion loss of approximately 4 dB for a 2x2 switch, including 6 dB from two external 3dB fiber couplers. Previous measurements of chip gain for devices from the same wafer are approximately 25 dB at 260 mA, with ~3-6 dB of polarization sensitivity. From these measurements, the coupling loss for the imaging configuration is estimated to be between -9 and -16 dB/facet. Approximately 4 dB of this coupling loss is due to spherical aberration, 1 dB due to magnification (modal size) mismatch, and 4-5 dB due to off axis aberrations. The remaining 7 dB variance between best and worst channels was caused by fiber movement during the epoxy curing cycle. Theoretical calculations of coupling loss predict that the off axis aberrations, and thus the total coupling efficiency, can be significantly increased by using closer center-to-center spacing for the amplifier array, and microball lenses instead of GRIN lenses. The measured signal isolation (signal-power-with-amplifier-ON/signal-power-with-amplifier-OFF) was 42 dB (Figure 3), and crosstalk (signal-power-in-incorrect-channel/signal-power-in-correct-channel, with all amplifiers ON) was less than -40 dB for all channels. The measured rise and fall times for a 0 to 300 mA current pulse were ~ 0.5 ns. Since the tilted-facet optical amplifiers used do not require any antireflection coatings to achieve facet reflectivities of $\leq 10^{-4}$ over the full optical spectrum [4], there was no difficulty in having the traveling wave optical bandpass of all amplifiers overlap (Figure 4).

*Summary*

In summary, a fast, low-loss, nonblocking, packaged 2x2 semiconductor optical amplifier switch has been demonstrated. The novel imaging approach taken to packaging this switch is a potential solution for fiber coupling other semiconductor switching or signal processing components in which multiple input or output waveguides are too closely spaced to permit direct fiber pigtailing.

*References*

[1] J. D. Evankow and R. Thompson, "Photonic Switching Modules Designed with Laser Diode Amplifiers," IEEE J. Selected Areas in Communications, 6 pp 1087-1095 (1988).

[2] S. Lindgren et al., "Loss-compensated optical y-branch switch in InGaAsP-InP," J. Lightwave Tech. 8 pp 1591-1595 (1990).

[3] I.H.White et al., "InGaAsP 400x200 μm active crosspoint switch operating at 1.5 μm using novel reflective y-coupler components," Electron. Lett. 26 pp 617-618 (1990).

[4] W. Rideout et al., "Ultra-low reflectivity semiconductor optical amplifiers without antireflection coatings," Electron. Lett 26 pp 36-37 (1990).

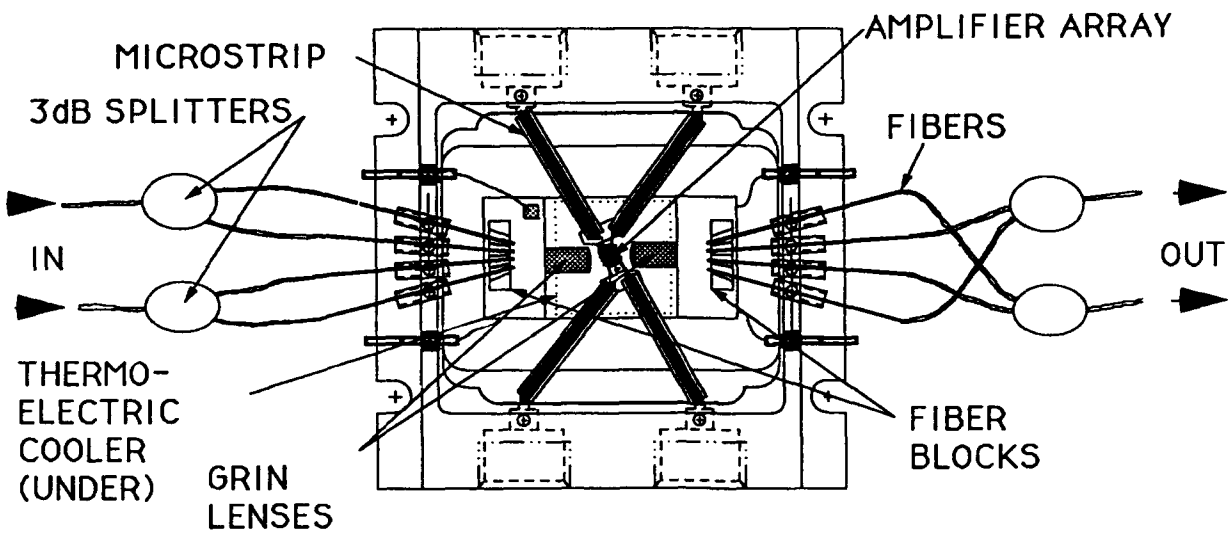


Figure 1 - Schematic of packaged, 2 x 2, semiconductor optical amplifier switch.

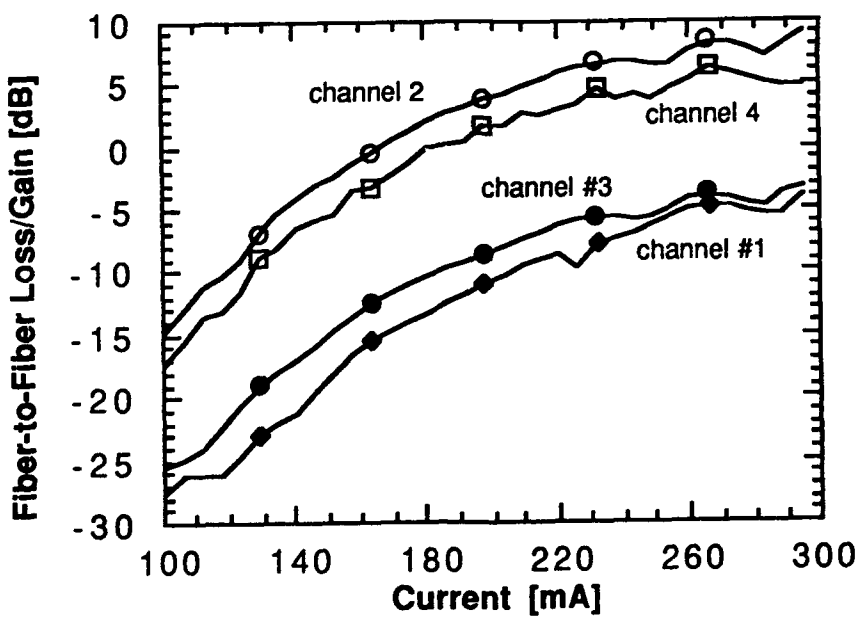


Figure 2 - Fiber-to-fiber gain for packaged semiconductor amplifier array. A polarization controller is used to rotate the input polarization to maximize the amplifier gain. The majority of the variation between channels is due to fiber movement during the epoxy curing cycle. To discriminate against amplified spontaneous emission, a modulated laser diode and lock-in were used to measure fiber-to-fiber gain.

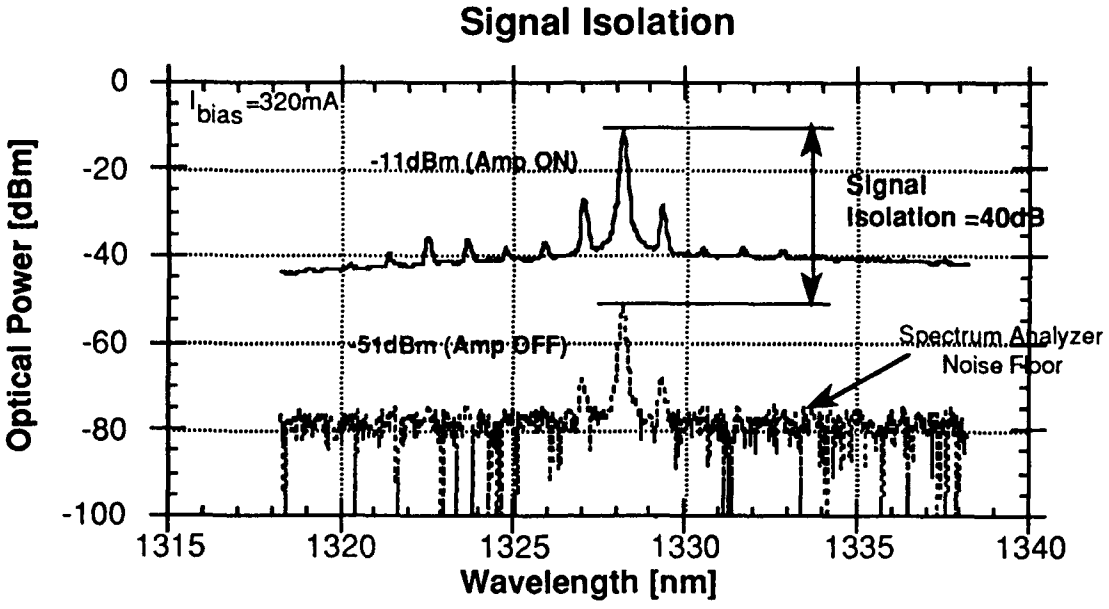


Figure 3 - Signal isolation (or ON/OFF ratio) for a given channel.

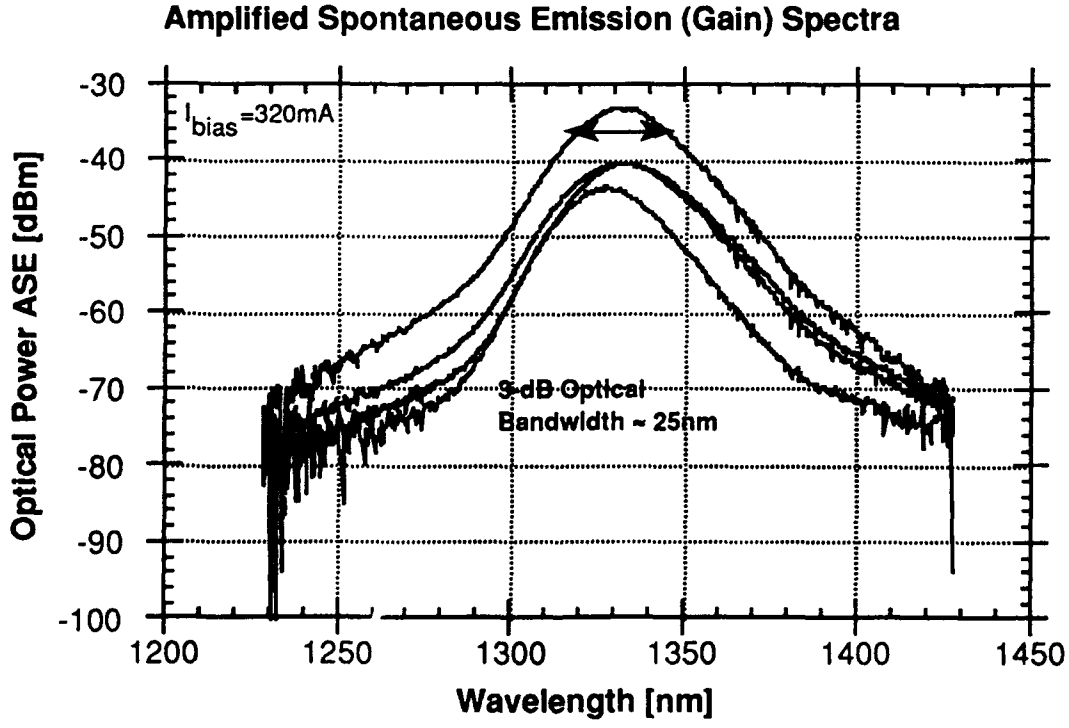


Figure 4 - Amplified spontaneous emission, or gain, as a function of wavelength for all 4 amplifiers. Since no antireflection coatings are required to achieve traveling wave performance (facet reflectivity ≤ -40 dB), the optical gain bandwidth of all channels is nearly identical.

# Fiber Amplifier Engineering

**FD** 2:15pm–3:15pm
Cabaret Room

W. L. Emkey, *Presider*
*AT&T Bell Laboratories, USA*

# Amplified Integrated Star Couplers with Zero Loss

Herman M. Presby and C. Randy Giles
AT&T Bell Laboratories
Crawford Hill Laboratory
Holmdel, NJ 07733
(201) 888-7150

Passive star couplers play a central role in the architecture of many high-speed, multiple-access optical networks. Although the use of a star coupler is possible under ideal conditions for networks with a large number of users, in practice, the size of the system is limited by the inherent 1/N splitting and excess loss of the coupler, the limited sensitivity of the receiver, and the finite available source power. A way to increase the number of users in a star network is with the use of erbium-doped fiber (EDF) amplifiers to compensate, at least to some degree, for the splitting and excess loss of the star.

Full compensation for the loss of large stars can be achieved by incorporating an EDF amplifier in each output port to amplify the signal. With such an arrangement, however, each output port requires its own EDF and associated pump laser and pump/signal combiner at a cost which can be prohibitive. Recently, an economical means of simultaneously pumping EDF's, placed at the input or output ports of the coupler, with a single laser source distributed through the star coupler itself was proposed [1]. In this way, many amplifiers can share the cost of a single pump laser and with the star acting as the pump/signal combiner, the need for a large number of these components is eliminated as well.

In this paper we utilize the principle of simultaneously pumping EDF's with one laser, distributing the pump through a 19×19 integrated star coupler [2]. We achieve 17.7 dB of gain and near quantum limited noise performance by pumping through one input port at the more efficient wavelength of 0.98$\mu$m and using very low gain-threshold EDF's. This fully compensates for the loss of the near wavelength-independent star and provides a potentially economical and compact network component and building block.

The experimental arrangement is shown in Figure 1. The integrated star coupler itself consists of two arrays of channel waveguides, fabricated using silica waveguides on a silicon substrate separated by a slab waveguide. The input array radiates into a planar "free-space" region, which is sufficiently long that the output array aperture is in the far field. When one of the input guides is excited it couples energy into the adjacent input waveguides in such a way that the far-field is nearly uniform over the N output guides. The efficiency of the integrated star coupler is approximately wavelength independent. The major effect of a change in wavelength is only to broaden somewhat, for longer wavelengths, or to confine slightly for shorter wavelengths, the radiated power distribution illuminating the receiving array. This will not have a significant effect on the couplers performance.

An erbium-doped fiber was attached by rotary splice to one of the output pigtails of the connectorized coupler as was a 0.98 pump source to one of the input ports. The pump consists of a Ti:Sapphire laser with a launched power into the coupler of 200 mW. A 1.55$\mu$m signal was also launched into one of the couplers input ports. Both the signal and the pump power are attenuated by the 1/N splitting and the excess loss of the coupler and its connectors. This varies somewhat with the channel used and has an average value about 17 dB. It is this loss that we would like to compensate with the EDF amplifier.

The particular EDF used has a gain threshold of somewhat less than 2 mW. To achieve 17 dB gain, about 5.5 mW of pump power is required. Some care was necessary to minimize splice losses and optimize the length of the EDF to maximize the gain for the available laser power.

The output optical spectrum for the amplified coupler with one input channel at $\lambda_s$ = 1552 nm is shown in Figure 2. The small-signal amplifier gain, G = 17.7 dB, fully compensated for the losses of the 19×19 integrated star coupler. Furthermore, very low-noise amplification was achieved using the 0.98$\mu$m pump wavelength. A near quantum-

limited amplifier excess noise factor, $n_{sp} = 1.04$ was estimated from the ASE power spectrum. In applications using all of the output ports, a length of EDF would be attached to each of the output port pigtails as indicated in Figure 1. In addition one would substitute a 0.98$\mu$m laser diode as the pump replacing the Ti:Sapphire laser used in this experiment. It is of course possible to increase the pump power by using more than one input port for pumping, at the price of reducing the number of available signal input channels.

Figure 3 shows the saturation performance of the star coupler for a single input channel. The small-signal insertion loss of the amplified star coupler was 0 dB, and increased to 4 dB for an output signal power $P_{out} = -0.2$ dBm without a significant change in the near quantum limited noise performance. This output signal power is also equal to the total saturated output power expected for a multi-channel application. Higher saturated output powers would be achieved for signal wavelengths at the amplifier gain peak $\lambda_s \sim 1530$ nm. Further improvement of the saturation power may be achieved using a more efficient EDF or increasing the pump power.

In conclusion, we have shown that it is possible to fully compensate for the loss of an integrated 19×19 star coupler with EDFA's in the output ports all pumped through the star itself with only one 0.98$\mu$m laser source connected to one of the input channels. When pumped with a laser diode the integrated star coupler and associated EDF's makes a very compact and economical system component. The fact that we pump at 0.98$\mu$m also means that the noise introduced into the system is minimized.

REFERENCES

1. A. E. Willner, A. A. M. Saleh, H. M. Presby, D. J. DiGiovanni and C. A. Edwards, to be published in IEEE Photonics Technology Letters.
2. C. Dragone, C. H. Henry, I. P. Kaminow and R. C. Kistler, IEEE Photonics Technology Letters, *Vol. 1,* No. 8, pp. 241-243, 1989.

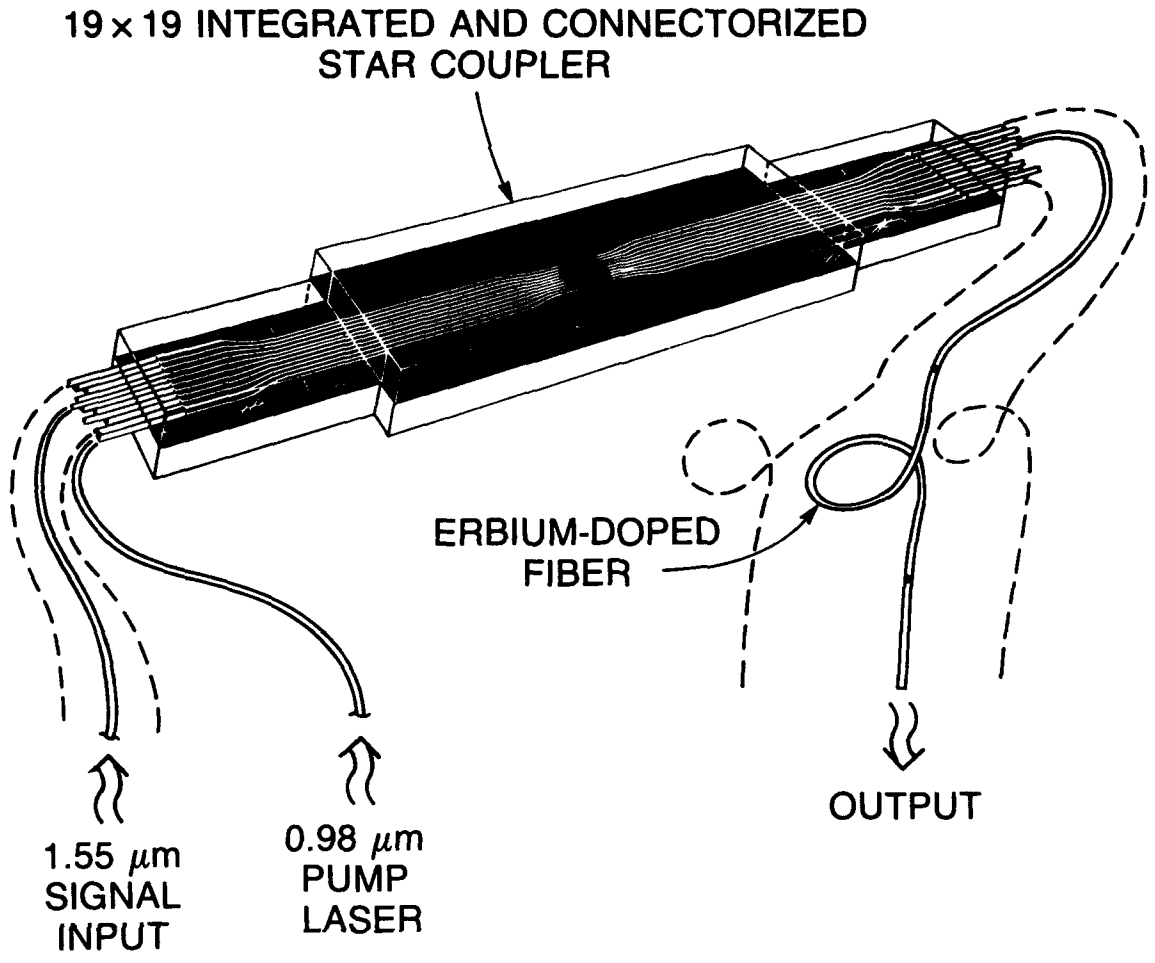


**FIGURE 1**

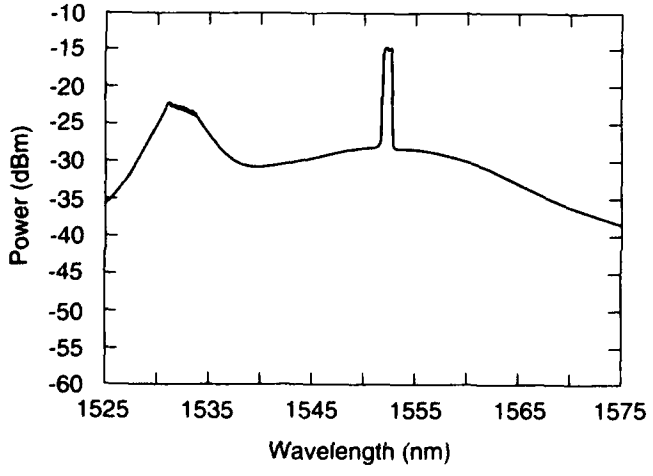


**FIGURE 2**

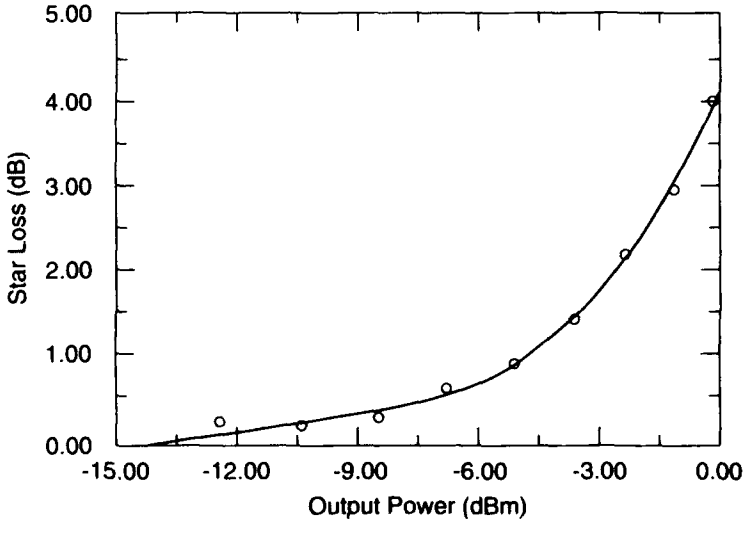


**FIGURE 3**

# Compact Size and High Output Power Er-doped Fiber Amplifier Modules Pumped With 1.48 μm MQW LDs

H.Takenaka, H.Okuno, M.Fujita, Y.Odagiri,
Y.Sunohara* and I.Mito*

Fiber Optic Communications Development Div.,
*Opto-Electronics Research Laboratories,
NEC Corporation

1753 Shimonumabe Nakahara-ku, Kawasaki, Kanagawa 211, JAPAN

## 1. Introduction

Er-doped fiber amplifiers(EDFAs) are very attractive for applications to the near-future optical communication systems[1].
High output power of +20 dBm was already reported by using 1.48 μm pump LD modules[2]. Increasing the signal output power from EDFA will be one of the important issues for such uses as the booster amplifiers in long-haul transmission systems and in optical distribution network systems.

In this paper, we report on development of an EDFA with signal output power more than +22 dBm by using high power 1.48 μm pump LDs and integrating passive optical components.
In addition, the components of the EDFA including an Er-doped fiber bobbin are installed in a small package to put it into practical use.

## 2. Optical components

### A) Pump LD Modules

Basically, the 1.48 μm LD module in this fiber amplifier comprises a DC-PBH MQW LD chip, an aspherical lens, a polarization maintaining fiber pigtail, and a thermo-electric cooler[3]. To get high pump power continuously, it is very important to realize an effective cooling performance of an LD package as well as to make an approach to obtain higher output power from the LD chip. For this purpose, we modified the LD package and reduce a thermal resistance between the LD chip and outside of the package.
This package , which is a metal cube with 5mm dimension, is directly soldered on a PELTIER cooler, and housed in a "butterfly" package. This enables us to get very stable operation even at fiber output power more than 100 mW in a wide range of ambient temperature from -20°C to 50°C.
We employed an aspherical lens with low wavefront aberration as low as 0.015λ. The resultant average LD-to-fiber coupling loss with thirty nine examples is 1.7 dB. Figure 1 shows the distribution of maximum output power from the pigtail.

B) WDM couplers

Reducing the insertion losses of passive components such as WDM, polarization coupler and optical isolator are very important to realize high performance EDFAs. For this purpose, we have newly developed integrated WDM - polarization coupler module with built-in polarization independent optical isolator as shown in Fig.2. PBS(polarization beam splitter) is used to combine pump powers from two LD modules. A shortwave pass filter(SPF) is added on the output surface of this PBS in order to filter out longer wavelength region of spontaneous emission of pump LD's. A dichroic mirror tilted by 22.5 deg is for multiplexing / demultiplexing a signal(1.552 μm) and a pump light(1.48 μm). To minimize the insertion loss of this coupler module, we use an Er-doped fiber as a pigtail which is to be spliced with Er-doped fiber(gain media). The lens system is designed to realize the mode matching between two ports with different mode field diameters. This fundamental configuration is used for both forward pumping and backward pumping with small modifications as shown in Fig.2.

We used aspherical lenses for coupling from port to port, and all the optical elements were welded in a metal box with 17 mm x 20 mm x 8 mm size by using Nd:YAG laser beam. The insertion loss was 1.4 dB in the signal beam path and 1.8 dB in the pump beam path, respectively.

## 3. The Amplifier Configuration and its Property

With pump LD modules and WDM couplers described above, we have realized compact EDFA modules. Figure 3 illustrates the configuration of the amplifier. We also show in Photo 1 the appearance of the amplifier, which was assembled in a 185 mm x 225 mm x 25 mm(1040 cc in volume)package. This amplifier employed four pump LDs to get higher saturation output power with the bidirectional pumping scheme, and total pump power launched into the Er-doped fiber was 345 mW . The fiber used was an alumina-silica Er-doped fiber with 1000 ppm Er concentration and 5000 ppm Al concentration. The mode field diameter was 5.0 μm .The fiber length was optimized to get the highest output power, and it was 80 m. Figure 4 shows the saturated signal output characteristics under different pump power conditions. With a signal input of +4 dBm at 1.552 μm , the amplifier output signal power of +22.3 dBm (170 mW) was obtained with net conversion efficiency of 69%.

## 4. Conclusion

We have developed compact size Er-doped fiber booster amplifiers by using newly designed pump LD modules and WDM couplers. The signal output power as high as +22.3 dBm has been achieved with total pump power of 345 mW .

These high output power amplifiers will be effective to expand the repeater spacing in long-haul systems.

## References

[1] K. Nakagawa, et al.,IEEE J.Lightwave Tech., vol 9(1991)pp..198 -208
[2] T.Sugie,et al.,Optical Amplifier and Their Application(Monterey,1990),paper PdP2-1
[3] M.Fujita, et al.,ibid.,paper WA4

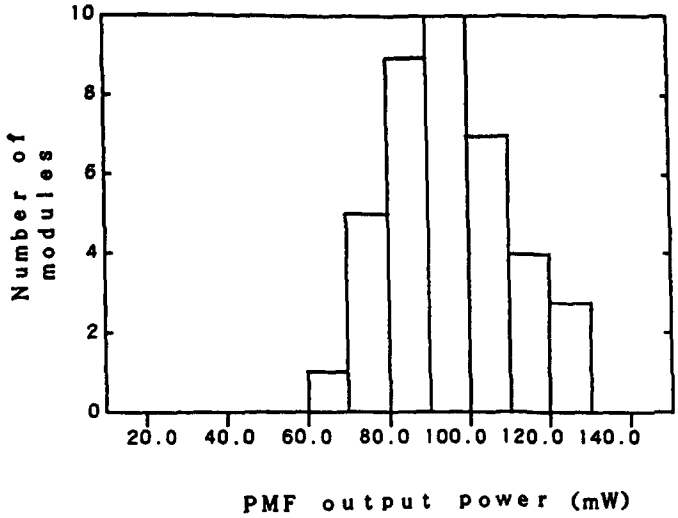


Fig. 1 Output power distribution of pump LD modules

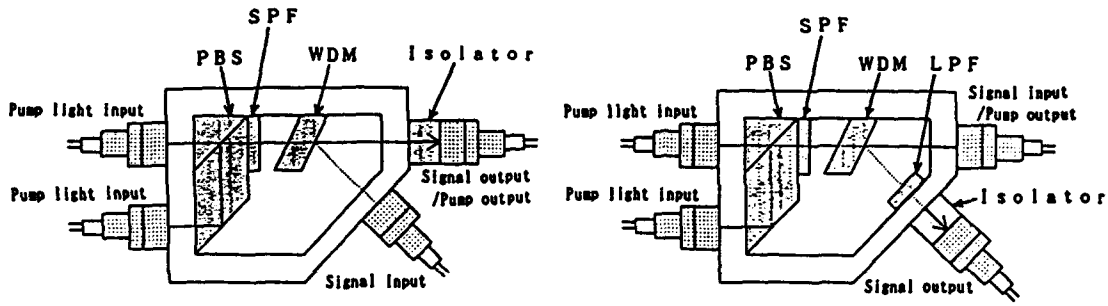


For forward pumping  For backward pumping

Fig. 2 WDM coupler configurations

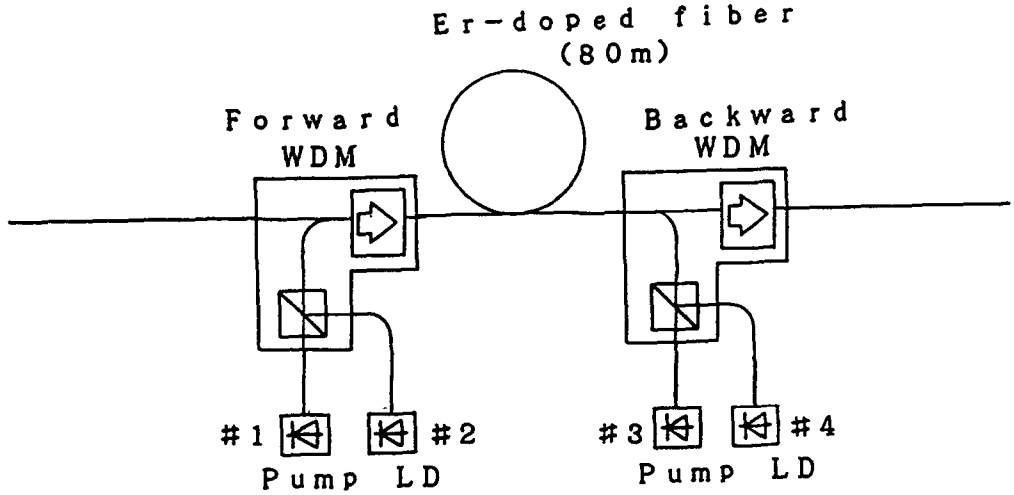


Fig. 3 Amplifier configuration

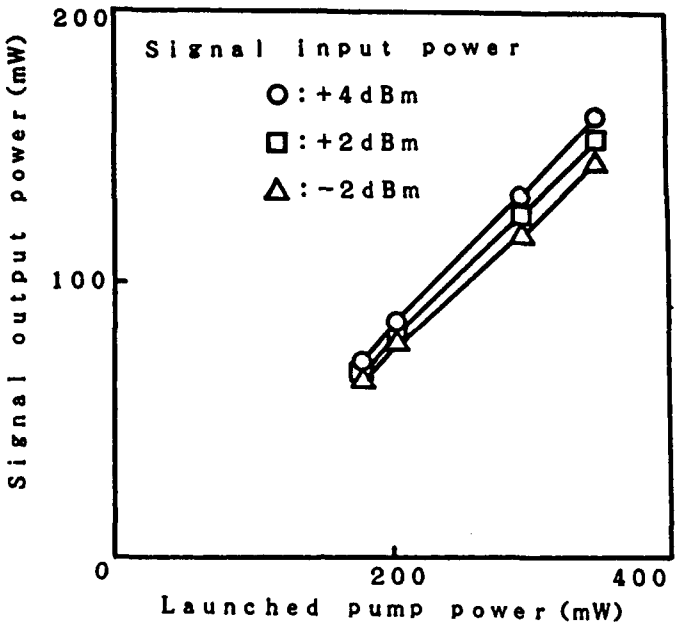


Fig. 4
Pump power-output power characteristics

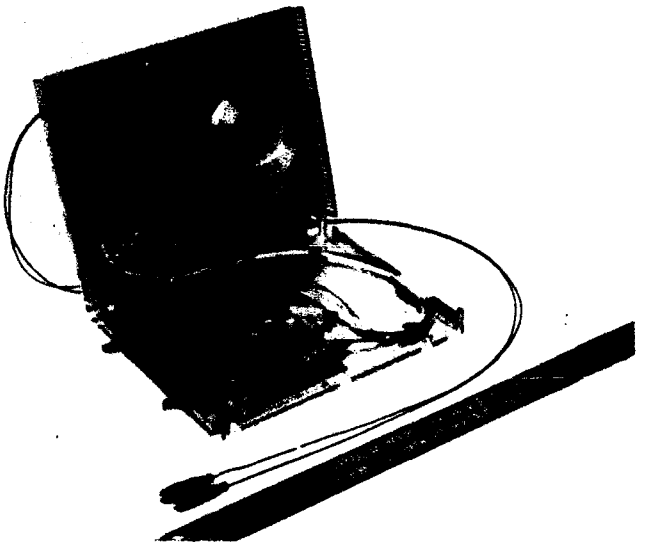

Photo. 1 Appearance of the amplifier

# High-Efficiency Erbium-Doped Fiber Amplifier using Mode Field Diameter Adjusting Technique

A.Wada, T. Sakai, D. Tanaka, T. Nozawa, R. Yamauchi

FUJIKURA Ltd.
1440 Mutsuzaki, Sakura-shi, Chiba 285, Japan

## Introduction

For efficient operation of an Er-doped fiber amplifier (EDFA) at 1.55 μm band it is essential to maximize the pump intensity in the Er-doped region because of the three level system [1]. A high NA structure of EDF is effective to reduce the mode field diameter (MFD) of the pump and to achieve strong pump intensity [2], and has resulted in excellent gain performance [3],[4]. In practical use, however, such small MFD fibers have a connection/splicing problem due to the mode field diameter mismatching. For example, approximately 1 dB splice loss is expected between an EDF with a 5 μm MFD and a conventional dispersion shifted fiber (DSF) with a 8 μm MFD. The smaller MFD of EDF, the higher splice loss. The increase of splicing loss causes noise figure degradation in pre-amplifiers and decreasing of conversion efficiency in booster amplifiers.

In this paper, we report the splicing loss less than 0.05 dB between an EDF with a small MFD and a conventional DSF. The MFD's have been adjusted by the thermal diffusion of core dopant after the splicing. We also describe the gain and noise characteristics of the EDFA with this adjusting technique.

## Mode field diameter adjusting technique

The MFD is magnified by thermal diffusion of the core dopant [5]. Change of core radius by thermal diffusion is expressed as $r_2 = (r_1 + 4Dt)^{1/2}$ [5], where $r_1$ and $r_2$ are radii before and after diffusion, D is a diffusion constant, and t is a diffusion time. The MFD is proportional to the core radius because the normalized frequency is not changed by the dopant diffusion [5]. Hence if the fibers with the different MFD's and with the same diffusion constants are spliced by fusion technique and then the spliced part is heated, the MFD's do not coincide with each other by thermal diffusion. We found that the diffusion constant of germanium in fluorine-doped glass is larger than that in non-doped silica glass. As a result, it is possible to adjust the MFD's of different fibers by heat treatment after splicing when the F-doped glass is used as cladding material of the Er-doped fiber. Fig.1 shows MFD change by thermal diffusion of Ge for two fibers; a Ge-doped silica core / F-doped silica cladding EDF; a Ge-doped silica core / non-doped

silica cladding DSF. The thermal diffusion constant of EDF is obviously larger than the that of DSF. The MFD's coincide with each other after ten minutes heating. Fig.2 shows the loss change of the splicing part between the EDF and DSF during the heating. The splice loss reached sufficiently low level after ten minutes heating. Using the above technique we spliced the EDF with external fibers. We call hereafter this MFD adjusted splicing part as a mode field diameter adjuster (MFDA).

## Configuration of Er-doped fiber amplifier

Fig.3 shows a configuration of the EDFA with the MFDA's. Depending on measuring items, either co-propagating or counter-propagating pump configuration was used. Small signal gain and noise figure were measured by co-propagating. Gain saturation and conversion efficiency were measured by counter-propagating. A 1.48μm semiconductor laser diode is used as pumping source and a dichroic mirror is used for combining the signal and pump light. An EDF used here is a Ge-doped core / F-doped cladding fiber having $\Delta$=1.5%, MFD= 5.1 μm, $\lambda$cut-off=1.1 μm, Er concentration=980 weight-ppm, Al concentration=4800 weight-ppm, and total absorption loss of 80.3 dB. We could realize $\Delta$=1.6% by using only Ge as a dopant, but used F-doped cladding for a reason mentioned above. The EDF is spliced through the MFDA to external DSF's.

## Gain and noise characteristics of Er-doped fiber with MFDA

Fig.4 shows signal gain characteristics of the EDFA for the signal input power of -40dBm at 1.552 μm; curve (a) shows gross gain (inside the EDF); curve (b) the gain including the splice loss of MFDA; curve (c) the gain including the splice loss of direct splicing. We can extract nearly full performance from the EDF with the MFDA. Fig.5 shows noise figure of the EDFA with MFDA. Noise figure less than 5.5 dB is obtained in the region from -40dBm to -20 dBm signal input power.

Fig.6 shows difference of conversion efficiency between the EDF's with and without MFDA. The gross conversion efficiency is also shown in Fig.6. The input signal wavelength and power are 1552 nm and -5 dBm, respectively. Here, the conversion efficiency $\eta$ is defined as $\eta = (P_{sig.out} - P_{sig.in}) / P_{pump}$. While without an MFDA, the conversion efficiency decreases to approximately 50%, with an MFDA, it decreases only a few percents from the gross value. Gain saturation characteristics of the EDF with MFDA's for different pump power are shown in Fig.7

## Conclusion

We have realized a splice loss less than 0.05 dB between an Er-doped fiber with 5 μm MFD and a conventional dispersion shifted fiber with 8 μm MFD by using mode field

diameter adjusting technique. We have demonstrated that nearly full performance can be drawn out from the high-NA EDF when mode field diameter adjusters are used.

## Reference

[1] J. R. Armitage, Appl. Opt. vol.27, p4831, 1988.

[2] M. Shimizu, Y. Yamada, M. Horiguchi, T. Takeshita, M. Okayasu, Electron. Lett., vol.26, p1641, 1990.

[3] M. Nakazawa, Y. Kimura, K. Suzuki, in Technical Digest on Optical Amplifiers and Their Applications(Optical Society of America, Washington, D.C., 1990), paper PDP1

[4] M. Shimizu, Y. Yamada, T. Takeshita, M. Horiguchi, in Technical Digest on Optical Amplifiers and Their Applications(Optical Society of America, Washington, D.C., 1990), paper MB2.

[5] K. Shiraishi, Y. Aizawa, S. Kawakami, J. Lightwave Technol., vol.8, p1151, 1990.

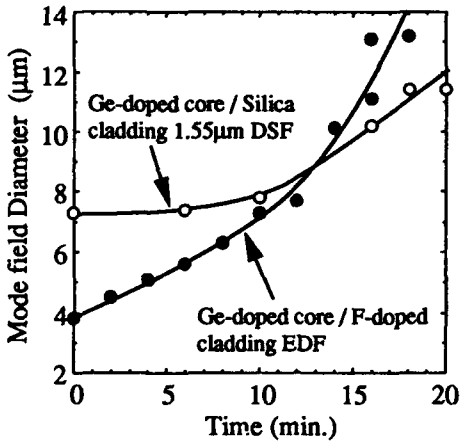


Fig.1 Change of mode field diameter by heating

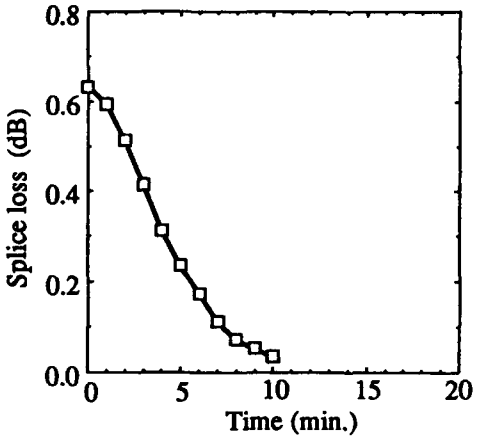


Fig.2 Loss change at splicing point between the EDF and 1.55μm DSF by heating.

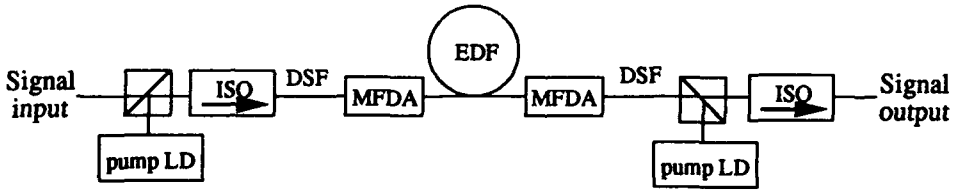


Fig.3 Configuration of the Er-doped fiber amplifier with mode-field-diameter adjusters (MFDA's)

Table I Structural parameters of Er-doped fiber used in the experiment

| | |
|---|---|
| Mode field diameter (@ 1.552μm), μm | 5.1 |
| Relative refractive index difference | 1.6 |
| cut-off wavelength, μm | 1.16 |
| Er concentration, weight-ppm | 980 |
| Al concentration, weight ppm | 4800 |
| Total absorption loss (@1.552μm), dB | 80.5 |

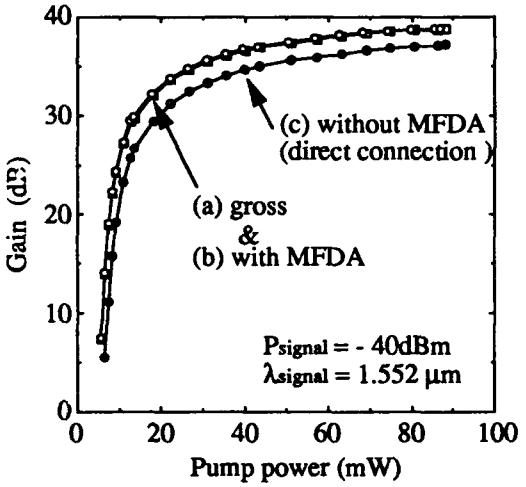


Fig.4 Comparison of small signal gains between the EDFA's with and without the MFDA.

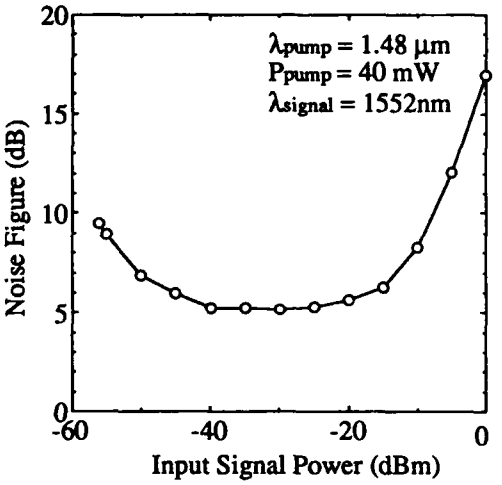


Fig.5 Noise figure of the EDFA with the MFDA.

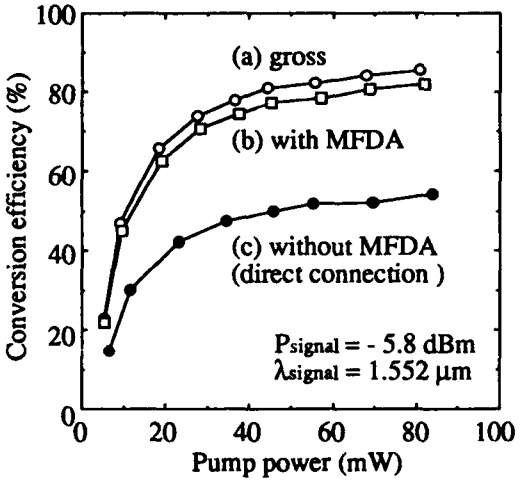


Fig.6 Comparison of conversion efficiencies between the EDFA's with and without the MFDA.

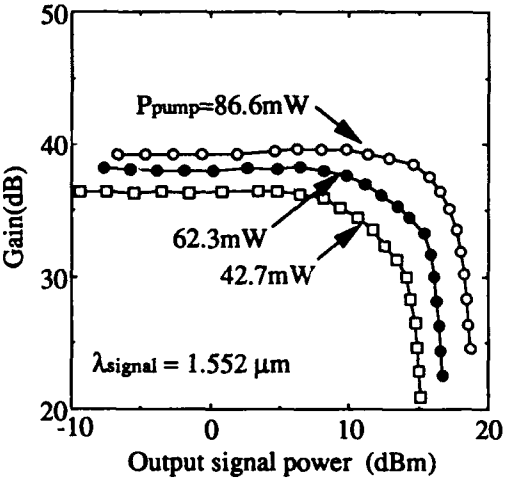


Fig.7 Gain saturation characteristics of the EDFA with MFDA.

# The Effect of Pump Induced Temperature Variation on Erbium-Doped Fiber Amplifiers

*S. NISHI, H. MASUDA, J. NAKAJIMA and K. AIDA*
**NTT Transmission Systems Laboratories**
1-2356, Take Yokosuka-shi Kanagawa, 238-03 Japan
Phone. +81-468-59-2545, Fax. +81-468-59-3396

*ABSTRACT*

The temperature increase of an erbium-doped fiber by 1.48μm pumping was measured. The mechanism of heat generation and its influence on amplification characteristics are discussed.

## *1. INTRODUCTION*

Erbium-doped fiber amplifiers (EDFAs) are very useful in optical communication systems. In order to obtain good performance, high power pumping is often required. Although, many studies[1][2] have increased the efficiency of pumping to signal energy conversion, a considerable part of the pump light power is converted to heat energy. It has also been reported that the gain of an EDFA is affected by temperature.[3][4] Therefore, it is important to study the effect of pump light on erbium-doped fiber (EDF) temperature. However, the heat generation of an EDF by the pump light has not been reported yet.

In this paper, we report the measured temperature increases of EDFs with a variety of packaging techniques. We discuss the mechanism of this heat generation and estimate its effect on amplification characteristics.

## *2. TEMPERATURE INCREASE OF EDF*

From the viewpoint of packaging space, EDFs should be set in very small containers. To gently hold fiber, a container can be made of a soft material such as sponge rubber. Generally, these materials have low heat conductivity. The difference between total optical input power (pump/signal) and optical output power (residual pump/amplified signal/amplified spontaneous emission) is converted into heat energy and warms up the EDF.

Figure 1 shows the experimental set up in which an EDF is pumped by 1.48μm laser diode light sources. Table 1 shows the main parameters of EDF tested. Figure 2 shows examples of measured temperature variation with various heat conditions and packaging techniques. The maximum pump power was 68mW and the maximum heat rise (about 5 degrees) occured with the tightest packaging configuration; EDF(A) wound in a 50mmϕ of sponge rubber. EDF(A) was tested with and without an opaque fiber cover and no difference in thermal response was noted ( see Figure 3 ). This means that almost all calorification occurs in fiber glass or its coat of expoxy resin. Figure 4 indicates that higher pump powers yield higher temperatures and require longer time to reach thermal stability.

## *3. DISCUSSION*

The mechanisms of heat Q generated in an EDF by a pump light are ;

(1) $Q_{sp}$ absorption of spontaneous emission radiated through lateral surfaces.



(2) $Q_{rel}$ due to the relaxation of three level system

(3) $Q_{abs}$ due to the absorption of pump light, which is not concerned with EDF amplification

(1) $Q_{sp}$ In the case of small signal power, spontaneous emission power $\Delta P_{sp}$, which generates in the section $\Delta z$ is given by following equation;

$$\Delta P_{sp} \propto \frac{P_p}{P_p+\varepsilon P_{th}} \Delta z$$

where $P_{th}=Ah\nu_p/(\varepsilon\sigma_p\tau_{12})$, $\varepsilon=\tau_{31}/(\tau_{32}+\tau_{31})$. A,h,$\nu_p$,$\sigma_p$ and $\tau_{ij}$ are effective interaction area, Planck's constant, frequency of pump light, pump absorption cross section, and characteristic life times from level i to j, respectively. Total spontaneous emission power $P_{sp}$ is given by integrating above equation along fiber length(z). For high power pumping region ($P_p>>P_{th}$), $\Delta P_{sp}$ is approximately constant, and $P_{sp}$ may saturate when launched pump power rises. In the case of EDF(A), $P_{th}$ is about 7.4mW and $\varepsilon$ approximates 1[5]. Using these values and the above equation, $\Delta P_{sp}$ is constant for $P_p(0)>50$mW. Figure 5 shows mean value of spontaneous emission power, which was measured by a photo diode set close to the wound EDF. In the region in which launched pump power $P_p(0)>50$mW, $P_{sp}$ saturates. However, temperature increase does not saturate even with launched pump powers over 50mW as shown in Figure 6. This suggests that $Q_{sp}$ is not dominant, in the case of high power pumping.

(2) $Q_{rel}$ According to the classical three level system, $Q_{rel}$ for no signal condition is given by

$$Q_{rel}=\frac{h\nu_{1.48}-h\nu_{1.54}}{h\nu_{1.54}} Q_{sp} \simeq 0.04\, Q_{sp}$$

Considering the up-conversion effect, $Q_{rel}$ is estimated to be larger than this value.

(3) $Q_{abs}$ Instead of measuring the loss at 1.48μm, we measured the loss at 1.3μm, because it is difficult to distinguish absorption due to erbium ions at 1.48μm. The loss of EDF(A) was 0.005dB/m at 1.3μm. If this attenuation is caused by OH radical absorption at 1.39μm, the loss value at 1.48μm nearly equals that at 1.3μm. The proportion of $Q_{abs}$ to total heat generation becomes large as launched pump power increases, because the erbium ions are pumped up and the section, over which strong pump light can reach, is extended. Figure 7 shows the dissipation of optical power in EDF for various pump powers. In the high power region, considerable absorption of pump power occurs.

Above discussion can be summarized qualitatively as Figure 8. Heat generation $Q_{sp}$ occurs in the fiber coat . While, $Q_{rel}$ and $Q_{abs}$ are generated in the core. The temperature difference $\Delta T_{c\text{-}s}$ between the core and outer surface of the fiber coat due to $Q_{rel}$ and $Q_{abs}$ is given by following equation;

$$\Delta T_{c\text{-}s}=\frac{1}{2\pi}\frac{Q_{rel}+Q_{abs}}{\tau L}\left\{\frac{ln(r_{eo}/r_{ei})}{\lambda_e}+\frac{ln(r_{go}/r_{gi})}{\lambda_g}\right\}$$

where $\Delta T$ ;temperature difference between core and outer surface of fiber coat

$r_{eo}$,$r_{ei}$,$r_{go}$ and $r_{gi}$;radius of coat outer,coat inner,glass outer and core, respectively

$\lambda_e$ and $\lambda_g$; heat conductivity of coat and glass, $\tau$;time, L;length

However, the temperature difference between core and coat surface is small in this case, because $Q_{rel}$ and $Q_{abs}$ are not so large compared with the heat conductivity of silica glass (about 1kcal/mhK) and epoxy resin (about 0.1kcal/mhK ). Therefore, the temperature increase is considered to occur uniformly in the EDF.

If the pump wavelength is 1.48μm and signal wavelength is 1.535μm, gain variation due to temperature increase has been estimated to be about -0.51(%/deg.).[3]

Using this value, 5 degrees of EDF temperature increase corresponds to about 0.6dB of gain decrease (for 25dB amplification). This effect is not so large, but we should pay attention to it, for example when accurate gain control is required for optical sensing etc., and when the EDF is packaged in an adiabatic container to maintain its a constant temperature.

## *4. CONCLUSION*

Self-warming of EDF pumped by 1.48μm laser diode was measured. Maximum temperature increase was 5 degrees with 68mW of pump power. The mechanisms of heat generatation in an EDF is discussed. Part of this calorification occurs within the core area, and local heating is very small. We should consider self-warming of EDF, in cases where very accurate gain control is required.

## *ACKNOWLEDGEMENT*

The authors wish to thank S. Shimada and H. Ishio for their encouragement. They also want to thank K. Hagimoto and H. Okamura for their valuable discussions.

[references]
[1] M.Shimizu et.al.,"0.98μm Laser Diode Pumped Erbium-Doped Fiber Amplifiers with a Gain Coeficient of 7.6 dB/mW",Topical Meeting on OAA 90,MB2,1990
[2] S.Nishi et.al.,"Highly Efficient Configuration of Erbium-Doped Fiber Amplifier",ECOC'90,MoG4.3,1990
[3] H.Masuda et.al.," Temperature Characteristics of Erbium-Doped Optical Fiber Amplifiers",Monograph Tech. Group Opt. Commun. Sys. IEICE Japan OCS90-22,1990
[4] M.Suyama et.al.,"Temperature Variation of Gain in a 1480nm-Pumped Erbium-Doped Fiber Amplifier", Topical Meeting on OAA 90,WD3,1990
[5] K.Nakagawa et.al.,"Trunk and Distribution Network Application of Erbium-Doped Fibers Amplifiers",IEEE J. of LT, Vol.9,No.2,p194,1991

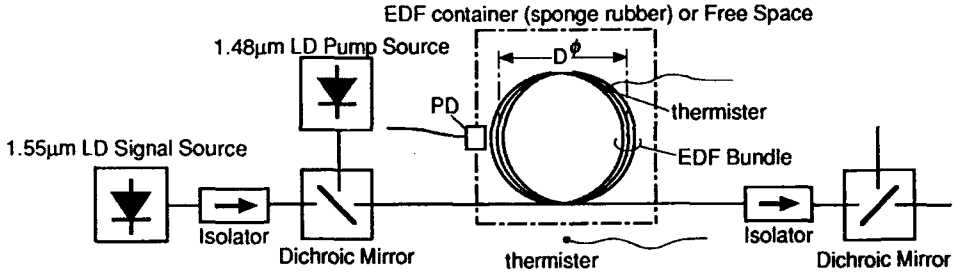


Figure 1 Experimental Set up

Table1 EDF parameters

| | EDF(A) | EDF(B) |
|---|---|---|
| Er concentration | 25ppm | 1200ppm |
| core diameter | 10.4μm | 6.6μm |
| clad dioameter | 124.1μm | 124.6μm |
| coat diameter | 0.4mm | 0.46mm |
| fiber length | 100m | 6.5m |
| coat material | UV epoxy | UV epoxy |

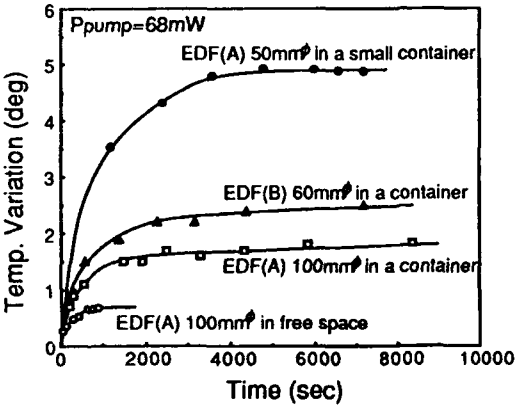


Figure 2 Temp. Variation of EDF

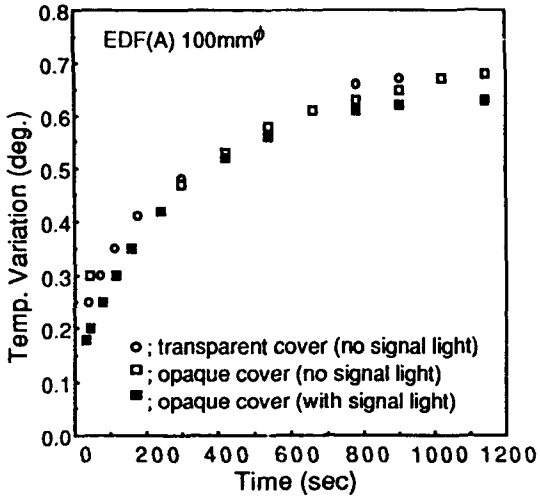


Figure 3 Temp. Variation of EDF in Space

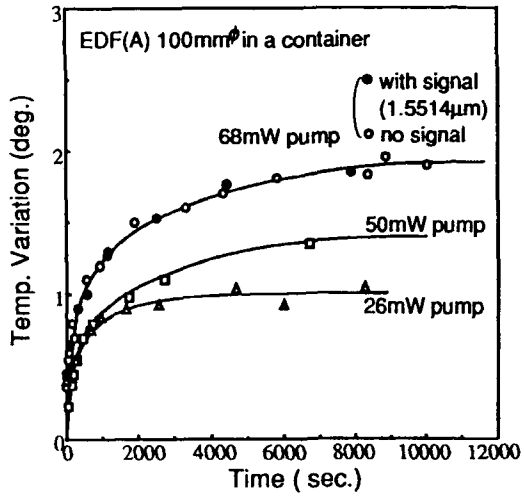


Figure 4 Temprature Variation of EDF in a Container

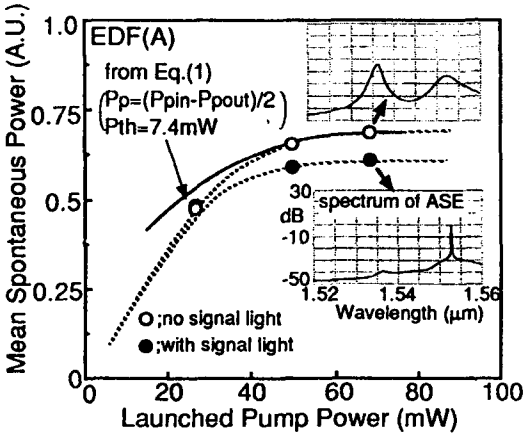


Figure 5 Spontaneous Emission Power

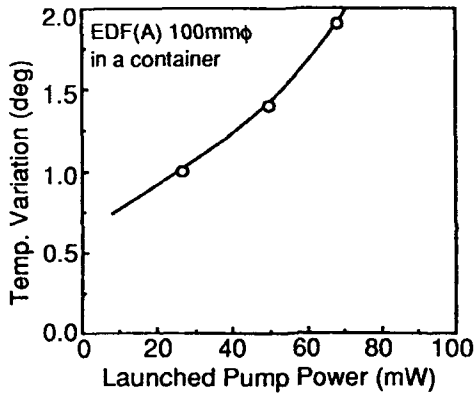


Figure 6 Steady State Temp. Increase vs. Pump Power

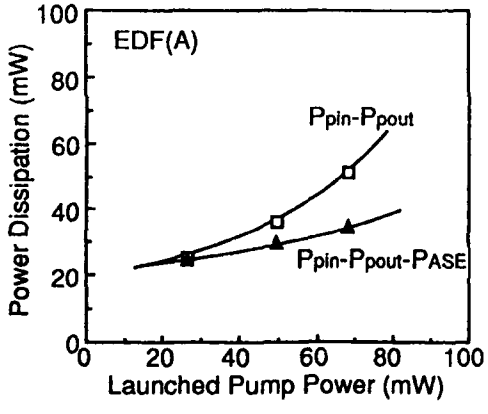


Figure 7 Optical Power Dissipation

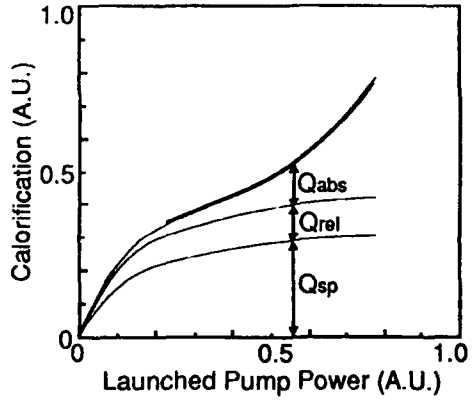


Figure 8 Qualitative Explanation of Calorification in EDF

# Novel System Techniques and Applications

**FE** 3:30pm–5:00pm
Cabaret Room

E. Eichen, *Presider*
*GTE Laboratories, USA*

# OTDR in Optical Amplifier Transmission Systems Using EDFAs Containing Optical Circulators

Yoshiaki Sato, Shigendo Nishi and Koh-ichi Aoyama
NTT Transmission Systems Laboratories

## 1. Introduction

Optical time domain reflectometry (OTDR) is an effective technique for locating breaks and for determining the loss distribution along a fiber [1][2]. However, OTDR can not be used with optical transmission lines containing traditional Er-doped fiber amplifiers (EDFAs) because EDFAs require optical isolators to eliminate signal reflection [3]-[5]. The returning backscattered light generated by the forward traveling probe pulse is blocked by optical isolators in each EDFA.

In this paper, we proposed a new EDFA containing optical circulators, which support both OTDR and digital signal transmission. Experimental results demonstrate that OTDR fault location and and 1.8Gb/s digital signal transmission can be carried out in the same optical transmission line containing three EDFAs.

## 2. Experimental setup

The configuration of the proposed EDFA is shown in Fig. 1. The EDFA is constructed with two Er-doped fibers, an isolator, a circulator and pump laser diodes. When only PUMP-1 is operated, the EDFA acts as a stable amplifier for signal transmission. Since PUMP-2 is not operated, EDF-2 acts as an optical attenuator. Even if reflection occurs at the output terminals, stable signal amplification is realized because the reflected light is attenuated by EDF-2. When OTDR is to be performed, EDF-2 is activated using PUMP-2. This requires the use of an independent supervisory line. The backscattered light of the transmission line fiber is led to the return transmission line through the optical circulator, EDF-2 and a fiber coupler. EDF-2 requires only small amplifier gain to compensate the loss of the detour route to the return transmission line. In this EDFA, the optical circulator is used as an isolator during signal transmission [6] and as a route changing component for the backscattered light during OTDR.

In the experiment, EDF-1 was 100m long and EDF-2 was 50m long. The ion concentration of EDF-1 and EDF-2 was 25ppm. The optical circulator characteristics were independent of input signal polarization state [7][8]. Its isolation and its excess loss between input and output ports was over 35dB and under 1dB respectively. The EDFA had a net gain of over 20dB which was achieved at a pump power of 40mW. The optical attenuation of the EDF-2 was 40dB during signal transmission.

Figure 2 shows the optical transmission line configuration used in this experiment. The total line length was 280.9km. Dispersion shifted fibers (DSF) with a loss of 0.2dB/km at 1.55μm were used as the transmission medium. The

loss of each segment which included a splice, an attenuator and a connector was about 17-19dB. The length of the fiber under test equaled that of the return fiber with the same number of transmission line segments.

Conventional OTDR equipment was used for fault location in the DSF-1. For DSF-2, DSF-3 and DSF-4, improved OTDR equipment was developed. Its optical probe pulses were generated from a 1.552μm distributed feedback laser diode (DFB-LD). The improved OTDR equipment has two ports, one for probe pulse launching and the other for receiving backscattered light. To eliminate amplified spontaneous emission power (ASE) from the first EDFA, an optical filter was set between the receiving port and the avalanche photodiode (APD). Its optical bandwidth was 1nm. The peak power of the probe pulse as injected into the optical fiber was +7.02dBm. The pulse width was 10μs. If only slight ASE is launched into the OTDR receiver, the DC-coupled electrical amplifier is saturated and small backscattered light was masked. This OTDR equipment used an AC-coupled electrical amplifier.

### 3. Experimental results and discussion

Figure 3 shows the observed OTDR waveform of the optical transmission line shown in Fig. 2. The OTDR waveform in Fig. 3(a) was observed by employing conventional OTDR equipment when only PUMP-1 was activated in each EDFA. When PUMP-1 and PUMP-2 were activated in each EDFA, the OTDR waveform of Fig. 3(b) was observed by employing the improved OTDR equipment. The dynamic range of this OTDR equipment was estimated at 25dB. The dynamic range in Fig. 3 (b) was smaller than this value. The reason is that the noise level of the OTDR rose due to ASE from the first EDFA. The backscattered trace from each transmission line segment was clearly observed. This results tells us the loss distribution of each repeater section and the gain of each EDFA. The indicated values correspond to those measured by an optical power meter and optical light source.

A 1.8Gb/s signal transmission was demonstrated using the optical transmission line setup shown in Fig. 2. Only PUMP-1 was activated in the each EDFA. A pseudorandom (PN $2^{15}$-1), 1.8Gb/s return to zero directly modulated optical signal was emitted from a 1.552μm DFB-LD optical transmitter. The transmitted signal was detected by an InGaAs-APD in the optical receiver. The measured Bit Error Rate (BER) performance is shown in Fig. 4. No evidence of an error rate floor was seen at levels as low as $10^{-11}$. The power penalty between 0km and after transmission with three EDFAs was about 1dB at a BER of $10^{-9}$. The power penalty was caused by S/N degradation of the multiple EDFAs.

### 4. Conclusion

A newly developed EDFA containing an optical circulator enables fault location using the return optical transmission lines of an optical transmission system. OTDR fault location and 1.8Gb/s signal transmission was demonstrated successfully in a 280.9km optical transmission line containing three EDFAs.

**Acknowledgements**

The authors would like to thank Dr. K. Nakagawa for his encouragement. The authors also would like to thank Dr. Y. Fujii for his useful discussion of optical circulators.

**References**

[1] S. D. Personick : Bell Sys. Tech. J. , Vol. 56, No. 3, p355, 1977.
[2] K. Aoyama, K. Nakagawa and T. Ito : IEEE J. Quantum Electron. , Vol. 17, No. 6, p862, 1981.
[3] K. Hagimoto, K. Iwatsuki, A. Takada, M. Nakazawa, M. Saruwatari, K. Aida and K. Nakagawa : Electronics Lett. , Vol. 25, No. 10, p662, 1989.
[4] K. Hagimoto, S. Nishi and K. Nakagawa : IEEE J. Lightwave Technol. , Vol. 8, No. 9, p1387, 1989.
[5] S. Saito, T. Imai, T. Sugie, N. Ohkawa, Y. Ichihashi and T. Ito : OFC'90, PD2, 1990.
[6] S. Nishi, K. Aida and K. Nakagawa : ECOC'90, MoG 4. 3, 1990.
[7] T. Matsumoto and K. Sato : Appl. Opt. No. 19, p108, 1980.
[8] Y. Fujii : IEEE J. Lightwave Technol. , to be Published.

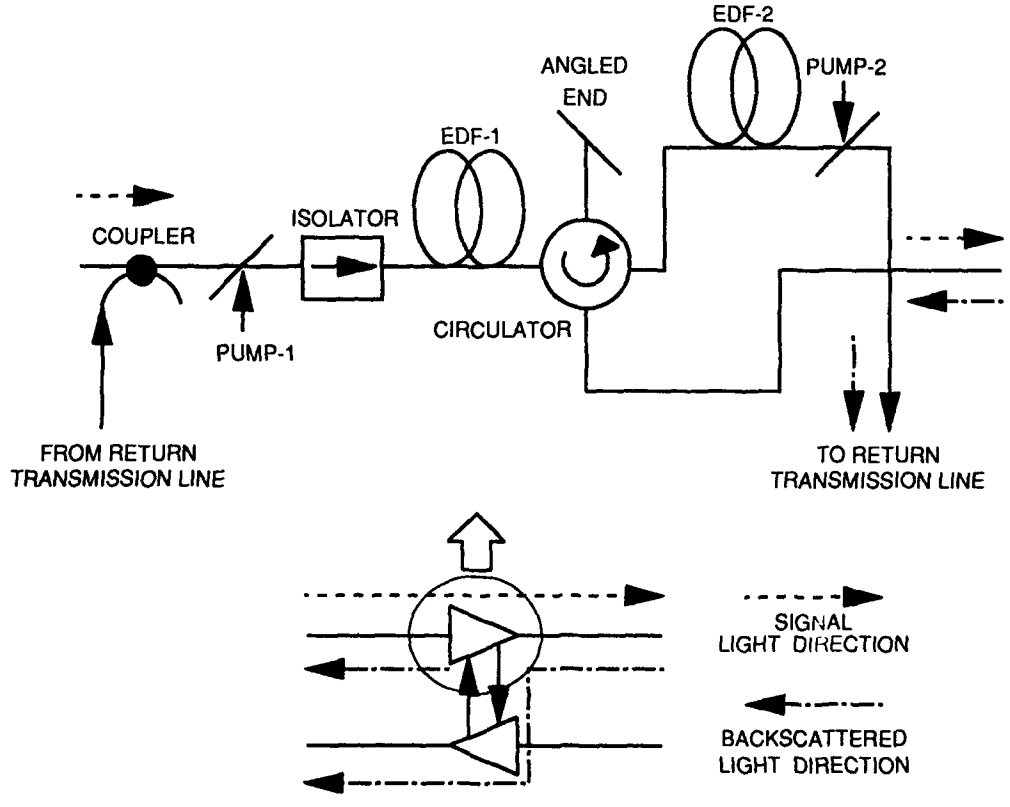


Fig.1 EDFA configuration.

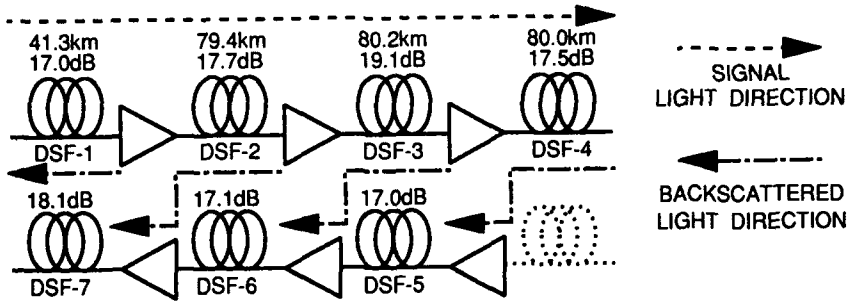


Fig.2 Experimental transmission line setup.

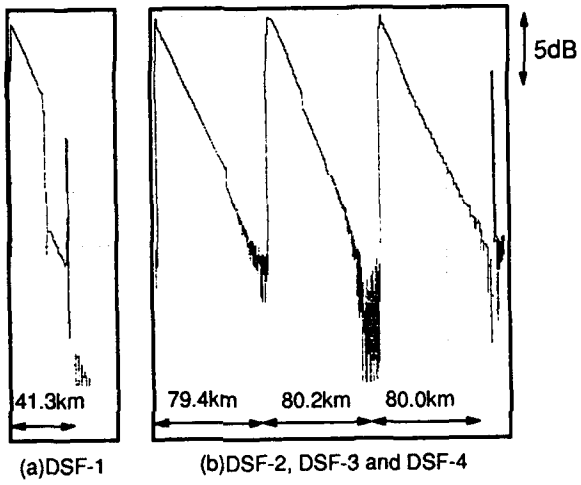


Fig.3 OTDR waveform.

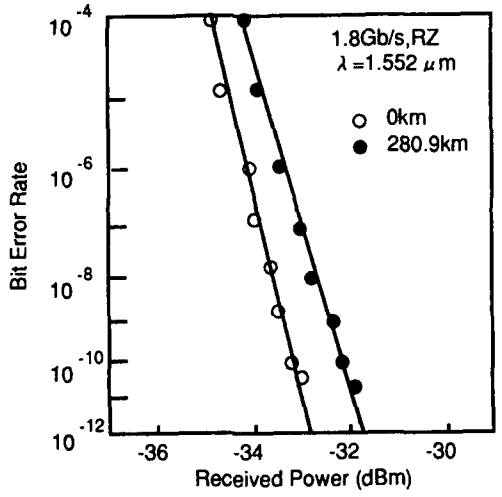


Fig.4 Bit error rate performance.

# MEASUREMENT OF POLARIZATION DISPERSION IN THE COMPONENTS OF IN-LINE ERBIUM DOPED FIBER AMPLIFIED LINKS

J.J. BERNARD, F. BRUYERE, J. GUILLON

ALCATEL ALSTHOM RECHERCHE
Route de Nozay, 91460 MARCOUSSIS - FRANCE

## ABSTRACT

An experimental investigation of polarization dispersion of an in-line erbium doped fiber amplified link has been carried out. Results show a non negligible contribution of the isolators.

## INTRODUCTION

Many results have been previously reported on polarization dispersion analysis and measurements in single-mode fibers [1-5]. The recent interest in long haul high bit rate transmission systems (transoceanic application) using non-regenerative in-line erbium doped fiber amplifiers (EDFA) requires a careful analysis of the polarization dispersion induced not only by the link fiber but also by the EDFA components, particularly the optical isolators and the 1.48/1.55 µm wavelength division multiplexers (WDM). Optical isolators using spatial splitting of the incoming lightwave into two polarization states, could have a non negligible contribution to the polarization dispersion of the overall link.
This paper presents, for the first time, the main results achieved for various optical components, including single-mode fibers, optical isolators and WDMs made by different technologies.

## DESCRIPTION OF THE TEST BENCH

Two major methods have been implemented so far for measuring polarization dispersion. One consists in observing the rotation of the Poincaré sphere under a frequency change of the source [1-2]. The other is based on the observation of the interferometric crosscorrelation obtained between the two principal states of polarization at fiber output [3-4]. Despite its relative complexity, this latter method permits high resolution, large dynamic range together with high measurement speed. This method has been used in the present work.
Figure 1 describes the test bench used for polarization dispersion measurement. The amplified spontaneous emission of a 40 m long, 1.48 µm pumped erbium doped fiber provides a 13 nm broadband source around 1.55 µm, having ~100 µm coherence length, allowing a time resolution better than the corresponding 0.3 ps coherence time.
A Mach-Zehnder interferometer splits the beam into two orthogonal linear states of polarization $E_1$ and $E_2$. In the fixed arm, the incoming lightwave is frequency shifted by mean of an acoustooptic modulator. In the mobile arm, a corner cube mounted on a translation stage controlled by a DC motor provides a variable delay $\tau_d$. The maximum value of $\tau_d$ determined by the largest mechanical displacement of the translation stage is 50 ps in this case. This corresponds to the maximum polarization dispersion that can be measured. The two orthogonal polarization states at interferometer output are recombined by a polarization beamsplitter and injected into the test fiber through a $\lambda/2$ rotating plate. This rotating plate is adjusted for the two incoming states of polarization to match the input principal states of polarization of the test fiber as well as possible. Polarization dispersion in single-mode fibers occurs due to the time delay $\tau_g$ between these two principal states evolving along fiber length.
A polarization analyzer is used at fiber end to optimize the amplitude of the detected crosscorrelation signal obtained between the two output principal states. A PINFET of - 43 dBm sensitivity is used as a receiver which, considering the 8 mW source output power, provides a dynamic range of 30 dB. DC motor control and signal acquisition are done via a personal computer.

Envelope detection at the heterodyne frequency gives :

$$S(\tau_d) = K \left\{ \sin^2\theta \,.\, |\sin 2\theta'| \,.\, \gamma(\tau_d + \tau_g) + |\sin 2\theta| \,.\, \sqrt{1 - \sin^2 2\theta' \,.\, \sin^2 \Delta\psi} \,.\, \gamma(\tau_d) + \cos^2\theta \,.\, |\sin 2\theta'| \,.\, \gamma(\tau_d - \tau_g) \right\}$$

where $\theta$ is the angle between the Stokes vector $\varepsilon_1$ of $E_1$ and $\varepsilon_i^+$ of the positive input principal state, and $\theta'$ the angle between the Stokes vector $\varepsilon_0^+$ of the positive output principal state and $\varepsilon_A$ of the analyzer (Figure 2). $\gamma(\tau)$ is the normalized mutual coherence function of $E_1$ and $E_2$, and K a constant. $\Delta\Psi$ is a phase constant.

It has been shown that a pulse at fiber input will couple energy proportionally to $\cos^2\theta$ to the positive input principal state and to $\sin^2\theta$ to the negative input principal state [6]. Thus, the normalized crosscorrelation part of the signal $S(\tau_d)$:

$$S_C(\tau) = \sin^2\theta \,.\, \gamma(\tau_d + \tau_g) + \cos^2\theta \,.\, \gamma(\tau_d - \tau_g)$$

can serve to measure the width $\sigma_{Sc}$ at fiber output of a pulse of initial duration $\sigma_\gamma$ equal to the coherence time $\tau_c$ of the source. $\sigma_{Sc}$ is given by : $\sigma_{Sc}^2 = \sigma_\gamma^2 + \sin^2 2\theta \,.\, \tau_g^2$.

Polarization dispersion can then be deduced : $D = \sqrt{\sigma_{Sc}^2 - \sigma_\gamma^2} = |\sin 2\theta| \,.\, \tau_g$

which shows that polarization dispersion vanishes if the pulse polarization at fiber input corresponds to one of the input principal states and is maximum if the pulse couples energy evenly between the two input principal states.

## EXPERIMENTAL INVESTIGATION OF POLARIZATION DISPERSION

A highly birefringent (HiBi) fiber first served for qualifying the bench. Then, various single-mode link fibers and EDFA constituents (optical isolators and WDMs) have been tested.

***High birefringence fiber :*** Figure 3 shows the typical correlation curves obtained for a 3 m long HiBi fiber. Polarization dispersion is given by the time interval between the autocorrelation peak and any of the two adjacent crosscorrelation peaks. In this specific case, polarization dispersion was 6.55 ps ( i.e. 2.2 ns/km), corresponding to an equivalent beat length of 2.38 mm (close to the indicative value of 2.45 mm given by the fiber manufacturer).

***Single-mode link fiber :*** Two kinds of single-mode fibers have been tested : conventional matched cladding (TAT9 type) and dispersion shifted fibers. These fibers were wound respectively on 30 and 21 cm diameter drums. Figure 4 shows the correlation curves obtained for a 40 km long dispersion shifted fiber. A polarization dispersion $\tau_g$ of 0.5 ps has been measured, corresponding to a normalized dispersion of 0.08 ps/$\sqrt{}$km. This dependence of polarization dispersion to the square root of fiber length is due to polarization mode coupling occuring in low birefringent fibers. A 27.5 km long TAT9 type fiber has also been tested. The polarization dispersion obtained was 0.45 ps (i.e. 0.085 ps/$\sqrt{}$km). These results are in good agreement with the typical value of 0.1 ps/$\sqrt{}$km usually published.

***Optical isolators :*** Optical isolators are used in various EDFA schemes to prevent undesirable optical feedback that could induce lasing effect. Most currently available devices are optimized in terms of isolation, return loss, insertion loss and polarization insensitivity. They are usually constituted of a YIG crystal inserted between two birefringent elements [7]. Any discrepancy between the optical paths of the two polarized light rays (ordinary and extraordinary) will result in polarization dispersion. Thus, the optical isolator could be a critical constituent of an EDFA with respect to polarization dispersion. Four different types of optical isolators have been investigated. All of them were pigtailed with a conventional single-mode fiber. We first made sure the observed correlation peaks were due to birefringence effect and not to any feedback from the interferometer or from the internal components of the isolator itself. Table 1 lists the results obtained for different types of optical isolators. A large variation of polarization dispersion was observed (from 0.3 ps to 7.5 ps). Figure 5 shows the correlation curve of the most dispersive isolator (7.5 ps). This corresponds roughly to the polarization dispersion of a 5000 km long fiber of 0.1 ps/$\sqrt{}$km normalized polarization dispersion.

The influence of the cumulated effect of the link fiber and the optical isolators has been investigated on a concatenated link composed of two 20 km long dispersion shifted fibers and two highly dispersive optical isolators spliced together. The correlation curve obtained (Figure 6) shows that the interferometric correlation method allows not only direct measurement of maximum polarization dispersion (15.5 ps), but also provides a versatile tool for accurate diagnosis of the polarization dispersion causes. Polarization dispersion of a single pulse propagating through a concatenated link is determined by the standard deviation of the correlation curve, after selecting the correlation peaks having physical significance, i.e. representing the actual time delays affecting the pulse.
Thus, for a concatenated link consisting of link fiber and optical isolators, the polarization principal states model does not apply. The correlation curve obtained cannot be explained only by the bandwidth validity limit of the polarization principal states. In this case, the effect of strong localized birefringence (from the optical isolators) perturbating the birefringence accumulation process in the link fiber needs to be considered both theoretically and experimentally.

***Wavelength division multiplexers :*** A complementary test has been achieved on a 1.48/1.55 μm WDM. As expected, no polarization dispersion could be observed on this component.

## LIMITATION DUE TO POLARIZATION DISPERSION IN AN EDF-AMPLIFIED LINK

For extremely long haul non regenerated systems (typically for transoceanic applications) working at very high bit rates (some Gbit/s) including a large number of in-line erbium doped fiber amplifiers associated to extremely low attenuation and chromatic dispersion single-mode fibers, polarization dispersion effect has to be accurately examined. As an example, taking a chromatic dispersion free fiber having a normalized polarization dispersion of 0.1 ps/√km and a length of 10,000 km, total fiber dispersion is then 10 ps. A 10 Gbit/s transmission bit rate requires the total link dispersion to be less than 20 ps (providing a margin of 150 % on the required electrical bandwidth of the system). These values show that the contribution to polarization dispersion of the optical isolators constituting the in-line EDFAs has to be minimized. The extreme value of 7.5 ps observed on a particular type of isolator would be probably too limitating on the required electrical bandwidth. Even in the case of optical isolators showing much lower polarization dispersion, a careful analysis of their cumulative effect needs to be undertaken.

## CONCLUSION

Polarization dispersion has been investigated in the constituents of an erbium doped fiber amplified link. It has been shown that, in addition to link fibers, optical isolators may have a non negligible contribution to the overall polarization dispersion. Furthermore, the interferometric correlation method implemented has proved to be a versatile tool both for accurate analysis and measurement of polarization dispersion.

**ACKNOWLEDGEMENT** : The authors are grateful to DAII for its financial support to this work.

## REFERENCES

[1] C.D. Poole and R.E. Wagner, "Phenomenological approach to polarisation dispersion in long single-mode fibres", Electronics Letters, Vol.22, No.19, 11th Sept. 1986, pp. 1029-1030.

[2] C.D. Poole *et al.*, "Polarization dispersion and principal states in a 147-km undersea lighwave cable", Journal of Lightwave Technology, Vol.6, No.7, July 1988, pp.1185-1190.

[3] N. Shibata *et al.*, "Spatial technique for measuring modal delay differences in a dual-mode optical fiber", Applied Optics, Vol.19, No.9, 1st May 1980, pp. 1489-1492.

[4] M. Tsubokawa *et al.*, "Evaluation of polarization mode coupling coefficient from measurement of polarization mode dispersion", Journ. of Lightw. Technol., Vol. LT-3, No.4, August 1985, pp.850-854.

[5] F. Curti *et al.*, "Statistical treatment of the evolution of the principal states of polarization in single-mode fibers", Journal of Lightwave Technology, Vol.8, No.8, August 1990, pp.1162-1166.

[6] G. De Marchis and E. Iannone, "Polarization dispersion in single-mode optical fibers : a simpler formulation based on pulse envelope propagation", Microwave and Optical Technology Letters, Vol.4, No.2, January 20 1991, pp.75-77.

[7] M. Shirasaki and K. Asama, "Compact optical isolator for fibers using birefringent wedges", Applied Optics, Vol.21, No.23, 1st December 1982, pp. 4296-4299.

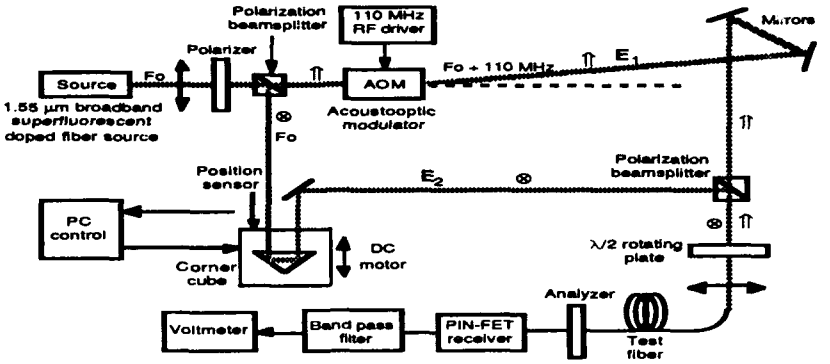


Figure 1 - Polarization dispersion measurement test bench

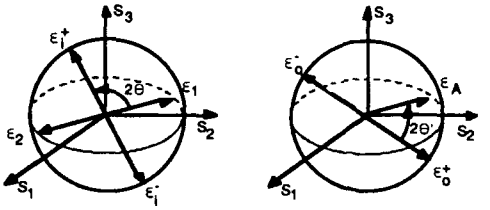


*Input* *Output*

Figure 2 - Poincaré sphere representation of polarization vectors

| Reference | Pol. disp. |
|---|---|
| Isolator A | 1.38 ps |
| Isolator B | < 0.6 ps |
| Isolator C | 1.13 ps |
| Isolator D | 7.5 ps |

Table 1 : Results obtained on different optical isolators

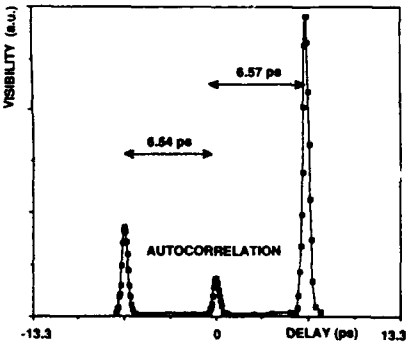


Figure 3 - Results obtained on a 3 m long polarization maintaining fiber

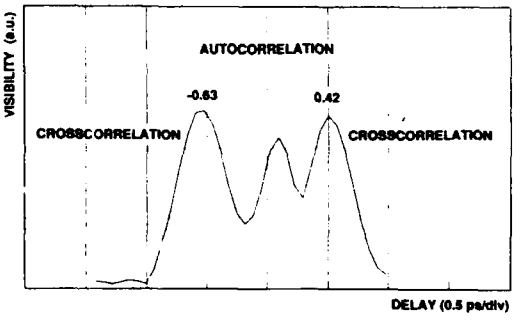


Figure 4 - Polarization dispersion measured on a 40 km long dispersion shifted fiber

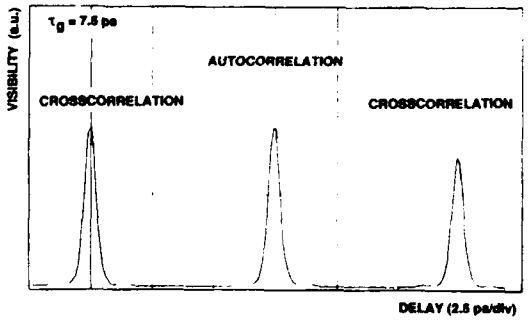


Figure 5 - Typical result obtained on a highly polarization dispersive optical isolator

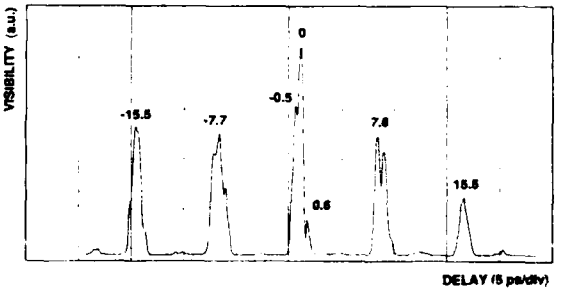


Figure 6 - Result obtained on a link composed of two optical isolators and two DS fiber sections

# Automatic Gain Control of Erbium-Doped Fiber Amplifier by Detecting Spontaneous Emission Power along the Fiber

**Kazuo Aida, Hiroji Masuda**

**NTT Transmission Systems Laboratories**
**1-2356, Take Yokosuka-shi Kanagawa, 238 Japan**

## *ABSTRACT*

EDFA gain control is achieved by detecting the spontaneous emission power radiated along the EDF and modulating the pump LDs with optoelectronic feedback.

## *INTRODUCTION*

Automatic gain control of Er-doped fiber amplifiers(EDFA) is required to compensate gain fluctuation and to increase the linear operation range for more reliable optical communication systems.

Previous AGC schemes with optelectronic feedback require the detection of the amplifier input and output power[1][2]. In such schemes, ASE power in the output may cause control error if high gain amplifiers are used.

In this paper, we propose a novel gain control scheme, which detects spontaneous emission power radiated along the EDF and modulates the pump LDs with optoelectronic feedback.

## *PRINCIPLE OF OPERATION*

The gain of an EDFA is given by the local gain r(z) along the EDF as follows[3],

$$G=\exp\{\int_0^L \gamma(z)dz\}, \qquad (1)$$

where the local gain is a function of position, pump power level and signal level along the EDF.

The local gain is related to the spontaneous emission power $P_{SE}(z)$ radiated along EDF and other constants as follows,

$$\gamma(z) = CP_{SE}(z) - \alpha_s, \qquad (2)$$

where

$$C = \frac{\eta\{\sigma_{emi}(\lambda_s) + \sigma_{abs}(\lambda_s)\}\tau}{h\nu_{SE}\pi(r_{Er})^2}, \quad \alpha_s = \eta\sigma_{abs}(\lambda_s)\rho,$$

$\eta$:overlap factor, $\sigma_{abs,emi}(\lambda_s)$ :absorption, emission cross-section,
$\tau$:spontaneous emission lifetime, $\rho$: $Er^{3+}$concentration
h:Plank constant, $\nu_{SE}$:average frequency of spontaneous emission
$r_{Er}$: $Er^{3+}$doped radius,

$\alpha_s$(small level signal loss of the EDF) and C are not a function of position, pump power or signal power along the EDF. From equation (1) and (2), the EDFA gain can be written as

$$G = \exp\{C\int_0^L P_{SE}(z)dz - \alpha_s L\}. \qquad (3)$$

Thus, EDFA gain can be controlled by using the integrated spontaneous emission power radiated along the EDF.

Figure 1 shows the basic automatic gain control scheme. The photodiode(s) within the integrating sphere detects and integrates the spontaneous emission power. By controlling pump power to maintain a constant integrated spontaneous emission(ISE) power level with the optoelectronic feedback loop, the gain of the EDFA is stabilized.

## *EXPERIMENTAL RESULTS*

The experimental arrangement for the integration and detection of spontanious emission power is shown in Figure 2(a). A 25 m high-NA center core doped EDF(Er concentration: 1000ppm, Al concentration: 5000ppm) with UV coat was coiled to a 100mm radius. One part of the coil was sandwitched between a mirror and a photodetector(4mm$^{\Phi}$). Because the EDF is coiled, the spontaneous emission power is sampled at intervals of about 310mm along the EDF. The EDF was pumped at1.48μm by LDs in a backward pumping scheme. Figure 2(b) shows the EDFA gain versus the integrated spontaneous emission(ISE) power for various input signal levels. This figure clearly shows that the ISE power is a good measure of the EDFA gain as predicted by equation (3), and also the simple experimental arrangement works well.

Figure 3 shows the ISE power and pump power versus input signal power under AGC operation. Figure 4 shows the EDFA gain versus input signal power level with and without AGC operation. The ISE power is kept constant up to an input signal power level of -10dBm by the modulation of pump LDs by the feedback loop. Pump power increases from 12mW for -50dBm input signal, to 38mW with a -10dBm input signal. The ISE power decreases with input signal power above -10dBm because of the pump power limitation of 38mW.

The 1 dB gain compression input signal power for the 20dB small signal gain EDFA is -22dBm without AGC, and -9dBm with AGC.

Thus, the linear operation range of the EDFA increases by 13dB with AGC.

## *CONCLUSION*

We have demonstrated a simple automatic EDFA gain control scheme by detecting the spontaneous emission power radiated along the EDF and modulating the pump LDs with optoelectronic feedback; input and output signal powers are not monitored. The AGC technique increases the linear operation range of the EDFA by 13dB.

## *ACKNOWLEDGEMENTS*

The authors wish to thank Dr. Sadakuni Shimada, Dr. Hideki Ishio and Dr. Kiyoshi Nakagawa for their encouragement.

## REFERENCES

[1]G.R.Giles et al., "Transient gain and cross talk in erbium-doped fiber amplifiers",

Optics Letters, Vol.14, No.16, p.880, 1989
[2]L. Eskildsen, et al.,"Automatic gain and power contral of semiconductor laser amplifiers", ECOC'90, pp.621-624, 1990
[3]P.R. Morkel et al.,"Theoretical modeling of erbium-doped fiber amplifiers with excited-state absorption", Optics Letters, Vol.14, No.19, p.1062, 1989

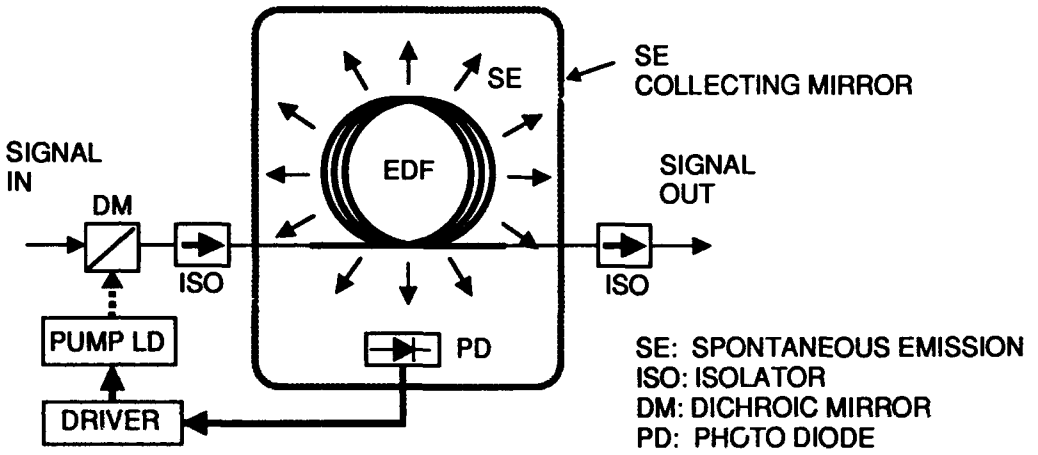


Fig. 1 Automatic gain control scheme by spontaneous emission detection

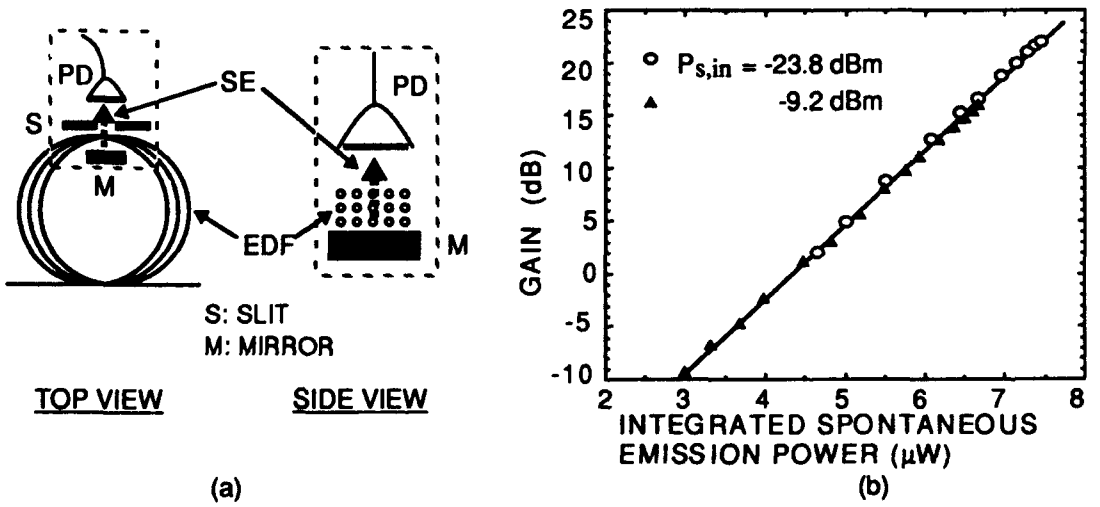


Fig. 2 EDFA gain as a function of integrated spontaneous emission power
(a) experimental arrangement, (b) experimental results

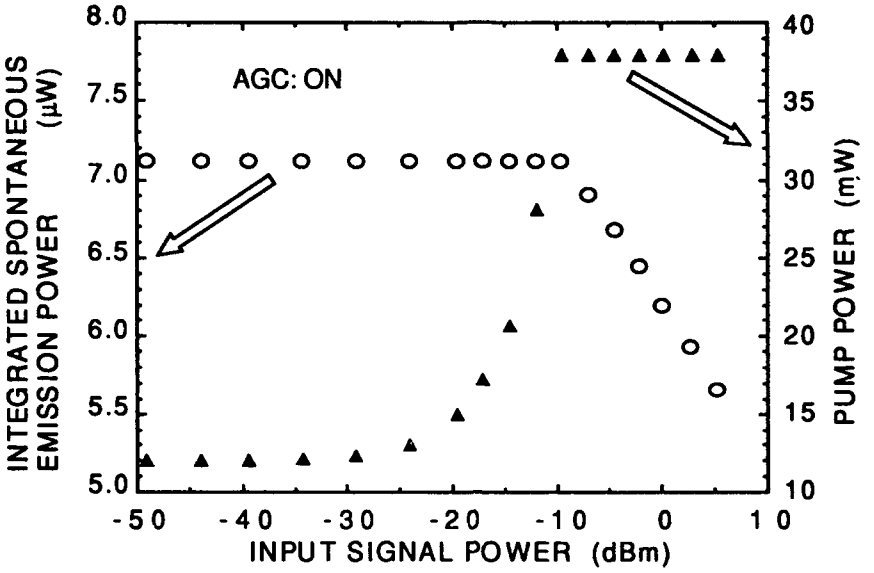


Fig. 3 Integrated spontaneous emission power and pump power versus input signal power with AGC

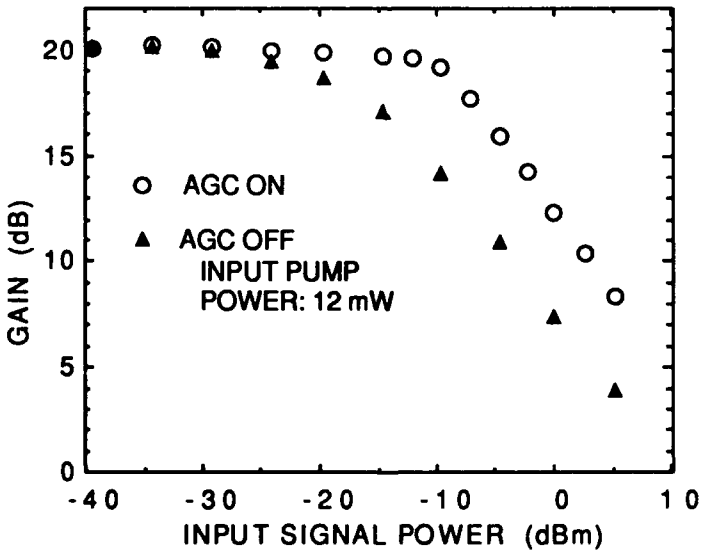


Fig. 4 EDFA gain versus input signal power with and without AGC. (Signal: 1.552 μm, Pump: 1.48 μm)

# Optimized Nonregenerative Repeater Using Cascaded Erbium-Doped and Raman Fiber Amplifier

S. L. Zhang and J. J. O'Reilly

School of Electronic Engineering Science

University of Wales, Bangor, U.K.

## 1. Introduction

Fiber-based optical amplifiers such as the erbium-doped fiber amplifier(EDFA) and Raman fiber amplifier(RFA) offer the attraction of high gain, low coupling loss and polarisation insensitivity. Hence their use in combination to form a nonregenerative repeater(NRR) deserves consideration. This paper provides a theoretical analysis and gain optimisation for this form of NRR. This arrangement is found to provide higher gain than either an EDFA or a RFA repeater alone and offer the potential of extending the NRR span to over 300 km.

## 2. Theoretical Analysis

The configuration of our proposed NRR is shown in Fig.1. As the RFA is more suitable for high power amplification, the configuration considered here is of an EDFA followed by a RFA, with the pump power travelling in the backwards direction serving as pump for both EDFA and RFA. The length of standard monomode fiber between the pump insertion point and the EDFA is $L_f$. This portion of fiber forms a RFA. The fiber length of the EDFA is $L_{ed}$.

For the EDFA, if the condition $P_s \ll P_{sat}$ is satisfied, the differential equations governing the pump and the signal[1] are as follows:

$$\frac{dP_p(z)}{dz} = \frac{\rho_0 \cdot \sigma_p}{\frac{P_s(z)}{P_p^{th}} + 1} \cdot P_p(z) \tag{1}$$

$$\frac{dP_s(z)}{dz} = \frac{\rho_0 \cdot \sigma_e \cdot (1-\eta)}{\frac{P_s(z)}{P_p^{th}} + 1} \cdot \frac{P_p(z)}{P_p^{th}} \cdot [P_s(z) + P_0] - \frac{\rho_0 \cdot \sigma_a \cdot (1-\eta)}{\frac{P_s(z)}{P_p^{th}} + 1} \cdot P_s(z) \tag{2}$$

where $P_p(z)$ and $P_s(z)$ are the pump and signal powers at s respectively, $P_{sat}$ is the homogeneous gain saturation power, $P_p^{th}$ is the pump power threshold, $\sigma_e$ and $\sigma_a$ are the fluorescence and absorption cross-sections at the signal wavelength, $\sigma_p$ is the absorption cross section at the pump wavelength, $\rho_0$ is the erbium concentration in the core region, $\eta$ is the signal mode/active core overlap factor. For the RFA, the pump and the signal satisfy the following differential equations[3]:

$$\frac{dP_p(z)}{dz} = \alpha_p \cdot P_p(z) + \frac{g \cdot P_p(z) \cdot P_s(z)}{A} \tag{3}$$

$$\frac{dP_s(z)}{dz} = -\alpha_s \cdot P_s(z) + \frac{\lambda_p}{\lambda_s} \cdot \frac{g \cdot P_p(z) \cdot P_s(z)}{A} \tag{4}$$

where $\alpha_p$ and $\alpha_s$ represent the fiber loss at pump and signal wavelengths, $\lambda_p$ and $\lambda_s$, respectively, A is the effective fiber core area, $g$ is the Raman gain coefficient.

$$g = \frac{g_0 \cdot (w/2)^2}{(\nu_p - \nu_s - \nu_0)^2 + (w/2)^2} \tag{5}$$

where $g_0$ is the peak Raman gain coefficient, $w$ is the full width at half-maximum of the Lorentisan lineshape of the Raman gain characteristic, $\nu_0$ is the Raman shift frequency, $\nu_s$ and $\nu_p$ are the signal and pump frequency respectively. By numerically solving the differential equations (1) to (4), the gain of our proposed EDFA-RFA repeater can be calculated.

## 3. Gain Optimization and Discussion

In order for the pump to operate efficiently for both the EDFA and RFA so that high gain can be achieved, a pump wavelength of 1.47 $\mu$m is selected. We note also that this pump wavelength is appropriate for the aluminosilicate $Er^{+3}$:glass EDFA which can be pumped at 1.46-1.47 $\mu$m. Let us consider now $L_f$, the fiber length of the RFA. For fixed pump power, increasing $L_f$ will increase the Raman gain but reduce the gain of the EDFA because of the reduction of pump power into the EDFA. Therefore, there should exist an optimised length of $L_f$ which will give maximum end to end gain $G_{BB} = 10 \cdot log10(P_{sout}/P_{sin})$ for the repeater. Besides the gain itself, an additional distance $L_f$ is also added to the repeater span. In order to estimate the maximum NRR span that can be realised, an equivalent gain $G_B$ is introduced. $G_B = G_{BB} + G_a = G_{BB} + L_f \cdot \alpha_s$, where $\alpha_s$ is the fiber loss at the signal wavelength. This relates to the NRR span by $L_B = G_B/\alpha_s$. Fig.2 shows how $L_{fo}$, the optimised fiber length $L_f$ for $G_{BB}$ and $G_B$, varies with pump power. It is seen that $L_{fo}$ is different for the two cases and is longer for optimising $G_B$ than

for optimising $G_{EE}$. To compare the cascade EDFA-RFA NRR with a single EDFA or RFA repeater, Fig.3 shows the optimised $G_E$ and $G_{EE}$ of our proposed NRR and the results obtained using only an EDFA or RFA. We see that the optimised EDFA-RFA NRR gives better performance than does the single EDFA or RFA NRR. The optimised $G_{EE}$ of 55dB or optimised $G_E$ of 61 dB can be achieved by 400mW pump power for 0.1 $\mu$W input signal power, which means that the output signal power can be as high as 30 mW and the maximun NRR span as long as 305km for 0.2dB/km loss single-mode fiber.

## 4. Conclusion

In this paper, a new cascade EDFA-RFA NRR configuration has been proposed and optimised. In this configuration, no additional components are needed other than for an EDFA NRR although higher pump powers are involved. The results show that this configuration offers, for the same pump power, improved performance compared with either the EDFA or RFA NRR used in isolation.

## References

[1] K. Aida et al.; *IEE Proceedings, vol.137, Pt.J, No.4, 1990, pp225-229*

[2] E. Desurvire et al.; *J. Lightwave Technol., vol.7, No.5, 1989, pp835-845*

[3] G. -D. Peng; *Electron. Lett., vol.26, no.5, 1990, pp334-335*

[4] E. Desurvire et al.; *Optics Letters, vol.14, No.22, 1989, pp1266-1268*

[5] S. T. Davey et al.; *IEE Proceedings, vol.136, Pt.J, No.6, 1989, pp302-306*

[6] E. Desurvire et al.; *Photonics Technology Letters, vol.2, No.3, 1990, pp208-210*

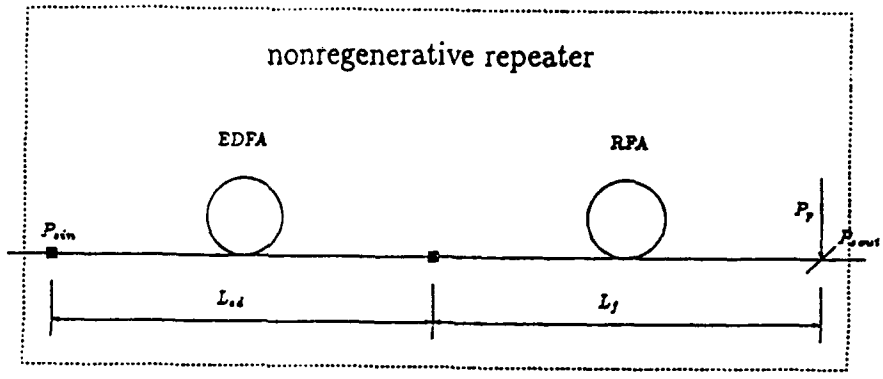


Fig.1 Configuration of EDFA and RFA Cascade Repeater

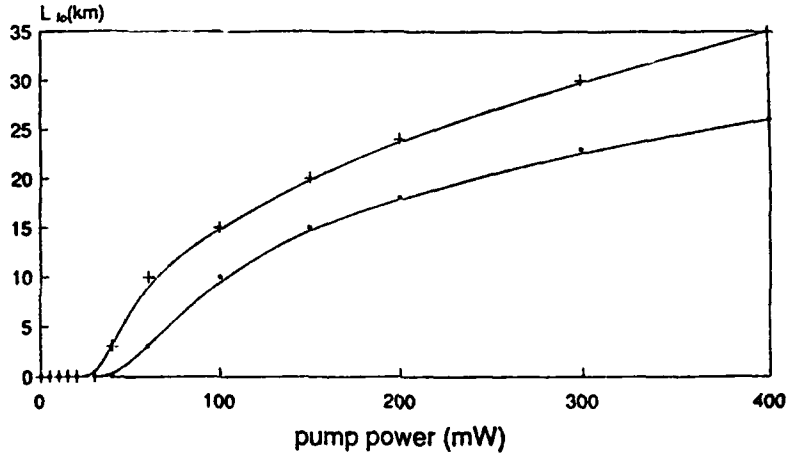


Fig.2 Optimized Fiber Length of RFA for $G_E$ and $G_{EE}$ Varies with Pump Power Values

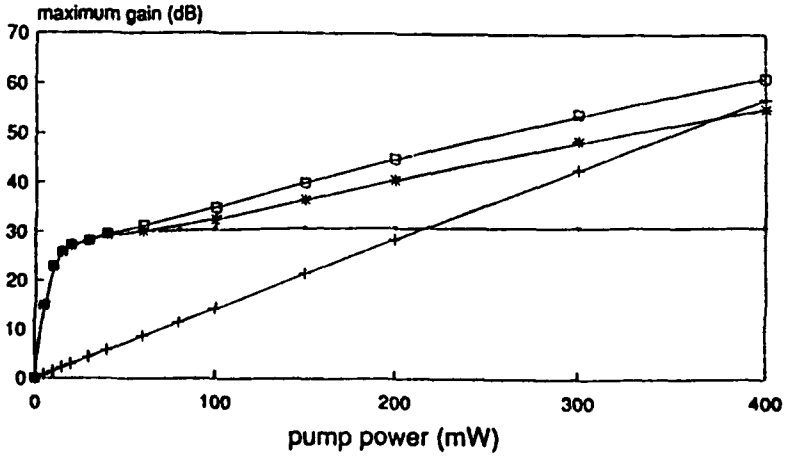


Fig.3 Comparison of the Optimized Gain of EDFA-RFA Cascade Repeater with That of Single EDFA or RFA Repeater

# An All-Optical Remote Gain Switching Scheme for Er-Doped Fiber Amplifiers

M. Zirngibl
AT&T Bell Laboratories
Crawford Hill Laboratory
Holmdel, New Jersey 07733
Phone: (908) 888-7153
Fax: (908) 888-7074

Er-doped fiber amplifiers (EDFA's) may find many potential application in optical networks due to their high gain, polarization insensitivity, low noise and immunity to cross-talk. They are especially useful in overcoming splitting losses in multiple access networks. Due to the very long $^4I_{13/2}$ lifetime of $Er^{3+}$, fast gain switching, which would be needed for packet switching for instance, is not possible with EDFA's. To direct traffic flow, however, slow gain switching schemes for EDFA's may still be very useful. The purpose of this letter is to demonstrate an optical feedback scheme, which allows remote switching of the gain, all-optically over the transmission fiber without the need for any electrical or mechanical control device.

Recently, we proposed an all-optical feedback loop, which efficiently stabilizes the gain in an EDFA [1]. In this scheme, a selected wavelength of the amplifier spontaneous emission (ASE) was coupled back to the input using linear components. Here, we insert a saturable absorber, in the form of an unpumped Er-doped fiber, into the feedback loop to form a non linear feedback loop (NFL). The EDFA with the NFL has two stable states: In the first, there is no ring-lasing since the unpumped Er-doped fiber highly absorbs the selected wavelength so that the ring is below threshold; in the second there is ring-lasing and the unpumped fiber is bleached by the optical power in the feedback loop. In the latter case, the signal gain in the EDFA is substantially depressed due to saturation by the ring-lasing. If the system is in the unlasing (gain-on) state, the ring-lasing can be switched on (and hence the gain switched off) by injecting a signal at the feedback wavelength. This signal first experiences high gain in the unsaturated amplifier and then it bleaches the Er-doped fiber in the NFL so that ring-lasing starts. Switching off the lasing (and hence switching on the EDFA gain) can be achieved by injecting a signal at a wavelength different from the feedback wavelength. This signal has to depress the EDFA gain below the threshold value required for ring-lasing.

The experimental set-up is shown in Fig. 1. The EDFA consists of 19.5m of a $Al_2O_3$:$GeO_2$:$SiO_2$ fiber with a small-signal peak gain of 34 dB. The amplifier is pumped through a wavelength selective coupler (WSC) at 1.48$\mu$m. The output of the EDFA is first isolated and then split by a wavelength independent 3 dB coupler (WIC) into an output branch and a feedback branch. In the feedback loop, an interference filter (IF) tuned to 1560nm with a 3 dB bandwidth of 1.2nm is inserted into a beam expander. The saturable absorber consists of 4m of a second piece of $Al_2O_3$:$GeO_2$:$SiO_2$ Er-doped fiber (EDF) whose small signal absorption coefficient at 1560nm was measured to be 5 dB/m. A second isolator prevents the backward ASE from entering into the feedback loop. Two signal channels are multiplexed with the NFL in a WIC and input to the EDFA through the WSC. The sources of the signal channels are a narrow bandwidth fiber laser (FL) tuned exactly to the feedback wavelength of 1560nm and a Fabry Perot laser diode (FP) whose frequency spectrum is centered around 1535nm. To study the dynamics of this switching scheme, the two signal

channels are chopped simultaneously in beam expanders. The EDFA output is monitored by an optical spectrum analyzer. A second output branch is filtered in a beam expander and detected by a Ge-photodetector. Ge-photodetectors are also used to monitor the signal power at $P_{sig}$ and the EDFA input at $P_{in}$.

The output spectra corresponding to the two bistable states of the EDFA-NFL scheme are displayed in Fig. 2. When the pump is first turned on, the system does not self-start lasing and the output spectrum for this case is given by the top curve in Fig. 2. The system is switched to lasing by injecting -24 dBm cw power (as measured at $P_{in}$) at 1560nm from the fiber laser, and remains lasing after removal of this signal. The output spectrum for this case is shown by the lower curve in Fig. 2. The lasing saturates the ASE by approximately 22 dB at the peak emission wavelength of 1530nm. The power in the feedback loop (as measured at $P_{in}$) was -8 dBm. Switching back to the non-lasing state is achieved by injecting -8.5 dBm (as measured at $P_{in}$) from the 1535nm laser diode. The ASE difference between the two states can not be exactly identified to the small signal gain difference due to the distributed generation of spontaneous emission over the whole fiber length. We therefore investigated the small signal gain difference at 1530nm by tuning the FL to this wavelength after switching on the ring-lasing. A net small signal gain difference of 26 dB between the two bistable states was found.

The dynamics of this switch was checked by alternatively injecting the switching signals by means of a chopper. The output IF was tuned to 1530nm so that the ASE peak power in a 1.2nm bandwidth was monitored by the Ge photodetector. The upper trace in Fig. 3 shows the two alternating input signals detected at $P_{sig}$ and the lower trace the time evolution of the ASE. As expected, the switching times of 10-50ms due to the long $^4I_{13/2}$ lifetime of the $Er^{3+}$.

As reported above, and also observed in Fig. 3, we need much more signal power to switch the lasing off than to switch it on. This is explained by the fact that the off-switching control signal has to decrease the already strongly saturated gain by an additional sufficiently large amount to depress the gain at the feedback wavelength below the minimum loss in the NFL. Therefore, the power of the switching-off signal has to be of the same order of magnitude as the ring-lasing power. In a real system, where it is not convenient to deal with high control signal power levels, this problem could be solved by selectively amplifying the switching-off control signal in a second EDFA.

The switching range in the presented scheme is limited by linear losses in the feedback loop like the WIC. In an optimized version, the multiplexing between signal input and output channel and feedback channel should be done with "loss-free" WSC's. In this case, a gain switching between transparency (1 dB) and unsaturated small signal gain could be theoretically achieved by using, in the feedback loop, an Er-doped fiber whose small signal loss compensates exactly the small signal gain in the EDFA at the feedback wavelength.

The author is grateful to A. A. M. Saleh for many helpful discussions.

## *REFERENCES*

[1] M. Zirngibl, "Gain Control in Erbium-Doped Fiber Amplifiers by an All Optical Feedback Loop", appeared in El. Letters, March 28, Issue 7, 1991.

*FIGURE CAPTIONS*

Figure 1 Experimental set-up. WSC = wavelength selective coupler, Be = beam expander, FL = fiber laser, FP = Fabry Perot laser diode, IF = interference filter, Is = Isolator, EDF = Er-doped fiber.

Figure 2 Output spectra of the bistable states. Upper curve: no lasing at feedback wavelength and high gain in the amplifier. Lower curve: lasing at feedback wavelength and low amplifier gain.

Figure 3 Switching dynamics. Upper trace: Control-signal input at $P_{sig}$, lower trace: ASE output at 1530nm in a 1.2nm bandwidth at $P_{ASE}$.

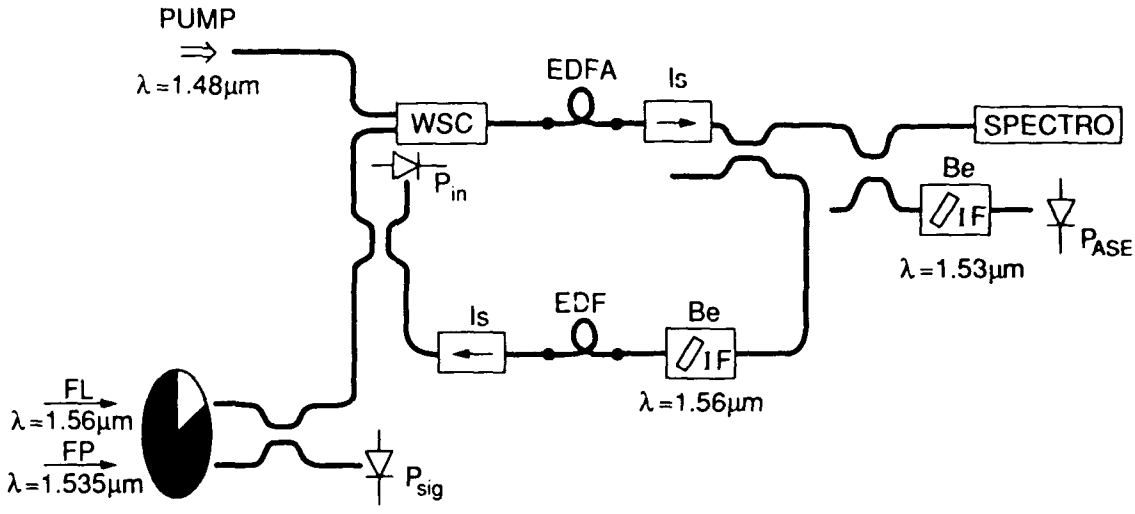


FIGURE 1

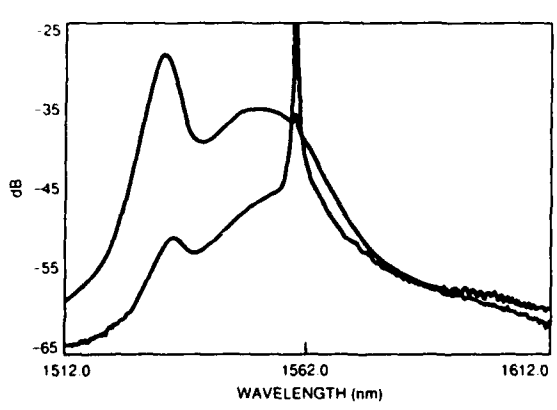


FIGURE 2

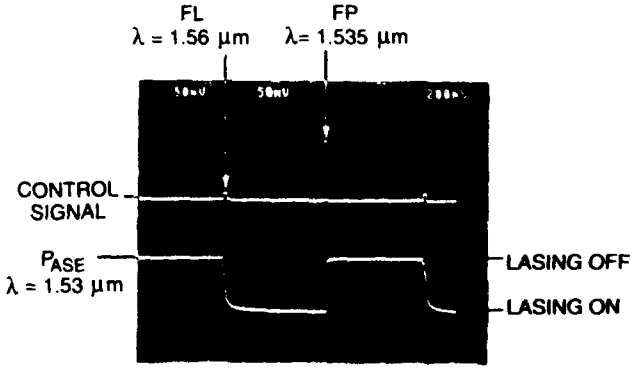


FIGURE 3

# Optical Amplifiers Operating in a Random Access Fiber Loop Optical Memory

G.Großkopf, L.Küller, R.Ludwig, W.Pieper, R.Schnabel, H.G.Weber
Heinrich-Hertz-Institut für Nachrichtentechnik Berlin GmbH
Einsteinufer 37, D-1000 Berlin 10, FRG

**Abstract:** In a fiber loop optical memory the applications of semiconductor laser amplifiers as switching elements and of Erbium doped fiber amplifiers as gain controlling elements are investigated.

**Introduction:** The use of fiber loops as recirculating delay lines or "optical memories" is discussed since several years /1 - 5/. One result of these investigations is, that optical amplifiers are required in the fiber loop, but that "ring laser" operation has to be avoided. The most straight forward solution of this problem is periodic gating of the loop. In Ref.5 the application of this technique enabled 160 Mbit/s data transmission at BER = $10^{-9}$ for one round trip and at BER = $10^{-4}$ for two round trips.

In Ref.6 transmission of a 1.7 Gbit/s signal (cell length 512 bit, $2^9$- 1 PRBS) was measured for constant signal power (-30 dBm) at the input of the fiber memory (point A in Fig. 1) with a constant BER = $10^{-9}$ for up to seven round trips in the loop. The number of round trips was only restricted by experimental constraints. The results in Ref.6 profited strongly from the appropriate use of a semiconductor laser amplifier (SLA) as switching element for the periodic gating and of an Erbium doped fiber amplifier (EDFA) as gain controller in the fiber loop. This paper reports on the operation of both devices in the fiber loop and on the properties of the optical memory.



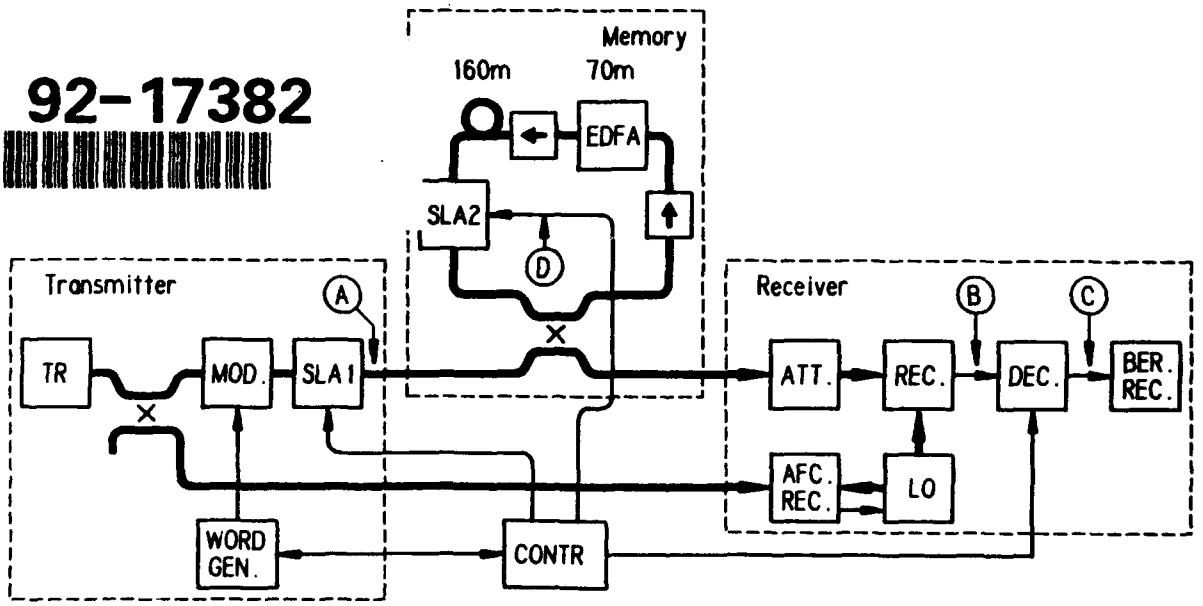


**Fig. 1:** Experimental set up consisting of the 4 parts: transmitter, fiber loop memory, receiver and control unit; thick lines are optical paths and thin lines are electrical paths

**Experiment:** Fig. 1 depicts the experimental set up used in Ref. 6. It consists of 4 parts: the transmitter, the memory, the receiver, and the control unit. The optical paths are indicated

by thick lines and the electrical paths by thin lines. The optical and electrical signals at the points A, B and D are depicted in Fig. 2. The transmitter output signal (A in Fig. 2) has two characteristic times, the packet length $\tau_P$ and the frame length $\tau_{FR}$. In the experiments, we used $\tau_P = 0.6\mu s$ and $\tau_{FR} = 9.64\mu s$.

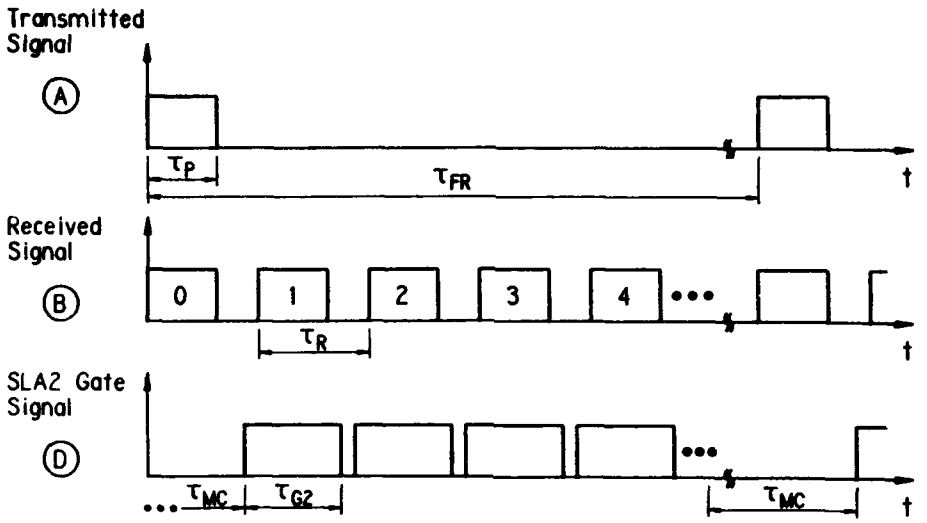


Fig. 2: Schematic of the optical and electrical signals at the points A, B and D indicated in Fig. 1

The ATM-cell is a fraction of the packet with the cell length $\tau_C < \tau_P$. In the experiment we used a $2^9$- 1 PRBS with $\tau_C = 512$ bit $(B_T)^{-1} = 0.301$ $\mu$s where the bit rate is $B_T = 1.7$ Gbit/s. The packet is generated by the gate SLA1, which is a semiconductor laser amplifier operating as optical switch and the ATM-cell is generated by the transmitter laser TR, the modulator MOD and the word generator WORD GEN. The timing of both the packet and the ATM-cell is controlled by the control unit CONT.

The signal B in Fig. 2 represents a train of packets seen by the receiver. The numbers n = 0, 1, 2 ... indicate the number of round trips in the loop. The number 0 designates the directly transmitted packet. In the DEC (decision circuit and gating unit) the signal B is gated such, that only the packet with the desired number n is received by the BER-receiver. The gate is controlled by the control unit CONT. In a more realistic system this gating operation is part of the memory and is performed in the optical domain.

In the transmitter and receiver parts, we used components of a coherent optical transmission system which was at hand /7/. In the transmitter part, TR is an external cavity laser and MOD is a $LiNbO_3$ phase modulator. Physically the ATM-cell is a phase modulated (DPSK) carrier wave. In the receiver part, REC is a balanced phase and polarization diversity receiver, which converts the optical packet train into an electrical packet train. Contrary to a more realistic direct detection system, our coherent system needs additional components: the gate SLA1, the local oscillator LO and the additional AFC path for the control of the intermediate frequency.

The memory consists of a fiber coil (lenght 160 m), a 3 dB fiber coupler, an Erbium doped fiber amplifier (EDFA, length 70 m) with optical isolators, and a semiconductor laser amplifier (SLA2) operating as optical switch. The SLA2 is switched periodically by the gating signal D as indicated in Fig. 2. The memory has 3 characteristic times, the round trip time $\tau_R$, which a packet needs for one circulation in the loop, the gating time $\tau_{G2} < \tau_R$ during which the SLA2 is in the transmission state and the memory clear time $\tau_{MC} > \tau_R$. In the experiment we used $\tau_R = 1.1\mu s$,

$\tau_{G2} = 0.7\mu s$ and $\tau_{MC} = 1.4\mu s$. The loop requires an automatic gain control. This operation is simply obtained by gain saturation in the EDFA. The control unit CONT is an essential part of the present experimental set up. But in a more realistic system it is replaced by a control unit which controls the memory part.

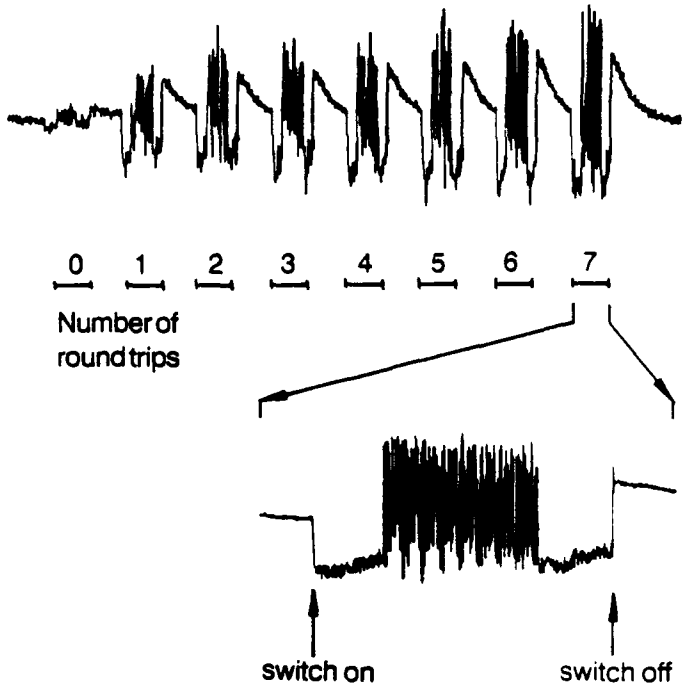


**Fig. 3:** Packet train measured at point B in Fig. 1. The number n denotes the number of round trips in the fiber loop. The signal with n = 7 is extracted in the lower part of this figure.

**Results:** Fig. 3 shows in the upper part an oscilloscope trace of the received packet train (signal in point B in Fig. 1). Indicated is the number n of round trips in the fiber loop of each received packet. Note that the directly transmitted packet (n = 0) has much less signal power than the packets that have circulated in the loop, because the loop has an effective gain. Gain saturation in the EDFA causes an approximately constant signal amplitude for $n \geq 1$. In the lower part of Fig. 3, the packet with n = 7 is extracted in order to display the switching behaviour of the SLA gate. This switching behaviour is depicted in detail in Fig. 4 for the switch "on" operation and in Fig. 5 for the switch "off" operation.

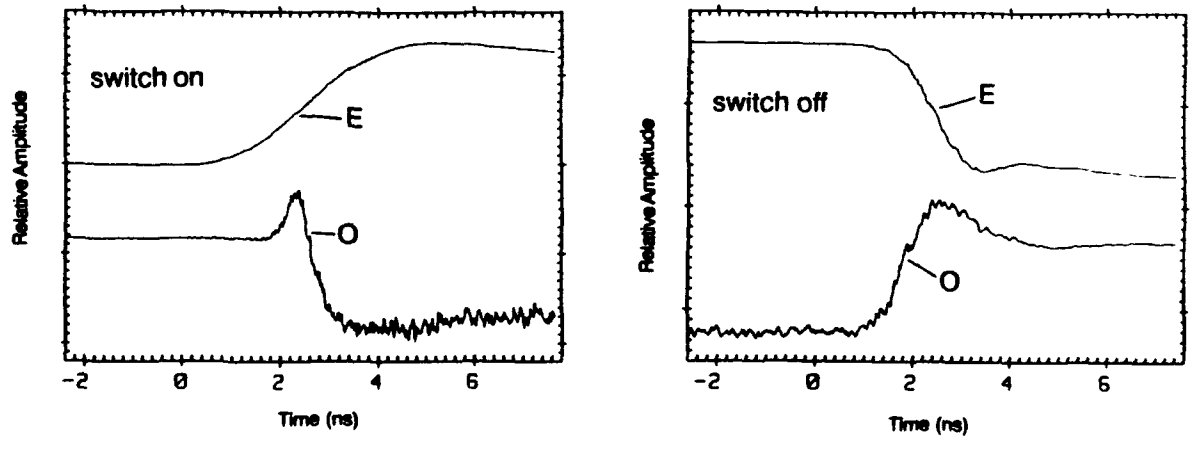


**Fig. 4 and 5:** Electrical gating signal (E) and measured switching response of the SLA gate (O) in the switch "on" and "off" operation.

In both figures trace E shows the electrical gating signal and trace O the response of the SLA gate at the receiver (position B of Fig. 1). As the receiver is a DPSK coherent optical receiver, it detects the amplitude and phase change of the optical signal associated with the switching operation in the SLA. It is evident from both figures that the switching times are less than 2 ns in both switching operations.

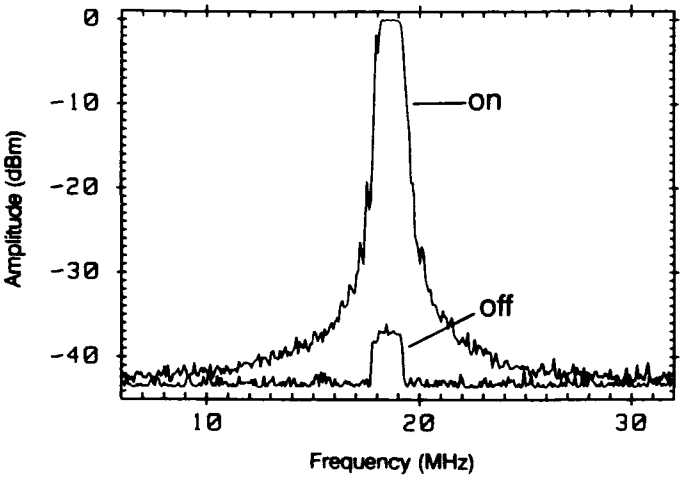


**Fig.6:** Measurement of the on/off ratio of the SLA gate

Figure 6 depicts the measured on/off ratio of the SLA gate. In this case an unmodulated carrier wave was transmitted through the SLA gate in the "on" and "off" position. Using a heterodyne receiver the intermediate frequency signal was displayed with a spectrum analyzer using maximum hold operation. An on/off ratio of 35 dB was obtained.

**Conclusion:** The operation of a semiconductor laser amplifier and of an Erbium doped fiber amplifier in a periodically gated fiber loop memory was investigated. The semiconductor laser amplifier provides a good on/off ratio and sufficient small switching times when operated as optical switch. The Erbium doped fiber amplifier turns out to be useful as gain controller because its saturation time constant is much larger than the round trip time of a packet in the fiber loop.

**Acknowledgement:** The authors are indebted to Dr.Edagawa from KDD (Japan) for providing the Erbium doped fiber. Support from our colleagues Mr.Heydt, Mr.Langenhorst, Mr.Eiselt, Mr.Dietrich, Mr.Molt and Mrs.Mikulski is friendly acknowledged. This work was supported by the Bundesminister für Forschung and Technologie of the Federal Republik of Germany under contract TK 04607.

**References**

1 R.A.Thompson, IEEE J.Selected Areas in Commun. Vol.6, No.7, (1988) 1096

2 M.I.Belovolov et al., Proc. Optical Computing 88 SPIE Vo.963, (1988), 90

3 S.Suzuki et al., Proc. Photonic Switching Topical Meeting, Salt Lake City, USA, (1989) paper FA3

4 G.Hodgkinson et al., Electron.Lett., Vol.26, No.16, (1990), 1262

5 C.Saxtoft, Proc. Photonic Switching Topical Meeting, Kobe, (1990), paper 14B-7(PD)

6 R.Ludwig et al., submitted to ECOC/IOOC 91, Paris

7 R.Langenhorst et al., IEEE Phot.Technol.Lett., (1991) in press

## GENERAL COCHAIRS

**Kiyoshi Nakagawa**
NTT Transmission Systems Laboratories, Japan

**David Payne**
University of Southampton, United Kingdom

**N. Anders Olsson**
AT&T Bell Laboratories, USA

## TECHNICAL PROGRAM COMMITTEE

### PROGRAM COCHAIRS

**Mike O'Mahony**
British Telecom Research Laboratories, United Kingdom

**Richard E. Wagner**
Bellcore, USA

### FIBER AMPLIFIERS AND FIBER COMPONENTS

**R. I. Laming,** *Chair*
University of Southampton, United Kingdom

**W. L. Emkey**
AT&T Bell Laboratories, USA

**E. Desurvire**
AT&T Bell Laboratories, USA

**G. Grasso**
Societa Cavi Pirelli SpA, Italy

**D. W. Hall**
Corning, Inc., USA

**C. A. Millar**
British Telecom Research Laboratories, United Kingdom

**W. J. Miniscalco**
GTE Laboratories, USA

**M. Nakazawa**
NTT Transmission Systems Laboratories, Japan

**M. Ogai**
The Furukawa Electric Company Ltd., Japan

**S. Poole**
University of Sydney, Australia

**H. Tanaka**
Mitsubishi Cable Industries Ltd., Japan

### SEMICONDUCTOR AMPLIFIERS AND PUMP LASERS

**K. Kurumada,** *Chair*
NSC Electronics Laboratories, Japan

**M. J. Adams**
British Telecom Research Laboratories, United Kingdom

**D. P. Bour**
David Sarnoff Research Center, USA

**G. Eisenstein**
Technion-Israel Institute of Technology, Israel

**T. Kamijoh**
OKI Electric Industry Company Ltd., Japan

**T. Kamiya**
University of Tokyo, Japan

**I. Mito**
NEC Corporation, Japan

**K. E. Stubkjaer**
University of Denmark, Denmark

**M. Suyama**
Fujitsu Ltd., Japan

**C. E. Zah**
Bellcore, USA

### SYSTEMS APPLICATIONS AND INSTALLATIONS

**C. R. Giles,** *Chair*
AT&T Bell Laboratories, USA

**K. Aida**
NTT Transmission Systems Laboratories, Japan

**J. Auge**
CGE, Marcoussis, France

**T. Hadjifotiou**
STC Technology Ltd., United Kingdom

**E. Eichen**
GTE Laboratories, USA

**R. Heidemann**
SEL/Alcatel, Federal Republic of Germany

**C. Lin**
Bellcore, USA

**J. J. O'Reilly**
University of Wales, United Kingdom

**Y. K. Park**
AT&T Bell Laboratories, USA

**S. Yamamoto**
KDD Meguro R&D Laboratories, Japan